Dual reactivity disulfide bridging reagents for antibody bioconjugation

Alina Anna Chrzastek

A thesis submitted in partial fulfilment of the requirements for the degree of Doctor of Philosophy

Supervisor: Prof James R. Baker

September 2022

Declaration

I, Alina Anna Chrzastek, confirm that the work presented in this thesis is my own. Where information has been derived from other sources, I confirm that this has been indicated in the thesis.

Alina Chrzastek

September 2022

Abstract

Antibody drug conjugates (ADCs) are monoclonal antibodies combined with drug moieties, these constructs jointly provide target specificity and potency. However, the majority of approved ADCs are heterogenous mixtures of species with different drug-to-antibody ratio (DAR) and conjugation sites, leading to species with varying toxicity profiles and pharmacokinetics. To overcome this problem, a major focus in the field is on creating homogenous ADCs. Approaches include engineering specific amino acid sequences that can be further used as a tag for enzymatic or chemical bioconjugation, however, these techniques are often laborious and costly.

Disulfide rebridging also known as disulfide stapling, represents an intriguing new method for site-selective bioconjugation on native antibodies. This involves reduction of disulfide bonds, which are then reconnected by rebridging reagents, creating homogenous conjugates. In our research group, we have previously reported that bis-thioesters are disulfide rebridging reagents that can be further exploited to transfer to nearby lysines, offering site-selective lysine conjugation.

In this work, further exploration of the thioester moiety has led to their application in creating multifunctional antibody fragment conjugates. A selection of novel bis-electrophiles containing the thioester moiety were synthesised and tested on a reduced antibody Fab fragment for their disulfide rebridging ability.

It was found that thioester containing reagents can be designed and used to insert a 'stable-labile' linkage between the two cysteines. The reactive labile handle was employed in a subsequent bioconjugation step *via* native chemical ligation with an *N*-terminal cysteine peptide that allows for construction of antibody peptide conjugates. A second strategy was also developed, where use of hydrazine as a ligating nucleophile enabled attachment of two separate cargos on each Fab cysteine, which can be exploited to insert variably cleavable linkers. The insertion of a 'stable-labile' handle with thioesters has demonstrated an enticing new chemical toolbox to enable facile production of diverse antibody conjugates.[1]

Impact statement

The advances in oncological therapies have led to the development of highly tailored antibody-drug conjugates (ADCs). ADCs utilise the specificity of monoclonal antibodies that have a very high affinity towards their particular target. The cytotoxic drugs commonly used in ADC therapies are extremely potent, and administration of the agent on its own could create unfavourable outcomes for the patient by also attacking healthy cells. Therefore, monoclonal antibodies have been selected as vectors, capable of targeting tumour cells while simultaneously delivering a potent cytotoxin. The majority of the approved ADCs, or those currently in clinical trials, are synthesised by modification of proteinogenic amino acid residues on the antibody. Although a range of amino acids can be targeted, lysine and cysteine residues are commonly used due to their highly nucleophilic amine and thiol groups respectively, which can react with electrophiles. Cysteine bioconjugation techniques give an unprecedented degree of site-selectivity and homogeneity whereas lysine conjugation leads to unselective and heterogenous conjugates, yet it is clinically validated.

Currently, there are eleven ADCs approved for human treatment, with eight of these approved in the past five years; making this a very exciting field to be working in. However, development of ADCs still present certain levels of challenge, namely the premature release of the linker-drug attachment in the bloodstream, the production of heterogenous species with different drug to antibody ratio (DAR), and the hydrophobicity of the payload. Thus, research within linker bioconjugation technologies is still ongoing to create successful new oncological treatments. The principal focus of this project was to identify novel site-selective bioconjugation methodologies for antibody conjugation that would lead to homogenous species and also allow for diverse functionalisation.

To achieve this, we developed a novel class of thioester containing reagents to target disulfide bonds; ideal handles for site-specific modification, through a rebridging and cross-linking mechanism. These reagents were then used towards new bioconjugation strategies. The insertion of the thioester moiety within the disulfide bridge in an antibody allowed for the introduction of further functionalities without the need of laborious chemical synthesis to produce one reagent containing the linker and the cargo.

Two key protocols were developed, one based on the principles of native chemical ligation allowing for a very convenient bioconjugation to generate antibody-peptide fusions. The second

protocol uses hydrazine as the ligating nucleophile that in turn enables attachment of two different cargos, which can be cleaved off in different cellular environments.

This work introduces a new class of reagents and new bioconjugation techniques that could have a beneficial impact on future research in academia and the pharmaceutical industry. Applications such as multi-labelling of protein conjugates with cleavable fluorophores, radiolabelling for imaging, or attachment of dual warhead drugs to reduce the chance of drug resistance are just some of the medical fields where these novel methodologies could be utilised.

Dla mamy

Acknowledgments

These last four years have been the hardest and the best in my life and I cannot imagine a better place and better group of people to share this journey with me. Everyone whom I met in the KLB 220 in the past four years has had some impact on my scientific research and experience at UCL.

First and the most I would like to thank Prof Jamie Baker. During our first meeting, I told Jamie that I have never done any chemistry, his eyes did not move for the longest 5 sec, but then he said 'okay, you will be fine'. I feel very lucky to have had such a supportive, enthusiastic, encouraging, and calm supervisor. Jamie is an exceptional mentor, who always pushed me out of my comfort zone, but was also there when I needed a guidance and help (sometimes a lot of it). Thank you for giving me this opportunity. I also want to thank Prof Vijay Chudasama for insightful comments and guidance throughout my PhD and his uninhibited sense of humour, without which the lab would not be the same.

Thanks to Dr Abil Aliev for providing the NMR support, Dr Kersti Karu for teaching me a lot about ins and outs of LCMS. Dr James Irving for his help during the biophysical assay. I am also grateful to Prof Stefan Howorka for conducting my upgrade *viva* examinations. I thank my examiners, Dr Daniele Castagnolo and Dr Louis Luk, for taking the time to read my thesis and carry out my *viva* examination.

The KLB has been a wonderful place to work, and without a doubt having 20 or so very unique personalities around, made the PhD journey doable. My first baby-steps into the chemistry world would not have gone smoothly if not for the enormous help from Dr Nafsika Forte, who patiently explained to me stuff ranging from what is that big bowl of hot water and that having too many peaks in your NMR is not always good. I thank Dr Archie Wall for deep conversations about certain boy with a scar on his forehead and guiding me through principles of TLC.

Certainly, the day-to-day lab-life would not be as pleasant as it was thanks to the two Senior Bakers: Muhammed and Yanbo. I would especially like to thank Muhammed Haque for being a '5 star' friend since day one of our rotations. Sharing a fumehood, office and finally one desk meant that I could not get rid of you. Thank you for all your science help and non-science chats, I am also very grateful to witness your first sip of coffee, that truly is a cherry on the top of my PhD. My dearest Yanbo Zhao, you have been a constant throughout our PhD journey, thank you

for showing me that there is more to life than just science, like influencing and eating out in fancy places. Thank you for giving me (and many other people) a hand when stuck in maths with your big calculator brain and thank you for being a superb friend.

Special thanks to Dr Roshni (Roshiniii, Rashniii, RMfH) Malde, for not only being an inspirational scientist but also a really good friend. Sharing your science wisdom in chemistry and also on how to win all the awards and medals was much appreciated, and much was learned from it. A big shout out to Luigia (Lula) Salerno for being the chilliest person I know and boosting my Animal Crossing Island life. Thanks to the youngest scientist I have ever worked with, Mikesh Patel for all the good laughs, games, and pranks. Your extensive knowledge about actors, movies, perfumes and chemistry mechanisms was very handy at times and will be missed by me.

The 'Baker-delight' or the 'Crème de la crème' was undoubtfully the Baker Group, each individual brought up something special to the table, like I was the funniest one, Nafiska the smartest one, Muhammed the prettiest one etc. All of you and each individually will always have a special place in my heart and the gap left by you all will be hard to fill up.

This section could not be complete without mentioning Usman Shabbir whose curiosity about other people life never stops to amaze me. We shared loads of good times together, snack breaks often guided by 'redpen' mischief, I will cherish those memories forever. Thanks to Nehaal Ahmed for introducing me to other, natural ways to achieve the 'bliss' moment, I will certainly be in touch.

I am also very grateful to all the past and present members of the Baker-Chudasama-Sheppards super group from the KLB 220; Dr Antoine Maruani (for his excellent baking skills), Dr André Shamsabadi (for his flag expertise), Dr Calise Bahou (for his introduction to gambling), Dr Faiza Javaid (for her world-wide gossip knowledge), Dr Richard Spears (for his immense science help and introduction to how to look for a job), Dr Steven Yap (excellent coffee discussions and being his forced 'plus one' to Housman Room events), Dr Fabien Thoreau (for help with coupling troubleshooting and shuffling expertise), Dr Dave Chisholm (for approving my music choices when others didn't), Dr Peter Szijj (for his LCMS know-how), Dr Matt Penny (for taking over my waste (trash) job and being a good friend), Dr Rachel Szpara (the best cake-bake-fairy), Dr Sahra St John-Campbell (for playing 'reggaeton' music and reminding me to get back to

Spanish), Dr Richard Procter (for cleaning the sink), Alex Furby (for his enormous trivia knowledge), Lea Rochet (excellent books recommendation), Ioanna Thanasi (for 'that' PD and help with the paper), Cliona McMahon (for demonstrating that you can indeed skate in the lab), Chapman Ho (unconventional fashion), Phyllida Britton (for being a first aider, yet stabbing herself on multiple occasions). I would also like to thank our visiting scientists Ilias Koutsopetras (for showing me the Greek essence) and Bianka Jackowska (for her help with ELISA optimisation).

I would like to extend my gratitude to my closest friends outside of the PhD: Maria Puiu, Paulina Brajer, Cristina Aller Garcia, Bahareh (Bee) Niknani, Marta Woldanski, Bozena De Becker, Xiao Wang, Yeannethe Ramos Calderon. Thank you all for checking up on me during the last four years, this meant a lot to me.

Undoubtfully, my deepest gratitude goes to my family, without whom I would not be able to start and finish this journey. Thanks to Rachith for his patience and the voice of wisdom. Special thanks to my brothers, Michał and Maciek for never failing to ask me when am I going to finish school. My ultimate gratitude goes to my parents Mirosława and Eugeniusz for supporting me and dealing with my emotional rollercoaster throughout the last four years.

Finally, I would like to thank myself, for making the decision to undertake PhD and going through the end:

"Last but not least, I wanna thank me
I wanna thank me for believing in me
I wanna thank me for doing all this hard work
I wanna thank me for having no days off
I wanna thank me for, for never quitting
I wanna thank me for just being me at all times"

Snoop Dogg

Table of contents

Abbreviations

Å	Angstrom
ACS	Antigen Combining Site
ADC	Antibody Drug Conjugate
Ala	Alanine
aq.	Aqueous
BBS	Borate Buffered Saline
BiTE	Bispecific T Cell Engager
BME	β-Mercaptoethanol
Boc_2O	Di-*tert*-butyl decarbonate
bsAbs	Bispecific Antibodies
CBTF	Sodium 4-((4-(cyanoethynyl)benzoyl)oxy)-2,3,5,6-tetrafluorobenzenesulfonate
$CDCl_3$	Deuterated Chloroform
CDRs	Complementary Determining Regions
CLT	Cysteine-to-Lysine Transfer
CMC	Chemistry, Manufacturing, and Control
COSY	Correlated Spectroscopy
CPP	Cell Penetrating Peptide
CuAAC	Copper-Catalysed Azide-Alkyne Cycloaddition
Da	Dalton
DAR	Drug-to-Antibody Ratio
DBM	Dibromomaleimide
DCM	Dichloromethane
DEPT	Distortionless Enhancement by Polarisation Transfer
DHAA	Dehydroascorbic Acid
DIPEA	*N*,*N*-Diisopropylethylamine
DMAP	4-Dimethylaminopyridine
DMF	*N*,*N*-Dimethylformamide
DMSO	Dimethyl Sulfoxide
DNA	Deoxyribonucleic Acid
DTT	Dithiothreitol
DTNB	5,5'-dithio-bis-(2-nitrobenzoic acid)
EDC	1-Ethyl-3-(3-dimethylaminopropyl)carbodiimide

EDTA	Ethylenediaminetetraacetic Acid
EEDQ	2-Ethoxy-1-ethoxycarbonyl-1,2-dihydroquinoline
EI	Electron Ionization
ELISA	Enzyme Linked Immunosorbent Assay
EMA	European Medical Agency
Eq.	Equivalents
ESI	Electrospray Ionization
EtOAc	Ethyl Acetate
Fab	Fragment Antigen Binding
FAR	Fluorophore-to-Antibody Ratio
Fc	Fragment Crystallisable
FcRn	Neonatal Fc Receptor
FDA	Food and Drug Administration
FGE	Formylglycine Generating Enzyme
g	Gram
GFP	Green Fluorescent Protein
GSH	Glutathione
h	Hour
HC	Heavy Chain
HER2	Human Epidermal Growth Factor Receptor 2
HL	Heavy Light
HMBC	Heteronuclear Multiple Bond Correlation
HOBt	Hydroxybenzotrazole
HPLC	High-Performance Liquid Chromatography
HRMS	High Resolution Mass Spectrometry
HRP	Horseradish Peroxidase
HSA	Human Serum Albumin
HSQC	Heteronuclear Single Quantum Coherence
kDa	Kilodalton
IR	Infrared
LC	Light Chain
LCMS	Liquid Chromatography Mass Spectrometry
LCMS/MS	Tandem Liquid Chromatography Mass Spectrometry

LRMS	Low Resolution Mass Spectrometry
M	Molar
mAb	Monoclonal Antibody
MeCN	Acetonitrile
MeOH	Methanol
MeOD	Deuterated Methanol
MESNa	2-Mercaptoethanesulfonate Sodium Salt
Me	Methyl
mg	Milligram
min	Minute
mL	Milliliter
mM	Millimolar
mmol	Millimole
mp	Melting Point
MPAA	4-Mercaptophenylacetic acid
MS	Mass Spectrometry
MWCO	Molecular Weight Cut-Off
m/z	Mass-to-Charge Ratio
NaOAc	Sodium Acetate
Net_3	Triethylamine
NCL	Native Chemical Ligation
NGM	Next Generation Maleimide
nM	Nanomolar
NMR	Nuclear Magnetic Resonance
NOESY	Nuclear Overhauser Effect Spectroscopy
ON	Overnight
qPCR	Quantitative Polymerase Chain Reaction
QTOF	Quadrupole Time-of-Flight
PABC	*para*-aminobenzyl carbamate
PB	Phosphate Buffer
PBS	Phosphate Buffer Saline
PD	Pyridazinedione
PDB	Protein Database

PEG	Polyethylene Glycol
Phe	Phenylalanine
PNGase F	Peptide: N-glycosidase F
PROTAC	Proteolysis Targeting Chimera
pM	Picomolar
ppm	Parts Per Million
RNA	Ribonucleic Acid
Rpm	Revolutions Per Minute
RT	Room Temperature
scFv	Single-Chain Fv
SDS-PAGE	Sodium Dodecyl Sulphate-Polyacrylamide Gel Electrophoresis
SMCC	Succinimidyl 4-(N-maleimidolmethyl) cyclohexane-1-carboxylate
SPAAC	Strain Promoted Azide-Alkyne Cycloaddition
SPh	Thiophenol
TAT	Trans-Activator of Transcription
TCEP	Tris(2-carboxyethyl)phosphine
TDC	THIOMAB-Drug Conjugate
TFA	Trifluoroacetic Acid
THF	Tetrahydrofuran
TLC	Thin Layer Chromatography
UAA	Unnatural Amino Acid
UV-Vis	Ultraviolet Visible Spectroscopy
μg	Microgram
μL	Microlitre
μM	Micromolar
μmol	Micromole
Val	Valine

Chapter 1: General introduction

1.1.1 Antibodies

Immunoglobulins, commonly known as antibodies, are glycoproteins that are part of the adaptive immune system and shield the host from diseased cells and pathogens. Antibodies can be classified into five different classes: IgA, IgD, IgE, IgG and IgM. The classification is based on their heavy chains that provide different serological properties and, as a result, different behaviour towards antigens. The most abundant IgG isotype is further categorised into four subclasses; IgG1, IgG2, IgG3, and IgG4.[2]

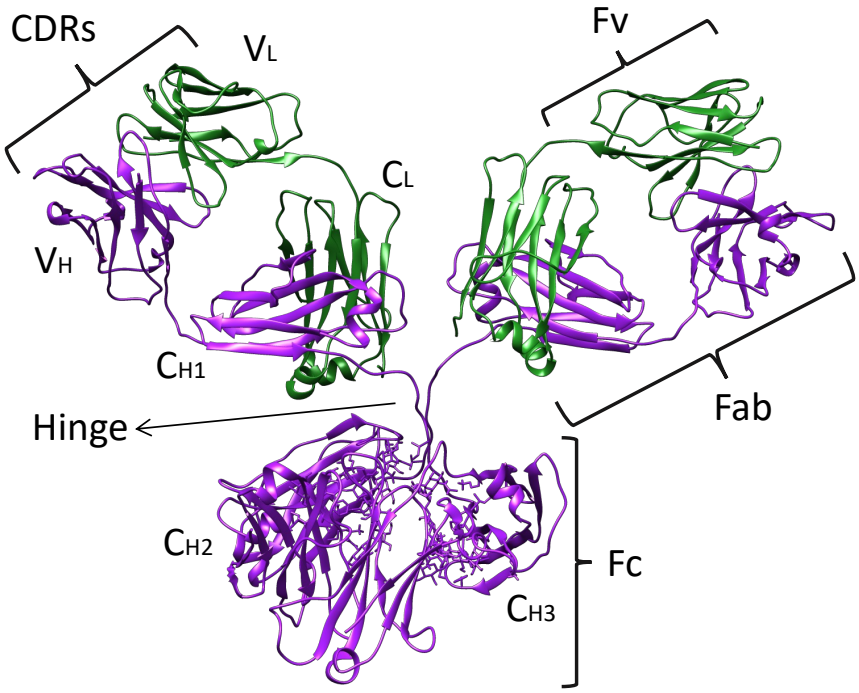

Figure 1. Full intact antibody IgG1 (PDB ID: 1IGY). Figure adapted from Harris *et al*.[3]

Antibodies are comprised of four polypeptides chains, two pairs of shorter 'light' chains (**Figure 1**, green) and two long 'heavy' chains (**Figure 1**, purple), further to that, heavy and light chains contain constant domains (CH or CL) and variable domains (VH or VL). The whole antibody can be divided into regions, comprising of the 'Fragment Antigen Binding' region (Fab) and the 'Fragment Crystallisable' region (Fc). The Fab fragment consists of the two *N*-terminal heavy domains (VH and CH1) and the light chain (VL and CL) that are linked together with inter-chain disulfide bonds (S-S). The top part of Fab region consists of variable domain known as the Fv region (VH and VL domain) and this is where the 'complementary determining regions' (CDRs)

are found.[4] The CDRs consist of three heavy and three light chain hypervariable loops creating a wide range of diversity through the variation of the nature of the binding surface and shape. The Fc region is comprised of two heavy chain constant regions (CH2 and CH3), and it is involved in modifying the immune system response to the formation of an antibody-antigen complex. Glycosylation occurs on the CH2 domain which is important for the antibody as it determines the antibody clearance from the body and it is present at the conserved regions of the Fc region.[2] The Fc region also contains a binding site for the Fc receptor (FcRn) which is involved in phagocytosis and antigen presentation, alongside the classical FcγR and complement pathway.[5] The chains composing antibodies are joined together by interchain disulfide bonds that create a flexible region called the hinge region, except IgM and IgD that lack the hinge region but contain an extra heavy chain domain.[6] The hinge region gives the antibody flexibility to bind to antigens effectively.

1.1.2 Monoclonal antibodies

The current advances in the development of monoclonal antibody (mAb) therapeutics have led to a significant rise in approved drugs in the past 30 years. Therapeutic antibodies express high specificity and affinity towards an antigen as well as showing fewer off-target side-effects when compared to small molecular weight compounds.[7] Currently, there are over 100 mAbs approved for human treatment in by FDA or EMA.[8] In 2018 there were 12 new mAbs therapeutics that received approval in the US or EU, with further 5 approved in 2019.[9] In comparison 2020 saw approval of 10 new mAbs and 19 in 2021[8]. To this day there are over 570 mAbs in various clinical phases[10] with the majority of mAbs on the market come from only one of the IgG subclasses, specifically IgG1 (79%) and having a kappa light chain (70%). The IgG1, and also in some cases IgG4, have a high activatory:inhibitory FcγR binding ratio which is optimal for clinical reagents.[11] Fully human mAbs account for 54% of approved antibodies with the rest being split between chimeric (14%) containing domains from different species (mostly murine) and humanised (32%) made up from human protein sequences.[12] Majority of approved mAbs were for cancer treatment (45%), the remaining was divided between immune-mediated disorders (27%), infectious diseases (8%), cardiovascular disorders (7%), and various other therapies.[8]

1.1.3 Antibody Drug Conjugates

Antibody drug conjugates (ADCs) are a result of modifying native monoclonal antibodies to allow for targeted delivery of highly potent therapeutics to specific cancerous cells.[13] Many nature-derived chemotherapeutic drugs are too toxic to be administered systematically, therefore these are attached to an antibody *via* a carefully designed linker (**Figure 2**). Ideally, ADCs carrying a potent drug should be efficiently internalised into the lysosome upon binding to the antigen on the surface of the tumour, followed by release through proteolytic, acid cleavage or disulfide reduction.[7] The idea of ADCs as a "magic bullet" has been around for decades, but the first regulatory approval was not until 2000 with the ADC Mylotarg.[7] There are currently 11 ADCs approved in the US or EU as of the end of 2021.[9]

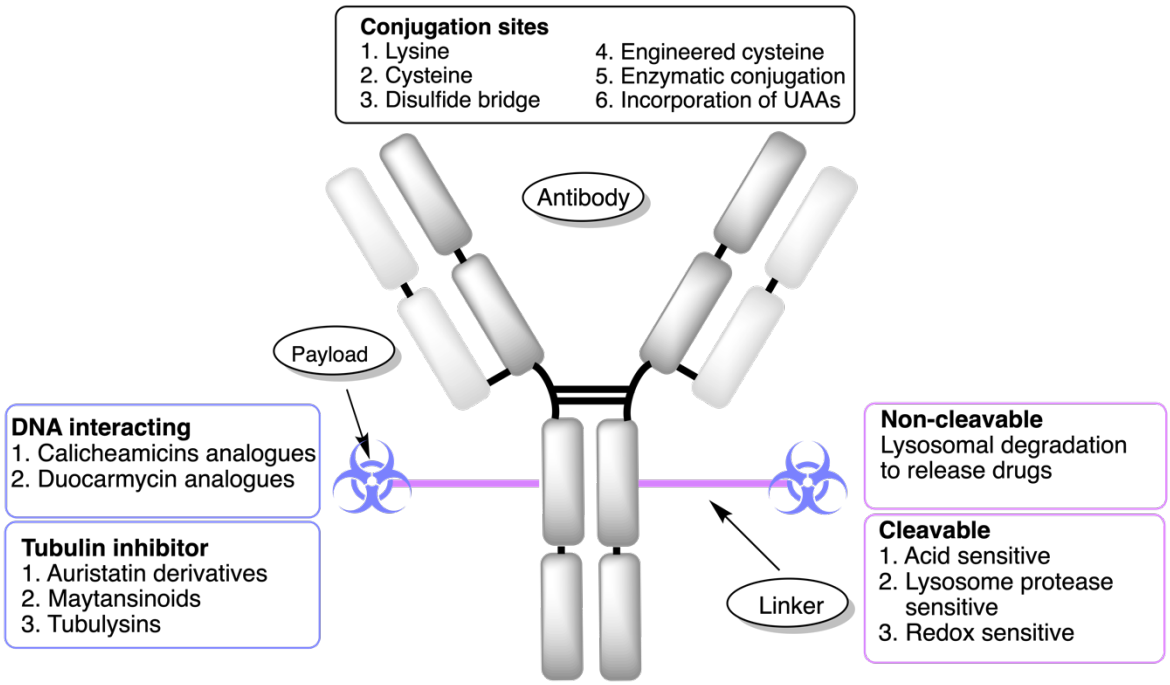

Figure 2. Schematic representation of a typical ADC design. Figure adapted from Grilo *et al*.[14]

The majority of the approved ADCs, or those currently in clinical trials, are synthesised by modification of native amino acid residues on the antibody. Bioconjugation is commonly achieved on lysine or cysteine residues, as these residues contain nucleophilic amine or thiol group respectively **(Figure 3)**.[15]

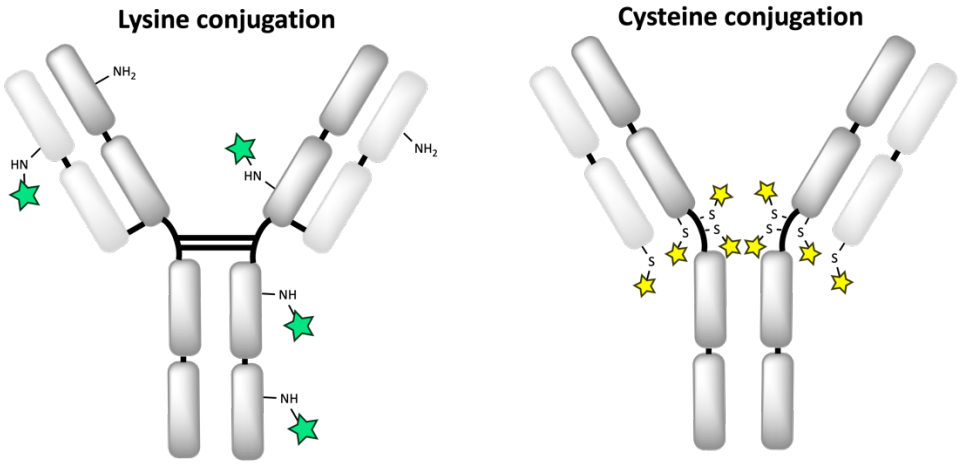

Figure 3. An illustration of antibody conjugation techniques, namely lysine and cysteine conjugation.

1.1.4 *In vivo* processing of ADC

ADCs are very complex biochemical platforms used in therapeutics field, combining the effect of antibodies and cytotoxic drugs thus expressing rare mechanisms of action and pharmacokinetic profiles. The simplest model describing ADC mode of action lists binding of the antibody to the target antigen, subsequent internalisation and lastly linker breakdown and intracellular drug release; however, each stage relies on more complex processes (**Figure 4**). After administration, the ADC exists as three major circulating components: the desired conjugate (which constitutes as the majority), native unconjugated antibodies and free payload molecules. The proportion of these three components can vary between ADCs, which often depends on the linker stability and final product purity, frequently this can change over days following drug administration.[16]

Vascular anatomy, transcapillary pressure gradients and stromal tissue components can be highly abnormal in solid tumours therefore large molecules such as ADC might have difficulties penetrating. Once extravasation from capillaries takes place, ADCs can reach tumour cells through passive diffusion, but this can lead to slow and heterogenous tissue penetration. Next, ADCs would bind to their target antigen and often this is not problematic as linkers are placed outside of the antigen-recognition domain of antibodies. ADCs would typically bind to their target with the same affinity as unconjugated native antibodies. The Fab fragment mediates the disrupting activity by inducing endocytosis and subsequent degradation of the target protein,

whilst the Fc region can orchestrate antibody-dependent cellular cytotoxicity (ADCC) and complement-dependent cytotoxicity.[16,17]

Once antigen binding takes place, internalisation of the ADC-antigen complex occurs through receptor-mediated endocytosis. ADC-antigen complex is then trafficked through endosomal and lysosomal pathways which is mediated by the organelle acidification. Acid-cleavable linkers are most likely to be released in early endosome, enzymatically cleavable linkers are degraded *via* proteolysis found in late endosomes or lysosomes, reducible linker release their payload principally upon exposure to glutathione, often found in higher concentration intracellularly.[18] Estimated time from antigen binding to payload release can be found in less than 24 h. Some ADCs are adept to exert a 'bystander effect' on neighbouring cells. Bystander killing may occur from ADC or a drug being released in the extracellular space. The bystander effect is dependent on ADC internalisation, type of linkers used and the physiochemical properties of the attached cytotoxic cargos.[16,17]

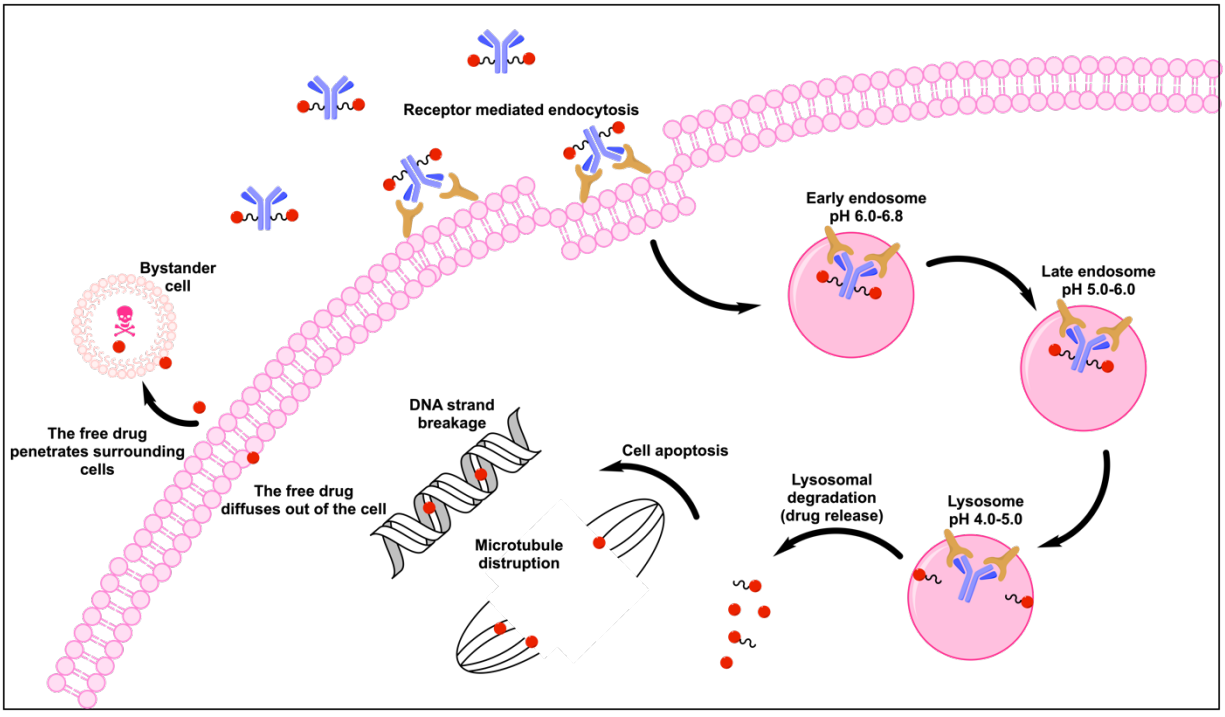

Figure 4. Typical pathway for ADC internalisation. The process begins with ADC binding with the target antigen on the cell surface leading to the internalisation of conjugate into the early endosome. As the pH drops down from near physiological to acidic in the lysosome this leads to degradation of the conjugate and subsequent release of the free cytotoxic drug into the cell. The free payload will cause cell death by specific mechanism of the drug used. Additionally, the free drug might diffuse out of the cell and enter neighbouring 'bystander' cell causing cell death.

1.1.5 Approved Antibody-Drug Conjugates

The first generation of ADCs was conjugated through non-cleavable linkers; however, these were shown to be less potent than the free drug. One of the examples of a first-generation ADC was Mylotarg that contained several disadvantages such as poor stability of the linker, relatively high proportion of unconjugated antibody and poor chemistry, manufacturing, and control (CMC) properties. The second generation of ADCs saw an improvement in several aspects namely better CMC, more potent chemotherapy drugs added, and improved cell targeting. Examples include Adcetris, Kadcyla, and Besponsa. Despite that, second generation of ADCs continued to suffer from off-target toxicity and variable clearance rates. The third generation of ADCs have seen improved site-selective conjugation that has led to more homogenous ADCs with a drug-to-antibody ratio (DAR) of two or more. These include Polivy, Padcev, Enhertu, and Trodelvy (**Table 1**).[14]

Table 1. Summary of approved ADCs.
AML – acute myeloid leukaemia; HL – Hodgkin lymphoma; ALCL – anaplastic large-cell lymphoma; HER2 BC – human epidermal growth factor receptor-2 breast cancer; ALL – acute lymphoblastic leukaemia; TNBC – triple-negative breast cancer; MM – multiple myeloma; DLBCL – diffuse large B-cell lymphoma.

	Mylotarg®	**Adcetris®**	**Kadcyla®**	**Besponsa®**	**Polivy™**	**Enhertu®**	**Padcev™**	**Trodelvy®**	**Blenrep®**	**Zynlonta™**	**Tivdak®**
Generic name	Gemtuzumab ozogamicin	Brentuximab vedotin	Ado-trastuzumab ematansine	Inotuzumab ozogamicin	Polatuzumab vedotin	Trastuzumab deruxtecan	Enfortumab vedotin-ejfv	Sacituzumab govitecan	Belantamab mafodotin	Loncastuximab tesirine	Tisotumab vedotin-tftu
Company	Pfizer	Seattle Genetics Inc.	Genentech/ Roche	Pfizer	Genentech/ Roche	Daiichi Sankyo Inc.	Astellas Pharma Inc.	Immunomedics	GSK	ADC Therapeutics	Seagen/ GenMab
Release date	2000; 2017	2011	2013	2017	2019	2019	2019	2020	2020	2021	2021
Target	CD33	CD30	HER2	CD22	CD79b	HER2	Nectin-4	Trop-2	BCMA	CD19	TF
mAb isotype	IgG4	IgG1	IgG1	IgG4	IgG1	IgG1	IgG1	IgG1	IgG1	IgG1	IgG1
Toxin	Calicheamicin	Auristatin (MMAE)	Maytansine (DM1)	Calicheamicin	Auristatin (MMAE)	Topoisomerase (DXd)	Auristatin (MMAE)	Topoisomerase (SN38)	Auristatin (MMAF)	PBD dimer	Auristatin (MMAE)
Conjugation site	Lysine	Cysteine	Lysine	Lysine	Cysteine	Cysteine	Cysteine	Cysteine	Cysteine	Cysteine	Cysteine
Release mechanism	Hydrazone + disulfide (cleavable)	Dipeptidic (cleavable)	Thioether (non-cleavable)	Hydrazone + disulfide (cleavable)	Dipeptidic (cleavable)	Peptidic (cleavable)	Dipeptidic (cleavable)	Peptidic (cleavable)	Maleimido-caproyl (non-cleavable)	Peptidic (cleavable)	Dipeptidic (cleavable)
DAR	av. 2-3	av. 4	av. 3.5	av. 6-7	av. 4	8	av. 4	8	av. 4	av. 2.3	av. 4
Clinical disease	AML	HL, ALCL	$HER2^{+2}$ BC	ALL	DLBCL	$HER2^{+}$ BC	Bladder cancer	TNBC	MM	DLBCL	Cervical cancer
References	[19, 20, 21, 22]	[23, 24, 25]	[26, 27, 28]	[29, 30, 31]	[29, 30, 31]	[32, 33, 34]	[35]	[36, 37]	[38, 39]	[40]	[41]

1.1.6 Fragment Antibody Drug Conjugate

Conventional, full-size ADCs have shown a great potential in the clinic, despite several drawbacks. Namely, the large size of typical IgG scaffold (~150 kDa) results in low tumour penetration, high systemic accumulation and slow clearance profiles.[42] Alternative, smaller fragment antibody drug conjugates are being developed (**Figure 5**). These include Fab-fragments, single-chain variable fragments (scFv), diabodies, nanobodies and humabodies.[43] The choice of antibody fragment, linker and payload is often disease depended. The smaller size of the antibody fragment is also beneficial for attachment of the cytotoxic payloads. DAR and the level of heterogeneity can impact the pharmacokinetics properties of the ADCs, resulting from multiple conjugation positions, thus finding an ideal location can be challenging. Higher DAR might seem to be preferable route; however, it is often accompanied by issues such as aggregation. Aggregation can lead to build-up of high molecular weight species and as a result it can inhibit binding to a receptor and can contribute towards toxicity due to alteration of clearance pathways. Even DAR 4 or 8 with hydrophobic payloads can lead to aggregation over time.

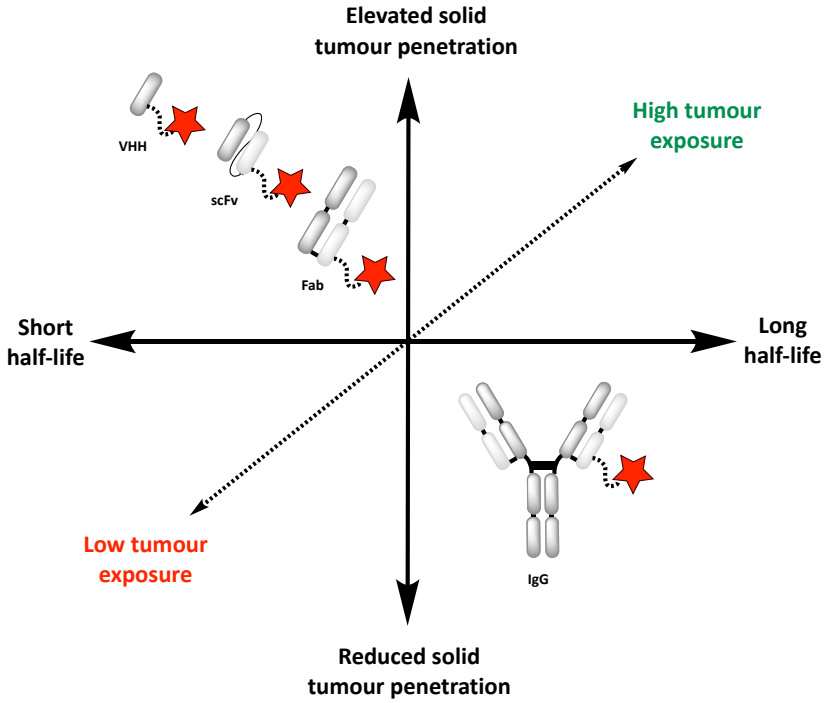

Figure 5. Simplified representation of different classes of fragment antibody drug conjugates. Figure adapted from Jager *et al*., 2021.[43]

Fab fragments comprise of variable and constant domains of immunoglobulin. These are linked by a single solvent accessible disulfide bond located at the C-terminus of the protein. Fab

fragments are commonly produced by proteolytic digestion of the whole IgG by proteases such as pepsin, papain, or ficin. Through this route, Fab' (light chain and heavy chain connected by single disulfide bond) and $F(ab)_2$ (two Fab fragment connected by hinge region) can also be isolated. Recombinant expression systems allow for production of bespoke Fab fragments, which may now consist of engineered or non-natural residues.[42] The advantageous aspect of Fab fragments is their small size, allowing for rapid transportation and *in vivo* penetration of the target, resulting in improved therapeutic effect. While the lack of the Fc fragment avoids the risk of unwanted bystander effect it can also reduce possibility of antibody-dependent cellular cytotoxicity (ADCC), antibody-dependent cellular phagocytosis (ADCP), or complement-dependent cytotoxicity (CDC), permitting the antibody fragment to bind to its target without activating the host's immune system.[18,44,45] The Fc domain interacts with the neonatal Fc receptor (FcRn), its natural ligand, which facilitates prolonged circulation of the whole IgG in the bloodstream. Therefore, antibody fragments lacking the Fc portion are often vulnerable to rapid systemic clearance rates. To improve this, poly(ethylene glycol) (PEG) chains can be added *via* conjugation strategies, resulting in prolonged *in vivo* half-life or human serum albumin.[46]

Combining different antibody fragments can generate bispecific antibodies (bsAbs) that in turn can target two different antigens on two different cells, or two different epitopes on the same antigen. The advantage of bsAbs is that these can recruit immune effector cells such as natural killer (NK) cells or T cells together with the tumour cell resulting in the efficient tumour cell killing.[47] An example of bsAbs are scFv fragments, that are still containing binding activity and are easily expressed in mammalian and bacterial cells, however, these can suffer from short *in vivo* half-life and rapid blood clearance. To overcome this, tandem scFv consisting of two scFv fragments fused together by a peptide linker were generated (VL_{mAbA}-VH_{mAbA}-VL_{mAbB}-VH_{mAbB}). To illustrate that, the bispecific T cell engager (BiTE) was developed that contains two scFv, one binding to CD3 on T cells and second binds to the antigen on tumour cells.[48,49]

1.1.7 Linkers for Antibody Drug Conjugates

The ideal linker design must balance the necessity for good internal stability during several days in circulation and efficient cleavage upon encountering the cell target. The linker design must consider factors such as attachment on the antibody, the number of attachment sites per molecule,

the polarity of the linker and cleavability. Linkers can be chemically designed based on cleavable and non-cleavable release triggers (**Figure 6**).[50]

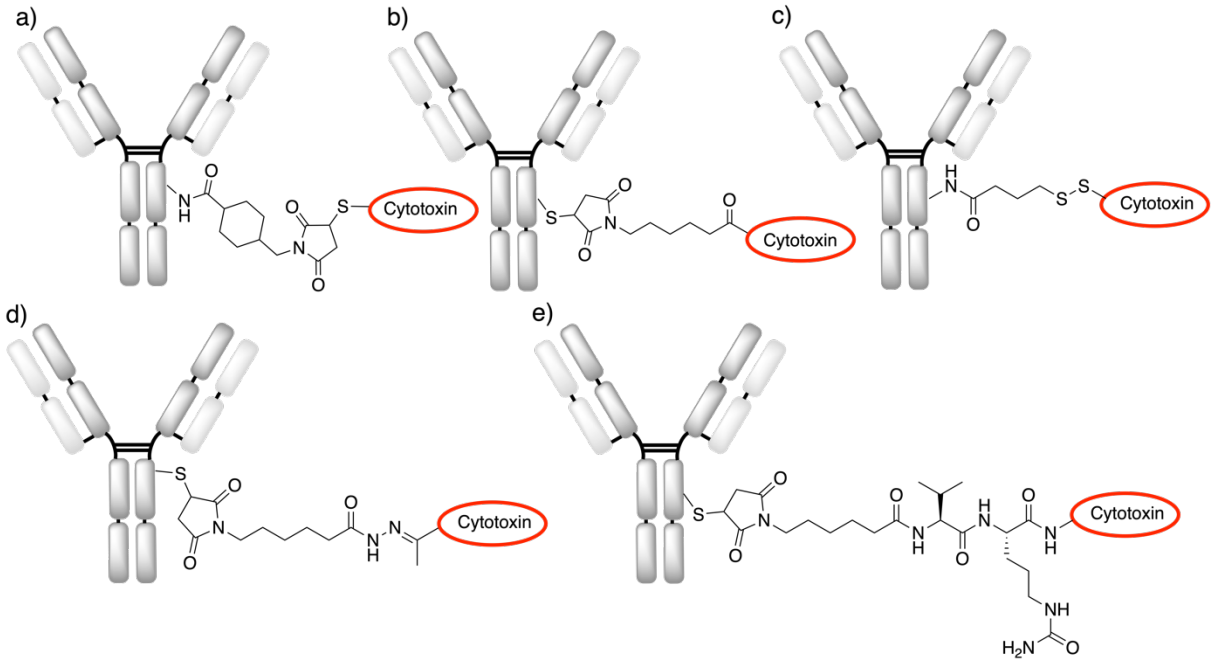

Figure 6. Example of ADC linker structures: a) SMCC thioether linker, b) maleimidocaproyl linker, c) disulfide cleavable linker, d) acid-sensitive hydrazone linker, e) lysosomal protease-sensitive/peptide-based linker.

1.1.7.1 Cleavable linkers

The success of cleavable linkers is based on the differences between physiological conditions of circulation and the intracellular conditions within targeted cells.[51] The endocytosis stage leads ADCs to the lysosomal phase that is characterised with its unique low pH and high concentration of hydrolytic enzymes. The cytosol of the cell is different from extracellular conditions due to the presence of high concentration of glutathione. Cleavable linkers exploit those conditions to release the drug at the target cell.[52]

1.1.7.1.1 Acid sensitive or acid labile linkers

Acid labile groups, for example hydrazones, can undergo hydrolysis upon entering the acidic cellular environment such as endosome (pH 5-6) and lysosome (pH 4.8), where the release of the cytotoxic payload will take place (**Scheme 1**). However, these linkers must remain stable in the

mildly alkaline environment, as found in the natural pH of systemic circulation.[53] Examples of this type of linkers can be seen in gemtuzumab ozogamicin (Mylotarg) and inotuzumab ozogamicin (Besponsa).[54]

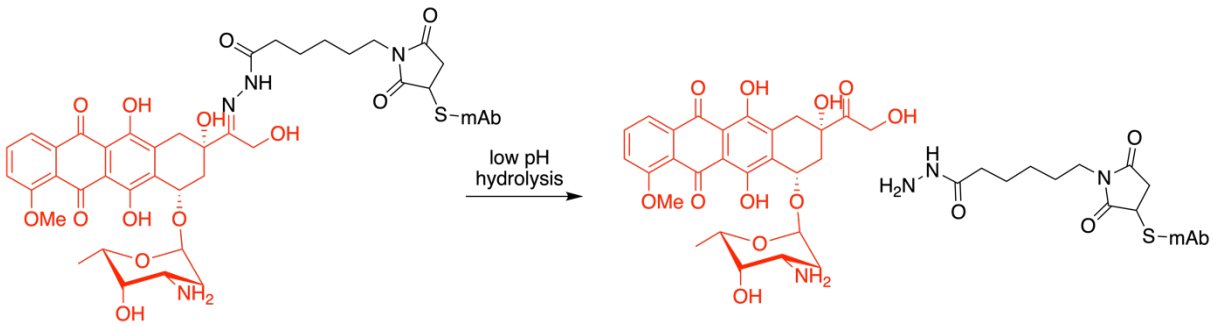

Scheme 1. The structural formula of BR96-doxorubicin.[55]

1.1.7.1.2 Enzymatically triggered linkers

Enzymatic linkers can be especially useful due to different enzyme expression levels found in diseased tissues in comparison to healthy tissues. This knowledge can be exploited when designing such a linker so the target substrate can be incorporated in their activable linker thus leading to controlled drug release and as an effect reduce their adverse side effects.

β-Glucuronidase/β-Galactosidase

β-Glucuronidase and β-galactosidase are key targets in cancer treatment due to their overexpression in malignant tumour cells. β-Glucuronidase is an enzyme that can catalyse the hydrolysis of a glucuronide from variety of substrates, whereases β-galactosidase catalyses hydrolysis of a galactoside. A β-galactosidase cleavable linker was designed, where first conjugate internalisation of the ADCs occurs through receptor-mediated endocytosis, following receptor-ligand interaction. The intercellular β-galactosidase-catalysed cleavage of the carbohydrate unit triggers the release of the drug *via* the self-immolative mechanism (**Scheme 2**).[56]

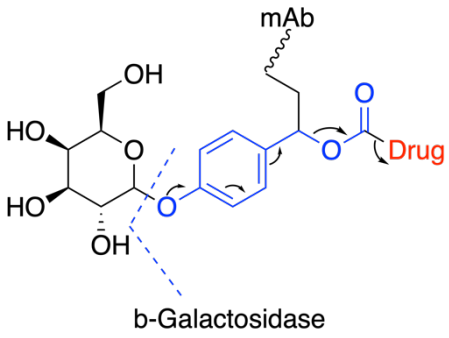

Scheme 2. β-Galactosidase-catalysed drug release mechanism.

Cathepsin B

Peptide-based linkers or lysosomal protease-sensitive linkers are amongst the most used linkers in ADC development. The reason for their wide application is due to the tumour cells exhibiting high expression of lysosomal proteases such as cathepsin B in comparison to the normal healthy cells. Cathepsin B (catB) enzyme is capable of cleaving the dipeptide bond as found in the valine-citrulline bond in Brentuximab vedotin (Adcetris), Polatuzumab vedotin (Polivy), Enfortumab vedotin-ejfv (Padcev), Sacituzumab govitecan (Trodelvy), Loncastuximab tesirine (Zynlonta), and Tisotumab vedotin-tftu (Tivdak). The advantage of the peptide-based linkers is their stability in acidic pH conditions and against other serum protease inhibitors, thus they demonstrate wide stability range in the systemic circulation, and only undergo cleavage upon reaching the target cells.[54] When designing the dipeptide linkers, two general trends were identified. A hydrophilic residue within the P_1 section is required for the increase in hydrolysis rate with basicity. The citrulline (Cit) is isoelectronic with Arg and it is commonly preferred over Arg due to synthetic ease, despite the lower basicity. Secondly, the hydrophobic residues Phe, Val and Ala often placed in P_2 to enable cleavage by cathepsin B whilst imparting plasma stability.[52] The *para*-aminobenzyl carbamate (PABC) linkage is often used as a self-immolative spacer, which undergoes spontaneous 1,6-elimination upon proteolysis to release the drug, CO_2 and aza-quinone methide (**Scheme 3**).

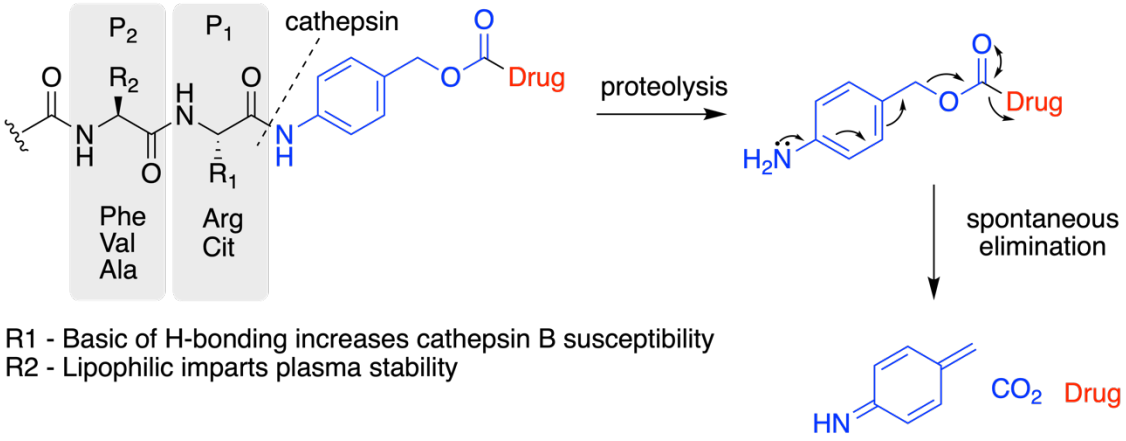

Scheme 3. The structure and cleavage mechanism of the Aaa-Aaa-PABC-Drug motif.

1.1.7.1.3 Glutathione-sensitive disulfide linkers

Glutathione-sensitive disulfide linkers offer another route for cleavable linkers through a specific target environment. This approach has been used in Mylotarg and Besponsa. Glutathione is a small thiol composed of L-glutamate, L-cysteine and glycine, that can be found in the intracellular setting such as cell cytoplasm (5 – 10 mM) or extracellular setting such as blood plasma (5 – 10 μM). Disulfide bonds are thermodynamically stable (bond energy of about 65 kcal/mol), but kinetically labile once in presence of thiol group.[57] Glutathione is released during tumour growth, and during hypoxia and other cell stressful conditions, therefore it is found in high concentration in those environments in comparison to normal cells.[58] As a result, disulfide linkers are stable in the blood flow, but can be selectively cleaved in the elevated concentration of glutathione, found in the tumour cells to release the cytotoxic cargo (**Scheme 3**).[54] The steric hindrance of disulfide bridges can be further optimised by adding an adjacent methyl group to prevent premature cleavage inside the cell as in *N*-hydroxysuccinimidyl-4-(2-pyridyldithio) butanoate linked to DM4 (SPDB–DM4), which is used in the ADC coltuximab ravtansine (currently Phase II of clinical trials).[50,57] Upon cleavage of the disulfide linker, the thiol is released which is subsequently methylated by the cellular methyltransferase activity, followed by the release of a drug. Alternatively, self-immolative designs can lead to release of unmodified drugs.[58]

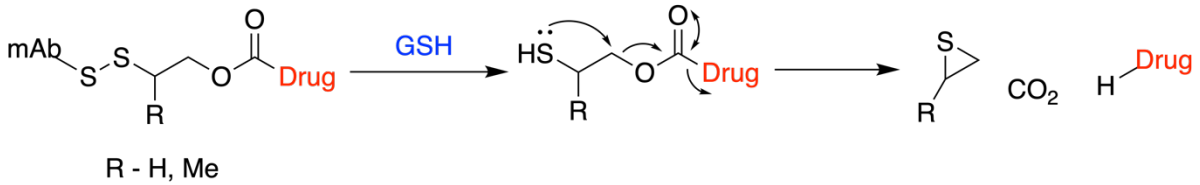

Scheme 4. Disulfide reduction and immolation of a disulfide-carbamate.

1.1.7.2 Non-cleavable linkers

In contrast, non-cleavable linkers only rely on the intracellular mechanisms for drug release such as lysosomal degradation.[59] Through the lysosomal proteases, the disintegration of the ADC takes place resulting in an 'amino acid-linker-drug' adduct, that then becomes an active moiety. Non-cleavable linkers often have prolonged half-lives and improved intracellular stability.[58] The proteolytic degradation of the ADC is followed by the release of the linker-drug moiety attached either to a cysteine or lysine residue of the degraded antibody,[54] however this often results in amino acid-linker-drug catabolite that are typically too polar to exhibit bystander effect and can show reduced potency when compared to cleavable linkers.[60] Non-cleavable linkers include thioether linkers, as found in ado-trastuzumab ematansine (Kadcyla) and Belantamab mafodotin (Blenrep).

1.1.8 Cytotoxic payloads

ADCs currently approved for therapy and clinically used are based on a limited number of toxic payloads targeting one of the following cellular structures: DNA, RNA, or tubulin filaments. DNA inhibitors include calicheamicins, duocarmycins and DNA crosslinkers (pyrrolobenzodiazepine dimers (PBD)). RNA targeting mostly involves amanitin, and tubulin inhibitors that are comprised of maytansinoids, auristatins, and taxol derivatives.[17]

Tubulin inhibitors

Most common tubulin inhibitors are auristatin derivatives. These include monomethyl analogues such as monomethyl auristatin E/F (MMAE and MMAF) that hinder microtubule polymerisation through binding to the vinca alkaloid binding domain, leading to cell apoptosis.[17] Both of these are derived from dolastatin 10 which was isolated from sea hare in 1970s.[61] MMAE and MMAF have slight structural differences that affect their ability to penetrate cell membranes. MMAF is

more hydrophilic due to its charged carboxylic terminus, thus unable to penetrate cell membranes, while MMAE is nonpolar and yields bystander effect *in vivo* due to its improved cell membrane permeability. Cellular IC_{50} for MMAE was found to be between 1-80 nM, while for MMAF was 60-120 nM.[60] MMAE has been utilised in FDA approved Adcetris, Polivy, Padcev and Tivdak, while MMAF was used in Blenrep **(Figure 7)**.[14]

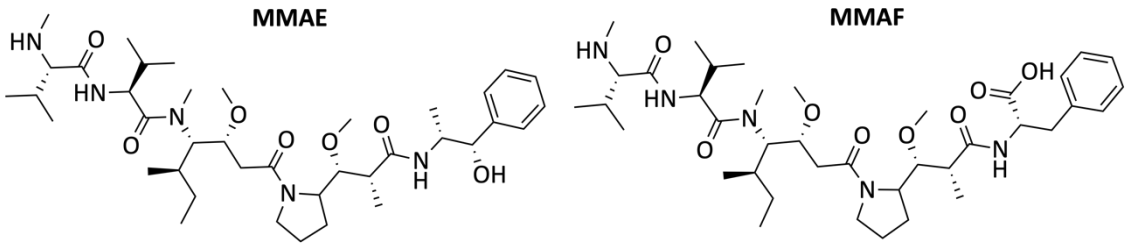

Figure 7. Chemical structure of auristatins MMAE and MMAF.

Maytansinoids (DMs) are derivatives of maytansine, a natural product isolated from African shrub *Maytenus ovatus* in 1972. These cytotoxins are structurally similar to rifamycin, geldanamycin, and ansatrienin as they all contain a 19-member lactam ring. The mode of action of maytansinoids is to disrupt microtubule polymerisation by binding to tubulin at or near the vinblastine-binding site, thus inducing mitotic arrest in the intoxicated cells.[62] Maytansinoid derivatives are very potent compounds requiring only picomolar concentrations for effectiveness, and these derivatives are split into two types - DM1 and DM4, notably, these can implement bystander effect *in vivo*.[17] Maytansinoid DM1 has been used in FDA approved ADC Kadcyla with cellular IC_{50} of 0.1-0.01 nM (**Figure 8**).[14,63,60] It is generally understood that the ADCs with maytansinoid are transported *via* endocytosis to the cytoplasm, followed by intracellular processing of the ADC, to release the lysyl-modified cytotoxic from DM1, thus resulting in anti-tubulin-associated cell death. The charged form of the DM1 drug is not membrane permeable and has no bystander effect. The limitations of tubulin-inhibiting drugs include indiscriminate cytotoxicity on proliferating cells, therefore non-dividing or quiescent cells are likely to escape the drug mechanism. Additionally, maytansinoid-based ADCs have hydrophobic character, therefore, the free form of the toxin is membrane permeable and could cause severe side effects from off-site toxicity. This can be managed by adding hydrophilic linkers containing a negatively charged alpha-sulfonic acid group or a short, polar polyethylene glycol (PEG) chain.[62]

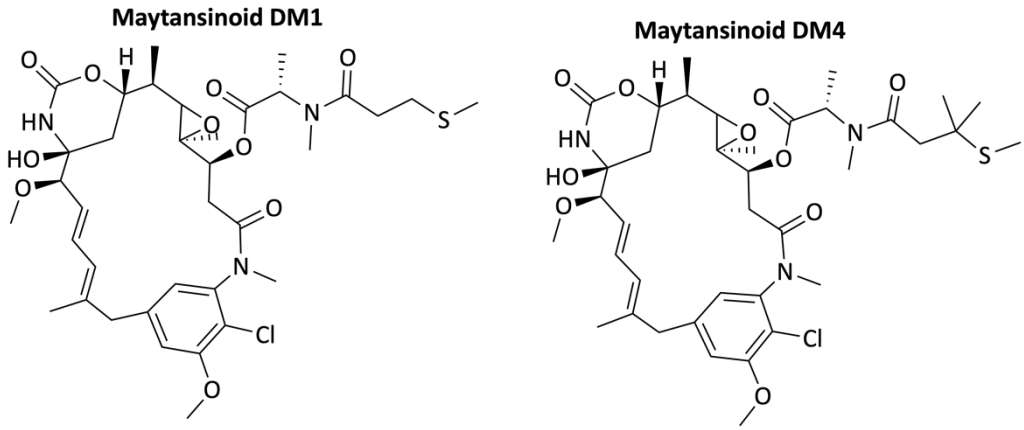

Figure 8. Chemical structure of Maytansinoid DM1 and DM4.

DNA inhibitors

Calicheamicins are isolated from actinomycete *Micromonospora echinospora calichensis*, discovered in the 1980s, and can induce DNA cleavage through binding into the minor groove of DNA.[62] These can lead to high potency and thus enable ADCs to target less abundant tumour antigens.[17] DNA damaging drugs such as calicheamicins have a narrow therapeutic effect and serious side effects that gives them limited clinical application. However, novel linker chemistry has overcome these issues and calicheamicins have been used in the FDA approved Mylotarg and Besponsa with cellular IC_{50} of 8-0.2 pM (**Figure 9**).[64,65,60] A new class of highly potent DNA minor grove interstrand crosslinking agents are pyrrolobenzodiazepine (PBD) dimers that showed a very good activity against solid and haematological tumours. The PBDs can also target antigens expressed in small amounts in malignant cells, resulting in lower required DARs. The PBD payload has recently been used in Zynlonta with IC_{50} of 8-0.2 pM, similar to calicheamicin.[60]

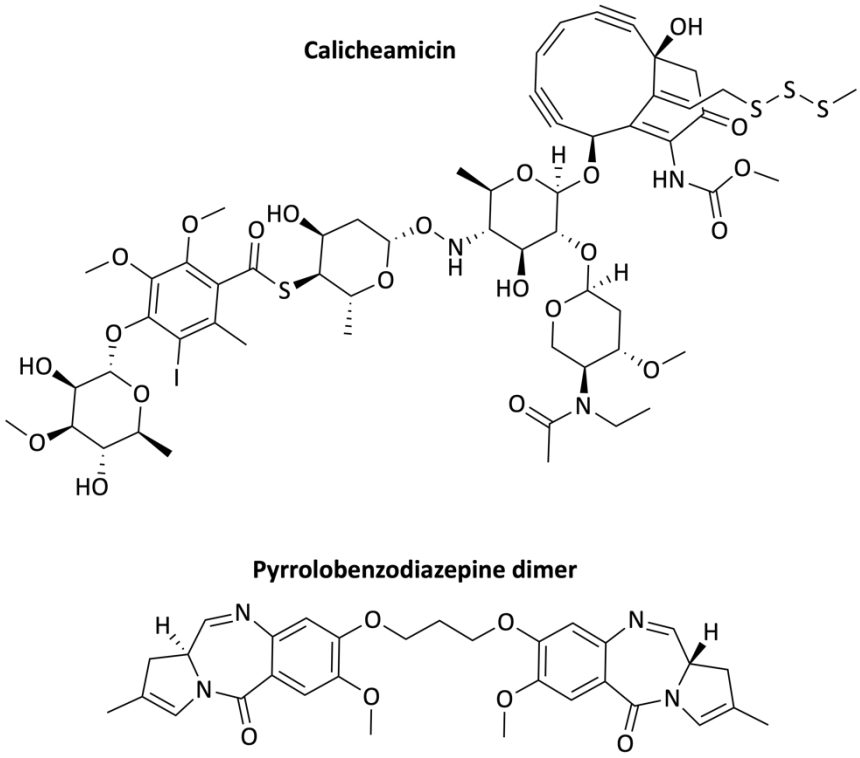

Figure 9. Chemical structure of *N*-acetyl-calicheamicin and pyrrolobenzodiazepine.

Another group of potent chemotoxins are topoisomerase I inhibitors such as irinotecan, which are often used for treatment of colorectal or gastric cancers. Topoisomerases are nuclear enzymes that are involved in DNA replication, transcription, chromosome segregation, and recombination. Examples of exatecan mesylate derivatives are DXd and SN-38. These are potent topoisomerase I inhibitors that bind to topoisomerase I-DNA cleavable complexes and stabilise them, leading to the induction of double-strand DNA break and subsequent apoptosis. The cytotoxic drug DXd is cleaved from the linker by lysosomal enzymes and released to attack tumour cells. DXd has been used in recently approved ADC Enhertu with IC_{50} of 0.8-0.04 nM,[66] while SN-38 was utilised in Trodelvy (**Figure 10**).[36,60]

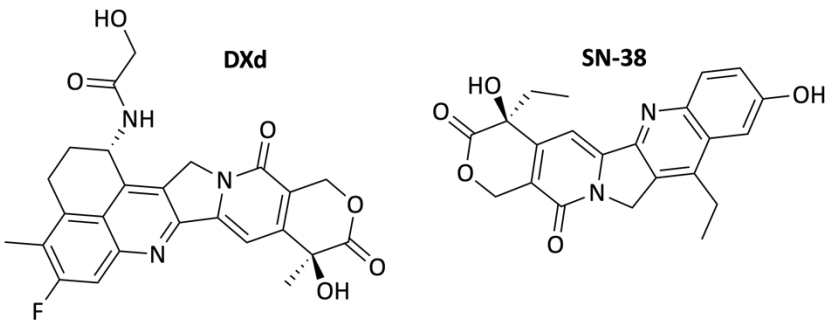

Figure 10. Chemical structures of topoisomerase I inhibitors DXd and SN-38.

1.2 Bioconjugation methods for ADCs

Bioconjugation strategies should ensure site-selective attachment to target proteins, whilst also ensuring a controlled number of additions, and avoid side-product formation. The linker molecules should ideally undergo the conjugation protocol in aqueous medium, near-physiological pH and at room temperature to maintain the tertiary structure of the protein. Lastly, the chemistry involved in the linker technology should be synthetically viable and result in blood plasma stability.[67]

Site-selective conjugation can be summarised in two categories: chemoselective and regioselective. Chemoselective conjugation can be achieved by exploiting the intrinsic reactivity of functional groups on proteins. For antibody conjugation the cysteine thiol (-SH) and lysine amino (ε-NH_2) are the most common targets for conjugation, due to their availabilities and nucleophilicities in solvent-accessible regions. Out of the current FDA-approved ADCs, three used the lysine conjugation approach whereas the remaining used cysteine conjugation. The regioselectivity conjugation focuses on targeting specific cysteine or lysine residues. Research efforts towards this goal have been extensive, however, they have yet to be used in FDA approved ADCs.[68] Alongside the cysteine and lysine, other amino acid side chains are being explored such as tyrosine,[69] tryptophan[70] and methionine.[71]

1.2.1 Lysine modification

Antibody modification through primary amino groups on lysine residues has been a popular ADC conjugation technique. The lysine's α-amino group is protonated under biological conditions (NH_3^+) while α-carboxylic acid group is deprotonated (COO^-) in the same conditions.
Lysine's side chain is composed of a linear four-carbon chain which is terminated with a primary amino group. The ε-amine of lysine possess a faintly higher ionisation point than the *N*-terminus α-amino group (pKa of ε-amine is found around 10.5, while α-amine is between 7.6-8.0), therefore this favours formation of positively charged ammonium groups at physiological pH.[68] Owing to its high abundance (~80-90 lysine on single antibody), lysine modification results in heterogenous ADCs. Reagents can randomly react with over 40 lysine residues that are solvent accessible in a typical IgG1.[72] This presents a concern as conjugation might lead to an increased heterogeneity, generating a pool of antibodies with a different number of attachments at different sites.[15] Despite that, lysine modification by acylation, typically using NHS esters, generates stable

amide bonds and it is widely used. Other reagents used for lysine conjugation include sulfonyl chlorides, isocyanates, isothiocyanates, epoxides and aldehydes (**Figure 11**).[73] Most commonly, basic pH conditions (pH > 8) are required to achieve the best yield due to amino groups having a high pKa (pKa ~10.5).[74] The extent of lysine modification can be controlled by limiting the reagent dose, namely equivalents or sub-stoichiometric reaction conditions that will lead to a decrease in modification yields.[74]

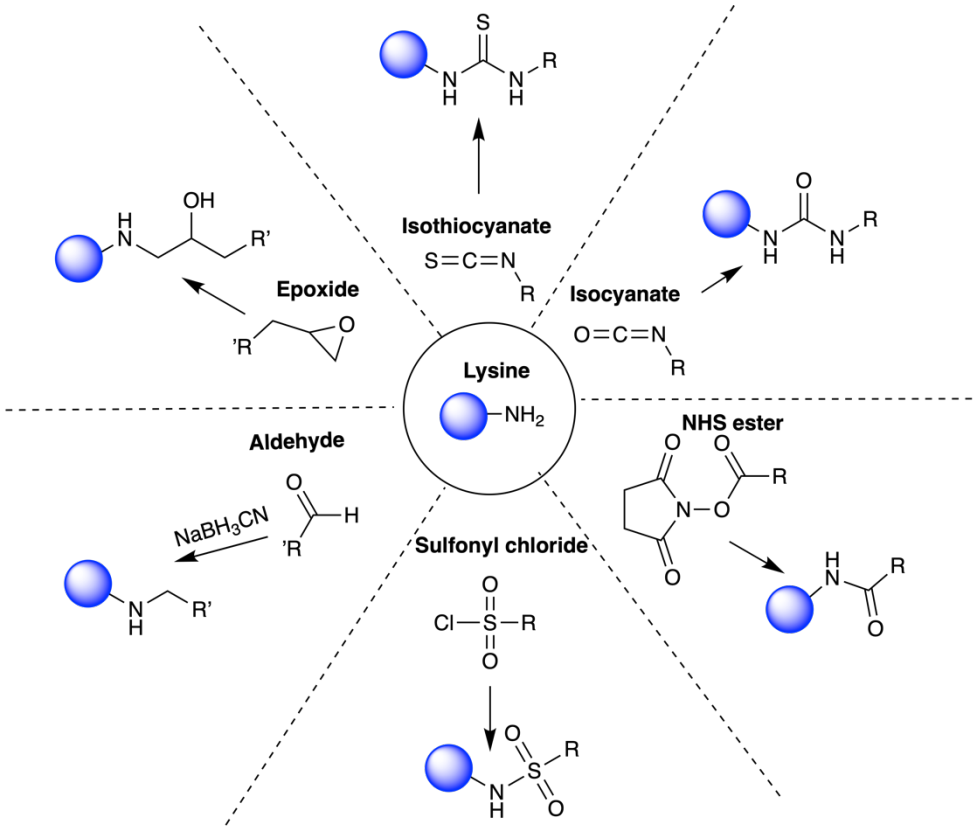

Figure 11. Selected examples of the most common lysine modification reagents.

NHS esters are very popular lysine acylation reagents (**Figure 11**). Formation of NHS esters helps to activate the parent carboxylic acid, which are easily substituted.[75] Reactions with primary amines and secondary amines leads to the formation of stable amide linkages. A broad application of heterobifunctional crosslinkers using an NHS ester on one end has been used for the preparation of several ADCs. Namely, a two-step process where a lysine on the antibody is first modified *via* the NHS ester to introduce a second reactive group, for example a maleimide, which is then conjugated to the drug linker that also contains a reactive handle such as a thiol. This approach has been seen in the development of Kadcyla.[76] Despite the wide popularity of

NHS esters, the drawback is that they can also react with other amino acids such as cysteine, serine, tyrosine, threonine and with the *N*-terminus of an antibody.

Isothiocyanates are highly selective for modifying ε-amine group in lysine side chain (**Figure 11**). The reaction proceeds through nucleophilic attack on the central electrophilic carbon within isothiocyanate group.[75] Allyl isothiocyanate was shown to form a stable lysine adduct on monoclonal antibody A4C7mAb[77] and more recently fluorescein isothiocyanate equipped with benzyl was selected for labelling lysine residues on antibody bioconjugates.[78] Isocyanates are similar to isothiocyanates with only difference an oxygen atom being replaced with sulphur. One of the application includes addition of the isocyanate group on one end and a maleimide group on the other end of a heterobifunctional linker.[79]

Another commonly used reactive group for lysine modification are sulfonyl chlorides (**Figure 11**). These are reactive acid derivatives with properties similar to carboxylates and acid chlorides. Sulfonic acid is too hindered to allow formation of bulky active intermediate, therefore, creation of sulfonyl chloride derivatives is the main chemistry. Commercially available sulforhodamine chloride dye are used for fluorescent labelling of amines.[80,81]

1.2.1.1 Site-selective modification of lysine residues

Recent advances have improved on chemoselectivity in lysine modification; however, site-selectivity is still challenging due to the high natural abundance of lysine. Site-selective modification of proteins is a strategy for modifying structures and functions of specific residues within the sequence of a protein, without altering other residues. Notably, new approaches are being developed with promising outcomes.

Recently, a study conducted by Forte *et al.*,[82] proposed a new methodology where transfer of an acylating agent from cysteine residues to proximal lysine residues was achieved. This strategy, termed as 'Cysteine-to-Lysine Transfer' (CLT), utilises the disulfide bond as a temporary "hook" employing the principles of native chemical ligation (NCL) (**Scheme 5**). The method uses readily available thioester reagents to react with cysteines which are first obtained from the reduction of the disulfide bridge in a Fab fragment. Following that, a transfer occurs at an elevated pH to a proximal lysine residue. Acylation was found to occur at two lysine residues out of three available in the HC region (K136, K221, K225), suggesting that DAR of 2.0 was possible. The investigated

reagents included alkyl thioester such as MESNa thioester and a bis-thioester. The CLT approach could give rise to a number of novel site-selective protein conjugations and thus construct highly homogenous antibody fragment conjugates.[82]

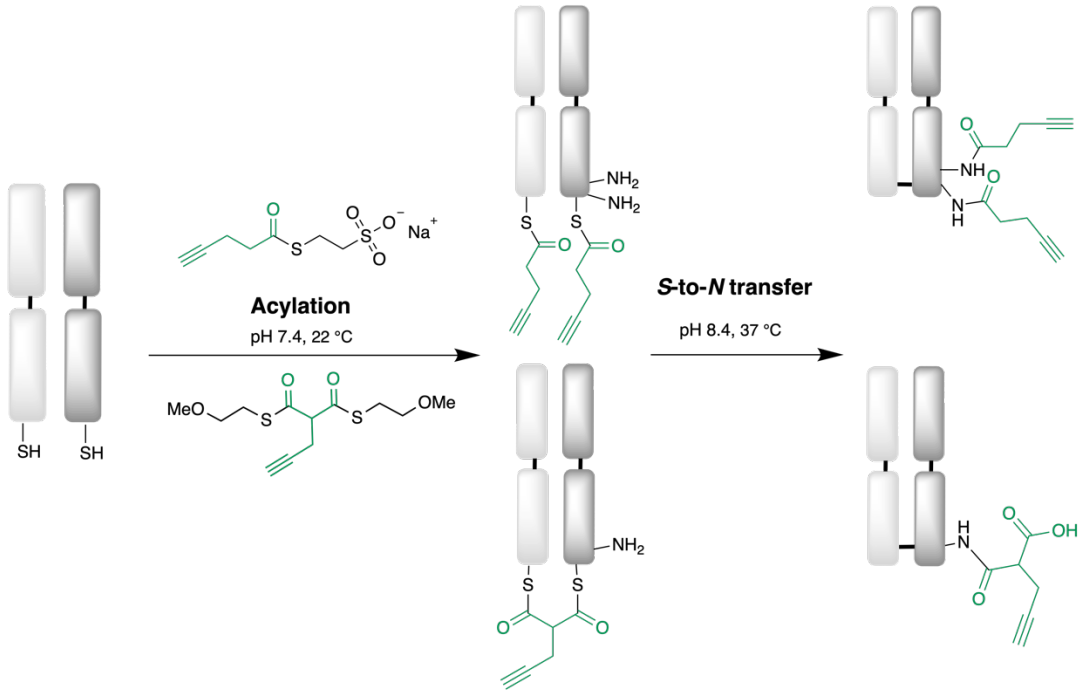

Scheme 5. Cysteine-to-Lysine transfer approach.[82]

Another example of site-selective modification of lysine residues is a peptide mediated modification on an antibody developed by biotech company Ajinomoto. The 'AJICAP' method enables regio-divergent functionalisation of specific lysine residues on an antibody, which can be achieved by changing a peptide sequence. The group has used a phage display technique to identify three peptides against human IgG. From this, one of them containing 17 amino acids (RGNCAYHKGQLVWCTYH) called AAPC 1 was selected because of its high affinity to the Fc region of the human IgG1 with a K_d value of 9 nM. The peptide was then chemically modified *via* the peptide's single lysine residue with dithiobis(succinimidyl propionate), which is useful for protein labelling. During the peptide design, any lysine residues were replaced with arginine to avoid any competition of the peptide lysine with the antibody lysine residues. Once the peptide is presented to the antibody, it binds to the Fc region. An NHS ester linker is then placed in near proximity to a lysine residue on the antibody where the transfer occurs forming an amide bond between the peptide-reagent and the antibody. Whilst the NHS ester group rapidly reacts with lysine residues, it is also prone to hydrolytic decomposition at natural pH, so this required further optimisation. The antibody was found to show optimal peptide conjugation with a buffer at pH

5.5, 20 °C for 1 h incubation time.[83] The success of the NHS linker design required the incorporation of the cleavable disulfide bond between the affinity peptide and the NHS ester. Once covalent antibody lysine modification takes place, the disulfides are reduced with TCEP, followed by treatment with dehydroascorbic acid (DHAA). DHAA facilitates the formation of the intermolecular disulfide bonds and does not interact with the thiol moiety of the chemical linker attached into the Fc region. Lastly, payload conjugation *via* a thiol-maleimide reaction occurs to install the SMCC linker with the DM1 cytotoxic drug. The MS/MS analysis revealed one lysine being modified on each heavy chain (K246 and K248) with average DAR of 1.9, showing site-specific lysine modification of antibodies (**Scheme 6**).[83, 84]

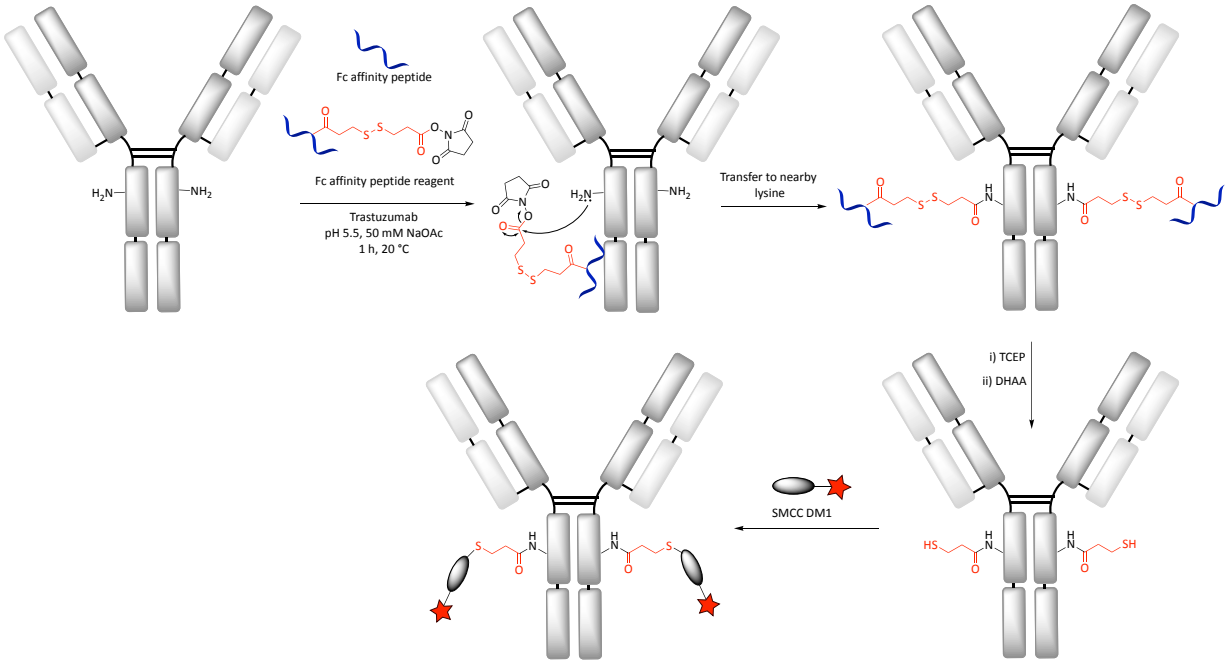

Scheme 6. Reaction conditions and synthesis of AJICAP ADC. A structure of SMCC linker is illustrated in the section 1.1.7, while DM1 can be found in section 1.1.8.

1.2.2 Cysteine modification

In antibodies, cysteine has a low natural abundance (1.5%) and is found in the form of disulfide bridges to stabilise the tertiary structure.[85,15] Formation of ADCs through cysteine conjugation improves homogeneity relative to lysine conjugation because of the fewer potential conjugation sites.[85,86] The cysteine conjugation approach typically involves partial reduction of the four antibody interchain disulfide bonds to generate up to eight reactive cysteine thiol groups. The

reduction is commonly achieved with dithiothreitol (DTT) or tris(2-carboxyethyl)phosphine (TCEP) followed by conjugation of a payload comprising of thiol-specific linkers.

One of the characteristics of free cysteine is unique high nucleophilicity. In physiological conditions, cysteine has a high tendency to form a nucleophilic thiolate ion (S^-).[87] The cysteine thiol group in aqueous buffer has a pKa~8 which is more acidic than other nucleophiles found in proteins, such as hydroxyl group of serine (pKa~13) or ε-amine of lysine (pKa~10).[88] Additionally, sulphur is a "softer" nucleophile than nitrogen or oxygen, resulting in the cysteine thiol/thiolate being more reactive than other soft nucleophiles.[89] Modification is commonly achieved by reaction of the thiol group with electrophiles such as maleimides, iodoacetamides, alkyl halides, and pyridyl disulfides (**Figure 12**).

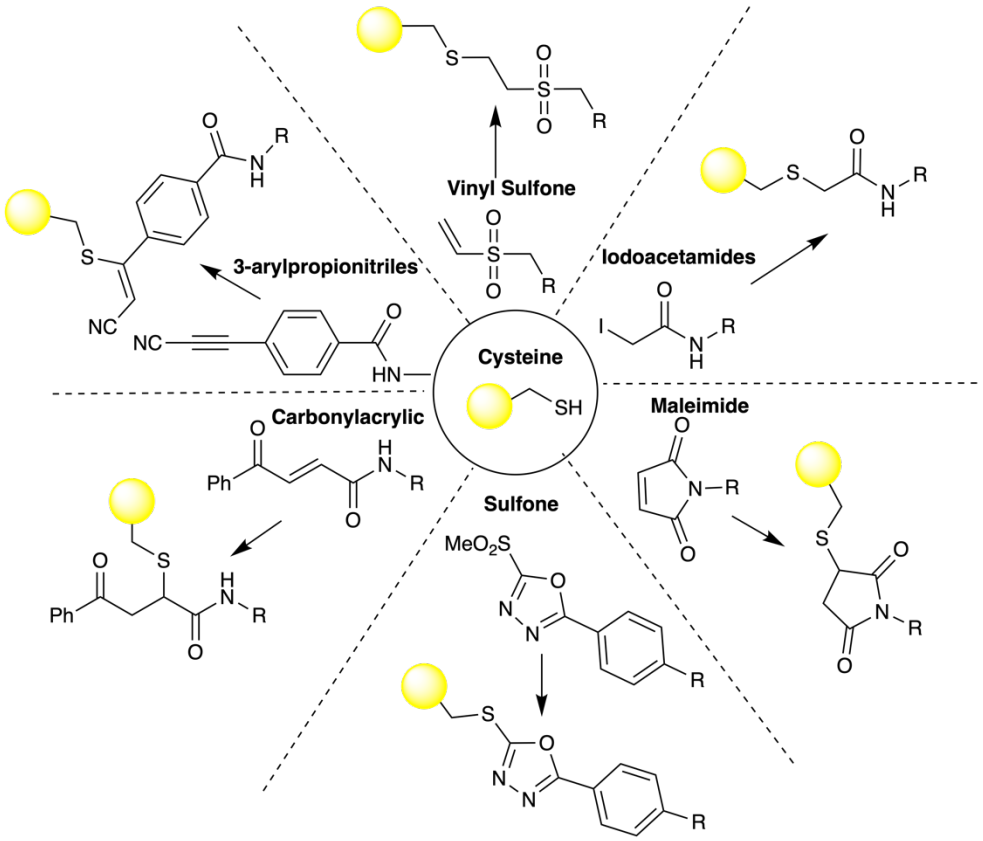

Figure 12. Selected examples of the most common cysteine modifications.

Alkyl halides derivatives are frequently used to create thiol-reactive compounds such as haloacetamides (**Figure 12**). Upon nucleophilic attack, the halogen group is easily displaced with the nucleophile to create an alkylated derivative. The order of reactivity of haloacetamides is I > Br > Cl > F, where iodide is a better leaving group among the halogens, due to its atomic radius,

whereas fluorine is unlikely to react at all.[90] Commercially available crosslinkers containing an iodoacetyl group are used in immobilisation kits, biotinylation reagents and mass spectrometry tags.[91] Iodoacetamides are used for alkylation of thiols to prevent the formation of disulfide bonds after antibody reduction and it is often employed for analytical purposes.[75]

The vinyl sulfone group may be used for conjugation with thiols in aqueous solution and mild conditions (**Figure 12**). In comparison to maleimides, vinyl sulfone groups are not as strong electrophiles, but efficiently couples with thiols under alkaline pH to yield stable β-thiosulfonyl linkages.[92] Previously, vinyl sulfones were exclusively used for PEGylation of proteins,[93] but this has since seen improvements and vinyl sulfones are now used a probes, chelating agents or fluorescent tags.[94]
Functionalised carbonylacrylic reagents (**Figure 12**) were used for irreversible site-selective modification of cysteine residues on antibodies. The approach is based on thiol-Michael-type addition of cysteines to carbonylacrylic reagents which are additionally equipped with cytotoxic payload. The reaction can proceed to completion with single molar equivalent forming a thioether bond and it is fully resistant to degradation in human plasma.[95]

Another example of cysteine conjugation is CBTF (**Figure 12**), that was developed as heterobifunctional reagent for amine-to-thiol coupling. Through that strategy, defined antibody conjugates with DAR of 4.0 were generated with significantly lower level of deconjugation of cytotoxic transfer in the human serum.[96]

Maleimide-functionalised reagents or linkers are the most frequently used for cysteine-based conjugation (**Figure 12**).[84] The maleimide double bond can undergo an addition reaction with sulfhydryl groups to generate a thioether bond. It was found that the reaction of maleimides with thiol at pH 7.0 proceeds at rate 1000 times greater than its reaction with amines.[97] Maleimide modification with thiols results in the formation of thiosuccinimide conjugates that are inherently unstable in plasma, due to their tendency towards retro-Michael addition. This leads to premature release of the maleimide-payload that can further react with thiols found in plasma or diffuse into nearby cells, which is linked to a reduction of efficacy and safety.[97] The hydrolysis of the thiosuccinimide ring in conjugate **B** to succinamic acid conjugate **C** improves stability and efficacy, however this often results in significantly lower yield of the hydrolysed thiol-stable conjugate caused by competing retro-Michael pathway (**Scheme 7**).

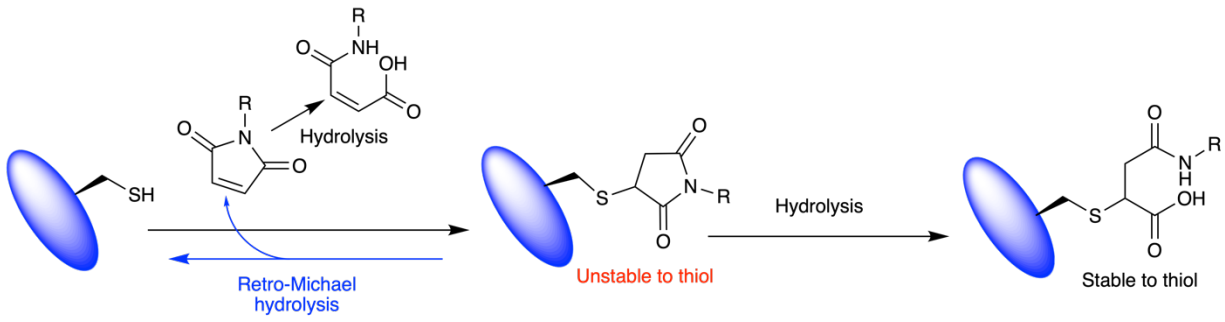

Scheme 7. Maleimide modification resulting in thiosuccinimide adduct followed by hydrolysis to achieve thiol stability.

More recently, bromomaleimides were found to selectively and rapidly react with cysteine residues to create thiomaleimides[98] that presents two points for chemical attachement, thus generating multifunctional bioconjugates. Bromomaleimides can react with thiol in an addition-elimination reaction to form a maleimide conjugate, which in comparison to succinimide conjugate, retains a double bond (**Scheme 8**, **A**). When exposed to high concentration of thiol, such as β-mercaptoethanol (BME) or glutathione (GSH), a conjugate addition to the double bond occurs, followed by a retro-Michael pathways, thus freeing the thiol (**Scheme 8**, **B**). In addition to reversibility achieved with excess of thiol, the retention of the double bond allows for a second point of attachement *via* another nucleophilic attack, such as stoichometric addition of different thiol to result in a dithiosuccinimide (**Scheme 8**, **C**). Thiomalemides can also undergo hydrolysis to give the stable acid and this blocks the retro-Michael competition reaction resulting in higher yield (**Scheme 8**, **D**).[99]

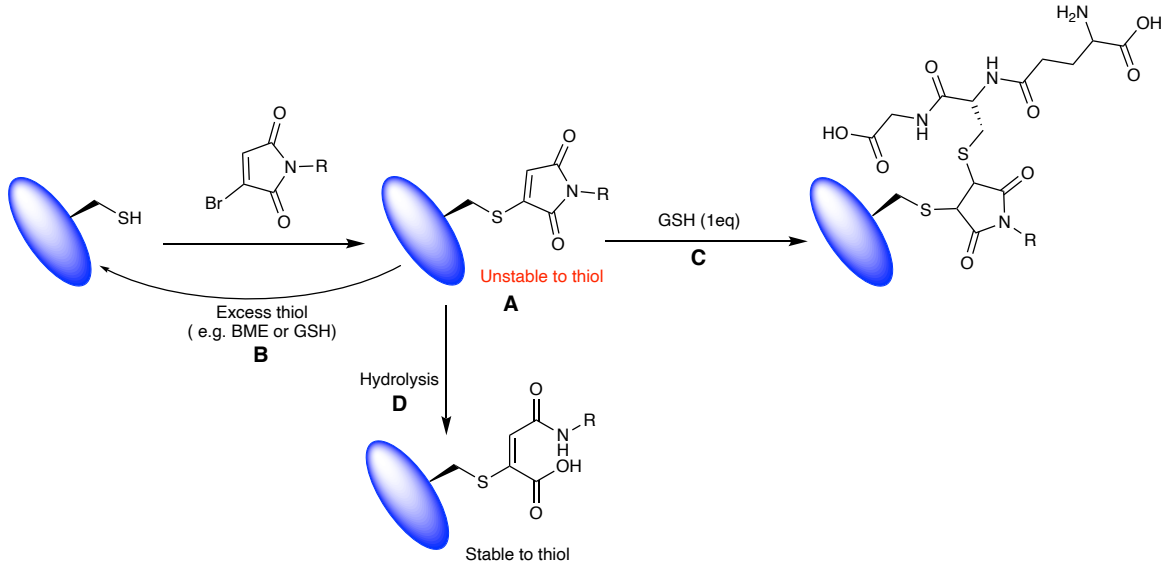

Scheme 8. Bromomaleimides modification with thiol.

1.2.3 Disulfide rebridging

An alternative way of site selective bioconjugation is through disulfide bridging or disulfide stapling. Large numbers of peptides and proteins consist of solvent accessible disulfide bond, which can be targeted by reduction and subsequent rebridging approaches that would lead to retention of the covalent bond between the two cysteine residues.[75] Some of the most prominent examples for the rebridging of disulfide bonds include next generation maleimides (NGMs),[100,101] pyridazinediones (PDs),[102,103] arylenedipropiolonitrile,[104] bis-sulfone,[105] divinylpyrimidine,[106] dichlorotetrazine,[107] and thiol-yne[108] (**Figure 13**).

The reduction of antibody disulfide bonds followed by a rebridging bioconjugation with bis-reactive reagents allows for reconnection of the polypeptide chains, whilst simultaneously introducing drug molecules or bioorthogonal functionalities, allowing for subsequent functionalisation of the linker.[109,84] Studies have also demonstrated that after reduction of the interchain disulfides, the individual protein chains in an antibody are still held together (including *in vivo*) by non-covalent interactions such as hydrogen bonding, van deer-waals and ionic bonds interactions. Therefore the lack of the disulfide bridge between the heavy chains does not affect the pharmacological properties of an ADC.[46]

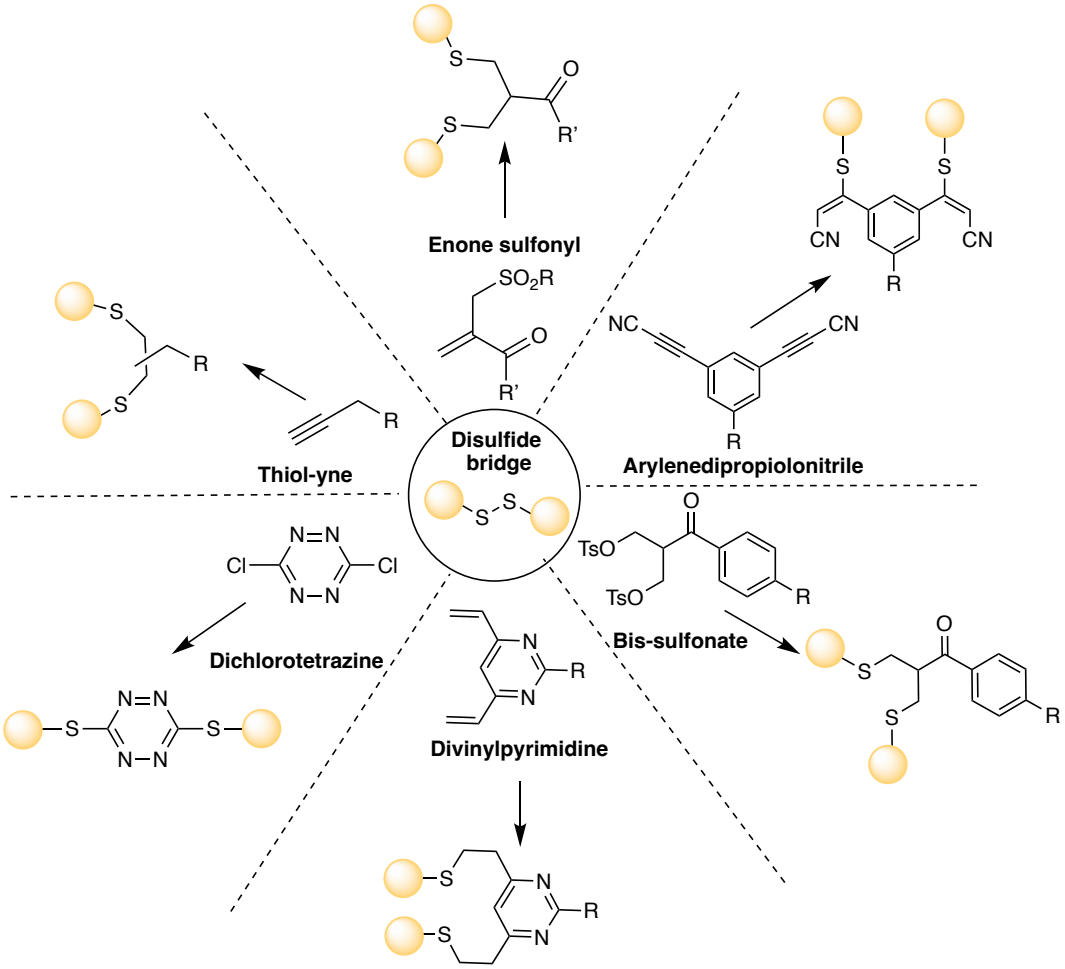

Figure 13. Selected examples of the most common disulfide modifications.

To illustrate an example of disulfide rebridging on a Fab fragment are enone sulfonyl reagents that have been found to be highly selective for thiol groups. The bis-sulfone undergoes bis-alkylation to conjugate, both freed thiols resulting in covalent rebridging of the disulfide bond *via* a three-carbon bridge. The method has been selected for site-specific conjugation with a wider range of therapeutic protein to improve the pharmacokinetic properties, whilst retaining activity (**Scheme 9**).

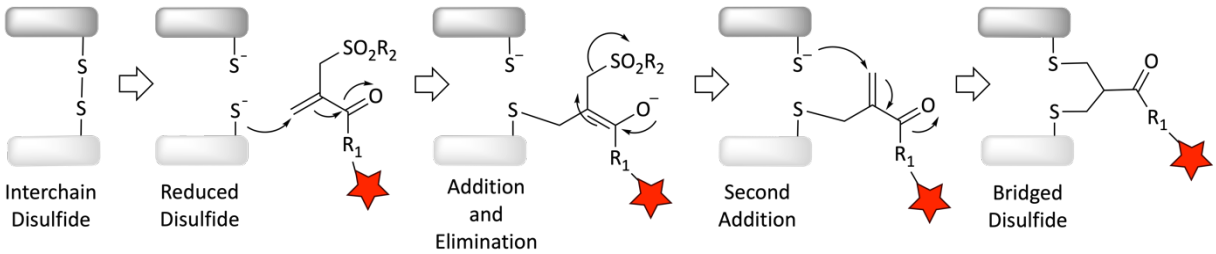

Scheme 9. Rebridging of inter-chain disulfides by bis-alkylation involving a sequence of Michael addition and elimination reactions. Scheme adapted from Basescu *et al*., 2014.[105]

At UCL, two effective class of disulfide rebridging reagents have been developed. A next generation of maleimides (NGMs), for the purpose of rebridging the reduced disulfide bonds, has broadened the scope of antibody modification.[110,111] NGMs contain leaving groups in the 3- and 4- position, such as bromine (Br) or thiophenol (SPh), thus allowing a reaction with two nucleophilic thiol groups as in the reduced disulfide bridge. The addition-elimination reaction introduces a 2-carbon bridge between the two thiols, retaining a double bond. The bridged conjugate can maintain the structural features of the antibody while introducing functionalisation (**Scheme 10**).[100]

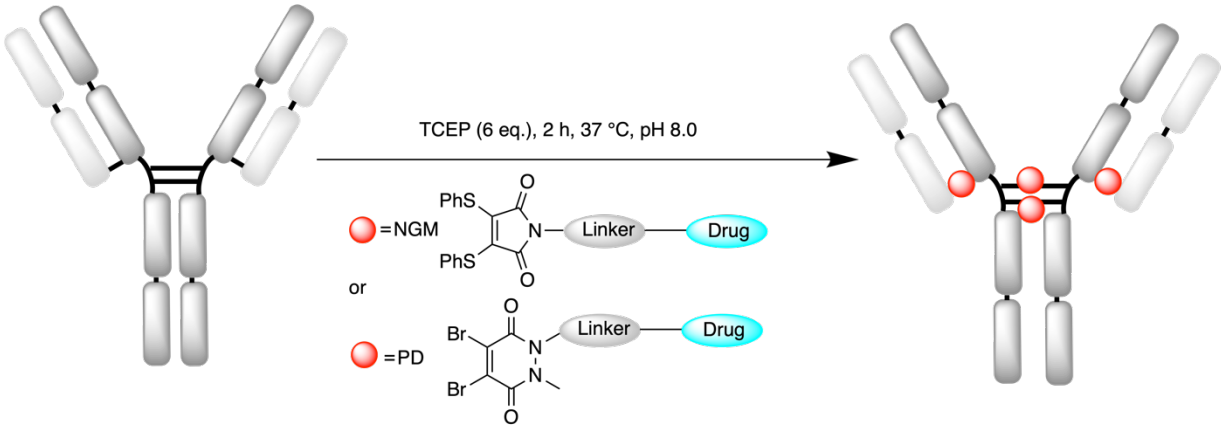

Scheme 10. Schematic representation of bridging of native antibody disulfide bonds with Next Generation Maleimide and pyridazinediones. Scheme adapted from Schumacher *et al*.[85]

NGMs have seen a wide range of applications. These include addition of reactive handles *via* dibromomaleimides in polymers,[112] PEGylation of proteins with dihalo- and dithiomaleimides,[85] nuclear imaging with a fluorescent azide and dithiomalemide-alkyne,[113] antibody-fragment diagnostic biotechnology using di-Br or di-SPh substituted maleimides,[114] photochemistry,[115] and photodynamic therapy.[116] Following this, dibromomaleimides have been shown to undergo conjugation to a native antibody and subsequent hydrolysis that essentially serves to 'lock' the conjugate as robustly stable maleamic acids with the reaction completed in just under 1 h. The dibromomaleimides can be presented with various linkers attached to the maleimide nitrogen such as an alkyne handle used for subsequent functionalisation steps (**Scheme 10**).[117]

The second class of reagents are pyridazinediones (PDs) that are structurally similar to NGMs, however PDs have the advantage of presenting four points of attachment, such as the two sp^2 carbons of the alkene moiety, which can react chemoselectively with free thiols through consecutive addition-elimination steps; and the two pyridazine nitrogens, that can be modified

with different bioorthogonal tags permitting for dual-labelling of the antibody (**Scheme 10**).[103,118] PDs were also shown to functionalise liberated thiols by disulfide bridging in clinically validated trastuzumab with monomethyl auristatin E (MMAE) to generate a stable ADC with controlled DAR 4 in an *in vitro* and *in vivo* environment.[119] Disulfide bridging offers great promise in the development of new ADCs but is yet to be validated in the clinic.

The section above was designed to provide a general overview of current antibody modification approaches and it is not an exhaustive list. Other books[120] and reviews[121,122,73,123,124,87] cover this area in a great depth.

1.2.4 Antibody engineering

In contrast to the conventional antibody conjugation through native lysine or cysteine residues, the pharmacological profile of an ADC can be improved by recombinantly inserting additional surface-exposed cysteines into antibodies, such as in the THIOMAB drug conjugate (TDC) system.[125] TDCs work by engineering cysteine residues into different but carefully selected positions on antibody heavy or light chain, for ease of coupling (**Figure 14**).[7] In comparison to commonly achieved heterogenous mixtures, TDCs demonstrated equivalent *in vivo* potency, improved pharmacokinetics and an expanded therapeutic window.[126] Antibodies produced using the TDC system are not immediately amenable for conjugation, but still require several steps for de-capping. The newly expressed cysteines are always capped with glutathione or some other thiol-bearing molecule, thus these need to be reduced to remove the cap. However, this can result in reduction of interchain disulfides, which require further treatment with DHAA.[126] ADCs with engineered cysteines at different locations on the IgG have different solvent accessibility and local charge. Studies performed in monkeys and rats showed better tolerance of TDC antibodies with a maleimide linker than conventional ADCs, however due to the highly solvent accessible site, the conjugated thiol-reactive linkers were lost due to maleimide exchange with reactive thiols present in glutathione, free cysteines and albumin. The next generation of TDCs were improved by mutation on the light chain.[50] An example of this technique is the vadastuximab talirine antibody, consisting of engineered cysteines and the pyrrolobenzodiazepine (PBD) dimer attached *via* a cleavable dipeptide linker (valine-alanine).[127]

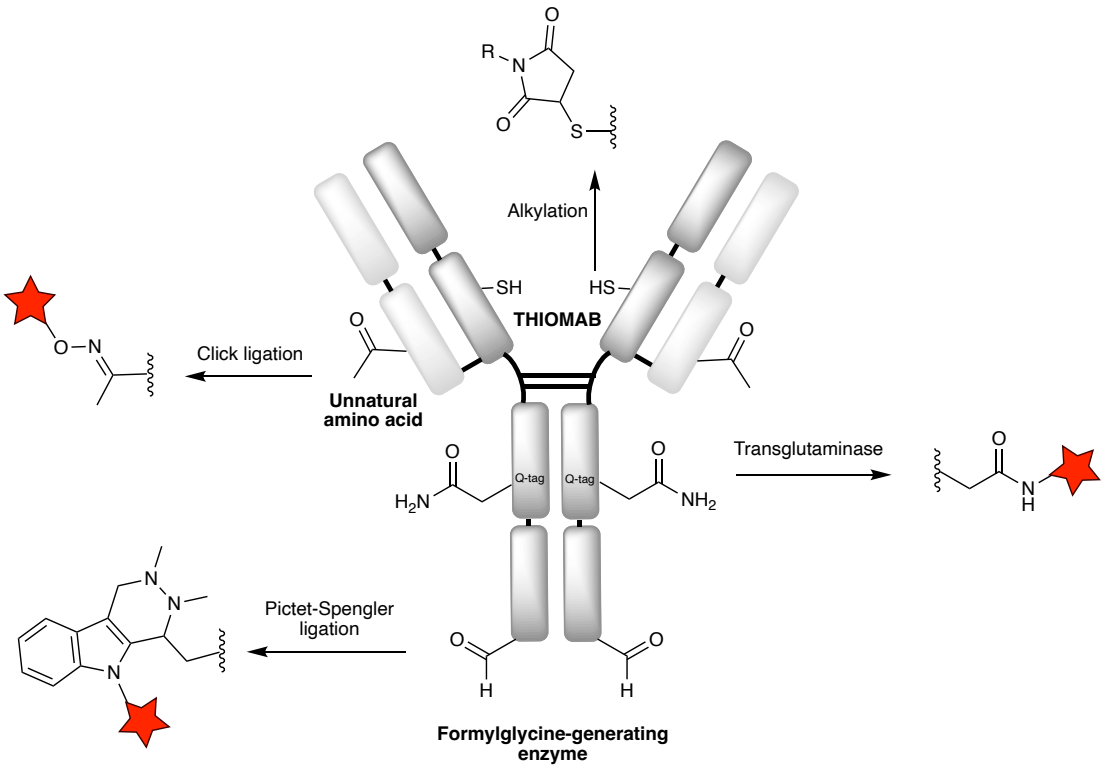

Figure 14. General schematic representation of engineering antibodies.

It is possible to incorporate unnatural amino acids (UAAs) during the transcription steps of antibody synthesis. This result in a structurally similar antibody as the wild type, however, offers a bioorthogonal functionality.[54] Genetically engineering of an orthogonal amber stop codon (TAG) at the site of desired UAA with a corresponding orthogonal tRNA/aminoacyl-tRNA synthase pair will introduce a UAA without interfering with native biochemical processes (**Figure 14**).[54] Despite this, modified antibodies containing UAAs expressed in mammalian cells such as CHO suffer from complications due to the high rate of amber stop codon usage, which leads to toxicity arising from unwanted amber products.[121]

Other methods for site specific antibody engineering uses bacterial derived enzymes that recognise a specific amino acid tag between four and fifteen residues. An example of this is formylglycine generating enzyme (FGE) that recognises a tag made of six residues motif (LCxPxR) and it oxidises the cysteine to formylglycine.[128] The resulting aldehyde can be further reacted with hydrazines or alkoxyamine to form hydrazones and oximes, respectively. Another example of tag-based approach is sortase-mediated transpeptidation which uses bacterial sortase A to catalyse ligation between LPXTG and polyglycine motif. Sortase ligation allows for fusing of proteins such as Fab fragment, albumin or GFP to LPETG tagged antibody. Lastly, microbial transglutaminases (MTGase) catalyse the acyl transfer reaction between the γ-carboxyamide

group of glutamine residues and other primary amines such as lysine, under the loss of ammonia.[15,58] Furthermore, unnatural tags can be integrated *via* chemoenzymatic methods which guarantees site-specific reactivity.[87] For example, SMARTag technology utilises an FGE that is capable of inserting functionality on the antibody after a specific amino acid sequence is recognised. Subsequently, the cysteine is converted into formylglycine and the engineered antibody can selectively react with aldehyde-specific compounds *via* the reaction based on the hydrazino-Pictet-Spengler ligation (**Figure 14**).[129]

1.2.5 Bioorthogonal modification of inserted functionalities

To study biomolecules in their native settings, chemist and biologist have developed an array of tools. These efforts have brought innovation such as the green fluorescent protein (GFP), whose widespread application was recognized with Nobel Prize in Chemistry.[130] Despite that, a number of biomolecules such as nucleic acids, lipids, glycans, or peptides cannot be monitored using genetically encoded reporters. For these reasons, bioorthogonal chemical modifications that do not interfere with biological process were developed, with the term originally coined by Bertozzi in 2003.[131]

The first bioorthogonal reaction involved the condensation of ketones or aldehydes that react with amine nucleophiles, which is enhanced by the α effect. The α effect is often described as high reactivity nucleophiles that possess an unshared pair of electrons adjacent to the nucleophilic atom.[132] Examples include aminooxy and hydrazide compounds which can form oxime and hydrazone linkages respectively under physiological conditions (**Scheme 11**). These carbonyl moieties have not been widely used for labelling of biomolecules because of competition with endogenous aldehydes and ketones such as in glucose and pyruvate.[128] Aldehydes can be introduced into cell-surface sialic acid residues by mild periodate oxidation which can be further captured by modified glycoproteins by reaction with aminooxybiotin followed by streptavidin chromatography.[133] Additionally, aniline can be used a catalyst to accelerate the reaction under neutral conditions.

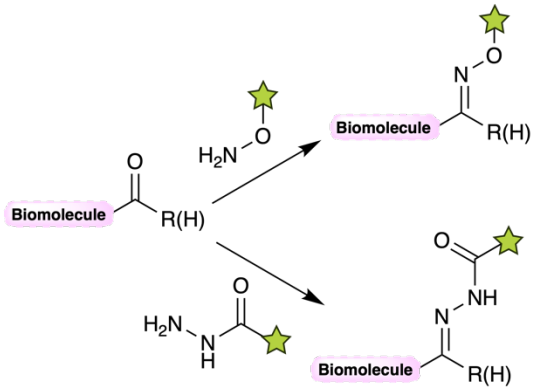

Scheme 11. Bioorthogonal reactions of aldehydes/ketones which can condense with aminooxy compound (top) or hydrazide compounds (bottom) to form a stable oxime or hydrazone linkages, respectively.

The first bioorthogonal reaction was reported by Bertozzi *et al*., and it is a modification of the classical Staudinger reaction of phosphines and azides.[134] The azide moiety has shown to be a powerful chemical reporter because unlike aldehydes or ketones, it is fully absent from any biological system. Azide group also exhibits orthogonal reactivity to most biological functional groups. The Staudinger reaction is a modification of the classical Staudinger reduction of azides with triphenylphospine. In this reaction, the triarylphosphine attacks the azido biomolecule, whereby releasing nitrogen from a four-coordinate transition state to yield aza-ylide, this then undergoes intramolecular attack on the ester, releasing methanol, and resulting in bicycle moiety. Upon hydrolysis, oxidation of the phosphine and formation of an amide bond occurs to yield a ligation product (**Scheme 12**).

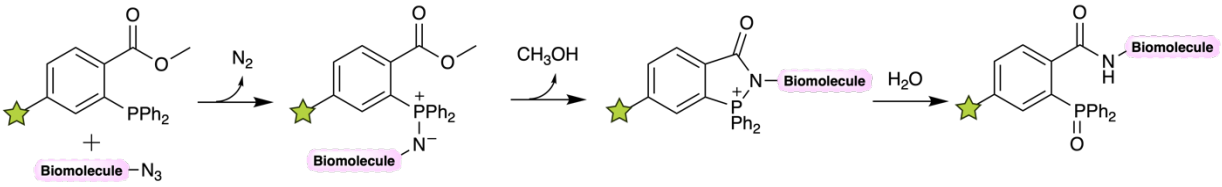

Scheme 12. The Staudinger ligation of azides and triarylphosphines.

Another example of bioorthogonal reaction was reported in 2001 by Sharpless[135] and Medal[136] research groups, a modification to a classical reaction in organic chemistry, the azide-alkyne Huisgen 1,3-dipolar cycloaddition. The main discovery was usage of Cu(I) catalyst that dramatically accelerated the cycloaddition of azide with terminal alkynes to generate 1,4-disubstituted 1,2,3-triazoles, this was achieved in aqueous conditions at room temperature. The copper-catalysed azide-alkyne cycloaddition (CuAAC) reaction takes advantage of the formation of copper acetylide to activate terminal alkynes towards reaction with azides (**Scheme 13**). The

CuAAC proceeds roughly seven orders of magnitude faster than the uncatalyzed cycloaddition, and this can be further accelerated by the use of specific ligand such as THPTA. Despite the usefulness of the CuAAC, it posed a problem in form of toxicity of copper in living systems. This can occur through Cu(I) generation of reactive oxygen species, which can lead to oxidative stress and biological damage, and as a result impairs the structural and functional integrity of biomolecules. To overcome this, it was demonstrated that the use of ligands such as THPTA can intercept and rapidly reduce reactive oxygen species without affecting the rate of CuAAC reaction.[137] The CuAAC reaction if often referred to as 'click chemistry' due to its efficiency, simplicity and selectivity.

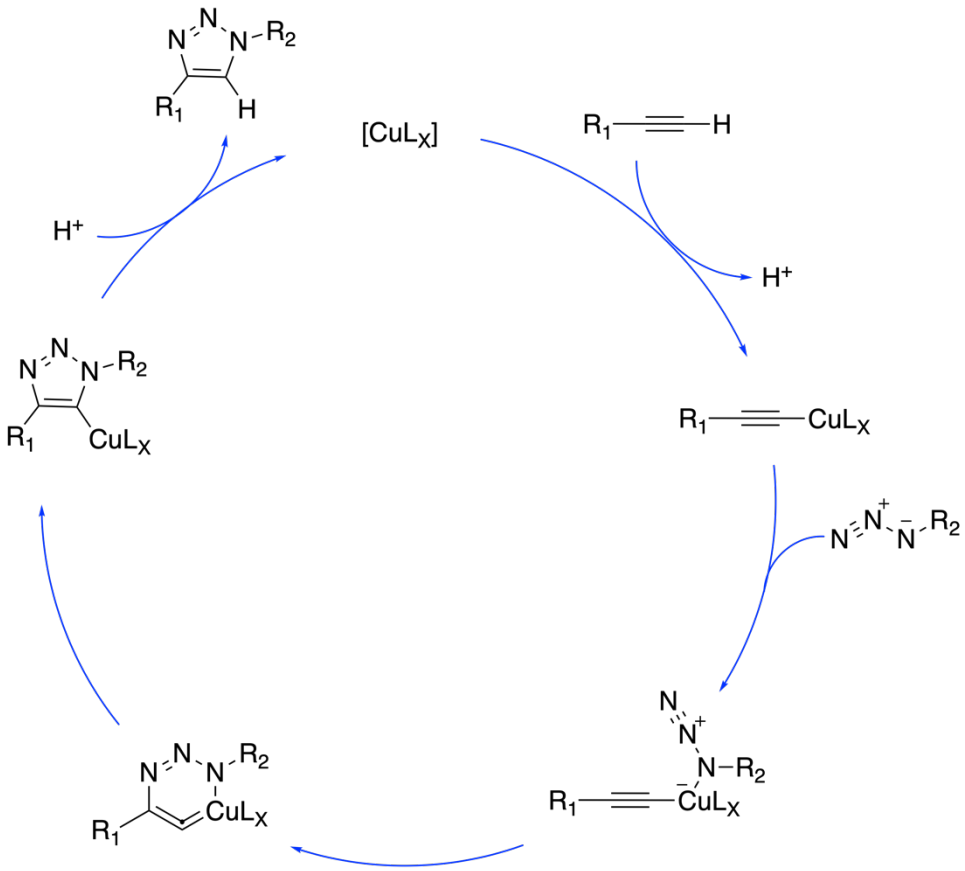

Scheme 13. An overview of the copper-catalysed azide-alkyne cycloaddition (CuAAC).

The CuAAC reaction works well for labelling of biomolecules, however it is largely unsuitable for labelling of living organisms, as mentioned earlier due to the toxicity of the Cu(I). Therefore, new azide-alkyne cycloaddition was sought to activate alkynes without the need of metal catalyst. Significant development was achieved by Wittig and Krebs who identified that cyclooctynes react rapidly with phenylazide to afford a single triazole product.[138] A new strain-promoted azide-

alkyne cycloaddition (SPAAC) was reported by Bertozzi *et al*.,[139] a reaction that did not require any catalysts or ligands, and is instead promoted by the bond angles of sp-hybridized carbons being 160°, which results in less distortion energy that is required to move towards the transition state (**Scheme 14**).[140] Despite that, the SPAAC was slower than CuAAC,[128] thus further optimisation, such as modifying the electron withdrawing groups at the propargylic position (DIFO), were explored. The addition of single fluorine atom showed electron withdrawing properties but with modest improvement of kinetic rates, whereas addition of difluorination afforded a dramatic 60-fold enhancement and showed comparable kinetics to CuAAC.[141] Improvement on SPAAC was also done by augmentation of strain energy through aryl ring (DIBO).[142] The reagent is non-toxic and has reaction kinetics similar to DIFO, whilst also being synthetically accessible, similarly to another reagent containing a cyclopropyl ring (BCN) fusion.[143] The vast functionality of these handles is unquestionable, however, limitations are also present, namely difficulty in synthesis and handling as well as undesirable oxidation of the strained alkyne.[128]

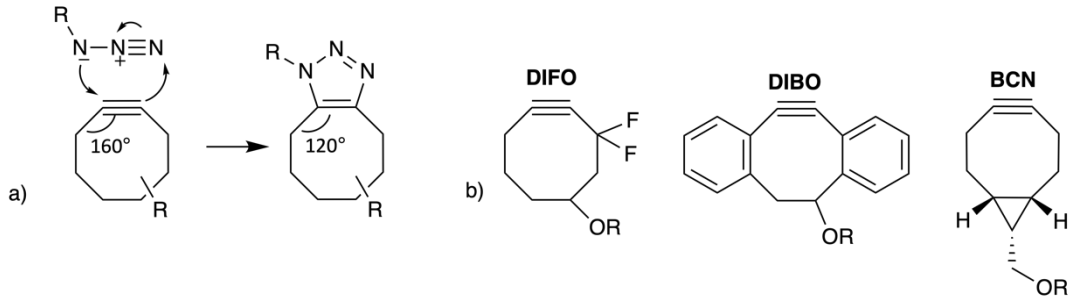

Scheme 14. Strain-promoted azide-alkyne cycloaddition (SPAAC); a) mechanism of SPAAC addition, b) examples of cyclooctynes.

1.3 Native Chemical Ligation

Native chemical ligation (NCL) is one of the most important techniques for site-selective protein modification in chemical biology. Two unprotected peptides in aqueous solutions can give rise to single covalently ligated product by undergoing chemoselective reaction through NCL. An *N*-terminal cysteine residue reacts with a *C*-terminal thioester-peptide through transthioesterification with the side-chain thiol. This results in a thioester intermediate, which spontaneously rearranges *via* a favourable five-membered ring. Then, an intramolecular nucleophilic attack by a nearby amino group of a cysteine residue results in formation of an amide bond at the ligation site Scheme **15**).[144]

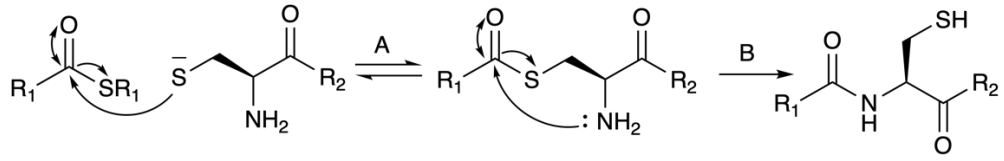

Scheme 15. The mechanism of Native Chemical Ligation. A) Initial reversible transthioesterfication reaction occurring between the new thioester peptide and *N*-terminal cysteine to produce a thioester-linker intermediate. B) Irreversible step where the thioester intermediate undergoes rapid intramolecular *S*-to-*N* acyl transfer rearrangement to form a native peptide bond at the ligation site.

The NCL system can be catalysed by the addition of a thiol. The thiol catalysts will reduce the disulfide bond formation and regenerate thioesters that can reversibly bind with internal cysteine molecules thus preserving the specificity of the reaction.[144] Common thiol catalysts are 1% benzyl mercaptan/3% thiophenol mix, or 2-mercaptoethanesulfonate sodium salt (MESNa) for chemically synthesised peptides thioesters or recombinant peptide-thioesters respectively.[145] The Kent group has investigated different thiol catalysts for improving the ligation rates and found that aryl thiols were the most effective catalyst. The aryl thiol such as 4-mercaptophenylacetic acid (MPAA) is also water soluble and lacks offensive odour as in comparison to the odorous, water insoluble thiophenol.[144] In NCL, the rate limiting step is the transthioesterfication with the thiol moiety of the side chain of the *N*-terminal cysteine.[144]

In terms of biological potential, NCL can occur at physiological pH and in aqueous solution. Additionally, it is a non-enzymatic and highly chemoselective reaction. NCL will only takes place between the *N*-terminal cysteine and *C*-terminal thioester, and no other interactions with other residues on the protein. Due to the initial transthioesterification, the *N*-terminal cysteine is capable of undergoing *S*-to-*N* acyl shift, thus there is no need for protecting groups. NCL can also be used for the attachment of chemical labels to proteins, for example fluorescein or biotin thioester derivatives.[146]

Thioesters

Thioesters have important roles as building blocks in organic chemistry and have been selected as intermediate for the synthesis of esters, b-lactones, peptides, b-lactams and ketones.[147] S-acylation is also a biochemical process by which a molecule is connected to another molecule *via* a thioester bond; for example for addition of fatty acids to cysteine residues within the peripheral membrane proteins. Additionally, peptides are commonly S-acylated using alkyl or

aryl thioester derivatives of palmitic acid, which have a vast application in mammalian cells.[148] Thioesters have also been explored for their therapeutic properties and literature examples lists candidates for few antibiotics,[149] treatment for high cholesterol,[150] and more recently inhibitors of SARS-CoV-2.[151]

In comparison to thioesters, esters have stabilised resonance structures where the lone pair of the singly bonded oxygen atom is delocalised into the carbonyl structure resulting in a partial double bond character and hindered rotation around the C-O single bond. A comparable resonance structure can be drawn for thioesters, but it does not improve their stability. This is due to poor orbital overlap of the 3p orbital of the sulphur atom and the 2p orbital of the carbon atom. Consequently, thioesters are more electrophilic and susceptible to nucleophilic attack and as a result this makes them excellent acyl transfer reagents.[152] Thioesters reactivity towards nucleophilic attack is due to their thermodynamic stability placing them in the middle of a reactivity scale, above unreactive amides and poorly reactive oxoesters but below overreactive carboxylic acid anhydrides and acyl chlorides. Thioesters were shown to be more than 100-fold more reactive towards the thiolate nucleophile compared to an oxoester.[153] Another advantage of this intermediate reactivity is the ability to transfer their acyl group under relatively mild conditions and within good time scales which are important features in the NCL reactions.[146]

Additionally, thioesters have shown to be "softer" acylating agents and are less likely to react with a "hard" hydroxide leading to good stability towards hydrolysis at natural pH, which is often selected for NCL reaction, whereas significant hydrolysis was reported at pH values greater than 8.0. The hydrolysis rate was further explored and it was found that pH-independent and base-catalysed hydrolysis rate are greater for aryl thioesters than for the alkyl thioesters.[146]

The most common way of synthesising a thioester is through an esterification reaction of an acyl compound, such as an acid anhydride, acid chloride or carboxylic acid with a thiol in the presence of a base.[152] However these may result in some drawbacks such as moisture-sensitive acyl chlorides and transformation of this into non-environmentally friendly halide anions.[147,154] Other explored pathways for the synthesis of thioesters include aldehydes where oxidising reagent is used[155] and acylation of thiols using range of catalysts (zeolites, NBS, CsF, triflates, rongalite, Lewis acid, zinc and ionic liquids).[156] Within the chemical biology field, *C*-terminal proteins modified into thioesters can be used for the semi-synthesis of different biological variants *via*

native chemical ligation.[157] Currently, there are no thioester containing reagents used for the formation of ADCs.

1.4 Project Aims

Previous work has demonstrated that bis-thioesters are effective disulfide rebridging reagents, yet literature research has shown that currently these type of reagents containing thioester are not being exploited for site-selective antibody modification. Therefore, the principal aim of this work was to identify new reagents containing a thioester motif that would extend the scope of disulfide rebridging as a new methodology for improved homogeneous bioconjugation. It was also proposed that installation of the thioester bond would allow for further modification of the conjugate, without the need of complex synthesis of the linker-attachment.

For the design of novel reagents, it was envisaged that bis-electrophiles containing two different functionalities would rapidly react with liberated thiols on the Fab antibody fragment. The challenge was to design thioester containing reagents that would rebridge reduced disulfide bonds while each thiol selectively reacts only with one of the functional handles. The installation of 'stable-labile' linkage would in turn allow for nucleophilic addition through native chemical ligation (NCL) mediated functionalisation (**Scheme 16**).

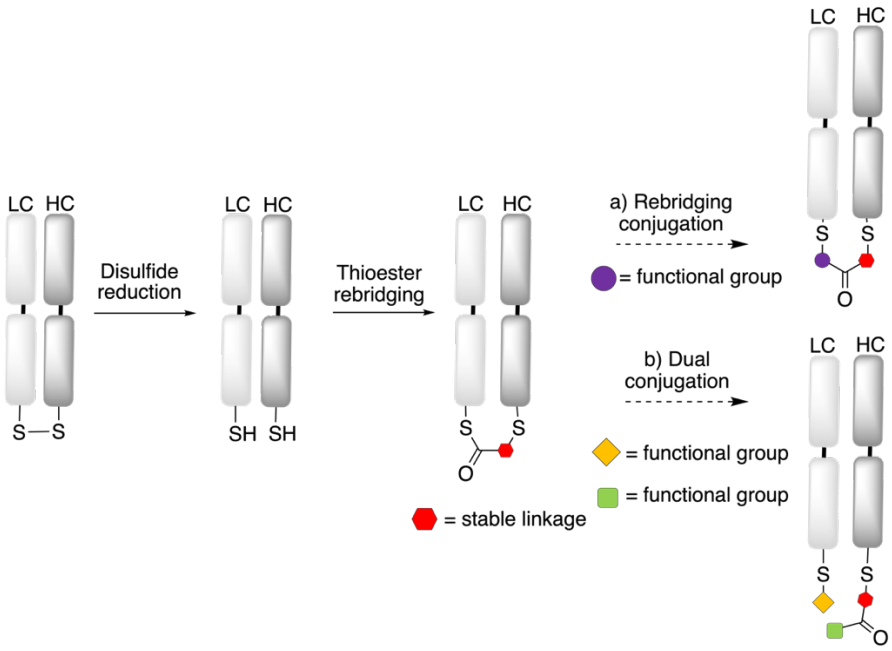

Scheme 16. Proposed strategy of disulfide rebridging with thioesters.

The purpose of Chapter 2 was to design and synthesise novel disulfide rebridging reagents containing two functional groups, one of them being the thioester moiety. It was important to

carefully design these bis-electrophilic reagents so no double addition would occur, instead giving a clean disulfide rebridging. The goal was also to understand how these reagents react towards thiols and their stability in physiological and elevated pH. The further functionalisation of 'stable-labile' linkages installed between two thiols was explored in Chapter 3, where principles of NCL were utilised for rebridging conjugation (**Scheme 16**, a). The key idea was to demonstrate that *N*-terminal cysteine peptides are only required for nucleophilic cargo addition, without the need of *C*-terminal thioesters as shown in the literature. In Chapter 4, the 'stable-labile' linkage was proposed to be expanded further by developing a dual conjugation protocol (**Scheme 16**, b). Here, it was suggested that the primary amine on the hydrazine would react with the thioester bond and as a result liberate the other cysteine thiol on the antibody which could go onto form a new disulfide bond. Overall, the resulting dually conjugated antibody fragment would incorporate two unique linkers, not achievable with current methodologies, that could be cleaved off at different cellular environments. The majority of the work presented here was accomplished by using a Fab fragment of HER2+ targeting breast cancer drug Trastuzumab, as this is an ideal platform due to a single solvent accessible disulfide bond. Lastly, the aim of Chapter 5 was to translate the newly developed methodologies on to a full antibody.

Chapter 2: Chemical synthesis of novel thioesters

2.1 Novel thioesters

To synthesise the designed thioesters, acyl chlorides were selected as starting materials due to their commercial availability and straightforward synthesis. To ensure the thioesters are widely applicable, the synthetic routes should be inexpensive and high yielding. Ideally, these novel thioesters should then react with reduced disulfide bonds rapidly, and only require near stoichiometric amounts of the reagent, to achieve complete conversion without side-product formation.

2.2 Synthesis of novel thioesters

To explore the proposed idea of a disulfide rebridging reagent, the two initial molecules chosen to be synthesised were α-chlorothioester **1** and α-bromothioester **2**. The idea was based on iodocetamide which is an excellent cysteine alkylating reagent, however, iodocetamide is known to alkylate other amino acids aside from cysteine.[158] Therefore, chlorine was selected as one of the functional group here as it showed a higher degree of specificity towards cysteine residues. These were both synthesised by a one-step addition-elimination reaction where chloroacetyl chloride or bromoacetyl bromide were reacted with methyl thioglycolate to result in compounds **1** and **2**, respectively (**Scheme 17**).

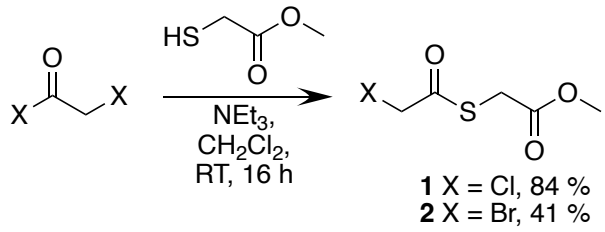

Scheme 17. Synthesis of α-chlorothioester **1** and α-bromothioester **2**.

Acrylic compounds or *α,β*-unsaturated carbonyl compounds are electrophilic at the carbonyl carbon and the *β*-carbon. They have also been shown to extensively react as Michael acceptors with thiols.[159] The reaction of a thiolate with a Michael acceptor results in a stable covalent bond between the *α,β*-unsaturated carbonyl moiety and the thiolate.[160] Currently there are no acrylic compounds containing a thioester bond in the literature where the *α,β*-unsaturated carbonyl could be used as a rebridging reagent. The most similar reagent used for rebridging is the bis-sulfone developed by Basescu *et al*.[105] For that reason, it was considered exciting to explore acrylic

thioesters. Reagent **3** was thus synthesised in one step by reacting methyl thioglycolate with acryloyl chloride in presence of triethylamine to afford acrylic thioester **3** in an acceptable yield (51%) (**Scheme 18**).

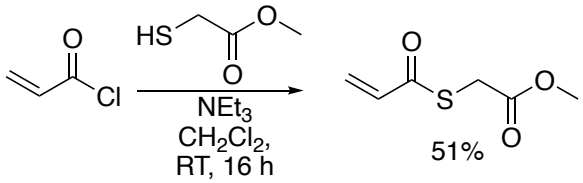

3

Scheme 18. Reaction scheme for the synthesis of methyl 2-(acryloylthio)acetate **3**.

The next reagent explored was a thioester with a halide-bearing aryl group. It was proposed that an S_NAr mechanism may be another viable route for a designed rebridging reagent. Benzene rings are usually electron rich, therefore nucleophilic attack on the aromatic ring is very difficult. On the aromatic ring, a strong electron-withdrawing group is required for the S_NAr reaction to increase the electrophilicity of the carbon electrophile and stabilise the Meisenheimer intermediate, such as a nitro group.[89] Studies done by Weerapana *et al*. has shown that aryl halide containing *para*-nitro benzene group are more reactive for covalent reaction with thiols *via* S_NAr mechanisms than the *meta*- or *ortho*- nitro groups,[124] therefore synthesis of a *para*-nitro benzene aryl halide was attempted. The synthesis of aryl-fluoro thioester **5** started with mixing of nitric acid with sulphuric acid at 0 °C followed by addition of 2-fluorobenzoyl chloride to afford an intermediate *2*-fluoro-5-nitrobenzoic acid **4** in a good yield (89%). The compound **4** was then mixed in DMF in the presence of EEDQ. Methyl thioglycolate was then added to the mixture and stirred ON resulting in the desired aryl-fluoro thioester **5** in a good yield (77%) (**Scheme 19**).

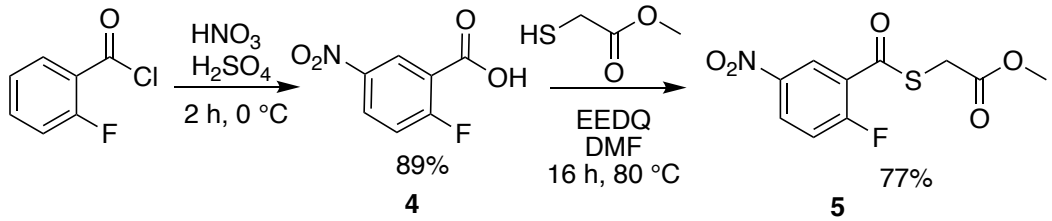

4 **5**

Scheme 19. Reaction scheme for the synthesis of methyl 2-((2-fluoro-5-nitrobenzoyl)thio)acetate **5.**

Lastly, a branched chloro-thioester was explored with an aim that a branched phenyl ring could be further functionalised by addition of a payload. Compound **6** was synthesised in similar manner as previous thioesters where α-chlorophenylacetyl chloride was added to methyl

thioglycolate and triethylamine in a one-pot reaction, resulting in the desired aryl-chloro thioester **6** in quantitative yield (**Scheme 20**).

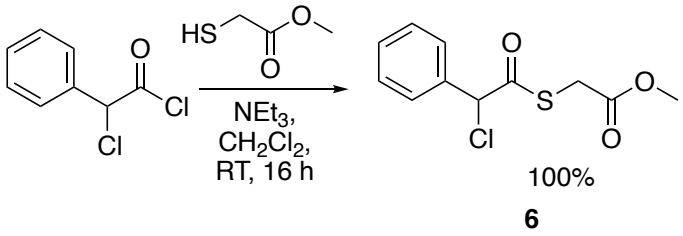

Scheme 20. Reaction scheme for the synthesis of methyl 2-((2-chloro-2-phenylacetyl)thio)acetate **6**.

2.3 Small molecule study of thioesters

To understand the relative thiol reactivity of the two functional groups in each structure a small molecule study was designed, where each reagent was initially reacted on *N*-Boc-Cys-OMe (50 mM phosphate buffer/ MeCN (80:20), pH 7.4), followed by purification and NMR analysis.

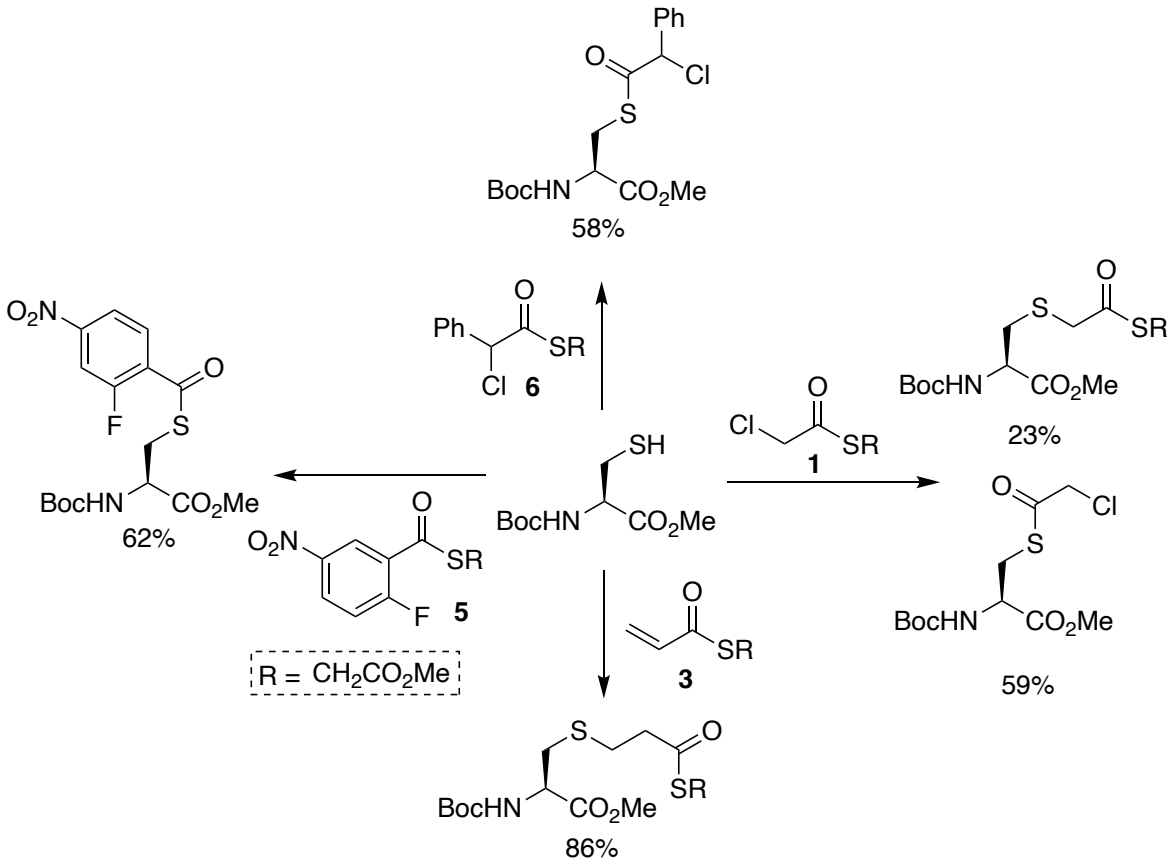

Scheme 21. Single amino acid study, using *N*-Boc-Cys-OMe and treating it with the dual-reactive reagents in phosphate buffer (50 mM/MeCN), pH 7.4.

Upon analysis of all the reactions, it was found that the product isolated for the compounds α-chlorothioester **1,** aryl-fluoro thioester **5**, and aryl-chloro thioester **6**, was achieved through transthioesterification which was taking place faster than the S_N2 or S_NAr reactions (**Scheme 21**). It is important to note that in the case of α-chlorothioester **1** a minor product formed by S_N2 displacement was also observed. In the case of acrylic thioester **3** the conjugate addition was faster than transthioesterification, which is consistent with the literature observation on thiol addition related with α,β--unsaturated thioesters.[161] In the cases where the yield is moderate, this was due to the full conversion not being achieved. Competing thiol oxidation was identified which prevented full conversion, therefore remaining starting material was recovered.

2.4 Fab reaction with thioesters

The successfully synthesised thioesters were then tested for their rebridging capability on the Fab fragment. In this study Fab moiety of HER2+ targeting breast cancer drug Trastuzumab was selected as this is an ideal platform due to a single solvent accessible disulfide bond. Fab fragment was obtained by in-house enzymatic digestion (full protocol is described in the experimental section). Optimisation was carried out by differing the equivalents of the thioesters added, reaction time and pH.

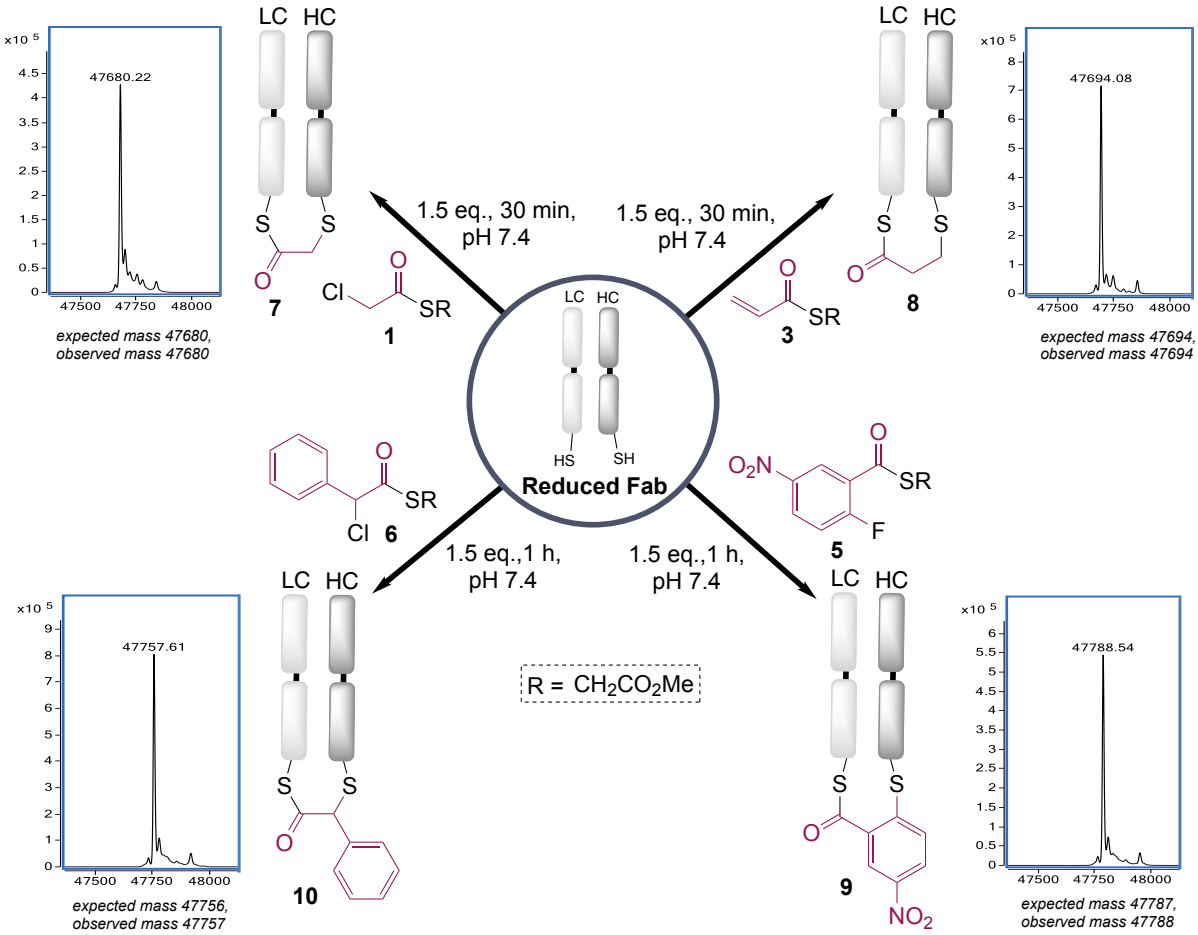

Scheme 22. Reduced Fab fragment, obtained by TCEP treatment, was then disulfide rebridged with selection of dual reactivity reagents.

Pleasingly, all thioesters rebridged the disulfide bond extremely well within 1 h at 22 °C, pH 7.4 with 1.5 eq. of reagents added (**Scheme 22**). This also demonstrated the rate enhancement for the bridging step, due to the proximity of the cysteine residue, was in fact sufficient to overcome the differential in reactivity of the two functional groups in the synthesised reagents; as no competing double addition was observed.

The α-bromothioester **2** required 5 eq. to achieve rebridging which was complete in 30 min at 22 °C (data presented in the experimental section). As bromine is a better leaving group than chlorine (I>Br>Cl>F), the need for more equivalents of compound **2** could be due to instability or degradation of the reagent by hydrolysis before it reacts with the cysteine residues. α-Chlorocarbonyl and α-bromocarbonyl compounds are known to be reactive towards cysteine site-chains, the additional presence of the thioester clearly enhances the reactivity of the molecule by providing two available electrophilic reactive sites.

For the rebridging of reduced Fab with acrylic thioester **3**, apart from the desired conjugate, an additional new species was also observed. The extra mass of +306 on the LC was postulated to be some kind of TCEP adduct (spectra not shown). Subsequently, rebridging of Fab with acrylic thioester **3** was repeated with removal of TCEP by ultrafiltration before adding the same number of equivalents of reagent **3.** The second attempt resulted in a significantly better outcome - the rebridged peak corresponding to conjugate **8** was present (observed mass 47694) and no native Fab was observed or unwanted addition on the LC or HC. Notably, no other thioester reagent cross-reacted with TCEP in the rebridging reaction, therefore the ultrafiltration step was only required for rebridging with reagent **3**.

A control experiment was also performed, where the Fab fragment was reacted with α-chlorothioester **1** under identical conditions, but without prior disulfide bond reduction, resulting in only native Fab observed (**Figure 15**).

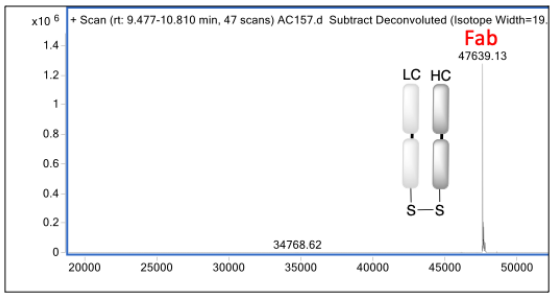

Figure 15. LCMS deconvoluted spectrum of control reaction with 1.5 eq. of α-chlorothioester **1** with Fab, without prior TCEP reduction.

2.5 Stability study of thioesters

Having successfully identified the conditions for disulfide rebridging with new thioesters, the stability of the resultant Fab conjugates towards increased hydrolysis was then evaluated. The results would give an appreciation of relative stability of these species and highlight whether hydrolysis is likely to be competing reaction to next bioconjugation step. Here base-mediated hydrolysis was investigated, where the pH of the conjugation buffer was increased from pH 7.4 to pH 8.5. The nucleophilic hydroxide attacks the carbonyl, followed by elimination of the thiol, leaving behind a carboxylic acid group. A possible side-reaction is expected leading to cysteine-to-lysine transfer thus forming conjugate **12** (HC) as drawn in **Scheme 23**.

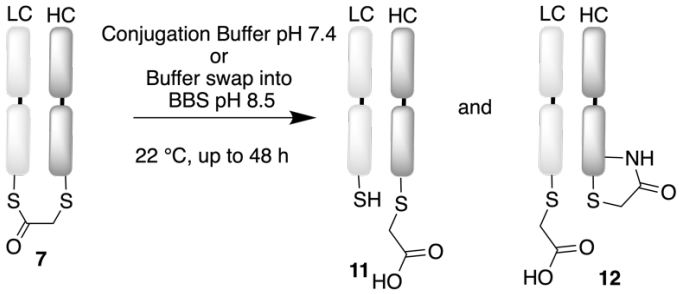

Scheme 23. Stability study of Fab conjugate **7** at pH 7.4 and pH 8.5.

The stability assay of Fab conjugate **7** was carried out with two buffers with different pH (**Scheme 23**). The initial timepoint at pH 7.4 shows expected rebridging of Fab, forming conjugate **7** and complete disappearance of native Fab (**Figure 16**, **a**). Following this, at the 24 h and 48 h timepoint the intensity of the rebridged peak **7** has decreased (**Figure 16**, **c** and **d**) with corresponding appearance of the native light chain **11**-LC, hydrolysed bridge species **12**-LC and **11**-HC, as well as small CLT conjugate peak **12**-HC (**Figure 16**, **d** and **f**). It is worth noting that the intensity of the peaks on LCMS does not correlate to their amount present, as any amount of light chain would be ionised much better under LCMS conditions. At 24 h and 48 h of reaction at pH 8.5, no rebridged conjugate **7** was observed, suggesting that the hydrolysis occurs within the initial 24 h of incubation at the elevated pH (**Figure 16**, **i** and **k**). A small CLT peak can be observed at 0 h (**Figure 16**, **h**), corresponding to CLT conjugate **12-**HC but it is not observed at the further timepoints, indicating it is a very minor species formed at this pH.

pH 7.4

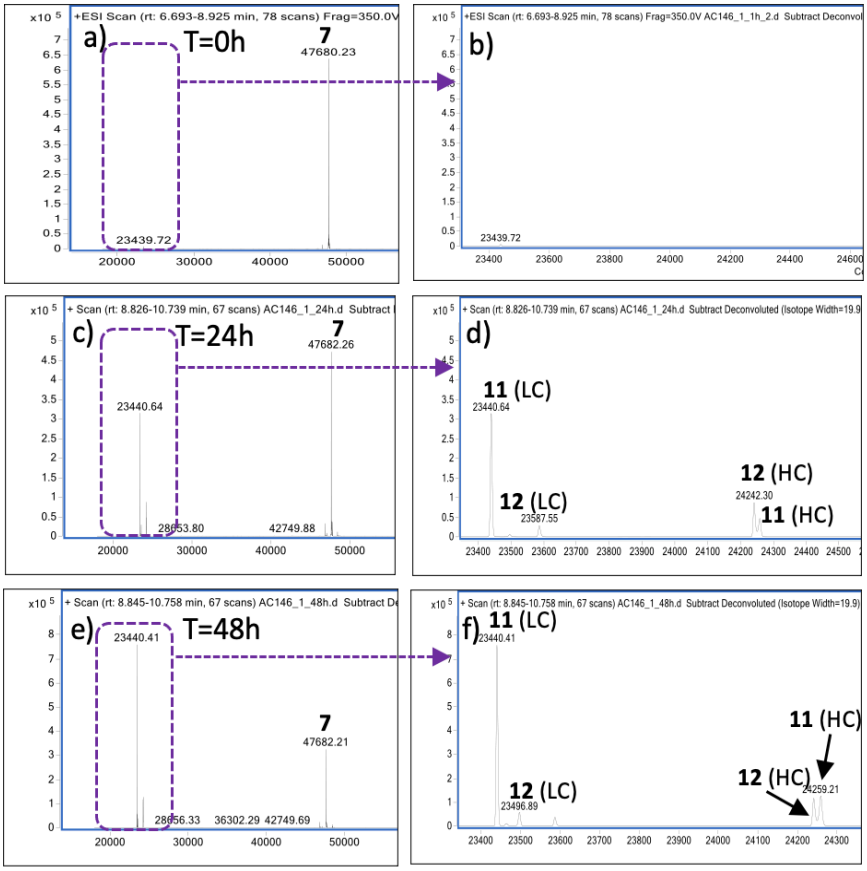
a)
T=0h
7
47680.23
23439.72
b)
23439.72
c)
T=24h
7
47682.26
23440.64
28053.80
42749.88
d)
11 (LC)
23440.64
12 (LC)
23587.55
12 (HC)
24242.30
11 (HC)
e)
T=48h
23440.41
7
47682.21
28056.33
36302.29
42749.69
f)
11 (LC)
23440.41
12 (LC)
23496.89
11 (HC)
12 (HC)
24259.21

pH 8.5

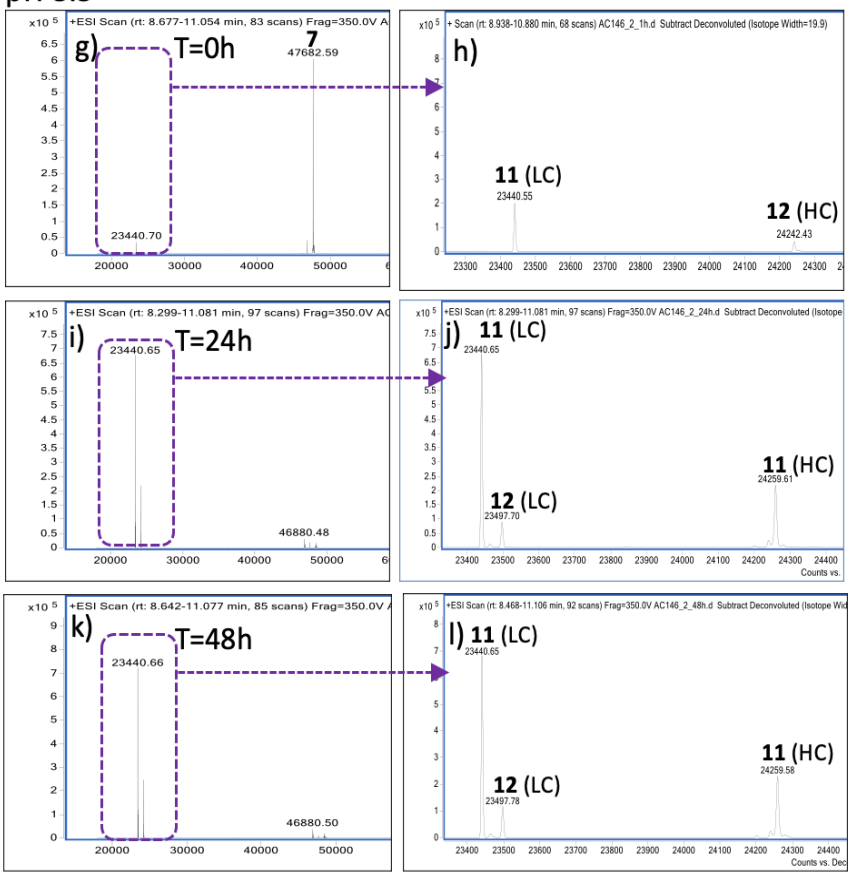
g)
T=0h
7
47682.59
23440.70
h)
11 (LC)
23440.55
12 (HC)
24242.43
i)
T=24h
23440.65
46880.48
j)
11 (LC)
23440.65
11 (HC)
24259.61
12 (LC)
23497.70
k)
T=48h
23440.66
46880.50
l)
11 (LC)
23440.65
11 (HC)
24259.58
12 (LC)
23497.78

Figure 16. Stability study of the Fab conjugate **7** at pH 7.4 and 8.5. Expected mass for **11** (LC) 23438, **11** (HC) 24259, **12** (LC) 23497, **12** (HC) 24242, Fab conjugate **7** expected mass 47680. a) deconvoluted ion series of Fab fragment at 0 h, pH 7.4, b) zoomed in spectrum of LC and HC at 0 h, pH 7.4, c) deconvoluted ion series of Fab fragment at 24 h, pH 7.4, d) zoomed in spectrum of LC and HC at 24 h, pH 7.4, e) deconvoluted ion series of Fab fragment at 48 h, pH 7.4, f) zoomed in spectrum of LC and HC at 48 h, pH 7.4, g) deconvoluted ion series of Fab fragment at 0 h, pH 8.5, h) zoomed in spectrum of LC and HC at 0 h, pH 8.5, i) deconvoluted ion series of Fab fragment at 24 h, pH 8.5, j) zoomed in spectrum of LC and HC at 24 h, pH 8.5, k) deconvoluted ion series of Fab fragment at 48 h, pH 8.5, l) zoomed in spectrum of LC and HC at 48 h, pH 8.5.

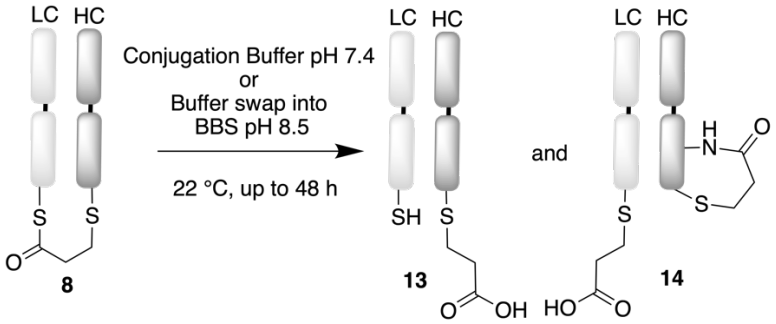

Scheme 24. Stability study of Fab conjugate **8** at pH 7.4 and pH 8.5.

The hydrolysis study for Fab conjugate **8** was set up as illustrated in **Scheme 24**. At pH 7.4 there is notable decrease in the intensity of the rebridged peak of conjugate **8** at the 24 h and 48 h of incubation (**Figure 17**, **c** and **e**), with appearance of native light chain **13**-LC and CLT on the heavy chain **14**-HC (**Figure 17**, **d** and **f**). At pH 8.5 complete hydrolysis was observed after 24 h of incubation (**Figure 17**, **i**). The hydrolysis of Fab conjugate **8** created with acrylic thioester **3** was found to be comparable with the one observed for Fab conjugate **7**.

pH 7.4

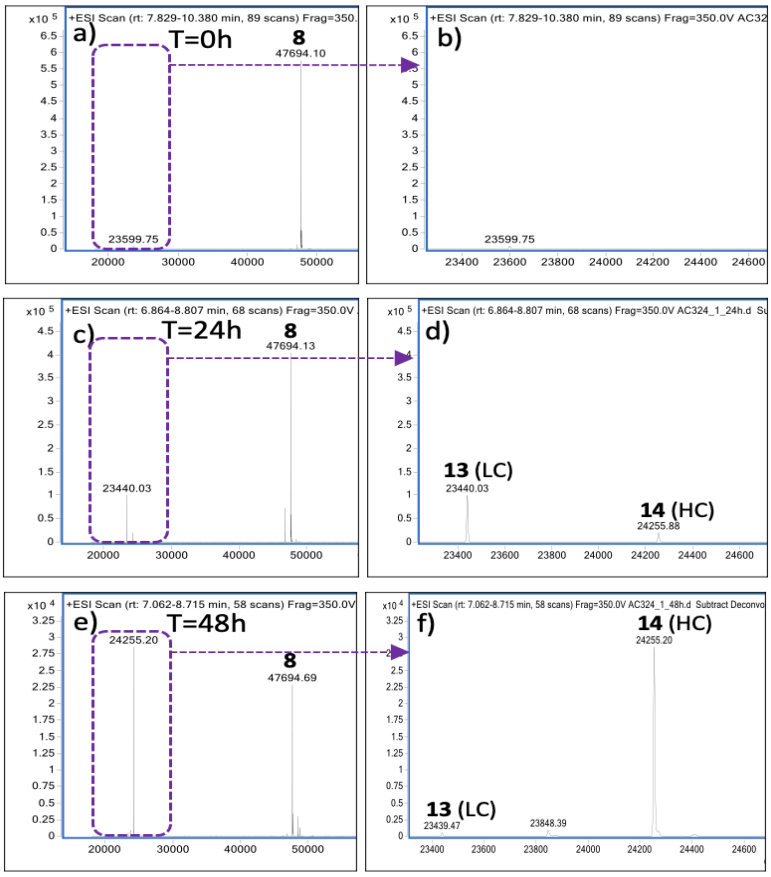
a)
T=0h
8
47694.10
23599.75
b)
23599.75
c)
T=24h
8
47694.13
23440.03
d)
13 (LC)
23440.03
14 (HC)
24255.88
e)
T=48h
24255.20
8
47694.69
f)
14 (HC)
24255.20
13 (LC)
23439.47
23848.39

pH 8.5

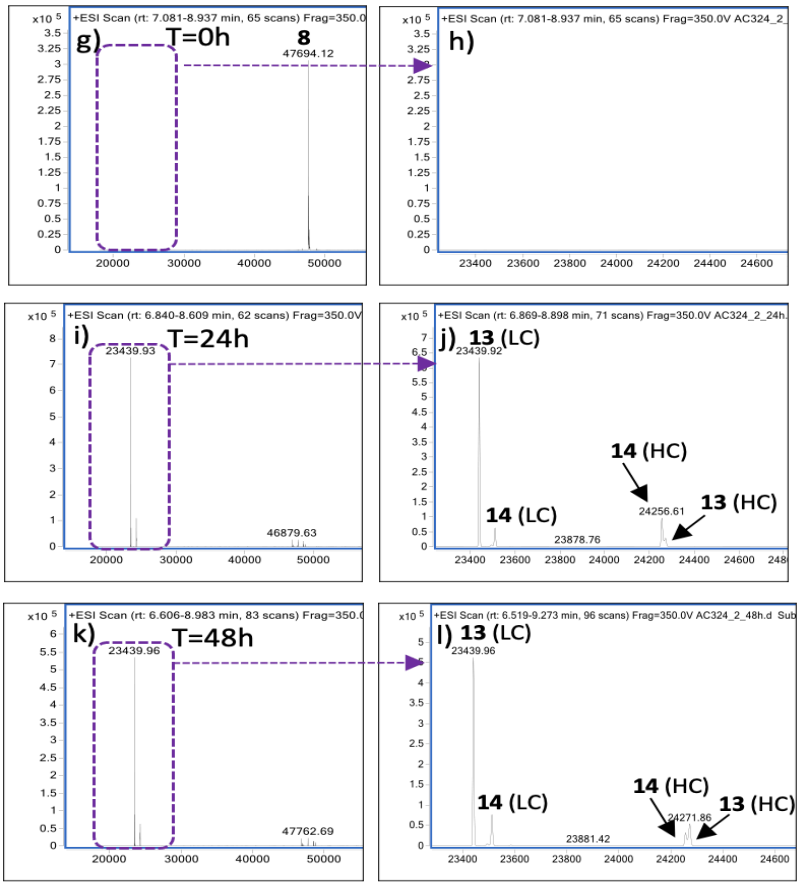
g)
T=0h
8
47694.12
h)
i)
T=24h
23439.93
46879.63
j)
13 (LC)
23439.92
14 (HC)
24256.61
13 (HC)
14 (LC)
23878.76
k)
T=48h
23439.96
47762.69
l)
13 (LC)
23439.96
14 (LC)
14 (HC)
24271.86
13 (HC)
23881.42

Figure 17. Stability study of the Fab conjugate **8** at pH 7.4 and 8.5. Expected mass for **13** (LC) 23438, **13** (HC) 24273, **14** (LC) 23511, **14** (HC) 24256, Fab conjugate **8** expected mass 47694. a) deconvoluted ion series of Fab fragment at 0 h, pH 7.4, b) zoomed in spectrum of LC and HC at 0 h, pH 7.4, c) deconvoluted ion series of Fab fragment at 24 h, pH 7.4, d) zoomed in spectrum of LC and HC at 24 h, pH 7.4, e) deconvoluted ion series of Fab fragment at 48 h, pH 7.4, f) zoomed in spectrum of LC and HC at 48 h, pH 7.4, g) deconvoluted ion series of Fab fragment at 0 h, pH 8.5, h) zoomed in spectrum of LC and HC at 0 h, pH 8.5, i) deconvoluted ion series of Fab fragment at 24 h, pH 8.5, j) zoomed in spectrum of LC and HC at 24 h, pH 8.5, k) deconvoluted ion series of Fab fragment at 48 h, pH 8.5, l) zoomed in spectrum of LC and HC at 48 h, pH 8.5.

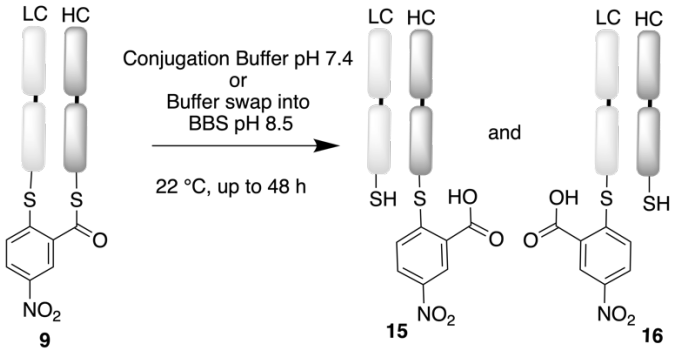

Scheme 25. Stability study of Fab conjugate **9** at pH 7.4 and pH 8.5.

Scheme 25 illustrates the condition for hydrolysis study of conjugate **9**. Here, conjugate **9** was generated with aryl-fluoro thioester **5**. The first two timepoints at 0 h and 24 h are comparable at pH 7.4, where the major species was the rebridged Fab **9** (**Figure 18**, **a** and **c**). There is some native light chain also observed in those two initial timepoints, this is likely unreacted minor species and not a result of the hydrolysis reaction (**Figure 18**, **b** and **d**). As expected, at pH 8.5 the peak intensity of rebridged species **9** has decreased, with corresponding hydrolysis on the light and heavy chain, **16**-LC and **15**-HC, however complete hydrolysis was not observed even after 48 h of incubation (**Figure 18**, **k**), suggesting a very good stability toward hydrolysis.

pH 7.4

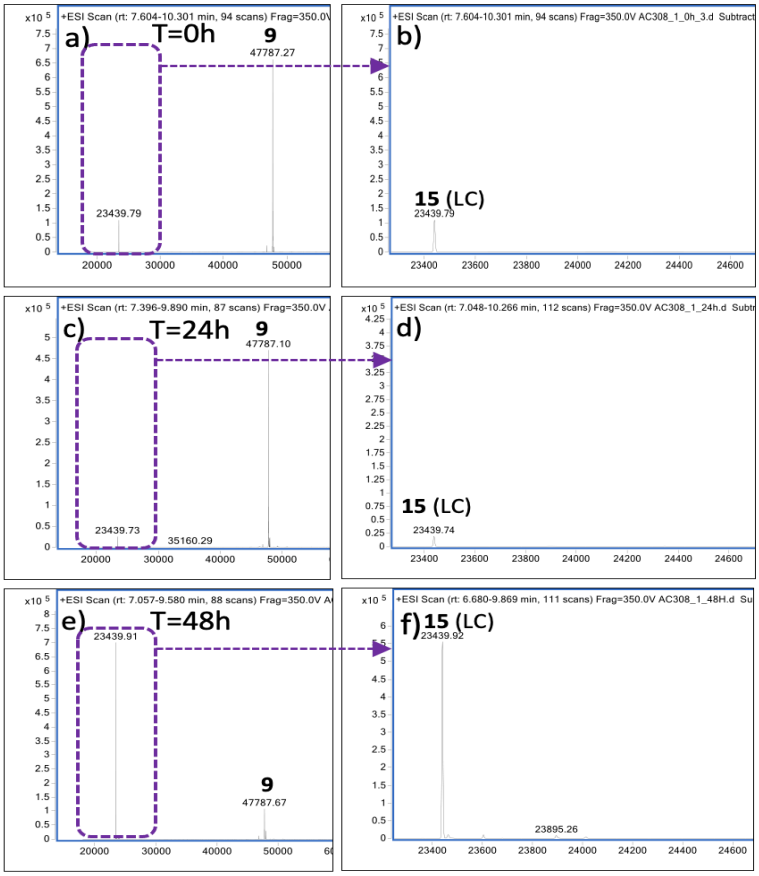
a)
T=0h
9
47787.27
23439.79
b)
15 (LC)
23439.79
c)
T=24h
9
47787.10
23439.73
35160.29
d)
15 (LC)
23439.74
e)
T=48h
23439.91
9
47787.67
f)
15 (LC)
23439.92
23895.26

pH 8.5

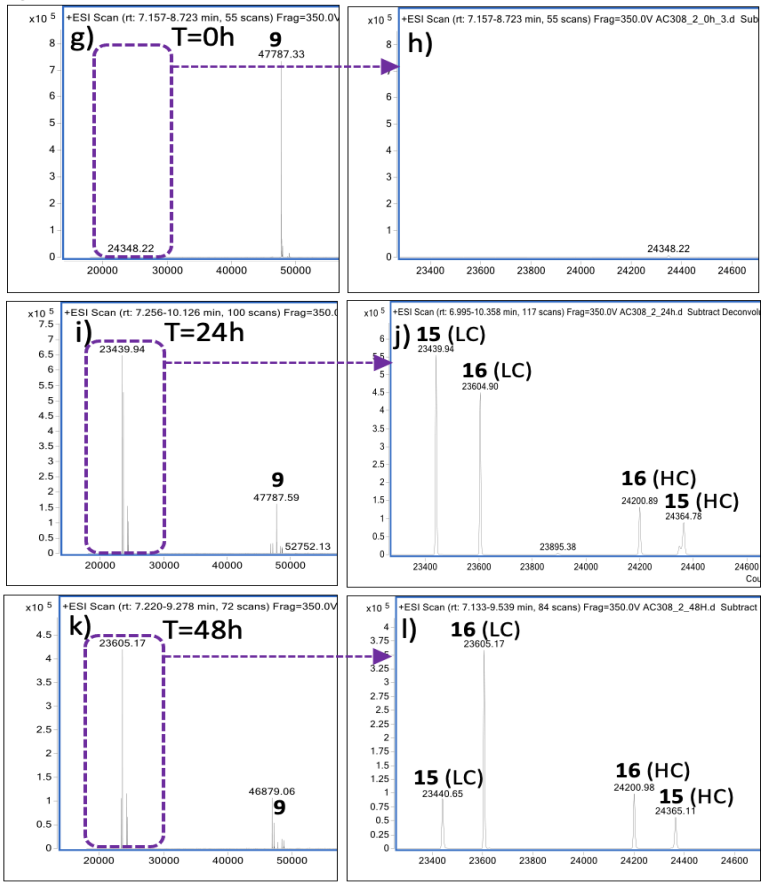
g)
T=0h
9
47787.33
24348.22
h)
24348.22
i)
T=24h
23439.94
9
47787.59
52752.13
j)
15 (LC)
23439.94
16 (LC)
23604.90
16 (HC)
24200.89
15 (HC)
24364.78
23895.38
k)
T=48h
23605.17
46879.06
9
l)
16 (LC)
23605.17
15 (LC)
23440.65
16 (HC)
24200.98
15 (HC)
24365.11

Figure 18. Stability study of the Fab conjugate **9** at pH 7.4 and 8.5. Expected mass for **15** (LC) 23438, **15** (HC) 24366, **16** (LC) 23604, **16** (HC) 24200, Fab conjugate **9** expected mass 47787. a) deconvoluted ion series of Fab fragment at 0 h, pH 7.4, b) zoomed in spectrum of LC and HC at 0 h, pH 7.4, c) deconvoluted ion series of Fab fragment at 24 h, pH 7.4, d) zoomed in spectrum of LC and HC at 24 h, pH 7.4, e) deconvoluted ion series of Fab fragment at 48 h, pH 7.4, f) zoomed in spectrum of LC and HC at 48 h, pH 7.4, g) deconvoluted ion series of Fab fragment at 0 h, pH 8.5, h) zoomed in spectrum of LC and HC at 0 h, pH 8.5, i) deconvoluted ion series of Fab fragment at 24 h, pH 8.5, j) zoomed in spectrum of LC and HC at 24 h, pH 8.5, k) deconvoluted ion series of Fab fragment at 48 h, pH 8.5, l) zoomed in spectrum of LC and HC at 48 h, pH 8.5.

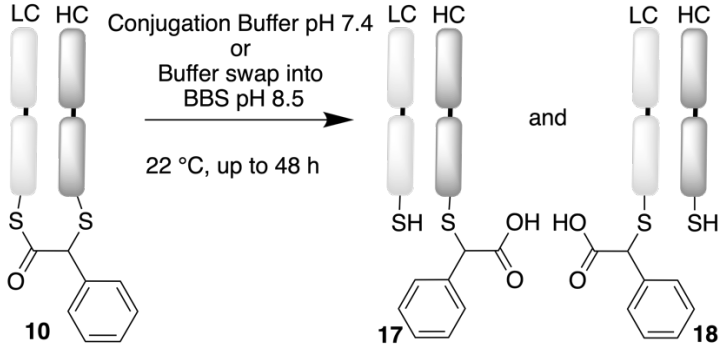

Scheme 26. Stability study of conjugate **10** at pH 7.4 and pH 8.5.

The Fab conjugate **10** hydrolysis study was prepared as illustrated in **Scheme 26**. At pH 7.4 there was no hydrolysis observed at any of the timepoints (**Figure 19**, **a**, **b** and **c**). Whilst at pH 8.5 a small level of hydrolysis was observed at the 48 h timepoint (**Figure 19**, **k**), indicating that Fab conjugate **10** is very stable and complete hydrolysis was not observed at the conditions selected for this study. The results from the hydrolysis reaction on the Fab conjugate **10**, generated by the aryl-chloro thioester **6** are comparable with the one obtained for the Fab conjugate **9**.

pH 7.4

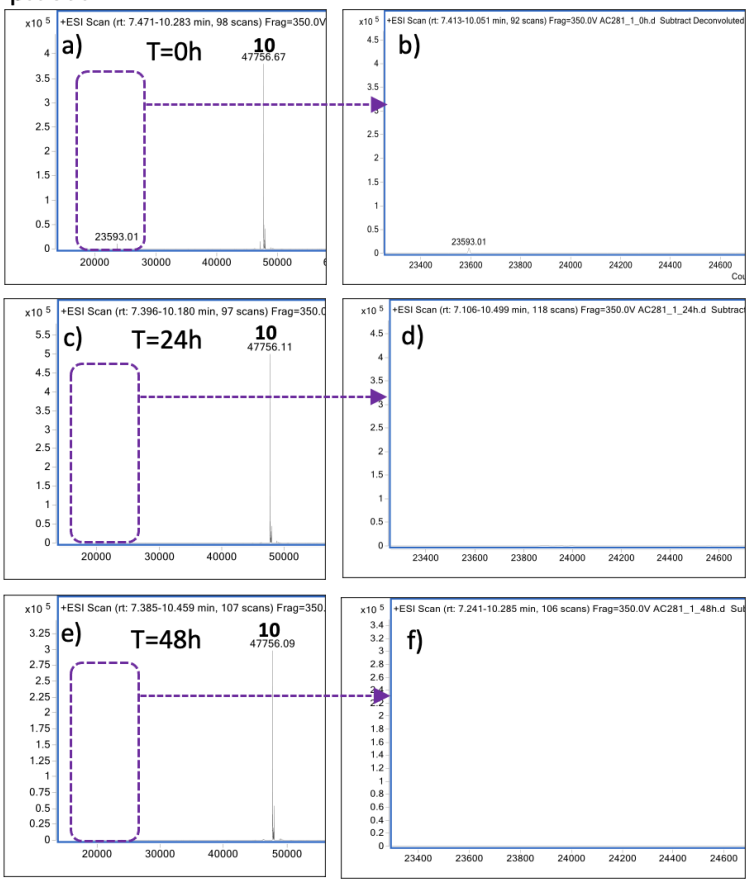
a)
T=0h
10
47756.67
23593.01
b)
23593.01
c)
T=24h
10
47756.11
d)
e)
T=48h
10
47756.09
f)

pH 8.5

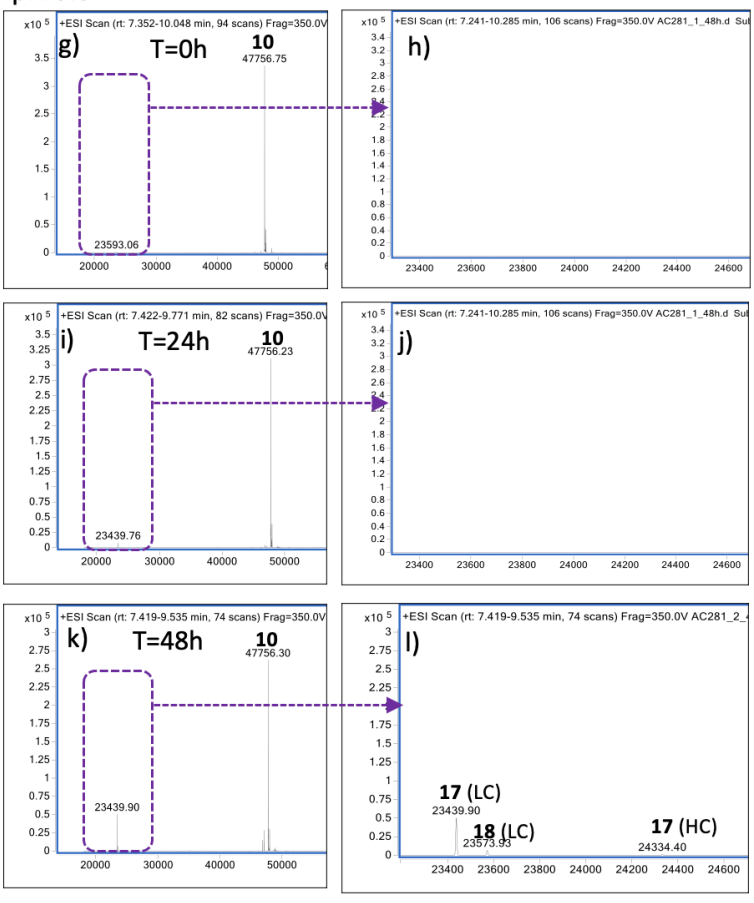
g)
T=0h
10
47756.75
23593.06
h)
i)
T=24h
10
47756.23
23439.76
j)
k)
T=48h
10
47756.30
23439.90
l)
17 (LC)
23439.90
18 (LC)
23573.93
17 (HC)
24334.40

Figure 19. Stability study of the Fab conjugate **10** at pH 7.4 and 8.5. Expected mass for **17** (LC) 23438, **17** (HC) 24335, **18** (LC) 23573, **18** (HC) 24200, Fab conjugate **10** expected mass 47756. a) deconvoluted ion series of Fab fragment at 0 h, pH 7.4, b) zoomed in spectrum of LC and HC at 0 h, pH 7.4, c) deconvoluted ion series of Fab fragment at 24 h, pH 7.4, d) zoomed in spectrum of LC and HC at 24 h, pH 7.4, e) deconvoluted ion series of Fab fragment at 48 h, pH 7.4, f) zoomed in spectrum of LC and HC at 48 h, pH 7.4, g) deconvoluted ion series of Fab fragment at 0 h, pH 8.5, h) zoomed in spectrum of LC and HC at 0 h, pH 8.5, i) deconvoluted ion series of Fab fragment at 24 h, pH 8.5, j) zoomed in spectrum of LC and HC at 24 h, pH 8.5, k) deconvoluted ion series of Fab fragment at 48 h, pH 8.5, l) zoomed in spectrum of LC and HC at 48 h, pH 8.5.

These overall hydrolysis studies showed the differing properties of the newly identified thioesters. Complete hydrolysis was achieved with the conjugates **7** and **8** at pH 8.5 within 24 h. Some acyl transfer (CLT), assumed to be on to nearby lysines, was also observed as a minor pathway competing with hydrolysis. Under pH 8.5 at the 24 h timepoint, the conjugate **9** had undergone only partial hydrolysis, while conjugate **10** was found intact. Intriguingly, hydrolysis of these conjugates serves to cap one cysteine residue out of a pair, which is not usually practicable using classical cysteine conjugation reagents.

2.6 Regioselectivity study of thioesters

The panel of new reagents generated desirable bridged Fab conjugates, each installing a thioester moiety that can be prospectively used as a handle for native chemical ligation (NCL). To explore that, bridged conjugate **7** was reacted with cysteine (25 eq.) and it was found to efficiently undergo a NCL conjugation, with LCMS confirming formation of conjugate **19** (**Figure 20**). As expected, the newly inserted cysteine had oxidised to form a disulfide bond with the remaining free cysteine side-chain of the Fab when left for longer incubation time, also to facilitate this step 5,5'-dithio-bis-(2-nitrobenzoic acid) (DTNB) was added here which essentially re-established the covalent bridge between the heavy and light chains. To understand the regioselectivity of the thioester reagents, as to whether the thioester is formed on the light or heavy chain, *N*-methylmaleimide was added to cap the free thiols during the intermediate step of the reaction. The LCMS analysis was carried out to investigate the ratio of the two regioisomer **20** and **21** formed upon bridging.

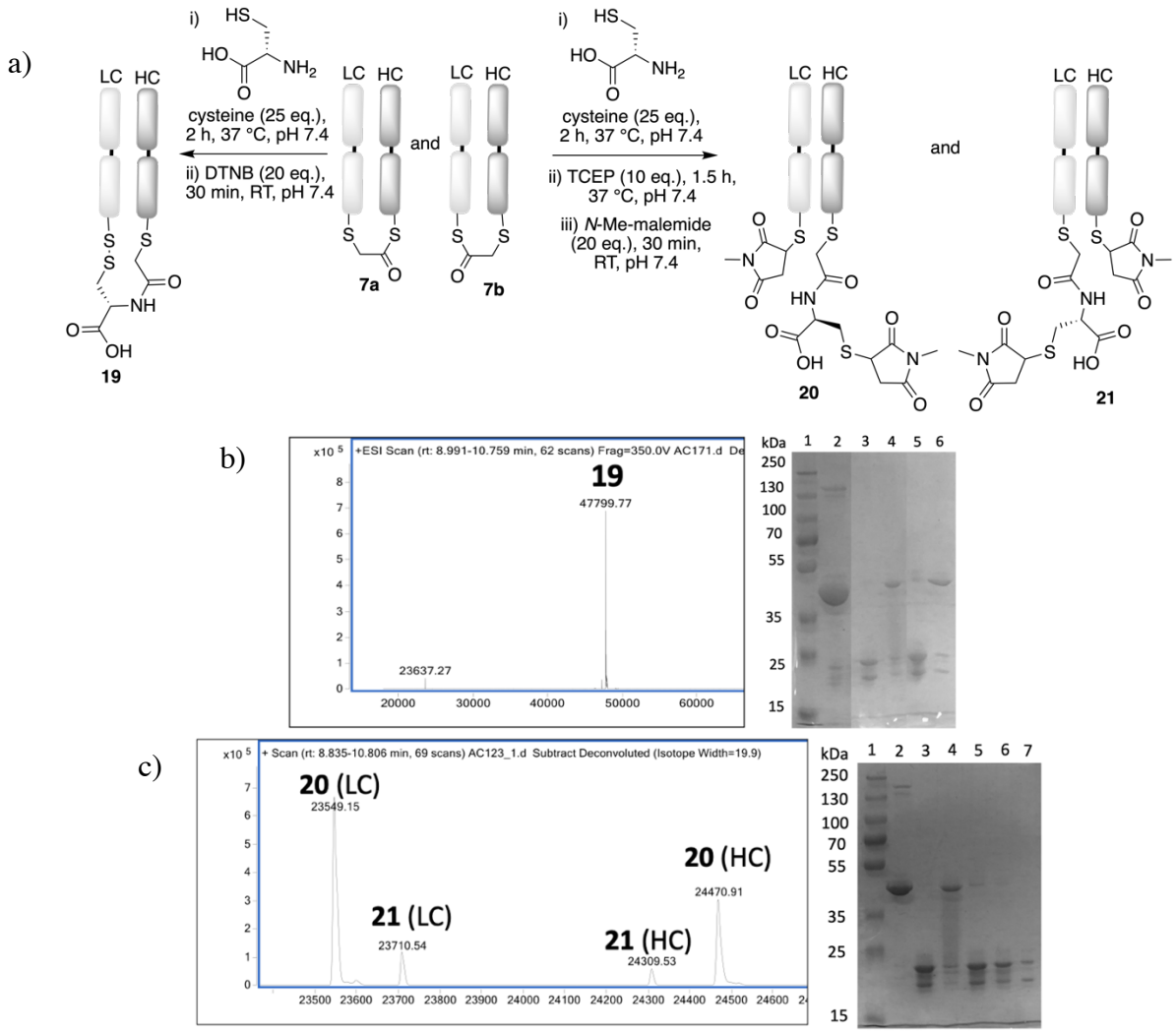

Figure 20. a) Analysis of native chemical ligation on conjugate **7** with cysteine and regioselectivity study with capped thiols; b) LCMS deconvoluted spectrum: Fab conjugate **7** reacted with cysteine formed conjugate **19** mass expected 47799, mass observed 47799; SDS-PAGE 1 – molecular marker, 2 – native Fab, 3 – TCEP reduction, 4 – rebridged Fab with **1**, 5 – cysteine addition, 6 – DTNB addition; c) LCMS zoomed in deconvoluted spectrum of regioselectivity study: **20** (LC) mass expected 23550, mass observed 23549, **21** (LC) mass expected 23711, mass observed 23710, **21** (HC) mass expected 24312, mass observed 24309, **20** (HC) mass expected 24473, mass observed 24470. SDS-PAGE 1 – molecular marker, 2 – native Fab, 3 – TCEP reduction, 4 – rebridged Fab with **1**, 5 – cysteine addition, 6 – 2nd TCEP treatment, 7 – *N*-Me-maleimide capping.

The LCMS data revealed an approximate 5:1 ratio of the external cysteine attached to the heavy chain compared to the light chain thus suggesting that the heavy chain thiol has higher selectivity towards the α-carbon by S_N2 reaction. This is possibly due to the heavy chain thiol having a lower pKa thus being more acidic, than the *C*-terminal light chain cysteine as *C*-terminal cysteine is known to have higher pKa and being less acidic, thus less reactive.[162] The SDS-PAGE analysis shows streaking and some presence of light and heavy chain in the rebridging lane. The reasons for these unusual results could be the effect of SDS-PAGE conditions. When running SDS-

PAGE, samples are heated to 80 °C for 5 min, therefore these harsh conditions may have cleaved off the labile thioester moiety.[163] This is consistent with having a hydrolytically unstable linkage treated at high temperatures under denaturating conditions, this observation was also found with other thioesters tested in this work.

This experiment was also performed at lowered and elevated pH (6.0 and 8.0) yet this show that it did not impact the regioisomer formation. Despite not being able to control the regioselectivity beyond the 5:1 ratio, this would not impact the future functionalisation steps as each regioisomer still installs a stable and labile linkage onto the Fab fragment. Therefore, conjugate **7** will be referred from here on as the major species, whilst acknowledging that a minor regioisomer will always be present as well.

The NCL assay with cysteine was then performed on the Fab conjugate **8** formed by acrylic thioester **3**. Interestingly, the LCMS data obtained for the determination of regioselectivity of conjugate **8** differs from the ones achieved with the Fab conjugate **7** (**Figure 21**).

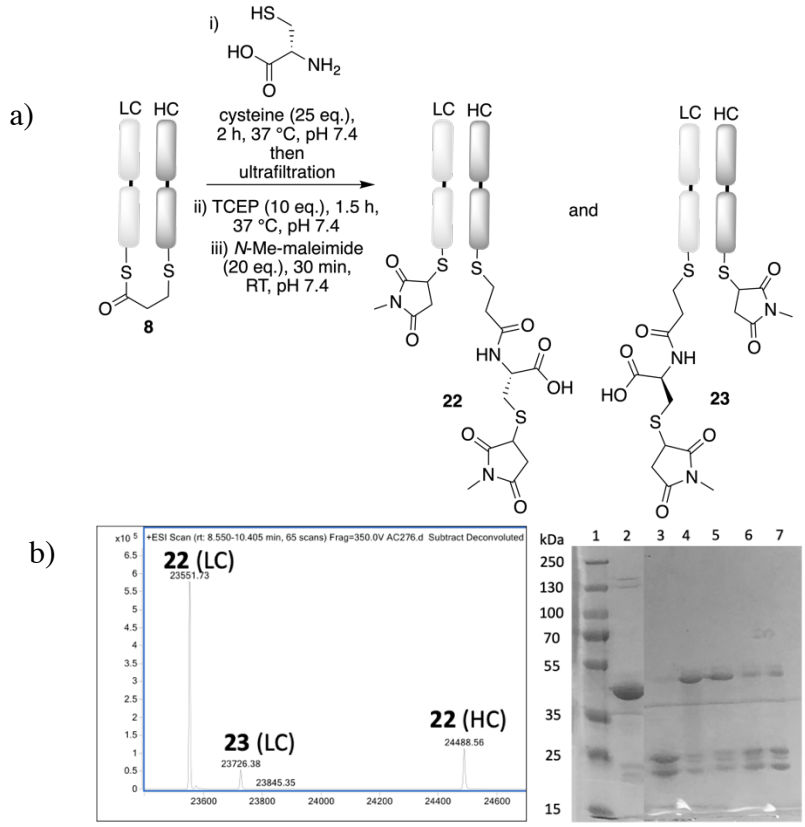

Figure 21. a) Analysis of native chemical ligation on conjugate **8** with cysteine capped thiols, b) LCMS deconvoluted spectrum: **22** (LC) mass expected 23550, mass observed 23551, **23** (LC) mass expected 23725, mass observed 23726, **23** (HC) mass expected 24312 but not

observed, **22** (HC) mass expected 24487, mass observed 24488. SDS-PAGE 1 – molecular marker, 2 – native Fab, 3 –TCEP reduction, 4 – rebridged with **3**, 5 – cysteine addition, 6 – 2nd TCEP reduction, 7 – *N*-Me-maleimide capping.

The only heavy chain species observed was one modified by cysteine **22**-HC, suggesting that is by far the predominant species formed. The light chain shows 12:1 ratio of unmodified light chain (**22**-LC) *vs*. modified with cysteine (**23**-LC), therefore approximate 12:1 selectivity of heavy chain conjugate can be inferred.

An NCL protocol was then employed on the aryl-fluoro Fab conjugate **9**. As with the previous regioselectivity study, a general protocol was initially used, however it was found that 25 eq. of cysteine was not sufficient to fully break the thioester bond, therefore harsher conditions had to be employed (**Figure 22**).

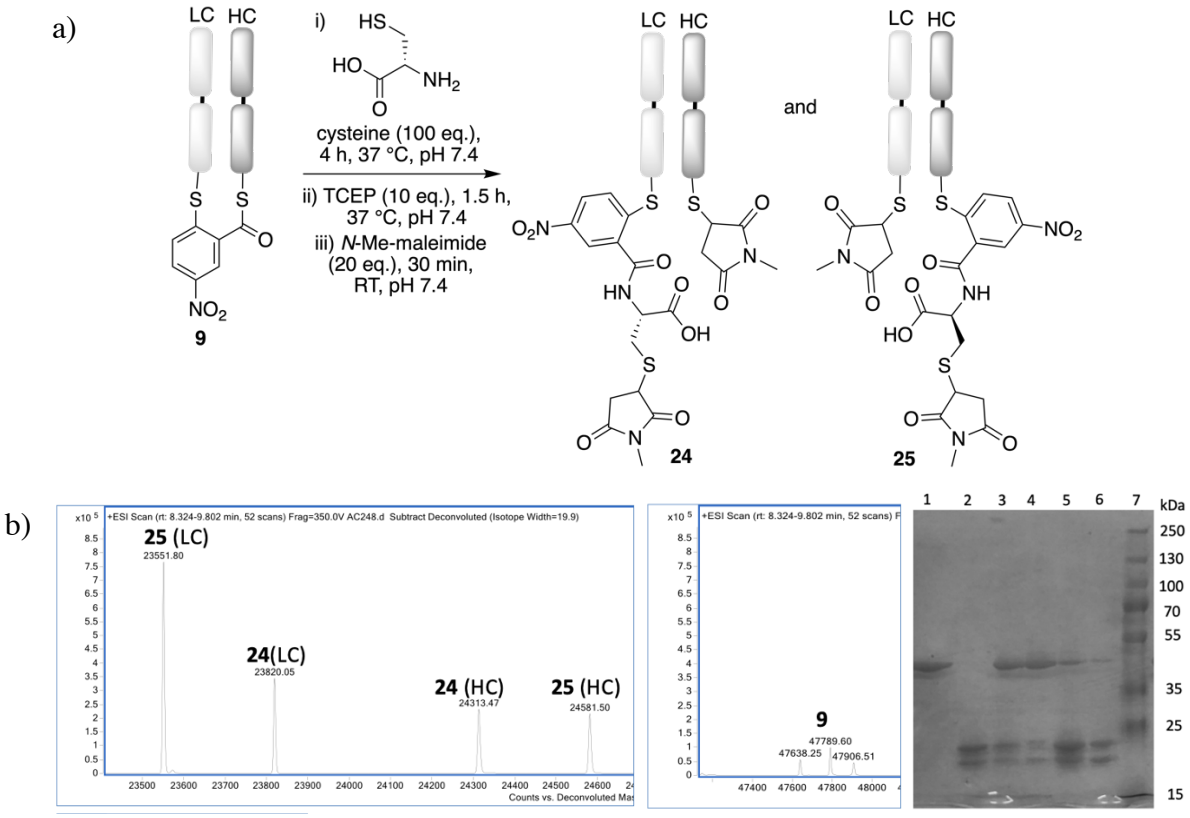

Figure 22. a) Analysis of native chemical ligation on conjugate **9** with cysteine capped thiols, b) LCMS deconvoluted spectrum: **25** (LC) mass expected 23550, mass observed 23551, **24** (LC) mass expected 23818, mass observed 23820, **24** (HC) mass expected 24312, mass observed 24313, **25** (HC) mass expected 24580, mass observed 24581. SDS-PAGE, 1 – native Fab, 2 – TCEP reduction, 3 – rebridged Fab with **5**, 4 – cysteine addition, 5 – 2nd TCEP reduction, 6 – *N*-Me-maleimide capping, 7 – molecular marker.

Even with 100 eq. Fab conjugate **9** was still present, notably as a minor peak on LCMS. The regioselectivity outcome was surprising to analyse as again it differed from the other thioesters

tested. Analysis by LCMS suggested an approximate 1:1 ratio of the additionally capped cysteine on the heavy chain **25**-HC *vs*. heavy chain with *N*-methylmaleimide **24**-HC. In the light chain area, the ratio was found to be approximately 2:1 of the light chain with *N*-methylmaleimide **25**-LC *vs*. light chain capped with cysteine **24**-LC. This suggested 1:1 and 2:1 ratio between either regioisomer being formed during bridging conjugation. Whereas with other thioesters such as α-chlorothioester **1** and acrylic thioester **3** the predominant regioisomer was the one with thioester formed on the light chain.

The last conjugate to analyse under the NCL protocol was the Fab conjugate **10** generated by the aryl-chloro thioester **6**. Similarly, as with Fab conjugate **9**, 25 eq. of cysteine was not enough to fully break the thioester bond and more stringent conditions were applied (**Figure 23**).

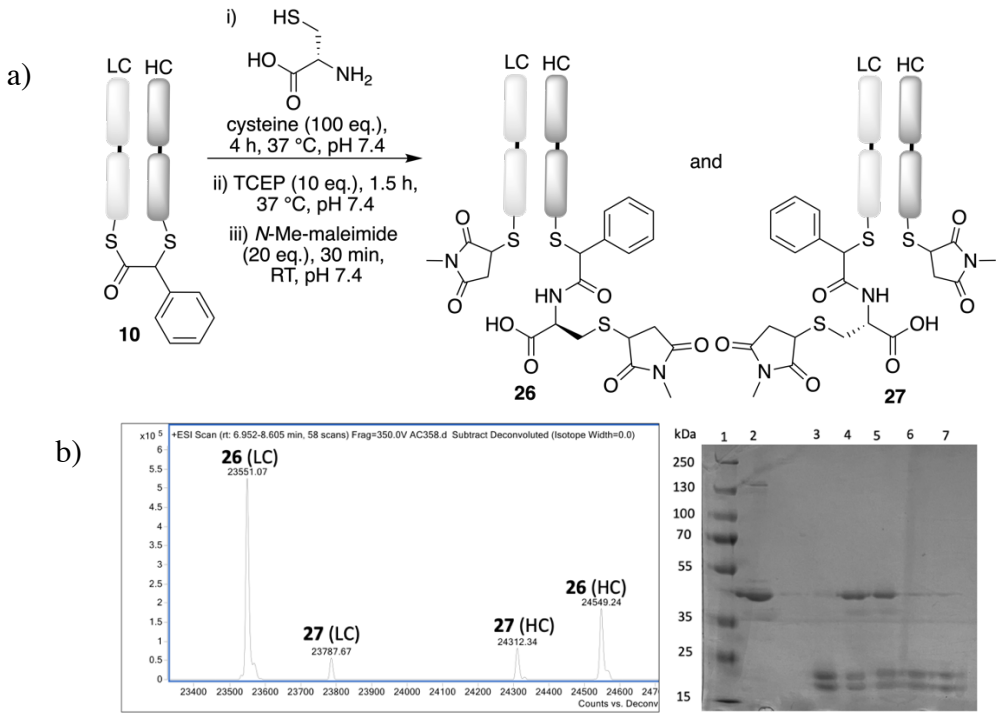

Figure 23. a) Analysis of native chemical ligation on conjugate **10** with cysteine capped thiols, b) LCMS deconvoluted spectrum: **26** (LC) mass expected 23550, mass observed 23551, **27** (LC) mass expected 23787, mass observed 23787, **27** (HC) mass expected 24312, mass observed 24312, **26** (HC) expected 24549, observed 24549. SDS-PAGE, 1 – molecular marker, 2 – native Fab, 3 – TCEP reduction, 4 – rebridged with **6**, 4 – cysteine addition, 6 – 2nd TCEP reduction, 7 – *N*-Me-maleimide capping.

LCMS analysis suggested an approximate 2:1 of additionally capped cysteine on the heavy chain **26**-HC compared with the heavy chain capped with *N*-methylmaleimide **27**-HC. For the light

chain, the ratio was approximately 7:1 of light chain capped with *N*-methylmaleimide **26**-LC *vs*. light chain capped with capped with cysteine **27**-LC.

The regioselectivity outcome in most of the cases resulted in the major product having thioester on the light chain, thus when undergoing NCL, the *N*-terminal cysteine would predominantly be found attached to the heavy chain with the highest selectivity achieved using acrylic thioester reagent **3** (~12:1). Ultimately, these regioisomer are unlikely to have significantly different properties given the similarity in the position of the attachments on the antibody fragment.

2.7 Summary and conclusion

To conclude, novel thioesters synthesised in this project showed marked advantages over current rebridging reagents, such as straight-forward chemical synthesis, affordable starting materials, and short reaction times. A sequential rebridging protocol is possible whereby TCEP removal is not required (except for acrylic thioester **3**). Bioconjugation with these thioesters is achievable at a wide range of pH, with near stoichiometric amount of conjugation reagents, short conversion times and room temperature conditions. The reagents are stable for at least 6 months as stock solutions in DMF, when stored at -20 °C, therefore this further saves the cost and labour required to make new stocks. The regioselectivity was found to vary between each conjugate with the highest identified using acrylic thioester. The thioester moiety was predominantly forming on the light chain cysteine. The stability data demonstrated that the major findings were aligned with the literature reports, where it is known that thioesters are stable at pH 7.4 and hydrolysis can be observed at the elevated pH such as 8.0 and above (**Scheme 27**).[146]

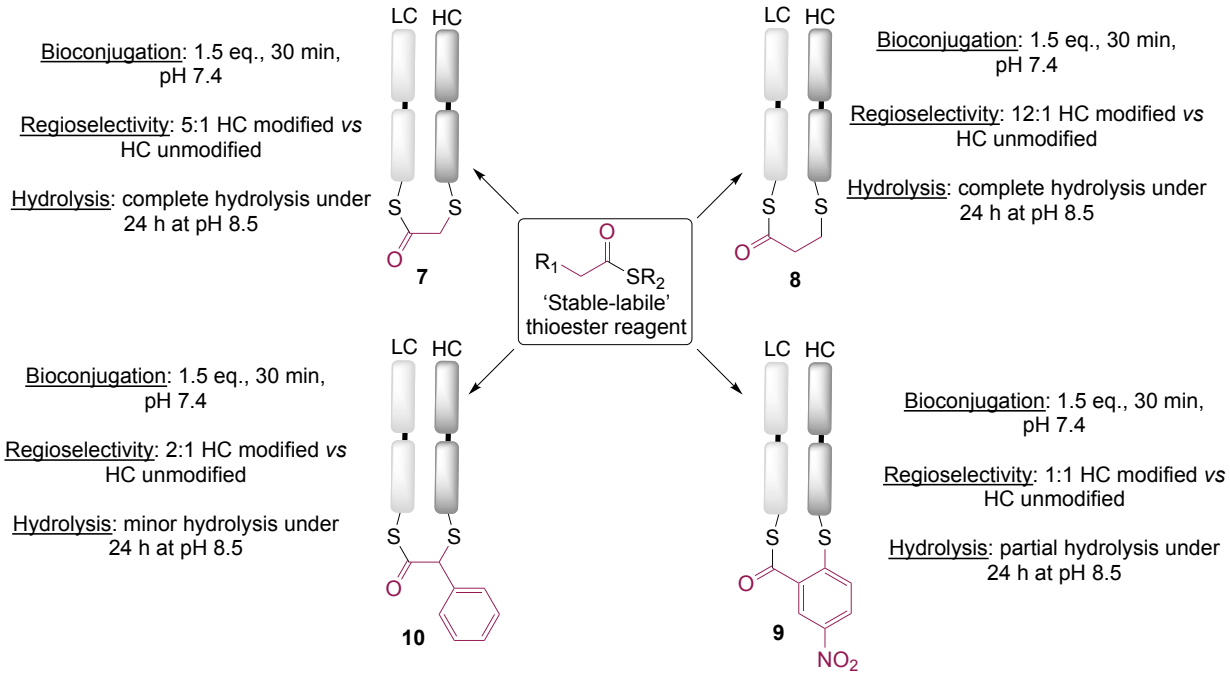

Scheme 27. Summary of the key findings for each new conjugate developed.

A cysteine thiol nucleophile, used in the NCL protocol (**Figure 20**), demonstrated a transposition of the chemical bond from the side chain thiol group to the α-amine group, making the thiol group of the cysteine available for subsequent chemoselective reaction. Thus, functionalised cysteine derivatives could be applied to enable late-stage modification. For example, an *N*-terminal cysteine containing peptide where the peptide could contain a cytotoxic cargo or have cell penetrating properties, and secondary modifications with thiol specific molecules such as NGM or PD containing an alkyne handle could be explored (**Scheme 28**).

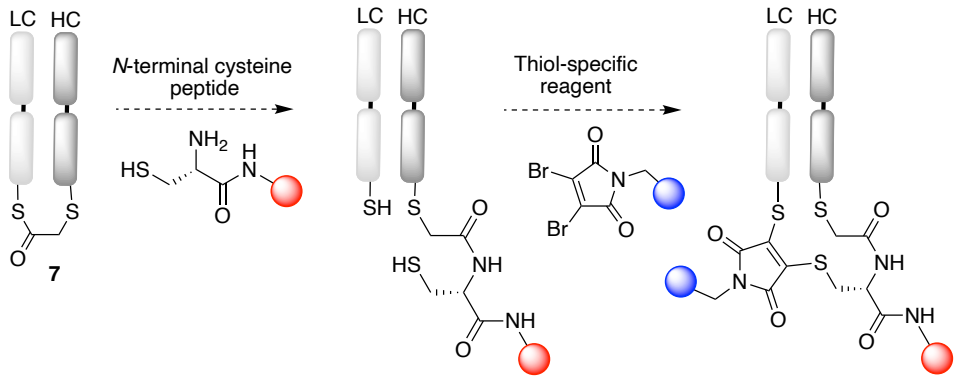

Scheme 28. Proposed further functionalisation of Fab conjugate **7** with *N*-terminal cysteine peptide, followed by further functionalisation with thiol specific reagent.

All thioesters synthesised here demonstrated corrected rebridging of the reduced Fab as mentioned earlier. Under the conditions for stability assay and the initial NCL protocol with cysteine, each thioester performed well however needing slightly different conditions, therefore α-chlorothioester **1** was selected as a main rebridging reagent to demonstrate the possible functionalisation. Notably, alkene thioester **3**, aryl-fluoro thioester **5**, and aryl-chloro thioester **6** are also capable of further functionalising, however data for that was not included here.

Chapter 3: Functionalisation of thioester moiety through Native Chemical Ligation

In common applications of NCL the protocol requires a *C*-terminal peptide thioester reacting with an *N*-terminal cysteinyl peptide to generate a new, native peptide bond.[146] The initial experiments in this work, with cysteine on bridged thioester validated NCL as a viable bioconjugation protocol, therefore it was then proposed to trial an approach where an antibody-fragment peptide bioconjugate is formed with a selection of *N*-terminal cysteine peptide.

3.1 Cell Penetrating Peptide – P-C218R

To test the NCL bioconjugation of Fab rebridged with α-chlorothioester **1**, a functional peptide was identified. Peptides such as Cell Penetrating Peptides (CPPs) are particularly attractive vectors, as they provide effective internalisation properties without causing membrane damage, and have been applied for the delivery of cytotoxic cargo to the cytosol, with CPP chemistry having improved over the years.[164] Various internalisation mechanisms of CPP have been reported including direct penetration across the plasma membrane followed by endosomal uptake *via* one or several endocytic pathways. When relatively high concentration of CPP is attached to small molecules such as fluorophores, a direct translocation is also observed.[165] CPP have particular application in cancer treatment due to the tumour microenvironment or other barriers blocking drug delivery to tumour cells, namely solid tumour, brain gliomas or pancreatic cancers. CPP can overcome a semipermeable hydrophobic barrier to promote effective drug delivery to the tissue.[166]

CPPs are commonly short, less than 30 amino acids long, and can be divided into cationic, amphipathic, and hydrophobic peptides.[167] Cationic CPPs are often rich in lysine, histidine, or arginine residues. Arginine residues are more suitable than lysine residues in terms of internalisation,[164] due to arginine's guanidine side chain that is capable of forming hydrogen bonds with phosphate, sulphate and carboxylate moieties. The positive charge of cationic CPPs leads to an excellent affinity with the cytoplasm under physiological conditions. The negatively charged cell membrane glycoprotein combined with the cationic CPPs is internalised into the cell through electrostatic interactions, subsequently, the CPP is internalised.[166] Single amino acid interactions are weak, therefore it was found that sequence of eight arginine residues have the highest membrane penetrating ability.[168]

Amphipathic CPPs are commonly chimeric peptides containing both polar and non-polar amino acid regions, with the non-polar regions mostly comprised of hydrophobic amino acid such as alanine, valine, leucine and isoleucine.[166] These can be further divided into primary amphipathic CPPs, which consist of cationic and hydrophobic sequences; or secondary amphipathic CPPs, which have one sequence ending with a hydrophobic moiety, and the other ending in a cationic, anionic, or polar moiety.[168]

Diverse cargo has been shown to be transported through biological barriers, using CPP including small drug molecules, proteins, and antibodies.[169] There are two main types of vectorisation – one involving covalent attachment to the CPP, and the other through nanoparticle formation with the cargo molecule.[170]

The P21 peptide was isolated by Dixon *et al.,* composed of 21 amino acid residues (KRKKKGKGLGKKRDPSLRK). The P21 peptide was shown to be a heparin-binding epidermal growth factor that has a strong affinity to heparin through that core 21 amino acid chain. The group then engineered an additional 8 arginine residues to the *C*-terminal end which significantly improved cell membrane binding, and, as a result intracellular targeting (P218R - KRKKKGKGLGKKRDPCLRKYKRRRRRRRR).[171] The P218R mutant was successfully used by Wall *et al*., to test a dual conjugation strategy by utilising the internal cysteine residue.[172] Ma and co-workers (Kings College, unpublished data) developed P-C218R, by modifying the original P21 peptide by inserting a cysteine residue at the *N*-terminal, and the aforementioned internal cysteine residue was replaced by serine. The P-C218R peptide was then selected here as a CPP model due to the *N*-terminal cysteine and potential penetrating properties.

In the first attempt at NCL bioconjugation on a thioester bridged Fab, 25 eq. of CPP was selected based on a previous assay (**Figure 20**), where 25 eq. of cysteine was ample to carry out the NCL in 2 h. Here, 25 eq., for 2 h incubation with the CPP was insufficient for complete conversion, as the rebridged Fab conjugate **7** was still present (data not shown). Despite that, the LCMS analysis of this reaction was encouraging as the intermediate conjugate **28** with an unoxidised thiol and peptide attached on HC was observed (**Figure 24**). This initial result indicated that the concept had worked as predicted, but bioconjugation conditions needed further optimisation.

Further adjustments to the protocol were carried out by varying the equivalents of the peptide and incubation time. The optimal conditions to achieve full conversion to conjugate **29** were found with 50 eq. of the P-C218R at 22 °C for 16 h, cleanly affording the reoxidised conjugate (**Figure 24**). The results confirmed functionalisation of the thioester construct is indeed feasible, allowing addition of various highly useful molecules containing an *N*-terminal cysteine.

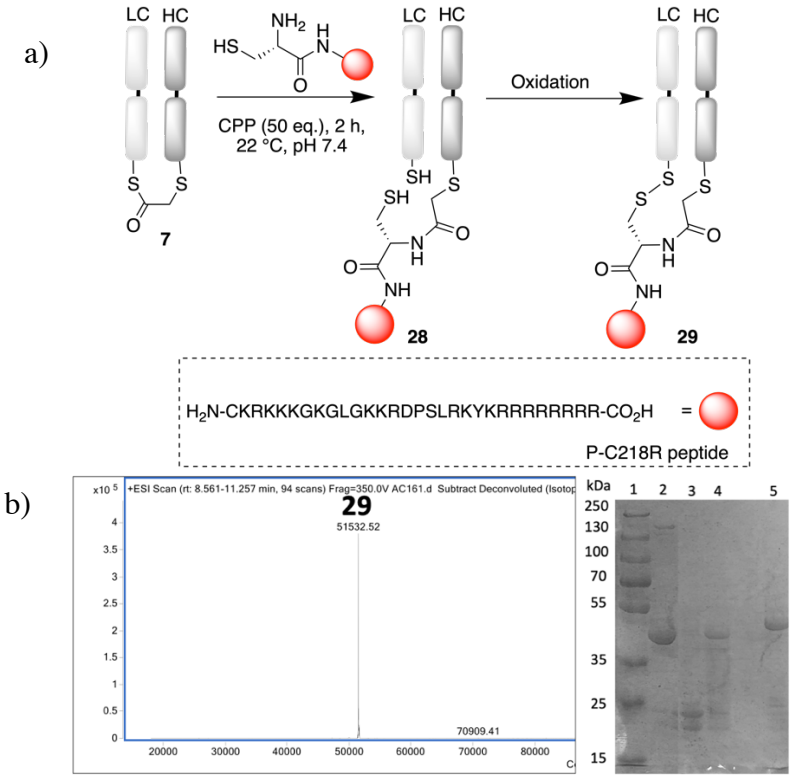

Figure 24. Functionalisation of Fab conjugate **7** with *N*-terminal cysteine peptide P-C218R through NCL, *N*-terminal cysteine reacts with the thioester bond on conjugate **7** forming intermediate construct **28**, followed by spontaneous disulfide oxidation thus forming conjugate **29**, mass expected 51532, mass observed 51532**.** SDS-PAGE 1 – molecular marker, 2 – native Fab, 3 – TCEP reduction, 4 – Fab rebridged with **1**, 5 – addition of P-C218R peptide.

3.2 Native Chemical Ligation on Fab thioester conjugate with P-C218R peptide and dibromomaleimide

An example of further functionalisation of Fab conjugate **7** can be demonstrated by the reaction with P-C218R peptide and a dibromomaleimide-strained alkyne linker (DBM-PEG-BCN). The DBM has been recently used for an antibody – PROTAC conjugate that mimics antibody-drug conjugates.[173]

Optimisation was first carried out to develop the protocol, in place of the P-C218R peptide, a cysteine was used to tailor the conditions. Pleasingly, 4 eq. of DBM-PEG-BCN was sufficient to achieve a full conversion to the desired conjugate (spectra not showed). Further improvements were also implemented for the NCL step by reducing the number of equivalents of the peptide (from 50 eq. to 25 eq.) and extending the incubation time (from 2 h to 16 h). The transthioesterification step was also enhanced by addition of the MPAA catalyst. To facilitate the quantitative hydrolysis of the maleimide component to the desired serum stable maleamic acid, an increase of incubation temperature was also implemented.[173] Lastly, the strained alkyne handle in the novel dibromomaleimide reagent was used for 'click chemistry' *via* copper-free strain-promoted azide-alkyne cycloaddition (SPAAC), which avoids the use of a copper that might induce toxicity to biological systems (**Figure 25**).[103] The Azide fluor 488 was then implemented and the whole conjugate was analysed by UV-Vis and LCMS spectra.

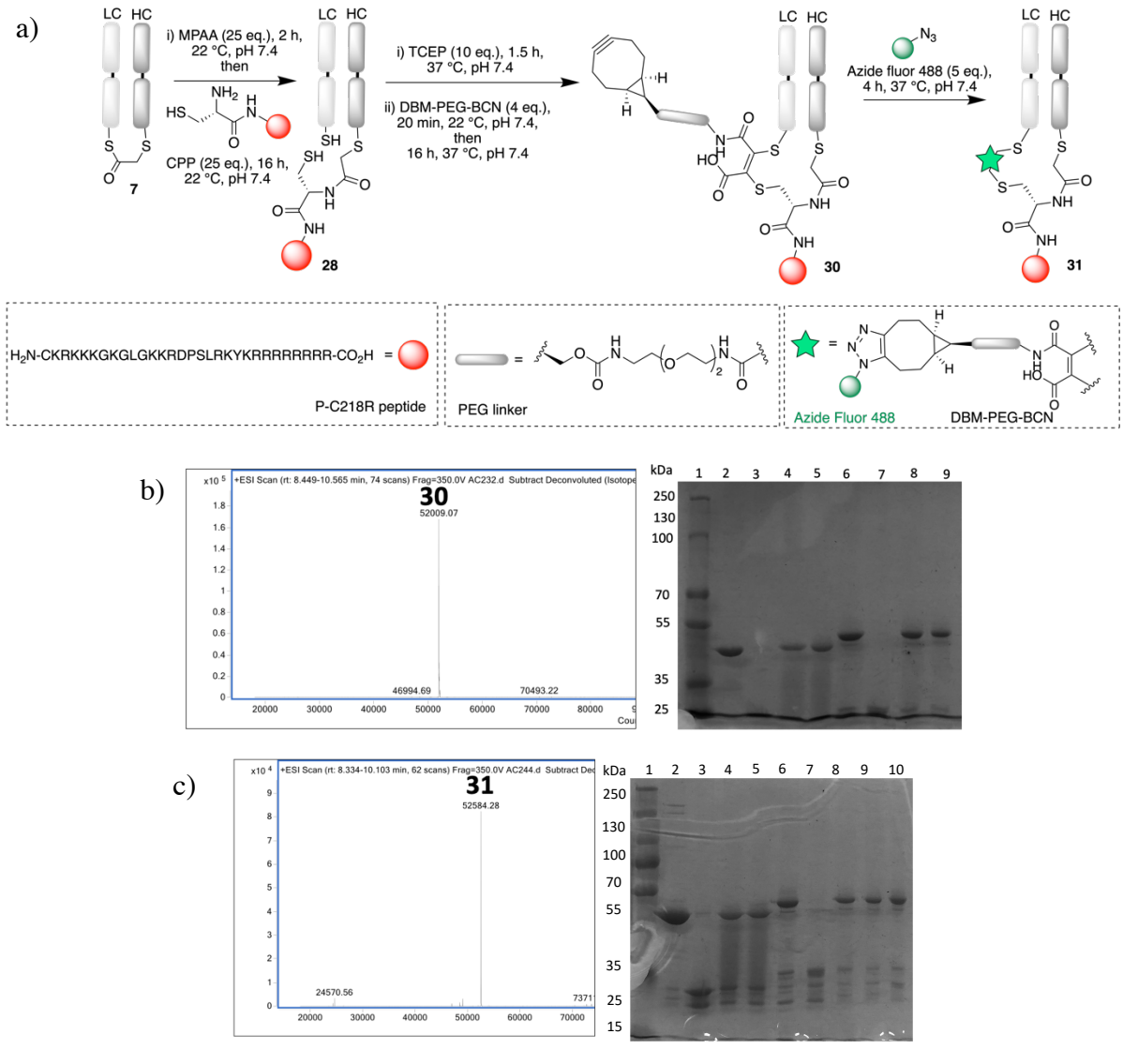

Figure 25. a) A full protocol for functionalisation of Fab conjugate **7** with P-C218R peptide, DBM-PEG-BCN and Azide fluor 488 to form Fab conjugate **31**, b) Deconvoluted ion series mass spectrum, Fab conjugate **30** mass expected 52009, mass observed 52009, SDS-PAGE 1 – molecular marker, 2 – native Fab, 3 – TCEP reduction, 4 – rebridged Fab with **1**, 5 – MPAA addition, 6 – P-C218R addition, 7 – 2nd TCEP reduction, 8 – DBM-PEG-BCN 20 min incubation, 9 - DBM-PEG-BCN 18 h incubation, c) Deconvoluted ion series mass spectrum, Fab conjugate **31** mass expected 52584, mass observed 52584. SDS-PAGE 1 – molecular marker, 2 – native Fab, 3 – TCEP reduction, 4 – rebridged Fab with **1**, 5 – MPAA addition, 6 – P-C218R addition, 7 – 2nd TCEP reduction, 8 – DBM-PEG-BCN 20 min incubation, 9 - DBM-PEG-BCN 18 h incubation, 10 – Azide fluor 488 addition.

The fluorophore-to-antibody ratio (FAR) was determined photometrically by obtaining the UV/Vis absorption reading of the conjugate **31** and using the following formula, where *Cf* is the correction factor for the absorbance of the Azide fluor 488 at 280 nm:

$$FAR = \frac{\frac{Abs_{505}}{\varepsilon_{505}}}{\frac{Abs_{280} - (Cf\ x\ Abs_{505})}{\varepsilon_{280}}} = \frac{\frac{0.479}{74000}}{\frac{0.714 - (0.11\ x\ 0.479)}{68590}} = 0.7$$

The FAR value of 0.7 was obtained, being close the loading calculated from the LCMS spectrum. The SDS-PAGE also confirms presence of a band within the expected mass area, >50 kDa (**Figure 25**). The SDS-PAGE also shows bands in the light and heavy chain area, notably these account for less than 10% in density when compared to the band corresponding to the conjugate **31**, and the species in the SDS-PAGE are not present in the LCMS spectra.

The functionalisation of the NCL platform comprising of conjugate **7** and an *N*-terminal cysteine containing peptide, could allow for the selective delivery of potent molecules. In this example, the strained alkyne permits for additional attachment of cargo *via* convenient SPAAC click chemistry. Further work on this peptide was not possible due to limited availability of the P-C218R, therefore a different CPP was investigated.

3.3 Cell Penetrating Peptide – TAT

A second cell penetrating peptide was employed in this work. A protein called the Trans-Activator of Transcription (TAT) has been identified to have the ability to enter and leave cells by a process called transduction. TAT is classified as a viral regulatory protein that was isolated from Human Immunodeficiency Virus 1 (HIV-1), which efficiently enters tissue-cultured cells and promote viral gene expression.[164] TAT binds to the viral nascent 5' leader RNA hairpin transactivation response element. The key domain of TAT peptide has been found between 49-

57 residues (RKKRRQRRR) of the entire protein. The sequence contains a nuclear localisation signal which is involved in the binding of TAR RNA. *In vitro* studies with the TAT peptide showed quick cell internalisation to all tissues in mice, including brain. Furthermore, six amino acids were added at the *N*-terminal end (CGISYGRKKRRQRRR) to facilitate chemical modification. TAT is a cationic peptide, rich in lysine, histidine, and arginine residues.[174] The TAT peptide has previously been used with anti-ED-B antibody fragment scFv(L19) to test whether the peptide would improve the crossing of endothelial barriers and thus increase tumour uptake, the results were reported to be positive in this aspect.[175] One of the major obstacles in successful ADC therapeutics is crossing the cell membrane and/or the endosomal membrane upon receptor mediated internalisation.[176] The TAT peptide could potentially bring benefits to the ADCs as it would improve antibody penetrations to cells and to efficiently reach the cytosol. Such a study is beyond the scope of this project, but the TAT peptide is thus of interest and will be employed in following bioconjugation studies.

The previously developed protocol for the first CPP - P-C218R was used as a starting point for this peptide conjugation, with further improvements namely increasing the temperature of the NCL step and removal of the MPAA catalyst. Preliminary data on this peptide suggested that MPAA did not improve the initial transthioesterification between this peptide and the thioester, though elevating the temperature for the overnight incubation step with the peptide increased the conversion to the desired conjugate.

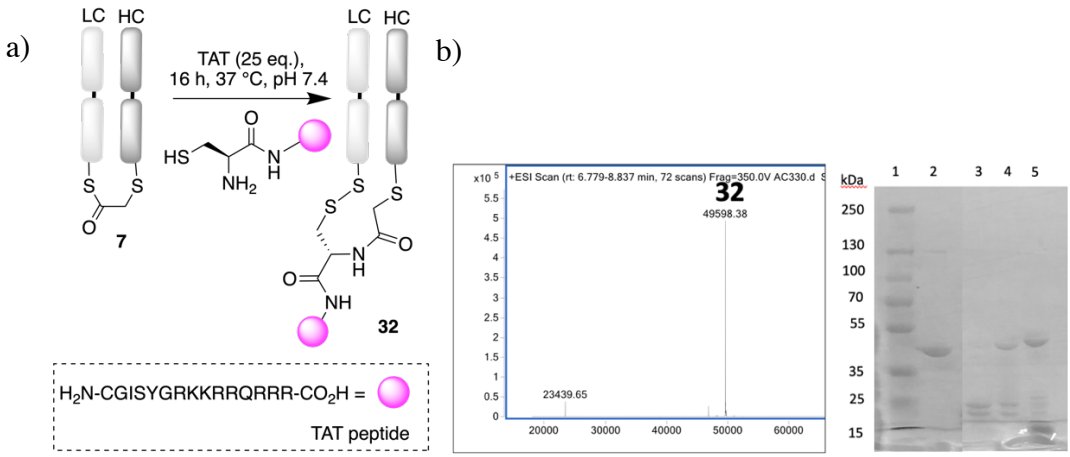

Figure 26. a) A full protocol for functionalisation of Fab conjugate **7** with TAT peptide, b) Deconvoluted ion series mass spectrum, Fab conjugate **32** mass expected 49600, mass observed 49598. SDS-PAGE 1 – molecular marker, 2 – native Fab, 3 – TCEP reduction, 4 – rebridged Fab with **1**, 5 – TAT addition.

The LCMS spectrum showed correct functionalisation of Fab conjugate **7** and the TAT peptide thus forming a new conjugate **32**. There is a small peak corresponding to the native light chain (observed mass 23439), however, its intensity is not indicative of amount as any light chain ionises well under MS conditions and is thus overrepresented in intensity (**Figure 26**).

3.4 Native Chemical Ligation on Fab thioester conjugate with TAT peptide and pyridazinedione

The TAT peptide worked well in the proposed NCL system, forming a new amide bond, and freeing up two thiols, one on the Fab chain and second from the *N*-terminal cysteine of the peptide. This allows for a second point of attachment, therefore in this experiment a diethyl dibromo pyridazinedione (PD-diEt)[118] compound was selected to first develop the protocol.

Recently, the pyridazinedione (PD) moiety has been extensively studied by our groups[103,177,178] and it was shown to have some advantages over alternative rebridging reagents. PD reagents are more serum stable for several days, as these do not react with high concentration of diverse thiol containing proteins such as human serum albumin (HSA) and glutathione (GSH). PDs were shown to be cleavable only under high concentrations of reactive thiols, for example 2-mercaptoethanol (BME). Lastly, the PD scaffold can incorporate two functional handles for use in bioorthogonal dual click reactions.[103]

a)

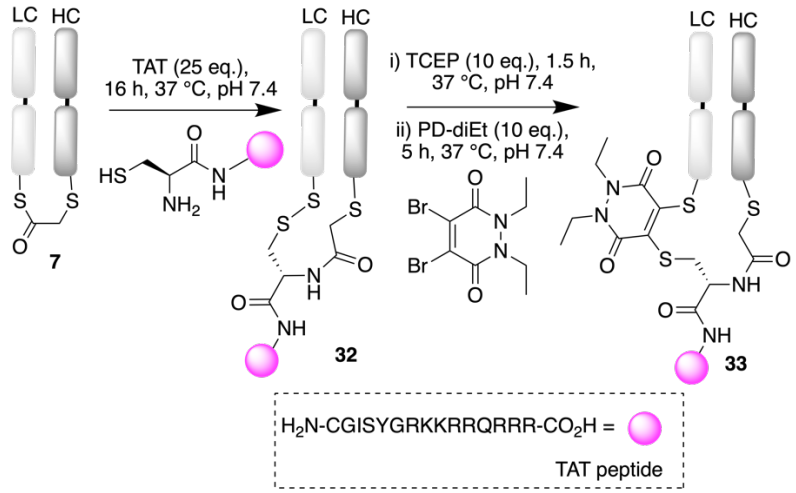

b)

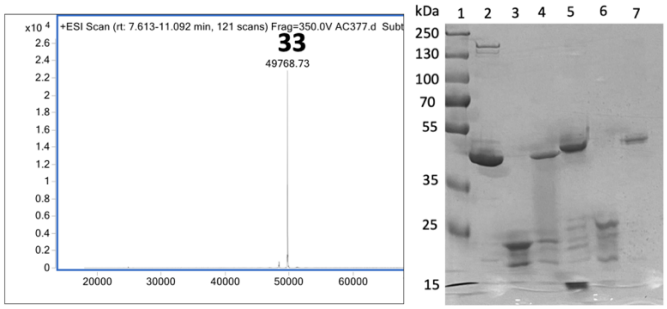

Figure 27. a) Further functionalisation of Fab conjugate **7** with TAT peptide and PD-diEt to form Fab conjugate **33**, b) Deconvoluted ion series mass spectrum, Fab conjugate **33** mass expected 49766, mass observed 49768. SDS-PAGE 1 – molecular marker, 2 – native Fab, 3 – TCEP reduction, 4 – rebridged Fab with **1**, 5 – TAT addition, 6 – 2nd TCEP reduction, 7 – PD-diEt addition.

The Fab TAT-PD-diEt conjugate **33** was successfully formed with PD-DiEt, with SDS-PAGE and LCMS showing correct reduction and consequent rebridging steps (**Figure 27**). Therefore, the use of functionalised strained alkyne PD-PEG-BCN[103] was proposed next, which is capable of SPAAC by attaching Azide fluor 488.

A stepwise protocol was employed here, where after NCL step with the TAT peptide, a PD-PEG-BCN was first added, and this resulted in a single species corresponding to the desired conjugate **34**. The conjugate **34** was then further functionalised with a fluorophore through copper-free click, following analysis on LCMS and SDS-PAGE (**Figure 28**).

a)

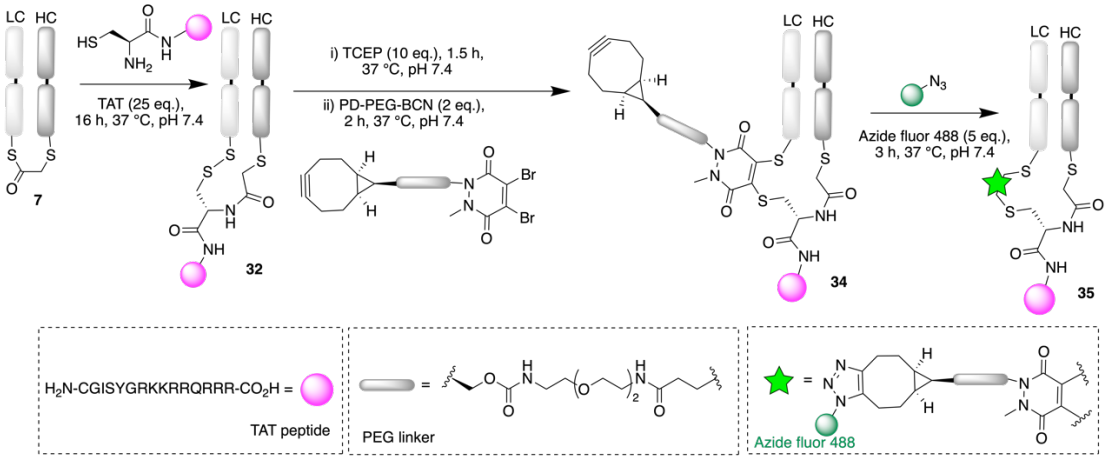

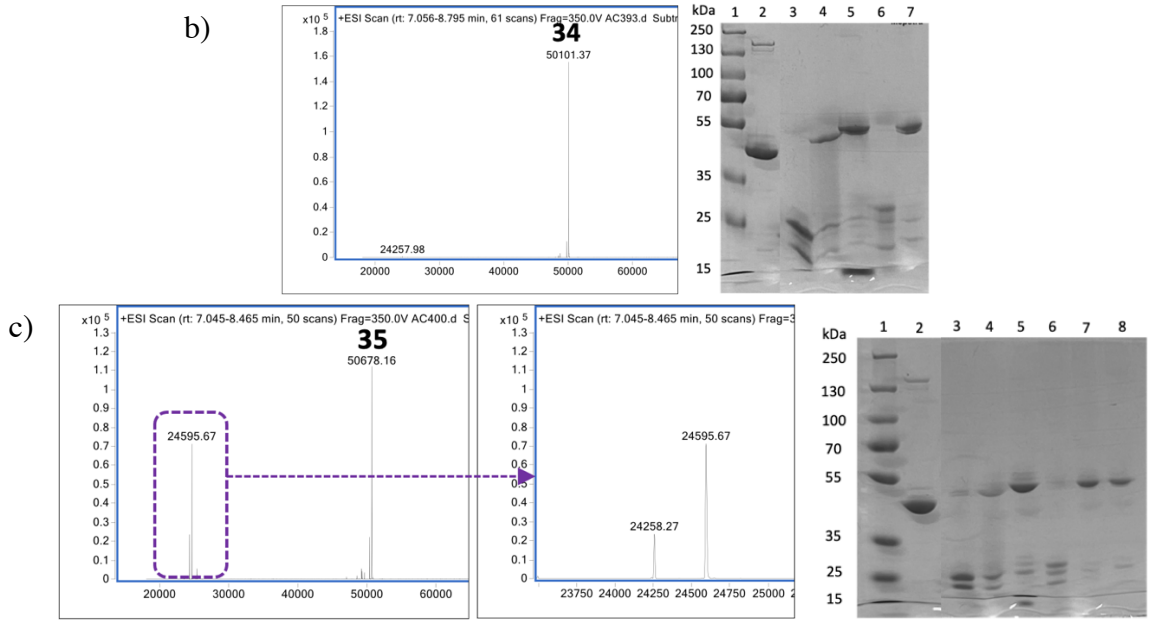

Figure 28. a) A protocol for formation of conjugate **35** by addition of TAT peptide, PD-PEG-BCN and Azide fluor 488, b) Deconvoluted ion series mass spectrum, Fab conjugate **34** expected 50102, observed 50101. SDS-PAGE 1 – molecular marker, 2 – native Fab, 3 – TCEP reduction, 4 – rebridged Fab with **1**, 5 – TAT addition, 6 – 2nd TCEP reduction, 7 – PD-PEG-BCN addition, c) Deconvoluted ion series mass spectrum, Fab conjugate **35** mass expected 50677, mass observed 50678, LC with PD(Br)-PEG-BCN and Azide fluor 488 mass expected 24594, mass observed 24596, HC hydrolysed bridged species mass expected 24259, mass observed 24257. SDS-PAGE 1 – molecular marker, 2 – native Fab, 3 – TCEP reduction, 4 – rebridged Fab with **1**, 5 – TAT addition, 6 – 2nd TCEP reduction, 7 – PD-PEG-BCN addition, 8 – Azide fluor 488 addition.

$$FAR\ of\ Abs_{505} = \frac{\frac{Abs_{505}}{\varepsilon_{505}}}{\frac{Abs_{280} - (Cf\ x\ Abs_{505})}{\varepsilon_{280}}} = \frac{\frac{1.55}{74000}}{\frac{1.83 - (0.11\ x\ 1.55)}{68590}} = 0.9$$

Overall, the strategy for the new non-native disulfide bond rebridged with PD reagent and then clicked with Azide fluor 488 to afford a fluorescently labelled antibody-peptide dual conjugate **35** worked very well. UV/Vis absorbance resulted in FAR of 0.9, thus providing further evidence of conjugation efficiency supported by the LCMS and SDS-PAGE data (**Figure 28**).

The light and heavy chain area on the LCMS spectrum shows additional peaks negligible (**Figure 28**, c), these can be attributed to light chain containing PD(Br)-PEG-BCN and a fluorophore attached. Additionally, heavy chain can be seen with some hydrolysed α-chlorothioester bridge **11** (HC) species. Upon analysing the SDS-PAGE *via* densitometry software, it shows that the rebridged Fab band accounts for more than 90%, therefore LC and HC bands density are negligible.

3.5 Native Chemical Ligation on Fab thioester conjugate with TAT peptide and dibromomaleimide

The work achieved with the DBM-PEG-BCN and the P-C218R peptide was then translated on to the TAT peptide with the utilisation of the protocols developed for the PD reagent. First the conjugate **36** was generated by reacting the DBM reagent with the two available thiols from the conjugate **32**. Upon achieving a stable conjugate formation *via* hydrolysis to the serum-stable maleamic acid, further functionalisation with the fluorophore was carried out.

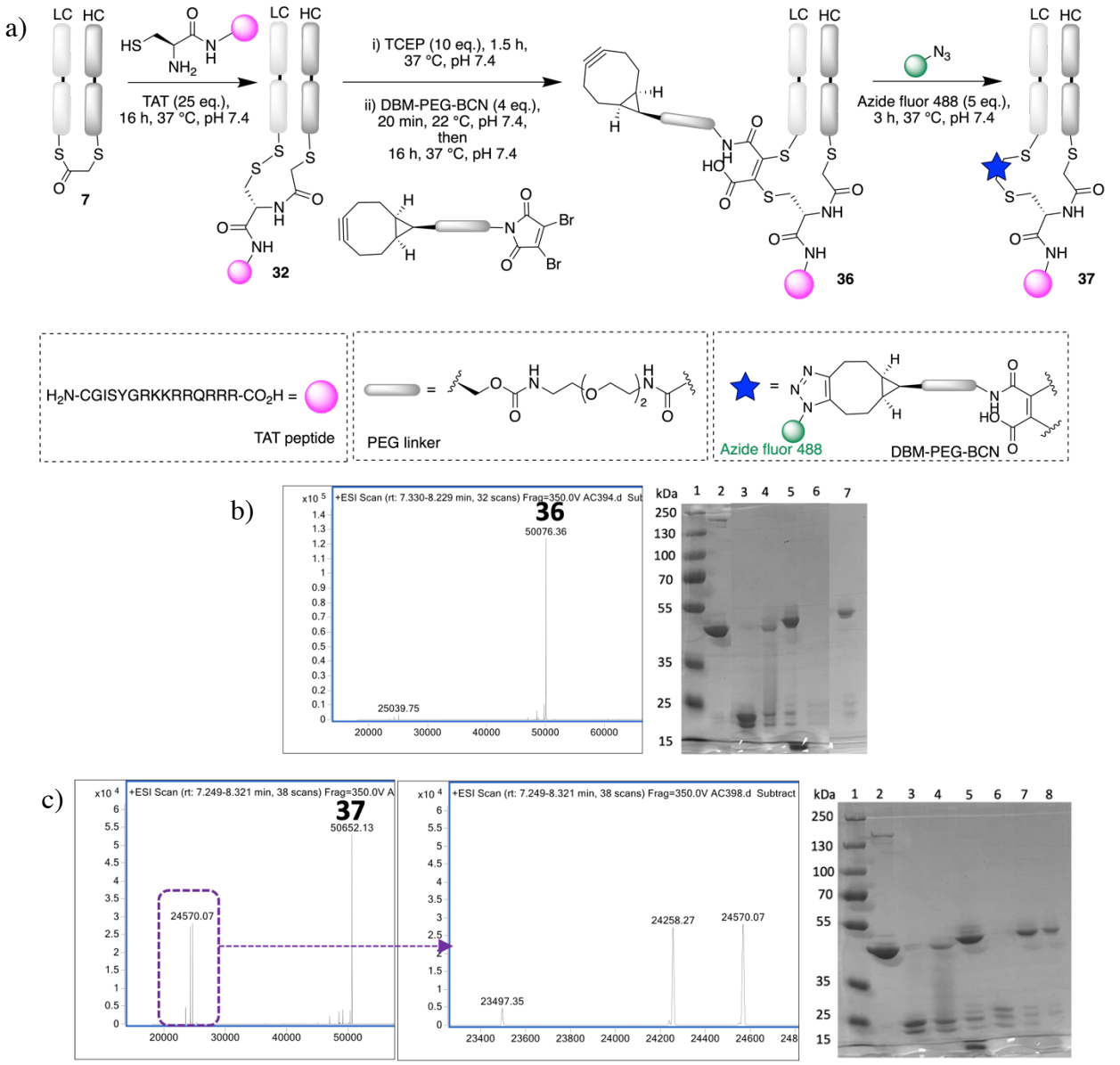

Figure 29. a) A protocol for formation of conjugate **37** by addition of TAT peptide, DBM-PEG-BCN and Azide fluor 488, b) Deconvoluted ion series mass spectrum, Fab conjugate **36** expected 50077, observed 50076. SDS-PAGE 1 – molecular marker, 2 – native Fab, 3 – TCEP reduction, 4 – rebridged Fab with **1**, 5 – TAT addition, 6 – 2nd TCEP reduction, 7 – DBM-PEG-

BCN 16 h addition, c) Deconvoluted ion series mass spectrum, Fab conjugate **37** mass expected 50652, mass observed 50652, LC with DBM(Br)-PEG-BCN and Azide fluor 488 mass expected 24569, mass observed 24570, HC hydrolysed bridging species mass expected 24259, mass observed 24258, LC hydrolysed bridging species mass expected 23497, mass observed 23497. SDS-PAGE 1 – molecular marker, 2 – native Fab, 3 – TCEP reduction, 4 – rebridged Fab with **1**, 5 – TAT addition, 6 – 2nd TCEP reduction, 7 – DBM-PEG-BCN addition, 8 – Azide fluor 488 addition.

$$FAR = \frac{\frac{Abs_{505}}{\varepsilon_{505}}}{\frac{Abs_{280} - (Cf\ x\ Abs_{505})}{\varepsilon_{280}}} = \frac{\frac{0.96}{74000}}{\frac{1.59 - (0.11\ x\ 0.96)}{68590}} = 0.6$$

The expected intermediate conjugate **36** and fully functionalised conjugate **37** was observed as per LCMS and SDS-PAGE analysis with FAR of 0.6 (**Figure 29**). Similarly as with the PD reagent, undesirable additions are being formed in the light and heavy chain area, which are not identified on the SDS-PAGE. Both light and heavy chain can be observed with the hydrolysed bridged species **12**-LC and **11**-HC, respectively (**Figure 29**, c). There is also peak corresponding to the DBM with single bromine and a fluorophore attached (observed mass 24570), species like that was also observed when using PD reagent. Based on the densitometry calculations of SDS-PAGE bands, the abundance of these is very low (less than 10%).

3.6 Stability assays

3.6.1 ELISA

Enzyme-linked immunosorbent assay (ELISA) was carried out on the native Fab and Fab conjugate **33,** containing a rebridging component conjugated to cysteine and PD-diEt to test affinity towards HER2 antigen. A 96-well polystyrene plate was coated first with HER2 antigen. Following that, native Fab and Fab conjugate were applied to it. Upon completing the incubation time with a secondary antibody linked to HRP, *o*-phenylenediamine HCl was added to quench the reaction. This was converted to 2,3-diaminophenazine by the enzyme HRP, which shows strong absorbance at 490 nm, allowing for spectrophotometric quantification of the antigen-binding activity of the Fab conjugate **33** and native Fab.

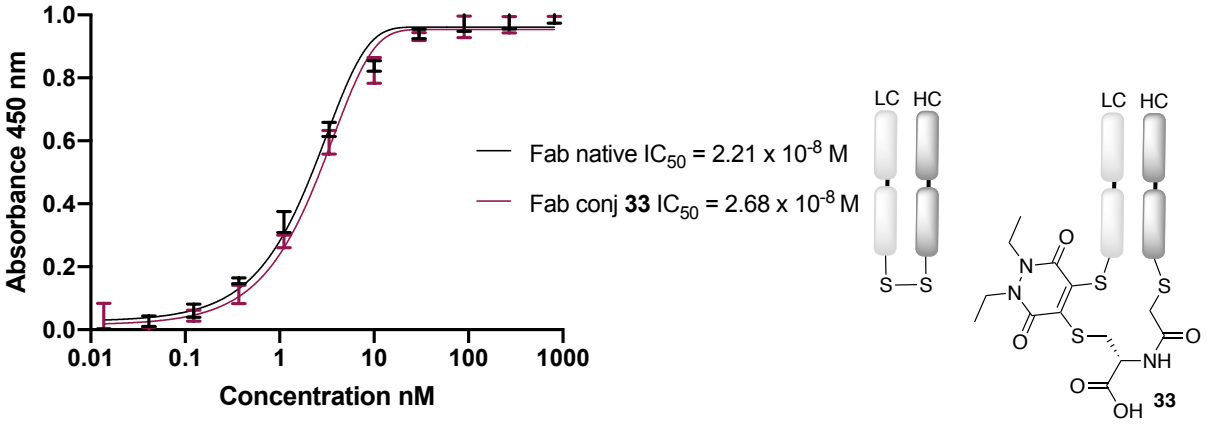

Figure 30. Binding activity to HER2 of trastuzumab native Fab and Fab conjugate **33** over concentration ranges from 810-0.0137 nM, absorbance was measured at 450 nm.

The Fab conjugate **33** showed comparable antigen binding activity to the native Fab (**Figure 30**). Previous reports exploring bridging of IgG1 interchain disulfide residues showed little to no impact on antigen binding, which is in line with findings in this study.[179,180]

3.6.2 Thermal Shift Assay

The stability of antibodies is governed by several factors such as disulfide bonds between two chains, non-covalent interaction between C_H2 and C_H3 domains, protein-protein interactions, and interactions between glycans located in the C_H2 domain of each heavy chain. In the Fab fragment, apart from interchain disulfide bond, non-covalent interactions help stabilise the structure namely ionic forces, hydrogen bonds, and van der Waal forces.[181]

The Thermal Shift Assay also known as Differential Scanning Fluorimetry is a key technique for assessing a stability of proteins or biophysical ligand screening. The methods use a dye, SYPRO Orange, that is quenched in an aqueous environment but becomes strongly fluorescent when bound to exposed hydrophobic regions of a protein. The hydrophobic groups may be exposed by heating of the protein mixture, leading to protein denaturation, therefore the thermal unfolding transition can be monitored spectrophotometrically leading to a shift in the midpoint of the unfolding transition i.e., the melting temperature (T_m).[182] Most commonly used environmental dyes have excitation/emission wavelengths outside of the range of widely available real-time PCR instruments (qPCR) that are equipped with fluorescence detection capabilities, whereases SYPRO Orange has fluorescence properties (λ_{ex} 470 nm/λ_{em} 570 nm) which is compatible with filters inside the qPCR instruments.[183]

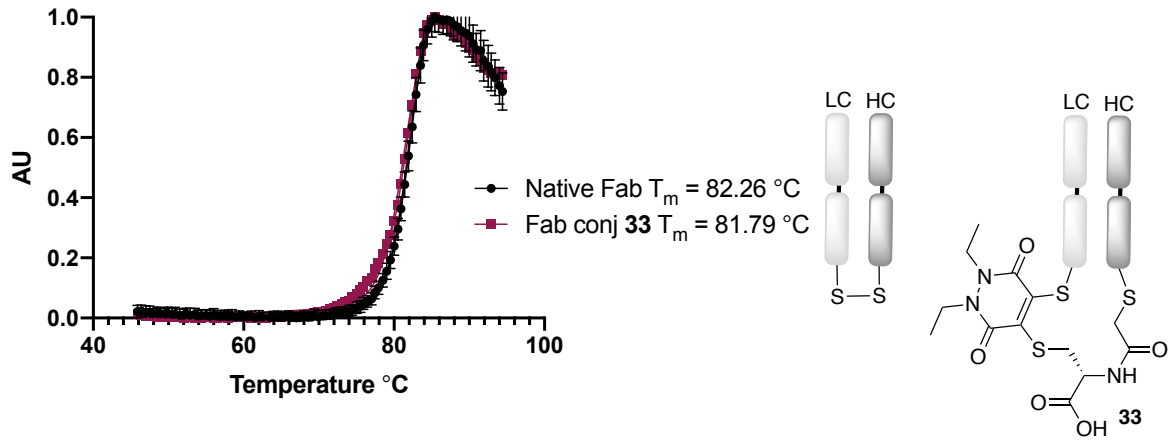

Figure 31. Thermal unfolding of native Fab and Fab conjugate **33** was monitored using SYPRO Orange. Data was collected in presence of 4 μM Fab concentration pH 7.4.

In a comparative experiment, melting temperatures (T_m) were calculated for native Fab and Fab conjugate **33** by conducting a thermal shift assay. An unfolding transition often described as a rightward shift[182] was observed in the intact and rebridged interchain covalent links resulting in minimal change to the melting temperatures for native Fab T_m = 82.26 °C and Fab conjugate **33** T_m = 81.79 °C (**Figure 31**). In the literature, there are reports of intact Trastuzumab antibody at pH 7.4 T_m = 85.3 °C, and Trastuzumab Fab fragment T_m = 82.4 °C,[13] which is in line with findings obtained here.

Interestingly, temperature-induced unfolding studies done on human IgG1 on its Fab and Fc fragment showed that there are two transitions states with the melting temperatures. The study reported T_m of 70 °C for Fab fragment at pH 5.5, and T_m of 66 °C and 82 °C for the Fc fragment, suggesting that the first unfolding event of the intact IgG is associated with melting of the C_H1 domain on the Fab fragment and C_H2 domain in the Fc fragment, whilst the second transition state represents mainly unfolding of the C_H3 domain.[184,185]

3.7 Summary and conclusion

In this strategy two liberated cysteine residues on the antibody fragment were reacted with a thioester containing molecule. Since α-chlorothioester **1** demonstrated excellent reactivity, stability and regioselectivity towards Fab fragment in Chapter 1, it was selected for further work as a model thioester for development of NCL strategy.

The initial NCL results on the Fab conjugate **7** with cysteine has shown the promising indication of the potential of *N*-terminal cysteine when reacted with thioester bridge on the Fab fragment. This idea was further explored in this section with Cell Penetrating Peptide containing *N*-terminal cysteine residue. Two peptides were studied, one 30 aa long (P-C218R) and one 15 aa long (TAT peptide) that allowed for unique peptide ligation. The *N*-terminal cysteine allows for implementation of the NCL method where the thiol of the cysteine peptide reacts with the thioester moiety on the Fab fragment through transthioesterification. This results in a thioester intermediate, which then is rearranged *via* a five-membered ring triggered by an intramolecular nucleophilic attack by a nearby amino group side chain within the *N*-terminal cysteine, resulting in a formation of an amide bond at the ligation site. The CPP brings its own functionality in the form of unlocking a pathway to penetrate solid tumours, as penetration is often challenging for monoclonal antibodies and ADCs. Nearly all of the existing therapeutic antibodies target cell-surface antigens which are overexpressed in malignant cells. Targeting intracellular antigens with functional and native antibodies is therefore difficult, hence CPP covalently attached to antibody could deliver the protein inside the cell and lead to on-demand release of the cargo.
Subsequent functionalisation with reagents such as NGMs (e.g., DBM-PEG-BCN with strained alkyne), or the more stable PDs such as PD-PEG-BCN, also containing strained alkyne allowing for SPAAC copper free click chemistry with fluorophore demonstrated effective and efficient protocol for dual modification. Smaller and more accessible linker payload as tested in this study (PDs and NGMs) allow for further addition of payloads, due to their unique handles, such as toxins and PEGs, the latter of which could improve solubility of the cargo, extend the half-life, and potentially reduce aggregation of the attachment.[67] The benefit of this technique is that any payload with thiol reactive handles can be added to the antibody, without the limiting step of first chemical synthesis of the whole linker-payload conjugate, which is often challenging to isolate and purify. Thermal stability and HER2 affinity biophysical assays showed that natively rebridging of the disulfide residues had no impact on the biophysical profile of the Fab fragment with key CDRs functions fully retained.

It is envisaged that this work will stimulate further efforts to appraise the secondary modification step of this approach, resulting in novel ADCs modified by disulfide rebridging and subsequent NCL. Other prospects of antibody peptide conjugate could also be explored, where the antibody target is found inside the cell allowing for intracellular delivery.

Chapter 4: Dual conjugation of thioesters with primary amine on Fab fragment

Rebridged Fab with α-chlorothioester **1** introduced a thioester functional group, which enables Fab functionalisation by addition of nucleophile as it was demonstrated in Chapter 3. The aim of this experiment was to screen several alternative nucleophiles that would react with thioester present on the rebridged Fab to facilitate further modification, whilst also freeing a thiol on the other chain leading to dual functionalisation (**Scheme 29**). The retention of the covalent bond between the two Fab chains is likely to afford extra stability, however there is no strong evidence that is essential for the various applications such as in development of antibody conjugates *via* cysteine modification, as the chains are still held together by intermolecular forces.[13]

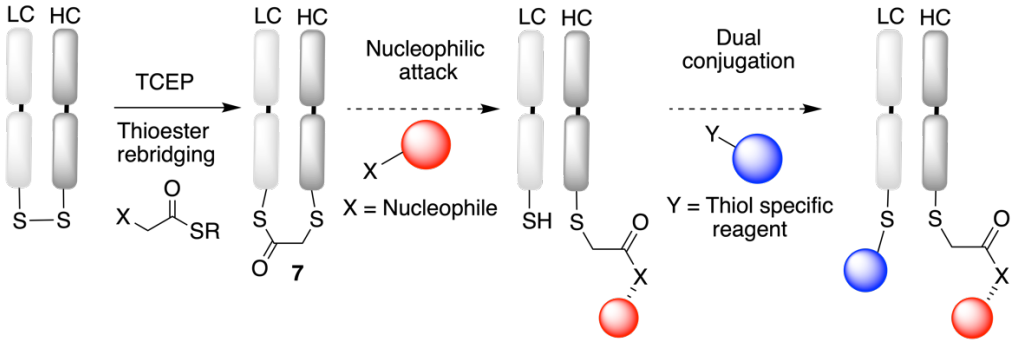

Scheme 29. Proposed strategy of disulfide rebridging with a two-carbon molecule containing a thioester, followed by nucleophilic attack leading to secondary ligation on the other chain.

4.1.1 Reaction of Fab thioester conjugate with amine nucleophiles

The selected nucleophiles should be primary or secondary amines that would react with a thioester by an intermolecular *S*-to-*N* acyl transfer to form an amide bond. The tested nucleophiles were selected based on their accessibility, nucleophilicity[132,186] and potential functionality. All the reactions with selected amines from **Table 2** were carried out at near physiological pH (pH 7.4), with 1000 eq. of the nucleophile. Reactions were incubated at 37 °C for up to 4 h and monitored by LCMS. Three examples from this study were selected to illustrate the results.

Table 2. Selected nucleophiles for reaction with thioester.

Name	Structure	Name	Structure
Aniline	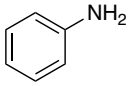	Hydroxylamine	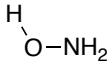
Propargylamine	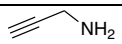	Hydrazine	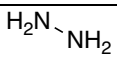
Benzylamine	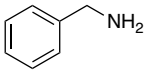	1,1-dimethylhydrazine	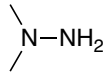
Piperidine	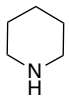	Methylhydrazine	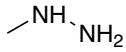
p-Anisidine	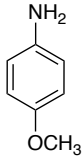	Benzhydrazide	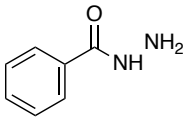

4.1.2 Hydrazine hydrate

The LCMS for the reaction with hydrazine hydrate resulted in proposed conjugate **38** (**Figure 32**), showing heavy chain with one addition of hydrazine attached to the rebridged species thus resulting in hydrazide moiety **38**-HC. This shows that hydrazine had successfully reacted with the rebridged thioester to form a hydrazide bond, present mostly on the HC. Large peak of unmodified light chain **38**-LC is expected as upon breaking the thioester bond the thiol on the LC would be liberated and potentially ready for second modification. The ~10% of unmodified heavy chain is due to regioisomer formation. The rebridged Fab **7** peak is not observed, confirming correct conversion.

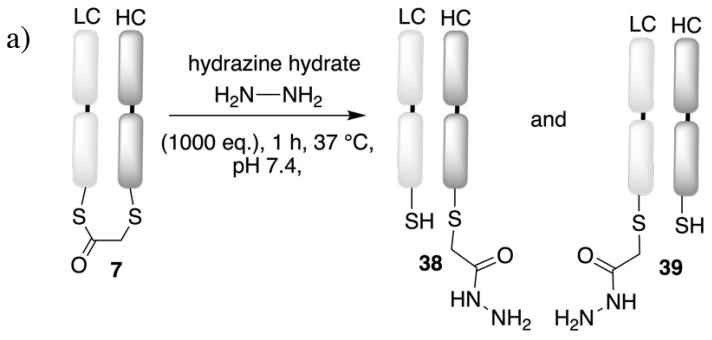

b)

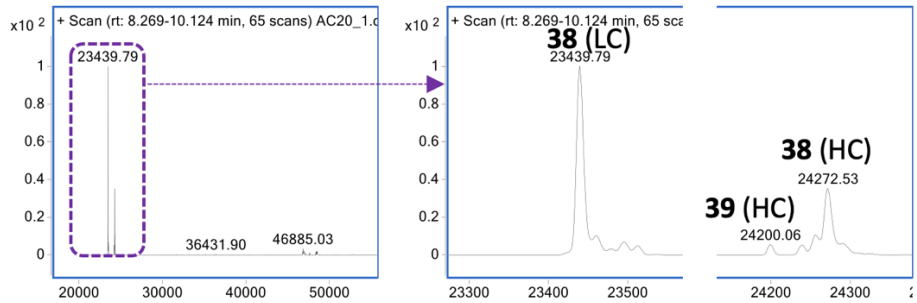

Figure 32. a) Formation of hydrazide conjugate **38** and **39**, b) LCMS analysis of Fab conjugate **7** reacted with hydrazine hydrate. Deconvoluted ion series mass spectrum; **38** (LC) mass expected 23438, mass observed 23439, **39** (HC) mass expected 24200, mass observed 24200, **38** (HC) mass expected 24272, mass observed 24272.

The advantages of using hydrazine include being bifunctional, as hydrazine have two reactive centres which are useful functionality for addition of other molecules, hydrazine reactivity is also enhanced by the α-effect. Additionally, hydrazine can be used for reaction with ketones or aldehydes to form hydrazones. Hydrazones can be designed to be hydrolytically unstable consequently lead to resulting bond being cleavable which are useful in bioconjugation.[187]

4.1.3 Propargylamine

Propargylamine was selected based on potential future uses of the alkyne handle with an azide through copper click chemistry. However, propargylamine showed no reactivity even at 1000 eq., and constructs **40** or **41** were not identified as proposed in **Figure 33**. Instead, the LCMS shows unmodified light and heavy chains. This is because of outcompeting hydrolysis of each of the corresponding chains caused release of the bridging molecule. The LCMS spectra is comparable to the one from conjugate **7** stability study (see section **2.5**). Additionally, some of the rebridged Fab conjugate **7** is still observed (expected 47680, observed 47680).

a)

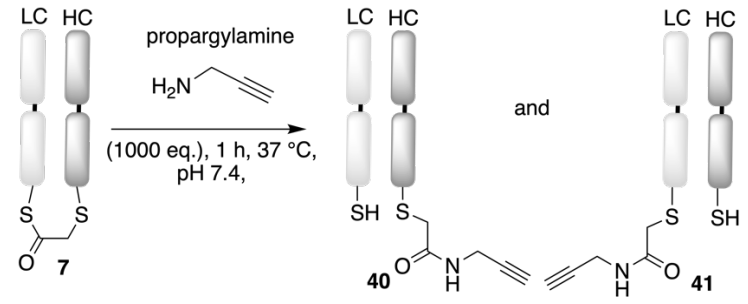

b)

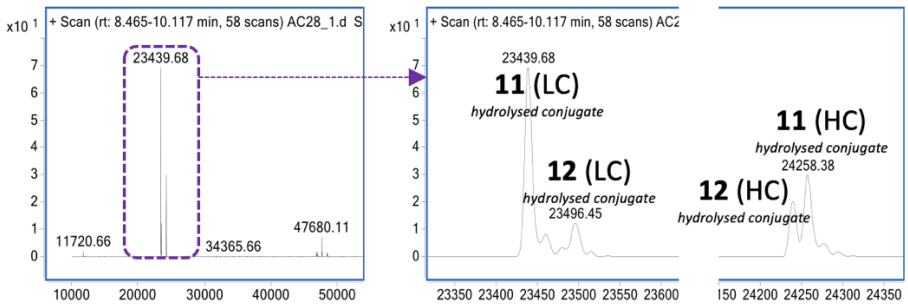

Figure 33. a) Formation of propargylamine conjugate **40** and **41**, b) LCMS analysis of Fab conjugate **7** reacted with propargylamine. Deconvoluted ion series mass spectrum; **40** (HC) mass expected 24296, mass not observed, **41** (LC) mass expected 23534, mass not observed, **11** (LC) mass expected 23438, mass observed 23439, **12** (LC) mass expected 23497, mass observed 23496, **12** (HC) mass expected 24200, mass observed 24200, **11** (HC) mass expected 24259, mass observed 24258.

As this reaction was carried out with 1000 eq. of a reagent with no indication of any conjugation, therefore any condition improvements would unlikely change the outcome of this reaction, thus propargylamine was deemed unsuitable as a modification reagent.

4.1.4 Hydroxylamine

The LCMS analysis of a reaction with hydroxylamine and thioester moiety showed a small modification forming desired conjugate **42**-HC when 1000 eq. was used as shown in **Figure 34**. However, hydrolysis was observed in both light and heavy chain with their corresponding native chains also present, no rebridged Fab was observed. In this study, hydroxylamine appeared to be a poorer nucleophile than hydrazine, meaning hydrolysis outcompetes thioester substitution, therefore this reagent was also not suitable for the dual conjugation protocol.

a)

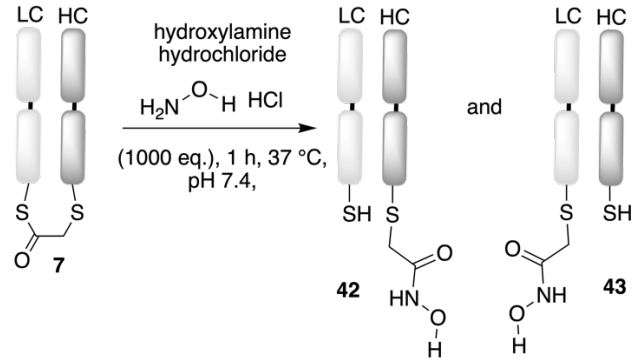

b)

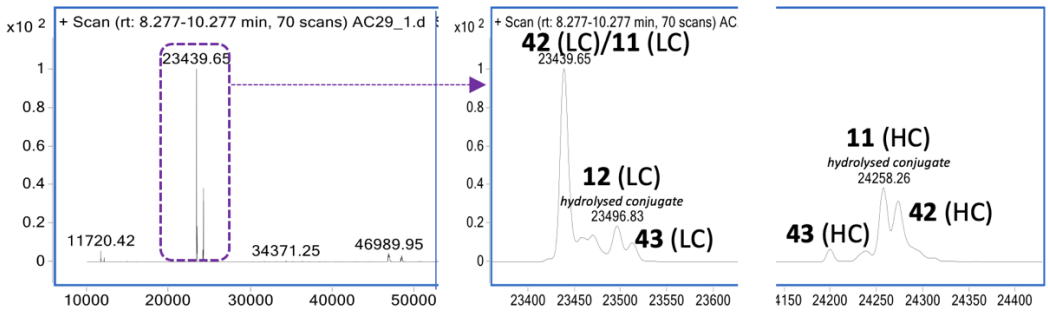

Figure 34. a) Formation of hydroxylamine hydrochloride conjugates **42** and **43**, b) LCMS analysis of Fab conjugate **7** reacted with hydroxylamine. Deconvoluted ion series mass spectrum; **42** (LC) mass expected 23438, mass observed 23439, **12** (LC) mass expected 23496, mass observed 23496, **43** (LC) mass expected 23510, mass observed 23513, **43** (HC) mass expected 24200, mass observed 24200, **11** (HC) mass expected 24259, mass observed 24258, **42** (HC) mass expected 24272, mass observed 24274.

Various other amine nucleophiles from **Table 2** were tested i.e., aniline, pyrrolidine, benzylamine, piperidine, p-anisidine, and benzhydrazide. However, all showed no reactivity and hydrolysis of the rebridged compound.

The aim of this assay was to identify a good nucleophile that would break the thioester bond thus freeing a thiol on the other chain, hydrazine was found to work efficiently for this purpose. The free thiol on the other chain can then be reacted either with thiol specific reagent such as maleimide or a disulfide containing reagent that would undergo thiol-disulfide exchange, whereas the hydrazide moiety can be further functionalised with ketone or aldehyde.

4.2 Dual conjugation with hydrazine and disulfide containing reagent

To explore the idea of dual functionalisation of the rebridged Fab conjugate **7** with hydrazine and disulfide containing reagent, Fab was rebridged with α-chlorothioester **1**, then a large excess of the hydrazine hydrate was added followed by MPAA-disulfide (**Figure 35**).

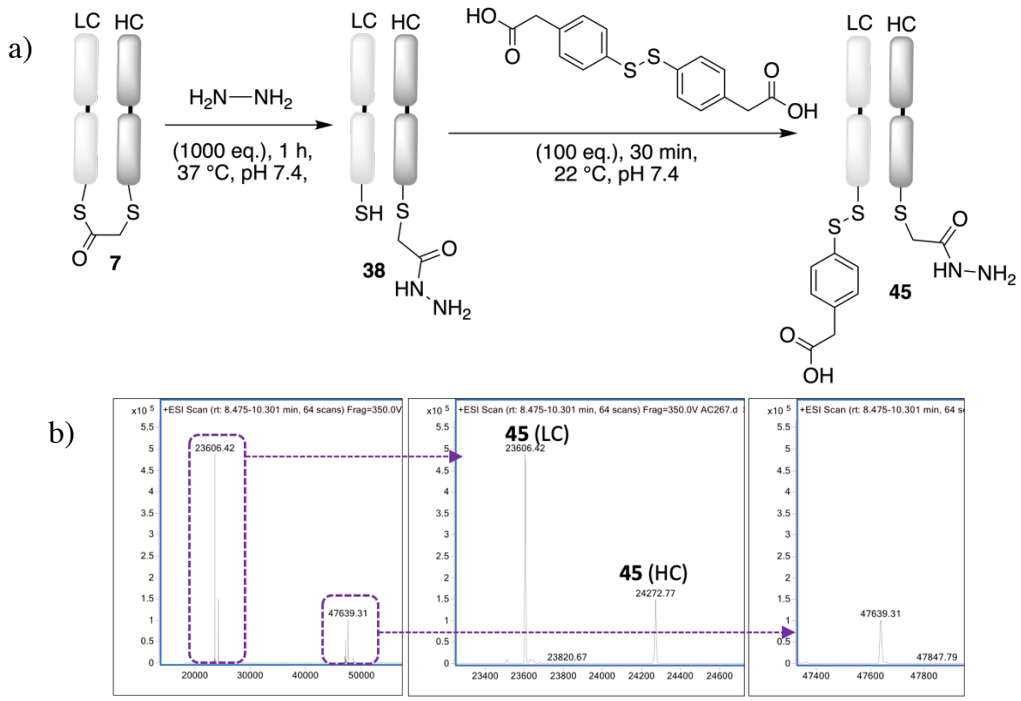

Figure 35. a) Development of the dual conjugation protocol with hydrazine and MPAA disulfide, b) LCMS analysis of Fab conjugate **7** reacted with hydrazine and MPAA disulfide. Deconvoluted ion series mass spectrum; **45** (LC) mass expected 23605, mass observed 23606, **45** (HC) mass expected 24272, mass observed 24272, native Fab mass observed 47639.

Upon analysis of the LCMS spectra, it was observed that the expected species have formed. There was no native LC or HC identified. The amine moiety from the hydrazine attacked the thioester on the Fab fragment thus formed a new hydrazide bond, **45**-HC. The LC peak shows addition of +167 Da corresponding to the disulfide formation between the LC thiol and the MPAA-disulfide, forming **45**-LC (**Figure 35**). In the Fab area, no rebridged Fab conjugate **7** peak was found, however native Fab reformation was observed. Based on the previous experiments, no native Fab was observed when using 1.5 eq. of the α-chlorothioester **1** with 1000 eq. of hydrazine hydrate, suggesting that the Fab reformation must have occurred during the experiment, potentially the second regioisomer LC thiolate attacking HC+MPAA species, or there is instability of the amide species, this needs to be explored further.

The initial aim of this protocol has been achieved, one chain was permanently modified with the hydrazine thus generating a hydrazide bond, **45**-HC, as well as being available for further modification. The other chain contained a new non-native disulfide bond, **45**-LC, which in general bioconjugations protocols is difficult to achieve on a single chain. It was then proposed to synthesise a functional reagent containing a disulfide bond with alkyne handle for functionality *via* click chemistry, and a good leaving group such as pyridyl. The pyridyl leaving group consists

of an electron-withdrawing pyridine ring, which draws electron density away from the adjacent sulphur, making it more electropositive and hence a better electrophile.

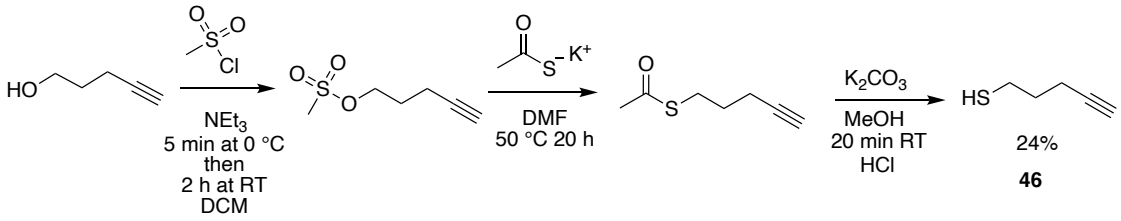

Scheme 30. Synthesis of pent-4-yne-1-thiol reagent **46**.

The protocol for synthesis of pent-4-yne-1-thiol **46** was followed as per published report in three step reaction,[188] affording desired compound **46** in 24% yield, **Scheme 30**.

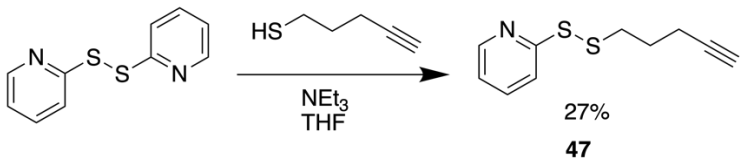

Scheme 31. Synthesis of pyridyldisulfide reagent **47**.

The target disulfide alkyne reagent **47** was synthesised in 27% yield by the addition of **46** to pyridyl disulfide (**Scheme 31**). With the reagent **47** in hand, conditions for thiol-disulfide exchange with free cysteine on the Fab fragment were evaluated (**Figure 36**).

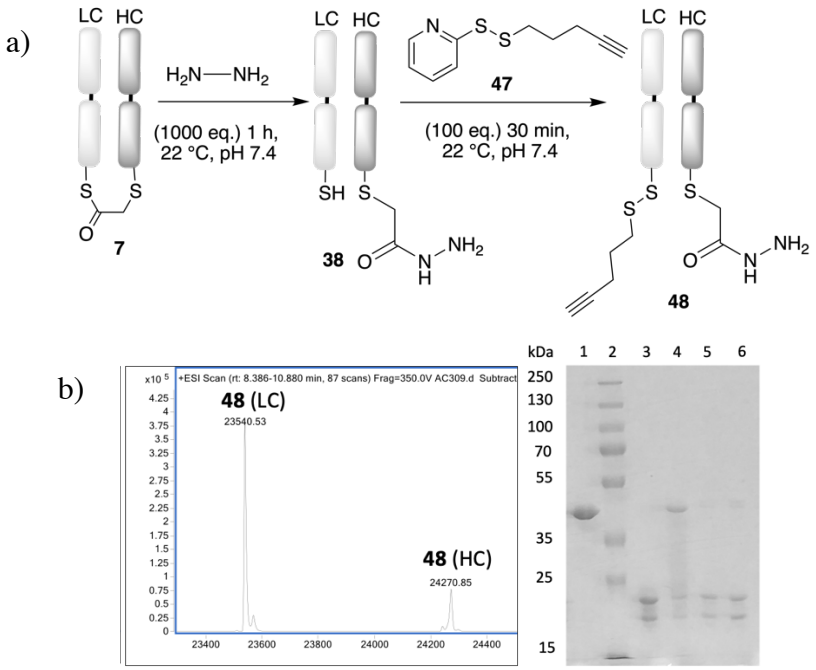

Figure 36. a) Dual conjugation protocol with hydrazine and pyridyldisulfide **47**, b) LCMS deconvoluted mass spectrum analysis of dual conjugation protocol. **48** (LC) mass expected 23537, mass observed 23540, **48** (HC) mass expected 24272, mass observed 24270. SDS-PAGE, 1 – native Fab, 2 – molecular marker, 3 – TCEP reduction, 4 – rebridged Fab with **1**, 5 – hydrazine addition, 6 – pyridyldisulfide addition.

The SDS-PAGE analysis showed correct reduction and subsequent rebridging of the Fab fragment, following disappearance of the Fab band on the gel, suggesting that the hydrazine step worked correctly. The LCMS spectrum resulted in the light chain peak with the alkyne addition **48**-LC and heavy chain with the hydrazide addition **48**-HC. No native or rebridged Fab was observed (**Figure 36**). The pyridyldisulfide alkyne undergoes thiol-disulfide exchange with the free chain thiol, the alkyne moiety has been selected here as a model, but this could be easily substituted with a different functional handle or a drug moiety. As the protocol for dual functionalisation has been encouraging, it was then envisaged to add double functionalities to the reactive handles. Namely, addition of a fluorophore azide to the alkyne handle and reaction of hydrazide with ketone or aldehyde.

4.3 Dual conjugation – hydrazone linker

To expand the dual conjugation protocol by incorporating a cleavable hydrazone bond, the hydrazine must be first reacted either with a ketone or aldehyde. The formation of the hydrazone bond commences by a proton-catalysed attack of the α-effect nucleophile, such as the hydrazide used in this study on the carbonyl atom of the electrophilic aldehyde or ketone. Following the proton transfer, the hemiaminal tetrahedral intermediate is formed. This then undergoes dehydration after protonation of the hydroxyl function. The reaction typically is done under acidic conditions.[189] In biological applications the ligation proceeds usually under physiological conditions which can be challenging due to the slow reaction rates at natural pH, therefore use of catalyst such as aniline can lead to more rapid bond formation.[189]

Proteinogenic amino acids found in proteins do not have aldehydes and ketones groups. Their reactivity with a wide range of nucleophiles makes them attractive handles for bioconjugation. Aldehydes reacting with amines can form imines, which is a reversible process, with equilibrium favouring the starting material. In comparison, hydrazones and oxime are less prone to hydrolysis resulting in more stable conjugates.[190]

It has been shown that the aromatic groups in the aldehyde/ketone region will stabilise the hydrazone bond due to resonance stabilisation.[191,189] Furthermore, a survey done on aryl aldehydes and ketones showed that electron-deficient carbonyl groups such as nitro, methoxy and chloro reacted more rapidly with hydrazine, in comparison to alkyl substrates.[192] The stability of the hydrazone bond can be influenced by various external factors, whereases the hydrolysis occurs significantly faster under acidic conditions and elevated temperatures. Hydrazone linkers have been shown to release their covalently bound payload mainly under the acidic conditions of specific organelles, namely endosomes (pH 5.5-6.2) or lysosomes (pH 4.5-5.0).[193] The hydrazone bond was utilised in the approved ADCs Besponsa and Mylotarg.[67]

To develop this protocol 20 eq. of phenylacetone was added to hydrazide **48** and left at 22 °C for 16 h. However, this showed no reactivity at all (data not shown), therefore an aldehyde was tested next. Benzaldehyde was chosen for this and as previously, a range of equivalents were evaluated, starting with 20 eq. for 16 h incubation under the same conditions as the ketone. Some modification on the heavy chain was observed, but full conversion was not attained (data not shown). Therefore, the conditions were altered by increasing the equivalents of the reagent to 50 eq. of benzaldehyde and adding aniline, which is commonly used as catalyst for hydrazone formation (**Figure 37**).[190]

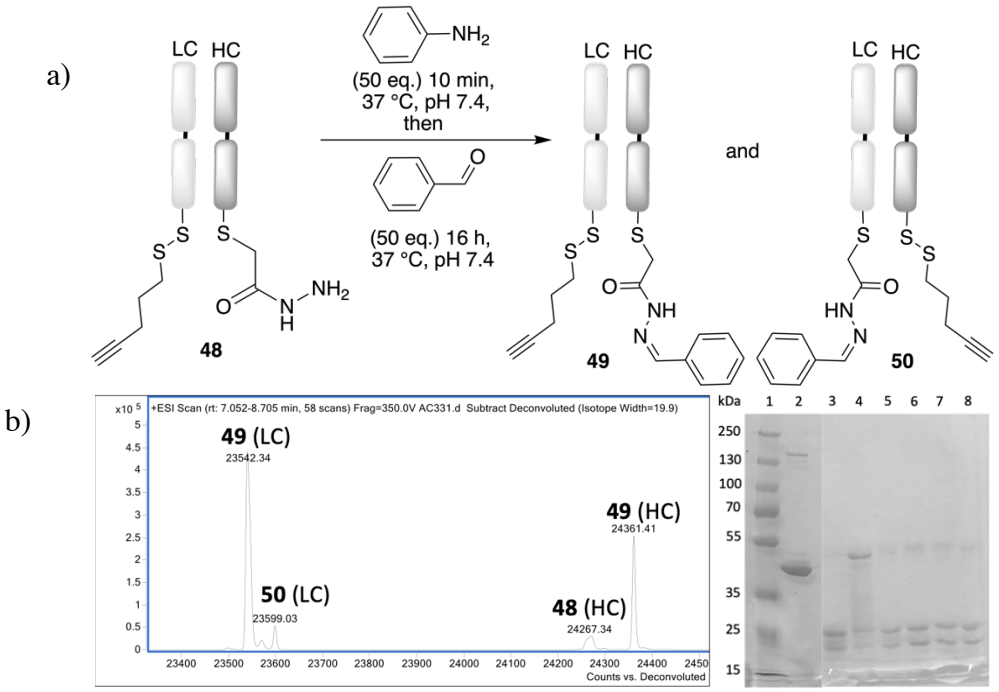

Figure 37. a) Dual conjugation protocol with hydrazine, pyridyldisulfide and a model aldehyde, b) LCMS deconvoluted mass spectrum analysis of dual conjugation protocol with benzaldehyde. **49** (LC) mass expected 23537, mass observed 23542, **50** (LC) mass expected 23599, mass observed 23599, **48** (HC) mass expected 24272, mass observed 24267, **49** (HC)

mass expected 24361, mass observed 24361. SDS-PAGE 1 – molecular marker, 2 – native Fab, 3 – TCEP reduction, 4 – rebridged Fab with **1**, 5 – hydrazine treatment, 6 – pyridyldisulfide addition, 7 – aniline addition, 8 – benzylaldehyde addition.

The heavy chain can be observed with the benzaldehyde addition **49**-HC aside minor heavy chain peak corresponding to unreacted hydrazide **48**-HC. The light chain shows an addition of the alkyne handle **49**-LC, there is also small peak in the light chain area corresponding to the second regioisomer with an aldehyde addition **50**-LC (**Figure 37**). It must be noted that as with all modification, the second regioisomer adduct is always there, however most of the time the peak intensity is not strong enough for the deconvolution algorithm to pick it up.

As the benzaldehyde data was encouraging, it was decided to synthesise two aldehyde bearing reagents, leading to a non-cleavable and a cleavable hydrazone handle. Biotin-PEG-aldehyde reagent was found to fit the purpose as not only it would generate the desired hydrazone cleavable/non-cleavable bond, but it will also allow for a pull-down assay with streptavidin/avidin beads that have high affinity towards biotin ($K_d = 10^{-14}$ mol L^{-1}).[194] The biotin-PEG-aldehyde reagent could mimic a toxic payload in this work, as toxic payload reagent availability and handling was not feasible at the time. The first aldehyde bearing reagent to be synthesised was the one with a phenyl ring and amide bond on the *para*-position to the aldehyde. This will generate a very stable bond due to the amide bond being a strong electron withdrawing group. As mentioned earlier, arylhydrazone on their own are stable under physiological temperature and pH[195] but the electron withdrawing groups will increase the reactivity of aldehyde in the hydrazone formation.[192] The short polyethylene glycol (PEG) was introduced because biotin binds better to streptavidin tag once there is a spacer between it and the attached protein (**Scheme 32**).

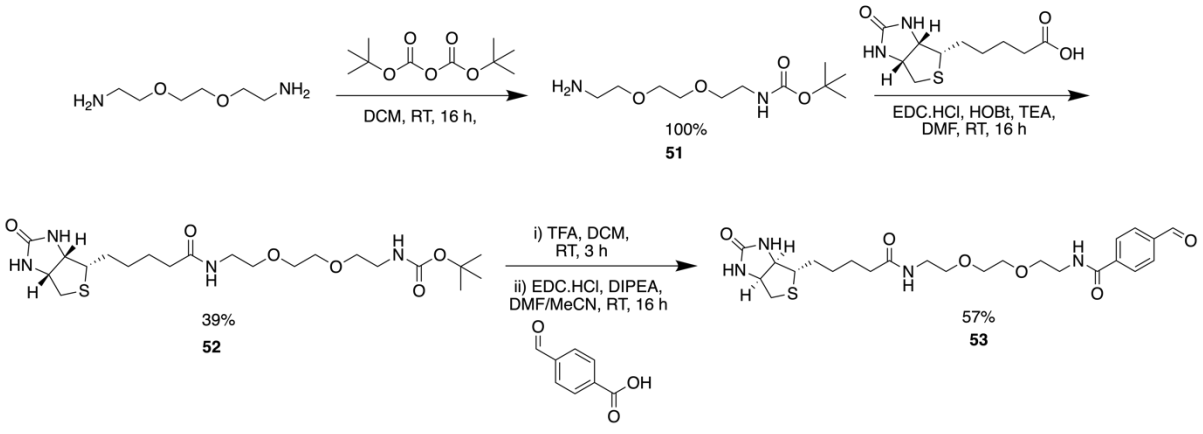

Scheme 32. Synthesis of biotin-PEG-aldehyde **53**.

The general protocol to synthesise biotin-PEG-aldehyde **53** was followed as per published reports, with some changes also incorporated.[194,196] First, the PEG used in this synthesis had an amine group on each end therefore one side had to be Boc protected, here amine PEG was used in excess resulting in compound **51** in 100% yield. This was then coupled to biotin in 39% yield, and finally the selected aldehyde was coupled to produce compound **53** in 57% yield (**Scheme 32**).

With the new biotin-PEG-aldehyde in hand, the reagent was added to the Fab conjugate **48** containing a hydrazide moiety on one chain and alkyne handle on the other. The dual conjugation protocol with pyridyldisulfide **47** and biotin-PEG-aldehyde **53** resulted in formation of desirable conjugate thus forming a new hydrazone bond (**Figure 38**). As expected, the second regioisomer is also observed on the light chain with bridged component, hydrazone, and biotin-PEG-aldehyde **53** (**55**-LC).

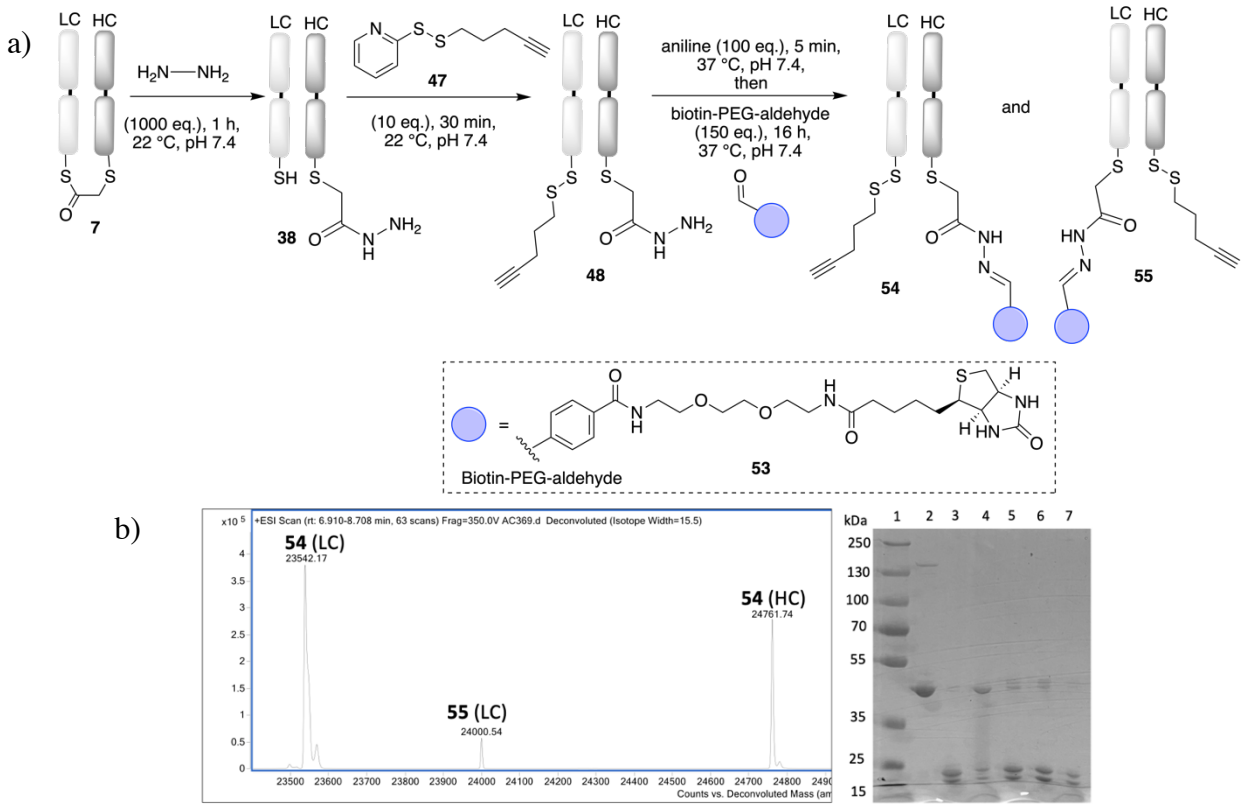

Figure 38. a) Fab conjugation with biotin-PEG-aldehyde **53** to form conjugate **54** and **55**, b) LCMS deconvoluted mass spectrum analysis of dual conjugation protocol with biotin-PEG-aldehyde **53**. **54** (LC) mass expected 23537, observed 23542, **55** (LC) mass expected 23999, mass observed 24000. **54** (HC) mass expected 24761, mass observed 24761. SDS-PAGE 1 – molecular marker, 2 – native Fab, 3 – TCEP reduction, 4 – rebridged Fab with **1**, 5 – hydrazine treatment, 6 – pyridyl disulfide addition, 7 – biotin-PEG-aldehyde **53** addition.

The second cleavable biotin-PEG-aldehyde **58** reagent to be synthesised was one that contained an extra carbon bond right after the phenyl ring on the *para*-position to the aldehyde, followed by the amide bond, this would have a slight electron donating effect and thus results in a cleavable hydrazone bond.

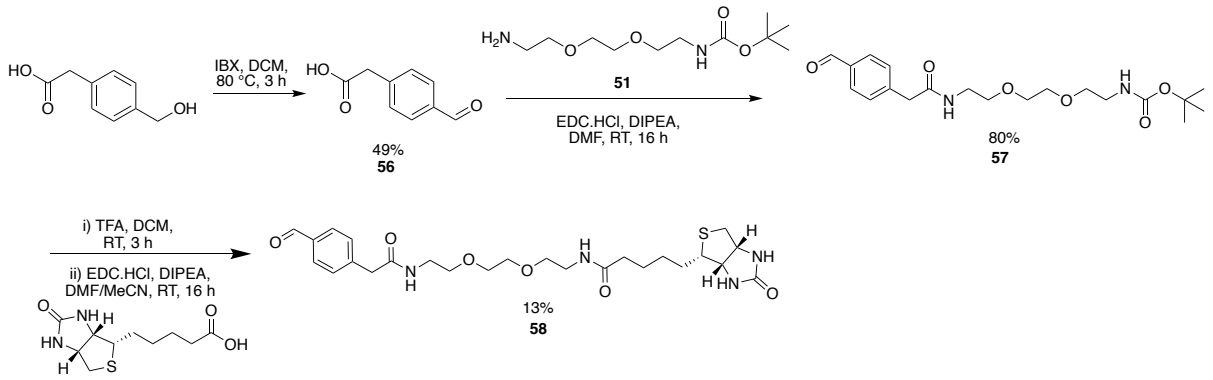

Scheme 33. Synthesis of cleavable biotin-PEG-aldehyde **58**.

The second biotin-PEG-aldehyde **58** was synthesised first by oxidising 2-(4-(hydroxymethyl)phenyl)acetic acid with 2-iodoxybenzoic acid (IBX) to generate aldehyde **56** in 49% yield. This was then mixed with Boc protected PEG **51** resulting in compound **57** in 80% yield. Lastly, this was coupled to biotin to produce biotin-PEG-aldehyde **58** in 13% yield (**Scheme 33**). The successfully synthesised second biotin-PEG-aldehyde **58** was then tested for the dual conjugation approach on Fab fragment (**Figure 39**).

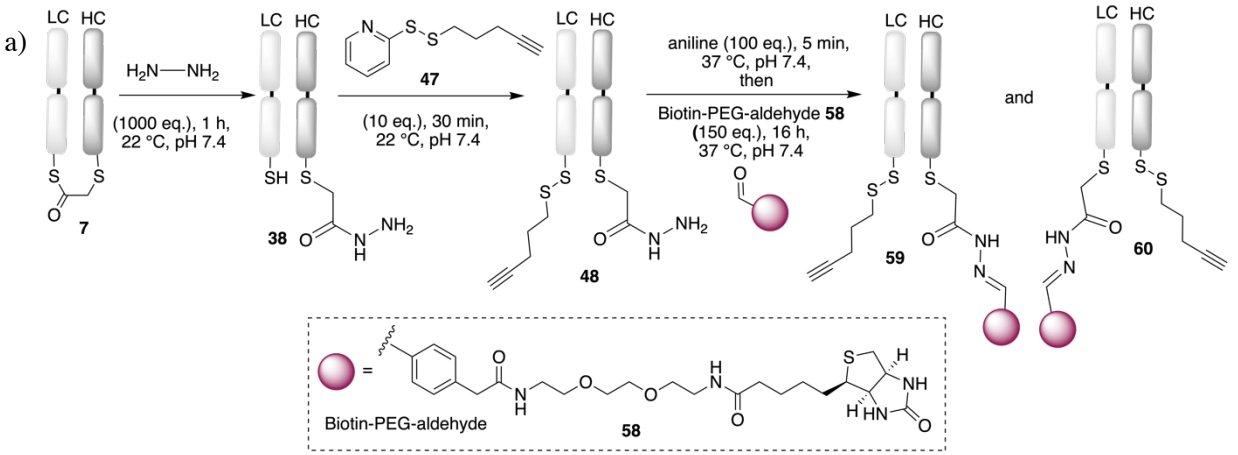

b)

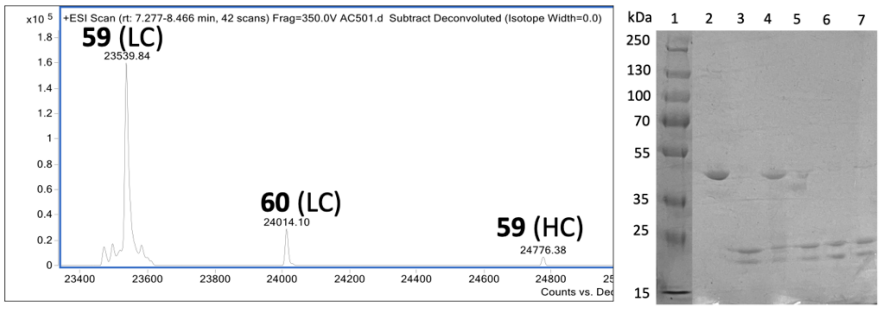

Figure 39. a) Fab conjugation with biotin-PEG-aldehyde **58** forming conjugate **59** and **60**, b) LCMS deconvoluted mass spectrum analysis of dual conjugation protocol with biotin-PEG-aldehyde **58**. **59** (LC) mass expected 23537, mass observed 23539, **60** (LC) mass expected 24013, mass observed 24014, **59** (HC) mass expected 24775, mass observed 24776. SDS-PAGE 1 – molecular marker, 2 – native Fab, 3 – TCEP reduction, 4 – rebridged Fab with **1**, 5 – hydrazine treatment, 6 – pyridyldisulfide addition, 7 – biotin-PEG-aldehyde **58** addition.

The light chain showed addition of the new disulfide bond with an alkyne handle **59**-LC, whereas the heavy chain peak corresponded to formation of the hydrazone bond with PEG and biotin **59**-HC, the formation of hydrazone bond has been observed with both of the aldehyde bearing reagents. A second regioisomer is also observed on light chain containing the hydrazone linker and biotin **60**-LC. No rebridged or native Fab was observed for both of the aldehydes reagents synthesised **53** and **58**, (**Figure 38** and **Figure 39**).

4.4 Dual conjugation – alkyne handle functionalisation with fluorophore

The alkyne addition on one of the chains represents a wide array of applicability for dual conjugate strategy. The most straightforward system is addition of an azide fluorophore *via* the CuAAC.[197] It was then proposed to add a fluorophore Azide fluor 488 that has been used in the previous chapters to demonstrated the practicality of the system.

The optimisation of the functionalisation platform started by using a typical CuAAC protocol where substrates were added: THPTA (50 eq.), $CuSO_4$ (10 eq.), Azide fluor 488 (10 eq.) and sodium ascorbate (final conc. 10 mM). This was incubated together with conjugate **48** at 22 °C for 16 h. After that time, biotin-PEG-aldehyde conjugation was undertaken as described before. The LCMS results indicated that the CuAAC did not work, the light chain still contained an unmodified alkyne handle and heavy chain contained the biotin conjugate (data not shown). The reasons for the unsuccessful click reaction were shortlisted as: the copper click reagents having expired; the conjugate was too hindered for the click to work; or the copper cross reacted with other reagents rendering it inactive. The CuAAC protocol was repeated with usage of different,

smaller azides namely azido-PEG-alcohol and benzyl azide alongside fresh reagent stocks, however the results were largely comparable. The click addition and formation of the triazole was not observed (data not shown). It was then suggested to try a direct conjugation protocol whereby the alkyne containing reagent **47** was mixed separately with the click reagents and this was then added directly into the Fab conjugate (**Scheme 34**).

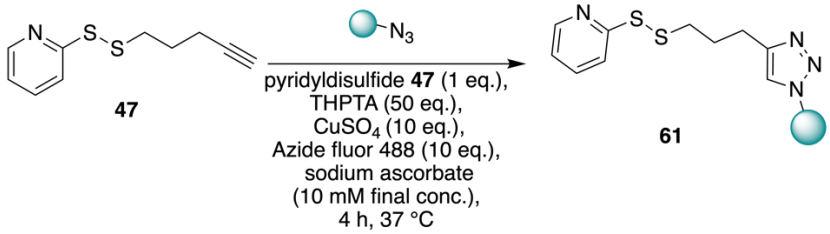

Scheme 34. Pre-conjugation click conditions for the formation of the dipyridyl disulfide with a fluorophore **61**.

Commonly, for direct conjugation or pre-conjugation click, the conjugate would have to be checked through UPLC, to confirm that indeed the reaction has worked, however in the case of copper click, it is not advisable to run a sample that still contains metals such a copper as this could have a negative effect on how the sample is being analysed. The purification of this conjugate was also not possible due to the small size. Fab conjugate was prepared, where Fab was reduced and rebridged with α-chlorothioester **1** followed by addition of hydrazine as before. Lastly the pre-click **61** was directly combined with the Fab conjugate, and this was further incubated at 22 °C for 4 h (**Figure 40**).

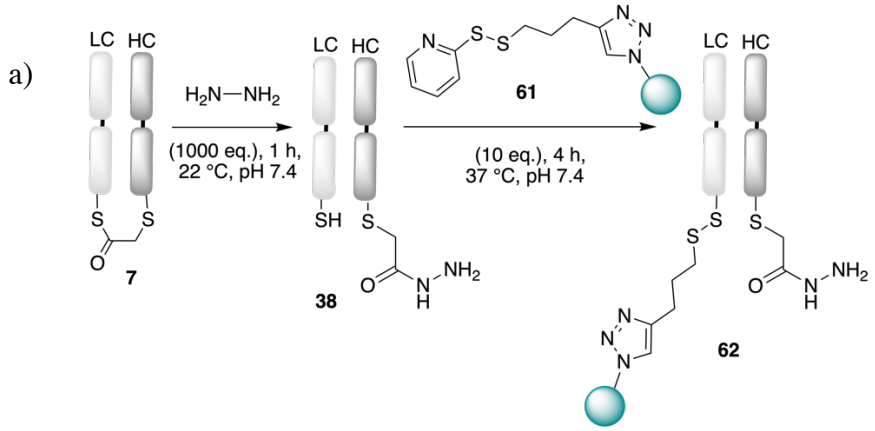

b)

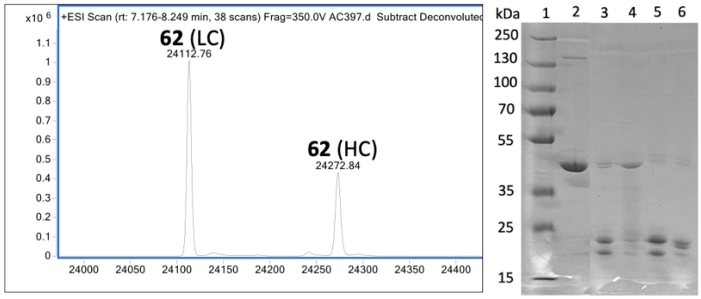

Figure 40. a) Protocol for Fab conjugate combined with the pre-click conditions, b) LCMS deconvoluted mass spectrum analysis of Fab conjugate combined with the pre-click conditions **61**. **62** (LC) mass expected 24112, mass observed 24112, **69** (HC) mass expected 24272, mass observed 24272. SDS-PAGE 1 – molecular marker, 2 – native Fab, 3 – TCEP reduction, 4 – rebridged Fab with **1**, 5 – hydrazine treatment, 6 – pre-click addition.

Both chains showed the expected conjugates, correct formation of triazole was observed on the light chain **62**-LC and hydrazide on the heavy chain **62**-HC (**Figure 40**). There was no native LC or HC observed, suggesting full conversion to the desirable conjugate has occurred. Additionally, the conjugate was analysed through UV/Vis resulting in FAR of 0.7.

$$FAR = \frac{\frac{Abs_{505}}{\varepsilon_{505}}}{\frac{Abs_{280} - (Cf\ x\ Abs_{505})}{\varepsilon_{280}}} = \frac{\frac{1.25}{74000}}{\frac{1.80 - (0.11\ x\ 1.25)}{68590}} = 0.7$$

Since the pre-conjugation click protocol was working in a desirable way, a full dual conjugation procedure was then employed where upon incubation of the pre-click **61** with Fab conjugate, the protocol was extended by addition of a catalyst aniline and a biotin-PEG-aldehyde **53** (**Figure 41**).

a)

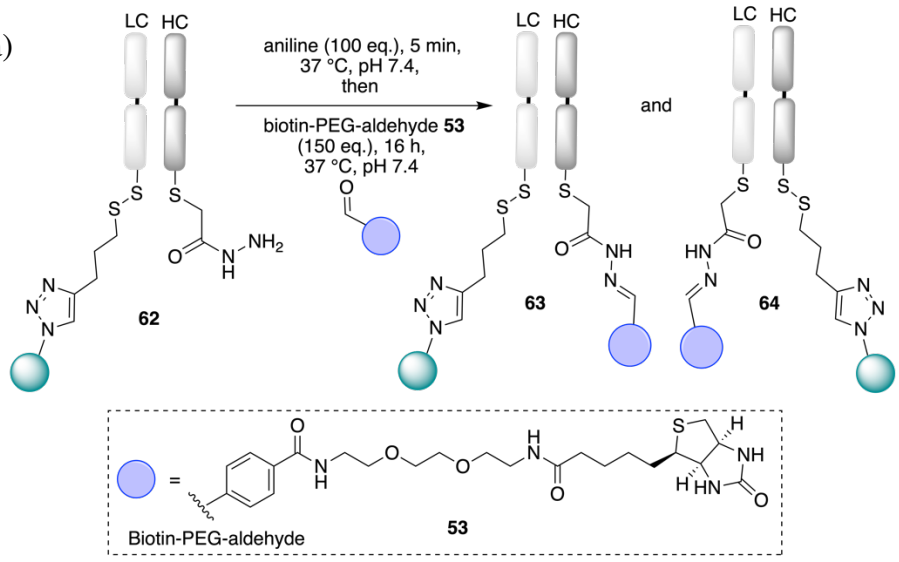

b)

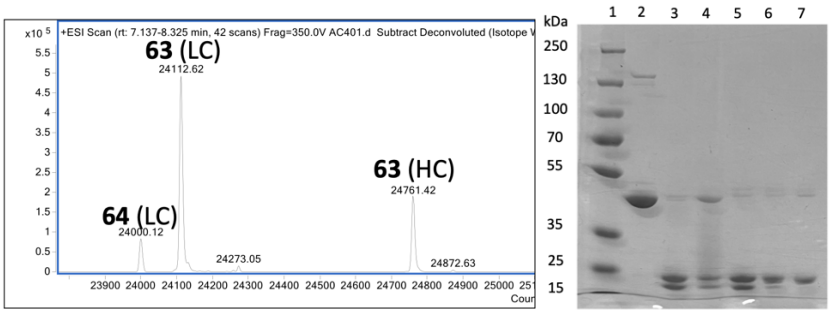

Figure 41. a) Complete dual conjugation strategy containing a pre-click alkyne-fluorophore and Fab conjugate with biotin-PEG-aldehyde forming conjugate **63** and **64**, b) LCMS analysis of the full protocol for dual conjugation. **64** (LC) mass expected 23999, mass observed 24000, **63** (LC) mass expected 24112, mass observed 24112, **63** (HC) mass expected 24761, mass observed 24761. SDS-PAGE 1 – molecular marker, 2 – native Fab, 3 – TCEP reduction, 4 – rebridged Fab with **1**, 5 – hydrazine treatment, 6 – pre-click treatment, 7 – biotin-PEG-aldehyde **53** addition.

The LCMS spectra showed clean results for dual conjugation protocol, light chain containing the triazole formation with the Azide fluor 488 **63**-LC, and the heavy chain with a hydrazone bond forming between the hydrazide and aldehyde containing PEG and a biotin **63**-HC (**Figure 41**). There is also the second regioisomer observed on the light chain containing the hydrazone-PEG-biotin conjugate **64**-LC. The SDS-PAGE analysis showed corrected reduction and subsequent formation of separate conjugates on light and heavy chain. The FAR was determined as before, using the UV/Vis absorption for the conjugate **63** resulting in FAR of 0.8.

$$FAR = \frac{\frac{Abs_{505}}{\varepsilon_{505}}}{\frac{Abs_{280} - (Cf\ x\ Abs_{505})}{\varepsilon_{280}}} = \frac{\frac{3.04}{74000}}{\frac{3.97 - (0.11\ x\ 3.04)}{68590}} = 0.8$$

The protocol was further tested on the second aldehyde **58** to demonstrate the addition of the fluorophore and formation of hydrazone bond. (**Figure 42**).

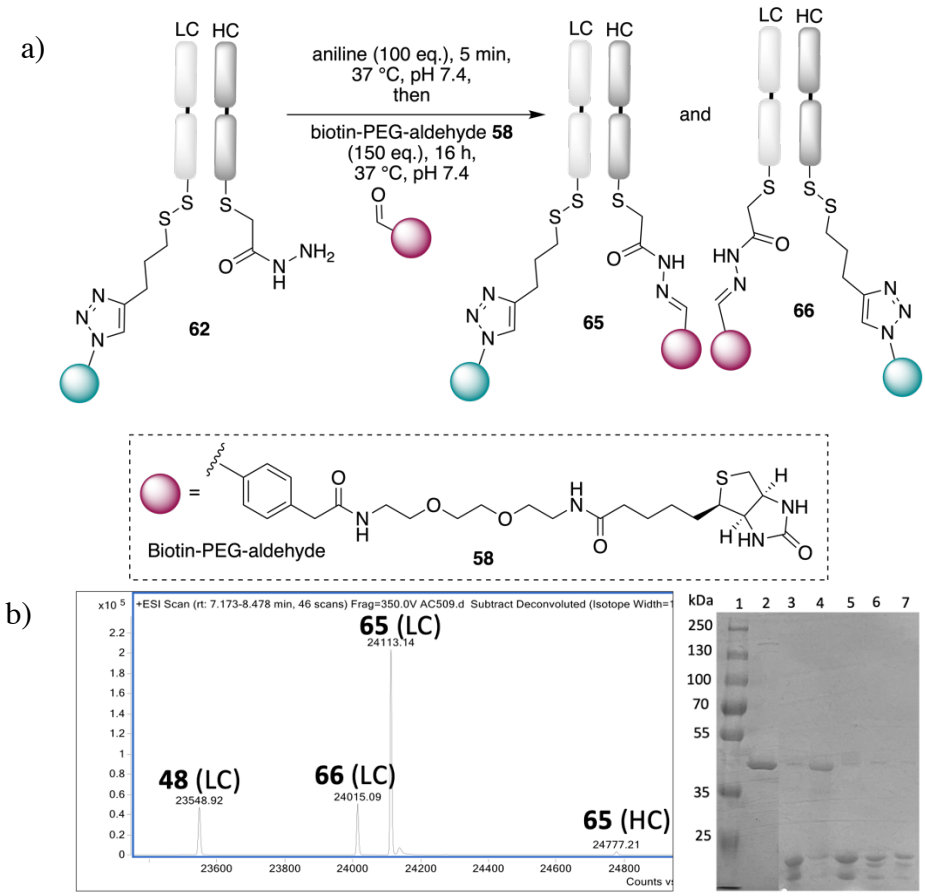

Figure 42. a) Complete dual conjugation strategy containing a pre-click alkyne-fluorophore and Fab conjugate with biotin-PEG-aldehyde **58**, forming Fab conjugate **65** and **66**, b) LCMS analysis of the full protocol for dual conjugation with biotin-PEG-aldehyde **58**. **48** (LC) mass expected 23537, mass observed 23548, **66** (LC) mass expected 24012, mass observed 24015, **65** (LC) mass expected 24112, mass observed 24113, **65** (HC) mass expected 24775, mass observed 24777. SDS-PAGE 1 – molecular marker, 2 – native Fab, 3 – TCEP reduction, 4 – rebridged Fab with **1**, 5 – hydrazine treatment, 6 – pre-click treatment, 7 – biotin-PEG-aldehyde **58** addition.

The LCMS spectra showed a clean results for dual conjugation protocol with the reagent **58**, light chain contained the triazole formation with the Azide fluor 488 (FAR = 0.8) **65**-LC, the heavy chain contained hydrazone bond forming between the hydrazide and aldehyde containing PEG and a biotin **65**-HC (**Figure 42**), a minor peak corresponding to light chain still containing alkyne handle was observed **48**-LC. There is also the second regioisomer observed on the light chain containing the hydrazone-PEG-biotin conjugate **66**-LC. The SDS-PAGE analysis showed corrected Fab reduction and subsequent formation of separate conjugates on light and heavy chain.

$$FAR = \frac{\frac{Abs_{505}}{\varepsilon_{505}}}{\frac{Abs_{280} - (Cf\ x\ Abs_{505})}{\varepsilon_{280}}} = \frac{\frac{1.69}{74000}}{\frac{2.28 - (0.11\ x\ 1.69)}{68590}} = 0.8$$

4.5 Dual conjugation cleavage of the disulfide bond – blood and early endosomal mimicking conditions

Disulfide bonds under bioconjugations conditions do not significantly cleave in buffer containing low concentration of GSH, which corresponds to the concentration of thiol in blood such as 5 μM. Upon increase of the GSH in the buffer to 5 mM, which is the concentration corresponding to cytosol environment of mammalian cells, the disulfide cleavage should be observed.[198] On-demand drug release in diseased environments is a very promising endeavour that not only would minimise off target toxicity but could improve efficiency of treatments. It was also found that in hypoxic tumour cells the GSH concentration can be up to four times higher.[199] This can be exploited by designing a reagent to form a new disulfide bond by programming redox responsiveness in the cellular environment. Additionally, studies on how steric hinderance of disulfide bond affects reducibility in disulfide linked antibody conjugate showed that when a methyl group is added to the α-carbon on the linker, the circulation time is extended considerably.[200]

The new non-native disulfide bond mostly observed on the light chain species offers a prospective cleavable linker. To demonstrate the cleavable properties of the linker developed in this study, an experiment was designed where the Fab conjugate **63** and **64** were incubated in a buffer containing high concentration of GSH. The Fab conjugates were prepared as previously, then these were buffer swapped into 5 mM GSH, at pH 6.5 to mimic the cytosol environment, and this was left at 37 °C for up to 8 h, following analysis on the LCMS as well as gel timepoints.

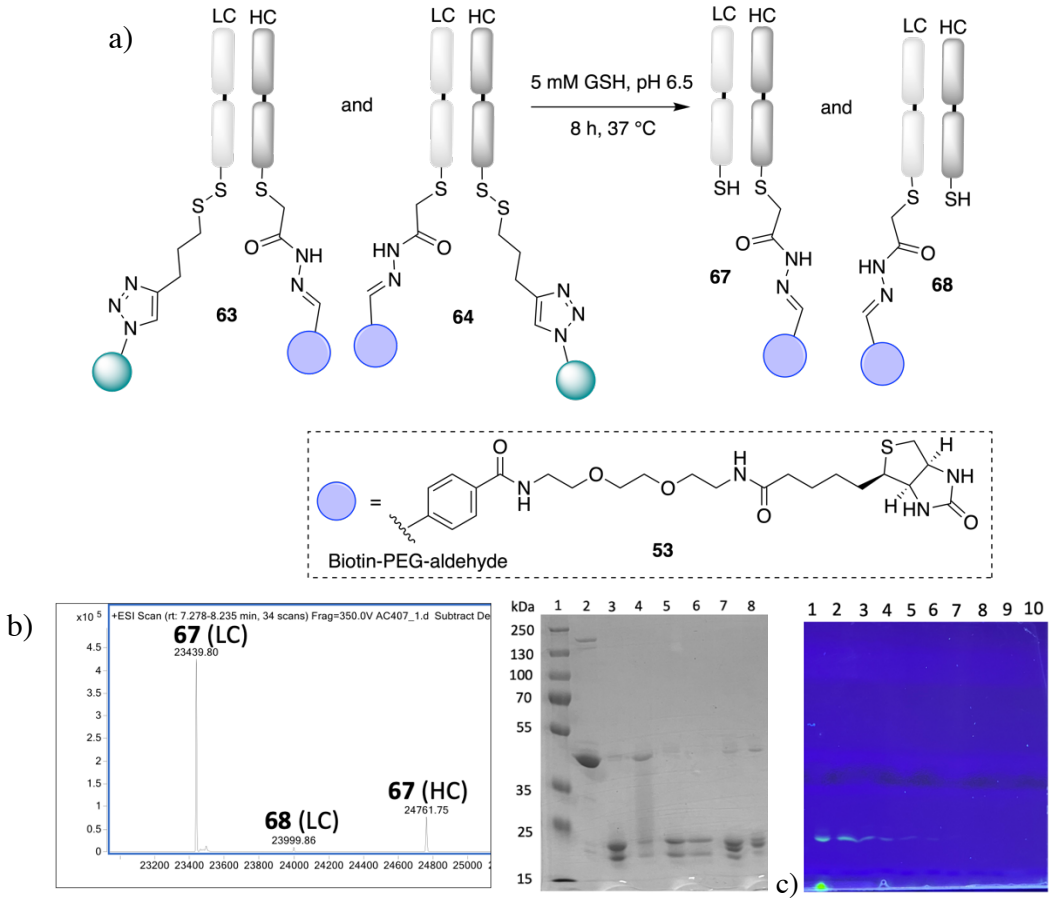

Figure 43. a) Early endosomal mimicking conditions for cleavage of the non-native disulfide bond in conjugate **63** and **64** with 5 mM GSH pH 6.5, b) LCMS analysis of the cleavage protocol for Fab conjugates **64** and **64**. **67** (LC) mass expected 23438, mass observed 23439, **68** (LC) mass expected 23999, mass observed 23999, **67** (HC) mass expected 24761, mass observed 24761. SDS-PAGE 1 – molecular marker, 2 – native Fab, 3 – TCEP reduction, 4 – rebridged Fab with **1**, 5 – hydrazine treatment, 6 – pre-click addition, 7 – biotin-PEG-aldehyde **53** addition, 8 – GSH 1 h incubation, c) UV scan of SDS-PAGE: 1 – pre-click, 2 – biotin-PEG-aldehyde **53**, 3 – GSH 1 h, 4 – GSH 2 h, 5 – GSH 3 h, 6 – GSH 4 h, 7 – GSH 5 h, 8 – GSH 6 h, 9 – GSH 7 h, 10 – GSH 8 h. Calculated densitometry analysis shows 52% decrease in the 1 h, 72% decrease in the 2 h, 86% decrease in 3 h, 92% decrease in 4 h, 100% decrease after 4 h.

The LCMS analysis shows native light chain **67**-LC, heavy chain containing biotin-PEG-aldehyde conjugate **67**-HC and light chain showing the second regioisomer with biotin-PEG-aldehyde **68**-LC. The overall results show the expected cleavage of the disulfide bond, whilst the hydrazone bond was not affected as expected (**Figure 43**). The gel scanned under UV light shows nearly 100% decrease in density of the fluorophore band after 4 h of incubation, this is in line with published reports for similar disulfide conjugates.[201,202] The calculated FAR resulted in 0.0, confirming a full cleavage of the fluorophore.

$$FAR = \frac{\frac{Abs_{505}}{\varepsilon_{505}}}{\frac{Abs_{280} - (Cf\ x\ Abs_{505})}{\varepsilon_{280}}} = \frac{\frac{0.02}{74000}}{\frac{0.50 - (0.11\ x\ 0.02)}{68590}} = 0.0$$

For the blood mimicking conditions, the developed Fab conjugates **63** and **64** were incubated in low concentration of GSH (**Figure 44**).

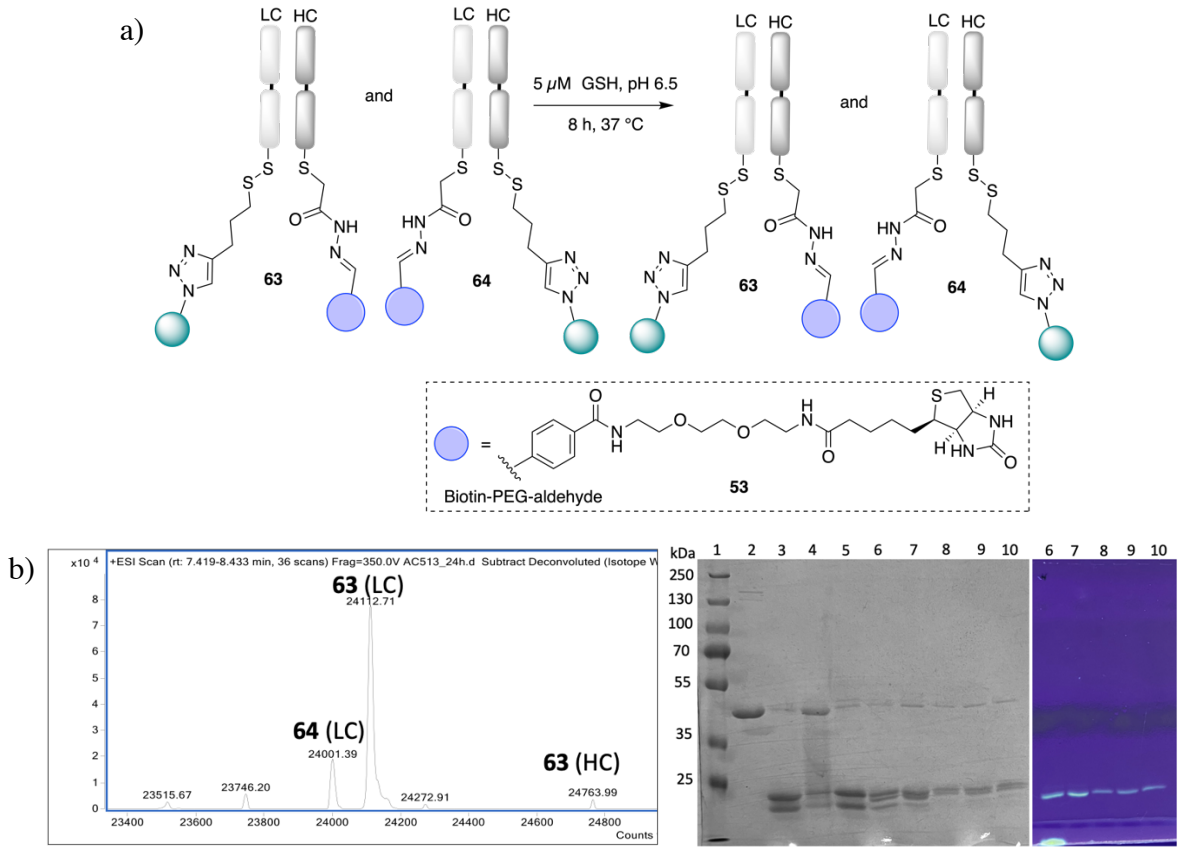

Figure 44. a) Blood mimicking conditions to demonstrate lack of cleavage of the non-native disulfide bond in Fab conjugates **63** and **64** with 5 μM GSH pH 6.5, b) LCMS analysis of the cleavage protocol for Fab conjugates **63** and **64** of the non-native disulfide bond with 5 μM GSH. LC with GSH mass expected 23745, mass observed 23746, **64** (LC) mass expected 23999, mass observed 24001, **63** (LC) mass expected 24112, mass observed 24112, **63** (HC) mass expected 24761, mass observed 24763. SDS-PAGE 1 – molecular marker, 2 – native Fab, 3 – TCEP reduction, 4 – rebridged Fab with **1**, 5 – hydrazine treatment, 6 – pre-click treatment, 7 – biotin-PEG-aldehyde **53**, 8 – GSH 4 h, 9 – GSH 8 h, 10 – GSH 24 h. Calculated densitometry analysis shows unchanged densitometry between lane 8 to 10.

The LCMS results show light chain peak corresponding to light chain with a fluorophore **63**-LC, therefore the disulfide cleavage did not occur, as estimated (**Figure 44**). The other peaks can be accounted for the heavy chain with the bridged component and biotin-PEG-aldehyde **63**-HC, as well the second regioisomer on the light chain **64**-LC. There is also a minor peak corresponding

to the light chain with alkyne handle, suggesting incomplete conversion during pre-click conditions (observed mass 23515) and second minor peak corresponding to the light chain with glutathione attached (observed mass 23746). Most likely this is being formed with unreacted light chain rather than the cleaved light chain. The SDS-PAGE analysis shows corrected reduction and subsequent rebridging. The UV scanned SDS-PAGE shows that lanes 8 to 10 where the fluorescence has not decreased between the timepoints taken (**Figure 44**). This was additionally confirmed by the FAR reading which resulted in 0.7.

$$FAR = \frac{\frac{Abs_{505}}{\varepsilon_{505}}}{\frac{Abs_{280} - (Cf\ x\ Abs_{505})}{\varepsilon_{280}}} = \frac{\frac{2.83}{74000}}{\frac{4.16 - (0.11\ x\ 2.83)}{68590}} = 0.7$$

4.6 Dual conjugation cleavage of the hydrazone bond – lysosomal mimicking conditions

The insertion of the hydrazone bond in the linker conjugate allows for cleavage of the payload at a particular environmental conditions namely late endosomes (pH 5.5-6.2) or lysosomes (pH 4.5-5.0).[193] The mechanism behind hydrolysis of the hydrazone bond involves first protonation of the imine hydrogen (**Scheme 35**, **A**) followed by a nucleophilic attack of a water molecule at the imine carbon (**Scheme 35**, **B**), then the tetrahedral carbinolamine intermediate is formed (**Scheme 35**, **C**) and lastly the intermediate is decomposed and cleaved off the C-N bond. The rate of hydrolysis is determined by the substituents adjacent to the hydrazone. For example, an electron-donating R-group can speed up the pH-dependent hydrolysis by boosting protonation of the imine nitrogen, which in turn activates the imine carbon to be more prone to nucleophilic attack from water, and thus the nitrogen can accept a pair of electrons from the imine bond to form the tetrahedral carbinolamine intermediate. Whereas, electron withdrawing R-groups will decrease the pH sensitivity towards nucleophilic attack by water.[203] Therefore, it is a very delicate balancing act to find the right group for desired pH-dependent hydrolysis and stability.[203]

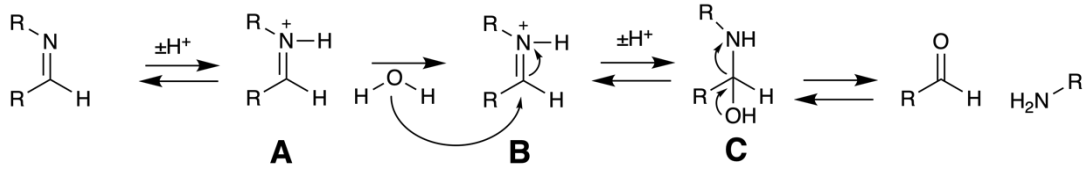

Scheme 35. Hydrolysis of the hydrazone bond.

To demonstrate the hydrazone bond, generated with the biotin-PEG-aldehyde reagent **53,** is not prone to acidic cleavage, an experiment was designed where the Fab dual conjugate was buffer swapped into 0.1 M sodium acetate pH 5.0 and incubated at 37 °C for 24 h. The results were then analysed on LCMS, UV/Vis and SDS-PAGE was scanned with fluorescent lamp (**Figure 45**).

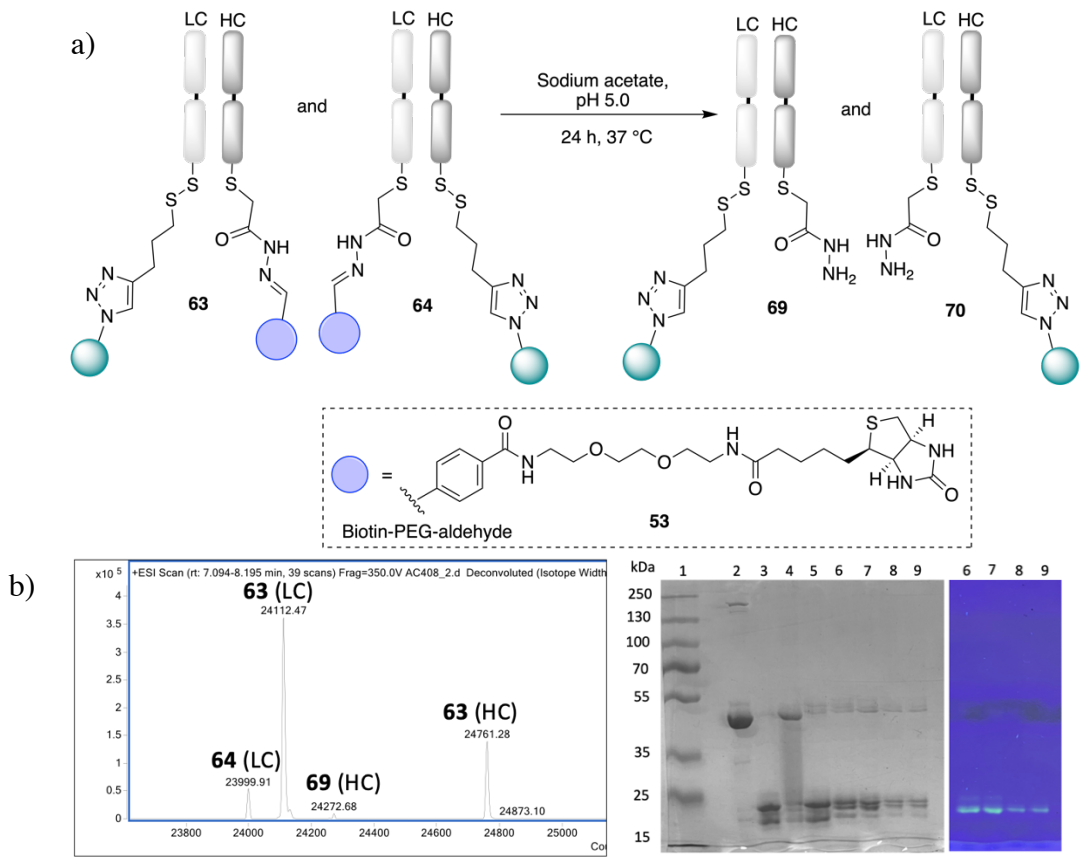

Figure 45. a) Acidic cleavage of the hydrazone bond from the Fab conjugates **63** and **64** with sodium acetate pH 5.0, b) LCMS analysis of the cleavage protocol for dual conjugation at pH 5.0 after 24 h incubation time at 37 °C. **64** (LC) mass expected 23999, mass observed 23999, **63** (LC) mass expected 24112, mass observed 24112, **69** (HC) mass expected 24272, mass observed 24272, **63** (HC) mass expected 24761, mass observed 24761. SDS-PAGE 1 – molecular marker, 2 – native Fab, 3 – TCEP reduction, 4 – rebridged Fab with **1**, 5 – hydrazine treatment, 6 – pre-click treatment, 7 – biotin-PEG-aldehyde **53**, 8 – 8 h incubation at pH 5.0, 9 – 24 h incubation at pH 5.0.

$$FAR = \frac{\frac{Abs_{505}}{\varepsilon_{505}}}{\frac{Abs_{280} - (Cf\ x\ Abs_{505})}{\varepsilon_{280}}} = \frac{\frac{2.57}{74000}}{\frac{3.50 - (0.11\ x\ 2.57)}{68590}} = 0.8$$

As anticipated, the cleavage of the hydrazone bond did not occur, there was no change observed in the heavy chain region **63**-HC (**Figure 45**). There is minor peak corresponding to heavy chain

with hydrazide attached, however it is more likely that this is unreacted species **69**-HC. The reaction was also left for longer incubation time and hydrazone cleavage was not observed. The light chain with the non-native disulfide bond and fluorophore attached remained unchanged **63**-LC, this was observed on the LCMS and the UV scanned SDS-PAGE. This lack of hydrazone cleavage was expected due to the strong electron withdrawing group on the *para*-position to the aldehyde, that makes the hydrazone bond very stable towards acid hydrolysis.

The Fab conjugate **63** and **64** were further pushed to test for their stability in more acidic buffer for any sign of cleavage at pH 4.0 for up to 72 h, and that also showed no cleavage, spectra were comparable with the one presented in **Figure 45**, (data not shown). Lastly, the Fab conjugate were also tested at pH 3.0 for up to 72 h. Cleavage at pH 3.0 has no real application for cleavable linkers, as such a low pH is not found in the lysosomal or cytoplasm environment. Therefore, this was just to test the limitation of the hydrazone bond generated with biotin-PEG-aldehyde **53**. The results from pH 3.0 cleavage study showed cleavage of the hydrazone bond and release of hydrazide moiety on the HC thus forming conjugate **69**-HC, however the second regioisomer with hydrazone bond **64**-LC, still showed minor peak with the biotin-PEG-linker attached (data not shown). This is an interesting finding on its own, suggesting that perhaps the hydrazone bond on the LC is more hindered than the one on the HC and potentially the bond is shielded from the water attack.

The hydrazone bond in the Fab conjugates **63** and **64** was thus found not be cleavable. Other application for this reagent or such a conjugate can be suggested. The biotin tag on one chain could also be used in sandwich ELISA set up, which is then reacted with streptavidin containing HRP, whilst the other chain could contain a cytotoxic cargo. This would be especially useful if the cargo contained a long linker that could potentially cover the Fab binding sites. Other application might include addition of a fluorophore on one side, thus allowing for tracking of the conjugate whereas the biotin could then be used for pull-down assay to remove the conjugate. The biotin-PEG-aldehyde **53** containing linker has been previously used for ELISA detection of semicarbazide (SEM) which is a break down product of nitrofurazone, a food additive used for treatment of gastrointestinal infection in poultry.[194]

The second biotin-PEG-aldehyde **58** synthesised here was then used to demonstrate the cleavage of the hydrazone bond. The second reagent contained an extra carbon bond between the aryl ring and the amide bond, resulting in a slight electron-donating effect, which should be sufficient to

make it viable for acid hydrolysis. Other changes to make the linker more hydrolytically unstable could be made by having an alkyl aldehyde, where the initial stability of the hydrazone bond is lower than an aryl derivative.

The reaction with Fab conjugate **63** and **64** was left at 37 °C for up to 72 h, with a gel timepoint taken at 24 h, 48 h and 72 h. The results were then analysed on LCMS and SDS-PAGE was scanned with fluorescent lamp (**Figure 46**).

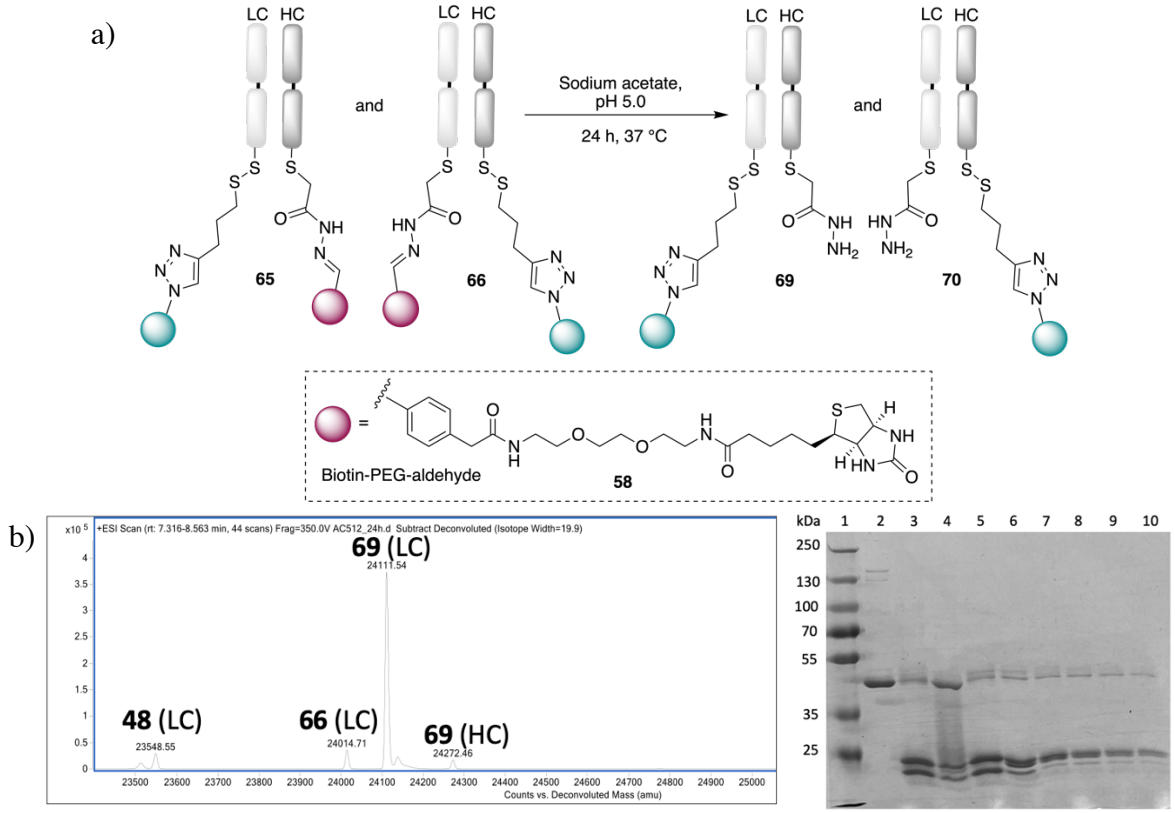

Figure 46. a) Acidic cleavage of the hydrazone bond from the Fab conjugate **65** and **66** with sodium acetate pH 5.0, b) LCMS analysis of the cleavage protocol for Fab conjugate **65** and **66** at pH 5.0 after 24 h incubation time at 37 °C. **48** (LC) mass expected 23537, mass observed 23548, **66** (LC) mass expected 24013, mass observed 24014, **69** (LC) mass expected 24112, mass observed 24111, **69** (HC) mass expected 24272, mass observed 24272. SDS-PAGE 1 – molecular marker, 2 – native Fab, 3 – TCEP reduction, 4 – rebridged Fab with **1**, 5 – hydrazine treatment, 6 – pre-click treatment, 7 – biotin-PEG-aldehyde **58** addition, 8 – pH 5.0/24 h incubation, 9 – pH 5.0/48 h incubation, 10 – pH 5.0/72 h incubation.

The LCMS spectra showed a full cleavage of the hydrazone bond in the first 24 h of incubation, thus releasing the hydrazide moiety on the heavy chain **69**-HC, the light chain showed the disulfide bond to be unaffected with the fluorophore still attached **69**-LC (**Figure 46**). Interestingly, the second regioisomer containing hydrazone bond with biotin remained intact **66**-LC. This could be related to the finding obtained with the non-cleavable aldehyde **53**, where even

at pH 3.0, the hydrazone bond on the light chain was not cleaved off, suggesting that the hydrazone bond is shielded from the water attack. There is also some light chain with the alkyne handle observed on the LCMS **48**-LC, indicating that the pre-click **61** did not reach the full conversion in this case. The FAR for the fluorophore addition resulted in 0.7, which is the value commonly achieved for this type of click in this project, suggesting that it was only minor amount left of the unreacted alkyne handle on the light chain.

$$FAR = \frac{\frac{Abs_{505}}{\varepsilon_{505}}}{\frac{Abs_{280} - (Cf\ x\ Abs_{505})}{\varepsilon_{280}}} = \frac{\frac{2.48}{74000}}{\frac{4.60 - (0.11\ x\ 2.48)}{68590}} = 0.7$$

4.7 Stability assays

4.7.1 ELISA

Enzyme-linked immunosorbent assay (ELISA) was carried out on reduced Fab (capped with *N*-Me-maleimide) and Fab conjugate **48** containing dual modification component to test affinity towards HER2 antigen. A 96-well polystyrene plate was coated first with HER2 antigen. Following that, capped Fab and Fab conjugate **48** were applied to it. Upon completing the incubation time with a secondary antibody linked to HRP, *o*-phenylenediamine was added. This was converted to 2,3-diaminophenazine by the enzyme HRP, that shows strong absorbance at 490 nm, allowing for spectrophotometric quantification of the antigen-binding activity of the Fab conjugate and native Fab. As it is presented in **Figure 47**, the Fab conjugate shows comparable antigen binding activity to the capped Fab.

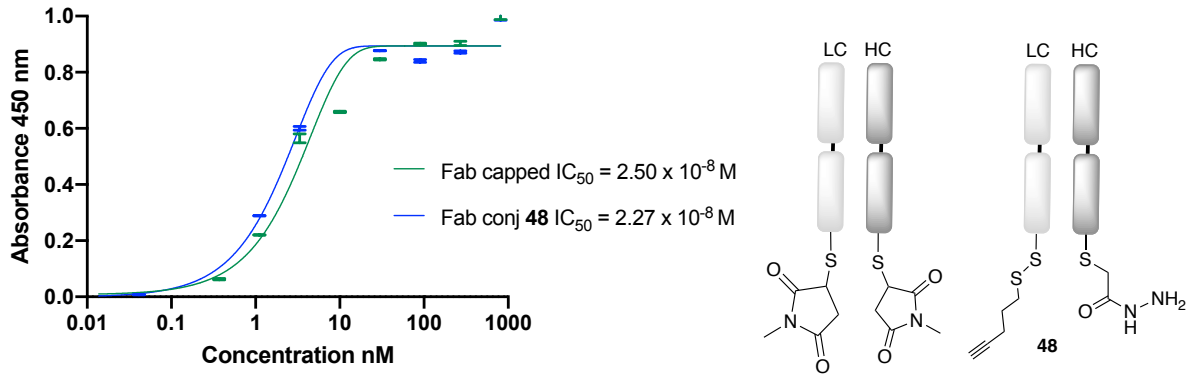

Figure 47. Binding activity to HER2 of trastuzumab native capped Fab and Fab conjugate **48** over concentration ranges from 810-0.0137 nM, absorbance was measured at 450 nm.

4.7.2 Thermal Shift Assay

In this study, capped Fab with *N*-Me-maleimide was analysed against Fab containing a hydrazide moiety on one chain and new non-native disulfide bond with an alkyne linker on the other side as illustrated in Fab conjugate **48.** The capped Fab showed T_m of 77.09 °C which is nearly 5 °C lower than native Fab containing disulfide bonds found in this study (see in section **3.6.2**). Furthermore, Fab conjugate **48**, also without native disulfide bond showed T_m of 75.56°C, a further 1.5 °C degree decrease (**Figure 48**).

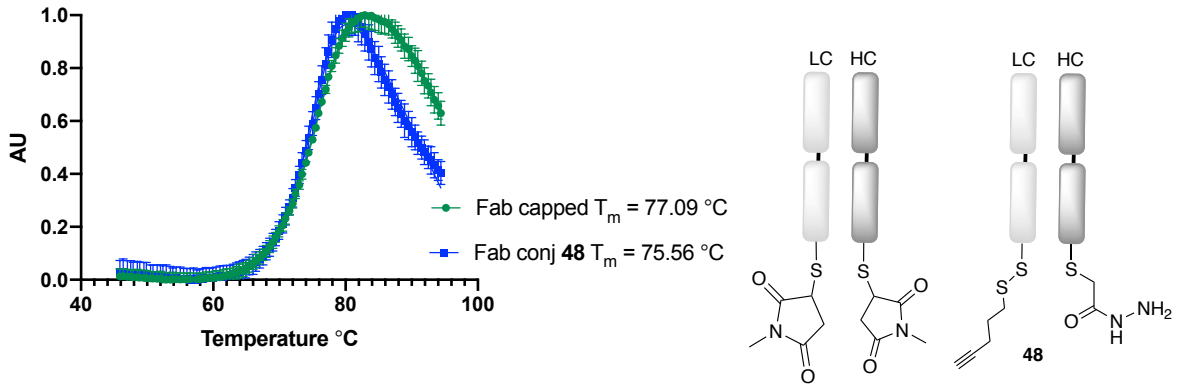

Figure 48. Thermal unfolding of capped Fab and Fab conjugate **48** was monitored using SYPRO Orange. Data was collected in presence of 4 µM Fab concentration pH 7.4 leading to rightward shift in the unfolding transition.

Currently, there are no reports in the literature of Trastuzumab Fab lacking native disulfide bonds or capped showing a thermal stability study. In one available report, full antibodies (human IgG1) containing kappa light chain were engineered to containing serine instead of cysteine and this resulted in T_m of 71 °C.[204] Another report of engineered Fabs with kappa light chain containing disulfide bonds at alternative positions or lack of them showed T_m of 78.5 °C for wild type Fab IgG1 and 72.5 °C for IgG1 without disulfide bonds.[205] A report of a mouse monoclonal antibody (H10) conjugated with various thiol specific linkers (SMCC, PEG8) resulted in T_m of the first transition state corresponding to the Fab fragment of 77.6 and 77.5 °C.[206] The lower T_m of reduced Fab in both of these reports could also be explained by the fact that these were not clinically validated antibodies which are commonly engineered to be more thermally stable. The decreased T_m for the dual modified conjugates in this study, without the native disulfide bonds was predictable as disulfide bond gives stabilising effect to the tertiary structure. Despite the lower thermal stability, the two chains are still held together through the strong intermolecular forces resulting in uninterrupted binding to the antigen as supported by the ELISA data.

4.8 Summary and conclusion

With the currently available thiol or disulfide specific reagents for antibody modification, both free thiols formed from reduction of disulfide bond are modified at the same time. A dual-modification strategy was developed in this project, where each thiol can be modified with two different payloads. Starting from the rebridged thioester, it was possible to generate disulfide and hydrazone modified species separately. The cleavage of these new species was explored to demonstrate that differentially cleavable linker can be introduced into such conjugates. The conjugate with new non-native disulfide bond was completely cleaved off at 37 °C after 4 h under cytoplasm-like conditions where the thiol concentration is high, while it remained undisturbed in blood-like conditions with low concentration of free thiol. The hydrazone bond was generated with two different linkers, yielding a cleavable (compound **58**) or a non-cleavable (compound **53**) hydrazone bond, respectively. The cleavable hydrazone bond was cleaved inside a lysosomal-like environment at 37 °C under 24 h.

In this project, it was not possible to add any of the FDA approved drugs (due to their extremely high toxicity), instead these were substituted with safer reagents such as fluorophore and PEG-biotin. It is acknowledged that once cytotoxic cargos would be added, additional stability and cleavability test would have to be performed. Despite the lack of a covalent link between the two chains, these are still held together by strong non-covalent interactions, which was confirmed by the biophysical assays. ELISA and melting point experiments demonstrated retention of binding to the antigen as well as relatively high thermal stability.

Chapter 5: Disulfide rebridging of native antibody with novel thioester

α-Chlorothioester **1** was shown to be an excellent rebridging reagent requiring near stoichiometric equivalents under mild conditions to achieve full modification of the Fab fragment. The next natural step for a rebridging reagent would be translation of the protocol onto a full antibody. If the full antibody rebridging was as successful as rebridging of the Fab, then this could be a very promising candidate for the construction of novel ADCs.

Initially, a control experiment was set up to see if reagent **1** would react non-specifically with the antibody, which could result in random addition on each chain. For that reason, a full antibody was buffer exchanged into conjugation buffer and incubated with 4.05 eq. of **1** for 1 h at 22 °C, without any initial reduction with TCEP.

The result from a control experiment (**Figure 49**) indicated that 4.05 eq. of reagent α-chlorothioester **1** did not cause any unwanted addition on native antibody, confirming that upon reducing the antibody with TCEP, α-chlorothioester **1** would react only with liberated thiols from the disulfide bonds.

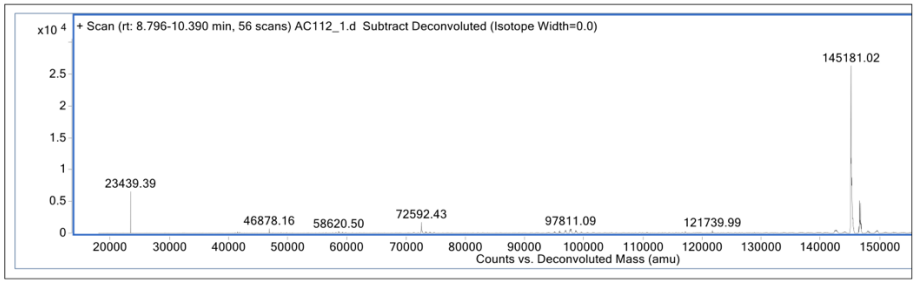

Figure 49. LCMS analysis of unreduced full antibody incubated with α-chlorothioester **1**. The presence of small peak corresponding to the LC is most likely due to LCMS fragmentation, no conjugation was observed on any of the chains. Native trastuzumab chain masses: LC expected 23438, observed 23439, HL expected 72585, observed 72592, Full Ab expected 145179, observed 145181.

To test the rebridging of full antibody, an experiment was then set out where disulfide bonds were reduced, followed by addition of reagent **1** (**Figure 50**).

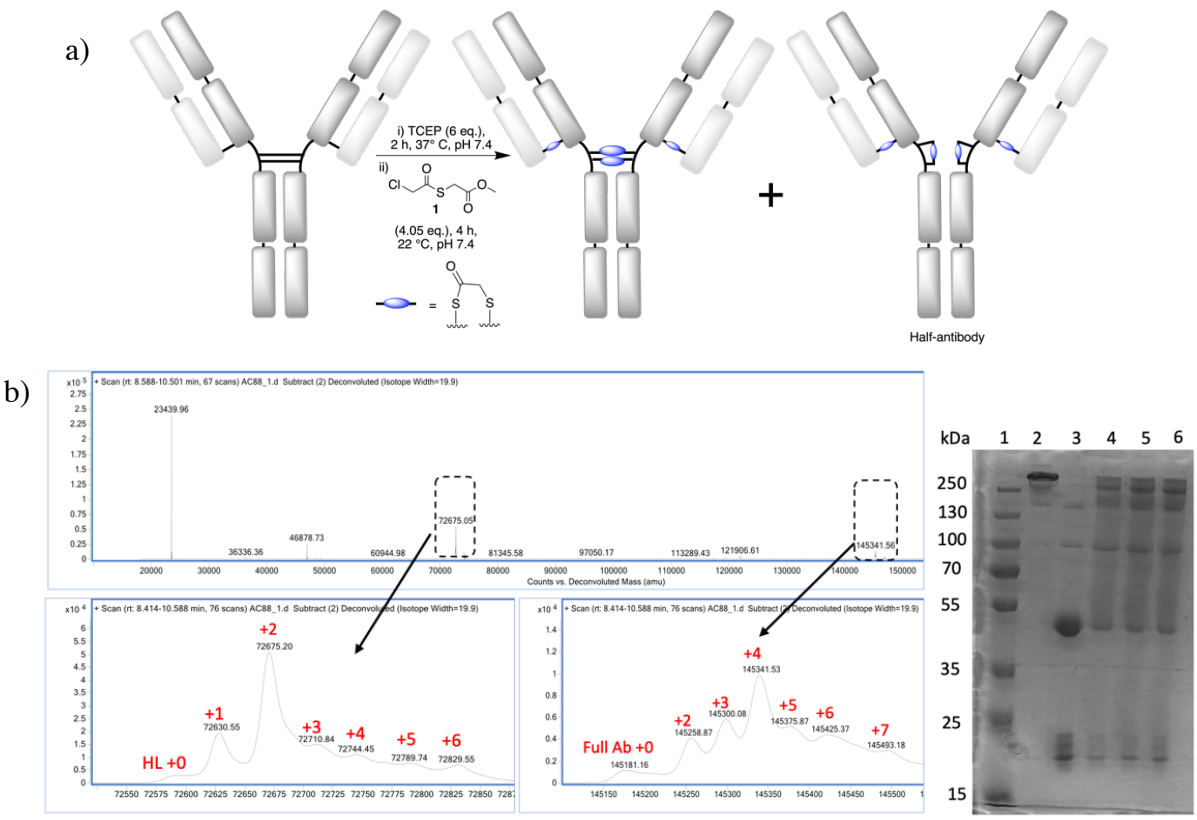

Figure 50. a) A protocol for rebridging of full antibody with α-chlorothioester **1**. The sequential bridging protocol can often yield a mixture of correctly and incorrectly rebridged half-antibody, due to formation of intrachain bridges, thus forming half-antibody, b) SDS-PAGE and LCMS analysis of full antibody rebridging with α-chlorothioester **1**. Deconvoluted ion series mass spectrum, zoomed in deconvoluted ion series mass spectrum, +0 native chain, +1/+2/+3 etc. refers to number of rebridging groups added per chain. Full rebridged antibody; mass expected 145349, mass observed 145341, HL rebridging mass expected 72672, mass observed 72675. SDS-PAGE 1 – molecular marker, 2 - native full antibody, 3 – TCEP reduction, 4 – rebridged with **1**-1 h, 5 – rebridged with **1**-2 h, 6 – rebridged with **1**-4 h.

LCMS deconvoluted spectrum shows addition of four rebridged species onto a full antibody, suggesting rebridging of four disulfide bonds. Other peaks can be assigned to modified heavy-light (HL) with double addition of the rebridging reagent (observed mass 72675) and unmodified LC (observed mass 23439). Multiple additions can also be identified on both HL and full antibody, counting to up to 3 extra additions on the full antibody. This is most likely cysteine-to-lysine transfer of the rebridged species as both would account for additional +42 mass. The double addition on HL (native HL 72588) suggests that half-antibody or disulfide scrambling has also occurred (**Figure 50**).

It was then proposed that altering conjugation conditions could produce a better selectivity of α-chlorothioester **1** on reduced full antibody. The follow up experiment included conditions such

as reducing antibody with TCEP as previously and incubation with 4.05 eq. of reagent **1** at 4 °C for 16 h and 12 °C for 5 h, however the results were largely unchanged and comparable with those achieved in the **Figure 50** (spectra not shown). This experiment was repeated with the other thioesters synthesised in this study and the results were similar, multiple addition of the bridging component was observed on HL and full antibody.

After several trials, it was clear that thioester rebridging on its own was not going to yield a clean conjugate by LCMS analysis, in contrast to that found with the Fab conjugation. The reason for that could be that despite removing an excess of rebridging reagent, the full antibody sample was left at 37 °C for 8-16 h in presence of PNGase F to promote deglycosylation of the glycans, therefore the thioester could either hydrolyse or transfer to nearby lysine in that time.

5.1 Native Chemical Ligation on full antibody

It was then suggested that the prolonged incubation of the rebridged antibody with α-chlorothioester **1** at elevated temperature is leading to the observed hydrolysis and CLT. To slow this process, it would be best to carry out the NCL functionalisation step directly before analysis. Therefore, antibody was reduced and rebridged as before, then a large excess of cysteine was added and left at 37 °C for 4 h (**Figure 51**).

a)

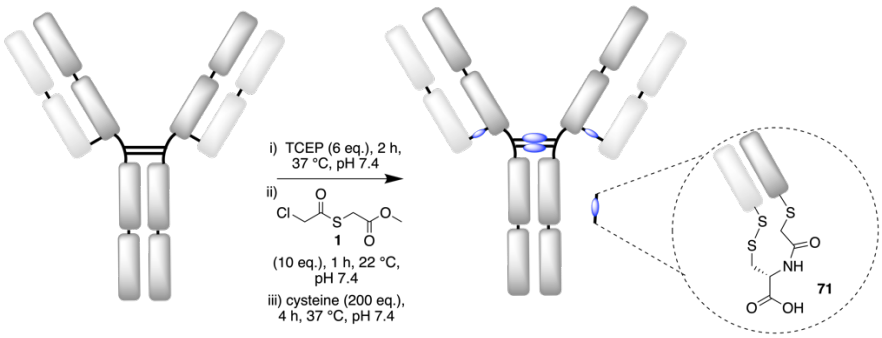

b)

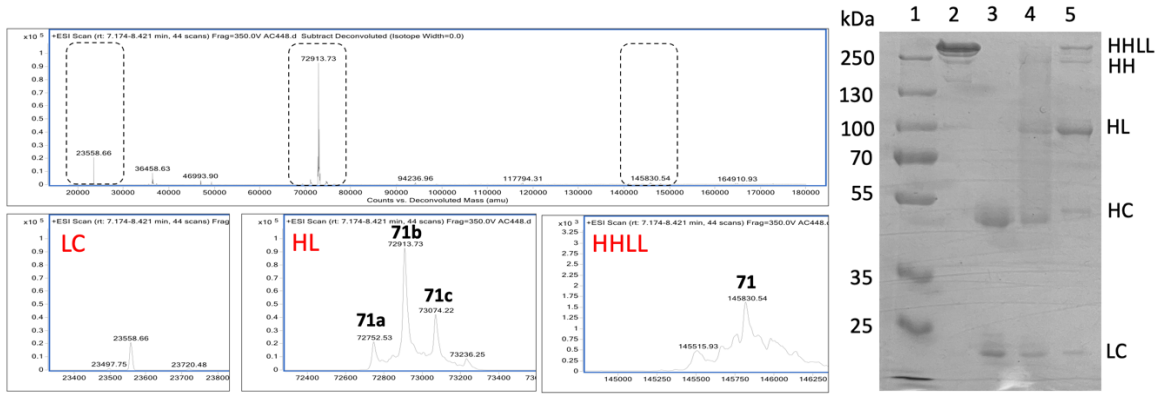

c)

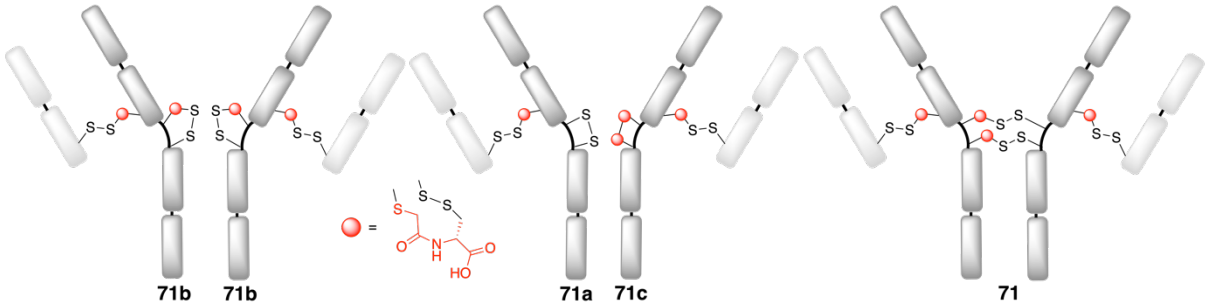

Figure 51. a) Rebridging of full antibody with α-chlorothioester **1** followed by addition of nucleophile cysteine to form a conjugate **71**, b) SDS-PAGE and LCMS analysis of forming conjugate **71**. Deconvoluted ion series mass spectrum, zoomed in deconvoluted ion series mass spectrum; LC and cysteine disulfide mass expected 23559, mass observed 23558; **79a**-HL mass expected 72746, mass observed 72752, **79b**-HL mass expected 72907, mass observed 72913, **79c**-HL mass expected 73068, mass observed 73074; **79** (HHLL) mass expected 145823, mass observed 145830. SDS-PAGE 1 – molecular marker, 2 - native full antibody, 3 – TCEP reduction, 4 – rebridging with **1**, 5 – cysteine treatment, c) Rebridging of full antibody with α-chlorothioester **1,** three possible formations observed in the HL area.

The LCMS spectra shows the main species to be the heavy-light antibody with two formation of the bridge-cysteine component **71b** (observed mass 72913) and full antibody with loading of four conjugates **71** (observed mass 145830). The LCMS is run under denaturating conditions with organic solvents which would break any non-covalent interactions, therefore HL appears are separate species, whereas in nature two HL will still be held together due to the strong intramolecular forces. Additionally, the HL species is smaller than the full antibody thus it is ionised better and it 'flies' better. The SDS-PAGE confirms that the main species are HL and full antibody (**Figure 51**).

The other minor peaks identified in the HL area correspond to HL **71a** as in **Figure 51**, **c**, where one addition of conjugate **71** is observed, mostly likely in the Fab region, and one native disulfide bond (in the hinge region) was left unreacted. The second minor species can be visualised as **71c**, where there is one formation of the conjugate **71** between two thiols. The other disulfide bond,

most likely in the hinge region, can be accounted for two bridge components and two cysteines oxidised together, with extra mass of +322. This is most likely formed due to the two regioisomers possible. In the hinge region two bridging reagents could have reacted with one heavy chain thiol by S_N2, thus the chlorine carbon would be substituted with a thiol, this would leave the labile linkage – thioester to be capped with cysteine. In that case, the two cysteines next to each other would oxidise thus forming **71c**. Due to the possible regioisomer formation, control of it will not be possible and mixture of conjugates might be formed in each reaction.

5.2 Functionalisation of rebridged full antibody with cysteine, pyridazinedione and fluorophore

To explore the NCL protocol on full antibody further, few steps were optimised namely the excess of cysteine was lowered to 50 eq. as this showed to be sufficient to achieve the same conversion as with 200 eq., then the antibody was treated with conditions as before followed by addition PD with Azide fluor 488 (**Figure 52**).

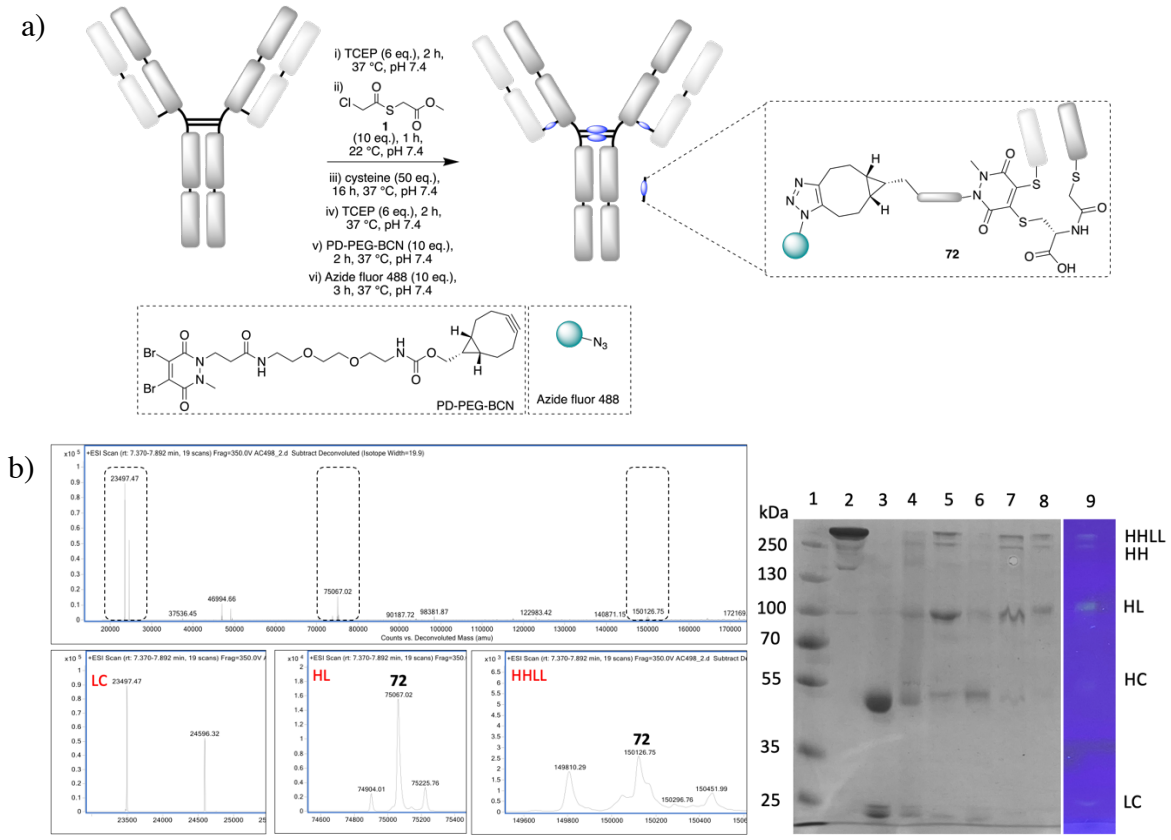

Figure 52. a) Rebridging of full antibody with α-chlorothioester **1** followed by addition of cysteine, PD-PEG-BCN and Azide fluor 488, forming conjugate **72**, b) SDS-PAGE and LCMS of conjugate **72**; Deconvoluted ion series mass spectrum, zoomed in deconvoluted ion series

mass spectrum; LC hydrolysed bridged species mass expected 23497, mass observed 23497, LC PD(Br)-BCN-Azide fluor 488 mass expected 24594, mass observed 24596; HL with one conjugate **72** and PD-BCN-Azide fluor 488 mass expected 74902, mass observed 74904, **72** (HL) mass expected 75065, mass observed 75067; HL with one conjugate **72** and bridge-cysteine-PD-BCN-Azide fluor 488-cysteine-bridge mass expected 75228, mass observed 75225; HHLL with two conjugate **72** and two PD-BCN-Azide fluor 488 mass expected 149813, mass observed 149810, **72** (HHLL) mass expected 150139, mass observed 150126. SDS-PAGE 1 – molecular marker, 2 – native full antibody, 3 – TCEP reduction, 4 – rebridging with **1**, 5 – cysteine treatment, 6 – 2nd TCEP reduction, 7 – PD-BCN addition, 8 – Azide fluor 488 addition, 9 – UV scan Azide flour 488.

The heavy light area shows a major species to be formation of two desired conjugates **72** (observed mass 75067) therefore forming half-antibody with loading of 2 (**Figure 52**). Full antibody area shows a major species with addition of four desired conjugates **72** (observed mass 150126), confirming loading of 4 for this modification. The SDS-PAGE shows that the HL and HHLL bands are the major bands in this experiment with UV scan also indicating that the fluorophore was attached mainly to the HL and HHLL. The LCMS spectra also shows two species in the LC area, one corresponding to hydrolysed bridged species while the other one is the light chain with PD-fluorophore moiety and one bromine. On the LCMS, both peaks show to be the major species; however due to their relatively small molecular size, they are ionised much better than larger species such as HL or full antibody. The SDS-PAGE confirms that these two peaks in fact are not major at all, as these are not visible on the lane 8, this is similar finding observed on the Fab fragment when using this protocol (**Figure 52**).

For the conjugates with fluorophore attached on the Fab fragment, reported in previous chapters, the absorbance readings for Abs_{280} and Abs_{505} were taken using the NanoDrop system. When the same step was taken for full antibody, it was found that the readings did not quite match, loading of 4 was not found despite LCMS data suggesting correct conjugation. Therefore, a full UV/Vis spectrum was read using spectrophotometer. Interestingly, it was observed that there was an additional small peak in the Abs_{480}, only observed in the full antibody conjugates. This finding was also confirmed with other members of the group who also detected the additional peak in their studies on full antibody conjugation with a fluorophore. It was suggested that due to multiple fluorophores attached to the antibody, the physical environment of these attached in the Fab region and hinge region are different, which might lead to shift of the fluorophore absorbance. When UV readings from Abs_{480} and Abs_{505} were combined the FAR yielded the desirable value.

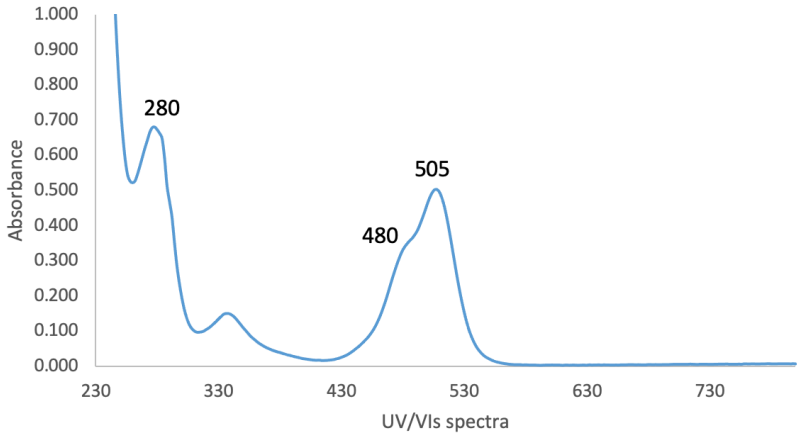

Figure 53. UV readings of the addition of Azide fluor 488 to the full antibody conjugate **72**. Absorbance readings for FAR calculations: Abs_{280} – 0.673, Abs_{480} – 0.330, Abs_{505} – 0.502. Absorbance readings for DAR calculations: Abs_{280} – 2.21 and Abs_{335} – 0.36. Calculated FAR – 3.9 and DAR – 3.7.

In the experiment where PD-PEG-BCN was added followed by click chemistry with the strained alkyne moiety and Azide fluor 488, it was important to read the Abs_{280} and Abs_{335} for the PD before the Azide fluor 488 is added, as PD will also slightly absorb at 505 nm, same as for Azide fluor 488. Therefore, DAR calculations were obtained first followed by FAR. In this experiment, DAR was 3.7 and FAR was 3.9, which is in line with the LCMS results suggesting overall DAR 4.

$$DAR = \frac{\varepsilon_{280}\ x\ Abs_{335}}{Abs_{280}\ x\ \varepsilon_{335}\ + (Cf\ x\ Abs_{335}\ x\ \varepsilon_{335})} = \frac{215380\ x\ 0.36}{2.21\ x\ 9100\ + (0.25\ x\ 0.36\ x\ 9100)} = 3.7$$

$$FAR\ of\ Abs_{505} = \frac{\frac{Abs_{505}}{\varepsilon 505}}{\frac{Abs_{280} - (Cf\ x\ Abs_{505})}{\varepsilon 280}} = \frac{\frac{0.502}{74000}}{\frac{0.673 - (0.11\ x\ 0.502)}{215380}} = 2.4$$

$$FAR\ of\ Abs_{480} = \frac{\frac{Abs_{480}}{\varepsilon 480}}{\frac{Abs_{280} - (Cf\ x\ Abs_{480})}{\varepsilon 280}} = \frac{\frac{0.330}{74000}}{\frac{0.673 - (0.11\ x\ 0.330)}{215380}} = 1.5$$

5.3 Native Chemical Ligation reaction of full antibody with TAT peptide

The conjugation of cysteine to the rebridged antibody with α-chlorothioester **1** showed a very promising result, therefore, TAT peptide was added in this experiment instead of cysteine and the previously optimised protocol was implemented.

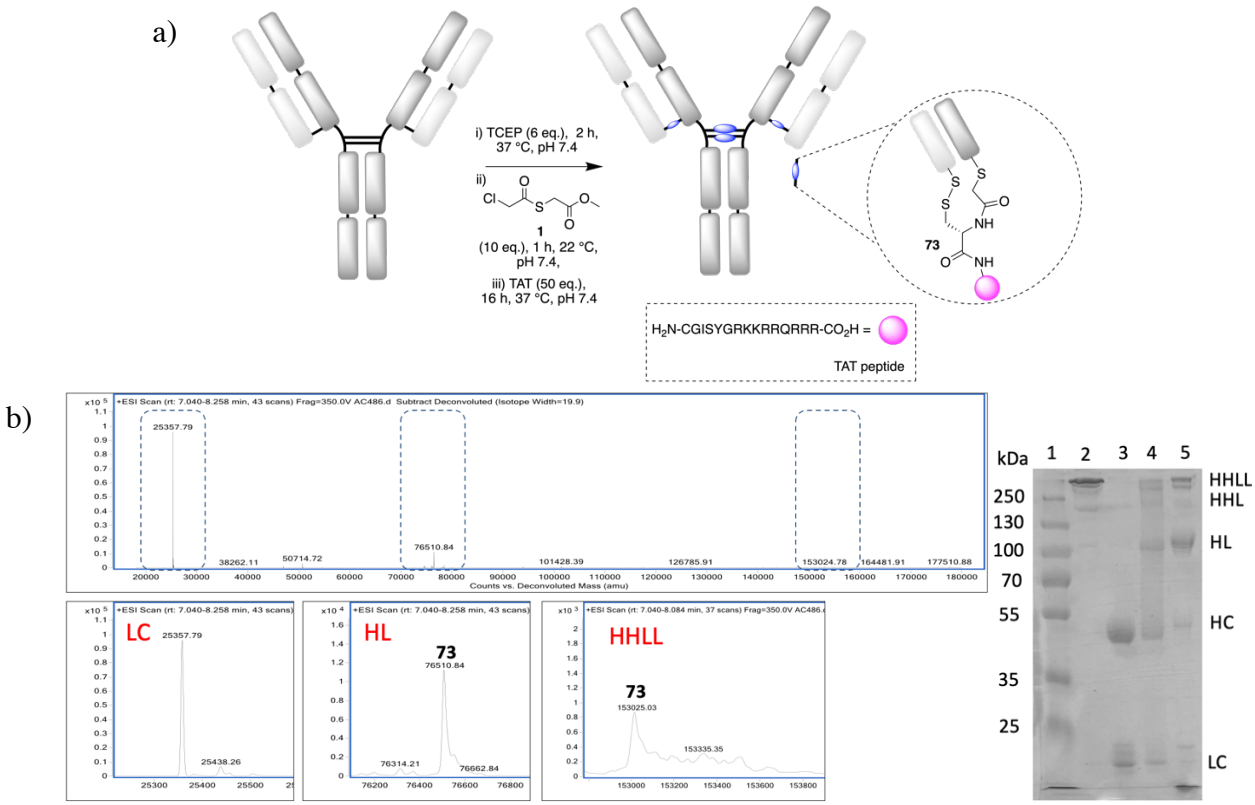

Figure 54. a) NCL strategy employed on full antibody with α-chlorothioester **1** followed by addition of TAT peptide forming conjugate **73**, b) SDS-PAGE and LCMS analysis of full antibody reaction with α-chlorothioester **1** and TAT peptide forming conjugate **73**. Deconvoluted ion series mass spectrum, zoomed in deconvoluted ion series mass spectrum; LC and TAT disulfide mass expected 25358, mass observed 25357; **73** (HL) mass expected 76509, mass observed 76510; **73** (HHLL) mass expected 153027, mass observed 153024. SDS-PAGE 1 – molecular marker, 2 – native full antibody, 3 – TCEP reduction, 4 – rebridging with **1**, 5 – TAT treatment.

The overall LCMS results show one peak in the HL area corresponding to formation of two conjugates **73** thus forming half-antibody (observed mass 76510) and one major peak in the full antibody area corresponding to four addition of conjugate **73** (observed mass 53024), resulting in overall calculated loading of 4 (**Figure 54**). The peak in the LC area can be accounted for TAT peptide forming a disulfide bond with LC thiol (observed mass 25357). The LCMS size of the peak is relatively high but again this is due to the LC being ionised much better than larger species. Additionally, SDS-PAGE shows that the major bands are the HL and HHLL conjugates, with a negligible amount in the LC.

The protocol was expanded further by reducing the new non-native disulfide bond and subsequently reacting that with PD-PEG-BCN.

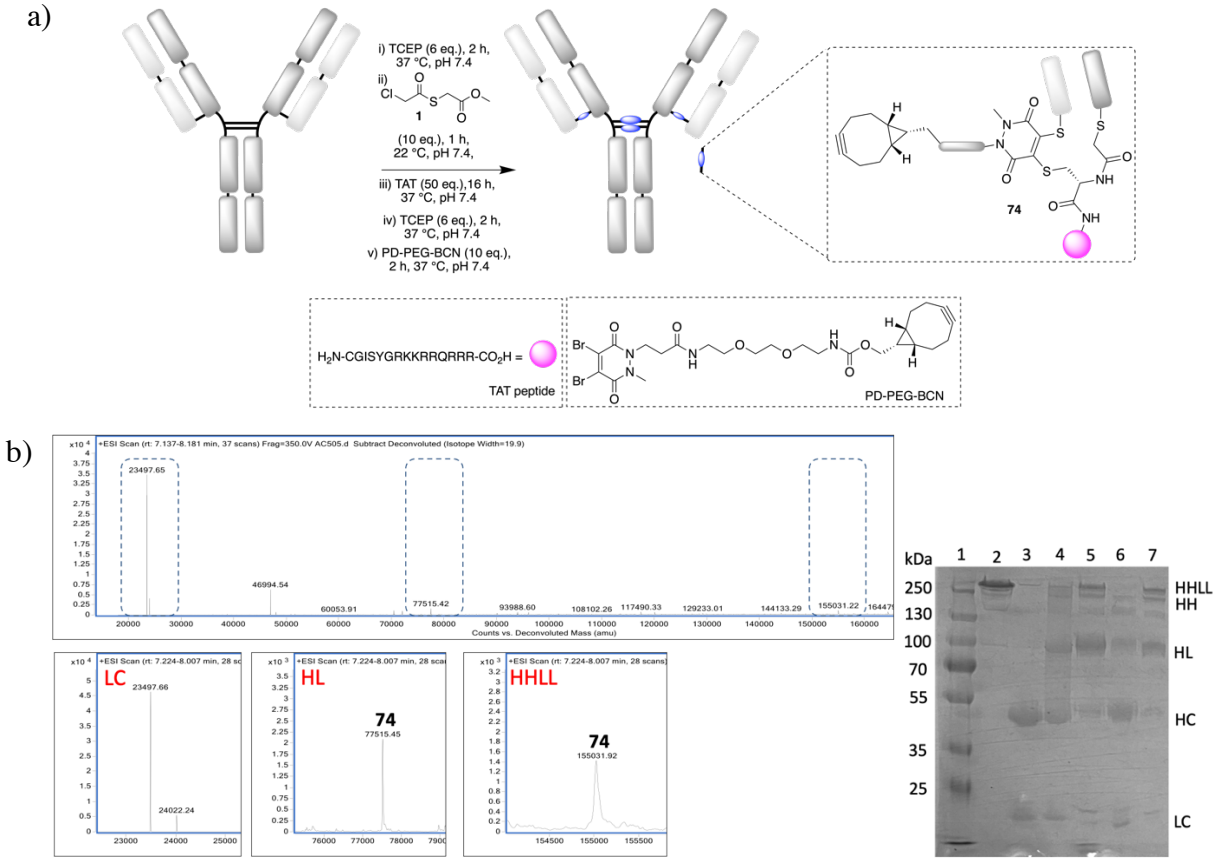

Figure 55. a) NCL strategy employed on full antibody with α-chlorothioester **1** followed by addition of TAT peptide and PD-PEG BCN forming conjugate **74**, b) SDS-PAGE and LCMS analysis of conjugate **74**; Deconvoluted ion series mass spectrum, zoomed in deconvoluted ion series mass spectrum; LC hydrolysed bridged species mass expected 23497, mass observed 23497, LC and PD(Br)-PEG-BCN mass expected 24019, mass observed 24022; **74** (HL) mass expected 77513, mass observed 77515; **74** (HHLL) mass expected 155035, mass observed 155031. SDS-PAGE 1 – molecular marker, 2 – native full antibody, 3 – TCEP reduction, 4 – rebridging with **1**, 5 – TAT treatment, 6 – 2nd TCEP reduction, 7 – PD-PEG-BCN addition.

The LCMS spectra shows full modification for both HL (observed mass 77515) and full Ab (observed mass 155031) with conjugate **75**, resulting in calculated loading (DAR) of 4. The loading was further calculated by measuring the absorbance for the PD moiety and this resulted in DAR of 3.5. This is also supported by the SDS-PAGE where HL and HHLL bands are the major species (**Figure 55**). In the LC area on the LCMS spectra, there is one peak corresponding to the hydrolysed bridged species (observed mass 23497) and the second peak is the addition of the PD-PEG-BCN-Br (observed mass 24022). This is a similar observation on the LC area as with other conjugations with TAT peptide and PDs or DBMs. These species are naturally ionised better due to their relatively smaller sizes, but LCMS is not quantitative therefore SDS-PAGE is a secondary tool to confirm that these are in fact minor occurrences.

$$DAR = \frac{\varepsilon_{280}\ x\ Abs_{335}}{Abs_{280}\ x\ \varepsilon_{335}\ + (Cf\ x\ Abs_{335}\ x\ \varepsilon_{335})} = \frac{215380\ x\ 0.16}{1.22\ x\ 9100 +\ (0.25\ x\ 0.36\ x\ 9100)} = 3.5$$

To fully develop the protocol for antibody modification through NCL with TAT peptide, PD-PEG-BCN was functionalised with a fluorophore through SPAAC.

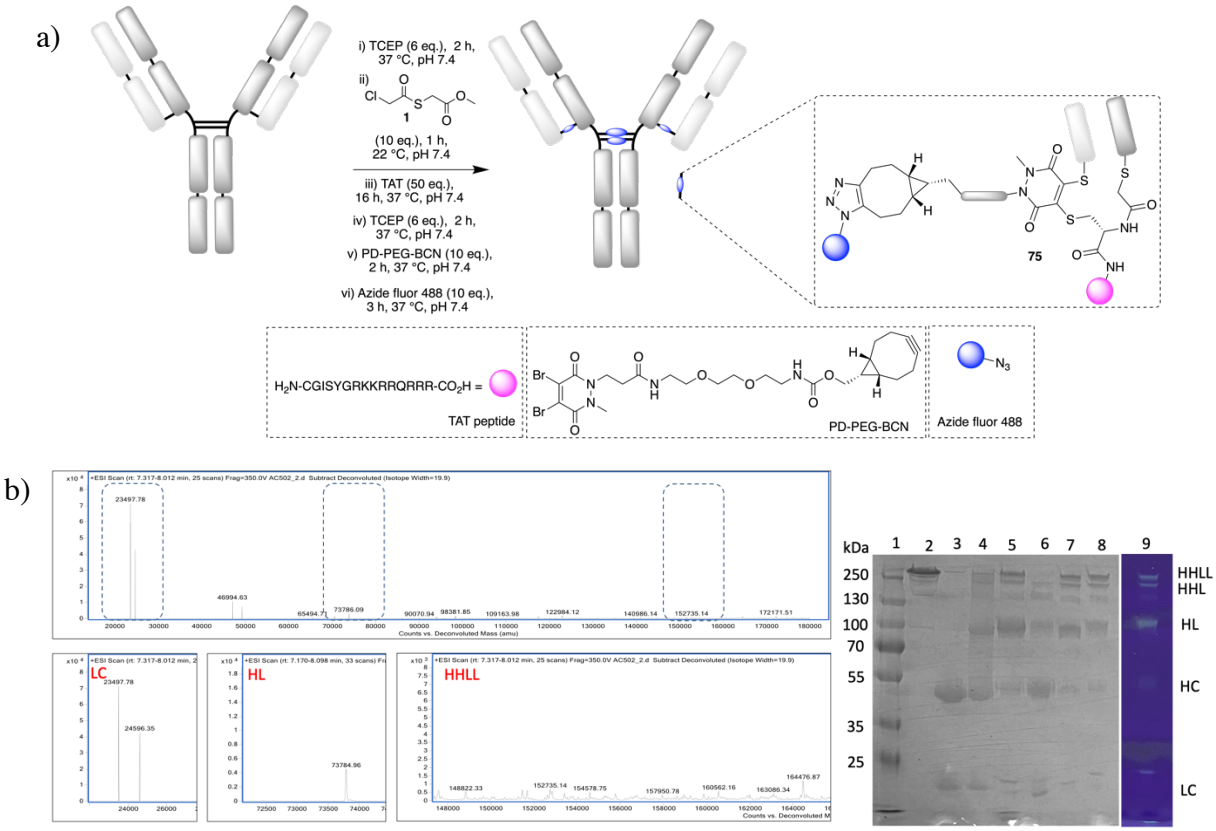

Figure 56. a) NCL strategy employed on full antibody with α-chlorothioester **1** followed by addition of TAT peptide, PD-PEG BCN and Azide fluor 488 forming conjugate **75**, b) SDS-PAGE and LCMS analysis conjugate **75**; Deconvoluted ion series mass spectrum, zoomed in deconvoluted ion series mass spectrum; LC hydrolysed bridged species mass expected 23497, mass observed 23497, LC with PD(Br)-PEG-BCN and Azide fluor mass expected 24594, mass observed 24596; HL peak mass observed 73784 cannot be identified. The expected mass for HL with two conjugates **75** was 78663, this mass is not observed. The expected mass for HHLL with four conjugates **75** was 157335, this mass is not observed. SDS-PAGE 1 – molecular marker, 2 – native full antibody, 3 – TCEP reduction, 4 – rebridging with **1**, 5 – TAT treatment, 6 – 2nd TCEP reduction, 7 – PD-PEG-BCN addition, 8 – Azide fluor 488 addition, 9 – UV scan.

The LCMS for this experiment was difficult to interpret, neither HL or HHLL area showed desired conjugate **75**, the LC area showed again hydrolysed bridged species and one addition of PD reagent still with one bromine attached (**Figure 56**). This experiment was repeated twice, and the same outcome was observed. The SDS-PAGE indicated that the HL and HHLL bands are the main species. Additionally, UV scan of the gel showed a fluorescence therefore adding another

level of confidence that the Azide fluor 488 was attached to the HL and HHLL species. Based on the intermediate steps for this conjugate where either just TAT peptide or TAT peptide and PD was added, the LCMS spectra showed the desired outcome. The loading and combined fluorophore reading indicated DAR of nearly 4 for the formation of conjugate **75** (**Figure 57**). The DAR and FAR readings were comparable between the repeats of this experiment. Perhaps the denaturating conditions of the LCMS have a negative impact on fluorophore addition on this conjugate and Native MS would be a better analytical method to analyse these results.

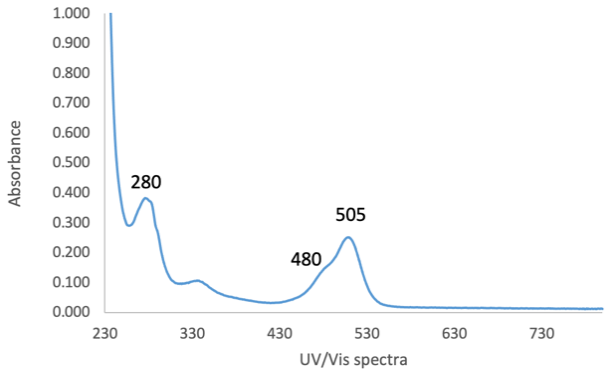

Figure 57. UV readings of the addition of Azide fluor 488 to the full antibody conjugate **75**. Absorbance readings for FAR calculations: Abs_{280} – 1.11, Abs_{480} – 0.56, Abs_{505} – 0.89. Absorbance readings for DAR calculations: Abs_{280} – 2.52 and Abs_{335} – 0.37. Calculated FAR – 4.2 and DAR – 3.4.

$$FAR\ of\ Abs_{505} = \frac{\frac{Abs_{505}}{\varepsilon_{505}}}{\frac{Abs_{280} - (Cf\ x\ Abs_{505})}{\varepsilon_{280}}} = \frac{\frac{0.890}{74000}}{\frac{1.11 - (0.11\ x\ 0.890)}{215380}} = 2.6$$

$$FAR\ of\ Abs_{480} = \frac{\frac{Abs_{480}}{\varepsilon_{480}}}{\frac{Abs_{280} - (Cf\ x\ Abs_{480})}{\varepsilon_{280}}} = \frac{\frac{0.560}{74000}}{\frac{1.11 - (0.11\ x\ 0.560)}{215380}} = 1.6$$

$$DAR = \frac{\varepsilon_{280}\ x\ Abs_{335}}{Abs_{280}\ x\ \varepsilon_{335}\ + (Cf\ x\ Abs_{335}\ x\ \varepsilon_{335})} = \frac{215380\ x\ 0.37}{2.51\ x\ 9100\ + (0.25\ x\ 0.37\ x\ 9100)} = 3.4$$

Despite the poor quality of the LCMS spectra for this assay, the functionalisation of the conjugate **7** on full antibody through NCL with *N*-terminal cysteine peptide as well as further thiol specific reagent is still a viable and achievable option. Loading of 4 was clearly observed when just TAT peptide was added and further functionalised with PD-PEG-BCN, which was the anticipated

result. The failure to obtain clear LCMS for the conjugate **75** was most likely due multiple regioisomers formation thus making the analysis challenging under denaturating conditions, therefore native MS would give an overall conjugate analysis.

5.4 Conclusion

In this project, the promising results of rebridging with thioesters and subsequent functionalisation of the new thioester bond on the Fab fragment demonstrated a vast extension of possibilities that can be achieved once the thioester moiety is installed between the two chains. The protocols were then translated onto a full antibody; however, despite overall promising results, these require more optimisation to achieve a clean conjugate. Implementing alternative characterisation methods could also be advantageous here.

The full antibody rebridged with α-chlorothioester **1** resulted in the desired species, however the thioester moiety had to be reacted with cysteine or an *N*-terminal cysteine peptide immediately through NCL, before analysis. The CPP was successfully installed on full antibody resulting in major species having loading of four peptides per antibody (DAR 4). Conjugates like that could potentially improve penetration to solid tumour cells, which is quite often challenging with just antibody itself. The antibody-peptide conjugate was further functionalised with PDs, which also resulted in desired species with an approximate loading of four. Taking advantage of the strained alkyne on the PD it was further modified with a fluorophore, however, the LCMS were difficult to characterise due to the challenge presented by the multiple regioisomers on full antibody. However, SDS-PAGE, UV scan and DAR/FAR calculations suggested that the formation of desired conjugate has occurred, nevertheless this protocol still requires further work. The dual conjugation strategy with hydrazine was also tested on the full antibody and this resulted in a mixture of regioisomers being formed (data not included), which are problematic to analyse with the tools available at the time of this project.

6.0 Conclusion and future outlook

This thesis has attempted to introduce a panel of disulfide rebridging reagents that each consisted of two functional groups with varying cysteine reactivity. The conjugation mechanism with cysteine included S_N2, conjugate addition and S_NAr that as a result rebridged the reduced disulfide bonds of Fab fragment efficiently by inserting 'labile-stable' linkage allowing for robust and reliable platform. The stable linkage inserts a thioether bond, whilst the labile one consists of a thioester that in turn allows for further functionalisation. The native chemical ligation system used here permits for attachment of *N*-terminal cysteine containing peptides which is a very convenient approach to generate antibody fragment-peptide conjugates thus eliminating the need to produce a *C*-terminal thioester. The successful insertion of CPP *via* NCL onto Fab fragment and full antibody could be enhanced by addition of a cytotoxic drug, which could improve tumour drug penetration. The newly developed trifunctional PD reagents can be equipped with two different drugs. The advantage of having two toxins with orthogonal mode of action is that these could inhibit mechanisms of drug resistance which is also a problem in oncological therapy.

The second system makes use of hydrazine as the ligating nucleophile that enables attachment of two separate cargos on each of Fab cysteine, the cargos can be designed to be cleavable at variable cellular environments, which gives an advantage towards the targeted treatment. The two toxins approach with two different targets could also be used in the dual-functionalisation protocol. The created platforms could also allow for multi-labelling of protein conjugates with cleavable fluorophores or radiolabelling which can be used for imaging applications. Initial data of disulfide rebridging on full antibody with four of the reagents is promising although, it still needs further work as four disulfide interchain found in full native antibody is a more complex system.

We believe that these two strategies developed here have expanded the scope of disulfide rebridging techniques, and also demonstrated the use of these practical methods which undoubtfully will have useful application in the field of antibody bioconjugation. Further functionalisation with relevant biological molecules such as drugs is an exciting next step that would further clinically validate the conjugates.

Some of the future work could also include:

a) Kinetics study could be performed between each thioester and the *N*-Boc-cysteine-OMe. Based on small molecule study with cysteine and each thioester we know where the initial conjugation takes place. However, in nearly all the cases the yield of the final product suggested that the reaction did not go to completion as starting material was also isolated. This is most likely due to the oxidation of thiol rendering the cysteine inactive, therefore small amount of reducing agent could be added, therefore allowing for completion of the reaction.

b) Small molecule study between α-chlorothioester (and other bis-electrophiles) and *N*-terminal cysteine-OMe could be undertaken to see whether transthioesterification will take place first between the cysteine thiol and the thioester **1**, followed by *S*-to-*N* acyl transfer forming an amide bond. Then it was proposed that free thiol would attack the chloride carbon position and thus cyclise the newly synthesised molecule. This could serve as a new method for *N*-terminal cysteine modification of peptides and proteins.

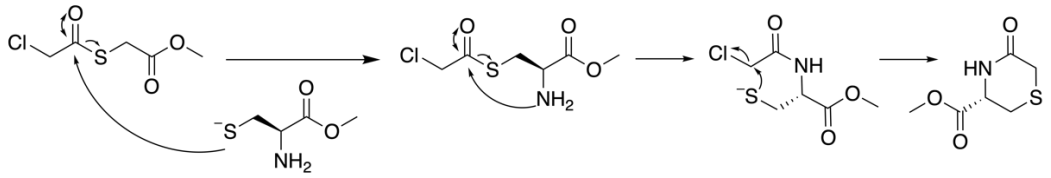

c) The aryl-chloro thioester **6** containing branched aryl group performed well on the Fab model for rebridging and stability. The experiment to determine regioselectivity showed that even with 100 eq. of cysteine nucleophile, the thioester bond was not fully cleaved off, suggesting a very stable linkage. Therefore, this could be used in an advantage to generate a two-carbon linker with a payload attached on it. The payload or a functional moiety could be added to the phenyl ring thus creating a functional disulfide rebridging reagent. Similar approach could be undertaken for the aryl-fluoro thioester **5** that also showed to be less prone to hydrolysis and requiring large excess of cysteine to break the thioester bond. Here also the phenyl ring could be functionalised with a payload. The alkene thioester **3** is also an intriguing compound, the payload could be inserted either at the α- or β-carbon. Functionalised alkene with an attachment on β-carbon and thioester has been reported but it was not tested as disulfide rebridging reagent,[161] alkene with a payload attached at the α-carbon has been reported for disulfide rebridging[105] but it does not contain thioester as second point of attachment, therefore these would be interesting compounds to synthesise and test on an antibody.

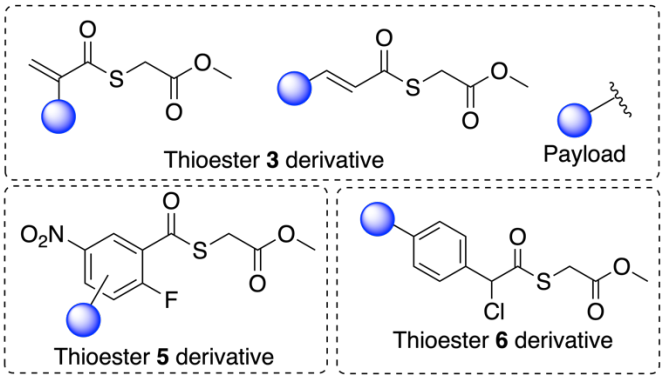

d) Chapter 3 explored the possibilities of an NCL strategy with cysteine and *N*-terminal cysteine peptide for functionalisation of the thioester moiety. After the first round of α-chlorothioester **1** followed by addition of the TAT peptide, a new non-native disulfide bond is generated. This was modified by thiol-specific reagents such as PDs and DBMs. Instead of these functional reagents, another α-chlorothioester **1** can be added to generate a second thioester moiety that again can be reacted with cysteine or an *N*-terminal cysteine peptide through NCL, adding yet another peptide. Preliminary data for this strategy with cysteine and TAT peptide showed that at least two rounds of addition (bridging component and cysteine) can be added, therefore we strongly believe that this is achievable (data not shown). The limits of the protocol as to how many peptides can be added are currently not explored.

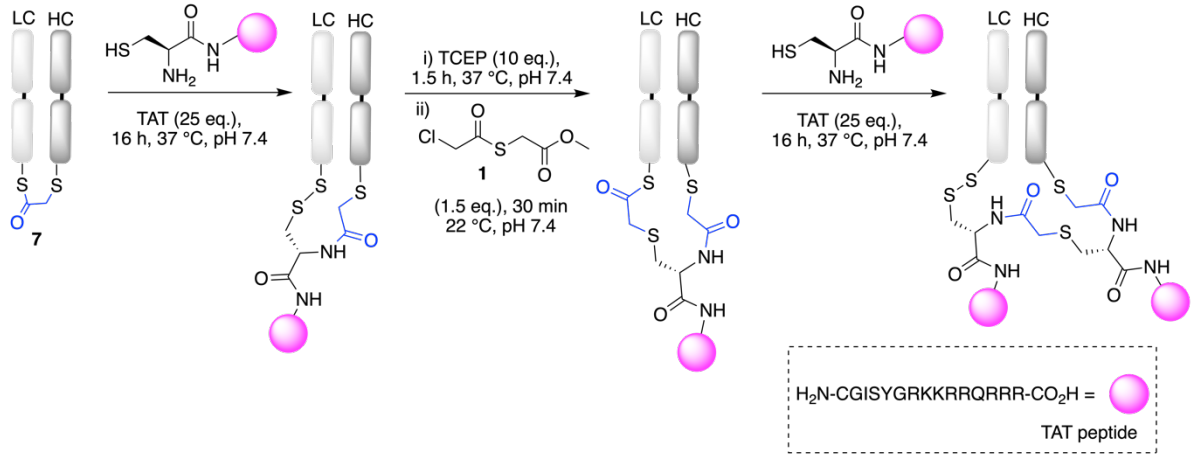

e) The dual conjugation protocol with hydrazine allowed for modification of two thiols liberated from a disulfide bond, which is usually very difficult to achieve with current approaches. The method worked well on the Fab fragment, and initial studies were performed on native antibody, however, these resulted in a large mix of species which was difficult to interpret by LCMS (data not shown). It was expected that there will be a mixture of species due to the possible regioisomer formed from α-chlorothioester **1**. However, more work needs to be done to optimise this reaction and correctly characterise the results.

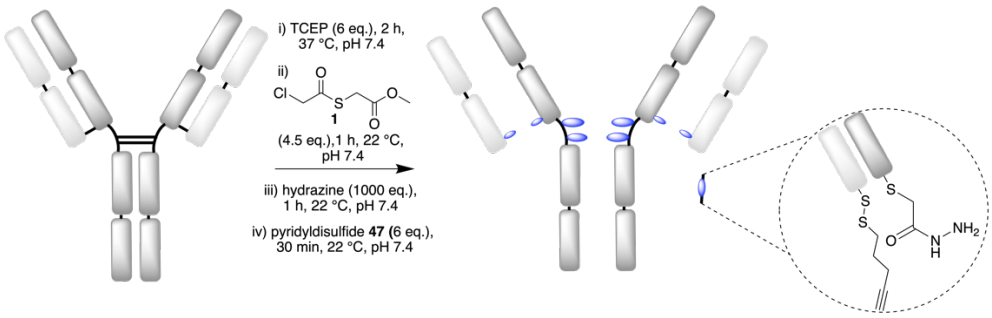

f) Both of the modification strategies explored here could be functionalised with an imaging agent. To study this, HER2-positive SKBR3 cells and HER2-negative MCF7 cells could be treated with conjugates containing fluorophore as was explored in this study, and internalisation of the ADC could be tracked by confocal microscopy imaging. The desirable outcome would show correct labelling and internalisation by the HER2-positive cells but not the HER2-negative cells. This would provide additional evidence, alongside an ELISA study that the dual conjugation protocol does not impact the antigen binding or internalisation.

g) To determine the wide use of the conjugate formed with CPP and generate bioactive ADCs, functionalisation of the PD linker with a cytotoxic warhead should also be undertaken. Monomethyl auristatin E (MMAE) could be selected as a payload as it is commonly used for generation of approved ADCs. An azide-functionalised MMAE payload comprised of cathepsin-cleavable valine-citrulline motif is key to allow to traceless release of the MMAE payload from the antibody followed by internalisation by the target cell.

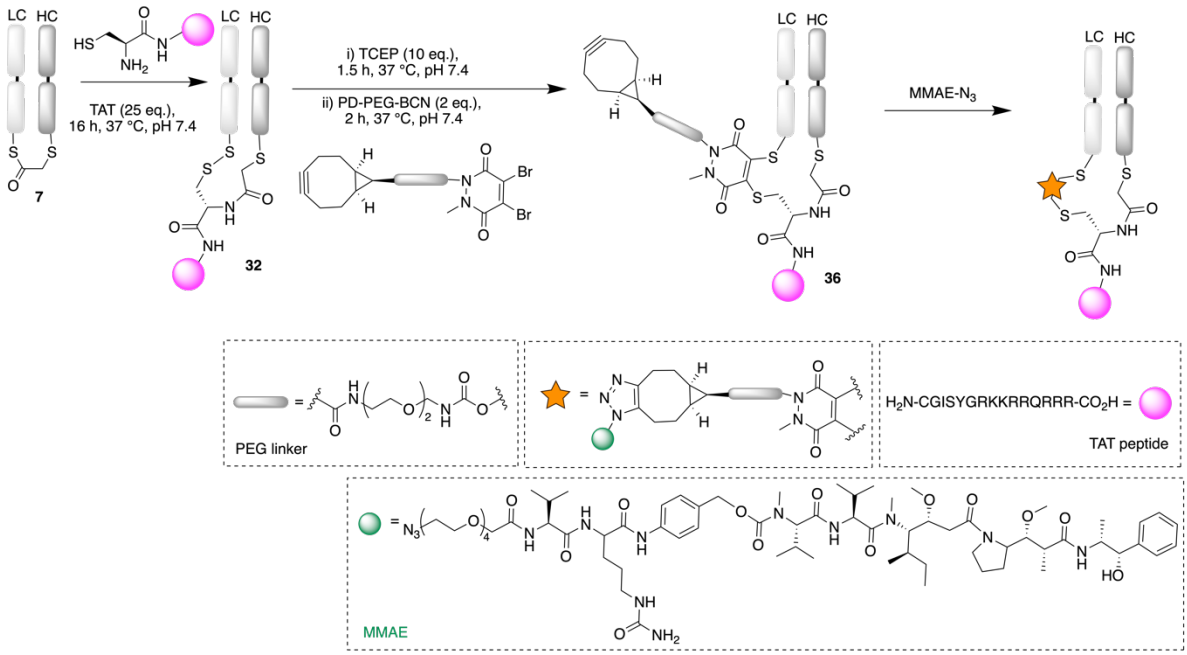

h) The functionalisation of thioester moiety with *N*-terminal cysteine peptide was showed to work well on both Fab and native antibody. The next natural step would be to test for the conjugate's aggregation behaviour, whilst having a cytotoxin attached. Hydrophobic entities such as linkers used for development of ADC can often induce protein aggregation. To explore that, conjugates would have to be analysed through size-exclusion chromatography to detect the level of aggregation, and this should be compared to unmodified protein. The analytical characterisation could also determine the DAR of the conjugates, which could add another level of confidence. Lastly, *in vitro* cytotoxicity of the conjugate with and without attached drug should also be studied again on HER2-postive and HER2-negative cell lines. Concentration-dependent cytotoxicity compared to trastuzumab alone could also be checked. Additionally, throughout this project only trastuzumab antibody was used, however other antibodies could also be used for verification of applicability of the methods developed here onto different clinical antibodies, such as Rituximab or Cetuximab.

7. Experimental section

7.1 Chemical synthesis general remarks

All chemical reagents and solvents were purchased from commercial sources; Sigma UK, Fisher UK or VWR UK and used as per manufacturer instructions. Buffers were prepared with double-deionised water and filter sterilised (0.20 μm). All chemical reactions were carried out at atmospheric pressure, under argon. Room temperature (RT) is defined as between 15-25 °C. The term *in vacuo* refers to organic solvent removal using Buchi rotary evaporator between 15-60 °C. Chemical reactions were monitored using thin layer chromatography (TLC) on pre-coated silica gel plates (254 μm) purchased from VWR, UK. Detection of synthesised compounds was done by UV (254 nm and 365 nm) or chemical stain ($KMnO_4$, ninhydrin, bromocresol blue). Flash column chromatography was carried out using pre-loaded FlashPure Eco Flex column on Biotage Isolera Spektra One flash chromatography system. ^{1}H NMR and ^{13}C NMR were obtained at ambient temperature on a Bruker Advance AMX600 instrument operating at 600 MHz or 700 MHz ^{1}H and 150 MHz for ^{13}C in the stated solvent. Chemical shifts (δ) are reported in parts per million (ppm) and coupling constants (*J*) in Hertz (Hz). The multiplicity of each signal is indicated as s-singlet, d-doublet, t-triplet, q-quartet, quin-quintet, m-multiplet (i.e., complex peak obtained due to overlap) or a combination of these. All assignments were made with the aid of DEPT, COSY, HSQC, HMBC, or NOESY corelation experiments. Infra-red spectra were recorded on a Bruker ALPHA FT-IR spectrometer operating in ATR mode, with frequencies given in reciprocal centimetres (cm^{-1}). The absorptions are characterised as s (sharp), br (broad), m (medium), w (weak). Melting points were taken on a Gellenkamp apparatus and are uncorrected. High and low resolution mass spectra were recorded on a VG70 SE mass spectrometer, operating in modes ESI, EI, or CI (+ or -) depending on the sample, at the Department of Chemistry, University College London. Buffers used in organic synthesis were prepared with double-deionised water and filter sterilised (0.20 μm); 50 mM Phosphate Buffer pH 6.75; 5 mM glutathione in 50 mM Phosphate Buffer, pH 6.5.

7.1.1 Synthesis and characterisation of compounds

Methyl 2-((2-chloroacetyl)thio)acetate (1)

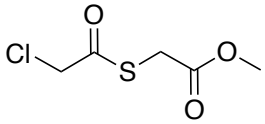

Methyl thioglycolate (0.28 mL, 3.14 mmol, 1.0 eq.) and triethylamine (0.44 mL, 3.14 mmol, 1.0 eq.) were combined in DCM (2.0 mL). The mixture was then added dropwise over 2 h into a stirring solution of chloroacetyl chloride (0.75 mL, 9.43 mmol, 3.0 eq.) in DCM (10.0 mL) and this was left ON. The reaction was performed at RT, under argon atmosphere and constant agitation. The solvent was then removed *in vacuo* and purification by column chromatography (gradient elution from 100% cyclohexane to 40% EtOAc in cyclohexane) afforded the target compound as light-yellow oil (484 mg, 2.65 mmol, 84% yield).

^{1}H NMR (700 MHz, $CDCl_3$) δ_H 4.22 (s, 2H, CH_2Cl), 3.72 (s, 2H, CH_2S), 3.71 (s, 3H, OCH_3); ^{13}C (150 MHz, $CDCl_3$) δ_C 193.2 (S*C*(O)), 168.6 (O*C*(O)), 53.1 (O*C*H$_3$), 47.9 (*C*H$_2$Cl), 31.7 (S*C*H$_2$); IR (oil) V_{max}/cm^{-1} 3003 (C-H), 2955 (C-H), 1794 (C=O), 1680 (C=O); LRMS (ESI) *m/z* (%) 183.0 ([^{35}M+H]$^+$, 100), 185.0 ([^{37}M+H]$^+$, 30); HRMS (ESI) *m/z* calculated for [$C_5H_7{}^{35}ClO_3S$] 182.9883, observed 182.9888.

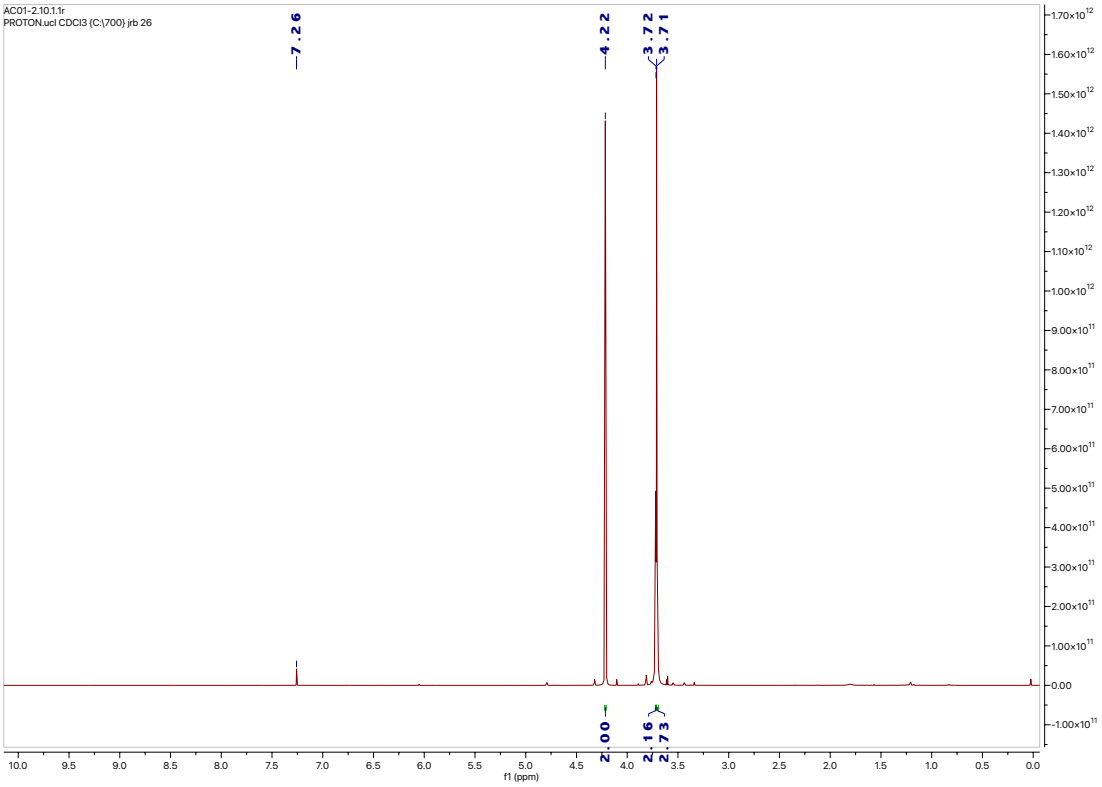

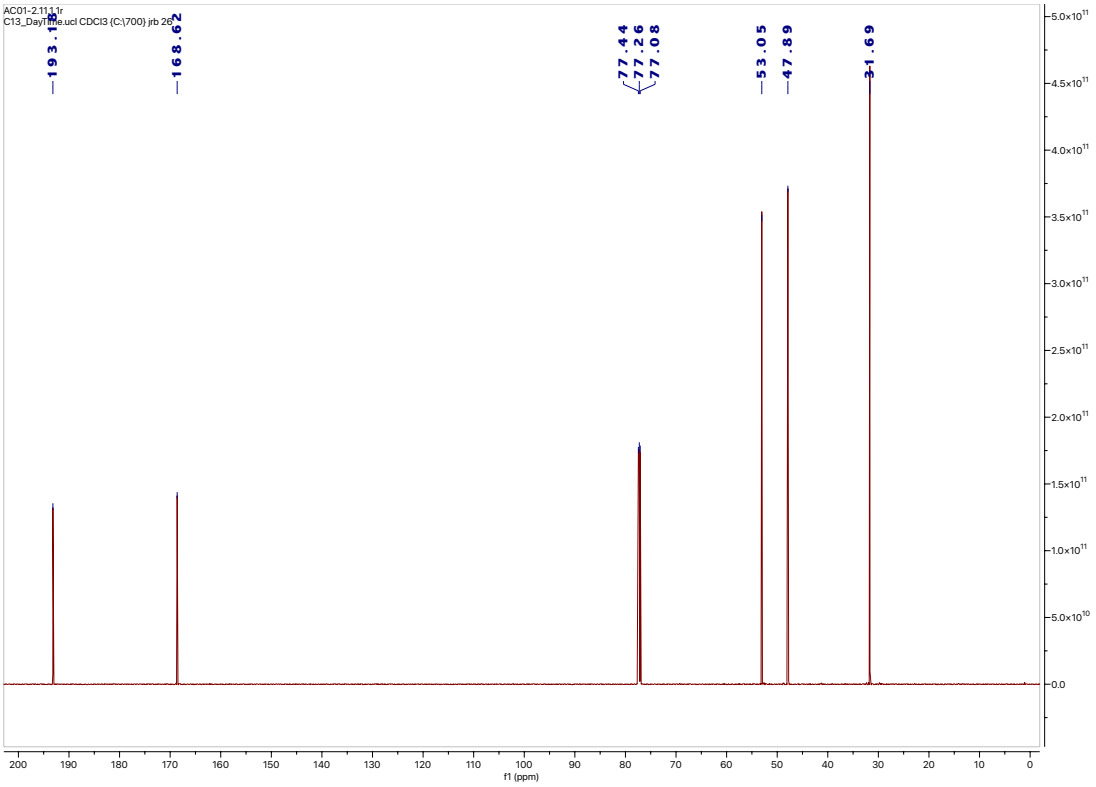

Methyl 2-((2-bromoacetyl)thio)acetate (2)

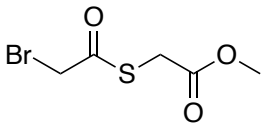

Methyl thioglycolate (0.20 mL, 2.24 mmol, 1.0 eq.) and triethylamine (0.31 mL, 2.24 mmol, 1.0 eq.) were combined in DCM (2.0 mL). The mixture was then added dropwise over 2 h time into a stirring solution of bromoacetyl bromide (0.98 mL, 11.2 mmol, 5.0 eq.) in DCM (10.0 mL) and this was left ON. The reaction was performed at RT, under argon atmosphere and constant agitation. The solvent was then removed *in vacuo* and purification by column chromatography (gradient elution from 100% cyclohexane to 40% EtOAc in cyclohexane) afforded the target compound as light-yellow oil (209 mg, 0.92 mmol, 41% yield).

^{1}H NMR (700 MHz, $CDCl_3$) δ_H 4.08 (s, 2H, CH_2Br), 3.76 (s, 2H, CH_2S), 3.75 (s, 3H, OCH_3); ^{13}C (150 MHz, $CDCl_3$) δ_C 191.6 (S*C*(O)), 168.7 (O*C*(O)), 53.1 (O*C*H$_3$), 33.1 (S*C*H$_2$), 32.3 (*C*H$_2$Br); IR (oil) V_{max}/cm^{-1} 3001 (C-H), 2953 (C-H), 1738 (C=O), 1678 (C=O); LRMS (ESI) *m/z* (%) 249.0

([^{79}BrM + Na]$^{+}$, 100), 250.0 ([^{81}BrM + Na]$^{+}$, 100), 228.0 ([M+H]$^{+}$, 15); HRMS (ESI) *m/z* calculated for [$C_5H_7{}^{79}BrO_3S$] 225.9372, observed 226.9372.

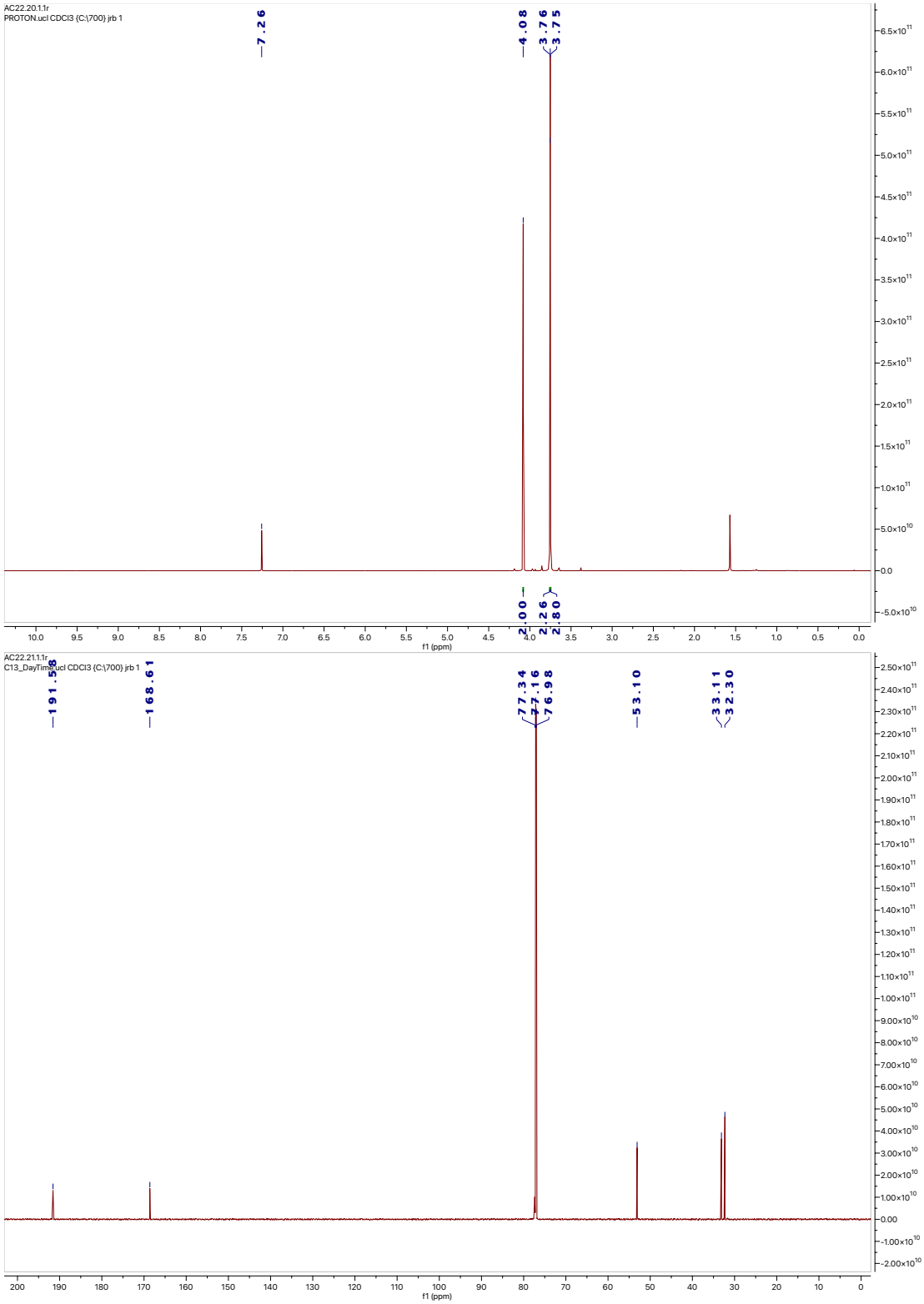

Methyl 6-(methoxycarbonyl)-2,2-dimethyl-4,10-dioxo-3-oxa-8,11-dithia-5-azatridecan-13-oate (S1) and methyl *N*-(*tert*-butoxycarbonyl)-*S*-(2-chloroacetyl)cysteinate (S2)

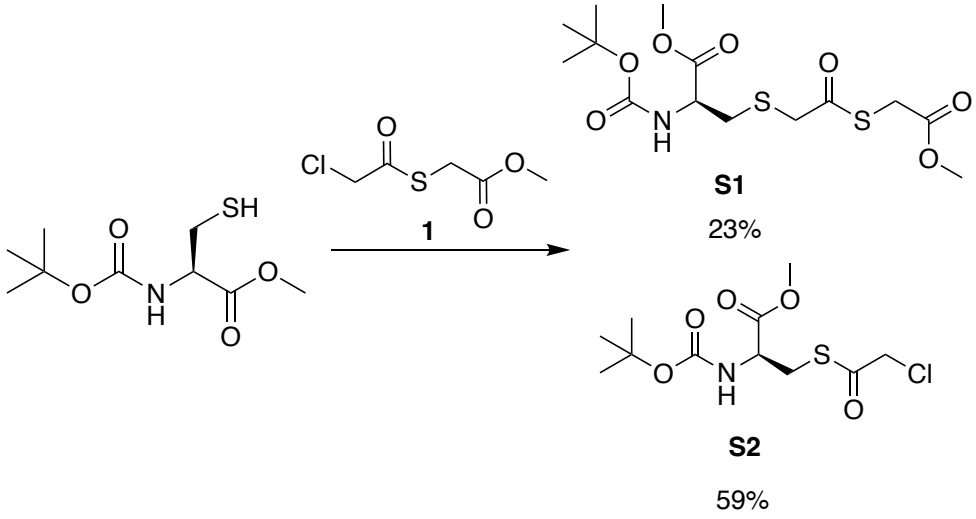

Methyl 2-((2-chloroacetyl)thio)acetate **1** (40 mg, 0.24 mmol, 1.1 eq.) was dissolved in 0.5 mL of MeCN followed by addition of 0.7 mL of 50 mM Phosphate Buffer pH 6.75 (addition of MeCN will increase pH to 7.4). *N*-Boc-L-cysteine methyl ester (50 mg, 0.22 mmol, 1.0 eq.) was then added and the mixture was stirred at RT for 3 h. The solvent was then removed *in vacuo* and purification by column chromatography (gradient elution from 100% cyclohexane to 30% EtOAc in cyclohexane) afforded compounds **S1** and **S2**.

S1 (clear oil, 19.8 mg, 0.05 mmol, 23% yield): ^{1}H NMR (600 MHz, $CDCl_3$) δ_H 5.41 (s, 1H, N*H*), 4.61-4.60 (m, 1H, C*H*), 4.24 (s, 2H, CH_2SCH_2), 3.78 (s, 3H, OCH_3), 3.75 (s, 3H, OCH_3), 3.75 (s, 2H, CH_2), 3.01-2.93 (m, 2H, CH_2SCH_2), 1.45 (s, 9H, (CCH_3)); ^{13}C (150 MHz, $CDCl_3$) δ_C 193.3 (S*C*(O)), 171.0 (O*C*(O)), 168.7 (O*C*(O)CH_2), 155.3 (O*C*(O)NH), 80.4 (O*C*), 54.9 (*C*H) 53.1 (O*C*H_3), 52.9 (O*C*H_3), 47.9 (*C*H_2SCH_2), 31.7 (C(O)S*C*H_2), 28.4 (C*C*H_3), 27.5 (CH_2SCH_2); IR (oil) V_{max}/cm^{-1} 2978 (C-H), 2954 (C-H), 1741 (C=O), 1705 (C=O), 1596 (C=O); LRMS (ESI) *m/z* (%) 282.0 ([M–Boc]$^+$, 55), 382.1 ([M+H]$^+$, 85), 404.1 ([M + Na]$^+$, 100); HRMS (ESI) *m/z* calculated for [$C_{14}H_{23}NO_7S_2$] 381.0915, observed 381.0988.

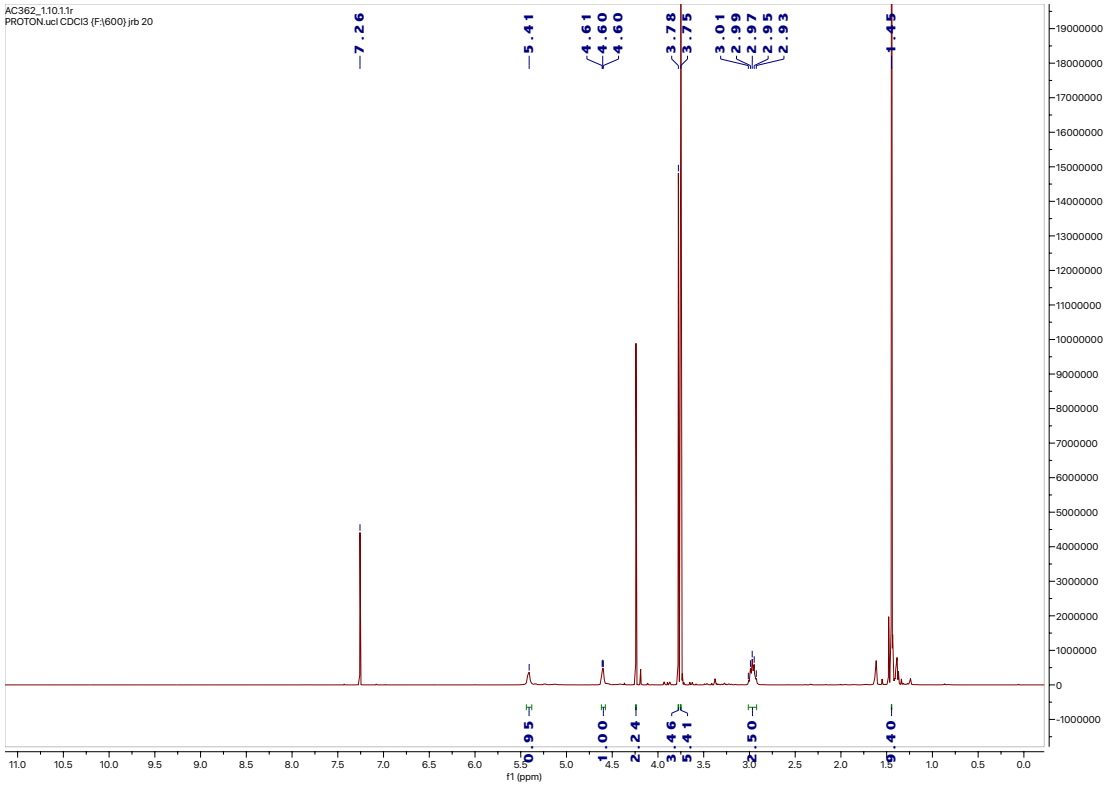

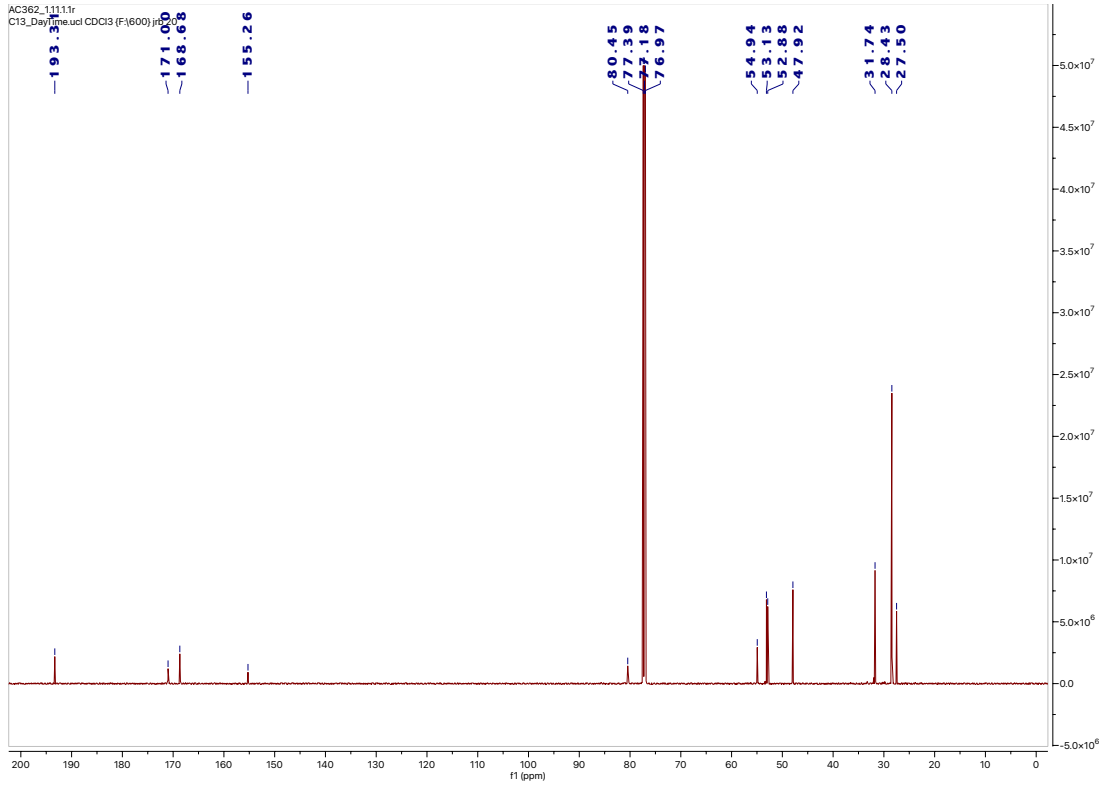

S2 (clear oil, 40.1 mg, 0.13 mmol, 59% yield): ^{1}H NMR (600 MHz, $CDCl_3$) δ_H 5.24 (s, 1H, N*H*), 4.57-4.54 (m, 1H, C*H*), 4.18 (s, 2H, ClCH_2), 3.75 (s, 3H, OCH_3), 3.48-3.45 and 3.36-3.33 (m,

2H, SCH_2), 1.43 (s, 9H, (CCH_3); ^{13}C (150 MHz, $CDCl_3$) δ_C 193.6 (S*C*(O)), 170.9 (O*C*(O)), 155.2 (O*C*(O)NH), 80.5 (O*C*), 53.0 (O*C*H_3), 52.8 (*C*H), 48.0 (SCH_2), 31.9 (Cl*C*H_2), 28.4 (C*C*H_3); IR (oil) V_{max}/cm^{-1} 2979 (C-H), 2954 (C-H), 1744 (C=O), 1706 (C=O); LRMS (ESI) *m/z* (%) 312.0 ([^{35}M+H]$^+$, 30), 314.0 ([^{37}M+H]$^+$, 10), 212.0 ([^{35}M – Boc]$^+$, 80); HRMS (ESI) *m/z* calculated for [$C_{11}H_{18}{}^{35}ClNO_5S$] 311.0594, observed 311.0484.

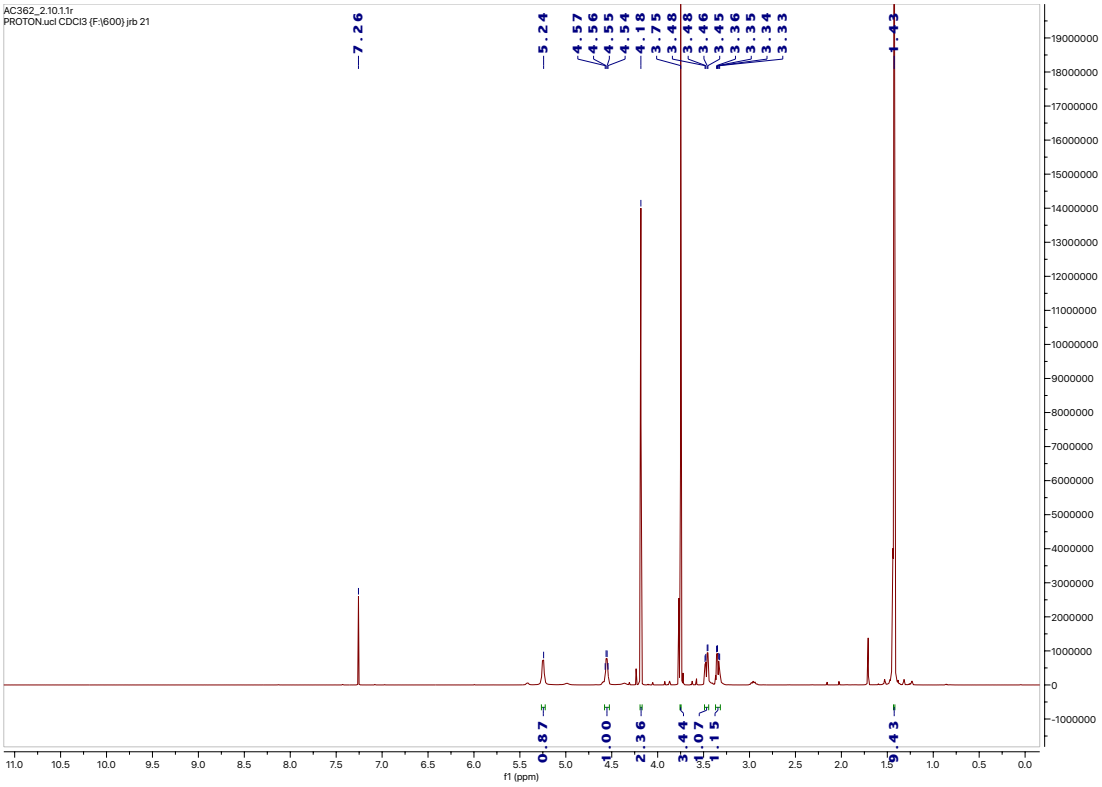

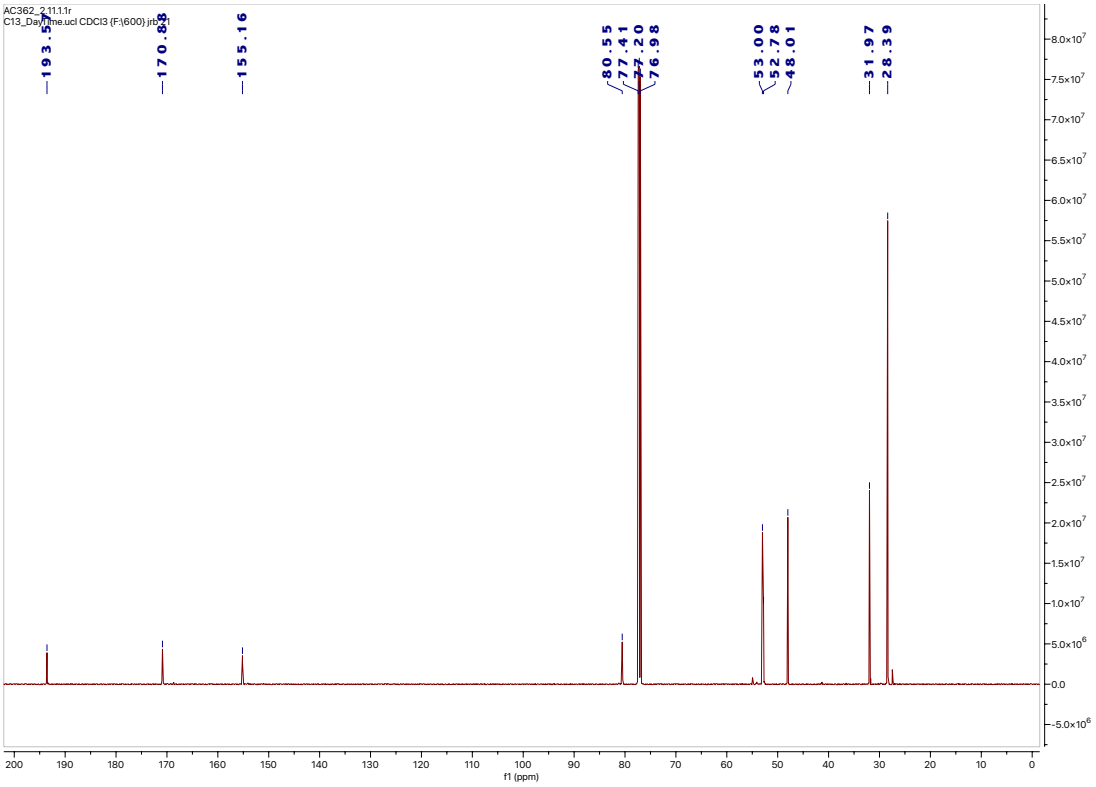

Methyl 2-(acryloylthio)acetate (3)

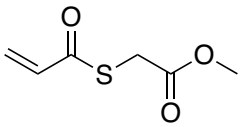

Methyl thioglycolate (0.20 mL, 2.24 mmol, 1.0 eq.) and triethylamine (0.17 mL, 2.24 mmol, 1.0 eq.) were combined in DCM (2.0 mL). The mixture was then added dropwise over 2 h into a stirring solution of acryloyl chloride (0.68 mL, 6.72 mmol, 3.0 eq.) in DCM (10.0 mL), this was left ON. The reaction was performed at RT, under argon atmosphere and constant agitation. The solvent was then removed *in vacuo* and purification by column chromatography (gradient elution from 100% cyclohexane to 30% EtOAc in cyclohexane) afforded the target compound as colourless waxy oil (183 mg, 1.14 mmol, 51% yield).

^{1}H NMR (600 MHz, $CDCl_3$) δ_H 6.42-6.33 (m, 2H, CHC*H*$_2$), 5.77 (dd, 1H, *J* = 9.7, 1.2 Hz, C*H*), 3.77 (s, 2H, SC*H*$_2$), 3.73 (s, 3H, OC*H*$_3$); ^{13}C (150 MHz, $CDCl_3$) δ_C 188.6 (S*C*(O)), 169.3 (O*C*(O)), 134.3 (CH*C*H$_2$), 128.0 (*C*H), 53.0 (O*C*H$_3$), 30.9 (S*C*H$_2$); IR (oil) V_{max}/cm^{-1} 2953 (C-H), 1737

(C=O), 1673 (C=O); LRMS (ESI) *m/z* (%) 161.0 ([M+H]$^+$, 100); HRMS (ESI) *m/z* calculated for [$C_6H_8O_3S$] 160.0194, observed 160.0268.

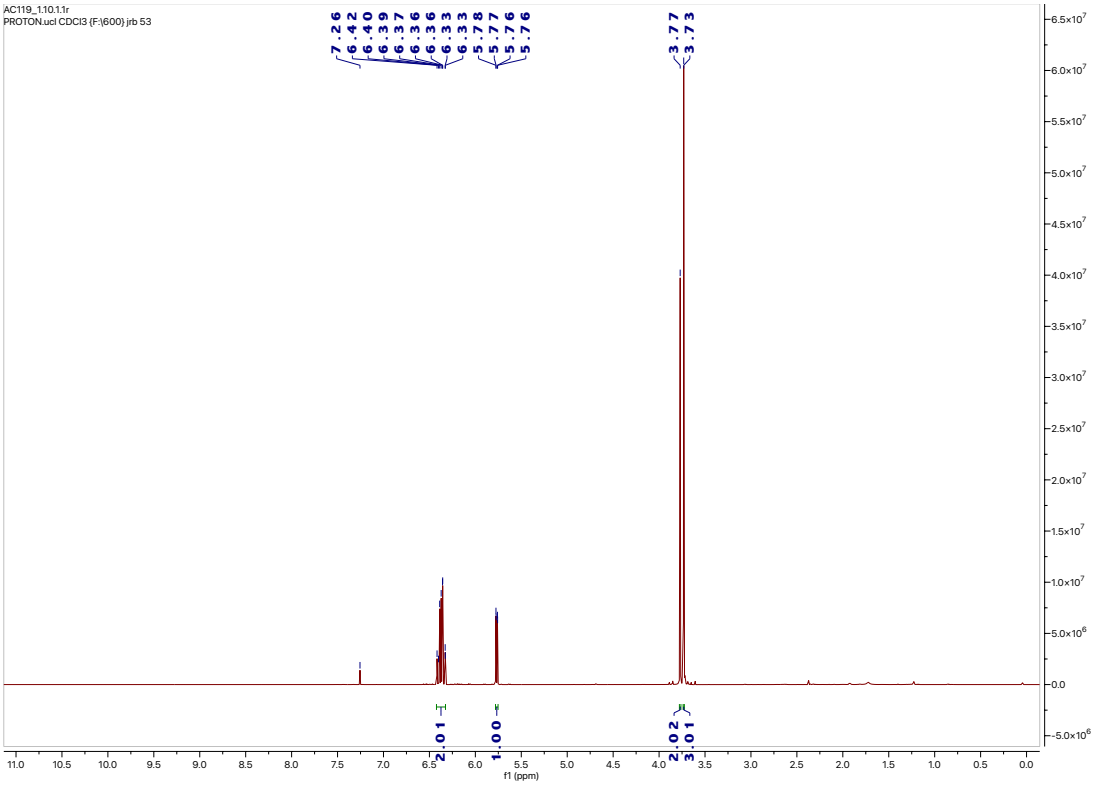

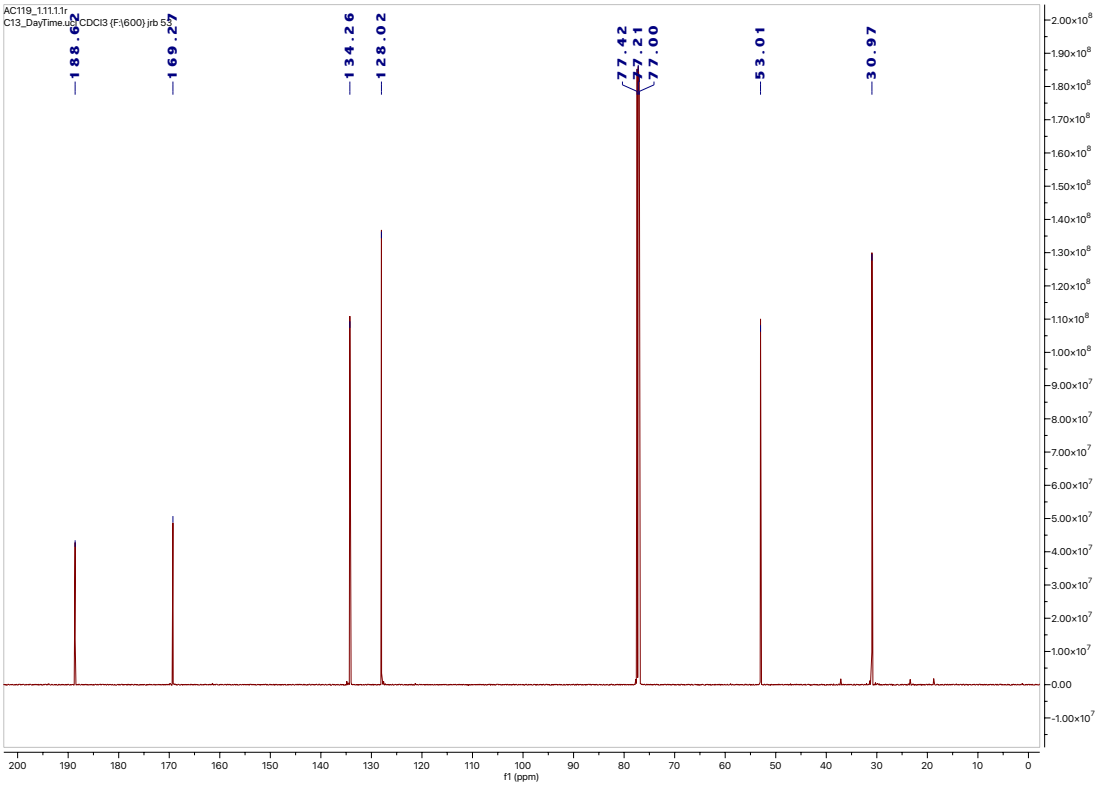

Methyl (*S*)-6-(methoxycarbonyl)-2,2-dimethyl-4,11-dioxo-3-oxa-8,12-dithia-5-azatetradecan-14-oate (S3)

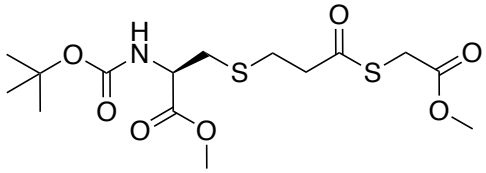

Methyl 2-(acryloylthio)acetate **3** (0.05 mL, 0.30 mmol, 3.0 eq.) was dissolved in 0.5 mL of MeCN followed by addition of 0.7 mL of 50 mM Phosphate Buffer pH 6.75 (addition of MeCN will increase pH to 7.4). *N*-Boc cysteine methyl ester (20 mg, 0.10 mmol, 1.0 eq.) was then added and the mixture was stirred for 3 h at RT. The solvent was then removed *in vacuo* and purification by column chromatography (gradient elution from 100% cyclohexane to 40% ethyl acetate in cyclohexane) afforded the target compound as clear oil (33.8 mg, 0.09 mmol, 86% yield*). *Minor solvent impurities observed in the NMR of ethyl acetate.

^{1}H NMR (600 MHz, $CDCl_3$) δ_H 5.37 (d, 1H, *J* = 8.1 Hz, N*H*), 4.53-4.50 (m, 1H, C*H*), 3.75 (s, 3H, OCH_3), 3.72 (s, 3H, OCH_3), 3.70 (s, 2H, SCH_2), 3.00-2.93 (m, 2H, CHCH_2S), 2.88-2.85 (m, 2H, CH_2CH_2), 2.82-2.80 (m, 2H, CHCH_2), 1.42 (s, 9H, CCH_3); ^{13}C (150 MHz, $CDCl_3$) δ_C 195.6 (S*C*(O)), 171.5 (NHCHO*C*(O)), 169.1 (O*C*(O)), 155.3 (CO*C*(O)), 80.4 (*C*), 53.4 (NH*C*H), 52.9 (O*C*H_3), 52.8 (O*C*H_3), 43.7 (*C*H_2CH_2), 34.9 (CH$_2$*C*H$_2$), 31.2 (S*C*H_2), 28.4 (S*C*H_3), 27.7 (CH*C*H_2); IR (oil) V_{max}/cm^{-1} 2977 (C-H), 2954 (C-H), 1741 (C=O), 1694 (C=O); LRMS (ESI) *m/z* (%), 396.1 ([M+H]$^+$, 100); HRMS (ESI) *m/z* calculated for [$C_{15}H_{25}NO_7S_2$] 395.1072, observed 395.1137.

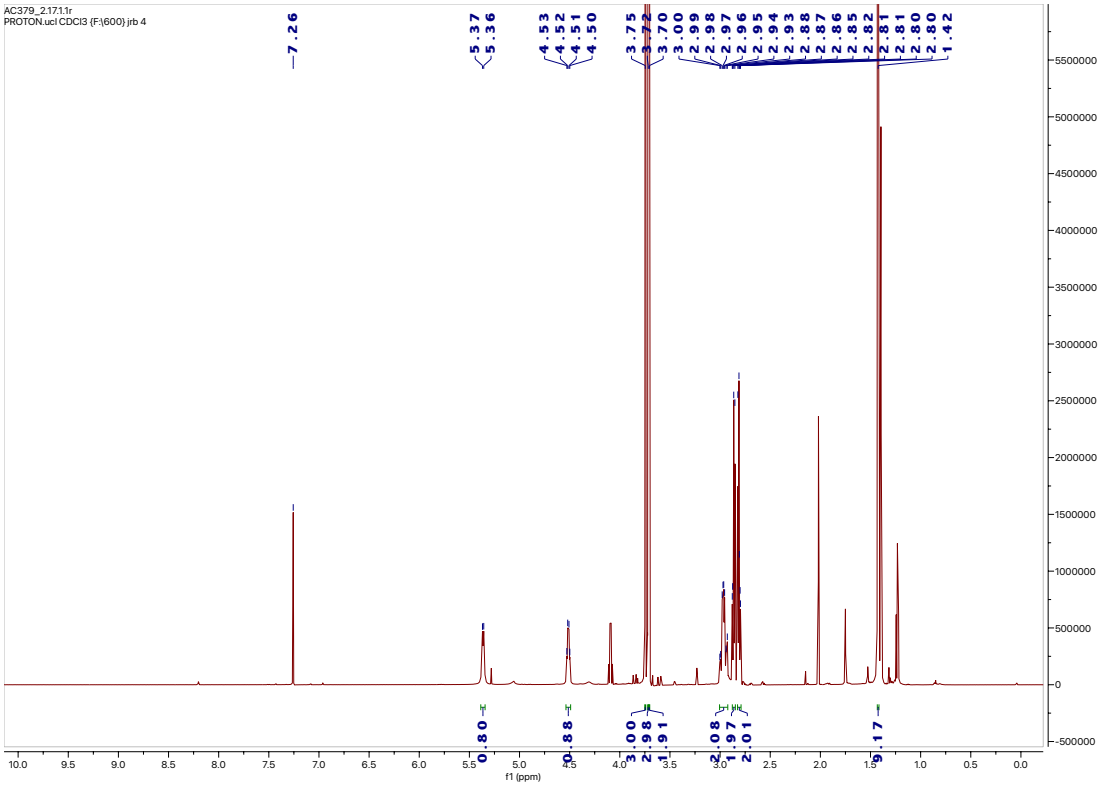
AC379_2.17.1.1r
PROTON.ucl CDCl3 {F:\600} jrb 4
7.26
5.37
5.36
4.53
4.52
4.51
4.50
3.75
3.72
3.70
3.00
2.99
2.98
2.97
2.96
2.95
2.94
2.93
2.88
2.87
2.86
2.85
2.82
2.81
2.81
2.80
2.20
1.42
0.80
0.88
3.00
2.98
1.91
2.08
1.97
2.01
9.17
f1 (ppm)

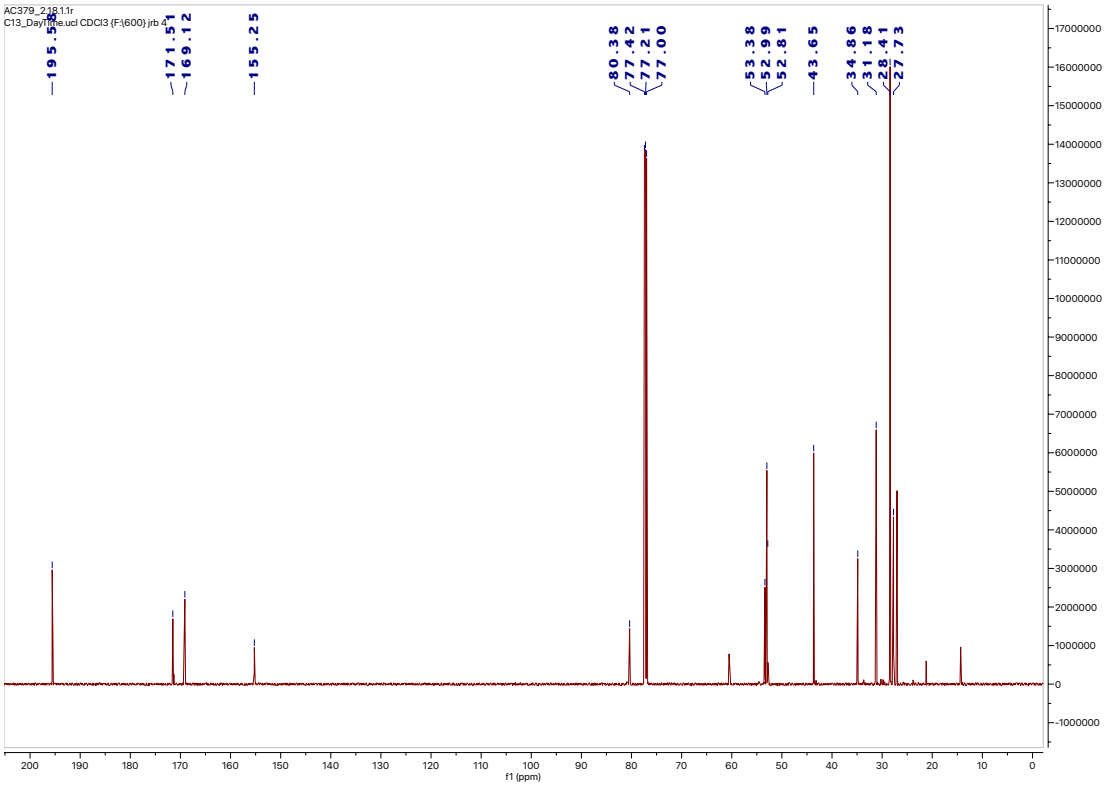
AC379_2.18.1.1r
C13_Daytime.ucl CDCl3 {F:\600} jrb 4
195.58
171.51
169.12
155.25
80.38
77.42
77.21
77.00
53.38
52.99
52.81
43.65
34.86
31.18
28.41
27.73
f1 (ppm)

2-fluoro-5-nitrobenzoic acid (4)

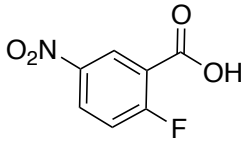

Nitric acid (0.42 mL, 10.1 mmol, 4.0 eq.) was cooled to 0 °C followed by a dropwise addition of sulphuric acid (0.54 mL, 10.1 mmol, 4.0 eq.). The mixture was stirred for 10 min, after which 2-fluorobenzoyl chloride (0.30 mL, 2.52 mmol, 1.0 eq.) was added and further stirred at 0 °C for 2 h. After this time, the solvent was removed *in vacuo* and the resulting yellow paste was dissolved in EtOAc (15 mL) and washed with H_2O (10 mL). The product was extracted with EtOAc (3 x 10 mL), dried ($MgSO_4$) and the solvent was removed *in vacuo*. The resulting solid was dry loaded on silica and purified by flash chromatography (gradient elution from 100% cyclohexane to 50% EtOAc in cyclohexane and 1% AcOH) to afford the target compound as white powder (413 mg, 2.23 mmol, 89% yield). *Minor solvent NMR impurity at 1.99 ppm can be assigned as acetic acid while impurity at 1.28 ppm is hexane.

^{1}H NMR (600 MHz, MeOD) δ_H 8.79-8.77 (m, 1H, ArC*H*), 8.49-8.46 (m, 1H, ArC*H*), 7.47 (t, 1H, *J* = 9.0 Hz, ArC*H*); ^{13}C (150 MHz, MeOD) δ_C 167.4 and 165.6 (*C*F), 165.1 and 165.0 (OH*C*(O)), 145.4 (*C*NO_2) 130.8 and 130.7 (NO_2C*C*HCH), 129.1 and 129.0 (NO_2C*C*HC), 121.7 and 121.6 (*C*C(O)OH), 119.8 and 119.6 (CF*C*H); IR (solid) V_{max}/cm^{-1} 2929 (C-H), 2858 (C-H), 1657 (C=O); LRMS (ESI) *m/z* (%) 186.0 ([M+H]$^+$, 100); HRMS (ESI) *m/z* calculated for [$C_7H_4FNO_4$] 185.0124, observed 185.0195.

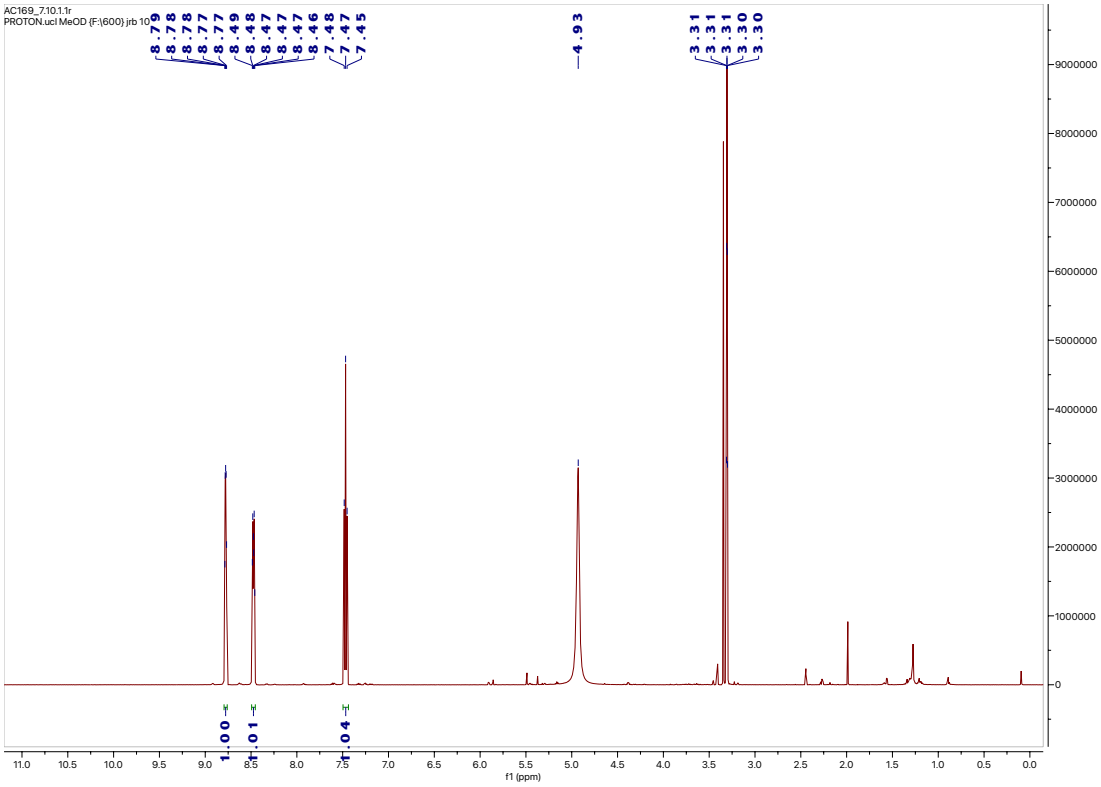
AC169_7.10.1.1r
PROTON.ucl MeOD {F:\600} jrb 10
8.79
8.78
8.78
8.77
8.77
8.49
8.48
8.47
8.47
8.47
8.46
7.48
7.47
7.45
4.93
3.31
3.31
3.31
3.30
3.30
1.00
1.01
1.04
f1 (ppm)

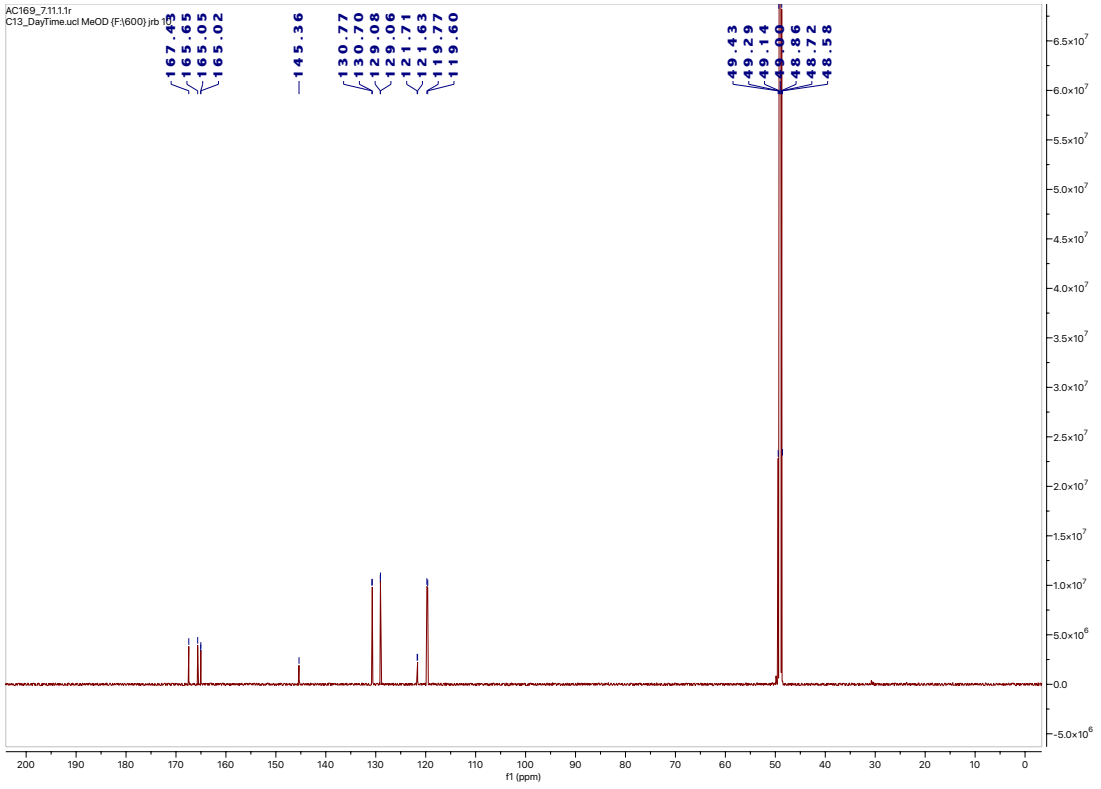
AC169_7.11.1.1r
C13_DayTime.ucl MeOD {F:\600} jrb
167.43
165.65
165.05
165.02
145.36
130.77
130.70
129.08
129.06
121.71
121.63
119.77
119.60
49.43
49.29
49.14
49.00
48.86
48.72
48.58
f1 (ppm)

methyl 2-((2-fluoro-5-nitrobenzoyl)thio)acetate (5)

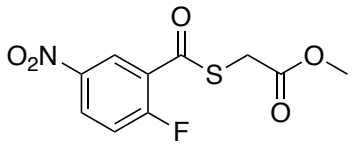

2-fluoro-5-nitrobenzoic acid **4** (200 mg, 1.08 mmol, 1.1 eq.) was dissolved in 5 mL of DMF followed by addition of N-Ethoxycarbonyl-2-ethoxy-1,2-dihydroquinoline (290 mg, 1.19 mmol, 1.2 eq.), this was stirred at RT for 30 min. Lastly, methyl thioglycolate (0.09 mL, 0.97 mmol, 1.0 eq.) was added and the mixture was left stirring ON at 80 °C. The solvent was then removed *in vacuo* and purification by column chromatography (gradient elution from 100% DCM to 10% methanol in DCM) afforded the target compound as yellow oil (205 mg, 0.75 mmol, 77%).

^{1}H NMR (600 MHz, $CDCl_3$) δ_H 8.79-8.78 (m, 1H, ArC*H*), 8.45-8.42 (m, 1H, ArC*H*), 7.38 (t, 1H, *J* = 9.2 Hz, ArC*H*), 3.92 (s, 2H, CH_2S), 3.79 (s, 3H, OCH_3); ^{13}C (150 MHz, $CDCl_3$) δ_C 185.3 and 185.3 (S*C*(O), 168.6 and 164.8 (*C*F), 163.0 (*C*(O)OCH_3), 144.3 (*C*NO_2), 129.9 and 129.8 (FCC*C*H_2), 126.2 and 126.1 (NO_2C*C*HCH), 125.4 and 125.3 (NO_2C*C*HC), 118.7 and 118.5 (NO_2CCH*C*H), 53.2 (O*C*H_3), 31.9 and 31.8 (C(O)*C*H_2S); IR (oil) V_{max}/cm^{-1} 3105 (C-H), 3076 (C-H), 2964 (C-H), 1744 (C=O), 1707 (C=O); LRMS (ESI) *m/z* (%) 274.0 ($[M + H]^+$, 100); HRMS (ESI) *m/z* calculated for [$C_{10}H_8FNO_5S$] 273.0107, observed 273.0175.

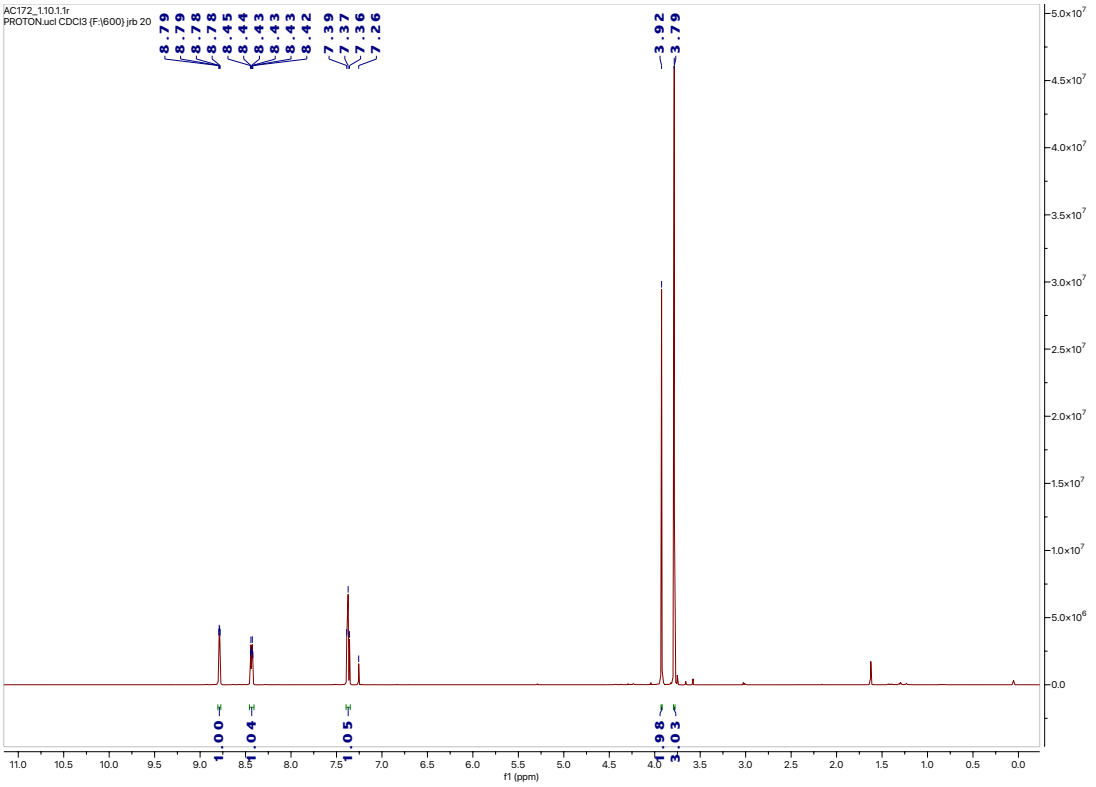
AC172_1.10.1.1r
PROTON.ucl CDCl3 {F:\600} jrb 20
8.79
8.79
8.78
8.78
8.45
8.44
8.43
8.43
8.42
7.39
7.37
7.36
7.26
3.92
3.79
1.00
1.04
1.05
1.98
3.03
f1 (ppm)

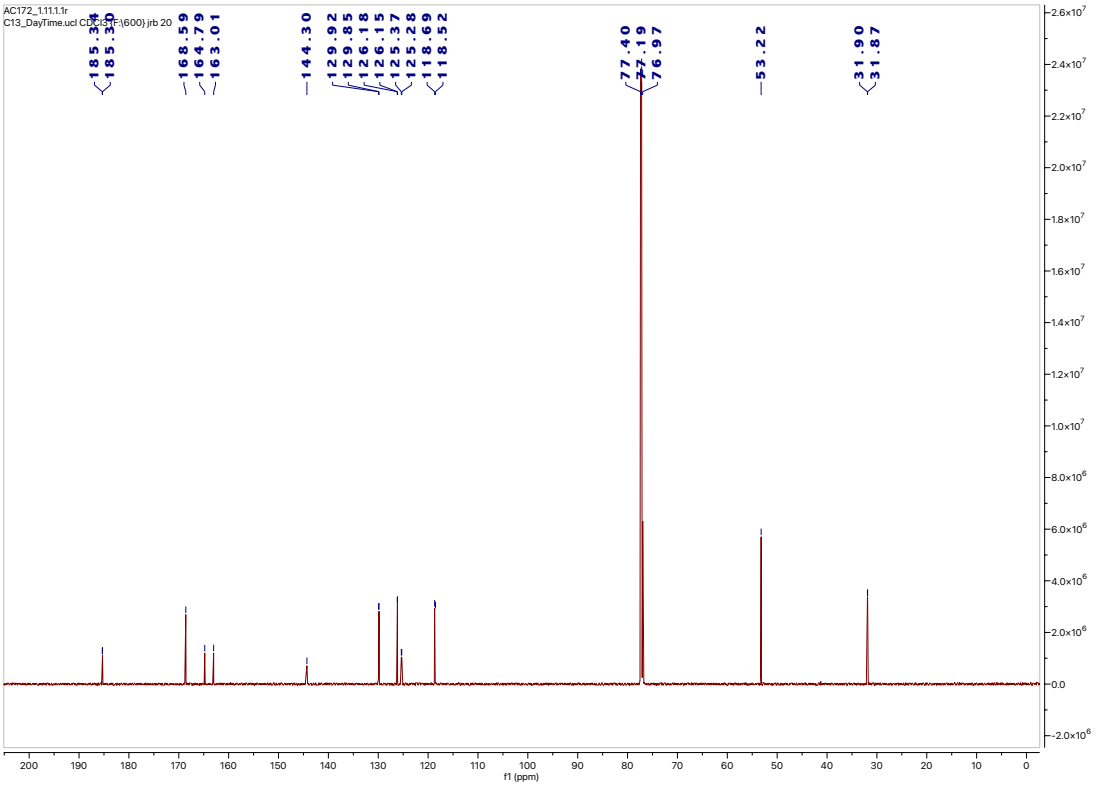
AC172_1.11.1.1r
C13_DayTime.ucl CDCl3 {F:\600} jrb 20
185.34
185.30
168.59
164.79
163.01
144.30
129.92
129.85
126.18
126.15
125.37
125.28
118.69
118.52
77.40
77.19
76.97
53.22
31.90
31.87
f1 (ppm)

Methyl *N*-(*tert*-butoxycarbonyl)-*S*-(2-fluoro-5-nitrobenzoyl)-*D*-cysteinate (S4)

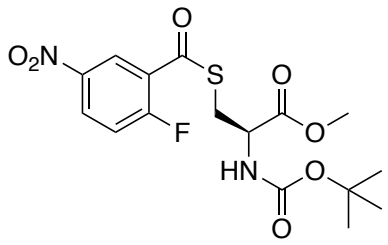

Methyl 2-((2-fluoro-5-nitrobenzoyl)thio)acetate **5** (60 mg, 0.20 mmol, 1.1 eq.) was dissolved in 0.5 mL of MeCN followed by addition of 0.7 mL of 50 mM Phosphate Buffer pH 6.75 (addition of MeCN will increase pH to 7.4). *N*-Boc cysteine methyl ester (40 mg, 0.18 mmol, 1.0 eq.) was then added and the mixture was stirred for 3 h at RT. The solvent was then removed *in vacuo* and purification by column chromatography (gradient elution from 100% cyclohexane to 40% ethyl acetate in cyclohexane) afforded the target compound as yellow oil (45 mg, 0.11 mmol, 62% yield).

^{1}H NMR (600 MHz, $CDCl_3$) δ_H 8.72-8.70 (m, 1H, ArC*H*), 8.42-8.39 (m, 1H, ArC*H*), 7.34 (t, 1H, *J* = 9.1 Hz, ArC*H*), 4.67-4.63 (m, 1H, C*H*), 3.78 (s, 3H, OCH_3), 3.67-3.64 and 3.53-3.48 (m, 2H, CHCH_2), 1.44 (s, 9H, CCH_3); ^{13}C (150 MHz, $CDCl_3$) δ_C 186.3 and 186.2 (S*C*(O)), 170.9 (*C*(O)OCH_3), 164.4 and 162.6 (*C*F), 155.2 (O*C*(O)NH), 144.2 (*C*NO_2), 129.7 and 129.6 (NO_2C*C*HCH), 126.1 and 126.0 (NO_2C*C*HCH), 118.6 and 118.5 (FC*C*H), 80.6 (O*C*), 53.1 (O*C*H_3), 52.8 (*C*H), 32.1 ((O)CS*C*H_2), 28.4 (C*C*H_3); IR (yellow powder) V_{max}/cm^{-1} 3101 (C-H), 3076 (C-H), 2964 (C-H), 1742 (C=O), 1690 (C=O), 1642 (C=O); LRMS (ESI) *m/z* (%) 403.0 ([M + H]$^+$, 100); HRMS (ESI) *m/z* calculated for [$C_{16}H_{19}FN_2O_7S$] 402.0897, observed 402.0977.

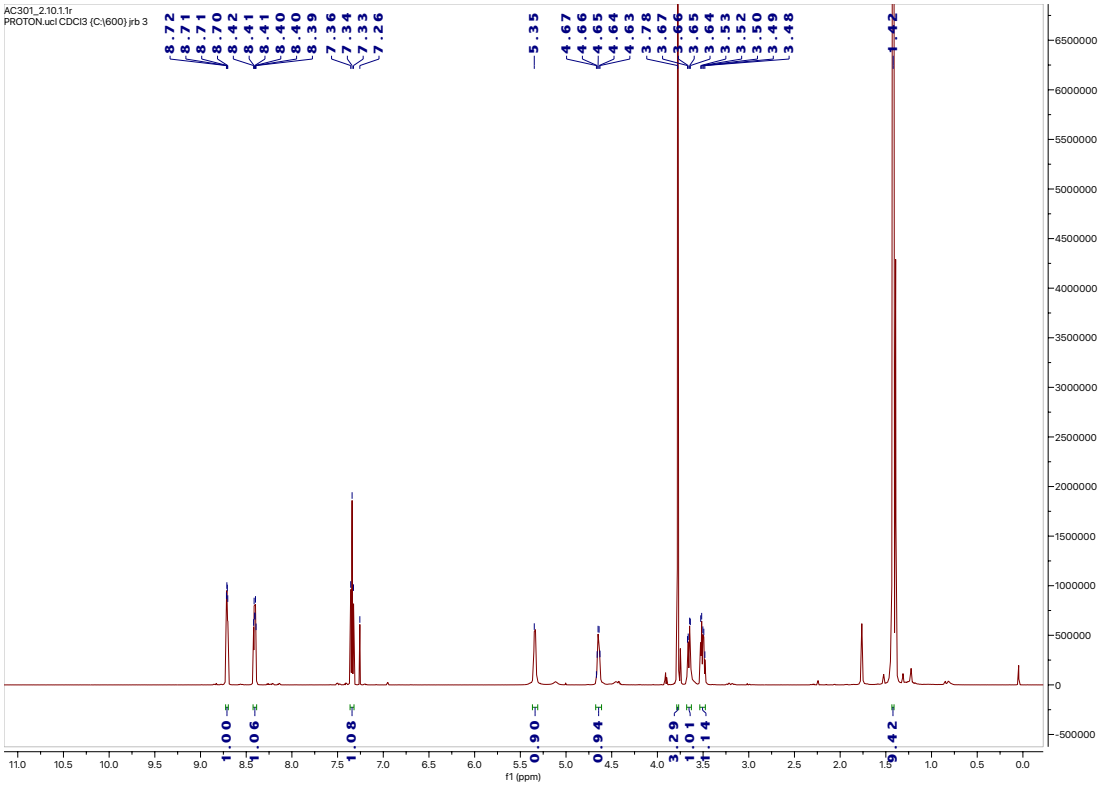
AC301_2.10.1.1r
PROTON.ucl CDCl3 (C:\600) jrb 3
8.72
8.71
8.71
8.70
8.42
8.41
8.41
8.40
8.40
8.39
7.36
7.34
7.33
7.26
5.35
4.67
4.66
4.65
4.64
4.63
3.78
3.67
3.66
3.65
3.64
3.53
3.52
3.50
3.49
3.48
1.42
1.00
1.06
1.08
0.90
0.94
3.29
1.01
1.14
9.42
f1 (ppm)

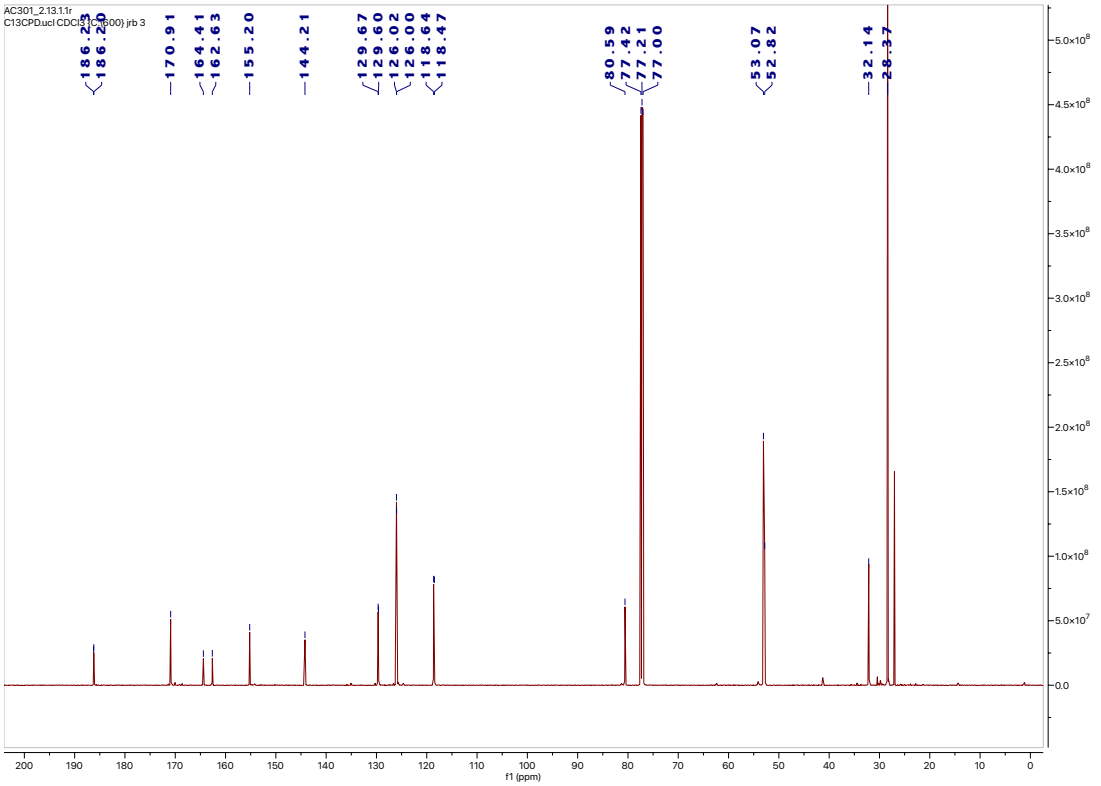
AC301_2.13.1.1r
C13CPD.ucl CDCl3 (C:\600) jrb 3
186.20
186.20
170.91
164.41
162.63
155.20
144.21
129.67
129.60
126.02
126.00
118.64
118.47
80.59
77.42
77.21
77.00
53.07
52.82
32.14
28.37
f1 (ppm)

methyl 2-((2-chloro-2-phenylacetyl)thio)acetate (6)

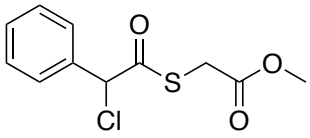

Methyl thioglycolate (0.20 mL, 2.24 mmol, 1.0 eq.) and triethylamine (0.31 mL, 2.24 mmol, 1.0 eq.) were combined in DCM (2.0 mL). The mixture was then added dropwise over 2 h time into a stirring solution of α-chlorophenylacetyl chloride (1.06 mL, 6.72 mmol, 3.0 eq.) in DCM (10.0 mL). The reaction was performed at RT, ON, under argon atmosphere and constant agitation. The solvent was then removed *in vacuo* and purification by column chromatography (gradient elution from 100% pet. ether to 30% ethyl acetate in pet. ether) afforded the target compound as light-yellow oil (698 mg, 2.70 mmol, quantitative yield).

^{1}H NMR (600 MHz, $CDCl_3$) δ_H 7.48-7.47 (m, 2H, ArC*H*), 7.40-7.38 (m, 3H, ArC*H*), 5.50 (s, 1H, C*H*Cl), 3.70 (s, 2H, CH_2S), 3.70 (s, 3H, OCH_3); ^{13}C (150 MHz, $CDCl_3$) δ_C 194.6 (S*C*(O)), 168.6 (O*C*(O)), 135.5 (Ar*C*H), 129.7 (Ar*C*H), 129.2 (Ar*C*H), 128.4 (Ar*C*H), 65.7 (*C*HCl), 53.1 (O*C*H_3), 32.3 (S*C*H_2); IR (oil) ν_{max}/cm^{-1} 2953 (C-H), 2844 (C-H), 1738 (C=O), 1679 (C=O); LRMS (ESI) *m/z* (%) 259.0 ([^{35}M+H]$^+$, 100), 261.0 ([^{37}M+H]$^+$, 35); HRMS (ESI) *m/z* calculated for [$C_{11}H_{11}{}^{35}ClO_3S$] 258.0117, observed 258.0197.

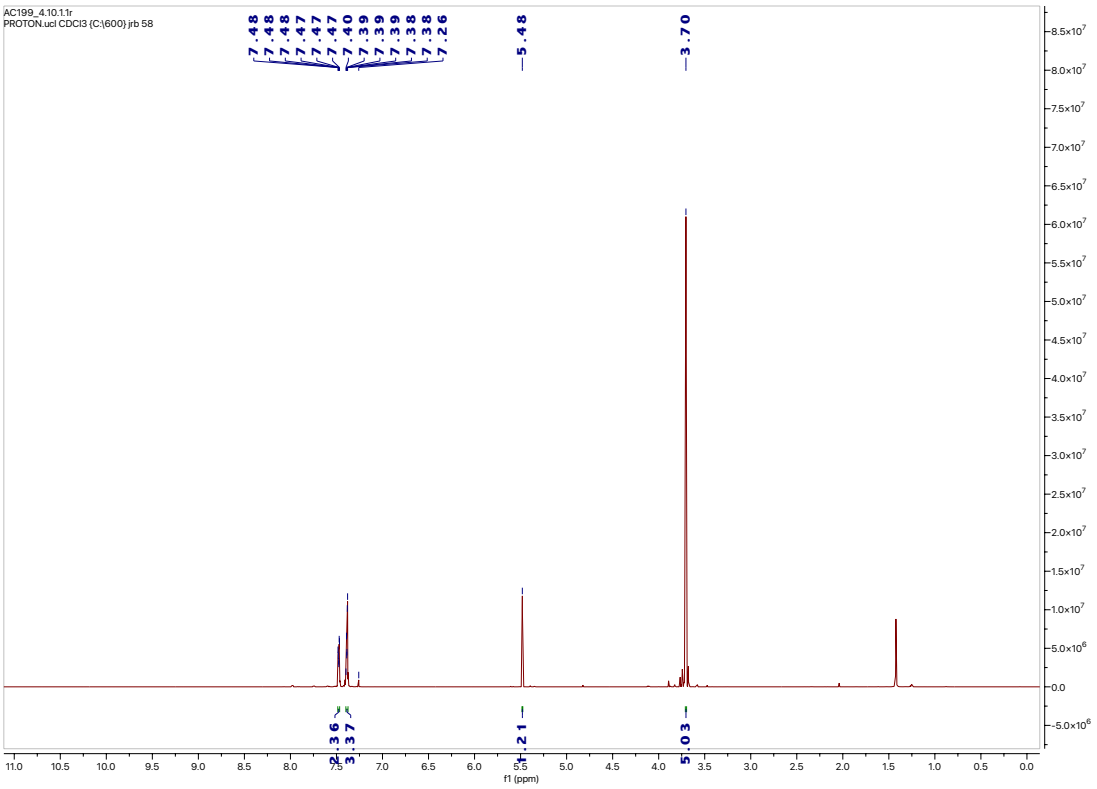

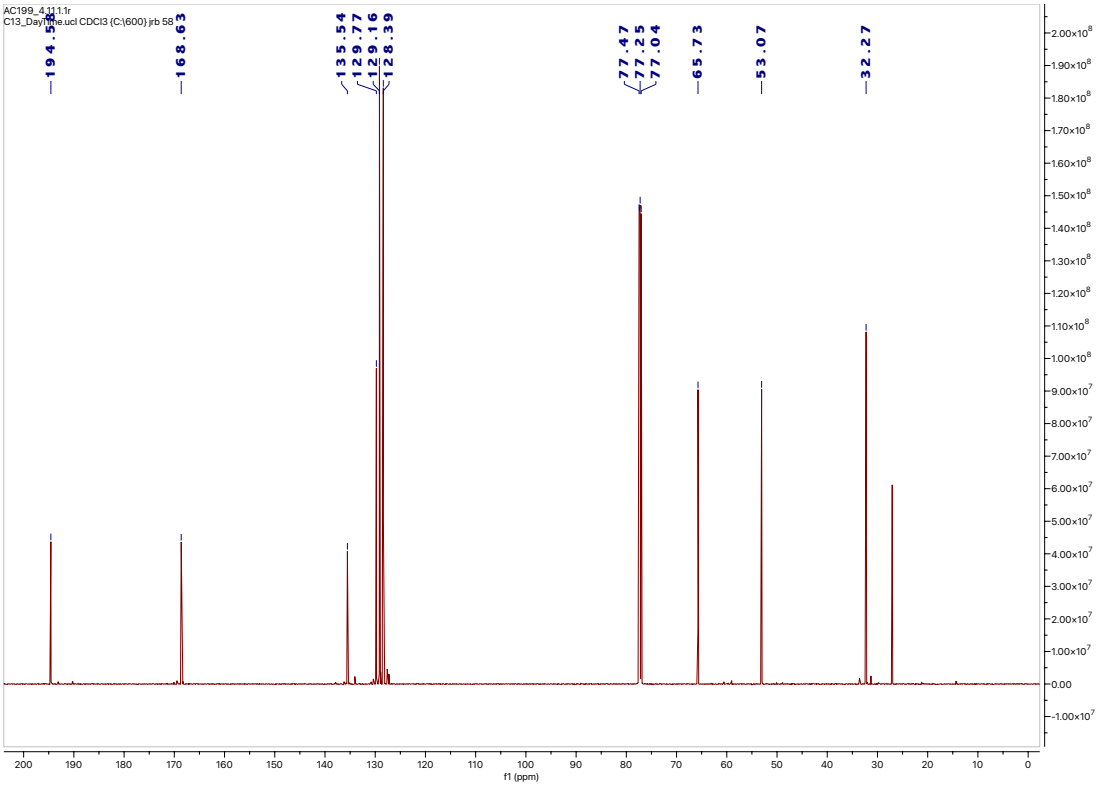

Methyl *N*-(*tert*-butoxycarbonyl)-*S*-(2-chloro-2-phenylacetyl)-*L*-cysteinate (S5)

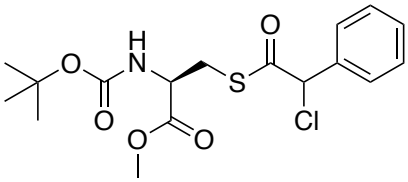

Methyl 2-((2-chloro-2-phenylacetyl)thio)acetate **6** (120 mg, 0.46 mmol, 1.1 eq.) was dissolved in 0.5 mL of MeCN followed by addition of 0.7 mL of 50 mM Phosphate Buffer pH 6.75 (addition of MeCN will increase pH to 7.4). *N*-Boc cysteine methyl ester (90 mg, 0.41 mmol, 1.0 eq.) was then added and the mixture was stirred for 3 h at RT. The solvent was then removed *in vacuo* and purification by column chromatography (gradient elution from 100% cyclohexane to 40% diethyl ether in cyclohexane) afforded the target compound as clear oil (93.1 mg, 0.24 mmol, 58% yield).

^{1}H NMR (600 MHz, CD_3CN) δ_H 7.49-7.48 (m, 2H, ArC*H*), 7.44-7.42 (m, 3H, ArC*H*), 5.72 (s, 1H, C*H*Cl), 4.33-4.32 (m, 1H, C*H*), 3.65 (s, 3H, OCH_3), 3.46-3.41 and 3.22-3.16 (m, 2H,

CH*C*H$_2$S), 1.39 (s, 9H, CC*H*$_3$); ^{13}C (150 MHz, CD$_3$CN) δ_C 195.8 (S*C*(O)), 171.8 (CH*C*(O)), 156.2 (NH*C*(O)), 137.1 (Ar*C*H), 130.6 (Ar*C*H), 130.1 (Ar*C*H), 129.3 (Ar*C*H), 80.4 (*C*), 66.3 (*C*HCl), 53.7 (NH*C*H), 53.2 (O*C*H$_3$), 32.3 (NHCH*C*H$_2$), 28.4 (C*C*H$_3$); IR (oil) V_{max}/cm^{-1} 2977 (C-H), 2954 (C-H), 1741 (C=O), 1694 (C=O); LRMS (ESI) *m/z* (%) 388.0 ([^{35}M+H]$^+$, 100), 390.0 (^{37}[M+H)$^+$, 33), 288.1 ([^{35}M-Boc]$^+$, 95), 410.1 [(^{35}M+Na]$^+$, 100); HRMS (ESI) *m/z* calculated for [$C_{17}H_{22}{}^{35}ClNO_5S$] 387.0907, observed 387.0979.

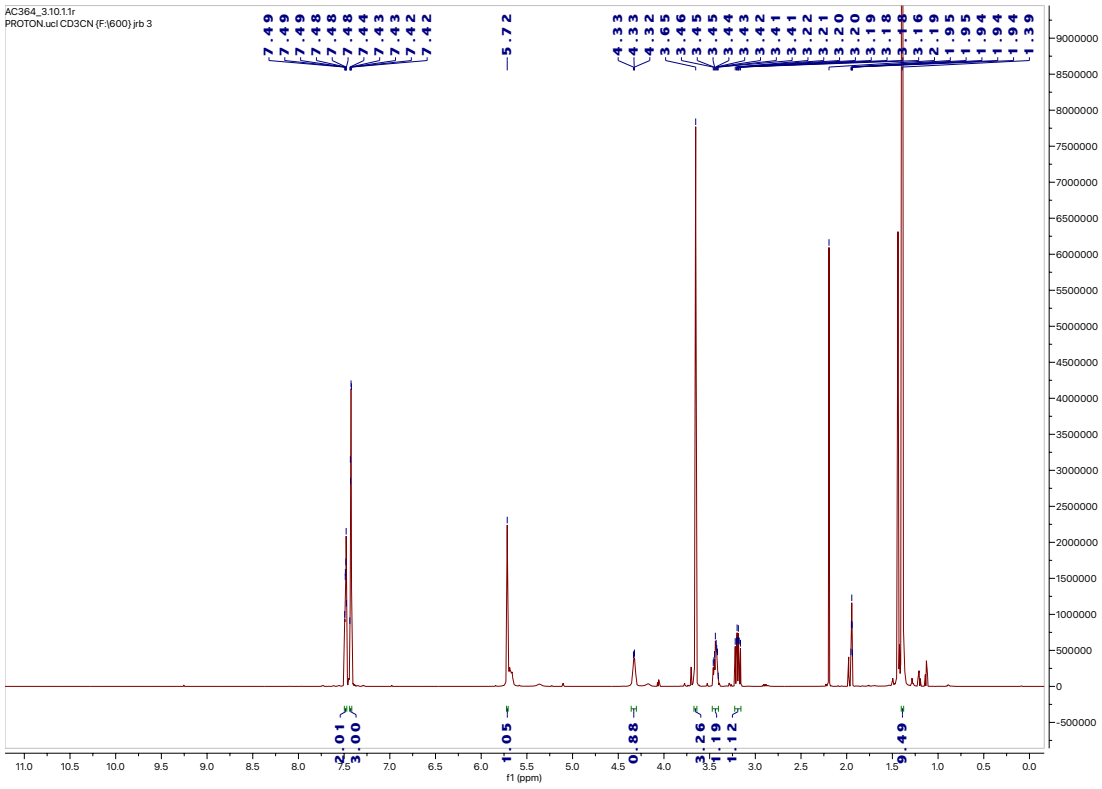

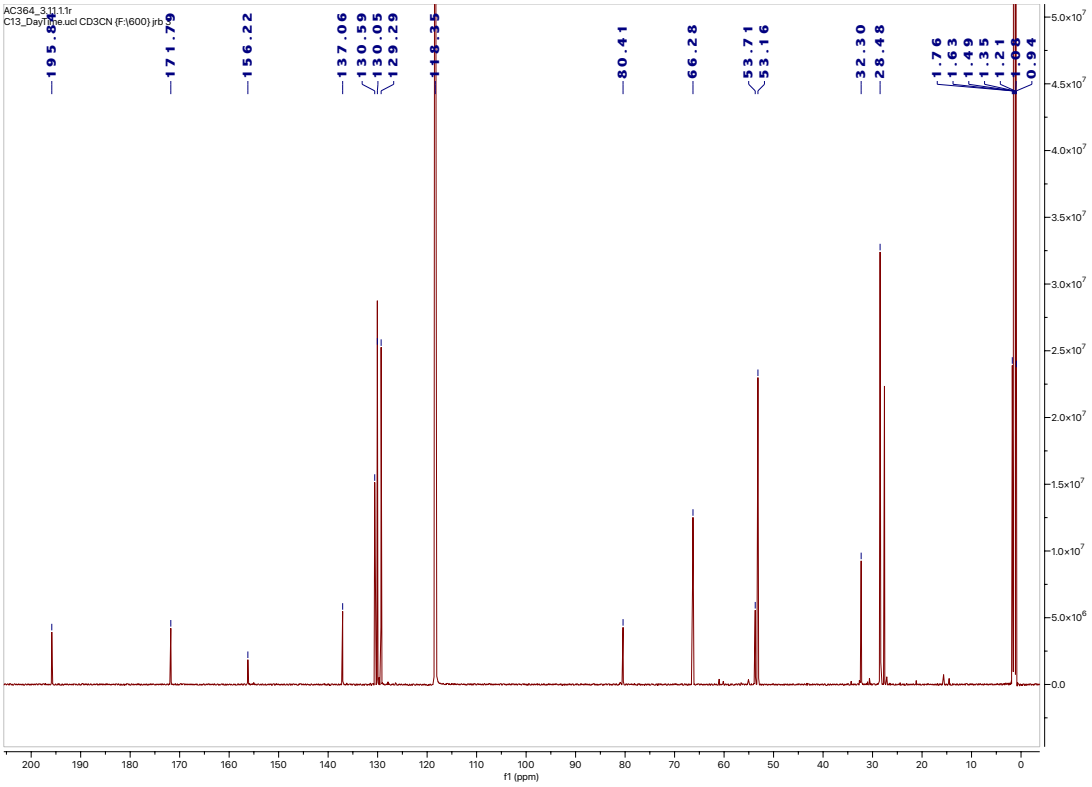

2,2'-(disulfanediylbis(4,1-phenylene))diacetic acid

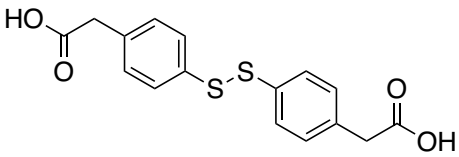

4-Mercaptophenylacetic acid (40 mg, 0.24 mmol, 2.0 eq.) was dissolved in 5 mL of MeCN, followed by addition of iodine (30 mg, 0.12 mmol, 1.0 eq.). The mixture was stirred at RT for 16 h. The solvent was then removed *in vacuo* and purification by column chromatography (gradient elution from 100% DCM to 15% MeOH in DCM with 1% AcOH) afforded the target compound as yellow powder (40 mg, 0.12 mmol, quantitative yield).

mp 76-78 °C ^{1}H NMR (600 MHz, MeOD) δ_H 7.45 (d, 4H, *J* = 8.3 Hz, ArC*H*), 7.25 (d, 4H, *J* = 8.4 Hz, ArC*H*), 3.58 (s, 4H, CH_2); ^{13}C (150 MHz, MeOD) δ_C 175.2 (*C*(O)OH), 136.6 (Ar*C*), 135.7 (Ar*C*H), 131.4 (Ar*C*H), 129.1 (Ar*C*), 41.3 (*C*H_2C(O)OH); IR (yellow powder) V_{max}/cm^{-1} 2987 (C-H), 2964 (C-H), 1781 (C=O)); LRMS (ESI) *m/z* (%) 334.0 ([M+H]$^+$, 100); HRMS (ESI) *m/z* calculated for [$C_{16}H_{14}O_4S_2$] 334.0333, observed 334.0326.

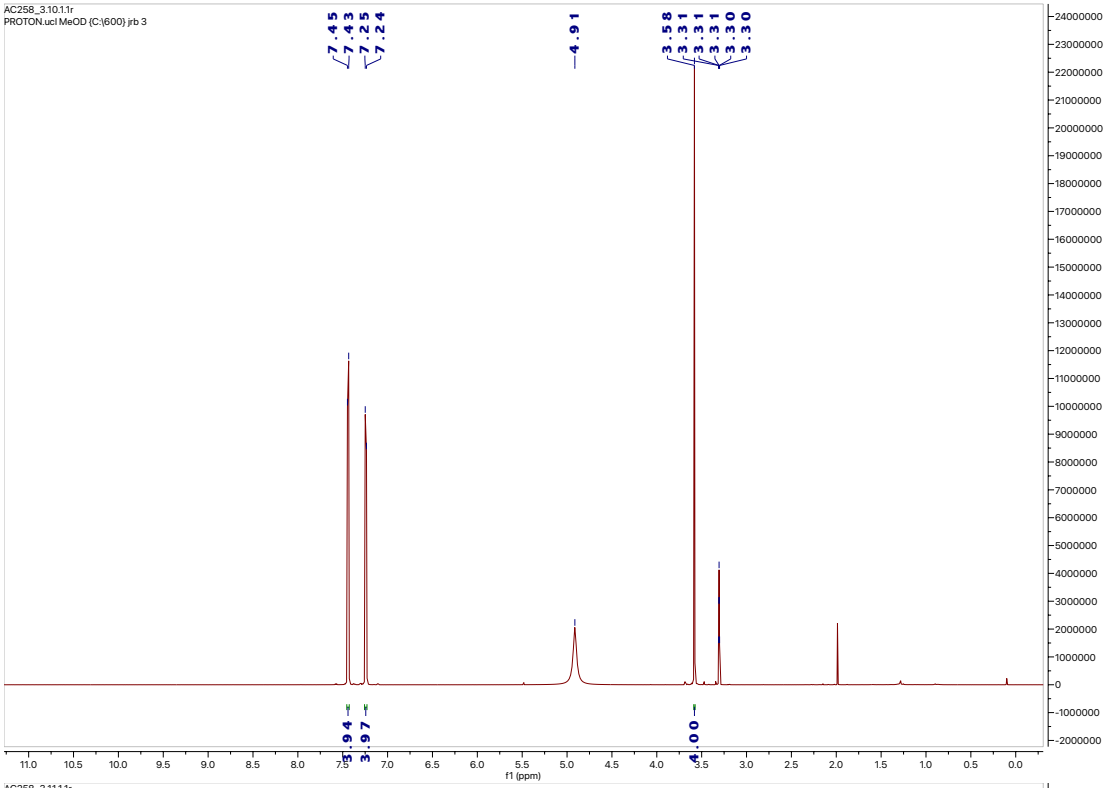
AC258_3.10.1.1r
PROTON.ucl MeOD {C:\600} jrb 3
7.45
7.43
7.25
7.24
4.91
3.58
3.31
3.31
3.31
3.30
3.30
1.94
3.97
4.00
f1 (ppm)

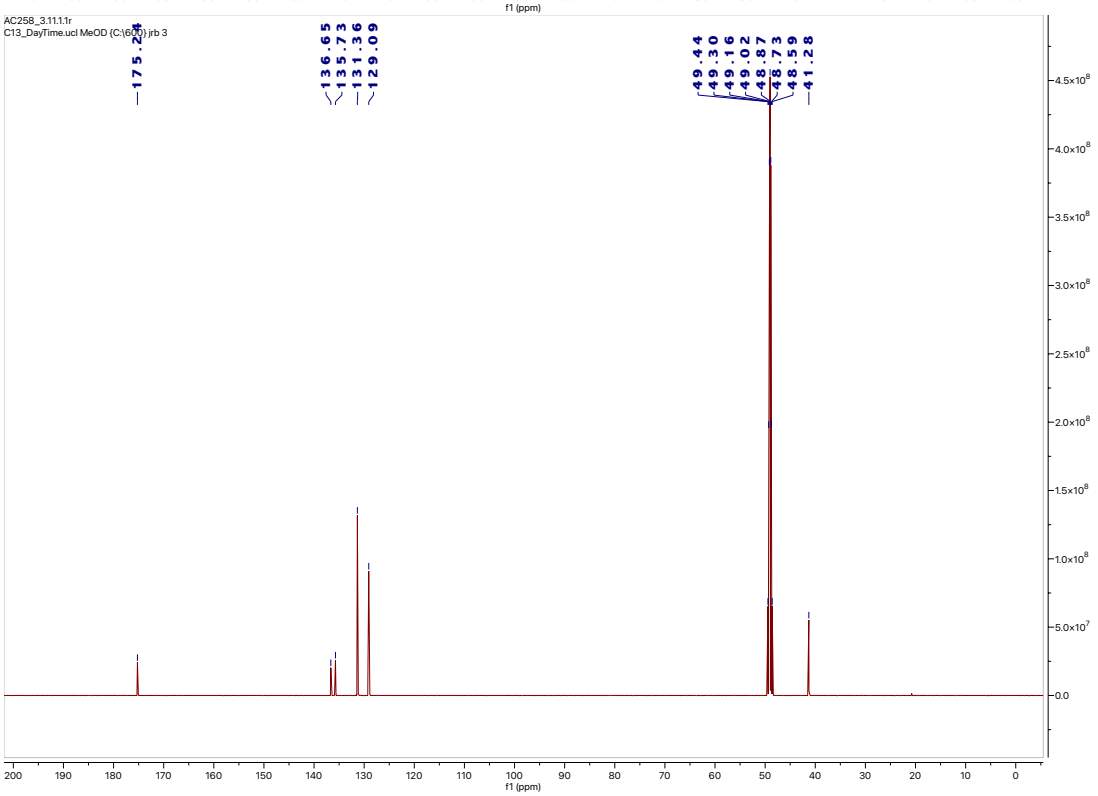
AC258_3.11.1.1r
C13_DayTime.ucl MeOD {C:\600} jrb 3
175.24
136.65
135.73
131.36
129.09
49.44
49.30
49.16
49.02
48.87
48.73
48.59
41.28
f1 (ppm)

Pent-4-yne-1-thiol[188] (46)

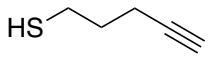

Methanesulfonylchloride (0.87 mL, 11.3 mmol, 1.5 eq.) was added over 5 min at 0 °C to a stirred solution of 4-pentyn-1-ol (0.70 mL, 7.5 mmol, 1.0 eq.) and triethylamine (1.34 mL, 15.0 mmol, 2.0 eq.) in DCM. After 5 min at 0 °C the reaction was warmed up to RT and stirred for 2 h. This was then washed with water (2 x 10 mL) and brine (1 x 10 mL), dried over $MgSO_4$, and concentrated *in vacuo*. The crude sulfonate was used without purification, and it was dissolved in DMF (47 mL), to which potassium thioacetate (900 mg, 7.87 mmol, 1.05 eq.) was added. The reaction mixture was heated up to 50 °C for 20 h, then diluted with DCM (40 mL). DMF was removed by repeated washing with water (4 x 10 mL). The combined organics were concentrated *in vacuo*.

Alongside that, in a separate flask a suspension of K_2CO_3 (380 mg, 2.75 mmol, 1.1 eq.) in MeOH (15 mL) was stirred for 20 min at RT. This was then added to the main crude thioacetate. The evolution of reaction was monitored by TLC. After 2 h, the reaction mixture was quenched with 1 M HCl until pH 2 was obtained and extracted with DCM (3 x 10 mL). The organic layer was washed with aq. NaCl, dried over $MgSO_4$, filtered, and concentrated *in vacuo*. The crude product was then purified using automatic column chromatography (gradient elution from 100% cyclohexane to 20% ethyl acetate in cyclohexane) afforded the target compound as light-yellow oil (179 mg, 1.79 mmol, 24% yield).

^{1}H NMR (600 MHz, $CDCl_3$) δ_H 2.79 (t, 2H, J = 7.0 Hz, SHCH_2), 2.33 (dt, 2H, J = 6.9, 2.7 Hz, CHCCH_2), 1.97 (t, 1H, J = 2.6 Hz, CH), 1.92 (quin, 2H, J = 7.4 Hz, SHCH$_2$CH_2); ^{13}C (150 MHz, $CDCl_3$) δ_C 83.4 (CH*C*), 69.3 (*C*HC), 37.5 (SH*C*H$_2$), 27.8 (CHC*C*H$_2$), 17.3 (SHCH$_2$*C*H$_2$); IR (oil) V_{max}/cm^{-1} 3292 (C-H), 2194 (CΞC); LRMS (ESI) *m/z* (%) 101.0 ([M + H]$^+$, 100); HRMS (ESI) *m/z* calculated for [C_5H_8S] 100.0346, observed 100.0419.

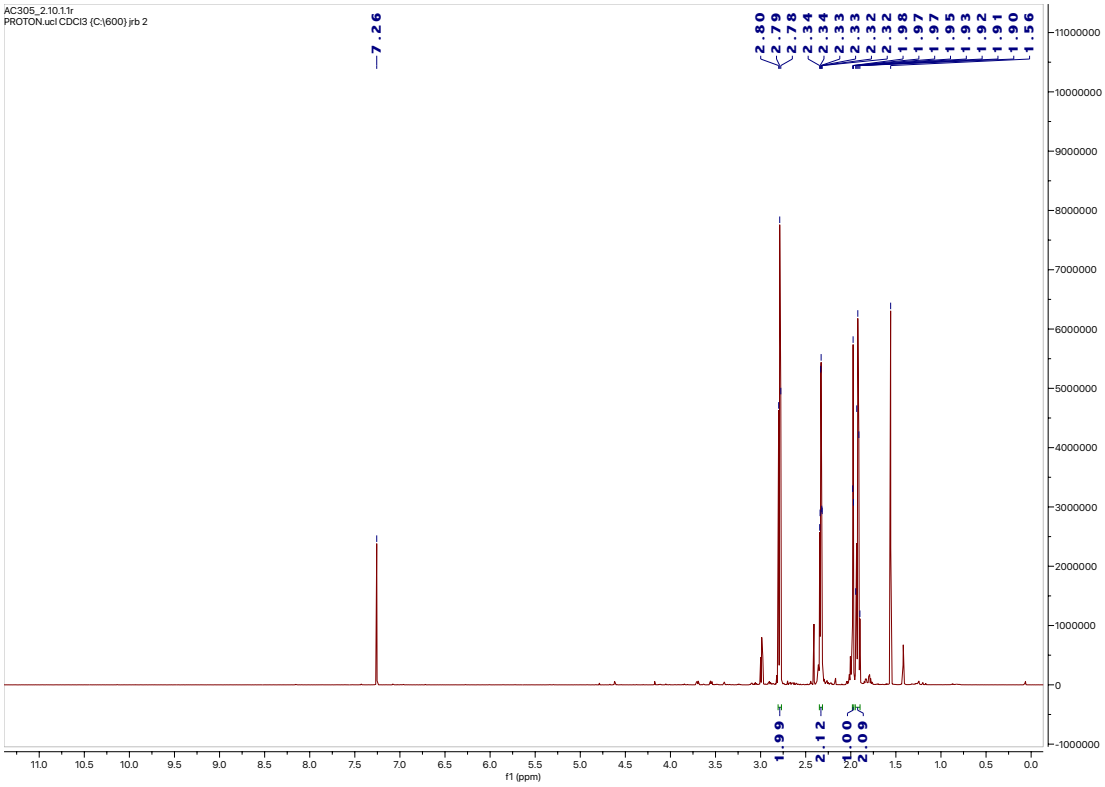
AC305_2.10.1.1r
PROTON.ucl CDCl3 (C:\600) jrb 2
7.26
2.80
2.79
2.78
2.34
2.33
2.32
1.98
1.97
1.95
1.93
1.92
1.91
1.90
1.56
1.99
2.12
1.00
2.09
f1 (ppm)

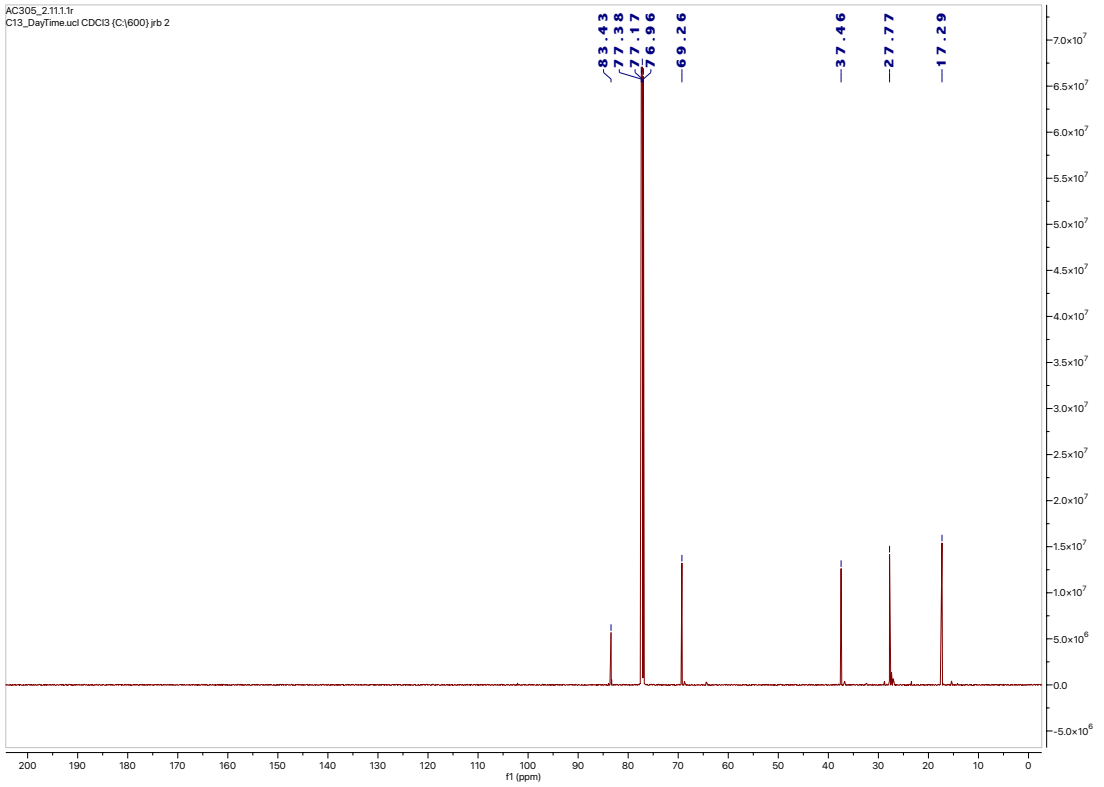
AC305_2.11.1.1r
C13_DayTime.ucl CDCl3 (C:\600) jrb 2
83.43
77.38
77.17
76.96
69.26
37.46
27.77
17.29
f1 (ppm)

2-(pent-4-yn-1-yldisulfaneyl)pyridine (47)

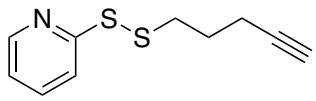

2,2'-dipyridyl disulfide (80 mg, 0.38 mmol, 1.25 eq.) was dissolved in 5 mL of 0 °C THF followed by addition of triethylamine (0.04 mL, 0.46 mmol, 1.5 eq.). To the cold mixture, pent-4-yne-1-thiol **46** (30 mg, 0.31 mmol, 1.0 eq.) was added and the reaction was allowed to come up to RT. The mixture was stirred at room temperature for 2 h. The crude product was then purified using automatic column chromatography (gradient elution from 100% cyclohexane to 30% ethyl acetate in cyclohexane) afforded the target compound as light-yellow oil (15 mg, 0.07 mmol, 23% yield).

^{1}H NMR (600 MHz, $CDCl_3$) δ_H 8.47 (d, 1H, *J* = 5.0 Hz, CCHC*H*), 7.71 (d, 1H, *J* = 8.2 Hz, CC*H*), 7.64 (td, 1H, *J* = 7.7, 1.9 Hz, CC*H*), 7.10-7.08 (m, 1H, CNCHC*H*), 2.91 (t, 2H, *J* = 7.2 Hz, SCH_2), 2.33 (dt, 2H, *J* = 6.9, 2.7 Hz, CHCCH_2), 1.95 (t, 1H, *J* = 2.7 Hz, C*H*), 1.93 (q, 2H, *J* = 6.9 Hz, SCH_2CH_2); ^{13}C (150 MHz, $CDCl_3$) δ_C 160.4 (*C*N), 149.8 (CN*C*H), 137.2 (CCH*C*H), 120.8 (C*C*H), 119.8 (CNCH*C*H), 83.2 (CH*C*), 69.4 (*C*HC), 37.5 (S*C*H_2), 27.5 ($SCH_2CH_2CH_2$), 17.3 ($SCH_2CH_2CH_2$); IR (oil) V_{max}/cm^{-1} 2926 (C-H), 2116 (CΞC), 1972 (C-H), w); LRMS (ESI) *m/z* (%) 210.0 ([M + H]$^+$, 100); HRMS (ESI) *m/z* calculated for [$C_{10}H_{11}NS_2$] 209.0332, observed 209.0410.

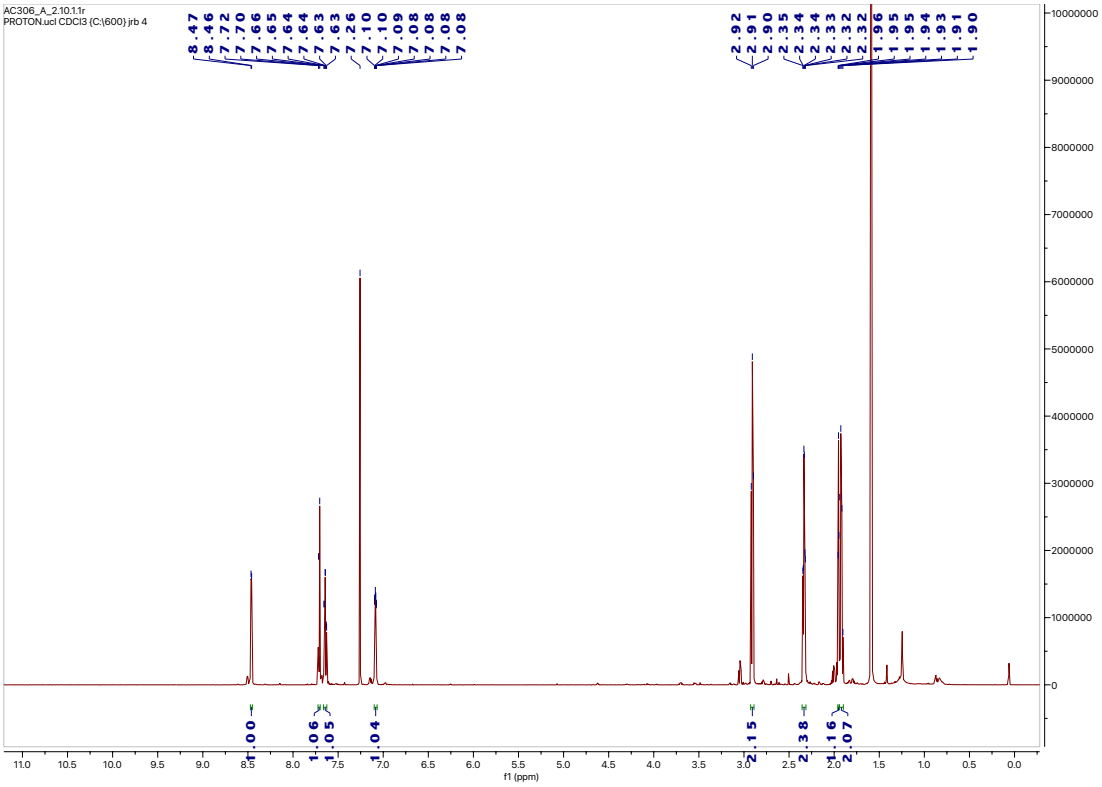
AC306_A_2.10.1.1r
PROTON.ucl CDCl3 (C:\600) jrb 4
8.47
8.46
7.72
7.70
7.66
7.65
7.64
7.64
7.63
7.63
7.26
7.10
7.10
7.09
7.08
7.08
7.08
7.08
2.92
2.91
2.90
2.35
2.34
2.34
2.33
2.32
2.32
1.96
1.95
1.94
1.93
1.91
1.90
1.00
1.06
1.05
1.04
2.15
2.38
1.16
2.07
f1 (ppm)

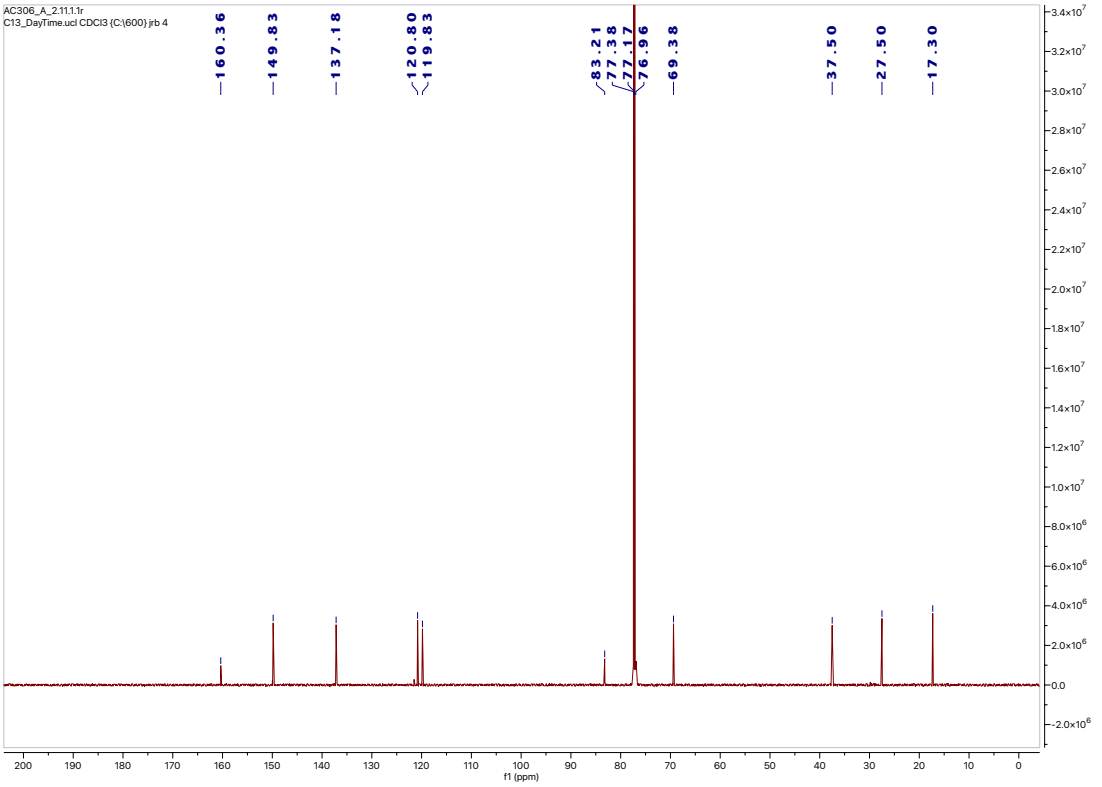
AC306_A_2.11.1.1r
C13_DayTime.ucl CDCl3 (C:\600) jrb 4
160.36
149.83
137.18
120.80
119.83
83.21
77.38
77.17
76.96
69.38
37.50
27.50
17.30
f1 (ppm)

tert-butyl (2-(2-(2-aminoethoxy)ethoxy)ethyl)carbamate[194] (51)

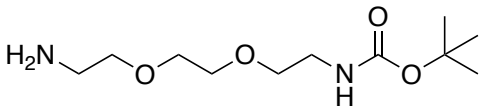

2,2'-(ethane-1,2-diylbis(oxy))bis(ethan-1-amine) (0.40 mL, 2.69 mmol, 5.0 eq.) was dissolved in 10 mL of DCM at 0 °C, followed by slow addition of di-tert-butyl-dicarbonate (120 mg, 0.54 mmol, 1.0 eq.) separately dissolved in 5 mL of DCM. The mixture was left at RT for 16 h, stirring. The crude was then washed with water (1 x 5 mL) and extracted with DCM (2 x 5 mL), dried over $MgSO_4$, and concentrated *in vacuo* that afforded the target compound as light-yellow oil (142 mg, 0.57 mmol, quantitative yield).

^{1}H NMR (600 MHz, $CDCl_3$) δ_H 5.17 (s, 1H, N*H*), 3.59 (s, 4H, OCH_2CH_2O), 3.52 (t, 2H, *J* = 5.2 Hz, OCH_2CH$_2$NH), 3.49 (t, 2H, *J* = 5.2 Hz, NH$_2$CH$_2$CH_2), 3.29 (d, 2H, *J* = 5.1 Hz, CH_2NH), 2.85 (t, 2H, *J* = 5.7 Hz, NH$_2$CH_2), 1.41 (s, 9H, CCH_3); ^{13}C (150 MHz, $CDCl_3$) δ_C 156.2 (NH*C*(O)), 79.3 (*C*), 73.6 (NH$_2$CH$_2$*C*H$_2$), 70.4 (O*C*H$_2$CH$_2$NH), 70.3 (OCH$_2$*C*H$_2$O), 41.9 (NH$_2$*C*H$_2$), 40.4 (*C*H$_2$NH), 28.5 (C*C*H$_3$); IR (oil) V_{max}/cm^{-1} 2924 (C-H), 1690 (C=H); LRMS (ESI) *m/z* (%) 249.2 ([M + H]$^+$, 100); HRMS (ESI) *m/z* calculated for [$C_{11}H_{24}N_2O_4$] 248.1736, observed 248.1808.

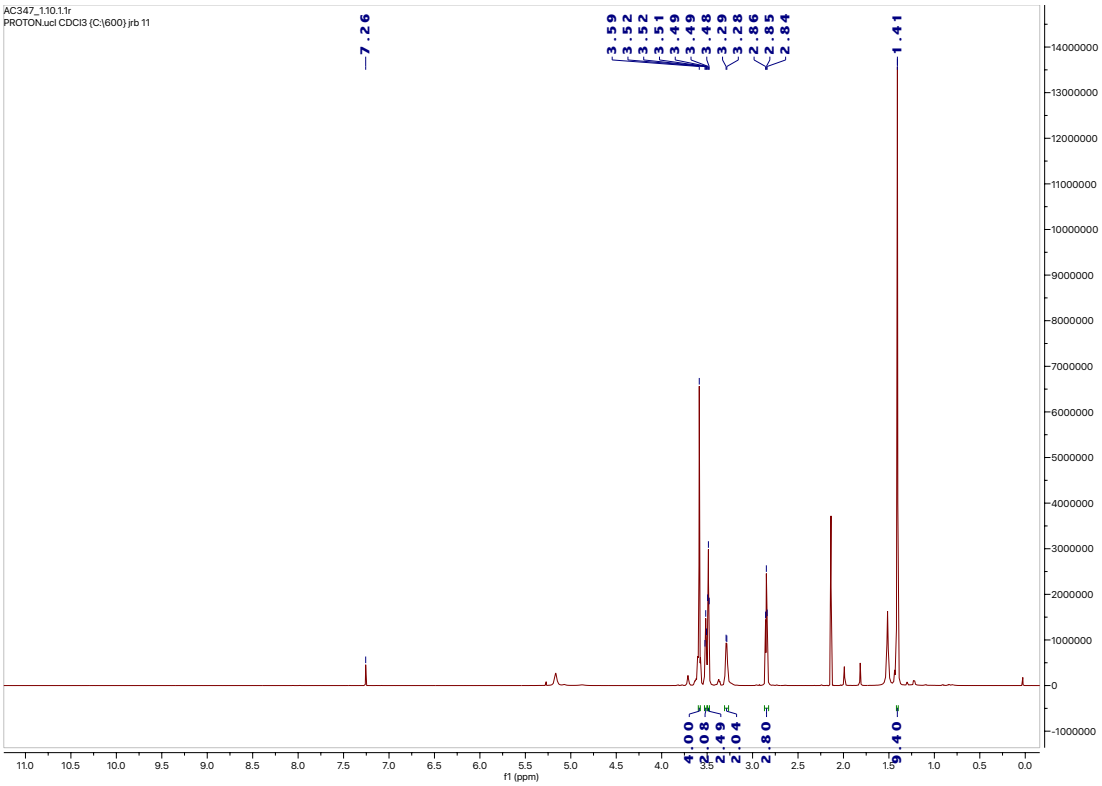

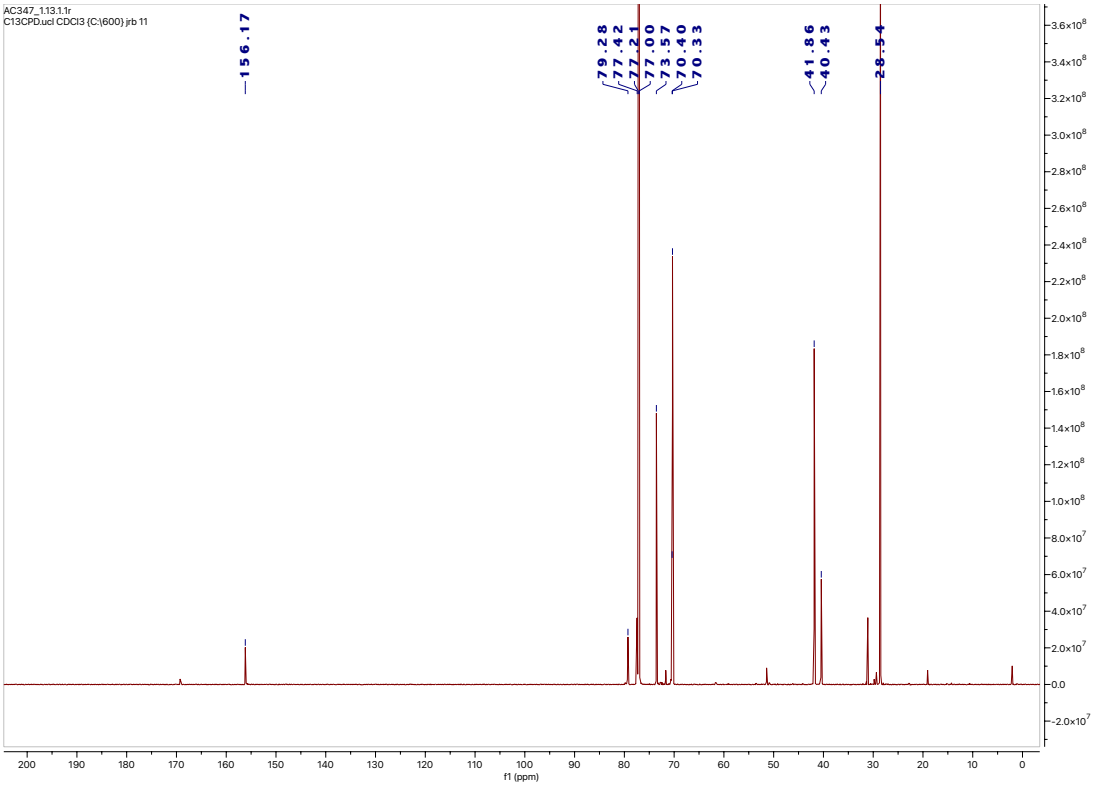

tert-butyl (2-(2-(2-(5-((3a*S*,4*S*,6a*R*)-2-oxohexahydro-1*H*-thieno[3,4-*d*]imidazol-4-yl)pentanamido)ethoxy)ethoxy)ethyl)carbamate[194] (52)

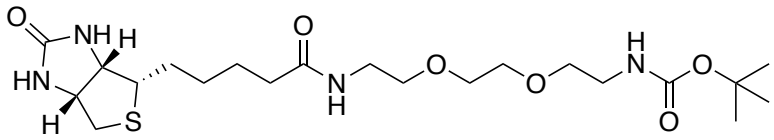

Biotin (140 mg, 0.57 mmol, 1.0 eq.) was first dissolved in 2 mL DMF, followed by addition of EDC.HCl (160 mg, 0.86 mmol, 1.5 eq.), HOBt (120 mg, 0.86 mmol, 1.5 eq.) and triethylamine (0.24 mL, 1.72 mmol, 3.0 eq.). This was stirred for 30 min at RT. Then PEG-Boc (**51**) (*tert*-butyl (2-(2-(2-aminoethoxy)ethoxy)ethyl)carbamate) was added, and the mixture was stirred for 16 h at RT. The solvent was then removed *in vacuo* and purification by column chromatography (gradient elution from 100% DCM to 30% methanol in DCM) afforded the target compound as white wax (106 mg, 0.22 mmol, 39% yield*). *Minor impurities observed in the aromatic region of the NMR, this was taken directly to the next step.

^{1}H NMR (700 MHz, MeOD) δ_H 4.50-4.48 (m, 1H, SCH$_2$C*H*), 4.32-4.29 (m, 1H, SCHC*H*), 3.61 (s, 4H, OC*H*$_2$C*H*$_2$O), 3.54 (t, 2H, *J* = 5.6 Hz, NHCH$_2$C*H*$_2$), 3.51 (t, 2H, *J* = 5.7 Hz, C*H*$_2$CH$_2$NH), 3.36 (t, 2H, *J* = 5.6 Hz, NHC*H*$_2$CH$_2$), 3.22 (t, 2H, *J* = 5.7 Hz, CH$_2$C*H*$_2$NH), 3.20-3.19 (m, 1H,

SC*H*), 2.92 (dd, 1H, *J* = 12.9, 4.9 Hz, SC*H*H), 2.71 (d, 1H, *J* = 12.9 Hz, SCH*H*), 2.22 (t, 2H, *J* = 7.4 Hz, CH_2C(O)NH), 1.76-1.56 (m, 6H, CHCH_2CH_2CH_2), 1.43 (s, 9H, CCH_3); ^{13}C (150 MHz, MeOD) δ_C 176.0 (CH_2C(O)NH), 166.0 (NH*C*(O)NH), 158.3 (NH*C*(O)O), 80.0 (*C*CH_3), 71.2 (NHCH_2CH_2), 71.0 (*C*H_2CH_2NH), 70.5 (OCH_2CH_2O), 63.3 (SCH*C*H), 61.5 (SCH_2*C*H), 56.9 (S*C*H), 41.2 (S*C*H_2), 41.0 (NH*C*H_2CH_2), 40.2 (CH_2*C*H_2NH), 36.7 (CHCH_2*C*H_2), 29.7 (CH*C*H_2), 29.4 (*C*H_2CH_2C(O)), 28.7 (C*C*H_3), 26.8 (*C*H_2C(O)); IR (gum) V_{max}/cm^{-1} 2932 (C-H), 2867 (C-H), 1690 (C=H); LRMS (ESI) *m/z* (%) 475.2 ([M + H]$^+$, 100); HRMS (ESI) *m/z* calculated for [$C_{21}H_{38}N_4O_6S$] 474.2512, observed 474.2586.

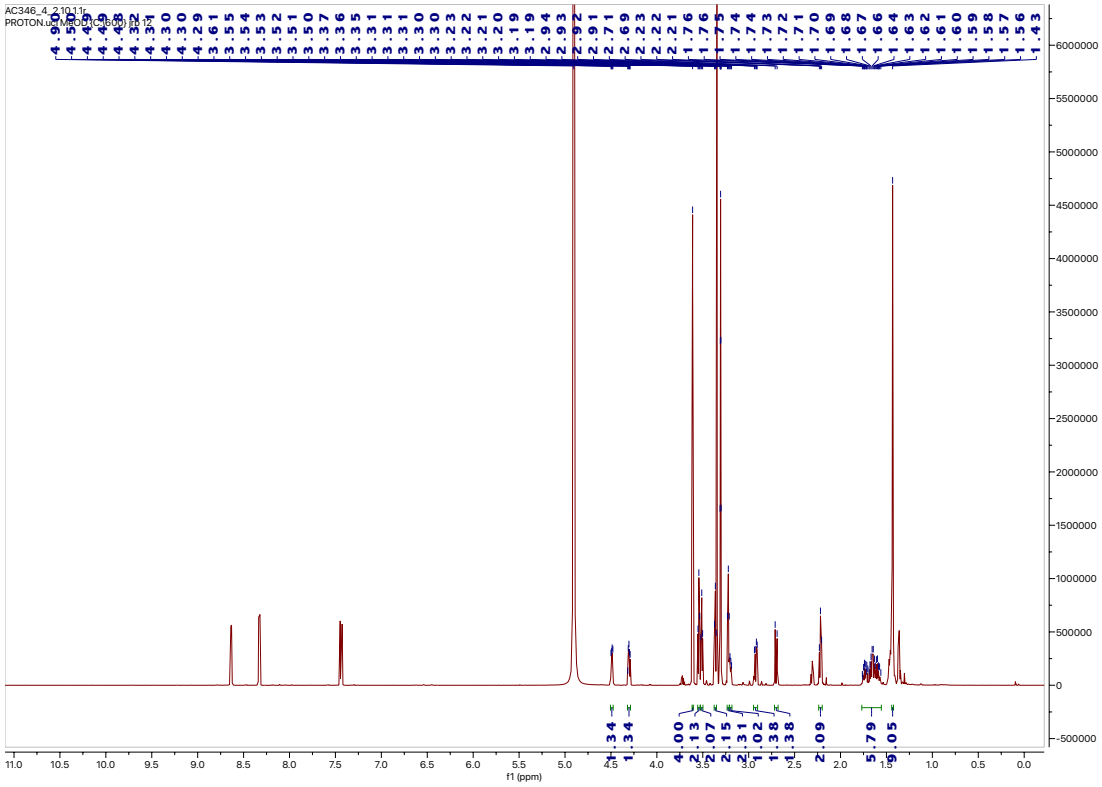

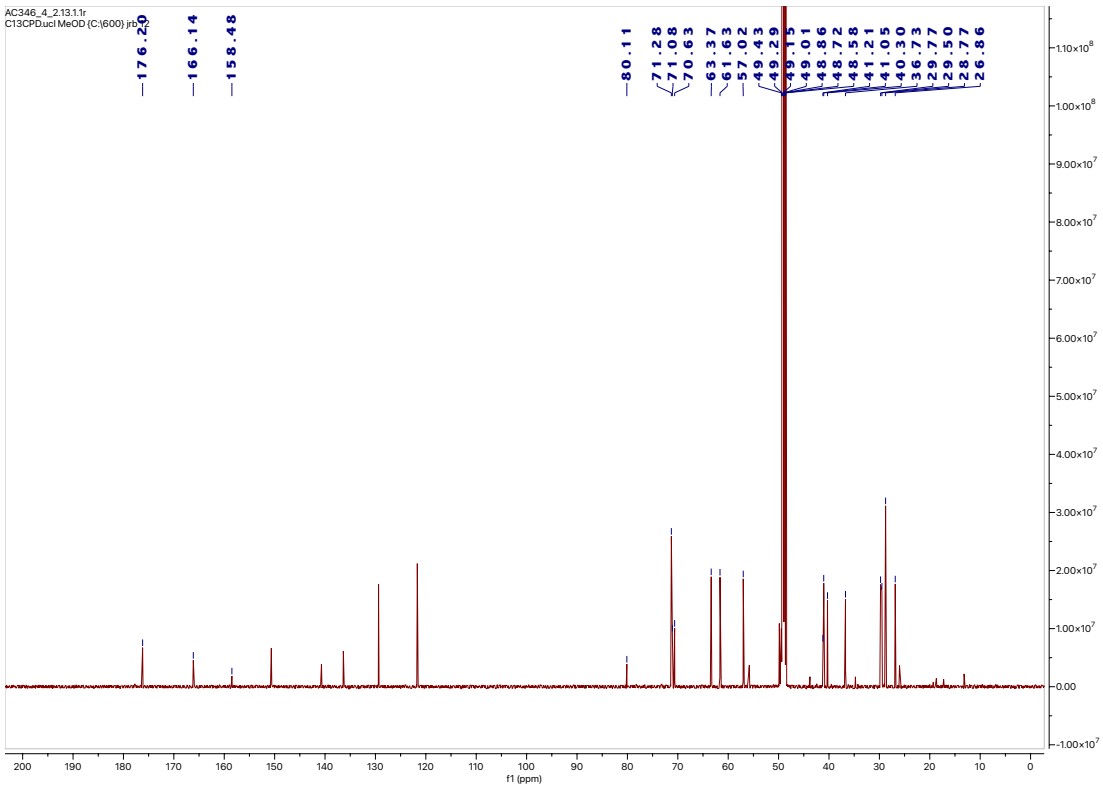

4-formyl-*N*-(2-(2-(2-(5-((3a*R*,4*R*,6a*S*)-2-oxohexahydro-1*H*-thieno[3,4-*d*]imidazol-4-yl)pentanamido)ethoxy)ethoxy)ethyl)benzamide[194] (53)

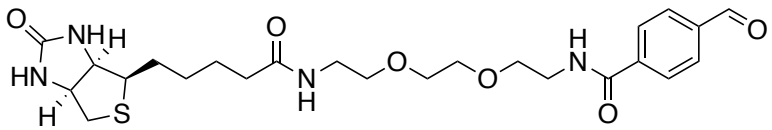

Impure Biotin-PEG-Boc **52** (60 mg, 0.12 mmol, 1.0 eq.) was dissolved in 1 mL of DCM followed by addition of 1 mL of TFA, this was stirred at RT for 2 h. After 2 h the solvent was removed *in vacuo*, and the mixture was washed with 3 x 5 mL of ethyl acetate to remove the TFA. In a separate flask, 4-formylbenzoic acid (40 mg, 0.26 mmol, 2.1 eq.) was dissolved in 0.5 mL of MeCN and 0.5 mL DMF. EDC.HCl (50 mg, 0.27 mmol, 2.2 eq.) and DIPEA (0.05 mL, 0.31 mmol, 2.5 eq.) were added and this was stirred for 30 min at RT. Lastly the acid mixture was added to the deprotected Biotin-PEG-NH_2 and the reaction was stirred at RT for 16 h. The solvent was then removed *in vacuo* and purification by column chromatography (gradient elution from 100% DCM to 30% methanol in DCM) afforded the target compound white gum (35.8 mg, 0.07 mmol, 57% yield*). *Impurities present in the NMR but are not observed in HRMS and bioconjugation reactions, the purity was found to be sufficient for protein labelling.

^{1}H NMR (600 MHz, DMSO-d) δ_H 10.08 (s, (1H, C*H*), 8.02 (d, 2H, *J* = 8.4 Hz, ArC*H*), 8.00 (d, 2H, *J* = 8.4 Hz, ArC*H*), 4.30-4.28 (m, 1H, SCH$_2$C*H*), 4.13-4.10 (m, 1H, SCHC*H*), 3.54-3.53 (m, 4H, OC*H*$_2$C*H*$_2$O), 3.51-3.50 (m, 2H, NHCH$_2$C*H*$_2$O), 3.45-3.43 (m, 2H, OC*H*$_2$CH$_2$NH), 3.18-3.15 (m, 2H, NHC*H*$_2$CH$_2$), 2.96 (t, 2H, *J* = 6.6 Hz, CH$_2$C*H*$_2$NH), 2.80 (dd, 1H, *J* = 12.7, 5.2 Hz, SCH*H*), 2.58 (d, 1H, *J* = 12.7 Hz, SC*H*H), 2.43 (d, 1H, *J* = 7.2 Hz, SC*H*), 2.05 (t, 2H, *J* = 7.7 Hz, C*H*$_2$C(O)NH), 1.51-1.42 (m, 4H, CHCH$_2$C*H*$_2$C*H*$_2$), 1.30-1.24 (m, 2H, SCHC*H*$_2$); ^{13}C (150 MHz, DMSO-d) δ_C 193.0 (*C*(O)H), 172.2 (CH$_2$*C*(O)NH), 165.5 (NH*C*(O)NH), 162.8 (CH$_2$*C*(O)C), 139.4 (NHC(O)*C*), 135.7 (*C*C(O)H), 129.5 (*C*HC*C*H), 128.0 (*C*HC*C*H), 69.6 (NHCH$_2$*C*H$_2$), 69.2 (*C*H$_2$CH$_2$NH), 68.8 (OC*H*$_2$*C*H$_2$O), 61.1 (SCH*C*H), 59.2 (SCH$_2$*C*H), 55.5 (S*C*H), 40.0 (SCH$_2$), 38.4 (NH*C*H$_2$CH$_2$), 38.3 (*C*H$_2$CH$_2$NH), 35.1 (CHCH$_2$*C*H$_2$), 28.2 (CH*C*H$_2$), 28.1 (*C*H$_2$CH$_2$C(O)), 25.3 (*C*H$_2$C(O)); IR (gum) V_{max}/cm^{-1} 2924 (C-H), 2825 (C-C), 1668 (C=O); LRMS (ESI) *m/z* (%) 507.2 ([M + H]$^+$, 100); HRMS (ESI) *m/z* calculated for [$C_{24}H_{34}N_4O_6S$] 506.2127, observed 507.2270.

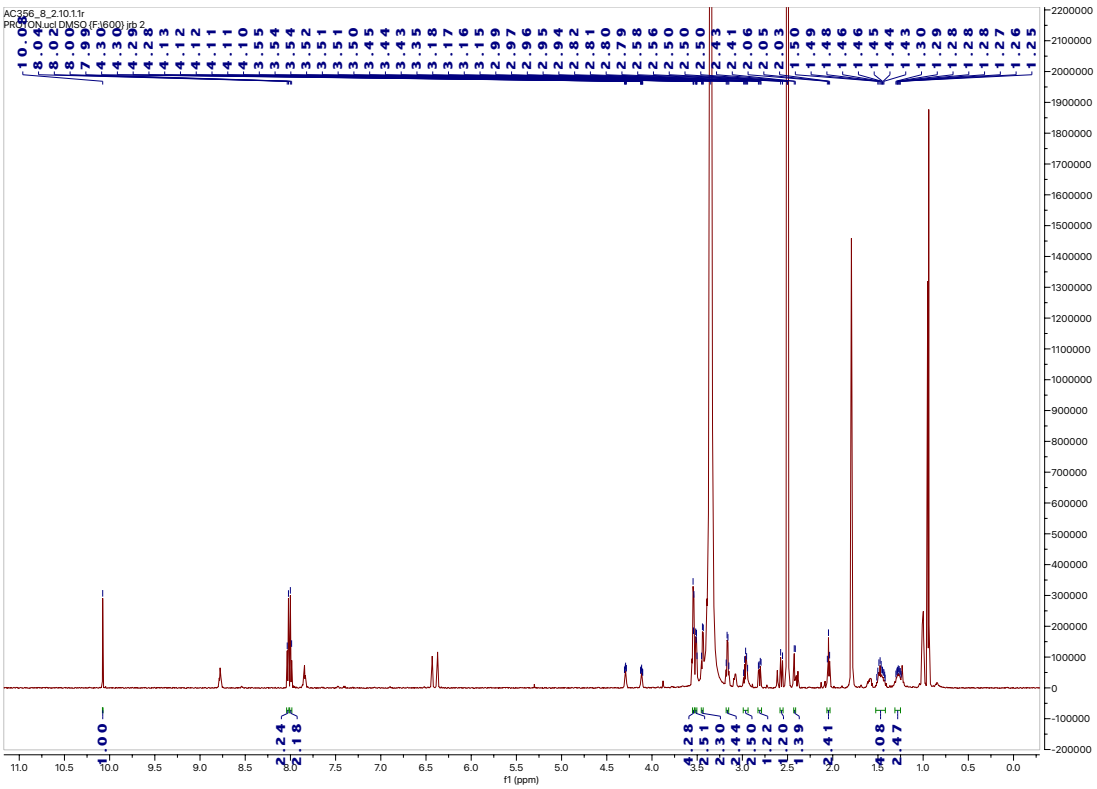

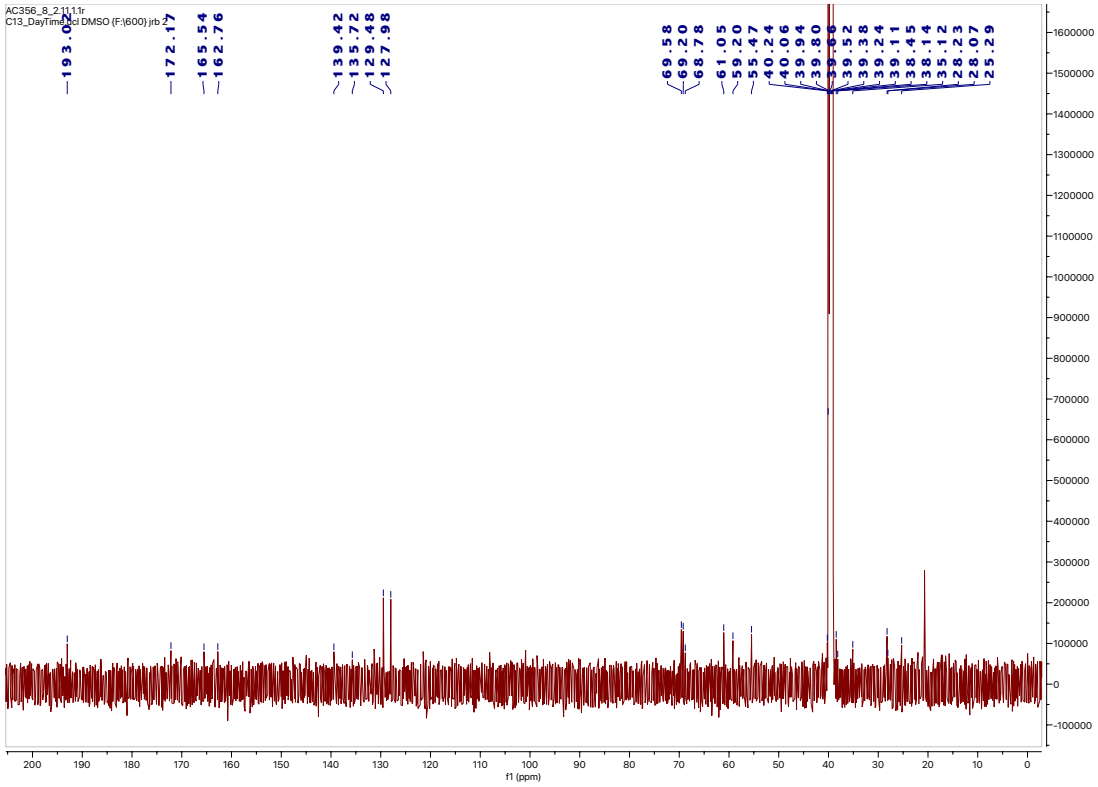

2-(4-formylphenyl)acetic acid (56)

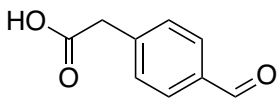

2-(4-(hydroxymethyl)phenyl)acetic acid (180 mg, 1.08 mmol, 1.0 eq.) was first dissolved in 10 mL ethyl acetate and heated to 80 °C, following that, 2-iodoxybenzoic acid (360 mg, 1.30 mmol, 1.2 eq.) was added and the mixture was stirred at 80 °C for 3 h. This was then washed with water (2 x 10 mL) and extracted with DCM (2 x 10 mL), dried over $MgSO_4$, and concentrated *in vacuo*. The crude product was then purified by column chromatography (gradient elution from 100% DCM to 10% methanol in DCM and 1% AcOH) afforded the target compound white powder (87.2 mg, 0.52 mmol, 49% yield). *Minor impurities observed in the aromatic region of the NMR, most likely from the starting material, this was taken directly to the next step.

mp 130-132 °C, ^{1}H NMR (600 MHz, $CDCl_3$) δ_H 10.0 (s, 1H, C(O)*H*), 7.85 (d, 2H, *J* = 8.2 Hz, ArC*H*), 7.46 (d, 2H, *J* = 8.2 Hz, ArC*H*), 3.75 (s, 2H, CH_2); ^{13}C (150 MHz, $CDCl_3$) δ_C 192.2 (*C*(O)H), 176.7 (*C*(O)OH), 140.3 (CH_2C), 135.6 (*C*C(O)), 130.4 (Ar*C*H), 130.3 (Ar*C*H), 41.2

(CH_2); IR (white powder) V_{max}/cm^{-1} 2848 (C-H), 1693 (C=O); LRMS (ESI) *m/z* (%), 165.1 ($[M+H]^+$, 100); HRMS (ESI) *m/z* calculated for $[C_9H_8O_3]$ 164.0473, observed 164.0547.

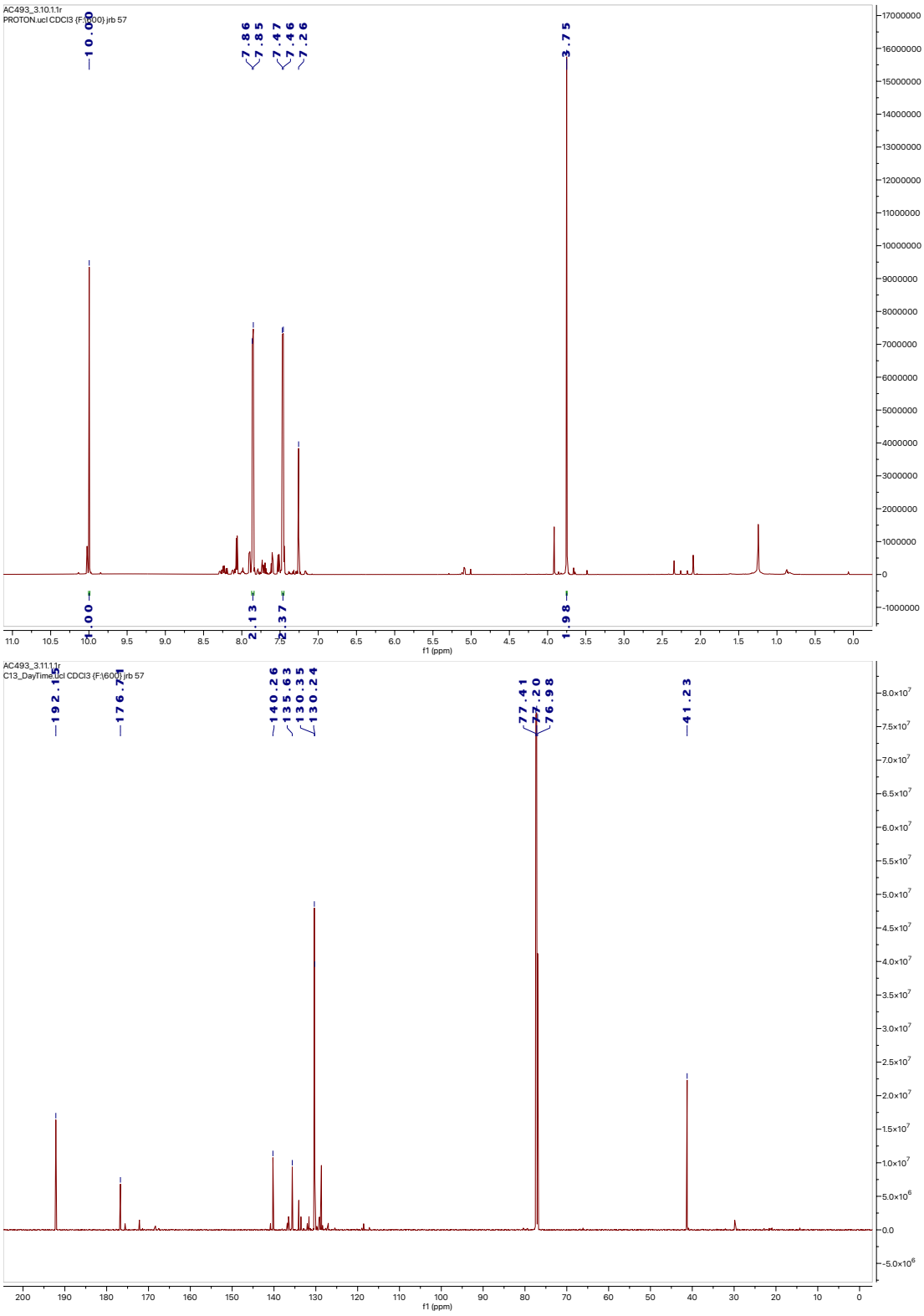

N-(2-(2-(2-aminoethoxy)ethoxy)ethyl)-2-(4-formylphenyl)acetamide (57)

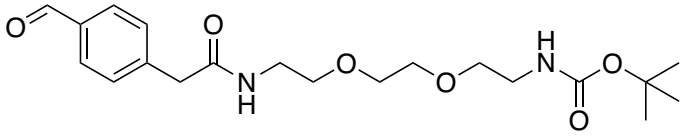

2-(4-formylphenyl)acetic acid **56** (70 mg, 0.41 mmol, 2.5 eq.) was dissolved in 1 mL DMF followed by EDC.HCl (40 mg, 0.19 mmol, 1.2 eq.) and DIPEA (0.06 mL, 0.32 mmol, 2.0 eq.). This was stirred for 30 min at RT. Then PEG-Boc (40 mg, 0.16 mmol, 1.0 eq.) was added, and the mixture was stirred for 16 h at RT. The solvent was then removed *in vacuo* and purified using automatic column chromatography (gradient elution from 100% DCM to 30% methanol in DCM) afforded the target compound as white gum (51.6 mg, 0.13 mmol, 81% yield). *Unknown impurities were found 2.34 ppm in ^{1}H and 129.2, 128.3 and 125.4 ppm in ^{13}C, this was taken directly to the next step.

^{1}H NMR (600 MHz, $CDCl_3$) δ_H 9.98 (s, 1H, C(O)*H*), 7.84-7.82 (m, 2H, ArC*H*), 7.46-7.26 (m, 2H, ArC*H*), 3.62 (s, 2H, CCH_2C(O)), 3.55 (s, 4H, OCH_2CH_2O), 3.53-3.52 (m, 4H, NHCH_2CH_2 and CH_2CH_2NH_2), 3.44 (q, 2H, *J* = 5.3 Hz, NHCH_2), 3.32-3.27 (m, 2H, CH_2NH_2) 1.43 (s, 9H, CH_3); ^{13}C (150 MHz, $CDCl_3$) δ_C 192.1, (*C*(O)H), 170.0 (CCH_2*C*(O)NH), 156.2 (NH*C*(O)O) 142.3 (CH_2*C*), 135.5 (*C*C(O)H), 130.1 (Ar*C*H), 130.1 (Ar*C*H), 79.6 (*C*), 70.4 (OCH_2*C*H_2O), 70.3 (NHCH_2*C*H_2O), 70.2 (OCH_2CH_2NH_2), 43.8 (C*C*H_2C(O)), 40.4 (NH*C*H_2), 39.6 (*C*H_2NH_2), 28.6 (CH_3); IR (gum) V_{max}/cm^{-1} 2924 (C-H), 2854 (C-H), 1700 (C=H), 1655 (C=O); LRMS (ESI) *m/z* (%) 295.2 ([M + H]$^+$, 100); HRMS (ESI) *m/z* calculated for [$C_{20}H_{30}N_2O_6$] 394.2103, observed 394.1653.

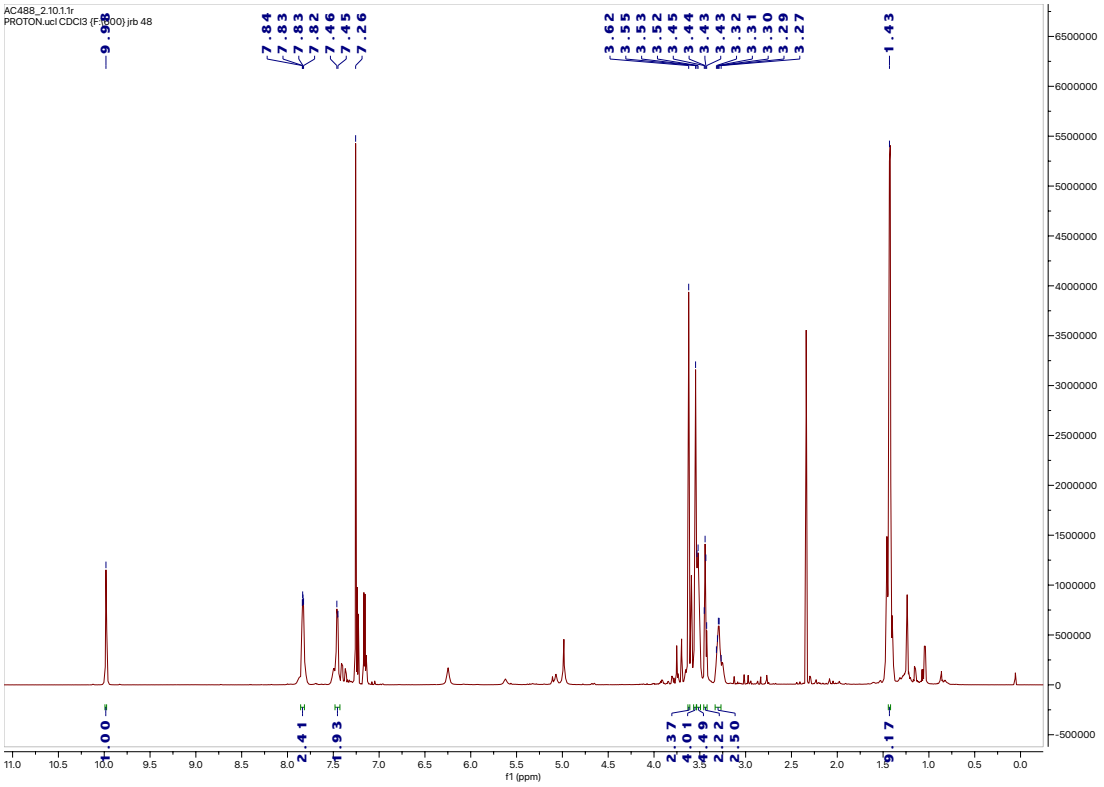
AC488_2.10.1.1r
PROTON.ucl CDCl3 {F:\600} jrb 48
9.93
7.84
7.83
7.83
7.82
7.46
7.45
7.26
3.62
3.55
3.53
3.52
3.45
3.44
3.43
3.43
3.32
3.31
3.30
3.29
3.27
1.43
1.00
2.41
1.93
2.37
4.01
4.49
2.22
2.50
9.17
f1 (ppm)

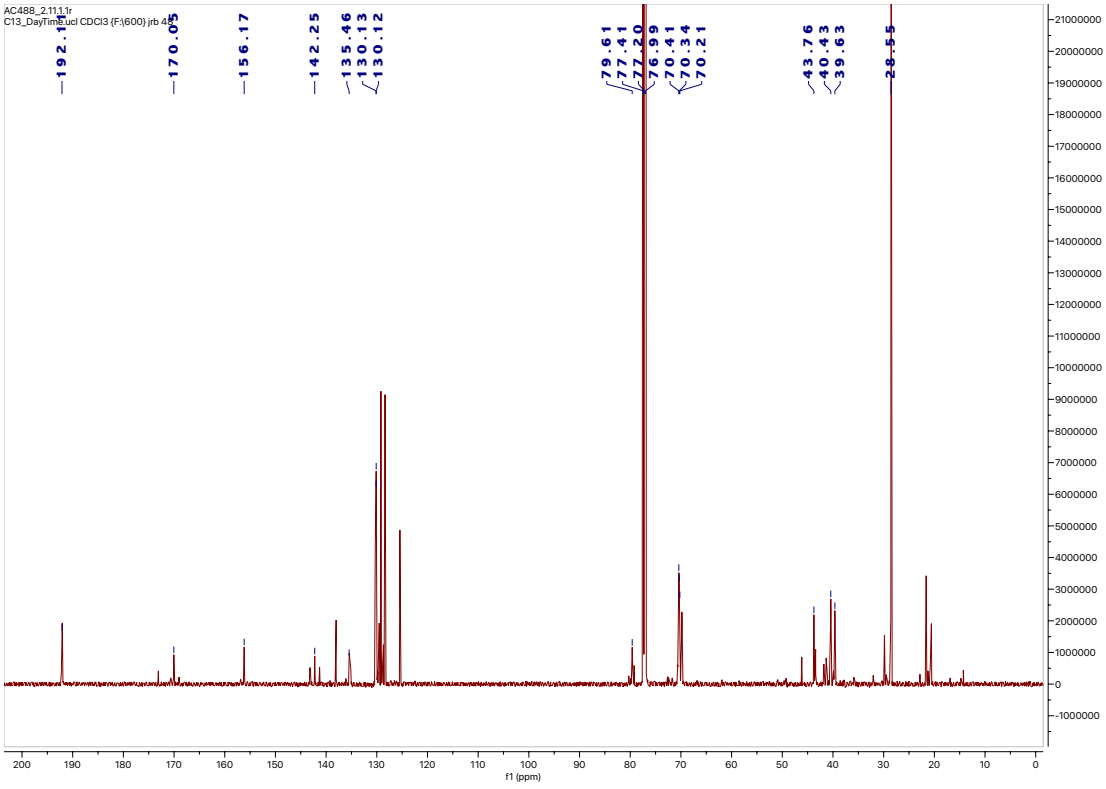
AC488_2.11.1.1r
C13_DayTime.ucl CDCl3 {F:\600} jrb 48
192.
170.05
156.17
142.25
135.46
130.13
130.12
79.61
77.41
77.20
76.99
70.41
70.34
70.21
43.76
40.43
39.63
28.55
f1 (ppm)

N-(2-(2-(2-(4-formylphenyl)acetamido)ethoxy)ethoxy)ethyl)-5-((3a*S*,4*S*,6a*R*)-2-oxohexahydro-1*H*-thieno[3,4-*d*]imidazol-4-yl)pentanamide (58)

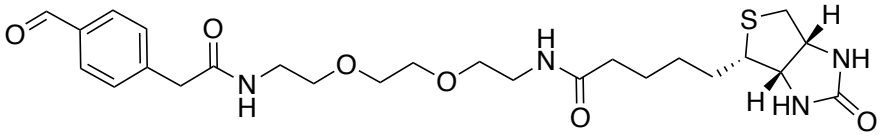

tert-butyl (2-(2-(2-(2-(4-formylphenyl)acetamido)ethoxy)ethoxy)ethyl)carbamate **65** (aldehyde-PEG-Boc) (40 mg, 0.10 mmol, 1.0 eq.) was first dissolved in 1 mL of DCM followed by addition of 1 mL of trifluoracetic acid, this was stirred at RT for 2 h. The mixture was then concentrated *in vacuo* and washed with ethyl acetate (3 x 10 mL). In a separate flask, biotin (50 mg, 0.21 mmol, 2.0 eq.) was dissolved in 1 mL of MeCN and 1 mL of DCM, followed by EDC.HCl (40 g, 0.21 mmol, 2.0 eq.) and DIPEA (0.05 mL, 0.31 mmol, 2.5 eq.), this was stirred for 30 min at RT. Lastly the acid mixture was added to the Biotin-PEG-NH_2 and the reaction was stirred for 16 h at RT. The solvent was then removed *in vacuo* and purified using automatic column chromatography (gradient elution from 100% DCM to 30% methanol in DCM) afforded the target compound white oil (21.9 mg, 0.04 mmol, 41% yield). *Minor impurities present in the aromatic region of the NMR but are not observed in HRMS and bioconjugation reactions, the purity was found to be sufficient for protein labelling

^{1}H NMR (600 MHz, MeOD) δ_H 9.96 (s, 1H, C(O)*H*), 7.86 (d, 2H, *J* = 8.2 Hz, ArC*H*), 7.51 (d, 2H, *J* = 8.2 Hz, ArC*H*), 4.49-4.47 (m, 1H, SCH_2CH), 4.29-4.27 (m, 1H, SCHC*H*), 3.63 (s, 2H, $CCH_2C(O)$), 3.60 (s, 4H, OCH_2CH_2O), 3.54-2.52 (m, 4H, $NHCH_2CH_2$ and CH_2CH_2NH), 3.38 (t, 2H, *J* = 5.2 Hz, $NHCH_2$), 3.35 (t, 2H, *J* = 5.4 Hz, CH_2NH), 3.20-3.17 (m, 1H, SC*H*), 2.90 (dd, 1H, *J* = 13.1, 5.1 Hz, SC*H*H), 2.70 (d, 1H, *J* = 13.1 Hz, SCH*H*), 2.21 (t, 2H, *J* = 7.2 Hz, $NHC(O)CH_2CH_2CH_2$), 1.75-1.54 (m, 6H, $SCHCH_2CH_2$ and $NHC(O)CH_2CH_2CH_2$); ^{13}C (150 MHz, MeOD) δ_C 193.2 (*C*(O)H), 176.7 ($NHC(O)CH_2$), 173.2 ($CCH_2C(O)NH$), 160.9 ($NHC(O)NH$), 141.1 (CH_2C), 134.1 (*C*C(O)H), 130.3 (Ar*C*H), 130.2 (Ar*C*H), 70.6 (OCH_2CH_2O), 69.9 ($NHCH_2CH_2O$), 69.8 (OCH_2CH_2NH), 62.7 (SCH*C*H), 60.9 (SCH_2CH), 56.3 (S*C*H), 43.1 ($CCH_2C(O)$), 40.4 (SCH_2), 39.9 ($NHCH_2$), 39.6 (CH_2NH), 36.1 ($SCHCH_2CH_2$), 29.1 ($NHC(O)CH_2$), 28.8 ($NHC(O)CH_2CH_2CH_2$), 26.2 ($NHC(O)CH_2CH_2CH_2$); IR (oil) V_{max}/cm^{-1} 2989 (C-H), 2924 (C-H), 1671 (C=O); LRMS (ESI) *m/z* (%) 521.2 ($[M + H]^+$, 100); HRMS (ESI) *m/z* calculated for $[C_{25}H_{36}N_4O_6S]$ 520.2355, observed 520.2426.

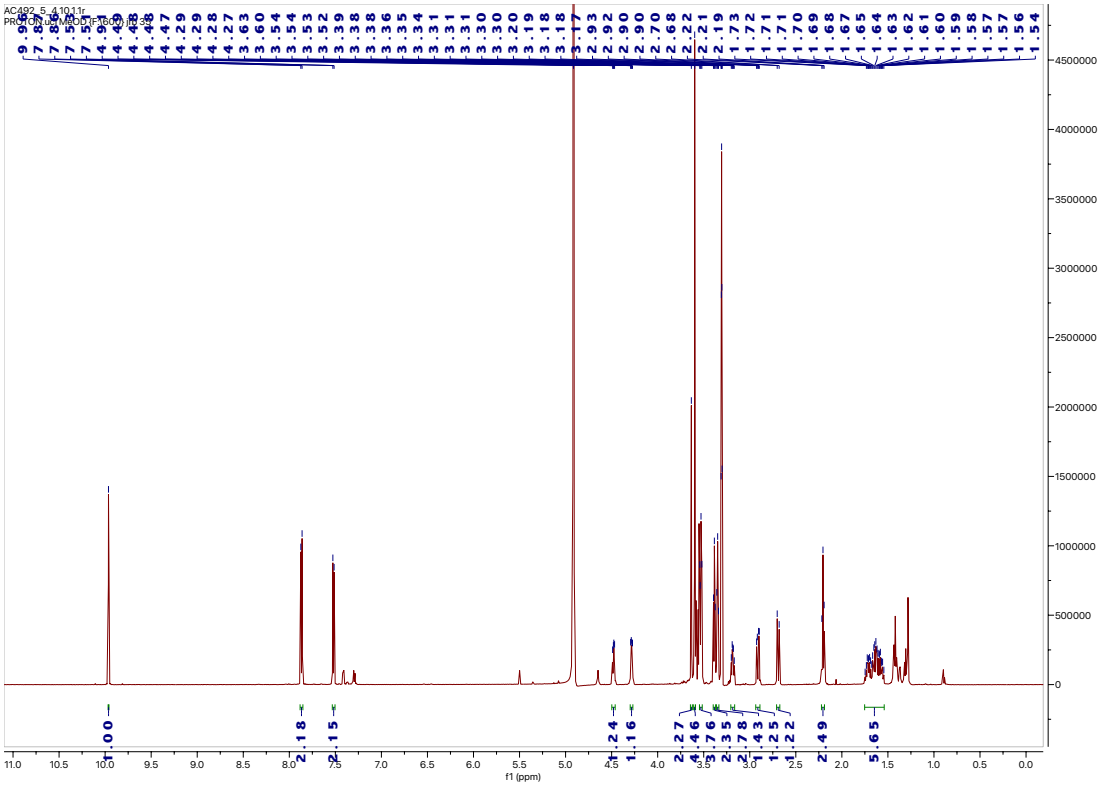

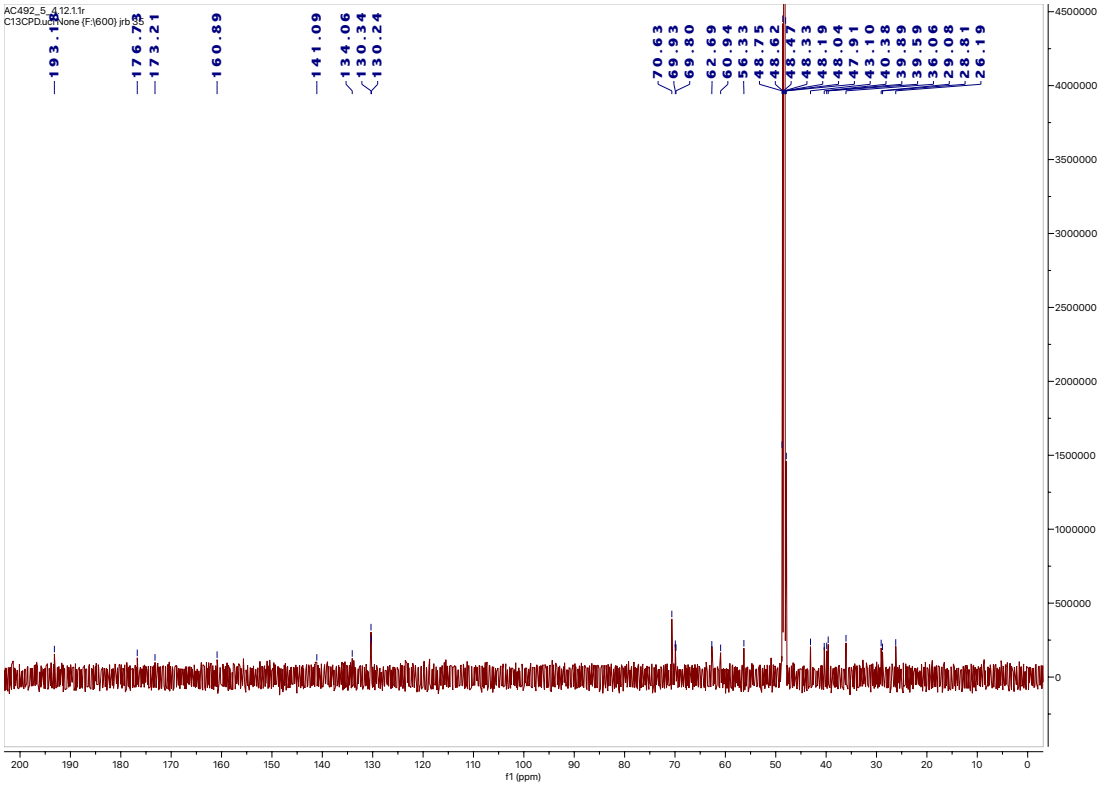

Bicyclo[6.1.0]non-4-yn-9-ylmethyl (2-(2-(2-(2-(3,4-dibromo-2,5-dioxo-2,5-dihydro-1*H*-pyrrol-1-yl)acetamido)ethoxy)ethoxy)ethyl)carbamate (S6)

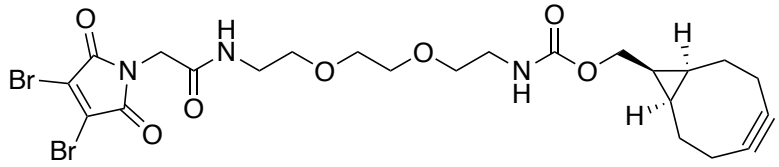

The compound was a kind gift from Dr Nafsika Forte. Full characterisation can be observed in Maneiro *et al*., 2020.[173]

((1*R*,8*S*,9*s*)-bicyclo[6.1.0]non-4-yn-9-yl)methyl (2-(2-(2-(3-(4,5-dibromo-2-methyl-3,6-dioxo-3,6-dihydropyridazin-1(2*H*)-yl)propanamido)ethoxy)ethoxy)ethyl)carbamate[103] (S7)

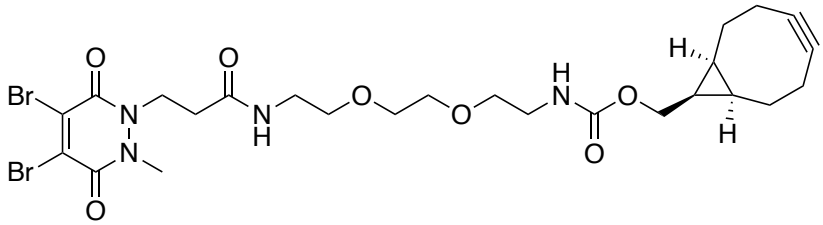

The compound was a kind gift from Ioanna Thanasi. Full characterisation can be observed in Bahou *et al*., 2021.[103]

4,5-Dibromo-1,2-diethyl-1,2-dihydropyridazine-3,6-dione (S8)

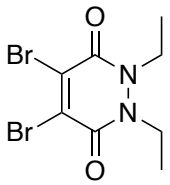

The compound was a kind gift from Ioanna Thanasi. Full characterisation can be observed in Bahou *et al*., 2021.[103]

7.2 Bioconjugation general marks

All conjugations experiments were performed in a standard polypropylene Eppendorf safe-lock tubes (1.5 or 2.0 mL) at atmospheric pressure with mixing at the temperature stated. All reagents and solvents were purchased from commercial sources; Sigma UK, Fisher UK or VWR UK and used as per manufacturer instructions. Buffers were prepared with double-deionised water and

filter sterilised (0.20 μm). Borate Buffer Saline (BBS) contains 50 mM sodium borate, 50 mM sodium chloride, and 5 mM ethylenediaminetetraacetic acid (EDTA) at pH 8.5 or 7.4. Phosphate Buffer Saline (PBS) tablet contains 10 mM phosphate, 138 mM NaCl, 2.7 mM KCl, pH 7.4. Conjugation Buffer contains 40 mM phosphate, 20 mM NaCl, 6 mM EDTA, pH 7.4. Ultrapure DMF was purchased from Sigma and stored under dry conditions.

Ultrafiltration was carried out using Amicon Ultra-4 Centrifugal Filter Units with molecular weight cut-off (MWCO) of 10 kDa or in Vivaspin 500 centrifugal concentrators (Sartorius, UK) with molecular weight cut-off (MWCO) of 10 kDa. Centrifugation was performed using Eppendorf 5415R fixed angle bench rotor operating at 14000 rcf at 20 °C or in an Eppendorf 5810 swing-bucket rotor centrifuge operating at 3220 rcf at 20 °C.
Peptide P-C218R sequence: CKRKKKGKGLGKKRDPSLRKYKRRRRRRRR, MW 3852.72; peptide TAT sequence: CGISYGRKKRRQRRR, MW 1920.25.

Trastuzumab (Ontruzant™) was purchased from UCLH in its clinical formulation (Samsung Bioepis, lyophilised). Expected mass was calculated according to MS data observed for IgG1 subunits and full antibody: full native antibody (HHLL) 145179, heavy-heavy light (HHL) 121740, heavy light (HL) 72585, heavy chain (HC) 49150, light chain (LC) 23438.[117] For Fab fragment expected masses are: Fab 47638, heavy chain (HC) 24200, light chain (LC) 23438. All masses listed are in Dalton unit (Da).

7.2.1 UV-Vis spectroscopy

UV-Vis spectroscopy was used to determine protein concentration using NanoDrop One/One Microvolume UV-Vis Spectrophotometer (Thermo Fisher) operating at RT. Sample buffer was used as blank for baseline correction with extinction coefficients: $\varepsilon_{280} = 68590\ M^{-1}\ cm^{-1}$ for Fab,[116] $\varepsilon_{505} = 74000\ M^{-1}\ cm^{-1}$ for Azide-fluor 488, $\varepsilon_{335} = 9100\ M^{-1}\ cm^{-1}$ for pyridazinedione (PD) scaffolds.[103] A correction factor at 280 nm of 0.25 for PD, 0.11 for Azide-fluor 488 was employed. Antibody Fab conjugate concentration was determined using the same extinction coefficient as for native trastuzumab Fab (PD were found to have negligible absorbance at 280 nm).

7.2.2 Trastuzumab antibody preparation

Before attempting antibody conjugations, a frozen stock of trastuzumab was taken from -20 °C. The aliquot was prepared in a form of 10 mg/mL (66.6 μM) in 0.5 mL. This was first buffer exchanged into conjugation buffer (40 mM phosphate, 20 mM NaCl, 6 mM EDTA, pH 7.4) *via* ultrafiltration (10 kDa MWCO), depending on subsequent steps. The concentration was then determined by UV/Vis absorbance. Trastuzumab concentration was adjusted to 30 μM (4.5 mg/mL) by adding appropriate amount of conjugation buffer to the buffer exchanged antibody. Aliquots of 30 μM in 50 μL were prepared and stored at -20 °C.

7.2.3 General procedure for the preparation of Trastuzumab (Ontruzant™) Fab fragment[207]

Trastuzumab (0.50 mL, 44.0 μM, 6.41 mg/mL) was buffer exchanged into sodium acetate (NaOAc) buffer (20 mM NaOAc, pH 3.1) *via* ultrafiltration (10 kDa MWCO), followed by determination of concentration. Immobilized pepsin (0.15 mL) was loaded onto a Pierce™ centrifuge column and also washed with NaOAc buffer (20 mM NaOAc, pH 3.1) three times. Trastuzumab (0.50 mL) was then added to the pepsin and the mixture was incubated at 37 °C for 5 h, under constant agitation (1,100 rpm). At the start at 4th hour of incubation, immobilised papain (0.65 mL) was loaded onto Pierce™ centrifuge column and activated with 10 mM DTT in digest buffer (50 mM phosphate, 150 mM NaCl, 1 mM EDTA, pH 6.8). This was incubated at 37 °C for 90 min under constant agitation (1,100 rpm). The resin was then removed from the digest using a Pierce™ centrifuge column and washed with digest buffer (3 × 0.4 mL, 50 mM phosphate, 150 mM NaCl, 1 mM EDTA, pH 6.8). The digest was combined with the washes and the volume was concentrated and adjusted to 0.5 mL. The resin containing papain was washed with digest buffer (4 × 0.4 mL, 50 mM phosphate, 150 mM NaCl, 1 mM EDTA, pH 6.8) without DTT, using a Pierce™ centrifuge column. Remove DTT buffer before adding the antibody. $F(ab')_2$ (0.5 mL) was added to the washed papain and the mixture incubated at 37 °C for 20 h under constant agitation (1,100 rpm). The resin was separated and washed with conjugation buffer (4 × 0.4 mL, 40 mM phosphate, 20 mM NaCl, 6 mM EDTA, pH 7.4). The digest was combined with the washes and the buffer was exchanged completely for conjugation buffer *via* ultrafiltration (10 kDa MWCO). The concentration was determined by UV/Vis absorbance and adjusted to 100 μM. Aliquots of Fab were stored at -20 °C for up to 6 months.

7.2.4 Sodium dodecyl sulphate – polyacrylamide gel electrophoresis (SDS-PAGE)

Protein conjugation reactions were monitored by 12% glycine-SDS-PAGE with 6% stacking gel under non-reducing conditions. Gels were prepared in-house by preparing 12% separating and 6 % stacking gel of components listed in **Table 3**. Gels can be stored at 4 °C for up to a month. Samples were mixed 1:1 with SDS non-reducing loading buffer (composition for 5X SDS: 10 g (8 mL) of glycerol, 4 mL dH_2O, 1.6 mL of 10% (w/v) SDS, 1 mL of 0.5 M Tris-HCl pH 6.8, 0.025 g Coomassie Brilliant Blue R-250) and heated at 75 °C for 5 min before loaded to the gel, each gel lane was loaded with 6 µL of 3 µg protein. For non-reducing samples, 5X loading dye consisting of 10 g (8 mL) of glycerol, 4 mL dH_2O, 1.6 mL of 10% (w/v) SDS, 1 mL of 0.5 M Tris-HCl pH 6.8, 0.025 g Bromophenol Blue, this was then diluted to 2X. For reducing samples, 5X loading dye consisted of 0.8 g of SDS, 4 mL glycerol, 2.5 mL of 0.5 M Tris buffer pH 6.8, 2.5 mL dH_2O, 2 mg Coomassie Brilliant Blue R-250 and dithiothreitol (DTT) (1 µL, 10 mM, 100 eq.). Prior to loading, all samples were briefly centrifuged at maximum speed for 10 sec, then boiled at 75 °C for 5 min, followed by a quick centrifugation at top speed for 10 sec to remove any condensation and were then loaded onto a gel. For reference, Page Ruler Plus Pre-Stained Protein Ladder (Thermo Scientific) was used. Gels were run at 200 V, 60 min at 1X running buffer. The 10X running buffer contained 30 g of Tris base, 144 g of glycine and 10 g of SDS in 1 L of dH_2O, with final pH of 8.3. Gels were stained in Coomassie Blue Stain: 10% Ammonium Sulphate (100 g), 0.1% Coomassie G-250 (500 mg), 3% Phosphoric Acid (30 mL), ethanol (200 mL), and water (1 L). Gels were de-stained with water. Densitometry analysis on SDS-PAGE was obtained by GelAnalyzer V 19.1 software. It should be noted that for all thioester containing bridged conjugates the SDS-PAGE lane is streaky, and whilst predominantly showing up as a rebridged Fab, there is also some detectable heavy and light chain species. This is consistent with having a hydrolytically unstable bridge treated at high temperatures under denaturing conditions, as some hydrolysis will be occurring during the analysis breaking the covalent linkage between the chains. Some of the SDS-PAGE gels included here, have had lanes cut out of the gel that included data not related to the specific experiments.

Table 3. Components of 12% SDS-PAGE gel. Listed volumes yield four gels.

Components	12% Separating	6% Stacking
dH_2O	7.95 mL	5.3 mL
Acrylamide	9.6 mL	2.0 mL
1.5 M Tris pH 8.8	6.0 mL	-
0.5 M Tris pH 6.8	-	2.5 mL
10% SDS	240 µL	100 µL
10% APS	240 µL	100 µL
TEMED	24 µL	10 µL

7.2.5 LCMS general remarks

The molecular masses of the conjugated, native antibodies and antibodies fragment was measured using Agilent 6510 QTOF LCMS system (Agilent, UK). Agilent 1200 HPLC system was built in with Agilent PLRP-S, 1000 Å, 8 µm, 150 mm x 2.1 mm column that was maintained at 60 °C. Protein sample (10 µl, ~ 5 µM) was separated on the column consisting of mobile phase A (water-0.1 % formic acid) and B (acetonitrile - 0.1% formic acid) using a gradient solution. The flow rate was adjusted to 300 µL/min.

Table 4. LCMS mobile phase A/B gradient elution

Time (min)	Solvent A (%)	Solvent B (%)
0	85	15
2	85	15
3	68	32
4	68	32
14	65	35
18	5	95
20	5	95
22	85	15
25	85	15

Agilent 6510 QTOF mass spectrometer was operated in a positive polarity mode, coupled with an ESI ion source. The ion source parameters were set up with a VCap of 3500 V, a gas temperature at 350 °C, a dry gas flow rate at 10 L/min and a nebulizer of 30 psig. MS Tof was acquired under conditions of a fragmentor at 350 V, a skimmer at 65 V and an acquisition rate at 0.5 spectra/s in a profile mode, within a scan range between 700 and 5000 m/z. The .d data was

then analysed by deconvoluting a spectrum to a zero charge mass spectra using a maximum entropy deconvolution algorithm within the MassHunter software version B.07.00.

7.2.6 LCMS sample preparation for full antibody

The sample was buffer exchanged into 50 mM ammonium acetate pH 7.0 by Zeba Spin as per manufacturer's instruction (Thermo Fisher). The antibody was first adjusted to 6.5 μM (1 mg/mL) in 100 μL and then deglycosylated with 1 μL PNGase F (NEB), at 37 °C for 16 h. The sample was diluted to 2.0 μM (0.2 mg/mL) with dH_2O and analysed. Analysis was also performed on native antibody as a control.

7.2.7 Enzyme-linked immunosorbent assay (ELISA) – Trastuzumab against HER2

A 96-well plate was coated for 16 h at 4 °C with HER2 (Sino Biological, 100 μL/well, 0.25 μg/mL solution in PBS), all wells except row D and H. After washing (3 × 0.1% Tween® 20 in PBS, followed by 3 × PBS), wells were blocked for 1 h at room temperature with 5% Marvel milk powder (Premier foods) in PBS (200 μL/well). The wells were then washed (3 × 0.1% Tween® 20 in PBS, followed by 3 × PBS), and the following dilutions of Fab conjugate were applied: 810 nM, 270 nM, 90 nM, 30 nM, 10 nM, 3.33 nM, 1.11 nM, 0.37 nM, 0.123 nM, 0.0412 nM, 0.0137 nM, prepared in 1% Marvel solution in PBS (100 μL/well), these were added to rows A to C – 1-11 and E to G – 1-11. The assay was then incubated at room temperature for 1 h. After 1 h, the plate was washed (3 × 0.1% Tween® 20 in PBS, followed by 3 × PBS), and the detection antibody (Anti-Human IgG, Fab specific-horseradish peroxidase (HRP) antibody, Sigma Aldrich, 1:5000 in 1% Marvel solution in 0.1% Tween® 20 in PBS) was added to the whole plate (100 μL/well), and incubated for 1 h at room temperature. After that, the plate was washed (3 × 0.1% Tween® 20 in PBS, followed by 3 × PBS), and *o*-phenylenediamine hydrochloride (Sigma-Aldrich, 100 μL/well, 0.5 mg/mL in a phosphate-citrate buffer with sodium perborate) was added to the whole plate, left for 15 – 30 min in dark (the colour development was monitored visually), room temperature. Once a yellow-orange colour was observed, the reaction was stopped by addition of HCl to the whole plate (4 M, 50 μL/well).

Absorbance was immediately measured at 450 nm and was corrected by subtracting the average of negative controls (i.e., PBS had been added to some of the wells instead of HER2 or instead

of the samples). Each sample was tested in triplicate and errors are shown as the standard deviation of the average. ELISA data was analysed with Graphpad Prism 8.0 (using equation Sigmoidal, 4PL, X is log(concentration)) and the values have been normalised.

7.2.8 Thermal Shift Assay

Melting temperature (T_m) of trastuzumab Fab conjugates was determined by thermal melt using Eppendorf qPCR equipment and Mastercycler software. Trastuzumab Fab conjugates were diluted to 4 µM in conjugation buffer pH 7.4 to give a final volume of 10 µL. SYPRO™ orange (Thermo Fischer) (1 µL, diluted 1:500 in conjugation buffer pH 7.4) was added to each sample before transferring to a 96-well PCR plate (Fischer Sci). Samples were heated in the range of 25–95 °C with ramping temperature at 1 °C /min. Thermal shift curves were analysed using Graph Pad Prism software to determine T_m (midpoint) values.

7.3 Bioconjugation reactions

7.3.1 Native Fab

Fab (30 μL, 100 μM, 4.76 mg/mL) in conjugation buffer was desalted (7 kDa MWCO, ZebaSpin) prior to LCMS analysis. Concentration was determined photometrically using ε_{280} = 68590 M^{-1} cm^{-1}.

a)

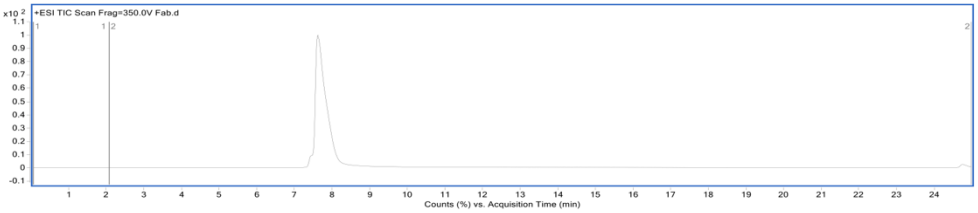

b)

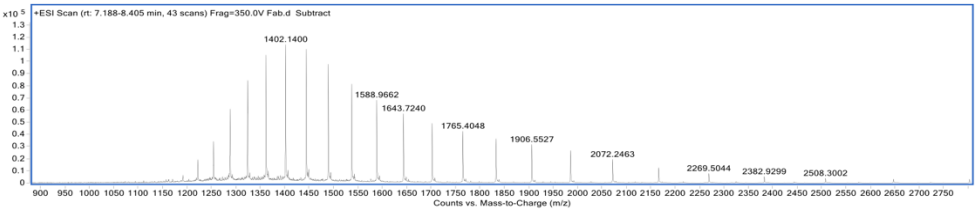

c)

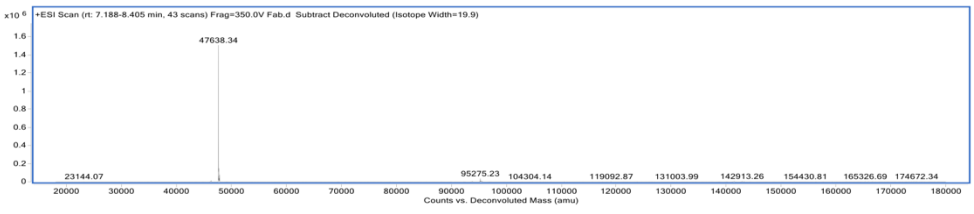

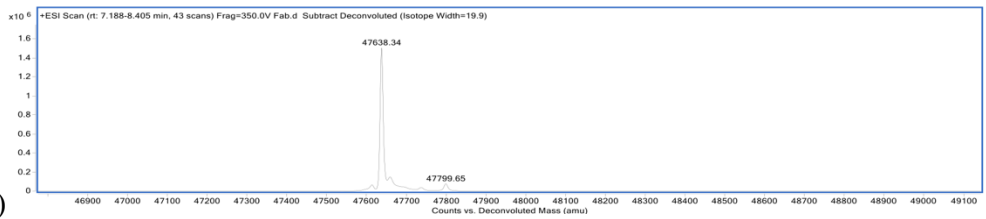

d)

Figure 58. LCMS analysis of native Fab; a) TIC, b) non-deconvoluted ion-series, c) full range deconvoluted ion series mass spectrum, d) zoomed in deconvoluted ion series mass spectrum; native Fab expected 47638, observed 47638.

7.3.2 Reduced Fab

Fab (30 μL, 100 μM, 4.76 mg/mL) in conjugation buffer was reduced with tris(2-carboxyethyl)phosphine (TCEP) (2 μL, 15 mM in diH_2O, 10 eq.) The mixture was incubated at 37 °C for 1.5 h, 300 rpm. Lastly, sample was desalted (7 kDa MWCO, ZebaSpin) prior to LCMS analysis. Concentration was determined photometrically using ε_{280} = 68590 M^{-1} cm^{-1}.

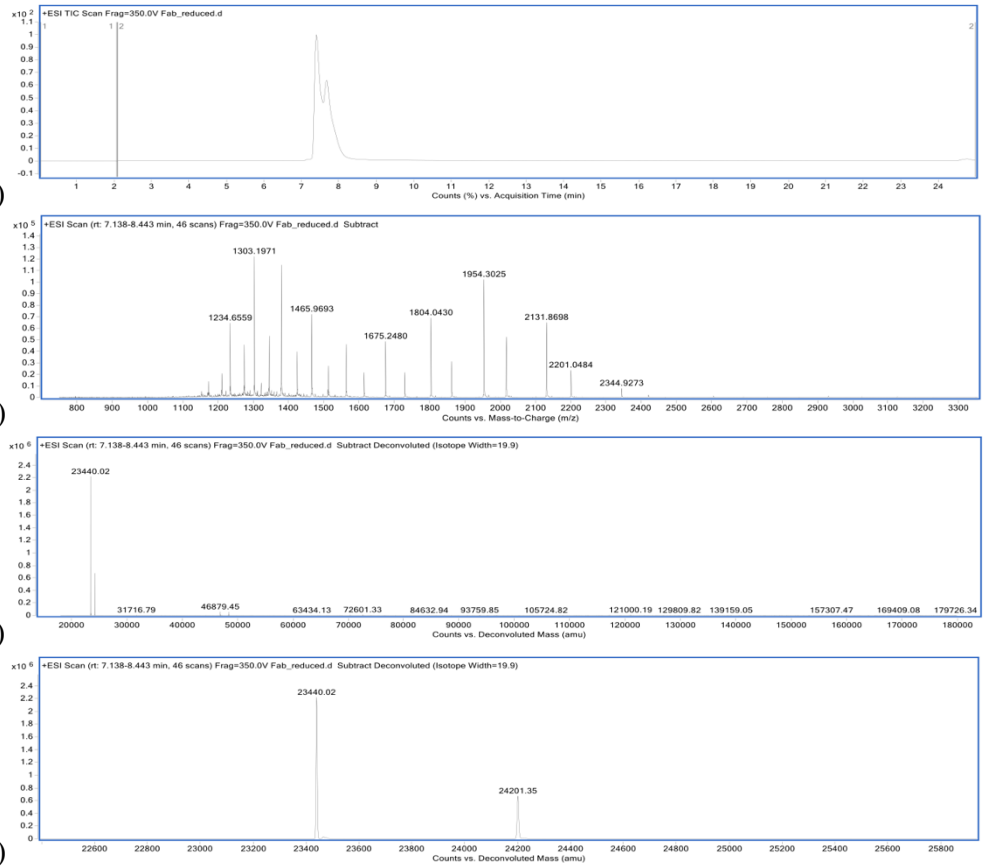

a)

b)

c)

d)

Figure 59. LCMS analysis of reduced Fab; a) TIC, b) non-deconvoluted ion-series, c) full range deconvoluted ion series mass spectrum, d) zoomed in deconvoluted ion series mass spectrum; native LC expected 23438, observed 23440, native HC expected 24200, observed 24201.

7.3.3 Rebridging of Fab with α-chlorothioester (1)

Fab (30 μL, 100 μM, 4.76 mg/mL) in conjugation buffer was reduced with tris(2-carboxyethyl)phosphine (TCEP) (2 μL, 15 mM in diH_2O, 10 eq.) The mixture was incubated at 37 °C for 1.5 h, 300 rpm. Following that, α-chlorothioester **1** (0.4 μL, 12 mM in DMF, 1.5 eq.) was added and incubated at 22 °C for 30 min. Lastly, sample was desalted (7 kDa MWCO, ZebaSpin) prior to LCMS analysis. Concentration was determined photometrically using ε_{280} = 68590 M^{-1} cm^{-1}.

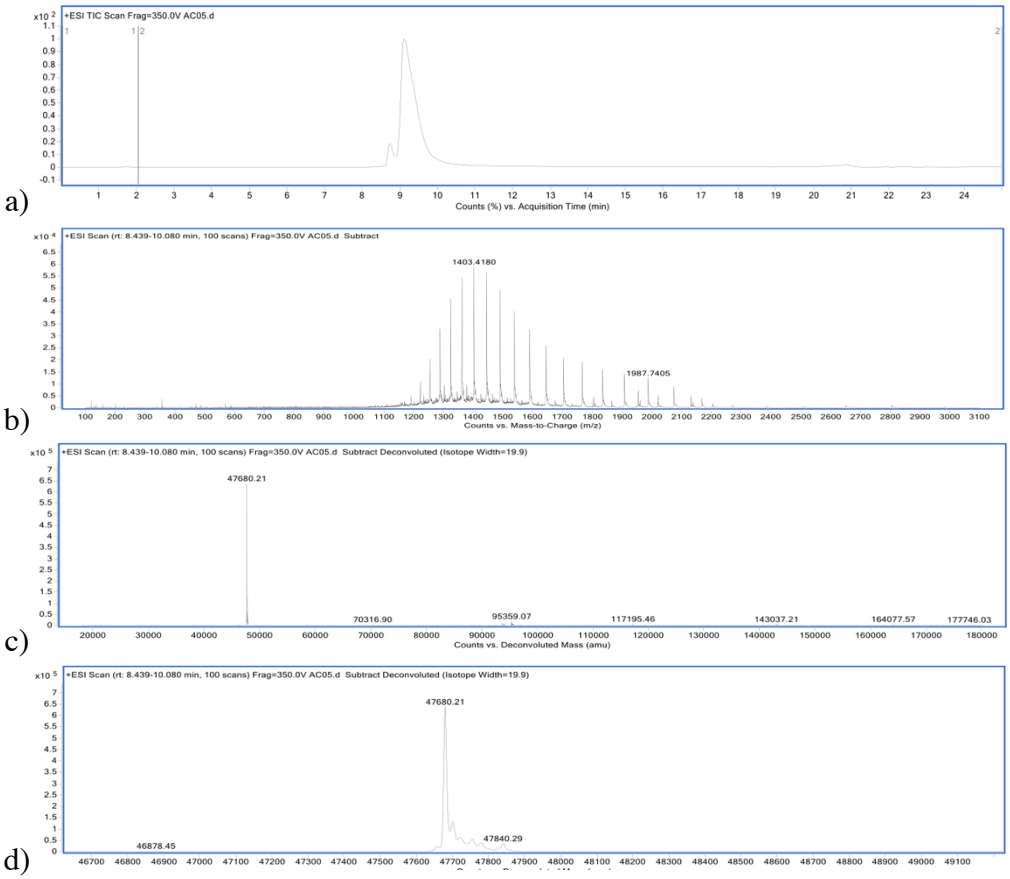

Figure 60. LCMS analysis of Fab rebridging with α-chlorothioester **1**; a) TIC, b) non-deconvoluted ion-series, c) full range deconvoluted ion series mass spectrum, d) zoomed in deconvoluted ion series mass spectrum; Fab conjugate **7** expected 47680, observed 47680.

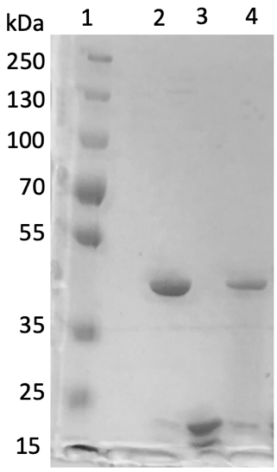

Figure 61. SDS-PAGE analysis Fab rebridging with α-chlorothioester **1**: 1 – marker, 2 – Fab native, 3 – TCEP reduction, 4 – rebridging with **1**.

7.3.4 Rebridging of Fab with α-bromothioester (2)

Fab (30 μL, 100 μM, 4.76 mg/mL) in conjugation buffer was reduced with tris(2-carboxyethyl)phosphine (TCEP) (2 μL, 15 mM in diH_2O, 10 eq.) The mixture was incubated at 37 °C for 1.5 h, 300 rpm. Following that, α-bromothioester **2** (0.3 μL, 56 mM in DMF, 5 eq.) was added and incubated at 22 °C for 30 min. Lastly, sample was desalted (7 kDa MWCO, ZebaSpin) prior to LCMS analysis. Concentration was determined photometrically using ε_{280} = 68590 M^{-1} cm^{-1}.

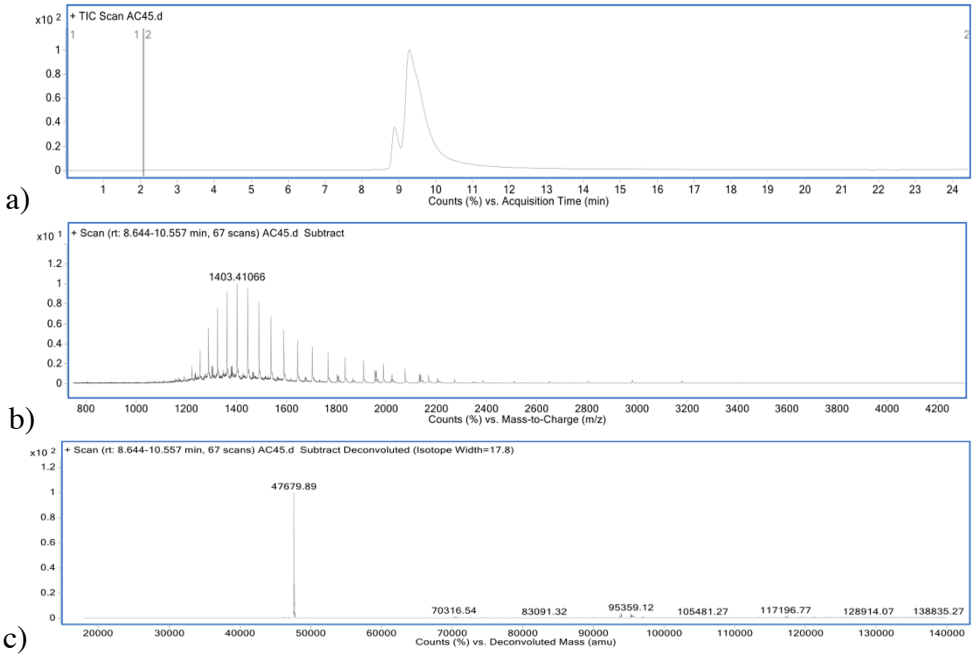

d)

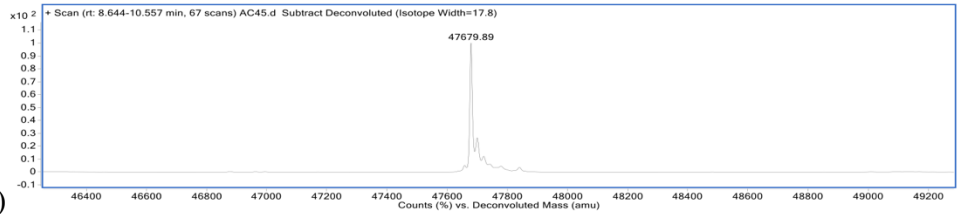

Figure 62. LCMS analysis of rebridging Fab with α-bromothioester **2**; a) TIC, b) non-deconvoluted ion-series, c) full range deconvoluted ion series mass spectrum, d) zoomed in deconvoluted ion series mass spectrum; rebridged Fab with α-bromothioester **2** expected 47680 observed 47679.

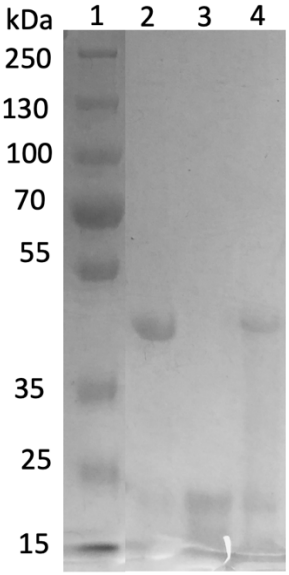

Figure 63. SDS-PAGE analysis Fab rebridging with α-bromothioester **2**: 1 – marker, 2 – Fab native, 3 – TCEP reduction, 4 – rebridging with **2**.

7.3.5 Stability study of Fab conjugate 7

Fab (30 μL, 100 μM, 4.76 mg/mL) in conjugation buffer was reduced with tris(2-carboxyethyl)phosphine (TCEP) (2 μL, 15 mM in diH_2O, 10 eq.) The mixture was incubated at 37 °C for 1.5 h, 300 rpm. Following that, α-chlorothioester **1** (0.4 μL, 12 mM in DMF, 1.5 eq.) was added and incubated at 22 °C for 30 min. For the samples tested at increased pH, the buffer was swapped (3 x ultrafiltration) after the initial 1 h rebridging with α-chlorothioester **1** into BBS buffer pH 8.5 and left for up to 48 h at 22 °C. Lastly, sample was desalted into HPLC grade water (7 kDa MWCO, ZebaSpin) prior to LCMS analysis. Concentration was determined photometrically using $\varepsilon_{280} = 68590\ M^{-1}\ cm^{-1}$.

pH 7.4

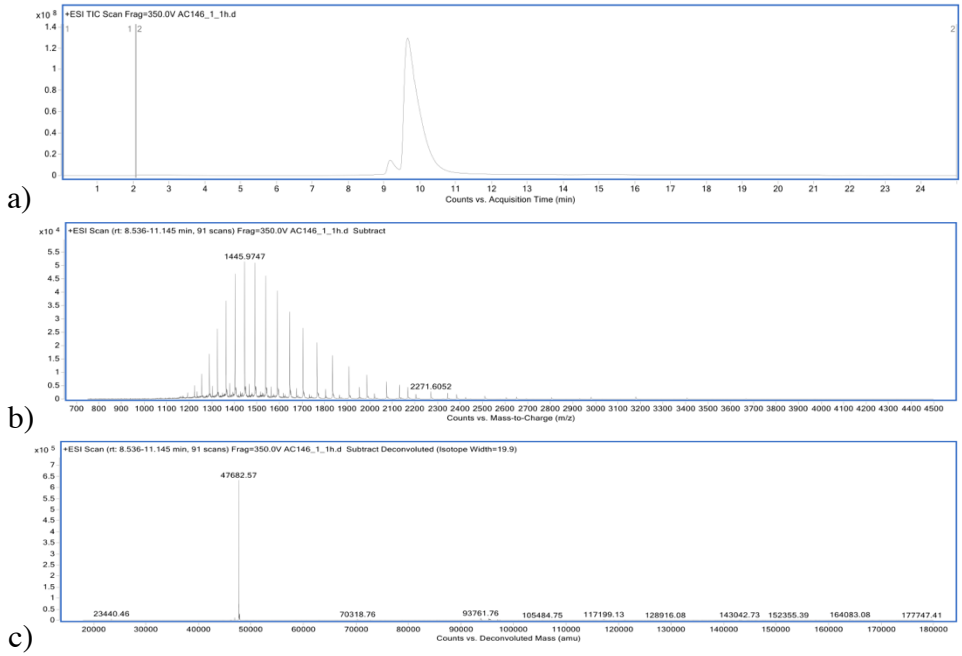

Figure 64. Stability study of Fab conjugate **7** at pH 7.4, 1 h; a) TIC, b) non-deconvoluted ion-series, c) full range deconvoluted ion series mass spectrum, Fab conjugate **7** expected 47680, observed 47682.

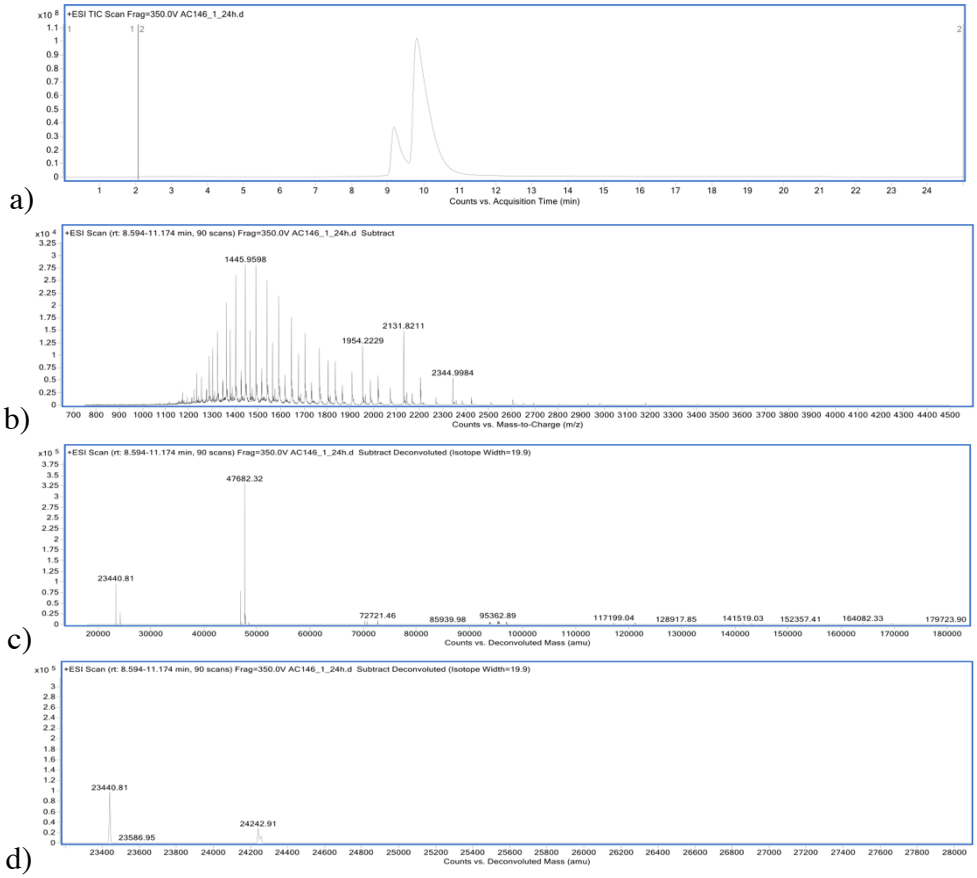

Figure 65. Stability study of Fab conjugate **7** at pH 7.4, 24 h; a) TIC, b) non-deconvoluted ion-series, c) full range deconvoluted ion series mass spectrum, d) zoomed in deconvoluted ion series mass spectrum.

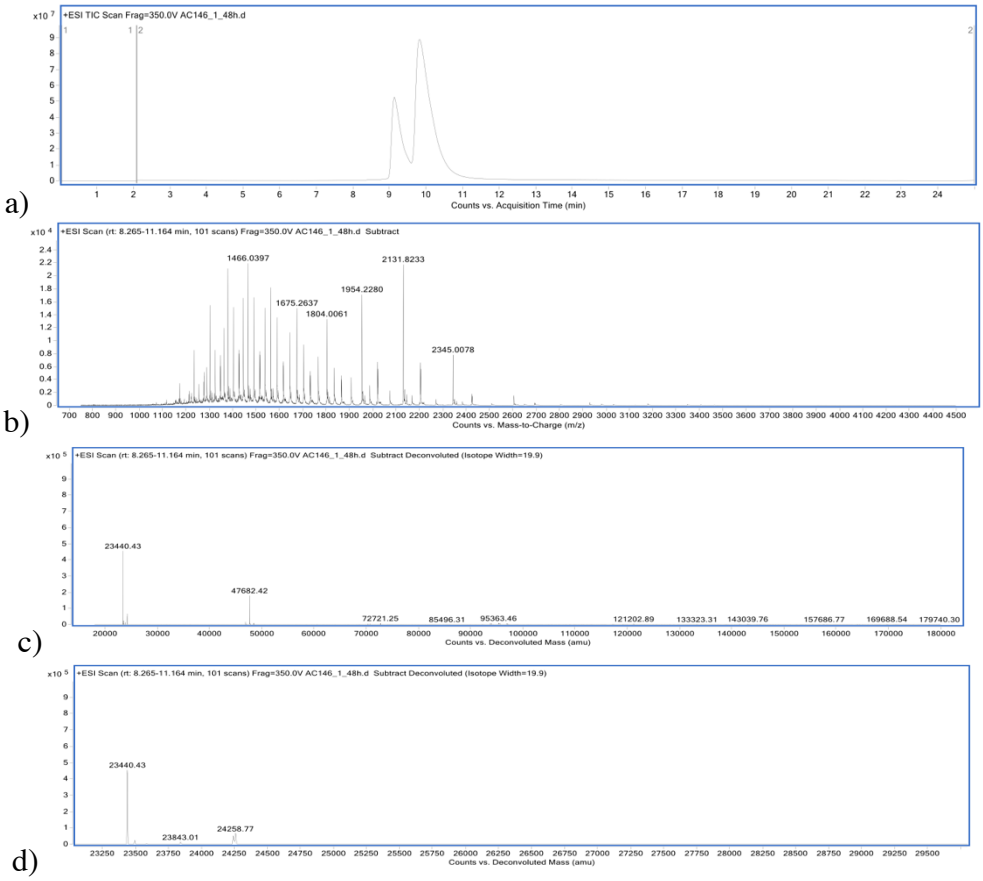

Figure 66. Stability study of Fab conjugate **7** at pH 7.4, 48 h; a) TIC, b) non-deconvoluted ion-series, c) full range deconvoluted ion series mass spectrum, d) zoomed in deconvoluted ion series mass spectrum.

pH 8.5

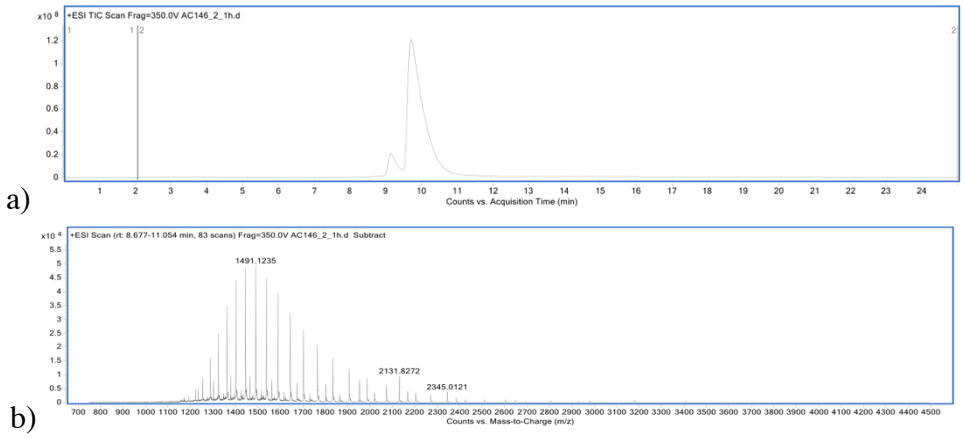

Figure 67. Stability study of Fab conjugate **7** at pH 8.5, 1 h; a) TIC, b) non-deconvoluted ion-series, c) full range deconvoluted ion series mass spectrum, d) zoomed in deconvoluted ion series mass spectrum.

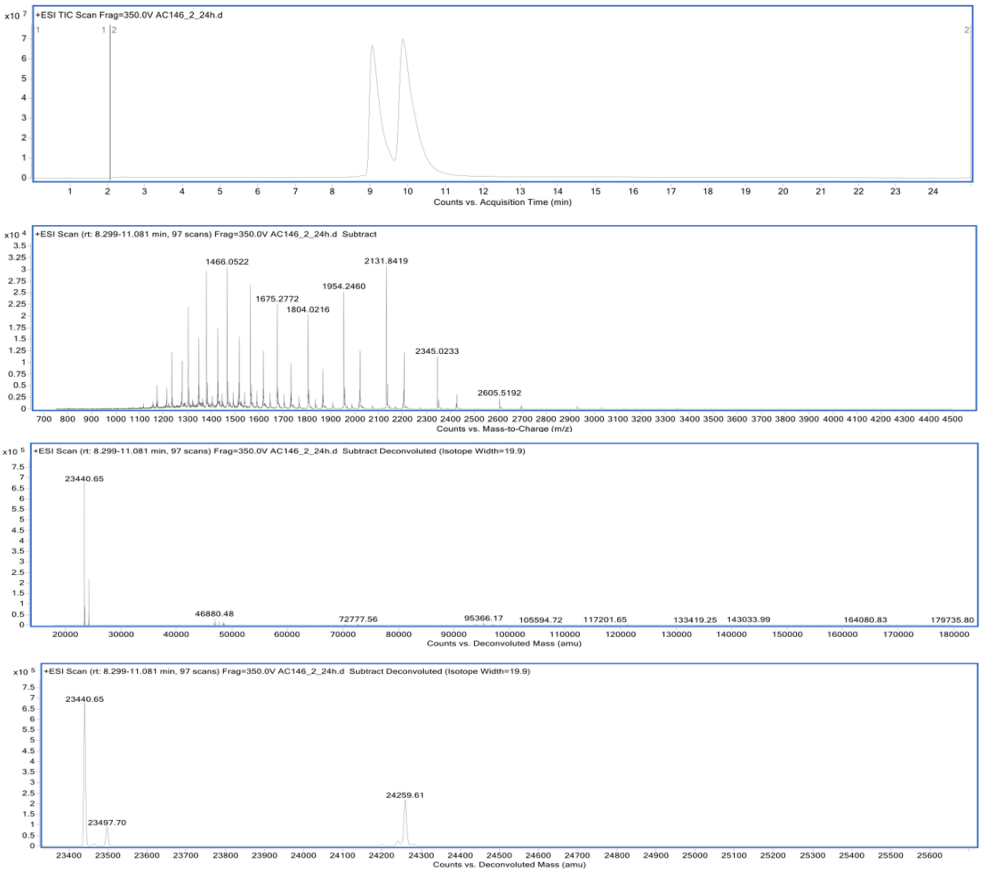

Figure 68. Stability study of Fab conjugate **7** at pH 8.5, 24 h; a) TIC, b) non-deconvoluted ion-series, c) full range deconvoluted ion series mass spectrum, d) zoomed in deconvoluted ion series mass spectrum.

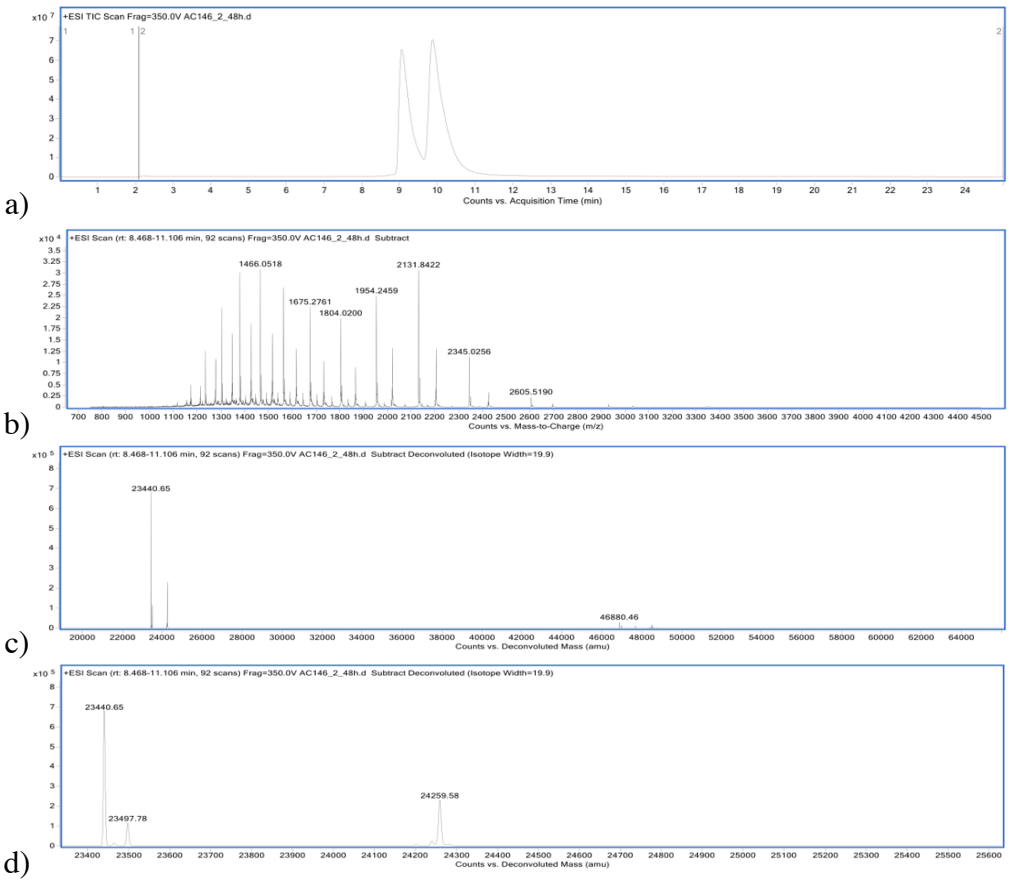

Figure 69. Stability study of Fab conjugate **7** at pH 8.5, 48 h; a) TIC, b) non-deconvoluted ion-series, c) full range deconvoluted ion series mass spectrum, d) zoomed in deconvoluted ion series mass spectrum.

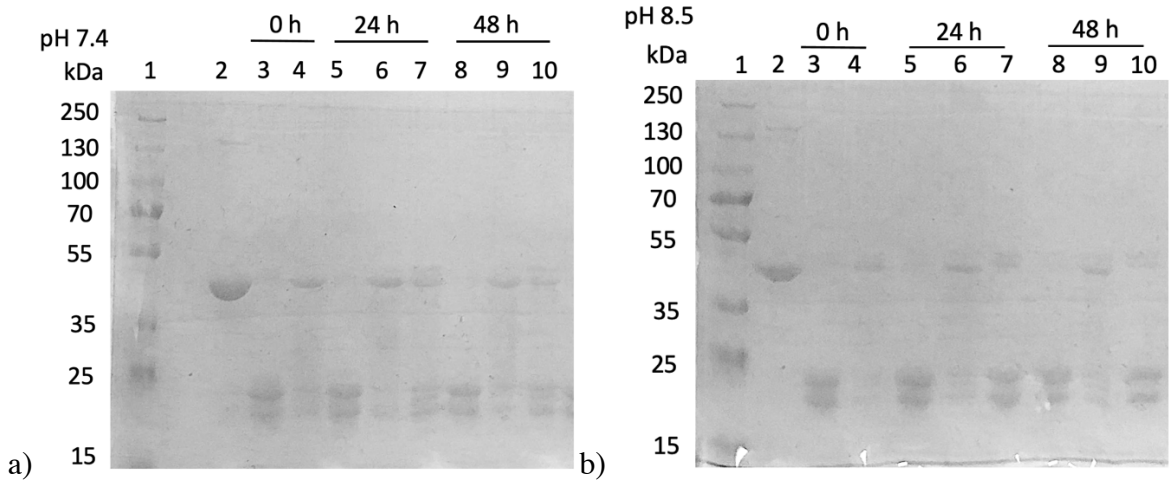

Figure 70. Stability study of Fab conjugate **7** at pH 7.4 and 8.5. SDS-PAGE: a) pH 7.4; 1 – molecular marker, 2 – native Fab, 3 – TCEP reduction, 4 – rebridging Fab with **1**, 5 – TCEP reduction, 6 – rebridging Fab with **1**, 7 – 24 h timepoint, 8 – TCEP reduction, 9 – rebridging Fab with **1**, 10 – 48 h timepoint; b) pH 8.5; 1 – molecular marker, 2 – native Fab, 3 – TCEP reduction, 4 – rebridging Fab with **1**, 5 – TCEP reduction, 6 – rebridging Fab with **1**, 7 – 24 h timepoint, 8 – TCEP reduction, 9 – rebridging Fab with **1**, 10 – 48 h timepoint.

7.3.6 Regioselectivity study α-chlorothioester (1) with cysteine

Fab (30 μL, 100 μM, 4.76 mg/mL) in conjugation buffer was reduced with tris(2-carboxyethyl)phosphine (TCEP) (2.0 μL, 15 mM in diH_2O, 10 eq.). The mixture was incubated at 37 °C for 1.5 h, 300 rpm. Following that, α-chlorothioester **1** (0.4 μL, 12 mM in DMF, 1.5 eq.) was added and incubated at 22 °C for 30 min. After that, L-cysteine (0.7 μL, 108 mM in diH_2O, 25 eq.) was added and left for at 37 °C, for 2 h, 300 rpm. Lastly, sample was desalted into HPLC grade water (7 kDa MWCO, ZebaSpin) prior to LCMS analysis. Concentration was determined photometrically using $\varepsilon_{280} = 68590\ M^{-1}\ cm^{-1}$.

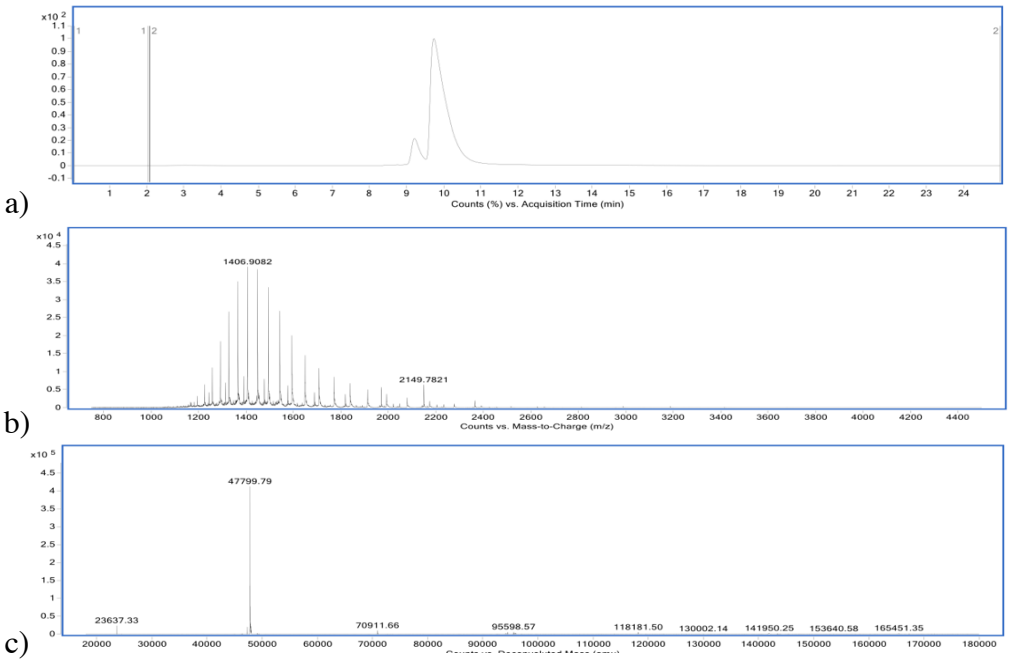

Figure 71. LCMS analysis of cysteine conjugate **19**; a) TIC, b) non-deconvoluted ion-series, c) full range deconvoluted ion series mass spectrum., Fab conjugate **19** expected 47799, observed 47799.

7.3.7 Regioselectivity study α-chlorothioester (1) with cysteine and *N*-Me-maleimide

Fab (20 μL, 80 μM, 3.81 mg/mL) in conjugation buffer was reduced with tris(2-carboxyethyl)phosphine (TCEP) (1.1 μL, 15 mM in diH_2O, 10 eq.) The mixture was incubated at 37 °C for 1.5 h, 300 rpm. Following that, α-chlorothioester **1** (0.2 μL, 12 mM in DMF, 1.5 eq.) was added and incubated at 22 °C for 30 min. After that, L-cysteine (0.4 μL, 108 mM in diH_2O, 25 eq.) was added and left at 37 °C, for 2 h, 300 rpm. After this period, the excess reagent was removed *via* ultrafiltration (10 kDa MWCO), into conjugation buffer, new Fab concentration was

determined, and TCEP reduction was performed again as before. To cap the free thiols, an excess of *N*-methylmaleimide was added (0.6 μL, 39 mM in diH_2O, 20 eq.). Lastly, sample was desalted (7 kDa MWCO, ZebaSpin) prior to LCMS analysis. Concentration was determined photometrically using $\varepsilon_{280} = 68590\ M^{-1}\ cm^{-1}$.

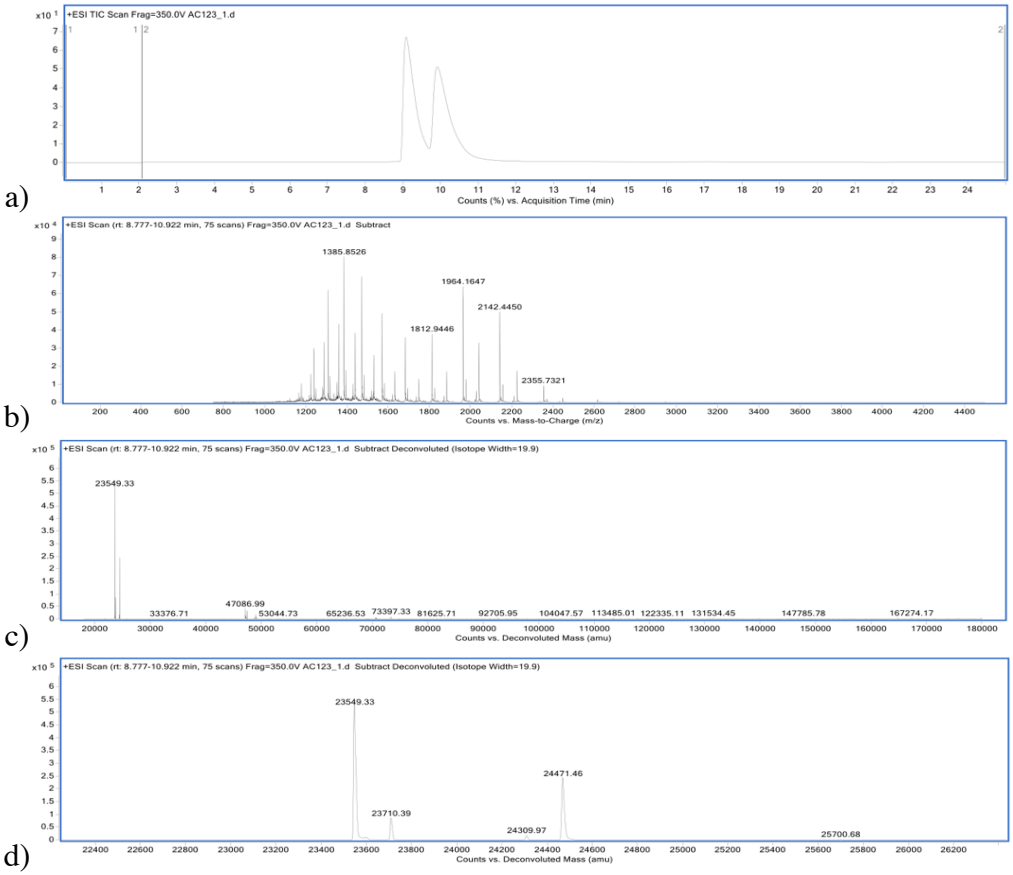

Figure 72. LCMS analysis of regioselectivity preference of α-chlorothioester **1**; a) TIC, b) non-deconvoluted ion-series, c) full range deconvoluted ion series mass spectrum, d) zoomed in deconvoluted ion series mass spectrum.

7.3.8 Rebridging of Fab with methyl 2-(acryloylthio)acetate (3)

Fab (30 μL, 100 μM, 4.76 mg/mL) in conjugation buffer was reduced with tris(2-carboxyethyl)phosphine (TCEP) (2 μL, 15 mM in diH_2O, 10 eq.). The mixture was incubated at 37 °C for 1.5 h, 300 rpm. The excess of TCEP was removed *via* ultrafiltration (10 kDa MWCO) into conjugation buffer and new Fab concentration was determined. Following that, methyl 2-(acryloylthio)acetate **3** (0.1 μL, 51 mM in DMF, 1.5 eq.) was added and incubated at 22 °C for 30 min. Lastly, sample was desalted (7 kDa MWCO, ZebaSpin) prior to LCMS analysis. Concentration was determined photometrically using $\varepsilon_{280} = 68590\ M^{-1}\ cm^{-1}$.

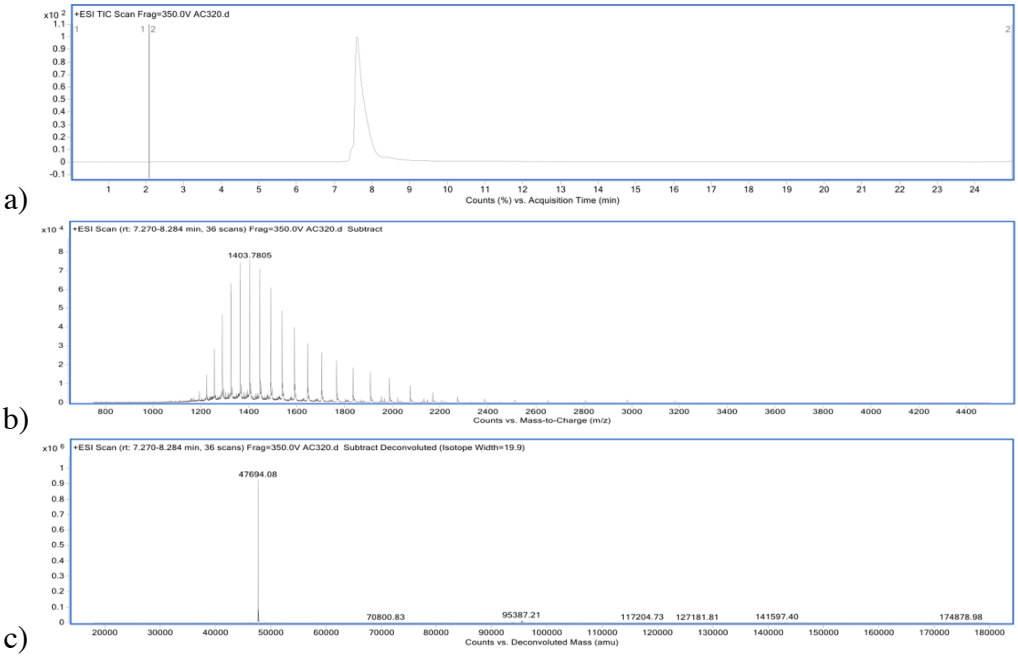

Figure 73. LCMS analysis of rebridging Fab with methyl 2-(acryloylthio)acetate **3**; a) TIC, b) non-deconvoluted ion-series, c) full range deconvoluted ion series mass spectrum of Fab conjugate **8** expected 47694, observed 47694.

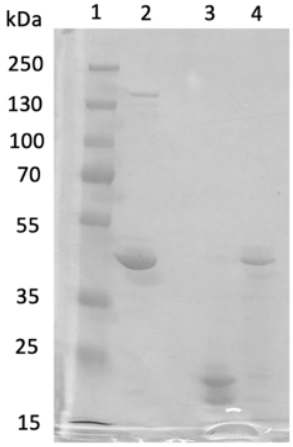

Figure 74. SDS-PAGE analysis Fab rebridging with acrylic thioester **3**: 1 – marker, 2 – Fab native, 3 – TCEP reduction, 4 – rebridging with **3**.

7.3.9 Stability study of Fab conjugate 8

Fab (30 μL, 100 μM, 4.76 mg/mL) in conjugation buffer was reduced with tris(2-carboxyethyl)phosphine (TCEP) (2 μL, 15 mM in diH_2O, 10 eq.). The mixture was incubated at 37 °C for 1.5 h, 300 rpm. The excess of TCEP was removed *via* ultrafiltration (10 kDa MWCO) into conjugation buffer, new Fab concentration was determined. Following that, methyl 2-(acryloylthio)acetate **3** (0.1 μL, 51 mM in DMF, 1.5 eq.) was added and incubated at 22 °C for 30 min. For the samples where increased pH was required, the buffer was swapped (3 x

ultrafiltration) after the initial 1 h rebridging with methyl 2-(acryloylthio)acetate into BBS buffer pH 8.5 and left for up to 48 h at 22 °C. Lastly, sample was desalted into HPLC grade water (7 kDa MWCO, ZebaSpin) prior to LCMS analysis. Concentration was determined photometrically using $\varepsilon_{280} = 68590\ M^{-1}\ cm^{-1}$.

pH 7.4

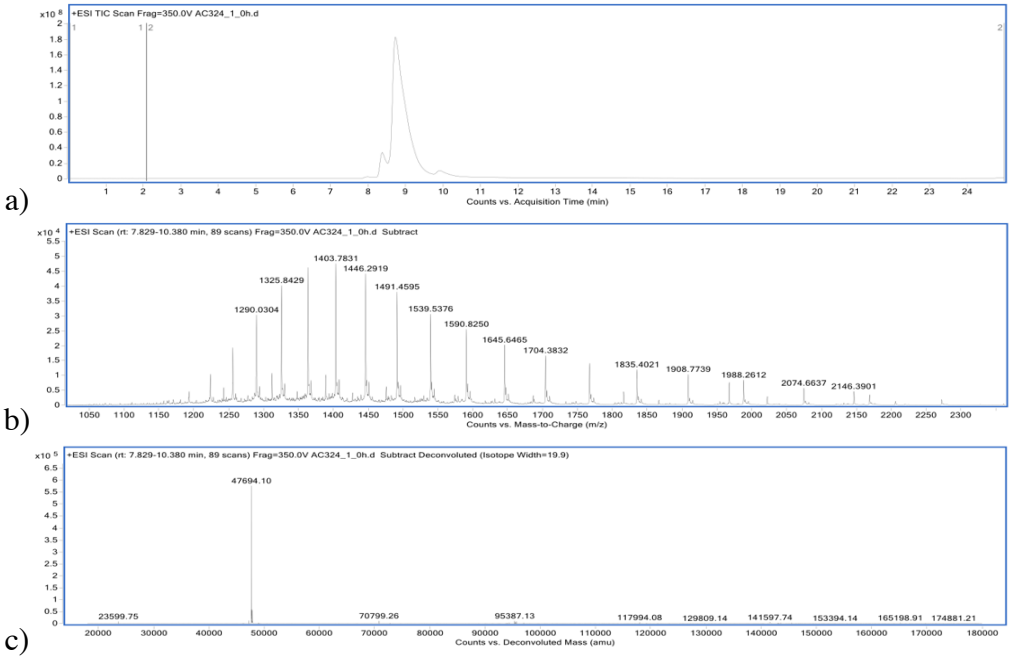

Figure 75. Stability study of Fab conjugate **8** at pH 7.4, 1 h; a) TIC, b) non-deconvoluted ion-series, c) full range deconvoluted ion series mass spectrum.

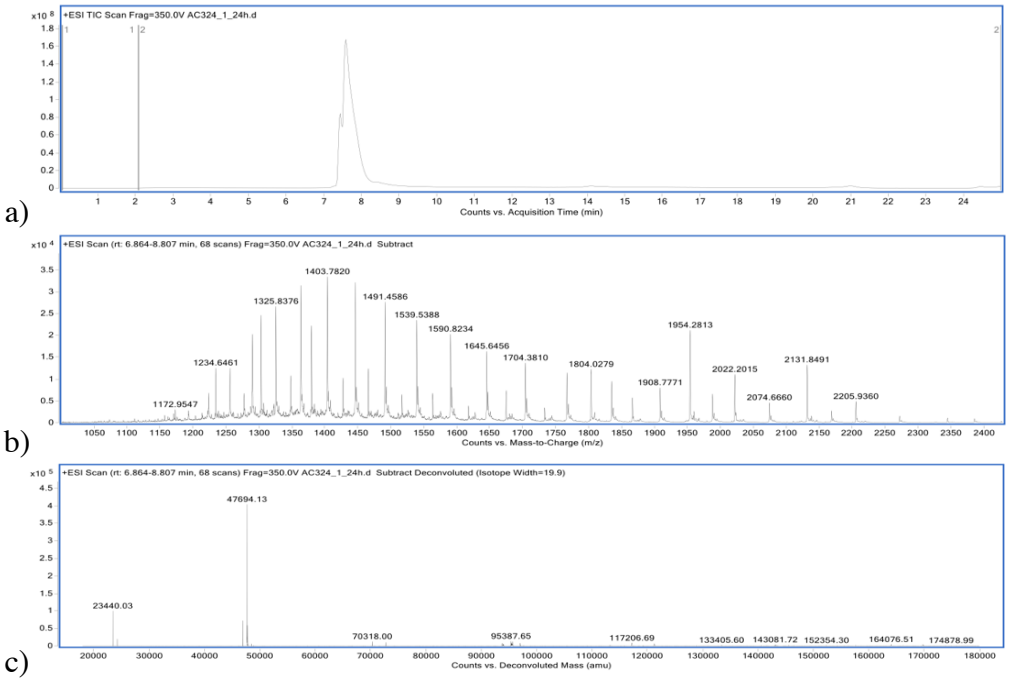

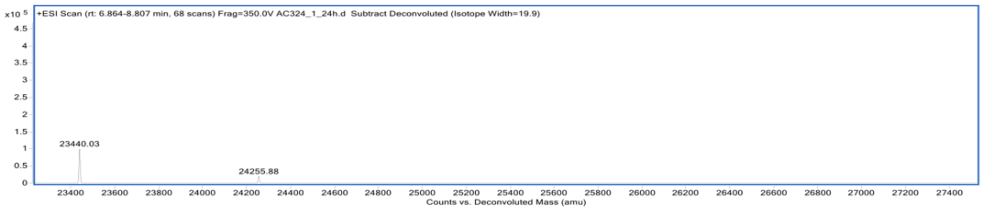

d)

Figure 76. Stability study of Fab conjugate **8** at pH 7.4, 24 h; a) TIC, b) non-deconvoluted ion-series, c) full range deconvoluted ion series mass spectrum, d) zoomed in deconvoluted ion series mass spectrum.

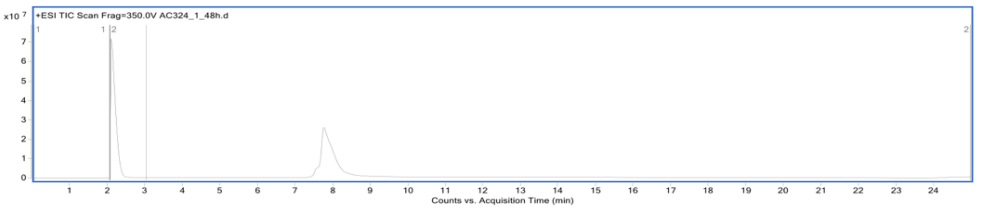

a)

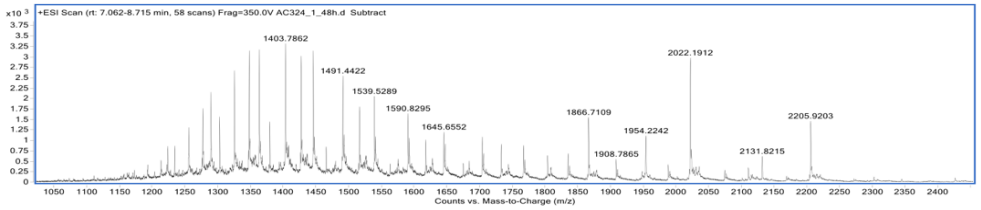

b)

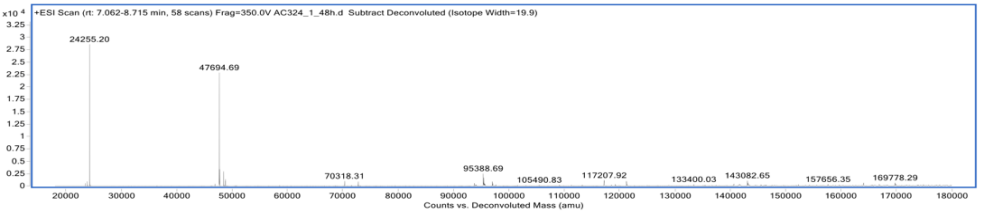

c)

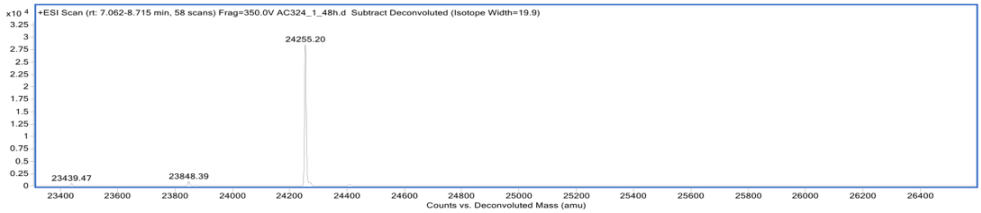

d)

Figure 77. Stability study of Fab conjugate **8** at pH 7.4, 48 h; a) TIC, b) non-deconvoluted ion-series, c) full range deconvoluted ion series mass spectrum, d) zoomed in deconvoluted ion series mass spectrum.

pH 8.5

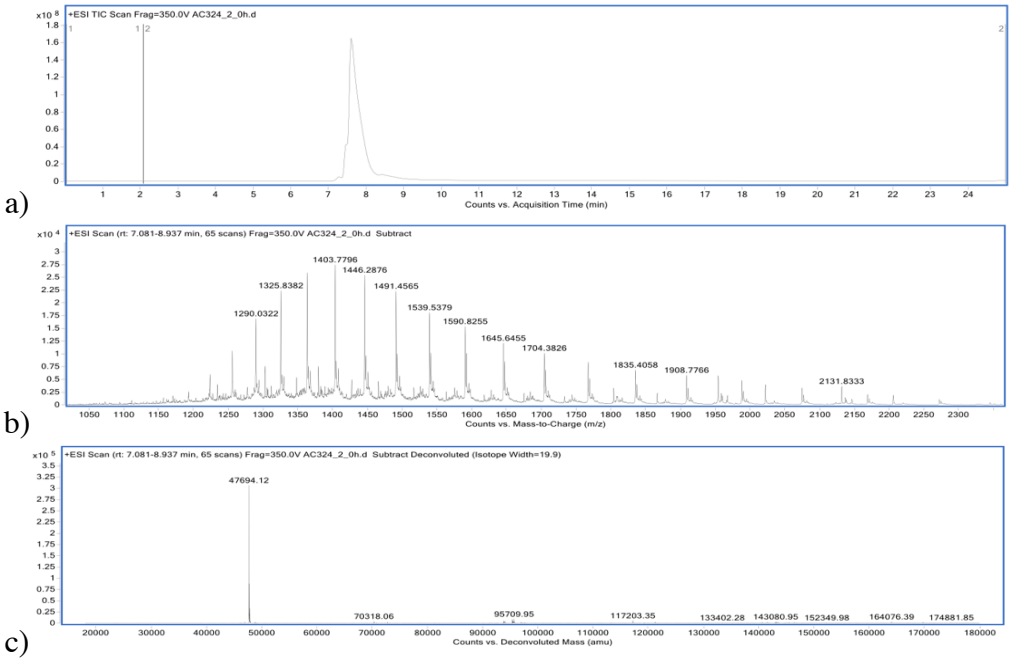

Figure 78. Stability study of Fab conjugate **8** at pH 8.5, 1 h; a) TIC, b) non-deconvoluted ion-series, c) full range deconvoluted ion series mass spectrum.

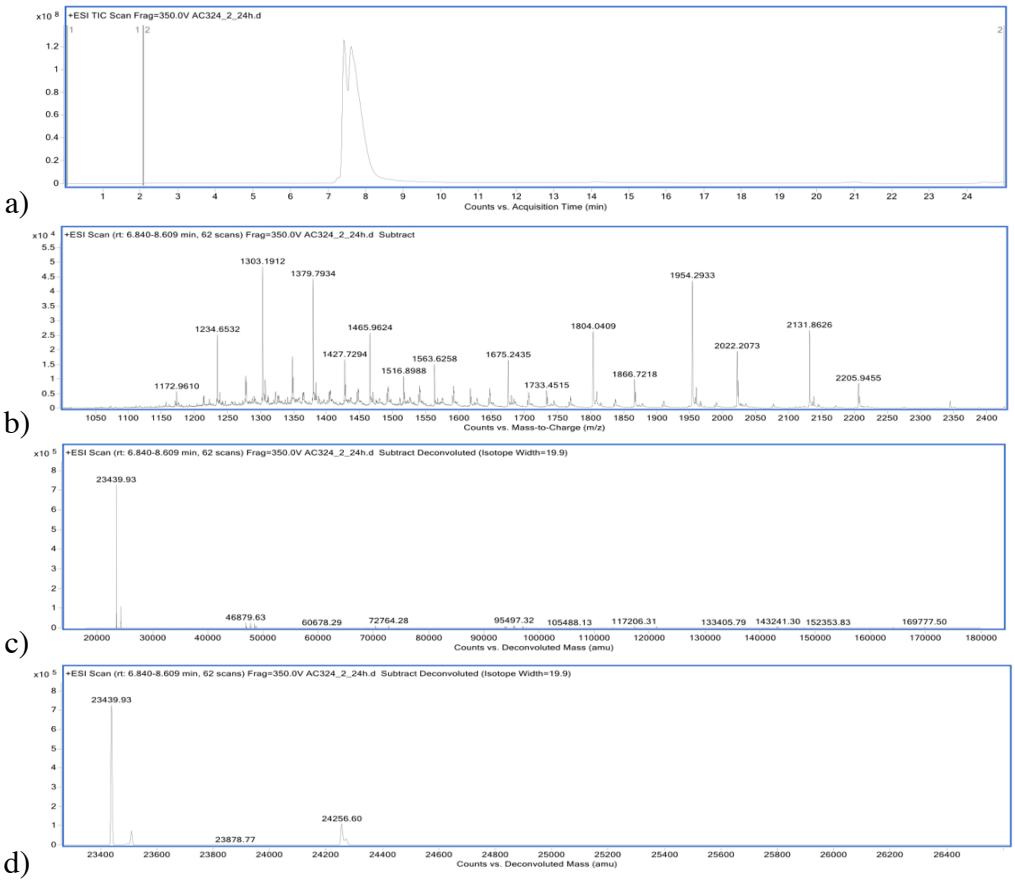

Figure 79. Stability study of Fab conjugate **8** at pH 8.5, 24 h; a) TIC, b) non-deconvoluted ion-series, c) full range deconvoluted ion series mass spectrum, d) zoomed in deconvoluted ion series mass spectrum.

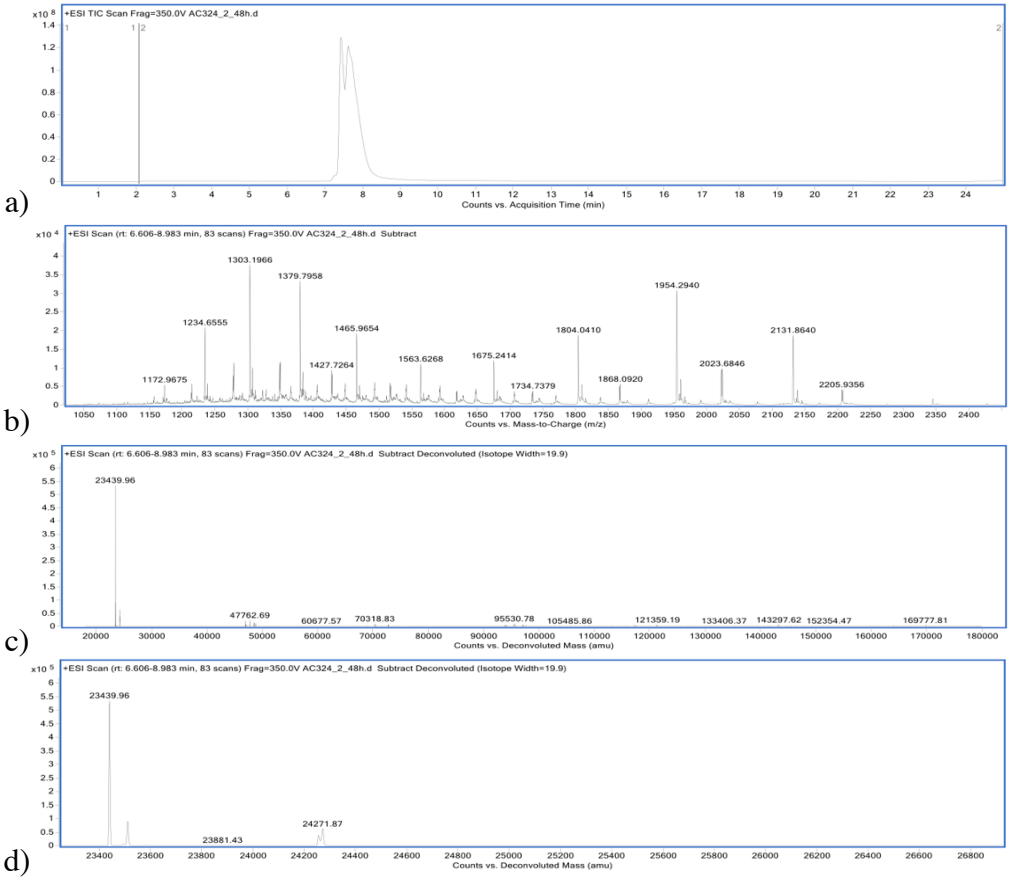

Figure 80. Stability study of Fab conjugate **8** at pH 8.5, 48 h; a) TIC, b) non-deconvoluted ion-series, c) full range deconvoluted ion series mass spectrum, d) zoomed in deconvoluted ion series mass spectrum.

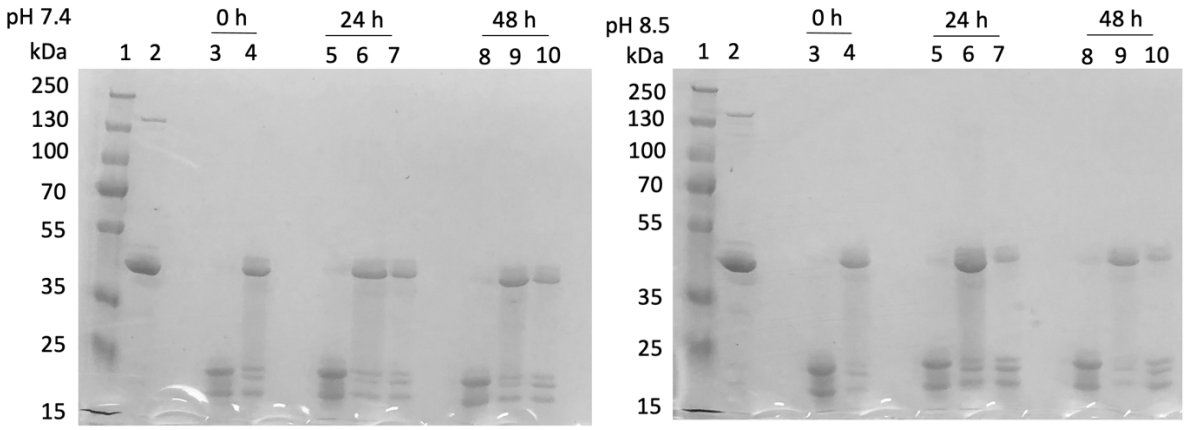

Figure 81. Stability study of Fab conjugate **8** at pH 7.4 and 8.5. SDS-PAGE: a) pH 7.4; 1 – molecular marker, 2 – native Fab, 3 – TCEP reduction, 4 – rebridging Fab with **3**, 5 – TCEP reduction, 6 – rebridging Fab with **3**, 7 – 24 h timepoint, 8 – TCEP reduction, 9 – rebridging Fab with **3**, 10 – 48 h timepoint; b) pH 8.5; 1 – molecular marker, 2 – native Fab, 3 – TCEP reduction, 4 – rebridging Fab with **3**, 5 – TCEP reduction, 6 – rebridging Fab with **3**, 7 – 24 h timepoint, 8 – TCEP reduction, 9 – rebridging Fab with **3**, 10 – 48 h timepoint.

7.3.10 Regioselectivity study of methyl 2-(acryloylthio)acetate (3) and cysteine and *N*-Me-maleimide

Fab (30 μL, 100 μM, 4.76 mg/mL) in conjugation buffer was reduced with tris(2-carboxyethyl)phosphine (TCEP) (2 μL, 15 mM in diH_2O, 10 eq.). The mixture was incubated at 37 °C for 1.5 h, 300 rpm. The excess of TCEP was removed *via* ultrafiltration (10 kDa MWCO) into conjugation buffer, new Fab concentration was determined. Following that, methyl 2-(acryloylthio)acetate **3** (0.4 μL, 11 mM in DMF, 1.5 eq.) was added and incubated at 22 °C for 30 min. After that, L-cysteine (0.5 μL, 108 mM in diH_2O, 25 eq.) was added and left at 37 °C, for 2 h, 300 rpm. After this period, the excess reagent was removed *via* ultrafiltration (10 kDa MWCO), into conjugation buffer and TCEP reduction was performed again as before. To cap the free thiols, an excess of *N*-methylmaleimide was added (0.9 μL, 39 mM in diH_2O, 20 eq.). Lastly, sample was desalted (7 kDa MWCO, ZebaSpin) prior to LCMS analysis. Concentration was determined photometrically using $\varepsilon_{280} = 68590\ M^{-1}\ cm^{-1}$.

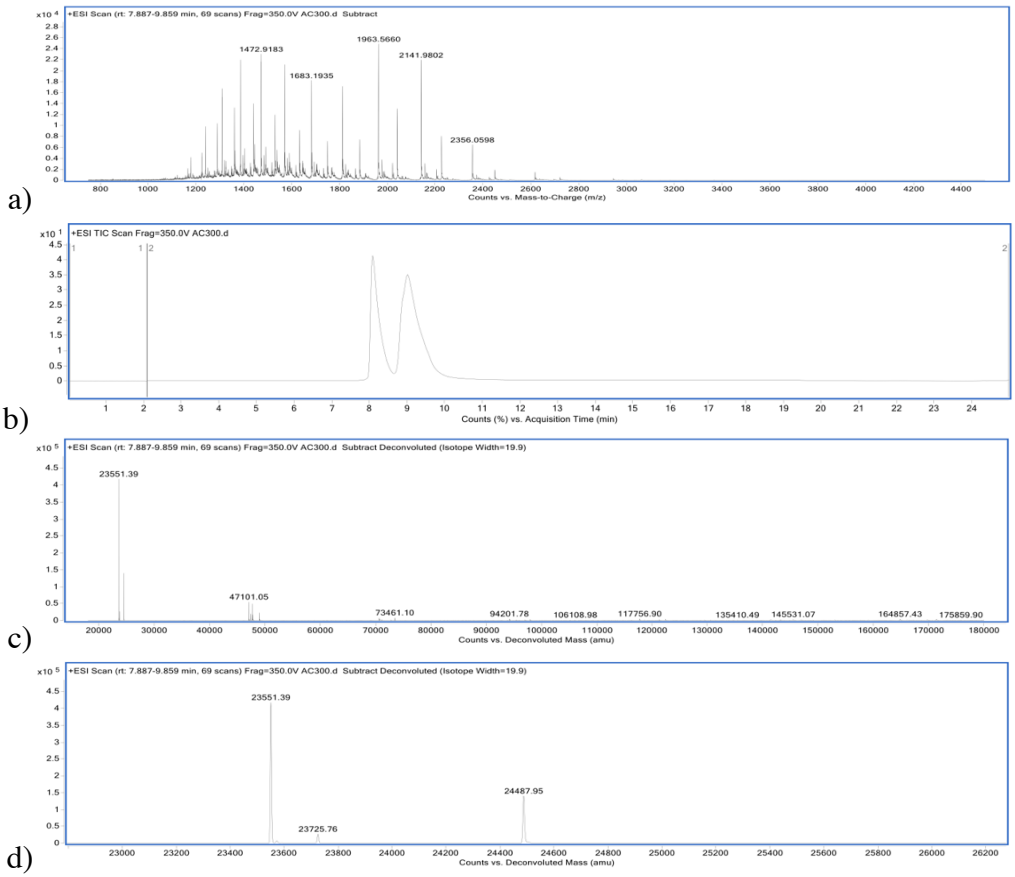

Figure 82. LCMS analysis of regioselectivity preference of methyl 2-(acryloylthio)acetate **3**; a) TIC, b) non-deconvoluted ion-series, c) full range deconvoluted ion series mass spectrum, d) zoomed in deconvoluted ion series mass spectrum.

7.3.11 Rebridging of Fab with methyl 2-((2-fluoro-5-nitrobenzoyl)thio)acetate (5)

Fab (30 μL, 100 μM, 4.76 mg/mL) in conjugation buffer was reduced with tris(2-carboxyethyl)phosphine (TCEP) (2 μL, 15 mM in diH_2O, 10 eq.). The mixture was incubated at 37 °C for 1.5 h, 300 rpm. Following that, methyl 2-((2-fluoro-5-nitrobenzoyl)thio)acetate **5** (0.2 μL, 23 mM in DMF, 1.5 eq.) was added and incubated at 22 °C for 1 h. Lastly, sample was desalted into HPLC grade water (7 kDa MWCO, ZebaSpin) prior to LCMS analysis. Concentration was determined photometrically using ε_{280} = 68590 M^{-1} cm^{-1}.

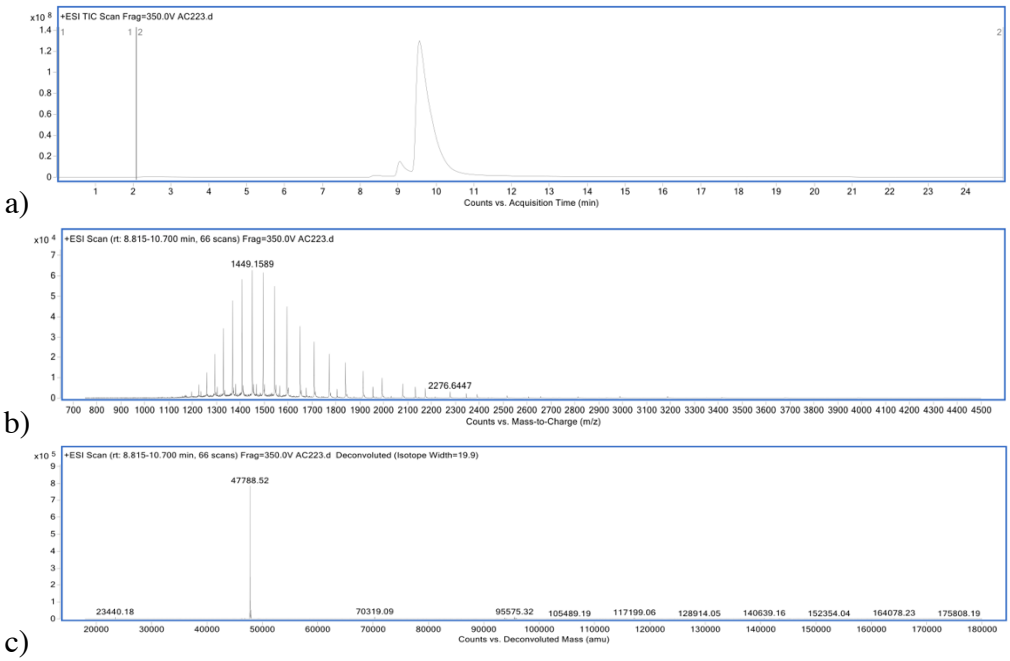

Figure 83. LCMS analysis of rebridging Fab with methyl 2-((2-fluoro-5-nitrobenzoyl)thio)acetate **5**; a) TIC, b) non-deconvoluted ion-series, c) full range deconvoluted ion series mass spectrum of Fab conjugate **9** expected 47787, observed 47788.

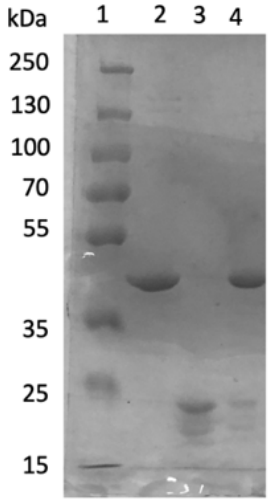

Figure 84. SDS-PAGE analysis Fab rebridging with aryl-fluoro thioester **5**: 1 – marker, 2 – Fab native, 3 – TCEP reduction, 4 – rebridging with **5**.

7.3.12 Stability study of Fab conjugate 9

Fab (30 μL, 100 μM, 4.76 mg/mL) in conjugation buffer was reduced with tris(2-carboxyethyl)phosphine (TCEP) (2 μL, 15 mM in diH_2O, 10 eq.). The mixture was incubated at 37 °C for 1.5 h, 300 rpm. Following that, methyl 2-((2-fluoro-5-nitrobenzoyl)thio)acetate **5** (0.2 μL, 23 mM in DMF, 1.5 eq.) was added and incubated at 22 °C for 1 h. For the samples where increased pH was required, the buffer was swapped (3 x ultrafiltration) after the initial 1 h rebridging with methyl 2-((2-fluoro-5-nitrobenzoyl)thio)acetate into BBS buffer pH 8.5 and left for up to 48 h at 22 °C. Lastly, sample was desalted into HPLC grade water (7 kDa MWCO, ZebaSpin) prior to LCMS analysis. Concentration was determined photometrically using ε_{280} = 68590 M^{-1} cm^{-1}.

pH 7.4

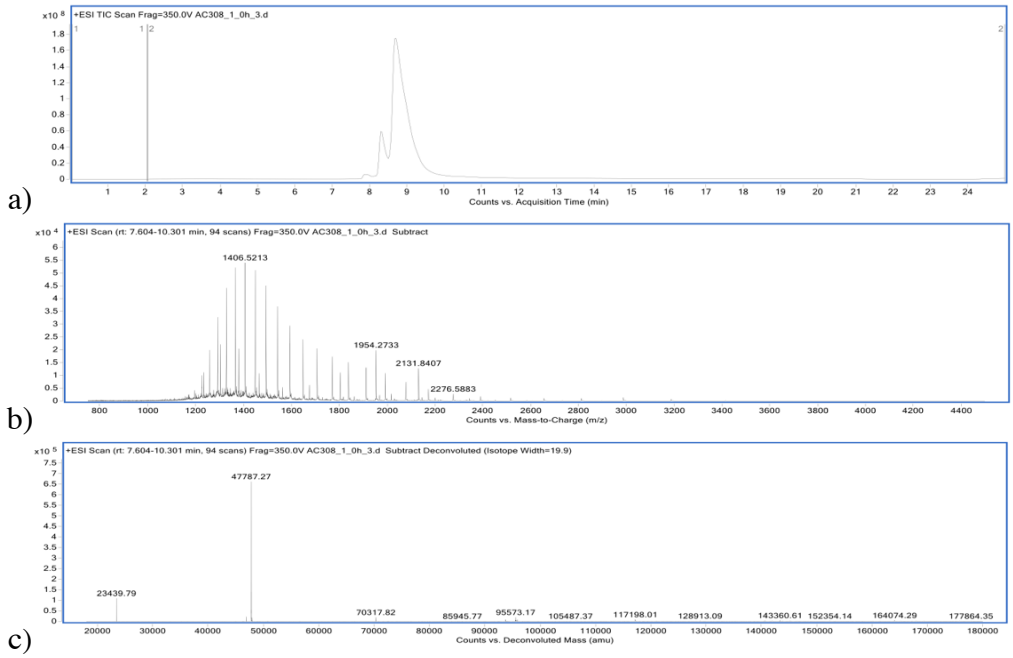

Figure 85. Stability study of Fab conjugate **9** at pH 7.4, 1 h; a) TIC, b) non-deconvoluted ion-series, c) full range deconvoluted ion series mass spectrum.

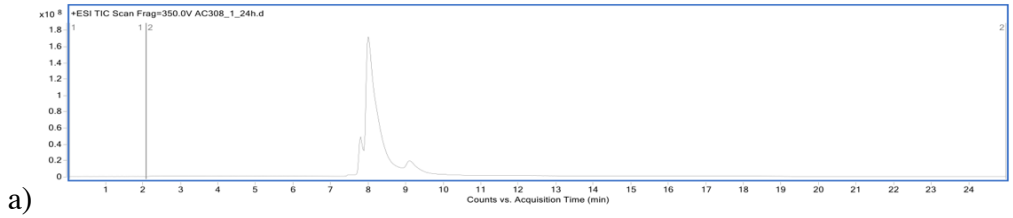

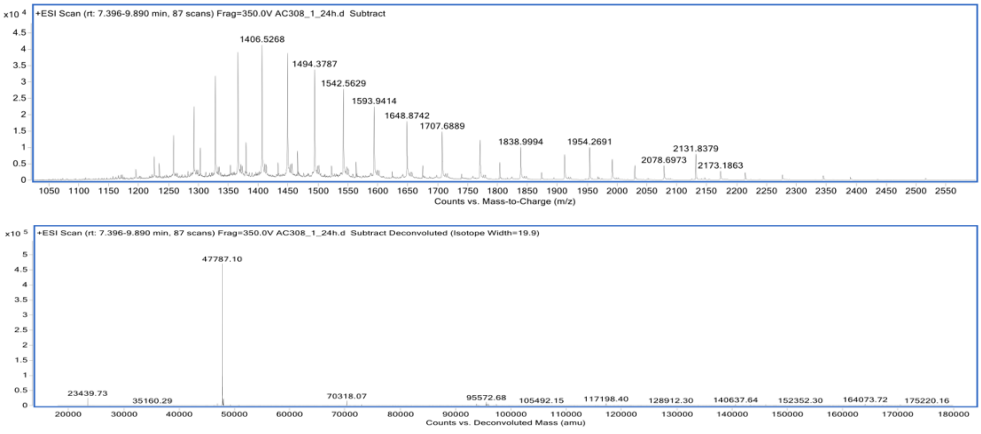

Figure 86. Stability study of Fab conjugate **9** at pH 7.4, 24 h; a) TIC, b) non-deconvoluted ion-series, c) full range deconvoluted ion series mass spectrum.

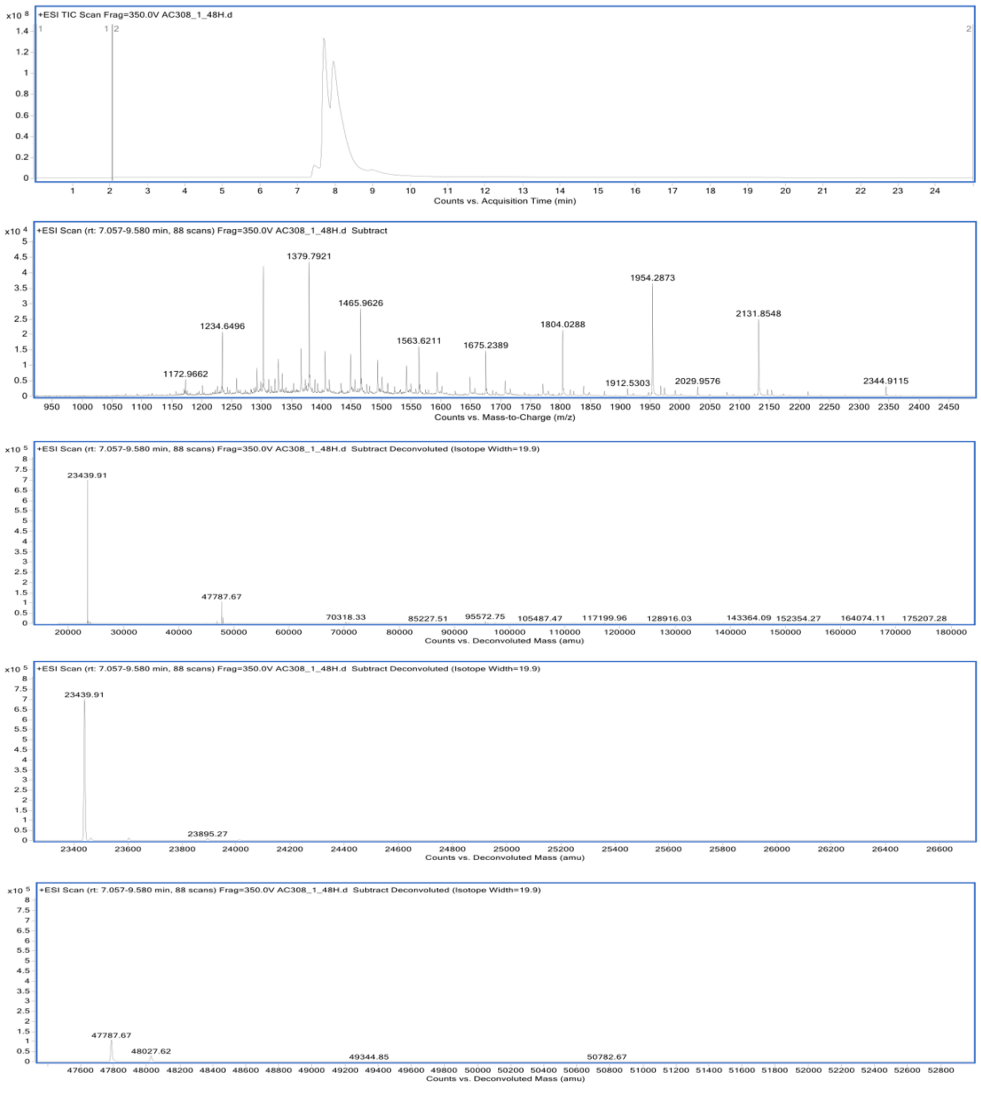

Figure 87. Stability study of Fab conjugate **9** at pH 7.4, 48 h; a) TIC, b) non-deconvoluted ion-series, c) full range deconvoluted ion series mass spectrum, d) zoomed in deconvoluted ion series mass spectrum, e) zoomed in deconvoluted ion series mass spectrum.

pH 8.5

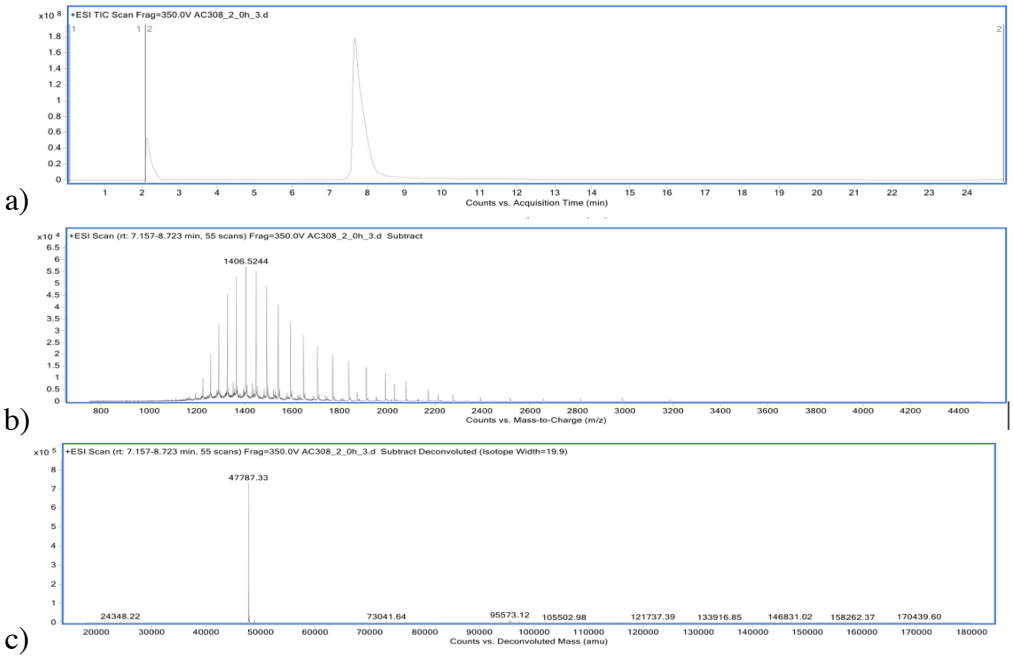

Figure 88. Stability study of Fab conjugate **9** at pH 8.5, 1 h; a) TIC, b) non-deconvoluted ion-series, c) full range deconvoluted ion series mass spectrum.

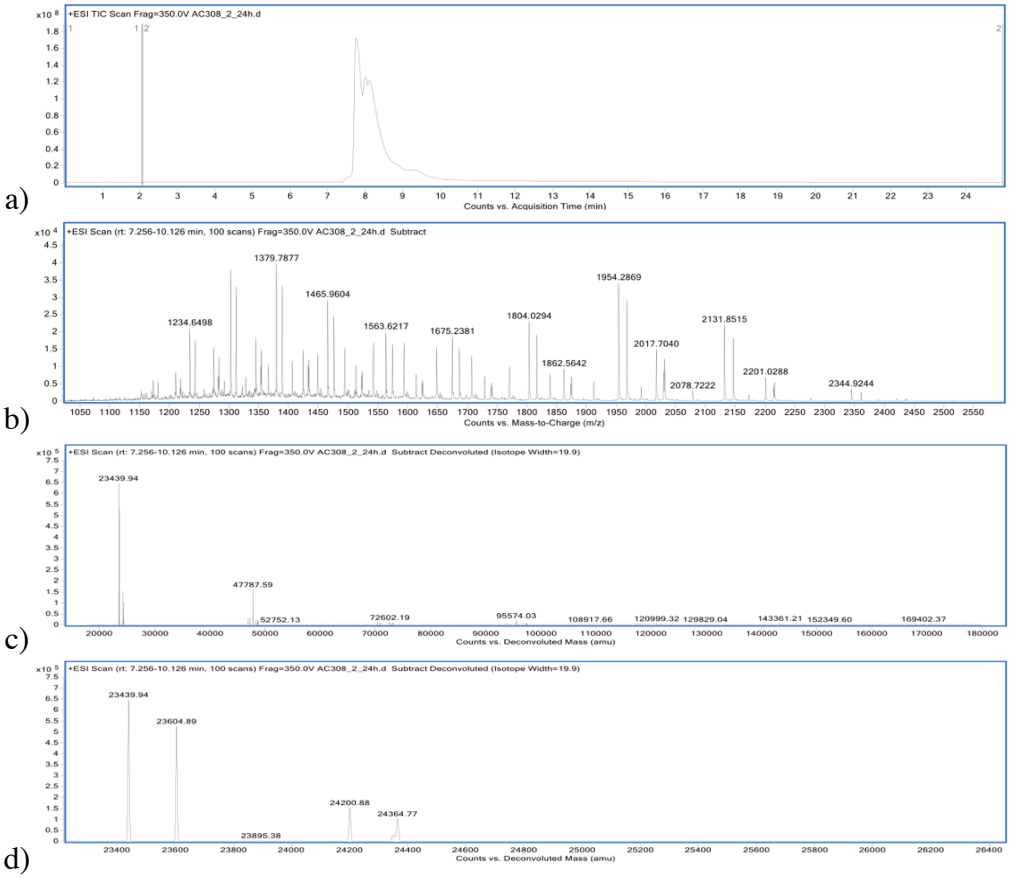

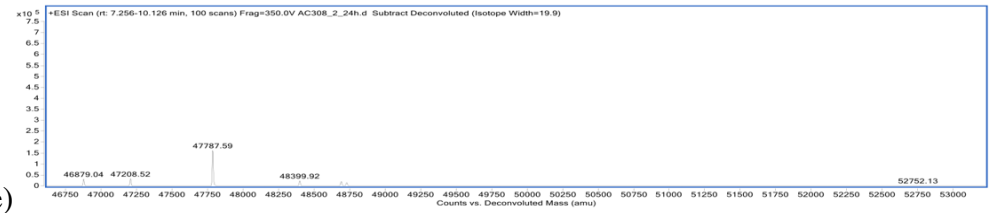

e)

Figure 89. Stability study of Fab conjugate **9** at pH 8.5, 24 h; a) TIC, b) non-deconvoluted ion-series, c) full range deconvoluted ion series mass spectrum, d) zoomed in deconvoluted ion series mass spectrum, e) zoomed in deconvoluted ion series mass spectrum.

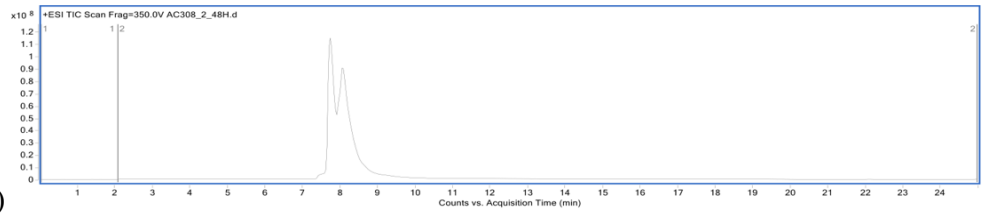

a)

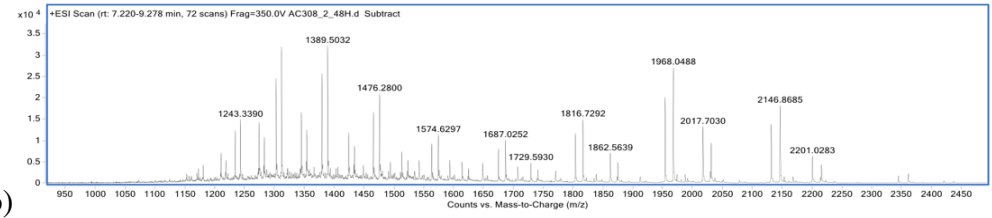

b)

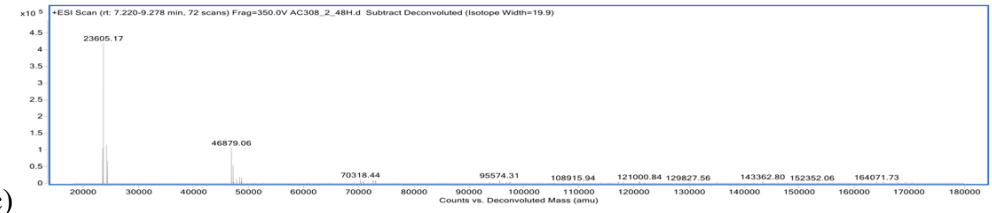

c)

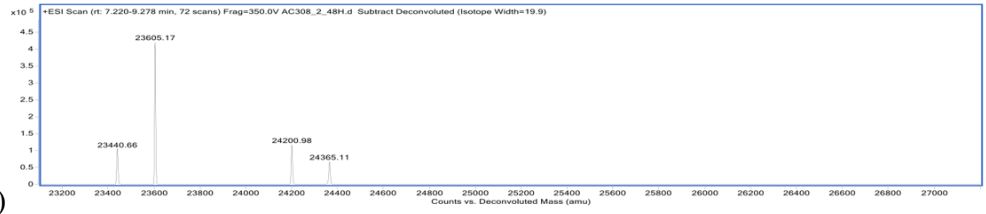

d)

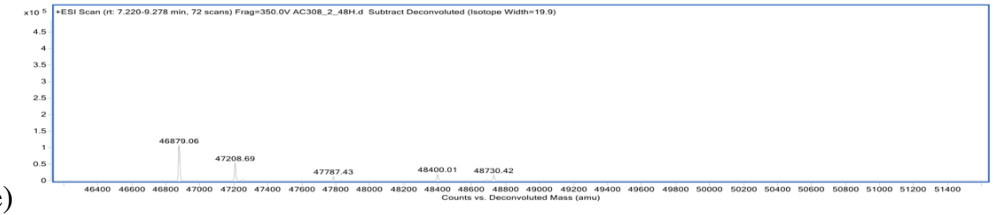

e)

Figure 90. Stability study of Fab conjugate **9** at pH 8.5, 48 h; a) TIC, b) non-deconvoluted ion-series, c) full range deconvoluted ion series mass spectrum, d) zoomed in deconvoluted ion series mass spectrum, e) zoomed in deconvoluted ion series mass spectrum.

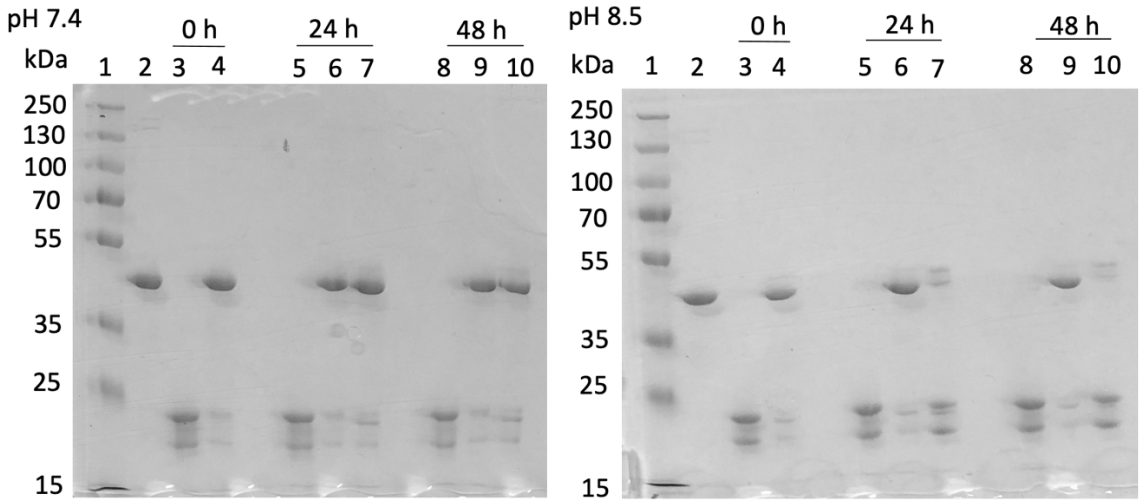

Figure 91. Stability study of Fab conjugate **9** at pH 7.4 and 8.5. SDS-PAGE: a) pH 7.4; 1 – molecular marker, 2 – native Fab, 3 – TCEP reduction, 4 – rebridging Fab with **5**, 5 – TCEP reduction, 6 – rebridging Fab with **5**, 7 – 24 h timepoint, 8 – TCEP reduction, 9 – rebridging Fab with **5**, 10 – 48 h timepoint; b) pH 8.5; 1 – molecular marker, 2 – native Fab, 3 – TCEP reduction, 4 – rebridging Fab with **5**, 5 – TCEP reduction, 6 – rebridging Fab with **5**, 7 – 24 h timepoint, 8 – TCEP reduction, 9 – rebridging Fab with **5**, 10 – 48 h timepoint.

7.3.13 Regioselectivity study of methyl 2-((2-fluoro-5-nitrobenzoyl)thio)acetate (5) and cysteine and *N*-Me-maleimide

Fab (30 μL, 100 μM, 4.76 mg/mL) in conjugation buffer was reduced with tris(2-carboxyethyl)phosphine (TCEP) (2 μL, 15 mM in diH_2O, 10 eq.). The mixture was incubated at 37 °C for 1.5 h, 300 rpm. Following that, methyl 2-((2-fluoro-5-nitrobenzoyl)thio)acetate **5** (0.2 μL, 23 mM in DMF, 1.5 eq.) was added and incubated at 22 °C for 1 h. After that, L-cysteine (2.8 μL, 108 mM in diH_2O, 100 eq.) was added and left at 37 °C, for 4 h, 300 rpm. After this period, the excess reagent was removed *via* ultrafiltration (10 kDa MWCO), into conjugation buffer, new Fab concentration was determined, and TCEP reduction was performed again as before. To cap the free thiols, an excess of *N*-methylmaleimide was added (1.1 μL, 39 mM in diH_2O, 20 eq.). Lastly, sample was desalted (7 kDa MWCO, ZebaSpin) prior to LCMS analysis. Concentration was determined photometrically using $\varepsilon_{280} = 68590\ M^{-1}\ cm^{-1}$.

a)

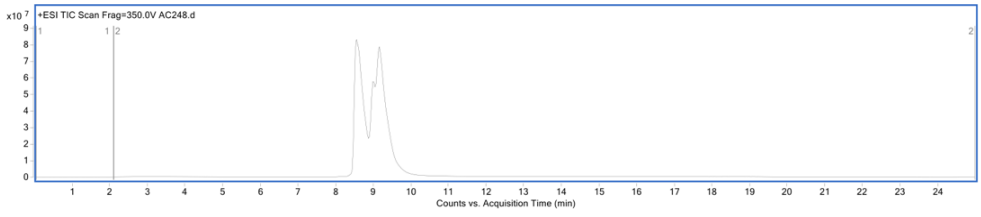

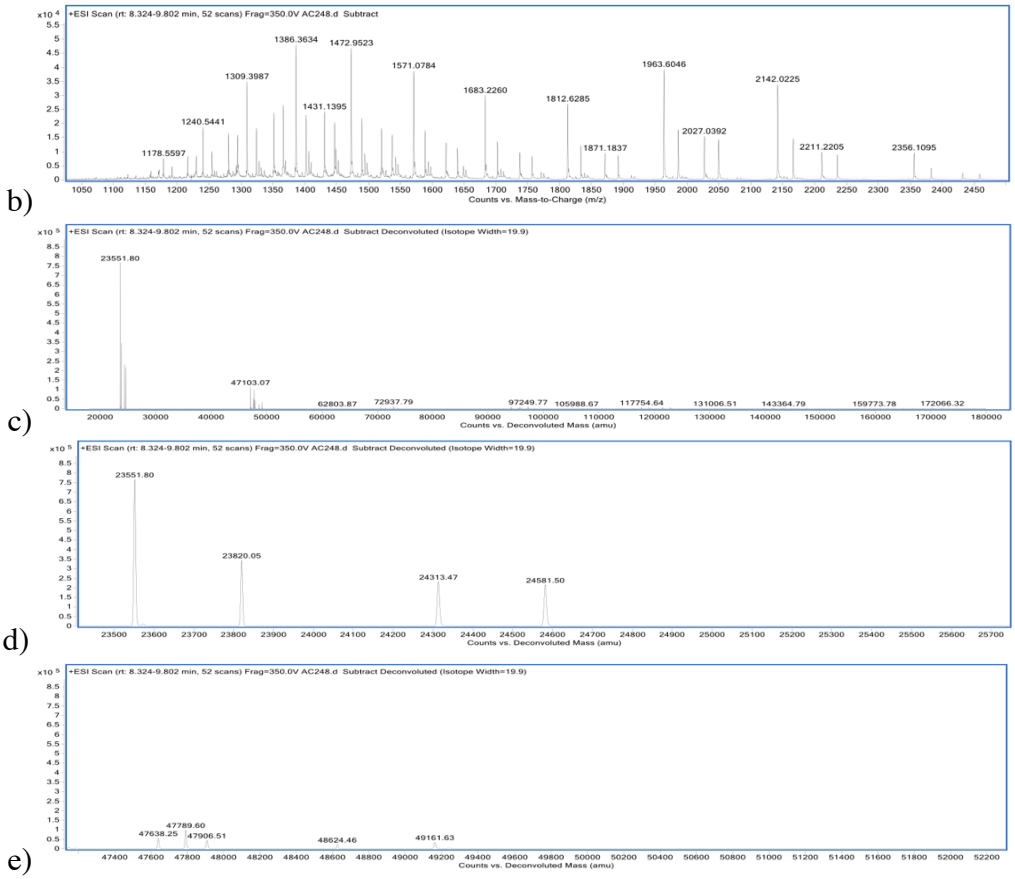

Figure 92. LCMS analysis of regioselectivity preference of methyl 2-((2-fluoro-5-nitrobenzoyl)thio)acetate **5**; a) TIC, b) non-deconvoluted ion-series, c) full range deconvoluted ion series mass spectrum, d) zoomed in deconvoluted ion series mass spectrum, e) zoomed in deconvoluted ion series mass spectrum.

7.3.14 Rebridging of Fab with methyl 2-((2-chloro-2-phenylacetyl)thio)acetate (6)

Fab (30 μL, 100 μM, 4.76 mg/mL) in conjugation buffer was reduced with tris(2-carboxyethyl)phosphine (TCEP) (2 μL, 15 mM in diH_2O, 10 eq.). The mixture was incubated at 37 °C for 1.5 h, 300 rpm. Following that, methyl 2-((2-chloro-2-phenylacetyl)thio)acetate **6** (0.1 μL, 43 mM in DMF, 1.5 eq.) was added and incubated at 22 °C for 1 h. Lastly, sample was desalted into HPLC grade water (7 kDa MWCO, ZebaSpin) prior to LCMS analysis. Concentration was determined photometrically using ε_{280} = 68590 M^{-1} cm^{-1}.

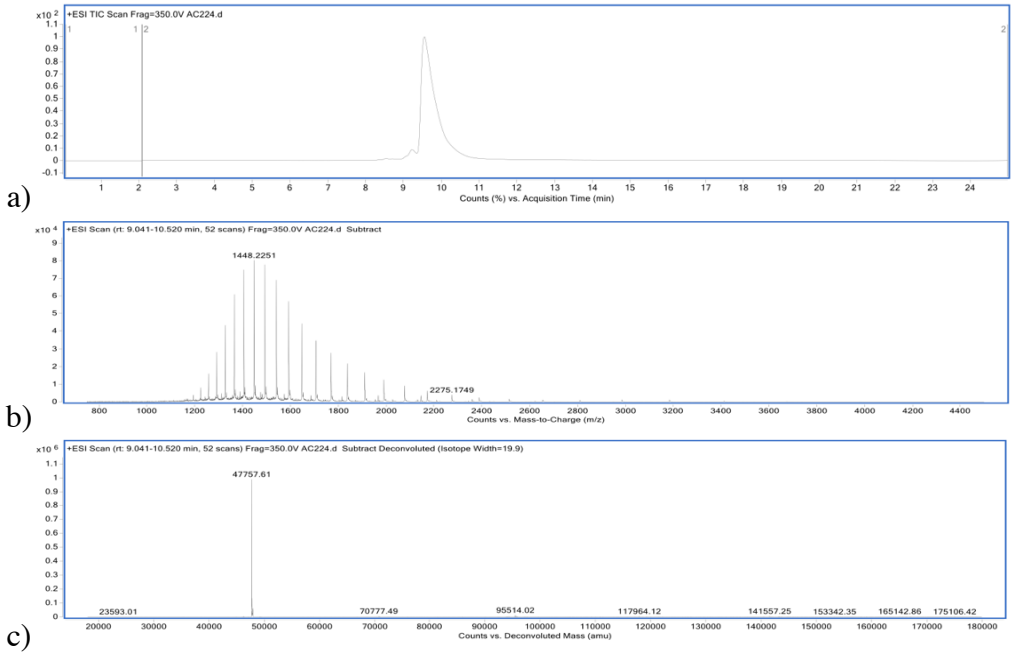

Figure 93. LCMS analysis of rebridging Fab with 2-((2-chloro-2-phenylacetyl)thio)acetate **6**; a) TIC, b) non-deconvoluted ion-series, c) full range deconvoluted ion series mass spectrum, Fab conjugate **10** expected 47756, observed 47757.

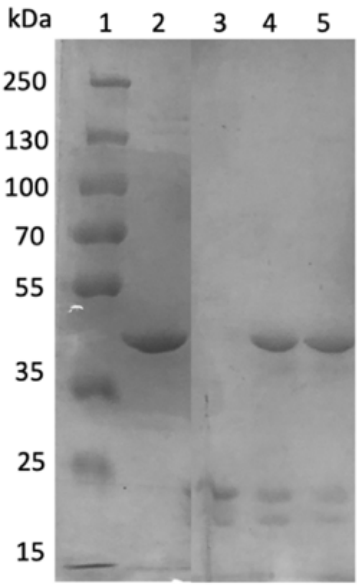

Figure 94. SDS-PAGE analysis Fab rebridging with aryl-chloro thioester **6**: 1 – marker, 2 – Fab native, 3 – TCEP reduction, 4 – rebridging with **6**.

7.3.15 Stability study of Fab conjugate 10

Fab (30 μL, 100 μM, 4.76 mg/mL) in conjugation buffer was reduced with tris(2-carboxyethyl)phoshpine (TCEP) (2 μL, 15 mM in diH_2O, 10 eq.). The mixture was incubated at 37 °C for 1.5 h, 300 rpm. Following that, methyl 2-((2-chloro-2-phenylacetyl)thio)acetate **6** (0.1 μL, 43 mM in DMF, 1.5 eq.) was added and incubated at 22 °C for 1 h. For the samples

where increased pH was required, the buffer was swapped (3 x ultrafiltration) after the initial 1 h rebridging with methyl 2-((2-chloro-2-phenylacetyl)thio)acetate into BBS buffer pH 8.5 and left for up to 48 h at 22 °C. Lastly, sample was desalted into HPLC grade water (7 kDa MWCO, ZebaSpin) prior to LCMS analysis. Concentration was determined photometrically using ε_{280} = 68590 M^{-1} cm^{-1}.

pH 7.4

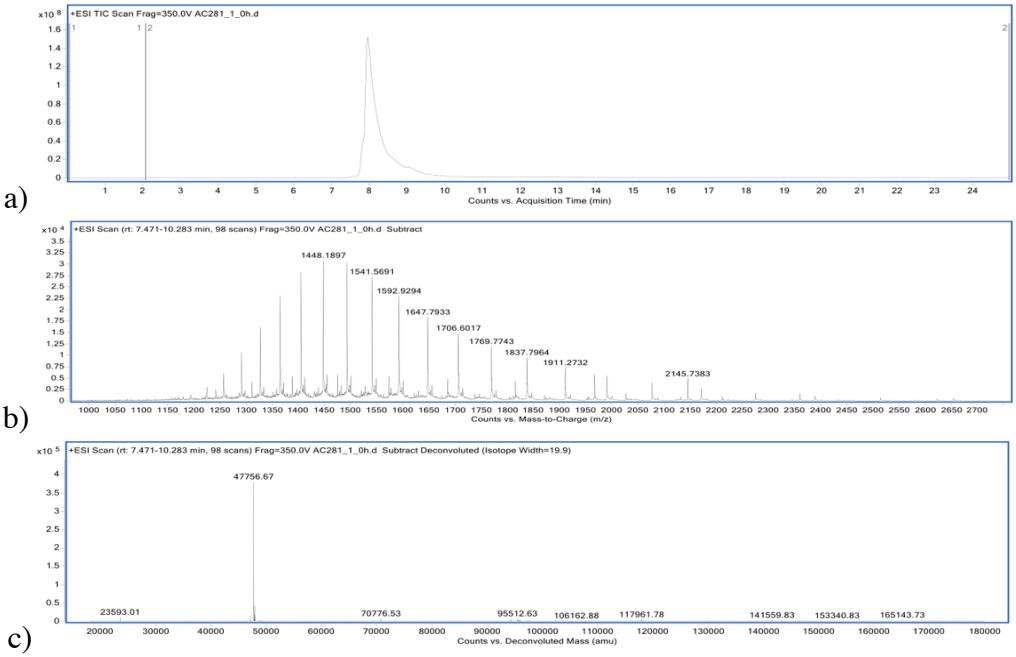

Figure 95. Stability study of Fab conjugate **10** at pH 7.4 for 1 h. a) TIC, b) non-deconvoluted ion-series c) full range deconvoluted ion series mass spectrum.

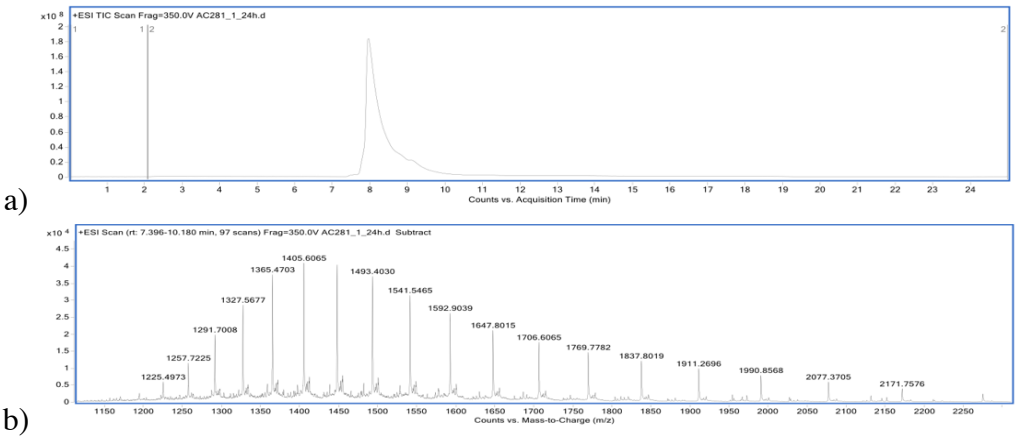

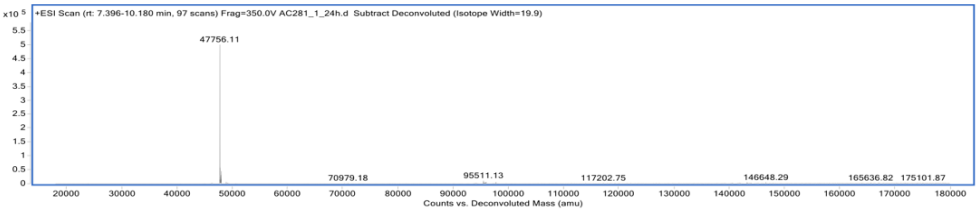

c)

Figure 96. Stability study of Fab conjugate **10** at pH 7.4 for 24 h. a) TIC, b) non-deconvoluted ion-series c) full range deconvoluted ion series mass spectrum.

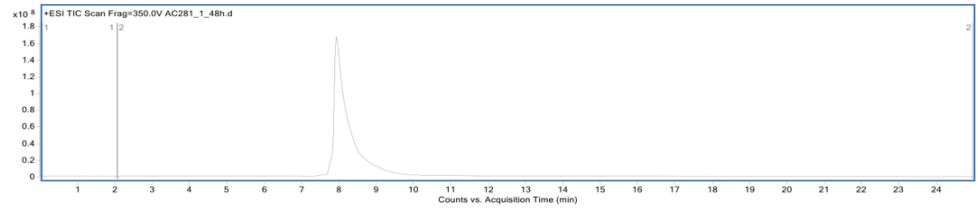

a)

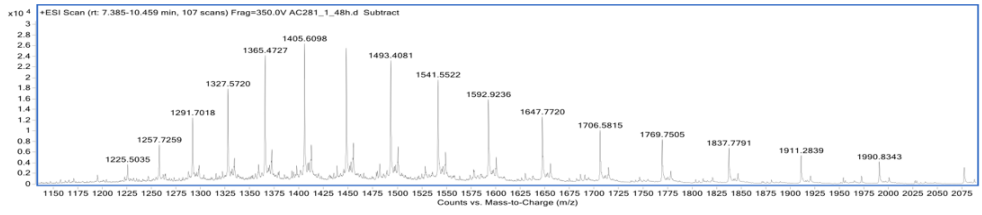

b)

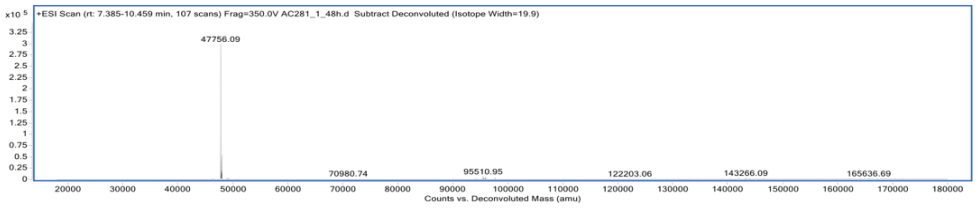

c)

Figure 97. Stability study of Fab conjugate **10** at pH 7.4 for 48 h. a) TIC, b) non-deconvoluted ion-series c) full range deconvoluted ion series mass spectrum.

pH 8.5

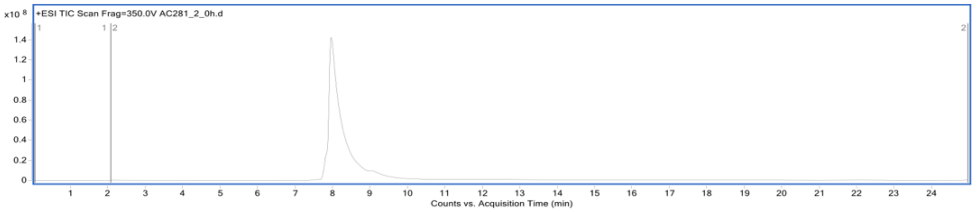

a)

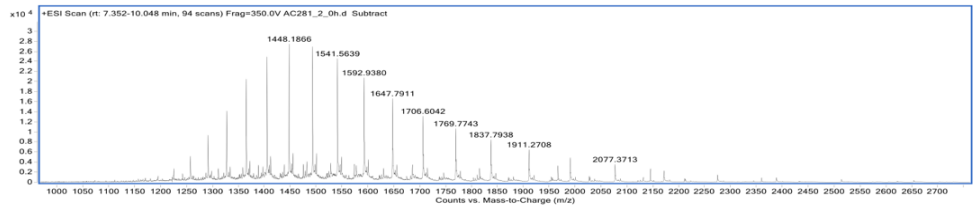

b)

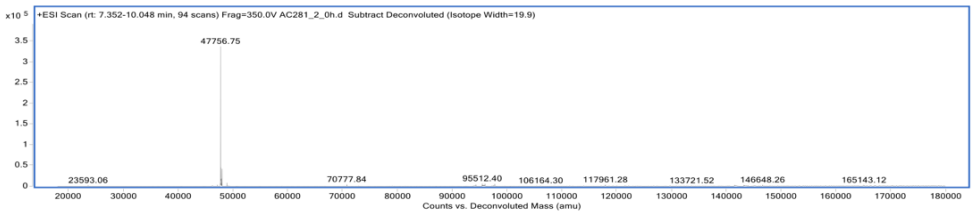

c)

Figure 98. Stability study of Fab conjugate **10** at pH 8.5 for 1 h. a) TIC, b) non-deconvoluted ion-series c) full range deconvoluted ion series mass spectrum.

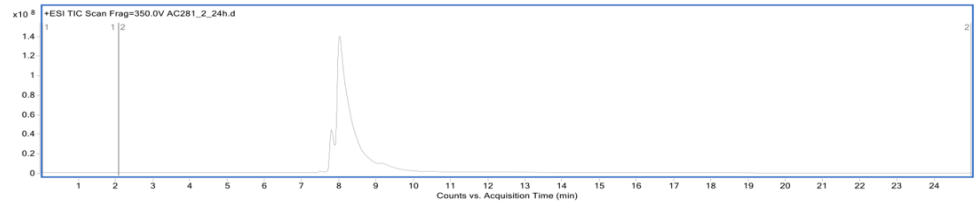

a)

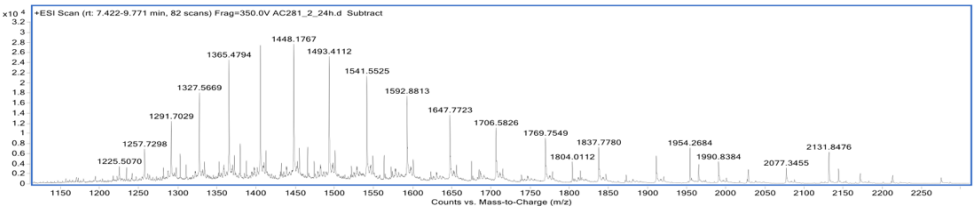

b)

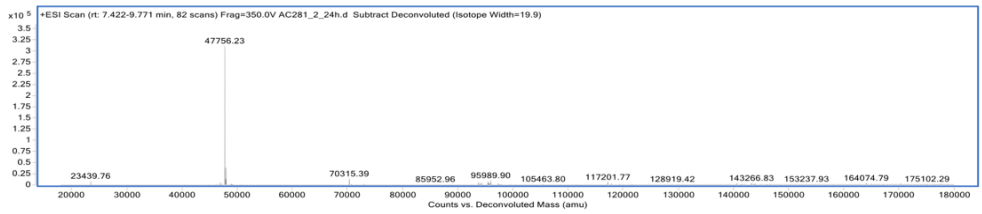

c)

Figure 99. Stability study of Fab conjugate **10** at pH 8.5 for 24 h. a) TIC, b) non-deconvoluted ion-series c) full range deconvoluted ion series mass spectrum.

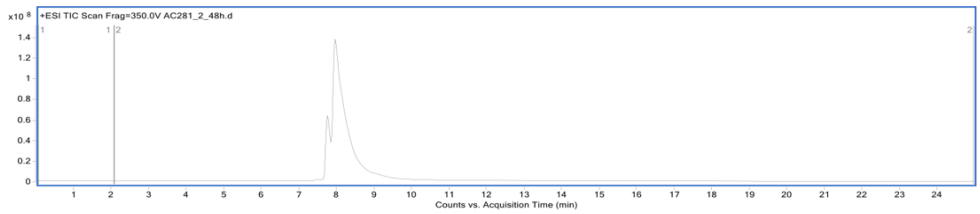

a)

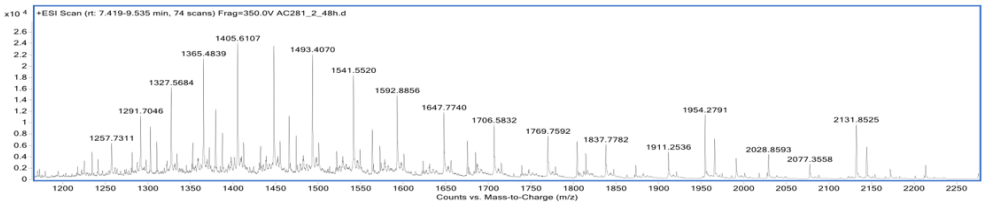

b)

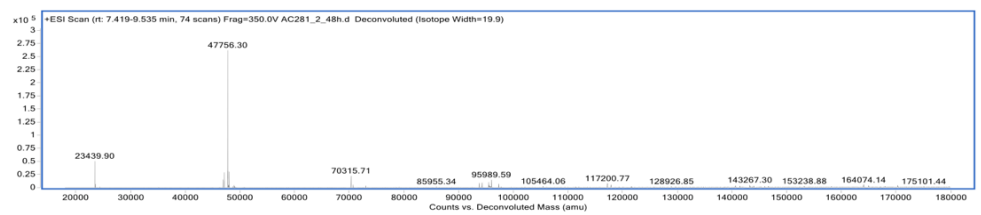

c)

d)

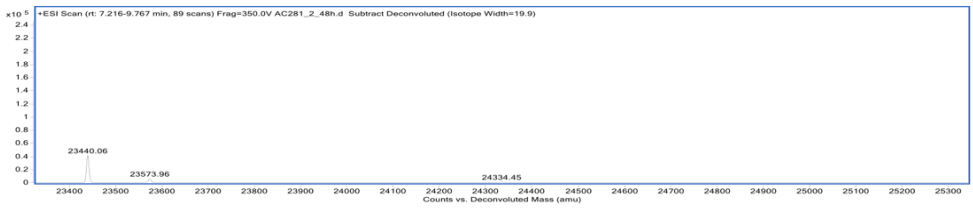

Figure 100. Stability study of Fab conjugate **10** at pH 8.5 for 48 h. a) TIC, b) non-deconvoluted ion-series c) full range deconvoluted ion series mass spectrum, d) zoomed in deconvoluted ion-series of LC and HC at 48 h.

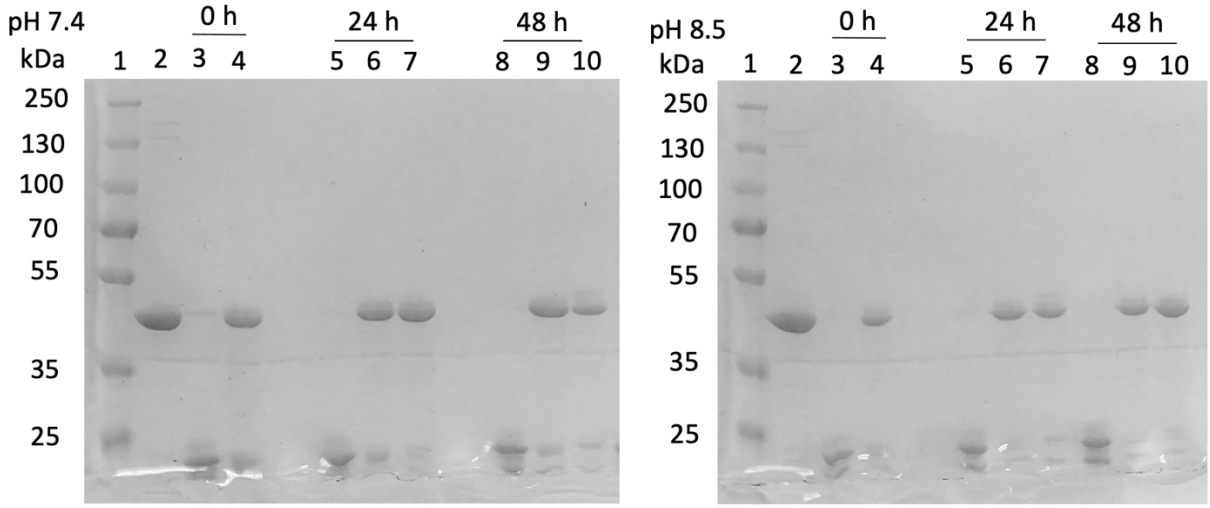

Figure 101. Stability study of Fab conjugate **10** at pH 7.4 and 8.5. SDS-PAGE: a) pH 7.4; 1 – molecular marker, 2 – native Fab, 3 – TCEP reduction, 4 – rebridging Fab with **6**, 5 – TCEP reduction, 6 – rebridging Fab with **6**, 7 – 24 h timepoint, 8 – TCEP reduction, 9 – rebridging Fab with **6**, 10 – 48 h timepoint; b) pH 8.5; 1 – molecular marker, 2 – native Fab, 3 – TCEP reduction, 4 – rebridging Fab with **6**, 5 – TCEP reduction, 6 – rebridging Fab with **6**, 7 – 24 h timepoint, 8 – TCEP reduction, 9 – rebridging Fab with **6**, 10 – 48 h timepoint.

7.3.16 Regioselectivity study of methyl 2-((2-chloro-2-phenylacetyl)thio)acetate (6) and cysteine and *N*-Me-maleimide

Fab (30 μL, 100 μM, 4.76 mg/mL) in conjugation buffer was reduced with tris(2-carboxyethyl)phosphine (TCEP) (2 μL, 15 mM solution in diH_2O, 10 eq.). The mixture was incubated at 37 °C for 1.5 h, 300 rpm. Following that, 2-((2-chloro-2-phenylacetyl)thio)acetate **6** (0.1 μL, 43 mM in DMF, 1.5 eq.) was added and incubated at 22 °C for 1 h. After that, L-cysteine (2.8 μL, 108 mM in diH_2O, 100 eq.) was added and left at 37 °C, for 4 h, 300 rpm. After this period, the excess reagent was removed *via* ultrafiltration (10 kDa MWCO), into conjugation buffer, new Fab concentration was determined, and TCEP reduction was performed again as before. To cap the free thiols, an excess of *N*-methylmaleimide was added (1.3 μL, 39 mM in diH_2O, 20 eq.). Lastly, sample was desalted into HPLC grade water (7 kDa MWCO, ZebaSpin)

prior to LCMS analysis. Concentration was determined photometrically using ε_{280} = 68590 M^{-1} cm^{-1}.

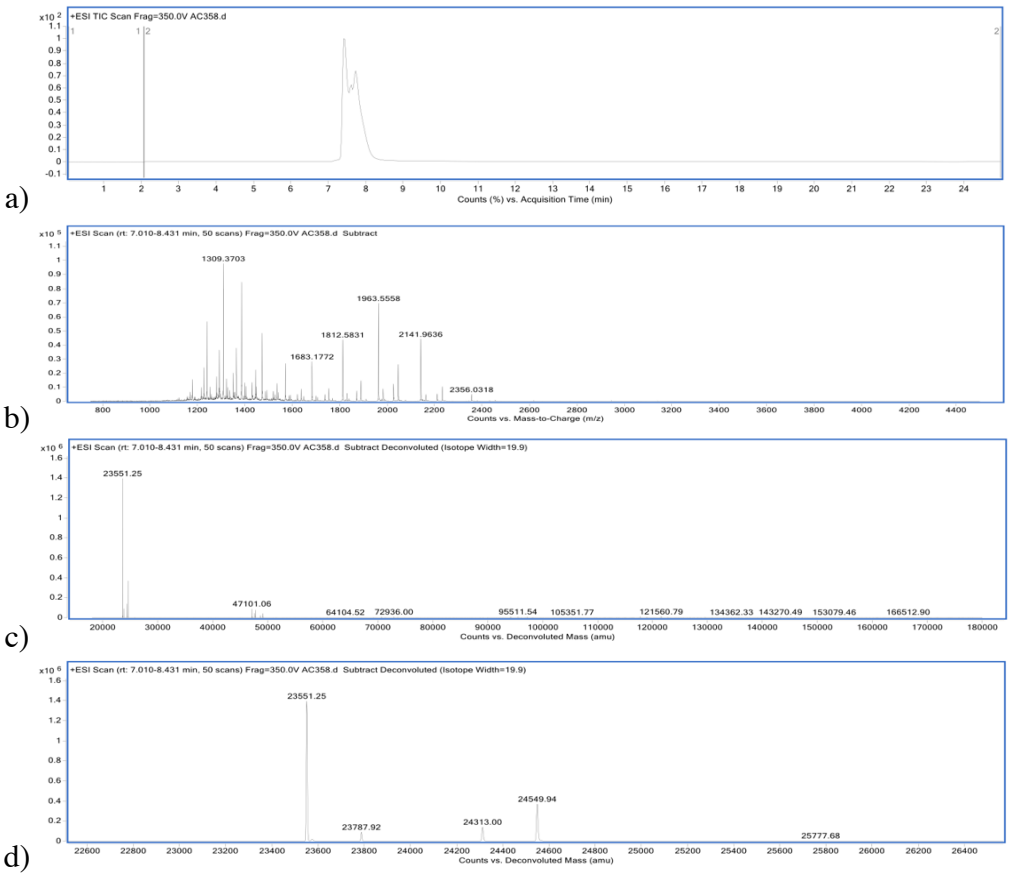

Figure 102. LCMS analysis of regioselectivity preference of 2-((2-chloro-2-phenylacetyl)thio)acetate **6**; a) TIC, b) non-deconvoluted ion-series, c) full range deconvoluted ion series mass spectrum, d) zoomed in deconvoluted ion series mass spectrum.

7.3.17 Cell Penetrating Peptide – P-C218R – reaction with Fab thioester conjugate

Fab (30 μL, 100 μM, 4.76 mg/mL) in conjugation buffer was reduced with tris(2-carboxyethyl)phosphine (TCEP) (2 μL, 15 mM in diH_2O, 10 eq.). The mixture was incubated at 37 °C for 1.5 h, 300 rpm. Following that, α-chlorothioester **1** (0.4 μL, 12 mM in DMF, 1.5 eq.) was added and incubated at 22 °C for 30 min. After that, P-C218R peptide (15 μL, 10 mM in diH_2O and 15 % MeCN, 50 eq.) was added and left at 37 °C for 16 h, 300 rpm. Lastly, sample was desalted into HPLC grade water (7 kDa MWCO, ZebaSpin) prior to LCMS analysis. Concentration was determined photometrically using ε_{280} = 68590 M^{-1} cm^{-1}.

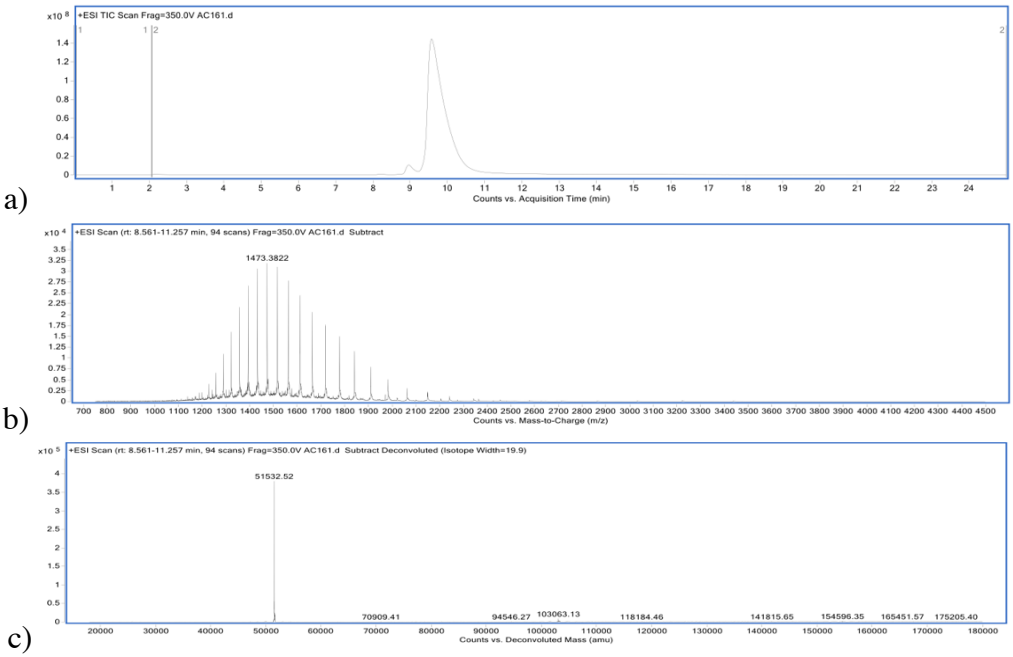

Figure 103. LCMS analysis of Fab conjugate **7** and P-C218R peptide, forming conjugate **29**; a) TIC, b) non-deconvoluted ion-series, c) full range deconvoluted ion series mass spectrum, Fab conjugate **29** expected 51532, observed 51532.

7.3.18 Reaction of Fab thioester conjugate with P-C218R peptide and DBM

Fab (30 μL, 100 μM, 4.76 mg/mL) in conjugation buffer was reduced with tris(2-carboxyethyl)phosphine (TCEP) (2 μL, 15 mM in diH_2O, 10 eq.). The mixture was incubated at 37 °C for 1.5 h, 300 rpm. Following that, α-chlorothioester **1** (0.2 μL, 24 mM in DMF, 1.5 eq.) was added and incubated at 22 °C for 30 min, then MPAA was added (2.5 μL, 30 mM, 25 eq.) and this was left at 22 °C for 2 h. After that, P-C218R peptide (7.5 μL, 10 mM in diH_2O and 15 % MeCN, 25 eq.) was added and left at 37 °C for 16 h, 300 rpm. Upon completion of this step, excess of the reagents was removed *via* ultrafiltration (10 kDa MWCO) into conjugation buffer, new Fab concentration was determined. TCEP reduction was performed again as before followed by removal of the excess of the reagent. Subsequently, DBM-PEG-BCN (0.9 μL, 10 mM in DMSO, 4 eq.) was added and first left at 22 °C for 20 min to conjugate then the sample was left at 37 °C for 16 h, 300 rpm to promote hydrolysis to 'lock' the conjugate as stable maleamic acids. Lastly, sample was desalted into HPLC grade water (7 kDa MWCO, ZebaSpin) prior to LCMS analysis. Concentration was determined photometrically using $\varepsilon_{280} = 68590\ M^{-1}\ cm^{-1}$.

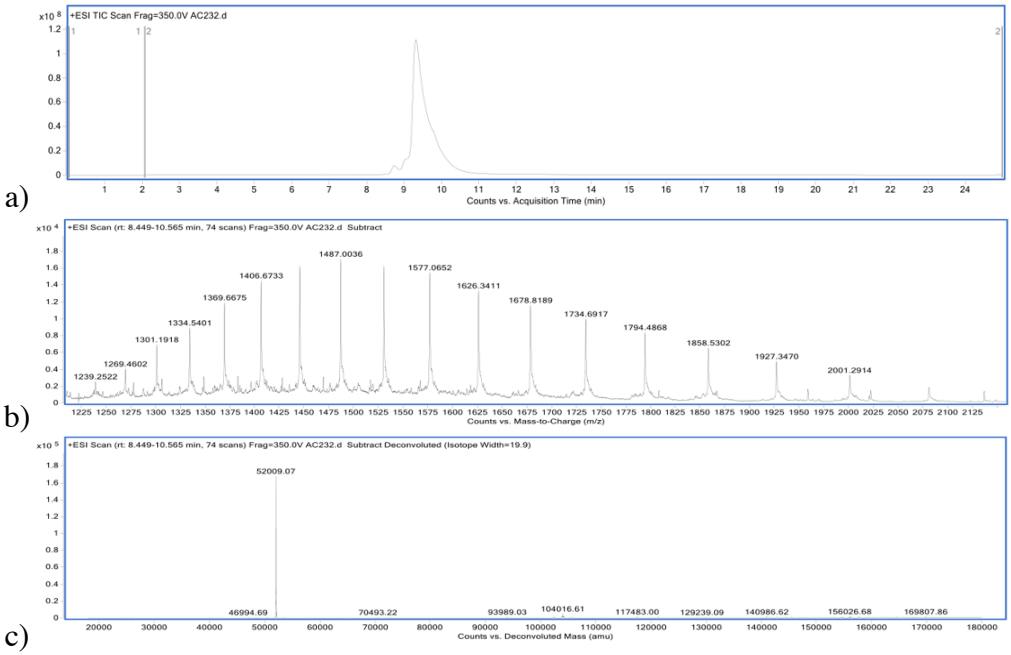

Figure 104. LCMS analysis of rebridged Fab with α-chlorothioester **1** and reacted with P-C218R peptide and DBM-PEG-BCN forming conjugate **30**; a) TIC, b) non-deconvoluted ion-series, c) full range deconvoluted ion series mass spectrum, Fab conjugate **30** expected 52009, observed 52009.

7.3.19 Reaction of Fab thioester conjugate with P-C218R peptide, DBM and fluorophore

Fab (30 μL, 100 μM, 4.76 mg/mL) in conjugation buffer was reduced with tris(2-carboxyethyl)phosphine (TCEP) (2 μL, 15 mM in diH_2O, 10 eq.). The mixture was incubated at 37 °C for 1.5 h, 300 rpm. Following that, α-chlorothioester **1** (0.2 μL, 24 mM in DMF, 1.5 eq.) was added and incubated at 22 °C for 30 min, then MPAA was added (2.5 μL, 30 mM, 25 eq.) and this was left at 22 °C for 2 h. After that, P-C218R peptide (7.5 μL, 10 mM in diH_2O and 15 % MeCN, 25 eq.) was added and left at 37 °C for 16 h, 300 rpm. Upon completion of this step, excess of the reagents was removed *via* ultrafiltration (10 kDa MWCO) into conjugation buffer, new Fab concentration was determined. TCEP reduction was performed again as before followed by removal of the excess of the reagent. Subsequently, DBM-PEG-BCN (0.8 μL, 10 mM in DMSO, 4 eq.) was added and first left at 22 °C for 20 min to conjugate then the sample was left at 37 °C for 16 h, 300 rpm to promote hydrolysis to 'lock' the conjugate as stable maleamic acids. This was followed by another ultrafiltration to remove excess of the reagent. Finally, Azide fluor 488 (0.8 μL, 10 mM in DMF, 5 eq.) was added and this was left in the dark at 37 °C for 4 h, 300 rpm. The excess reagent was then removed using a desalting column (PD Minitrap G-25, GE Healthcare) followed by ultrafiltration (10 kDa MWCO) into conjugate buffer to concentrate the

sample. Lastly, sample was desalted into HPLC grade water (7 kDa MWCO, ZebaSpin) prior to LCMS analysis. Concentration was determined photometrically using $\varepsilon_{280} = 68590\ M^{-1}\ cm^{-1}$.

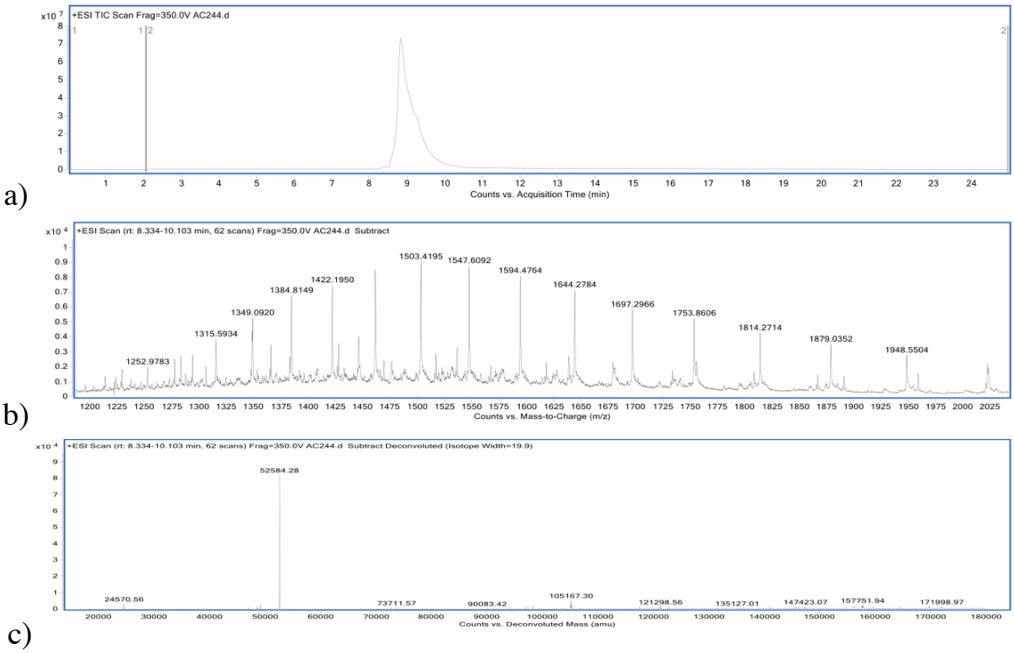

Figure 105. LCMS analysis of rebridged Fab with α-chlorothioester **1** and reacted with P-C218R peptide, DBM-PEG-BCN, and Azide Fluor 488 forming conjugate **31**; a) TIC, b) non-deconvoluted ion-series, c) full range deconvoluted ion series mass spectrum, Fab conjugate **31** expected 52584, observed 52584.

7.3.20 Cell Penetrating Peptide – TAT – reaction on Fab thioester conjugate

Fab (30 μL, 100 μM, 4.76 mg/mL) in conjugation buffer was reduced with tris(2-carboxyethyl)phosphine (TCEP) (2 μL, 15 mM in diH_2O, 10 eq.). The mixture was incubated at 37 °C for 1.5 h, 300 rpm. Following that, α-chlorothioester **1** (0.2 μL, 24 mM in DMF, 1.5 eq.) was added and incubated at 22 °C for 30 min. After that, TAT peptide (7.5 μL, 10 mM in diH_2O and 15 % MeCN, 25 eq.) was added and left at 37 °C for 16 h, 300 rpm. Lastly, sample was desalted into HPLC grade water (7 kDa MWCO, ZebaSpin) prior to LCMS analysis. Concentration was determined photometrically using $\varepsilon_{280} = 68590\ M^{-1}\ cm^{-1}$.

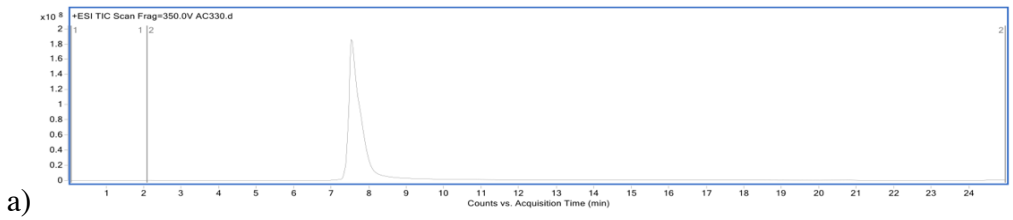

b)

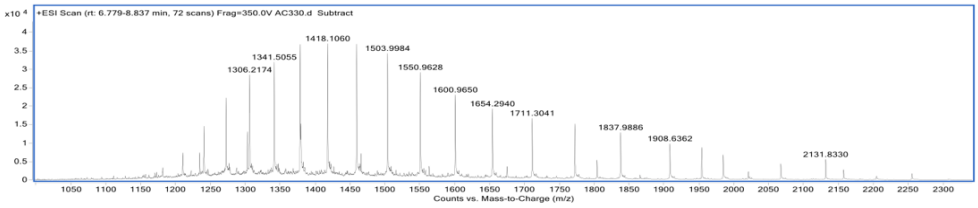

c)

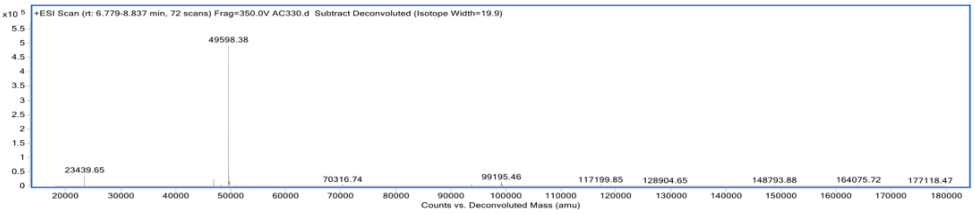

Figure 106. LCMS analysis of rebridged Fab with α-chlorothioester **1** and reacted with TAT peptide forming conjugate **32**; a) TIC, b) non-deconvoluted ion-series, c) full range deconvoluted ion series mass spectrum, native LC expected 23438, observed 23440, Fab conjugate **32** expected 49600, observed 49598.

7.3.21 Reaction of Fab thioester conjugate with TAT peptide and PD-diEt

Fab (30 μL, 100 μM, 4.76 mg/mL) in conjugation buffer was reduced with tris(2-carboxyethyl)phosphine (TCEP) (2 μL, 15 mM in diH_2O, 10 eq.). The mixture was incubated at 37 °C for 1.5 h, 300 rpm. Following that, α-chlorothioester **1** (0.2 μL, 24 mM in DMF, 1.5 eq.) was added and incubated at 22 °C for 30 min. After that, TAT peptide (7.5 μL, 10 mM in diH_2O and 15 % MeCN, 25 eq.) was added and left at 37 °C for 16 h, 300 rpm. Upon completion of this step, excess of the reagents was removed *via* ultrafiltration (10 kDa MWCO) into conjugation buffer, new Fab concentration was determined. TCEP reduction was performed again as before followed by removal of the excess of the reagent. Subsequently, PD-diEt (1.8 μL, 10 mM in DMSO, 10 eq.) was added and left at 37 °C for 5 h, 300 rpm. Lastly, sample was desalted into HPLC grade water (7 kDa MWCO, ZebaSpin) prior to LCMS analysis. Concentration was determined photometrically using $\varepsilon_{280} = 68590\ M^{-1}\ cm^{-1}$.

a)

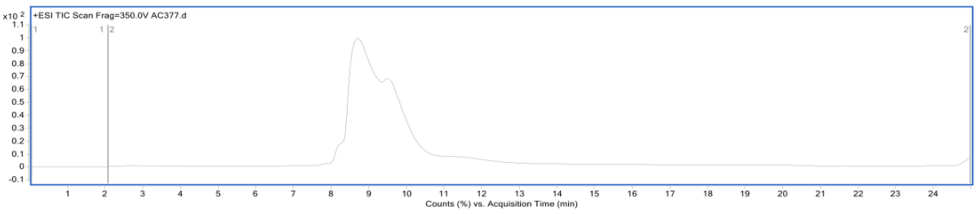

b)

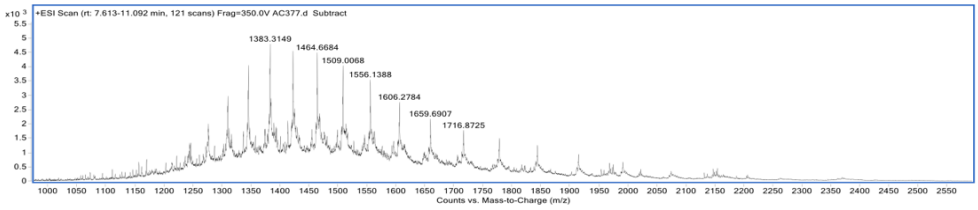

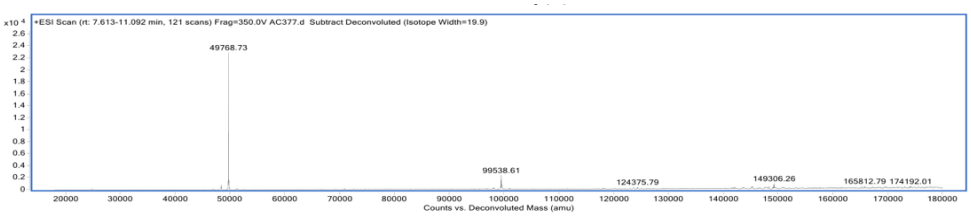

c)

Figure 107. LCMS analysis of Fab conjugate **7** reacted with TAT peptide and PD-diEt forming conjugate **33**; a) TIC, b) non-deconvoluted ion-series, c) full range deconvoluted ion series mass spectrum, Fab conjugate **33** expected 49766, observed 49768.

7.3.22 Reaction of Fab thioester conjugate with TAT peptide and PD

Fab (30 μL, 100 μM, 4.76 mg/mL) in conjugation buffer was reduced with tris(2-carboxyethyl)phosphine (TCEP) (2 μL, 15 mM in diH_2O, 10 eq.). The mixture was incubated at 37 °C for 1.5 h, 300 rpm. Following that, α-chlorothioester **1** (0.2 μL, 24 mM in DMF, 1.5 eq.) was added and incubated at 22 °C for 30 min. After that, TAT peptide (7.5 μL, 10 mM in diH_2O and 15 % MeCN, 25 eq.) was added and left at 37 °C for 16 h, 300 rpm. Upon completion of this step, excess of the reagents was removed *via* ultrafiltration (10 kDa MWCO) into conjugation buffer, new Fab concentration was determined. TCEP reduction was performed again as before followed by removal of the excess of the reagent. Subsequently, BCN-PD (0.2 μL, 20 mM in DMSO, 2 eq.) was added and left at 37 °C for 2 h, 300 rpm. Lastly, sample was desalted into HPLC grade water (7 kDa MWCO, ZebaSpin) prior to LCMS analysis. Concentration was determined photometrically using $\varepsilon_{280} = 68590\ M^{-1}\ cm^{-1}$.

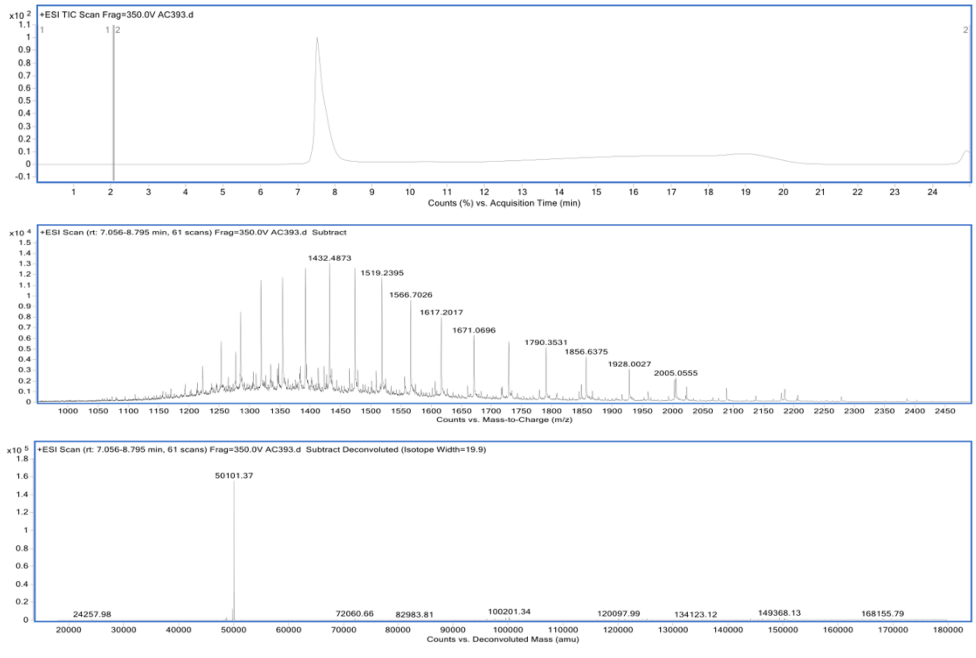

a)

b)

c)

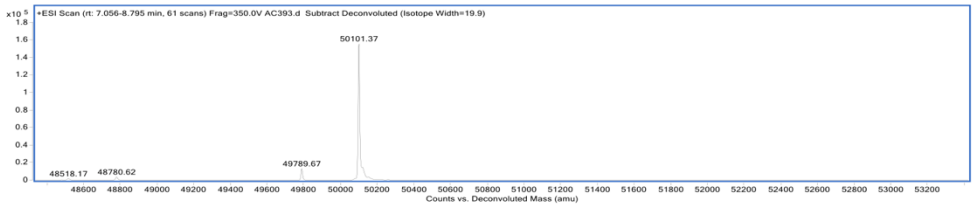

d)

Figure 108. LCMS analysis of Fab conjugate **7** reacted with TAT peptide, and PD-PEG-BCN forming conjugate **34**; a) TIC, b) non-deconvoluted ion-series, c) full range deconvoluted ion series mass spectrum, Fab conjugate **34** expected 50102, observed 50101. The minor peak 49789 is undefined, but it is notably not present, and therefore not associated with, the key TAT peptide conjugation step.

7.3.23 Reaction of Fab thioester conjugate with TAT peptide, PD and fluorophore

Fab (30 μL, 100 μM, 4.76 mg/mL) in conjugation buffer was reduced with tris(2-carboxyethyl)phosphine (TCEP) (2 μL, 15 mM in diH_2O, 10 eq.). The mixture was incubated at 37 °C for 1.5 h, 300 rpm. Following that, α-chlorothioester **1** (0.2 μL, 24 mM in DMF, 1.5 eq.) was added and incubated at 22 °C for 30 min. After that, TAT peptide (7.5 μL, 10 mM in diH_2O and 15 % MeCN, 25 eq.) was added and left at 37 °C for 16 h, 300 rpm. Upon completion of this step, excess of the reagent was removed *via* ultrafiltration (10 kDa MWCO) into conjugation buffer, new Fab concentration was determined. TCEP reduction was performed again as before followed by removal of the excess of the reagent. Subsequently, BCN-PD (0.2 μL, 20 mM in DMSO, 2 eq.) was added and left at 37 °C for 2 h, 300 rpm. This was followed by another ultrafiltration to remove excess of the reagent. Finally, Azide fluor 488 (0.7 μL, 10 mM in DMF, 5 eq.) was added and this was left in the dark at 37 °C for 2 h, 300 rpm. The excess reagent was then removed using a desalting column (PD Minitrap G-25, GE Healthcare) followed by ultrafiltration (10 kDa MWCO) into conjugate buffer to concentrate the sample. Lastly, sample was desalted into HPLC grade water (7 kDa MWCO, ZebaSpin) prior to LCMS analysis. Concentration was determined photometrically using $\varepsilon_{280} = 68590\ M^{-1}\ cm^{-1}$.

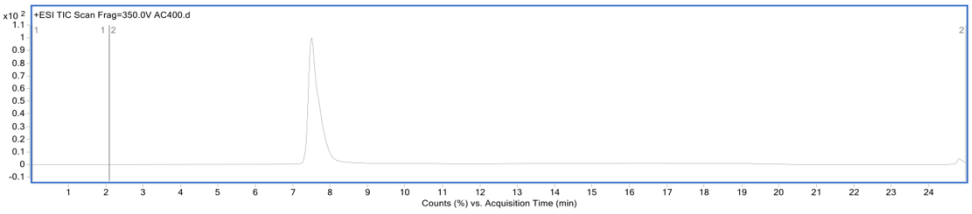

a)

b)

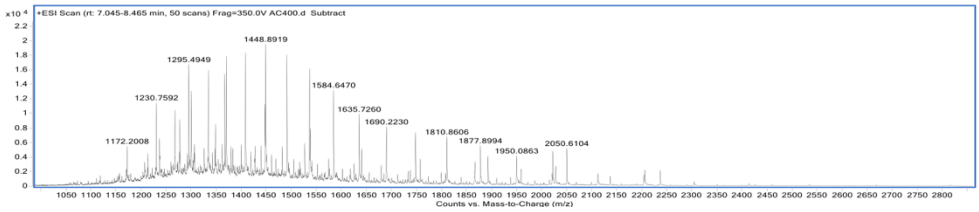

c)

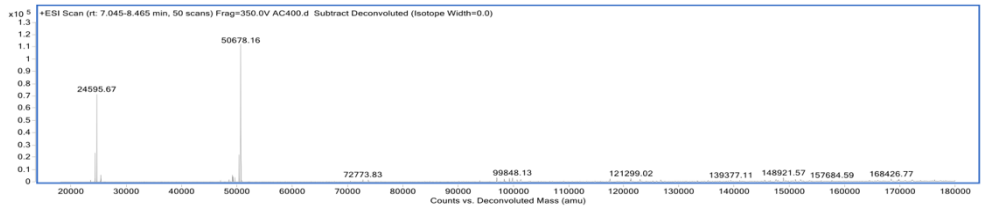

d)

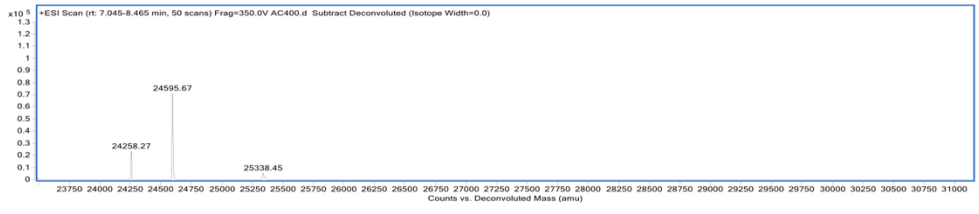

e)

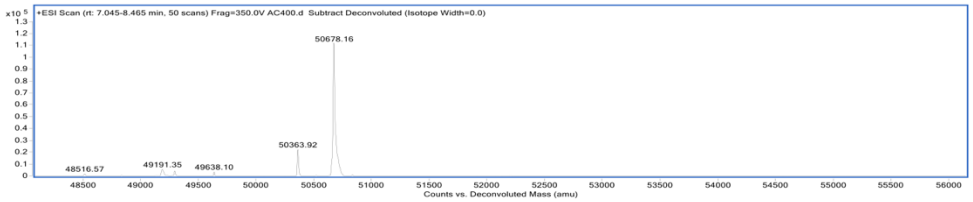

Figure 109. LCMS analysis of Fab conjugate **7** reacted with TAT peptide, PD-PEG-BCN, and Azide fluor 488 forming conjugate **35**; a) TIC, b) non-deconvoluted ion-series, c) full range deconvoluted ion series mass spectrum, d) zoomed in deconvoluted ion series mass spectrum, HC hydrolysed bridged species expected 24259, observed 24258, LC with PD(Br)-PEG-BCN and Azide fluor 488 expected 24594, observed 24595, e) zoomed in deconvoluted ion series mass spectrum, Fab conjugate **35** expected 50677, observed 50678. The minor peak 50363 is undefined, but it is notably not present, and therefore not associated with, the key TAT peptide conjugation step.

7.3.24 Reaction of Fab thioester conjugate with TAT peptide and DBM

Fab (30 μL, 100 μM, 4.76 mg/mL) in conjugation buffer was reduced with tris(2-carboxyethyl)phosphine (TCEP) (2 μL, 15 mM in diH_2O, 10 eq.). The mixture was incubated at 37 °C for 1.5 h, 300 rpm. Following that, α-chlorothioester **1** (0.2 μL, 24 mM in DMF, 1.5 eq.) was added and incubated at 22 °C for 30 min. After that, TAT peptide (7.5 μL, 10 mM in diH_2O and 15 % MeCN, 25 eq.) was added and left at 37 °C for 16 h, 300 rpm. Upon completion of this step, excess of the reagents was removed *via* ultrafiltration (10 kDa MWCO) into conjugation buffer, new Fab concentration was determined. TCEP reduction was performed again as before followed by removal of the excess of the reagent. Subsequently, DBM-PEG-BCN (1.1 μL, 10 mM in DMSO, 4 eq.) was added and first left at 22 °C for 20 min to conjugate then the sample

was left at 37 °C for 16 h, 300 rpm to promote hydrolysis to 'lock' the conjugate as stable maleamic acids. Lastly, sample was desalted into HPLC grade water (7 kDa MWCO, ZebaSpin) prior to LCMS analysis. Concentration was determined photometrically using ε_{280} = 68590 M^{-1} cm^{-1}.

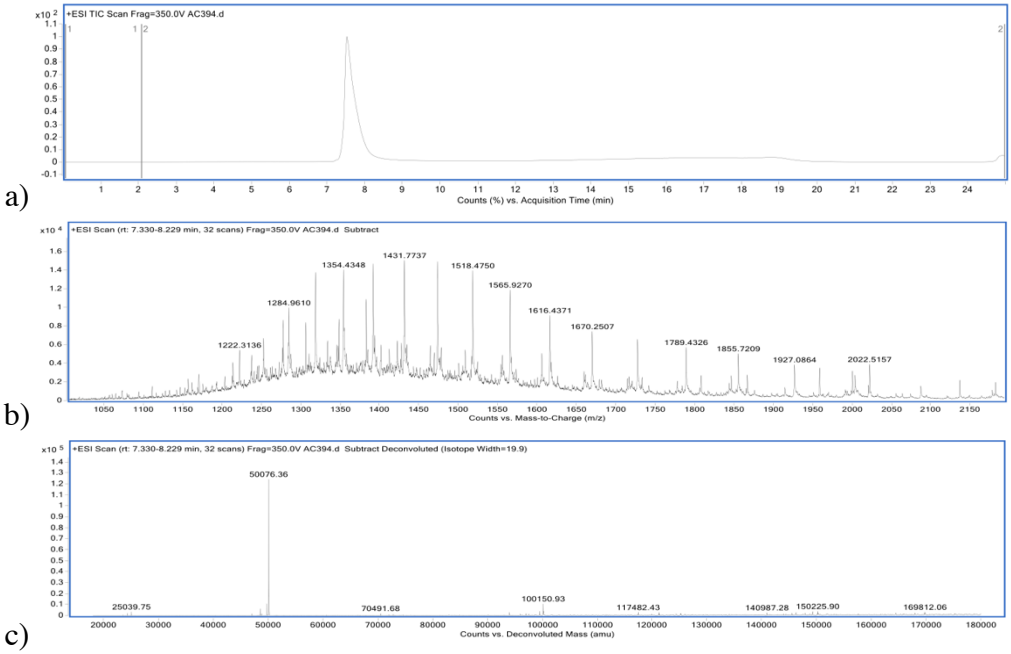

Figure 110. LCMS analysis of Fab conjugate **7** reacted with TAT peptide and DBM-PEG-BCN forming conjugate **36**; a) TIC, b) non-deconvoluted ion-series, c) full range deconvoluted ion series mass spectrum, Fab conjugate **36** expected 50077, observed 50076.

7.3.25 Reaction of Fab thioester conjugate with TAT peptide, DBM and fluorophore

Fab (30 μL, 100 μM, 4.76 mg/mL) in conjugation buffer was reduced with tris(2-carboxyethyl)phosphine (TCEP) (2 μL, 15 mM in diH_2O, 10 eq.). The mixture was incubated at 37 °C for 1.5 h, 300 rpm. Following that, α-chlorothioester **1** (0.2 μL, 24 mM in DMF, 1.5 eq.) was added and incubated at 22 °C for 30 min. After that, TAT peptide (7.5 μL, 10 mM in diH_2O and 15 % MeCN, 25 eq.) was added and left at 37 °C for 16 h, 300 rpm. Upon completion of this step, excess of the reagents was removed *via* ultrafiltration (10 kDa MWCO) into conjugation buffer, new Fab concentration was determined. TCEP reduction was performed again as before followed by removal of the excess of the reagent. Subsequently, DBM-PEG-BCN (0.9 μL, 10 mM in DMSO, 4 eq.) was added and first left at 22 °C for 20 min to conjugate then the sample was left at 37 °C for 16 h, 300 rpm to promote hydrolysis to 'lock' the conjugate as stable

maleamic acids. This was followed by another ultrafiltration to remove excess of the reagent. Finally, Azide fluor 488 (0.7 μL, 10 mM in DMF, 5 eq.) was added and this was left in the dark at 37 °C for 3 h, 300 rpm. The excess reagent was then removed using a desalting column (PD Minitrap G-25, GE Healthcare) followed by ultrafiltration (10 kDa MWCO) into conjugate buffer to concentrate the sample. Lastly, sample was desalted into HPLC grade water (7 kDa MWCO, ZebaSpin) prior to LCMS analysis. Concentration was determined photometrically using ε_{280} = 68590 M^{-1} cm^{-1}.

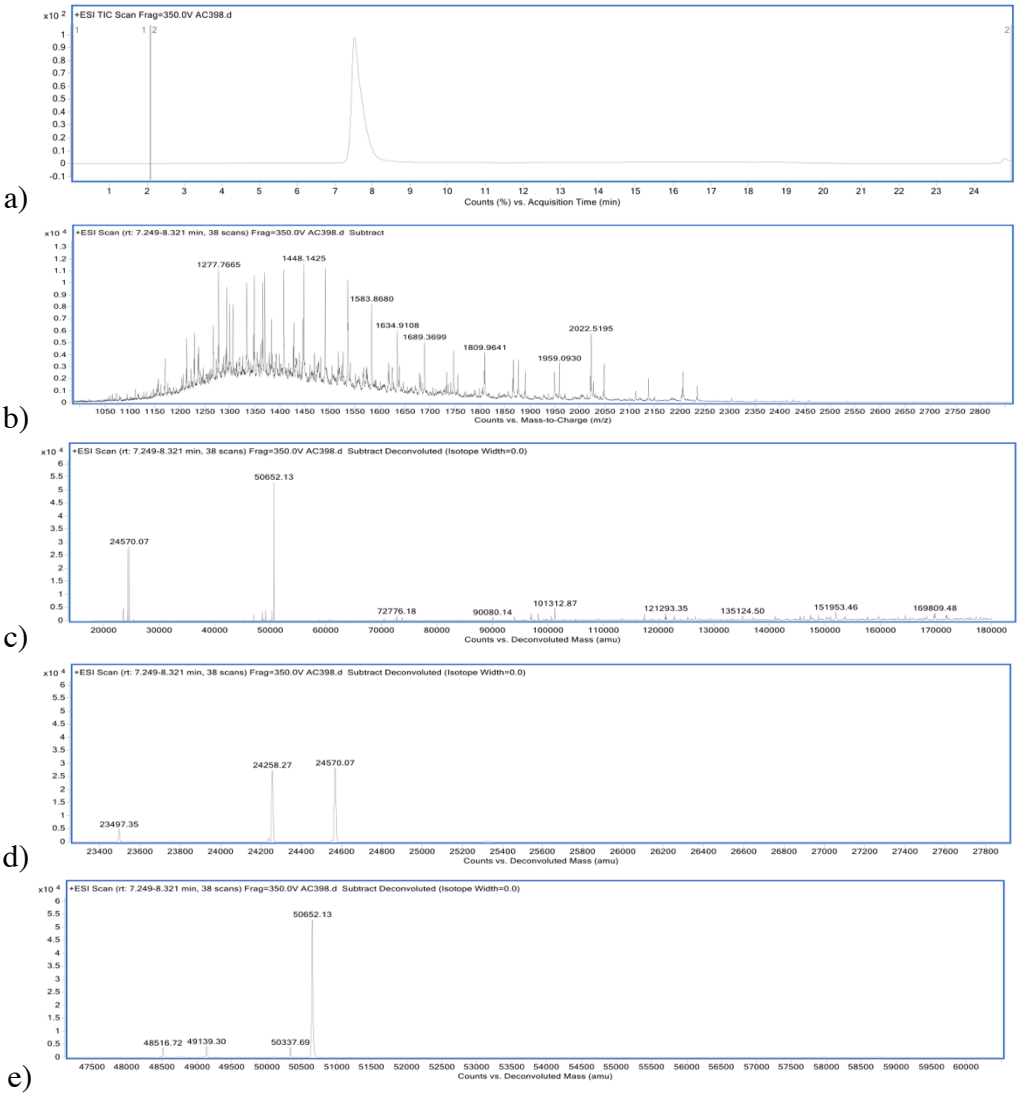

Figure 111. LCMS analysis of Fab conjugate **7** reacted with TAT peptide, DBM-PEG-BCN, and Azide Fluor 488 forming conjugate **37**; a) TIC, b) non-deconvoluted ion-series, c) full range deconvoluted ion series mass spectrum, d) zoomed in deconvoluted ion series mass spectrum, LC hydrolysed bridged species expected 23497, observed 24258, LC with DBM(Br)-PEG-BCN and Azide Fluor 488 expected 24569, observed 24570, e) zoomed in deconvoluted ion series mass spectrum, Fab conjugate **37** expected 50652, observed 50652. The minor peak 50337 is undefined, but it is notably not present, and therefore not associated with, the key TAT peptide conjugation step.

7.3.26 Reaction of Fab thioester conjugate with hydrazine hydrate

Fab (30 μL, 100 μM, 4.76 mg/mL) in conjugation buffer was reduced with tris(2-carboxyethyl)phosphine (TCEP) (2 μL, 15 mM in diH_2O, 10 eq.) The mixture was incubated at 37 °C for 1.5 h, 300 rpm. Following that, α-chlorothioester **1** (0.4 μL, 12 mM in DMF, 1.5 eq.) was added and incubated at 22 °C for 30 min. After that, hydrazine hydrate (3.0 μL, 1.0 M in DMF, 1000 eq.) was added and left at 37 °C, for 2 h, 300 rpm. Lastly, sample was desalted (7 kDa MWCO, ZebaSpin) prior to LCMS analysis. Concentration was determined photometrically using $\varepsilon_{280} = 68590\ M^{-1}\ cm^{-1}$.

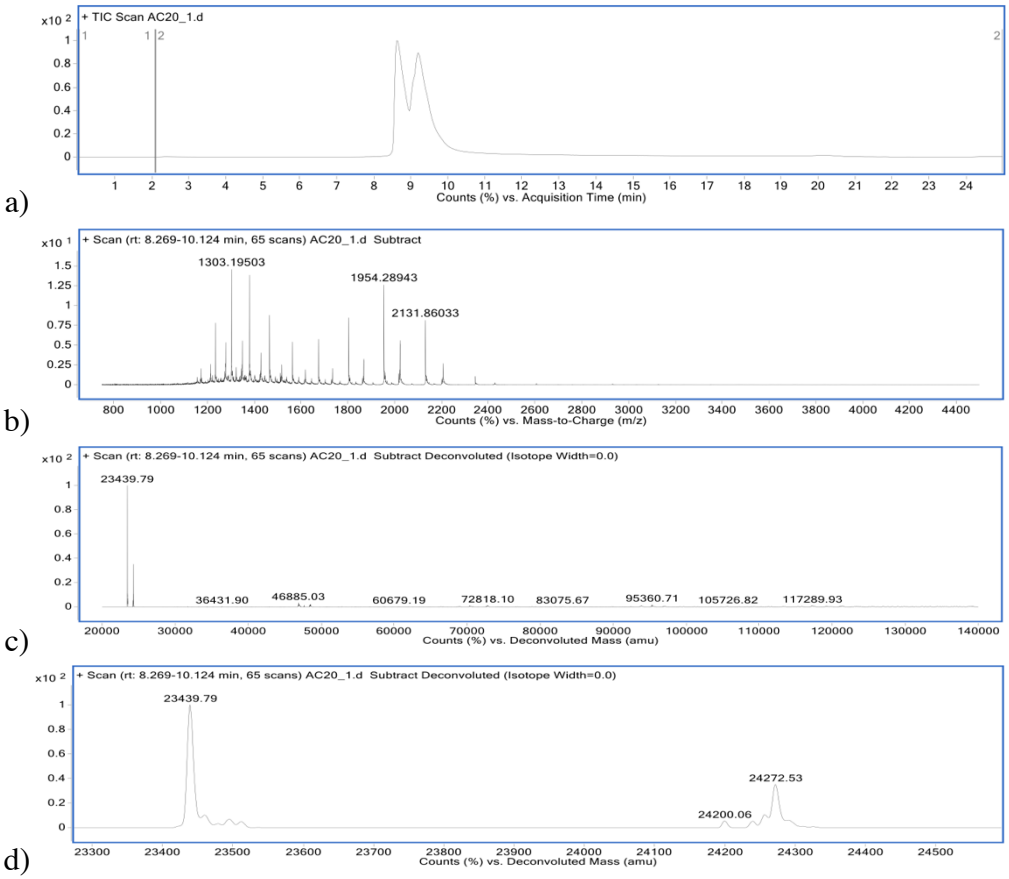

Figure 112. LCMS analysis of Fab conjugate **7** with hydrazine hydrate; a) TIC, b) non-deconvoluted ion-series, c) full range deconvoluted ion series mass spectrum, d) zoomed in deconvoluted ion series mass spectrum.

7.3.27 Reaction of Fab thioester conjugate with propargylamine

Fab (30 μL, 100 μM, 4.76 mg/mL) in conjugation buffer was reduced with tris(2-carboxyethyl)phosphine (TCEP) (2 μL, 15 mM in diH_2O, 10 eq.) The mixture was incubated at 37 °C for 1.5 h, 300 rpm. Following that, α-chlorothioester **1** (0.4 μL, 12 mM in DMF, 1.5 eq.)

was added and incubated at 22 °C for 30 min. After that, propargylamine (3.0 μL, 1.0 M in DMF, 1000 eq.) was added and left at 37 °C, for 2 h, 300 rpm. Lastly, sample was desalted (7 kDa MWCO, ZebaSpin) prior to LCMS analysis. Concentration was determined photometrically using $\varepsilon_{280} = 68590\ M^{-1}\ cm^{-1}$.

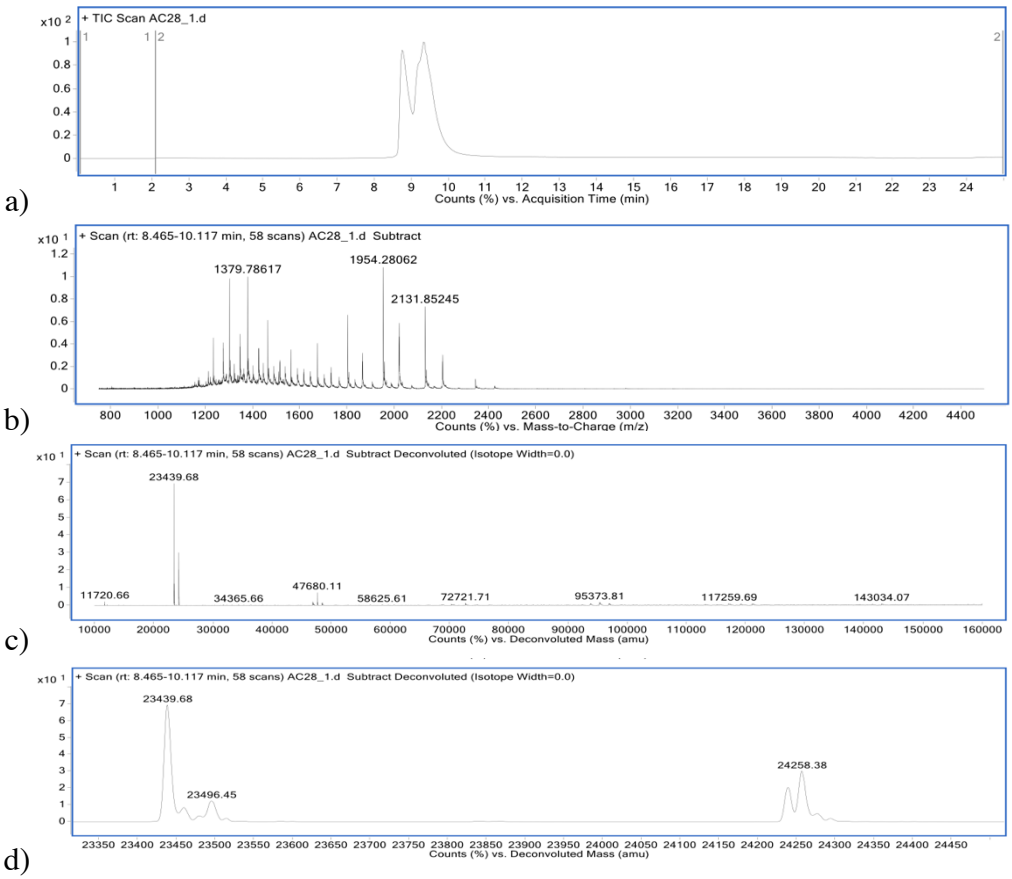

Figure 113. LCMS analysis of Fab conjugate **7** with propargylamine; a) TIC, b) non-deconvoluted ion-series, c) full range deconvoluted ion series mass spectrum, d) zoomed in deconvoluted ion series mass spectrum.

7.3.28 Reaction of Fab thioester conjugate with and hydroxylamine

Fab (30 μL, 100 μM, 4.76 mg/mL) in conjugation buffer was reduced with tris(2-carboxyethyl)phosphine (TCEP) (2 μL, 15 mM in diH_2O, 10 eq.) The mixture was incubated at 37 °C for 1.5 h, 300 rpm. Following that, α-chlorothioester **1** (0.4 μL, 12 mM in DMF, 1.5 eq.) was added and incubated at 22 °C for 30 min. After that, hydroxylamine (3.0 μL, 1.0 M in DMF, 1000 eq.) was added and left at 37 °C, for 2 h, 300 rpm. Lastly, sample was desalted (7 kDa MWCO, ZebaSpin) prior to LCMS analysis. Concentration was determined photometrically using $\varepsilon_{280} = 68590\ M^{-1}\ cm^{-1}$.

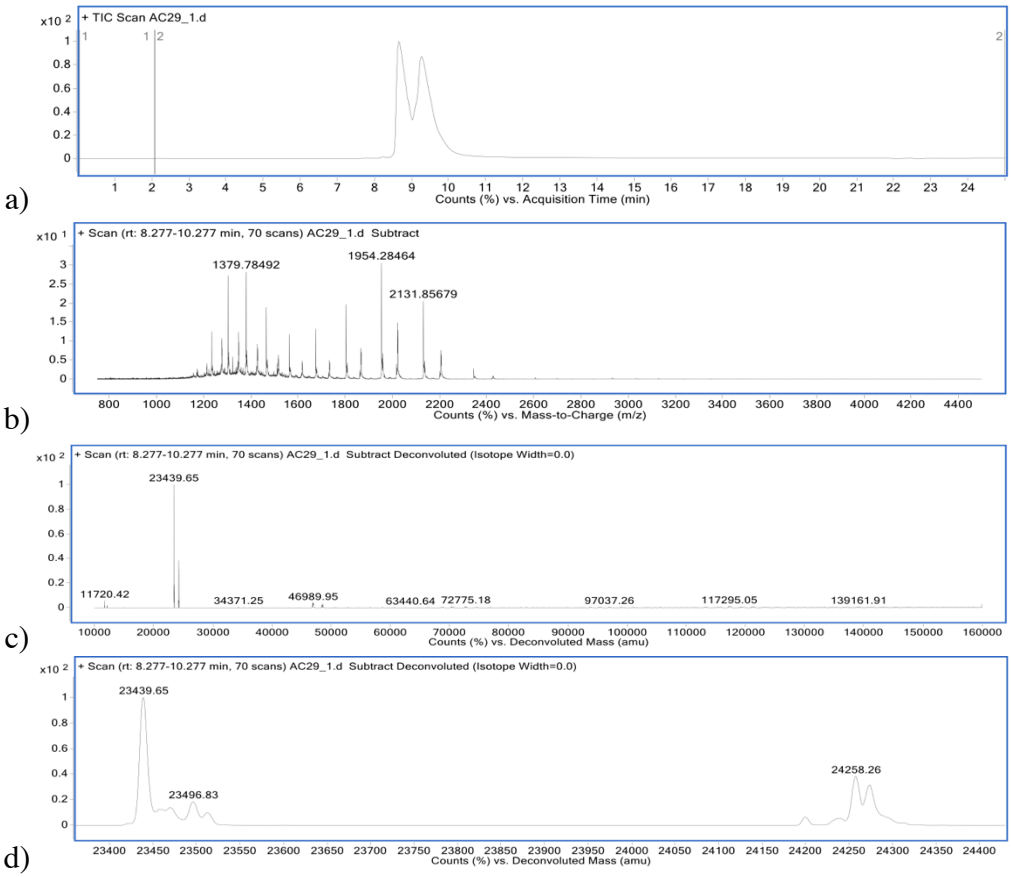

Figure 114. LCMS analysis of Fab conjugate **7** with hydroxylamine; a) TIC, b) non-deconvoluted ion-series, c) full range deconvoluted ion series mass spectrum, d) zoomed in deconvoluted ion series mass spectrum.

7.3.29 Dual conjugation reaction of Fab thioester conjugate with MPAA disulfide and hydrazine

Fab (30 μL, 100 μM, 4.76 mg/mL) in conjugation buffer was reduced with tris(2-carboxyethyl)phosphine (TCEP) (2 μL, 15 mM in diH_2O, 10 eq.). The mixture was incubated at 37 °C for 1.5 h, 300 rpm. Following that, α-chlorothioester **1** (0.2 μL, 24 mM in DMF, 1.5 eq.) was added and incubated at 22 °C for 30 min. Excess of the reagents was removed *via* ultrafiltration (10 kDa MWCO) into conjugation buffer, new Fab concentration was determined. Followed addition of hydrazine hydrate (3.0 μL, 1.0 M in DMF, 1000 eq.) at 22 °C, 1 h, 300 rpm, then MPAA disulfide (1.55 μL, 141 mM, 100 eq.) was added and left at 37 °C for 30 min. Lastly, sample was desalted into HPLC grade water (7 kDa MWCO, ZebaSpin) prior to LCMS analysis. Concentration was determined photometrically using $\varepsilon_{280} = 68590\ M^{-1}\ cm^{-1}$.

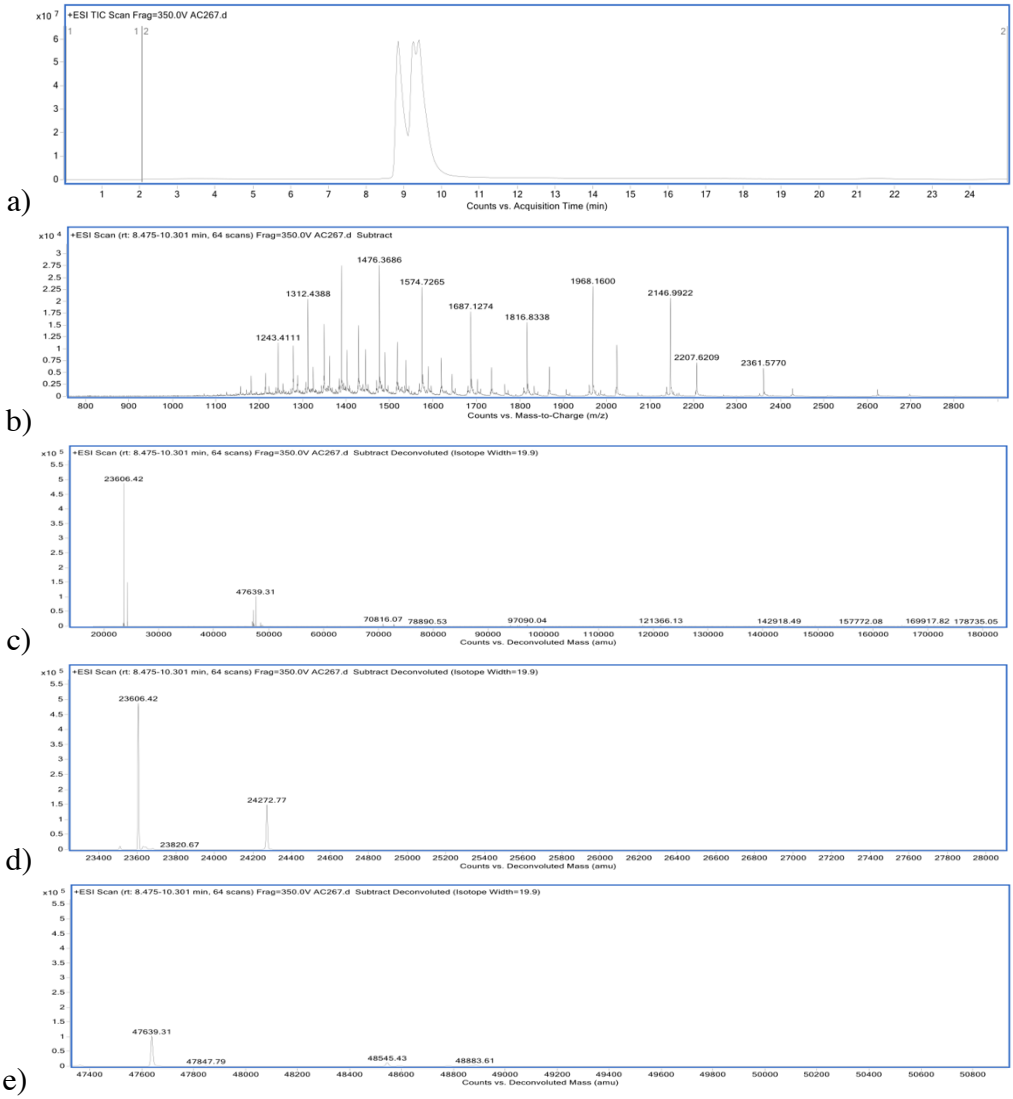

Figure 115. LCMS analysis Fab conjugate **7** with hydrazine hydrate and MPAA disulfide; a) TIC, b) non-deconvoluted ion-series, c) full range deconvoluted ion series mass spectrum, d) zoomed in deconvoluted ion series mass spectrum.

7.3.30 Dual conjugation reaction of Fab thioester conjugate with hydrazine and pyridyldisulfide (47)

Fab (30 μL, 100 μM, 4.76 mg/mL) in conjugation buffer was reduced with tris(2-carboxyethyl)phosphine (TCEP) (2 μL, 15 mM in diH_2O, 10 eq.). The mixture was incubated at 37 °C for 1.5 h, 300 rpm. Following that, α-chlorothioester **1** (0.2 μL, 24 mM in DMF, 1.5 eq.) was added and incubated at 22 °C for 30 min. Excess of the reagents was removed *via* ultrafiltration (10 kDa MWCO) into conjugation buffer, new Fab concentration was determined. Followed by addition of hydrazine hydrate (2.0 μL, 1.0 M in DMF, 1000 eq.) at 22 °C, 1 h, 300 rpm and pyridyldisulfide **47** (2.4 μL, 81 mM in DMF, 100 eq.) at 22 °C, 30 min, 300 rpm. Lastly,

sample was desalted into HPLC grade water (7 kDa MWCO, ZebaSpin) prior to LCMS analysis. Concentration was determined photometrically using $\varepsilon_{280} = 68590\ M^{-1}\ cm^{-1}$.

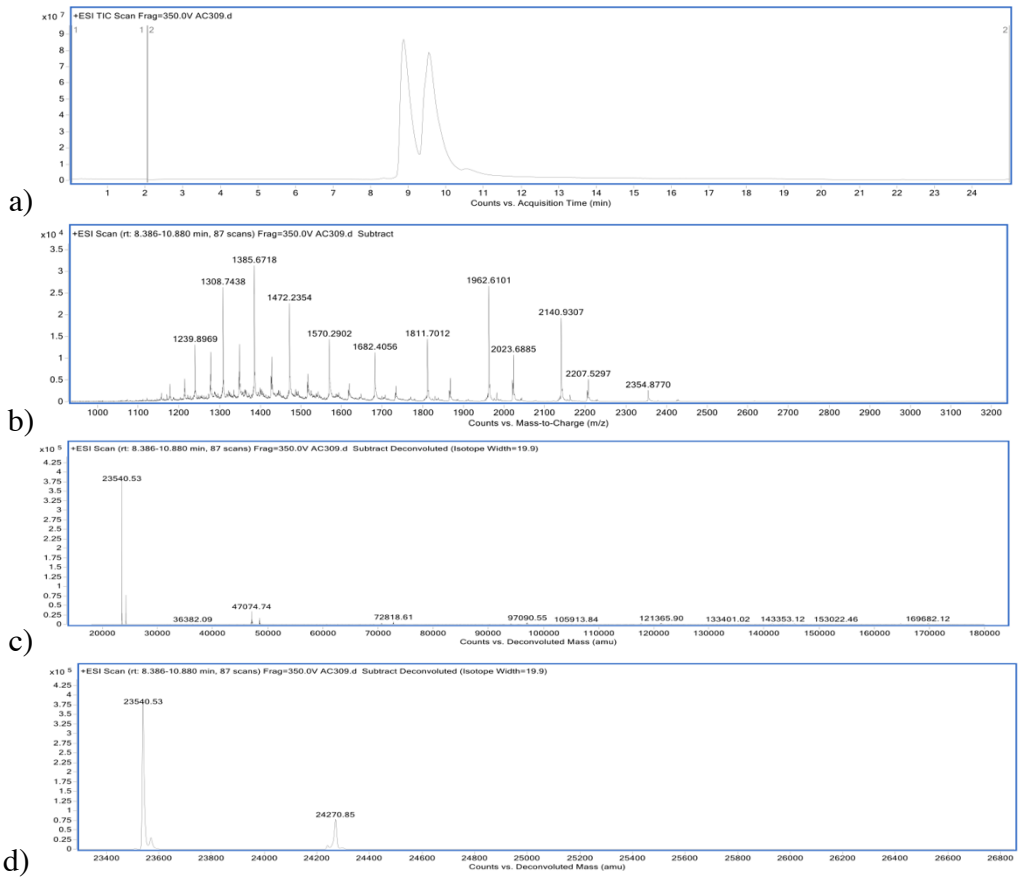

Figure 116. LCMS analysis Fab conjugate **7** reacted with hydrazine hydrate and pyridyldisulfide **47**; a) TIC, b) non-deconvoluted ion-series, c) full range deconvoluted ion series mass spectrum, d) zoomed in deconvoluted ion series mass spectrum.

7.3.31 Dual conjugation reaction of Fab thioester conjugate with hydrazine, pyridyldisulfide (47) and model aldehyde

Fab (30 μL, 100 μM, 4.76 mg/mL) in conjugation buffer was reduced with tris(2-carboxyethyl)phosphine (TCEP) (2 μL, 15 mM in diH_2O, 10 eq.). The mixture was incubated at 37 °C for 1.5 h, 300 rpm. Following that, α-chlorothioester **1** (0.2 μL, 24 mM in DMF, 1.5 eq.) was added and incubated at 22 °C for 30 min. Excess of the reagents was removed *via* ultrafiltration (10 kDa MWCO) into conjugation buffer, new Fab concentration was determined. Followed by addition of hydrazine hydrate (1.6 μL, 1.3 M in DMF, 1000 eq.) at 22 °C, 1 h, 300 rpm and pyridyldisulfide **47** (2.5 μL, 81 mM in DMF, 100 eq.) at 22 °C, 30 min, 300 rpm. This was followed by ultrafiltration into conjugation buffer. Subsequently, aniline (0.2 μL, 370 mM in DMF, 50 eq.) was added and benzaldehyde (0.6 μL, 133 mM in DMF, 50 eq.), this was left at

37 °C, for 16 h, 300 rpm. Lastly, sample was desalted into HPLC grade water (7 kDa MWCO, ZebaSpin) prior to LCMS analysis. Concentration was determined photometrically using ε_{280} = 68590 M^{-1} cm^{-1}.

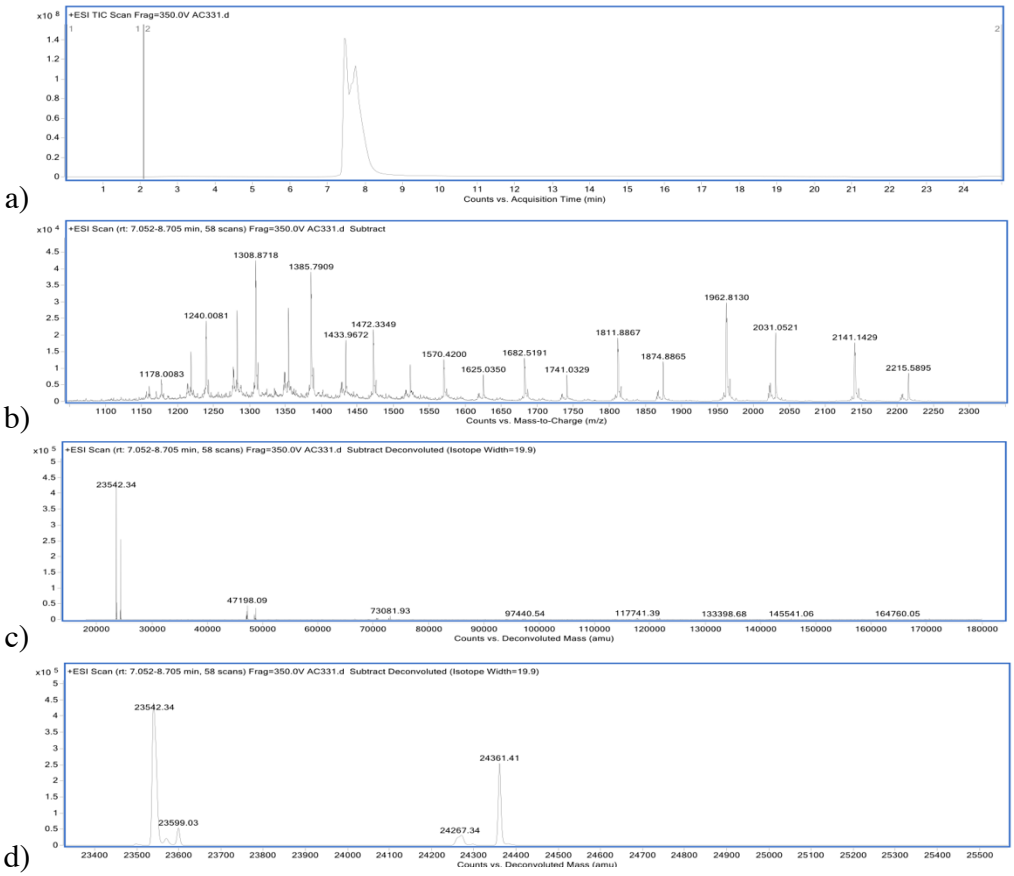

Figure 117. LCMS analysis of Fab conjugate **7** reacted with hydrazine, pyridyldisulfide **47**, and benzaldehyde; a) TIC, b) non-deconvoluted ion-series, c) full range deconvoluted ion series mass spectrum, d) zoomed in deconvoluted ion series mass spectrum.

7.3.32 Dual conjugation reaction of Fab thioester conjugate with hydrazine, pyridyldisulfide (47) and biotin-PEG-aldehyde (53)

Fab (30 μL, 100 μM, 4.76 mg/mL) in conjugation buffer was reduced with tris(2-carboxyethyl)phosphine (TCEP) (2 μL, 15 mM in diH_2O, 10 eq.). The mixture was incubated at 37 °C for 1.5 h, 300 rpm. Following that, α-chlorothioester **1** (0.2 μL, 24 mM in DMF, 1.5 eq.) was added and incubated at 22 °C for 30 min. Excess of the reagents was removed *via* ultrafiltration (10 kDa MWCO) into conjugation buffer, new Fab concentration was determined. Followed by addition of hydrazine hydrate (0.8 μL, 2.7 M in DMF, 1000 eq.) at 22 °C, 1 h, 300 rpm and pyridyldisulfide **47** (2.7 μL, 81 mM in DMF, 100 eq.) at 22 °C, 30 min, 300 rpm. This was followed by ultrafiltration into conjugation buffer. Subsequently, aniline (0.5 μL, 370 mM

in DMF, 100 eq.) was added and biotin-aldehyde **53** (6.2 μL, 48 mM in DMF, 150 eq.), this was left at 37 °C, for 16 h, 300 rpm. Lastly, sample was desalted into HPLC grade water (7 kDa MWCO, ZebaSpin) prior to LCMS analysis. Concentration was determined photometrically using $\varepsilon_{280} = 68590\ M^{-1}\ cm^{-1}$.

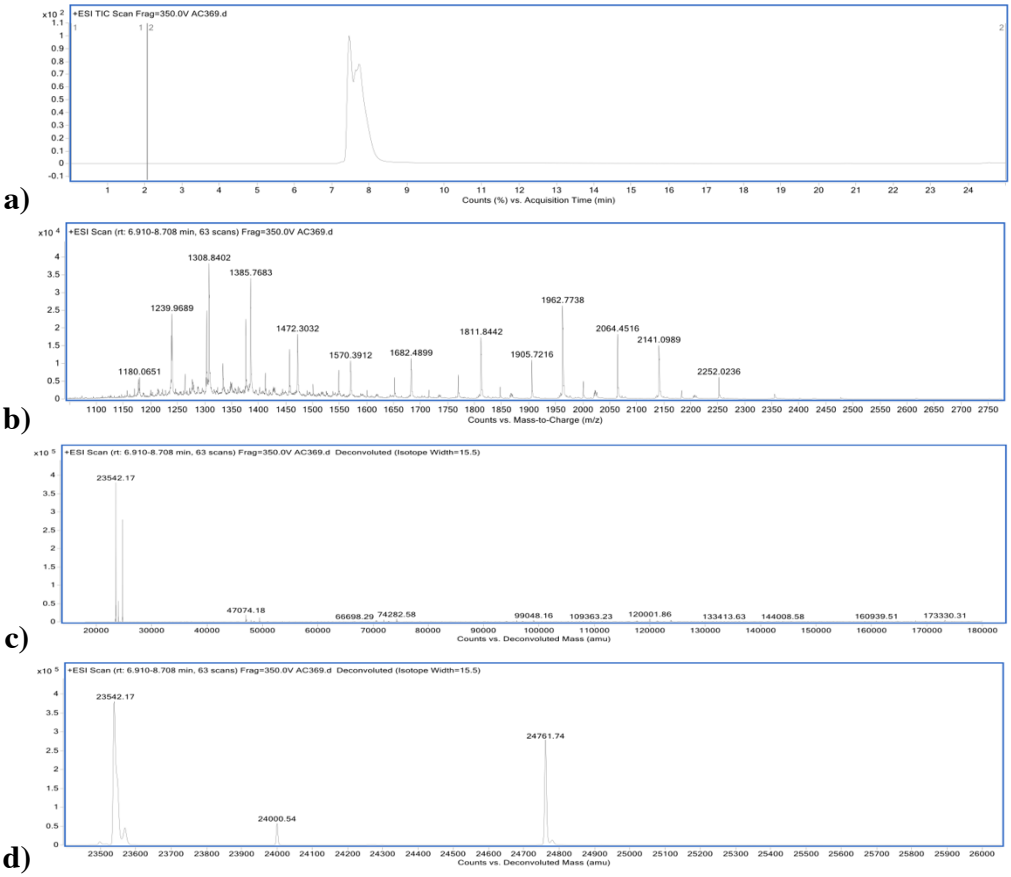

Figure 118. LCMS analysis of Fab conjugate **7** reacted with hydrazine, pyridyldisulfide **47**, and biotin-PEG-aldehyde **53**; a) TIC, b) non-deconvoluted ion-series, c) full range deconvoluted ion series mass spectrum, d) zoomed in deconvoluted ion series mass spectrum.

7.3.33 Dual conjugation reaction of Fab thioester conjugate with hydrazine, pyridyldisulfide (47) and biotin-PEG-aldehyde (58)

Fab (30 μL, 100 μM, 4.76 mg/mL) in conjugation buffer was reduced with tris(2-carboxyethyl)phosphine (TCEP) (2 μL, 15 mM in diH_2O, 10 eq.). The mixture was incubated at 37 °C for 1.5 h, 300 rpm. Following that, α-chlorothioester **1** (0.2 μL, 24 mM in DMF, 1.5 eq.) was added and incubated at 22 °C for 30 min. Excess of the reagents was removed *via* ultrafiltration (10 kDa MWCO) into conjugation buffer, new Fab concentration was determined. Followed by addition of hydrazine hydrate (1.1 μL, 2.1 M in DMF, 1000 eq.) at 22 °C, 1 h, 300 rpm and pyridyldisulfide **47** (0.3 μL, 81 mM in DMF, 10 eq.) at 22 °C, 30 min, 300 rpm. This

was followed by ultrafiltration into conjugation buffer. Subsequently, aniline (0.5 μL, 370 mM in DMF, 100 eq.) was added and biotin-aldehyde **58** (1.4 μL, 208 mM in DMF, 150 eq.), this was left at 37 °C, for 16 h, 300 rpm. Lastly, sample was desalted into HPLC grade water (7 kDa MWCO, ZebaSpin) prior to LCMS analysis. Concentration was determined photometrically using $\varepsilon_{280} = 68590\ M^{-1}\ cm^{-1}$.

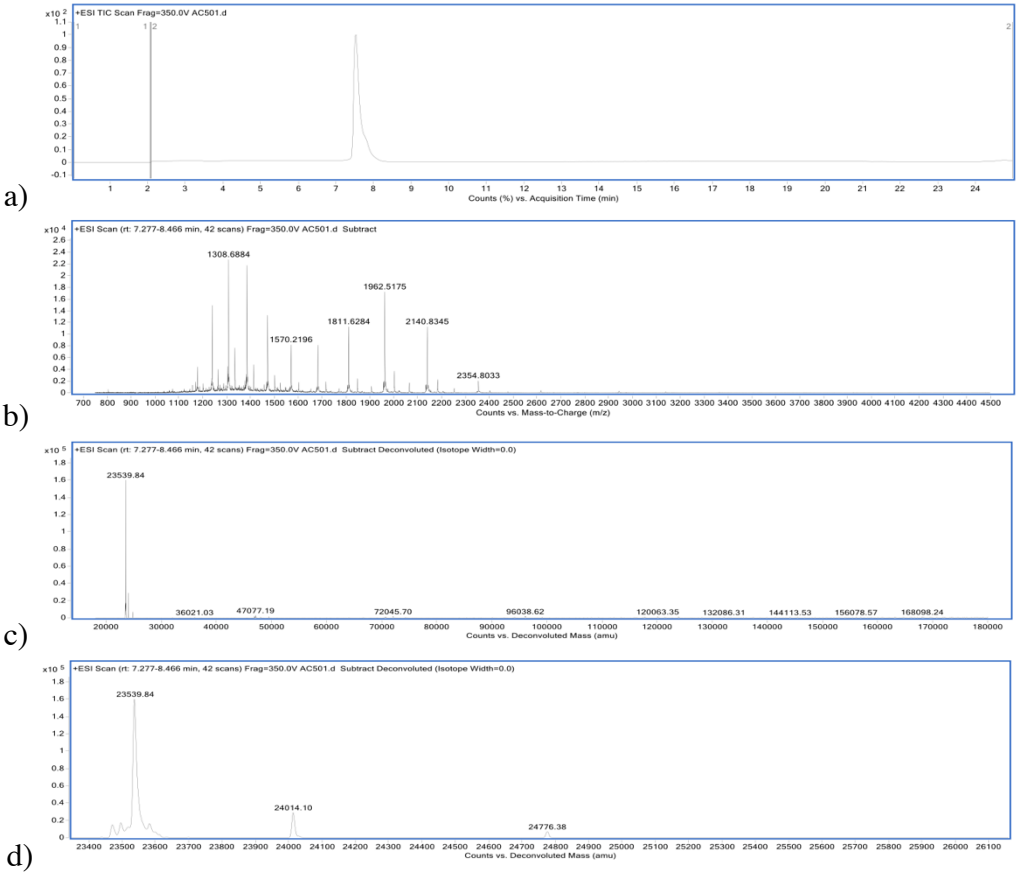

Figure 119. LCMS analysis Fab conjugate **7** reacted with hydrazine, pyridyldisulfide **47**, and biotin-PEG-aldehyde **58**; a) TIC, b) non-deconvoluted ion-series, c) full range deconvoluted ion series mass spectrum, d) zoomed in deconvoluted ion series mass spectrum.

7.3.34 Dual conjugation reaction of Fab thioester conjugate with hydrazine and pre-click

To a solution of the pyridyldisulfide alkyne **47** (0.31 μL, 81 mM in DMF, 1 eq.), THPTA (2.5 μL, 100 mM in diH_2O, 10 eq.), $CuSO_4$ (2.5 μL, 20 mM in diH_2O, 2 eq.), Azide fluor 488 (5 μL, 10 mM in DMF, 2 eq.), and sodium ascorbate (1.2 μL, 100 mM in diH_2O, final conc. 10 mM) was added and stirred at 37 °C for 4 h, 300 rpm. In meantime, Fab (30 μL, 100 μM, 4.76 mg/mL) in conjugation buffer was reduced with tris(2-carboxyethyl)phosphine (TCEP) (2 μL, 15 mM in

diH_2O, 10 eq.). The mixture was incubated at 37 °C for 1.5 h, 300 rpm. Following that, α-chlorothioester **1** (0.2 μL, 24 mM in DMF, 1.5 eq.) was added and incubated at 22 °C for 30 min. Followed by addition of hydrazine hydrate (1.1 μL, 2.2 M in DMF, 1000 eq.) at 22 °C, 1 h, 300 rpm and ultrafiltration into conjugation buffer. After this, a pre-conjugated fluorophore alkyne **61** was added to the Fab conjugate and this was further mixed at 22 °C for 4 h, 300 rpm. The excess reagent was then removed using a desalting column (PD Minitrap G-25, GE Healthcare) followed by ultrafiltration (10 kDa MWCO) into conjugate buffer to concentrate the sample. Lastly, sample was desalted into HPLC grade water (7 kDa MWCO, ZebaSpin) prior to LCMS analysis. Concentration was determined photometrically using $\varepsilon_{280} = 68590\ M^{-1}\ cm^{-1}$.

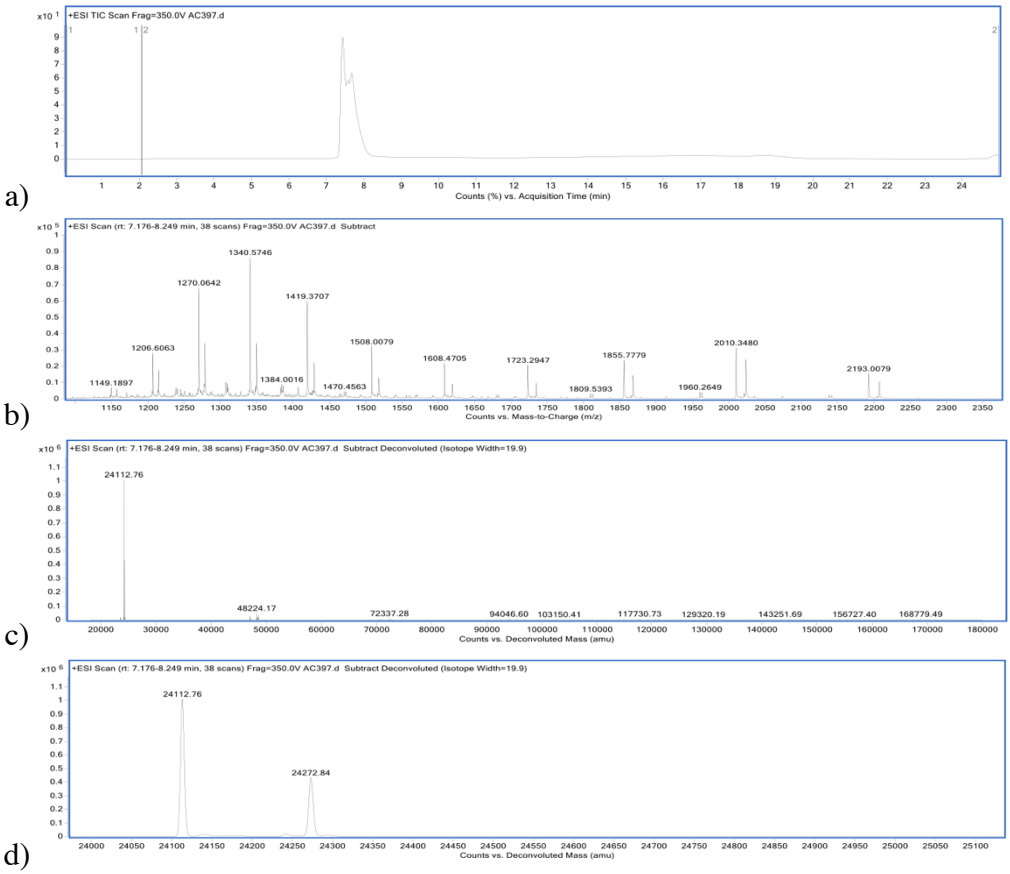

Figure 120. LCMS analysis of Fab conjugate **7** reacted with hydrazine, pre-click with pyridyl disulfide and Azide Fluor 488 **61**; a) TIC, b) non-deconvoluted ion-series, c) full range deconvoluted ion series mass spectrum, d) zoomed in deconvoluted ion series mass spectrum.

7.3.35 Dual conjugation reaction of Fab thioester conjugate with hydrazine, pre-click, and biotin-PEG-aldehyde (53)

To a solution of the pyridyldisulfide alkyne **47** (0.31 μL, 81 mM in DMF, 1 eq.), THPTA (2.5 μL, 100 mM in diH_2O, 10 eq.), $CuSO_4$ (2.5 μL, 20 mM in diH_2O, 2 eq.), Azide fluor 488 (5 μL,

10 mM in DMF, 2 eq.), and sodium ascorbate (1.2 μL, 100 mM in diH_2O, final conc. 10 mM) was added and stirred at 37 °C for 4 h, 300 rpm. In meantime, Fab (30 μL, 100 μM, 4.76 mg/mL) in conjugation buffer was reduced with tris(2-carboxyethyl)phosphine (TCEP) (2 μL, 15 mM in diH_2O, 10 eq.). The mixture was incubated at 37 °C for 1.5 h, 300 rpm. Following that, α-chlorothioester **1** (0.2 μL, 24 mM in DMF, 1.5 eq.) was added and incubated at 22 °C for 30 min. Followed by addition of hydrazine hydrate (1.0 μL, 2.5 M in DMF, 1000 eq.) at 22 °C, 1 h, 300 rpm and ultrafiltration into conjugation buffer, new Fab concentration was determined. After this, a pre-conjugated fluorophore alkyne **61** was added to the Fab conjugate and this was further mixed at 22 °C for 4 h, 300 rpm. The excess reagent was then removed using a desalting column (PD Minitrap G-25, GE Healthcare) followed by ultrafiltration (10 kDa MWCO) into conjugate buffer to concentrate the sample. Subsequently, aniline (0.4 μL, 370 mM in DMF, 100 eq.) was added and biotin-aldehyde **53** (4.9 μL, 48 mM in DMF, 150 eq.), this was left at 37 °C, for 16 h, 300 rpm. Lastly, sample was desalted into HPLC grade water (7 kDa MWCO, ZebaSpin) prior to LCMS analysis. Concentration was determined photometrically using $\varepsilon_{280} = 68590\ M^{-1}\ cm^{-1}$.

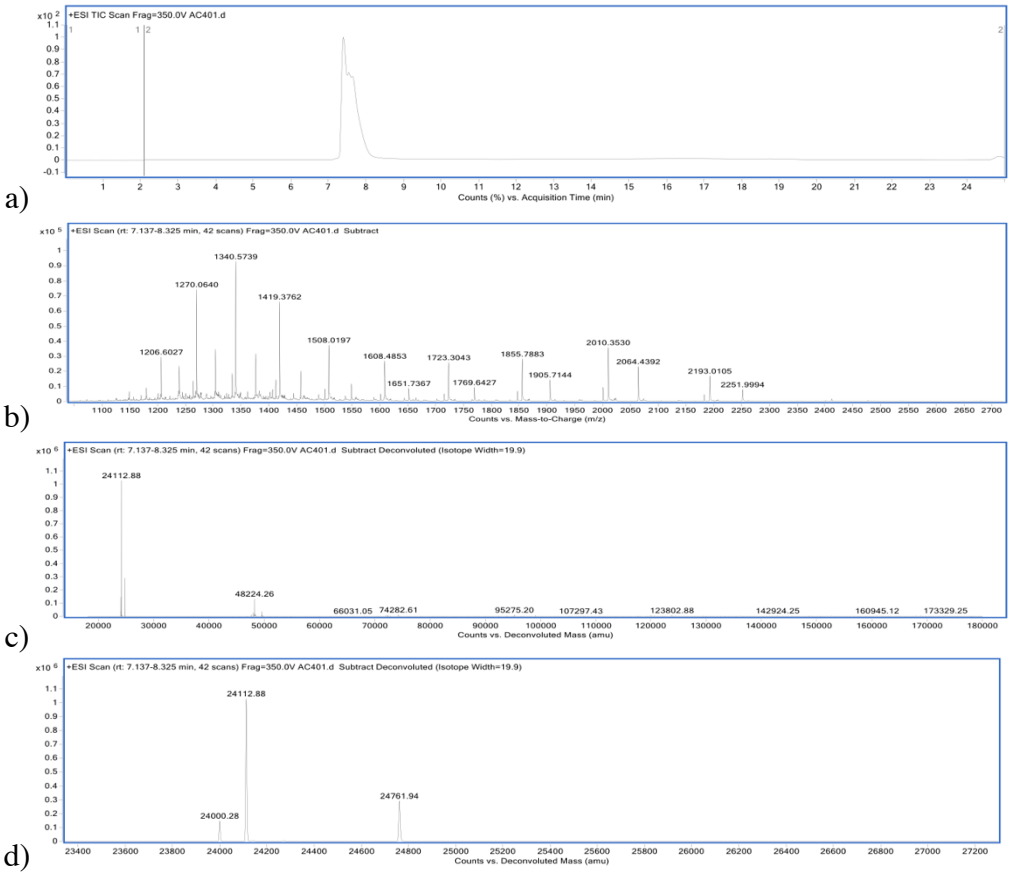

Figure 121. LCMS analysis Fab conjugate **7** reacted with hydrazine, pre-click with pyridyl disulfide and Azide fluor 488 **61**, and biotin-PEG-aldehyde **53**; a) TIC, b) non-deconvoluted

ion-series, c) full range deconvoluted ion series mass spectrum, d) zoomed in deconvoluted ion series mass spectrum.

7.3.36 Dual conjugation reaction of Fab thioester conjugate with hydrazine, pre-click, and biotin-PEG-aldehyde (58)

To a solution of the pyridyldisulfide alkyne **47** (0.31 μL, 81 mM in DMF, 1 eq.), THPTA (2.5 μL, 100 mM in diH_2O, 10 eq.), $CuSO_4$ (2.5 μL, 20 mM in diH_2O, 2 eq.), Azide fluor 488 (5 μL, 10 mM in DMF, 2 eq.), and sodium ascorbate (1.2 μL, 100 mM in diH_2O, final conc. 10 mM) was added and stirred at 37 °C for 4 h, 300 rpm. In meantime, Fab (30 μL, 100 μM, 4.76 mg/mL) in conjugation buffer was reduced with tris(2-carboxyethyl)phosphine (TCEP) (2 μL, 15 mM in diH_2O, 10 eq.). The mixture was incubated at 37 °C for 1.5 h, 300 rpm. Following that, α-chlorothioester **1** (0.2 μL, 24 mM in DMF, 1.5 eq.) was added and incubated at 22 °C for 30 min. Followed addition of hydrazine hydrate (1.3 μL, 2.2 M in DMF, 1000 eq.) at 22 °C, 1 h, 300 rpm and ultrafiltration into conjugation buffer, new Fab concentration was determined. After this, a pre-conjugated fluorophore alkyne **61** was added to the Fab conjugate and this was further mixed at 22 °C for 4 h, 300 rpm. The excess reagent was then removed using a desalting column (PD Minitrap G-25, GE Healthcare) followed by ultrafiltration (10 kDa MWCO) into conjugate buffer to concentrate the sample. Subsequently, aniline (0.7 μL, 370 mM in DMF, 100 eq.) was added and cleavable biotin-aldehyde **58** (1.8 μL, 208 mM in DMF, 150 eq.), this was left at 37 °C, for 16 h, 300 rpm. Lastly, sample was desalted into HPLC grade water (7 kDa MWCO, ZebaSpin) prior to LCMS analysis. Concentration was determined photometrically using ε_{280} = 68590 M^{-1} cm^{-1}.

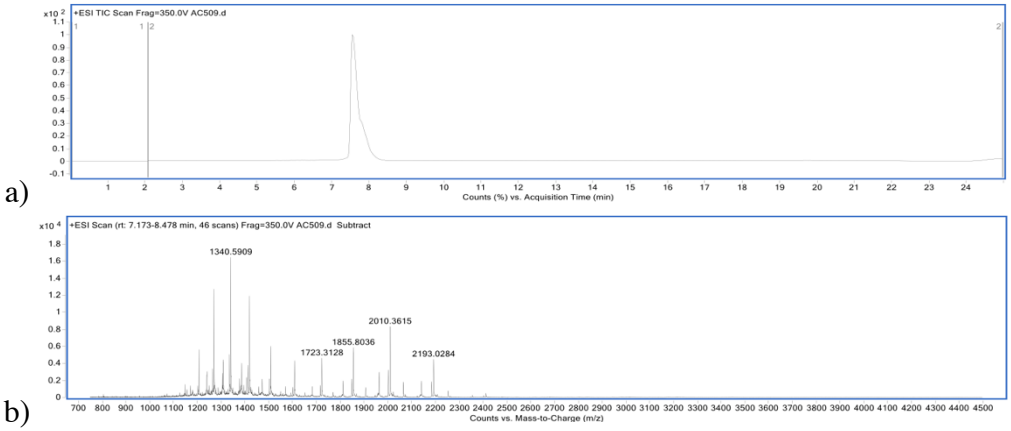

c)

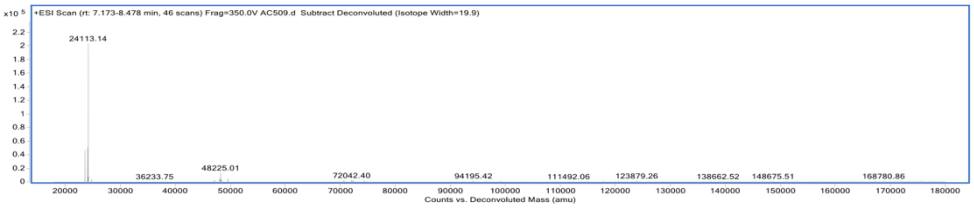

d)

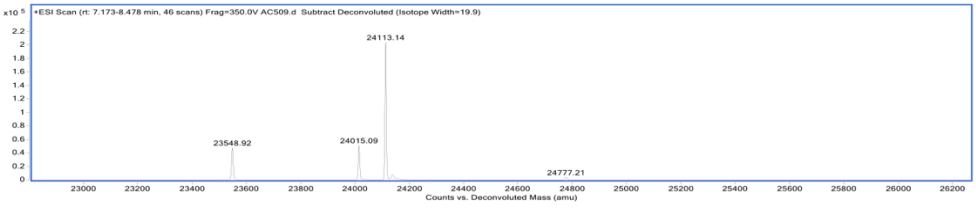

Figure 122. LCMS analysis of Fab conjugate **7** reacted with hydrazine, pre-click with pyridyl disulfide and Azide fluor 488 **61**, and biotin-PEG-aldehyde **58**; a) TIC, b) non-deconvoluted ion-series, c) full range deconvoluted ion series mass spectrum, d) zoomed in deconvoluted ion series mass spectrum.

7.3.37 Dual conjugation cleavage of the disulfide bond – early endosomal mimicking conditions

To a solution of the pyridyldisulfide alkyne **47** (0.31 μL, 81 mM in DMF, 1 eq.), THPTA (2.5 μL, 100 mM in diH_2O, 10 eq.), $CuSO_4$ (2.5 μL, 20 mM in diH_2O, 2 eq.), Azide fluor 488 (5 μL, 10 mM in DMF, 2 eq.), and sodium ascorbate (1.2 μL, 100 mM in diH_2O, final conc. 10 mM) was added and stirred at 37 °C for 4 h, 300 rpm. In meantime, Fab (30 μL, 100 μM, 4.76 mg/mL) in conjugation buffer was reduced with tris(2-carboxyethyl)phosphine (TCEP) (2 μL, 15 mM in diH_2O, 10 eq.). The mixture was incubated at 37 °C for 1.5 h, 300 rpm. Following that, α-chlorothioester **1** (0.2 μL, 24 mM in DMF, 1.5 eq.) was added and incubated at 22 °C for 30 min. This was followed by addition of hydrazine hydrate (1.35 μL, 1.9 M in DMF, 1000 eq.) at 22 °C, 1 h, 300 rpm and ultrafiltration into conjugation buffer, new Fab concentration was determined. After this, a pre-conjugated fluorophore alkyne **61** was added to the Fab conjugate and this was further mixed at 22 °C for 4 h, 300 rpm. The excess reagent was then removed using a desalting column (PD Minitrap G-25, GE Healthcare) followed by ultrafiltration (10 kDa MWCO) into conjugate buffer to concentrate the sample. Subsequently, aniline (0.6 μL, 370 mM in DMF, 100 eq.) was added and biotin-aldehyde **53** (6.3 μL, 48 mM in DMF, 150 eq.), this was left at 37 °C, for 16 h, 300 rpm. The conjugate was then buffer swapped into phosphate buffer with 5 mM glutathione (GSH) pH 6.5 and it was left for up to 8 h. Lastly, sample was desalted into HPLC grade water (7 kDa MWCO, ZebaSpin) prior to LCMS analysis. Concentration was determined photometrically using $\varepsilon_{280} = 68590\ M^{-1}\ cm^{-1}$.

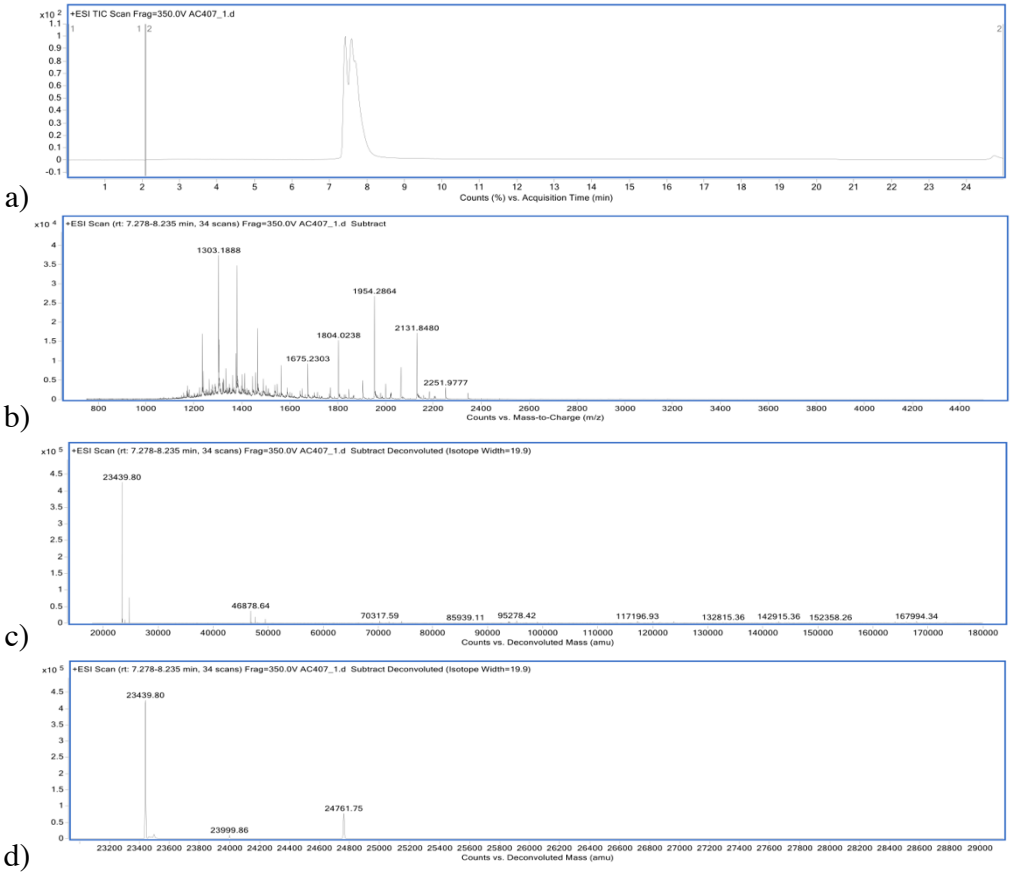

Figure 123. LCMS analysis of disulfide cleavage of conjugate **63** and **64** at 37 °C after 8 h, 5 mM GSH; a) TIC, b) non-deconvoluted ion-series, c) full range deconvoluted ion series mass spectrum, d) zoomed in deconvoluted ion series mass spectrum.

7.3.38 Dual conjugation cleavage of the disulfide bond – blood mimicking conditions

To a solution of the pyridyldisulfide alkyne **47** (0.31 μL, 81 mM in DMF, 1 eq.), THPTA (2.5 μL, 100 mM in diH_2O, 10 eq.), $CuSO_4$ (2.5 μL, 20 mM in diH_2O, 2 eq.), Azide fluor 488 (5 μL, 10 mM in DMF, 2 eq.), and sodium ascorbate (1.2 μL, 100 mM in diH_2O, final conc. 10 mM) was added and stirred at 37 °C for 4 h, 300 rpm. In meantime, Fab (30 μL, 100 μM, 4.76 mg/mL) in conjugation buffer was reduced with tris(2-carboxyethyl)phosphine (TCEP) (2 μL, 15 mM in diH_2O, 10 eq.). The mixture was incubated at 37 °C for 1.5 h, 300 rpm. Following that, α-chlorothioester **1** (0.2 μL, 24 mM in DMF, 1.5 eq.) was added and incubated at 22 °C for 30 min. This was followed by addition of hydrazine hydrate (1.3 μL, 2.4 M in DMF, 1000 eq.) at 22 °C, 1 h, 300 rpm and ultrafiltration into conjugation buffer, new Fab concentration was determined. After this, a pre-conjugated fluorophore alkyne **61** was added to the Fab conjugate and this was further mixed at 22 °C for 4 h, 300 rpm. The excess reagent was then removed using a desalting column (PD Minitrap G-25, GE Healthcare) followed by ultrafiltration (10 kDa MWCO) into

conjugate buffer to concentrate the sample. Subsequently, aniline (0.7 μL, 370 mM in DMF, 100 eq.) was added and biotin-aldehyde **53** (7.5 μL, 48 mM in DMF, 150 eq.), this was left at 37 °C, for 16 h, 300 rpm. The conjugate was then buffer swapped into 5 μM glutathione (GSH) pH 6.5 and it was left for up to 24 h. Lastly, sample was desalted into HPLC grade water (7 kDa MWCO, ZebaSpin) prior to LCMS analysis. Concentration was determined photometrically using ε_{280} = 68590 M^{-1} cm^{-1}.

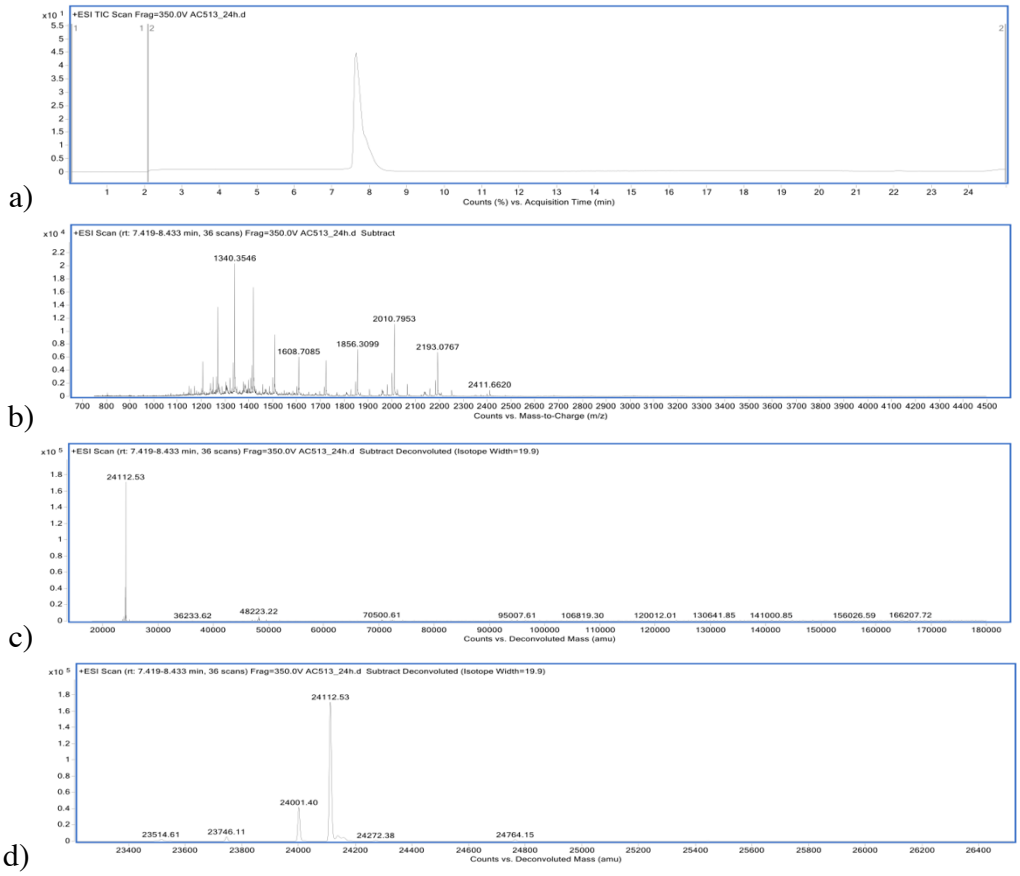

Figure 124. LCMS analysis of disulfide cleavage of conjugate **63** and **64** at 37 °C after 24 h, 5 μM GSH; a) TIC, b) non-deconvoluted ion-series, c) full range deconvoluted ion series mass spectrum, d) zoomed in deconvoluted ion series mass spectrum.

7.3.39 Dual conjugation reaction - hydrazone cleavage with biotin-PEG-aldehyde (53)

To a solution of the pyridyldisulfide alkyne **47** (0.31 μL, 81 mM in DMF, 1 eq.), THPTA (2.5 μL, 100 mM in diH_2O, 10 eq.), $CuSO_4$ (2.5 μL, 20 mM in diH_2O, 2 eq.), Azide fluor 488 (5 μL, 10 mM in DMF, 2 eq.), and sodium ascorbate (1.2 μL, 100 mM in diH_2O, final conc. 10 mM) was added and stirred at 37 °C for 4 h, 300 rpm. In meantime, Fab (30 μL, 100 μM, 4.76 mg/mL) in conjugation buffer was reduced with tris(2-carboxyethyl)phosphine (TCEP) (2 μL, 15 mM in

diH_2O, 10 eq.). The mixture was incubated at 37 °C for 1.5 h, 300 rpm. Following that, α-chlorothioester **1** (0.2 μL, 24 mM in DMF, 1.5 eq.) was added and incubated at 22 °C for 30 min. Followed by addition of hydrazine hydrate (1.4 μL, 1.9 M in DMF, 1000 eq.) at 22 °C, 1 h, 300 rpm and ultrafiltration into conjugation buffer, new Fab concentration was determined. After this, a pre-conjugated fluorophore alkyne **61** was added to the Fab conjugate and this was further mixed at 22 °C for 4 h, 300 rpm. The excess reagent was then removed using a desalting column (PD Minitrap G-25, GE Healthcare) followed by ultrafiltration (10 kDa MWCO) into conjugate buffer to concentrate the sample. Subsequently, aniline (0.5 μL, 370 mM in DMF, 100 eq.) was added and biotin-aldehyde **53** (6.3 μL, 48 mM in DMF, 150 eq.), this was left at 37 °C, for 16 h, 300 rpm. After this, sample was buffer swapped (3 x vivaspin) into sodium acetate pH 5.0 buffer and left for up to 72 h at 37 °C. Lastly, sample was desalted into HPLC grade water (7 kDa MWCO, ZebaSpin) prior to LCMS analysis. Concentration was determined photometrically using $\varepsilon_{280} = 68590\ M^{-1}\ cm^{-1}$.

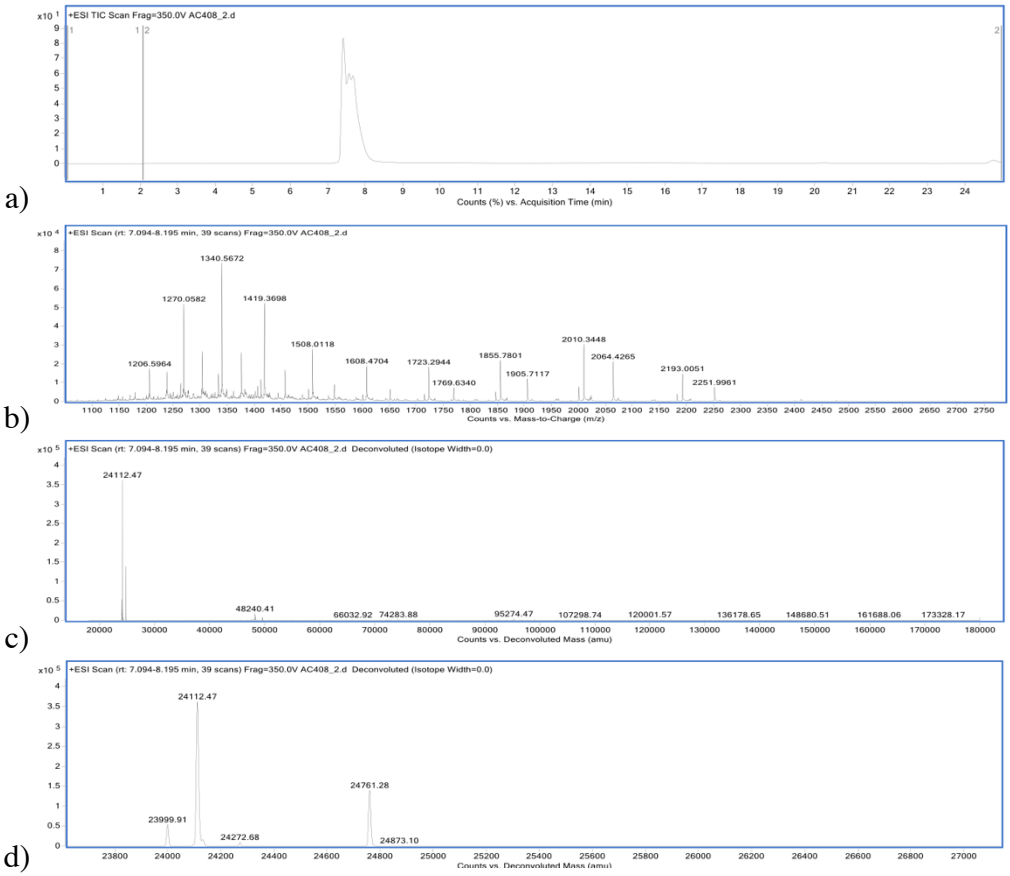

Figure 125. LCMS analysis of hydrazone cleavage of conjugate **63** and **64** at 37 °C after 24 h; a) TIC, b) non-deconvoluted ion-series, c) full range deconvoluted ion series mass spectrum, d) zoomed in deconvoluted ion series mass spectrum.

7.3.40 Dual conjugation reaction with - hydrazone cleavage of biotin-PEG-aldehyde (58)

To a solution of the pyridyldisulfide alkyne **47** (0.31 μL, 81 mM in DMF, 1 eq.), THPTA (2.5 μL, 100 mM in diH_2O, 10 eq.), $CuSO_4$ (2.5 μL, 20 mM in diH_2O, 2 eq.), Azide fluor 488 (5 μL, 10 mM in DMF, 2 eq.), and sodium ascorbate (1.2 μL, 100 mM in diH_2O, final conc. 10 mM) was added and stirred at 37 °C for 4 h, 300 rpm. In meantime, Fab (30 μL, 100 μM, 4.76 mg/mL) in conjugation buffer was reduced with tris(2-carboxyethyl)phosphine (TCEP) (2 μL, 15 mM in diH_2O, 10 eq.). The mixture was incubated at 37 °C for 1.5 h, 300 rpm. Following that, α-chlorothioester **1** (0.2 μL, 24 mM in DMF, 1.5 eq.) was added and incubated at 22 °C for 30 min. Followed addition of hydrazine hydrate (1.3 μL, 2.4 M in DMF, 1000 eq.) at 22 °C, 1 h, 300 rpm and ultrafiltration into conjugation buffer, new Fab concentration was determined. After this, a pre-conjugated fluorophore alkyne **61** was added to the Fab conjugate and this was further mixed at 22 °C for 4 h, 300 rpm. The excess reagent was then removed using a desalting column (PD Minitrap G-25, GE Healthcare) followed by ultrafiltration (10 kDa MWCO) into conjugate buffer to concentrate the sample. Subsequently, aniline (0.7 μL, 370 mM in DMF, 100 eq.) was added and biotin-aldehyde **58** (1.8 μL, 208 mM in DMF, 150 eq.), this was left at 37 °C, for 16 h, 300 rpm. After this, sample was buffer swapped (3 x vivaspin) into sodium acetate pH 5.0 buffer and left for 72 h at 37 °C. Lastly, sample was desalted into HPLC grade water (7 kDa MWCO, ZebaSpin) prior to LCMS analysis. Concentration was determined photometrically using ε_{280} = 68590 M^{-1} cm^{-1}.

a)

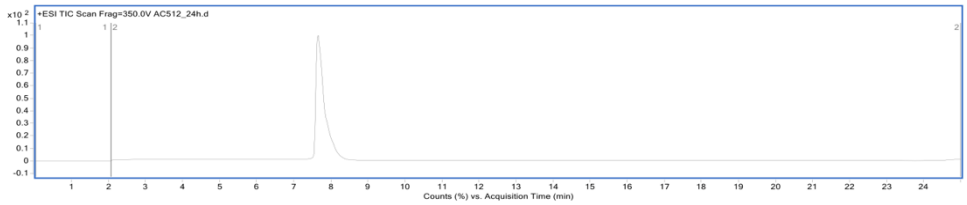

b)

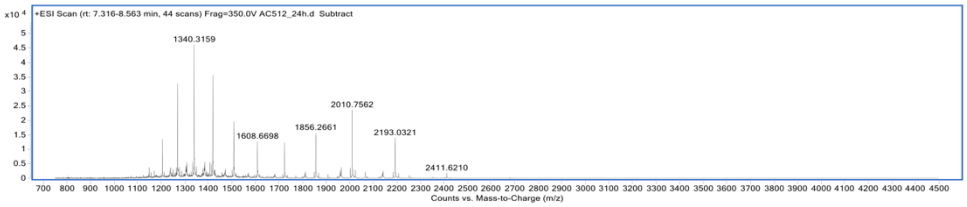

c)

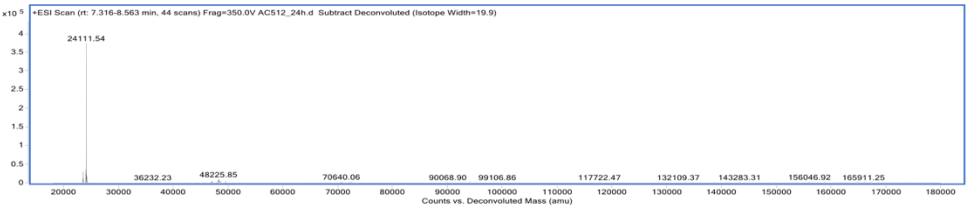

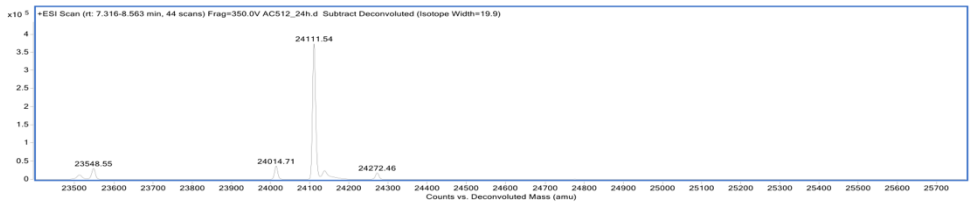

d)

Figure 126. LCMS analysis of hydrazone cleavage of conjugate **65** and **66** at 37 °C after 24 h; a) TIC, b) non-deconvoluted ion-series, c) full range deconvoluted ion series mass spectrum, d) zoomed in deconvoluted ion series mass spectrum.

7.3.41 Native full antibody

Trastuzumab full antibody (50 μL, 30 μM, 4.35 mg/mL) in conjugation buffer was buffer swapped into 50 mM ammonium acetate pH 7.0 (7 kDa MWCO, ZebaSpin) and adjusted to 6.5 μM following addition of 0.5 μL of PNGase F, the reaction was left at 37 °C for 16 h. Prior LCMS analysis the sample was adjusted to 2 μM with 50 mM ammonium acetate pH 7.0. Concentration was determined photometrically using $\varepsilon_{280} = 215380\ M^{-1}\ cm^{-1}$.

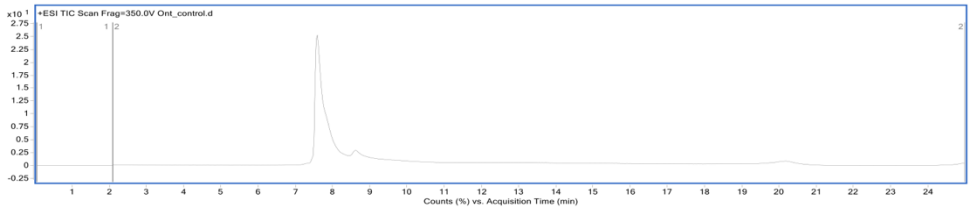

a)

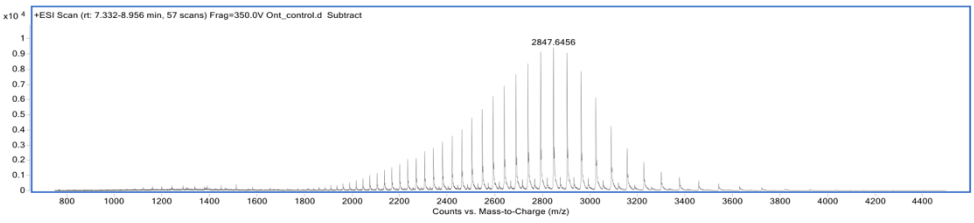

b)

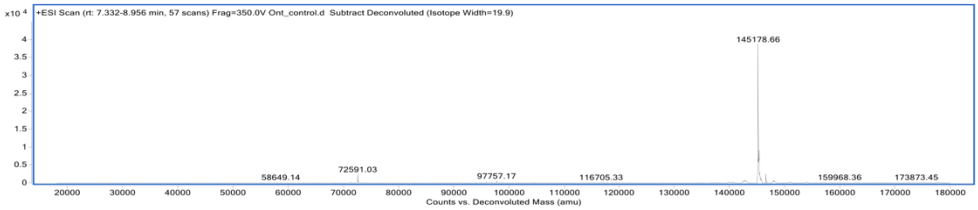

c)

Figure 127. LCMS analysis of native full antibody; a) TIC, b) non-deconvoluted ion-series, c) full range deconvoluted ion series mass spectrum, native full antibody observed 145178.

7.3.42 Reduced full antibody

Trastuzumab full antibody (50 μL, 30 μM, 4.35 mg/mL) in conjugation buffer was buffer swapped into 50 mM ammonium acetate pH 7.0 (7 kDa MWCO, ZebaSpin) and adjusted to 6.5 μM with 50 mM ammonium acetate pH 7.0, following addition of 0.5 μL of PNGase F, the reaction was left at 37 °C for 16 h. Then it was educed with tris(2-carboxyethyl)phosphine (TCEP) (0.6 μL, 15 mM in diH_2O, 6 eq.). Prior LCMS analysis the sample was adjusted to 2 μM with 50 mM ammonium acetate pH 7.0. Concentration was determined photometrically using ε_{280} = 215380 M^{-1} cm^{-1}.

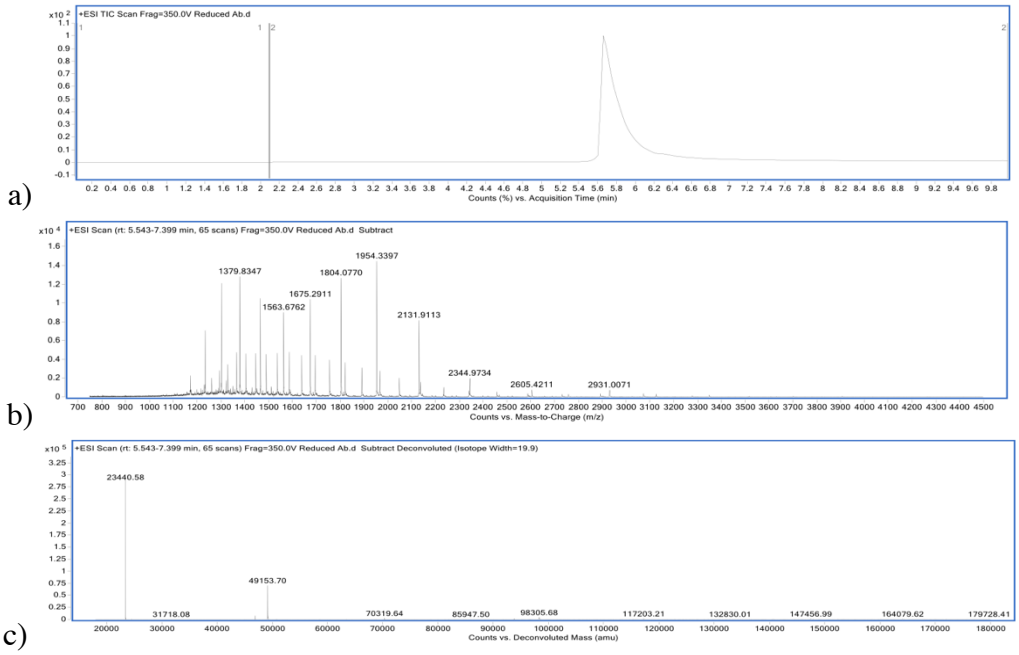

Figure 128. LCMS analysis of reduced full antibody; a) TIC, b) non-deconvoluted ion-series, c) full range deconvoluted ion series mass spectrum, light chain observed 23440, heavy chain observed 49153.

7.3.43 Control reaction of full antibody with α-chlorothioester (1)

To Trastuzumab full antibody (50 μL, 30 μM, 4.35 mg/mL) in conjugation buffer, α-chlorothioester **1** (0.5 μL, 12 mM in DMF, 4.05 eq.) was added and incubated at 22 °C for 1 h. Lastly, sample was buffer swapped into 50 mM ammonium acetate pH 7.0 (7 kDa MWCO, ZebaSpin) and adjusted to 6.5 μM following addition of 0.5 μL of PNGase F, the reaction was left at 37 °C for 16 h. Prior LCMS analysis the sample was adjusted to 2 μM with 50 mM ammonium acetate pH 7.0. Concentration was determined photometrically using ε_{280} = 215380 M^{-1} cm^{-1}.

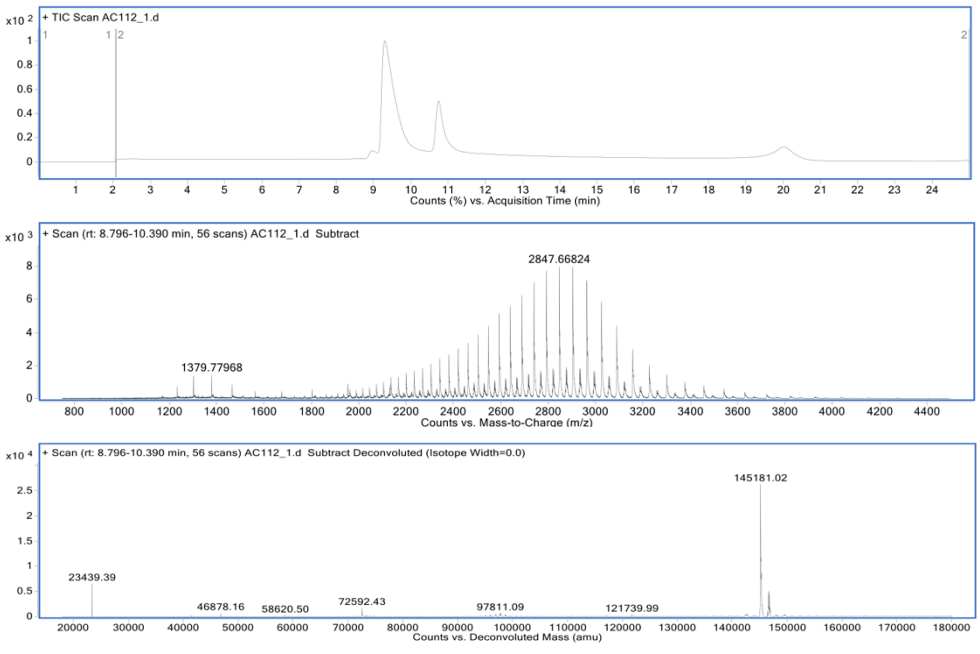

Figure 129. LCMS analysis of control reaction with α-chlorothioester **1** on full antibody; a) TIC, b) non-deconvoluted ion-series, c) full range deconvoluted ion series mass spectrum, native LC expected 23438, observed 23439, native HL expected 72585, observed 72592, native full antibody expected 145179, observed 145181.

7.3.44 Rebridging of full antibody with α-chlorothioester (1)

Trastuzumab full antibody (50 μL, 30 μM, 4.35 mg/mL) in conjugation buffer was reduced with tris(2-carboxyethyl)phosphine (TCEP) (0.6 μL, 15 mM in diH_2O, 6 eq.). Following that, α-chlorothioester **1** (0.5 μL, 12 mM in DMF, 4.05 eq.) was added and incubated at 22 °C for 1 h. Lastly, sample was buffer swapped into 50 mM ammonium acetate pH 7.0 (7 kDa MWCO, ZebaSpin) and adjusted to 6.5 μM, following addition of 0.5 μL of PNGase F, the reaction was left at 37 °C for 16 h. Prior LCMS analysis the sample was adjusted to 2 μM with 50 mM ammonium acetate pH 7.0. Concentration was determined photometrically using ε_{280} = 215380 M^{-1} cm^{-1}.

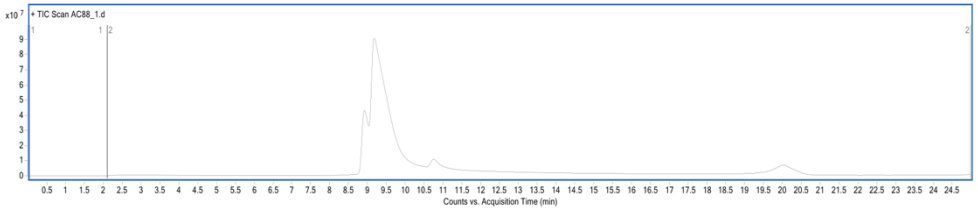

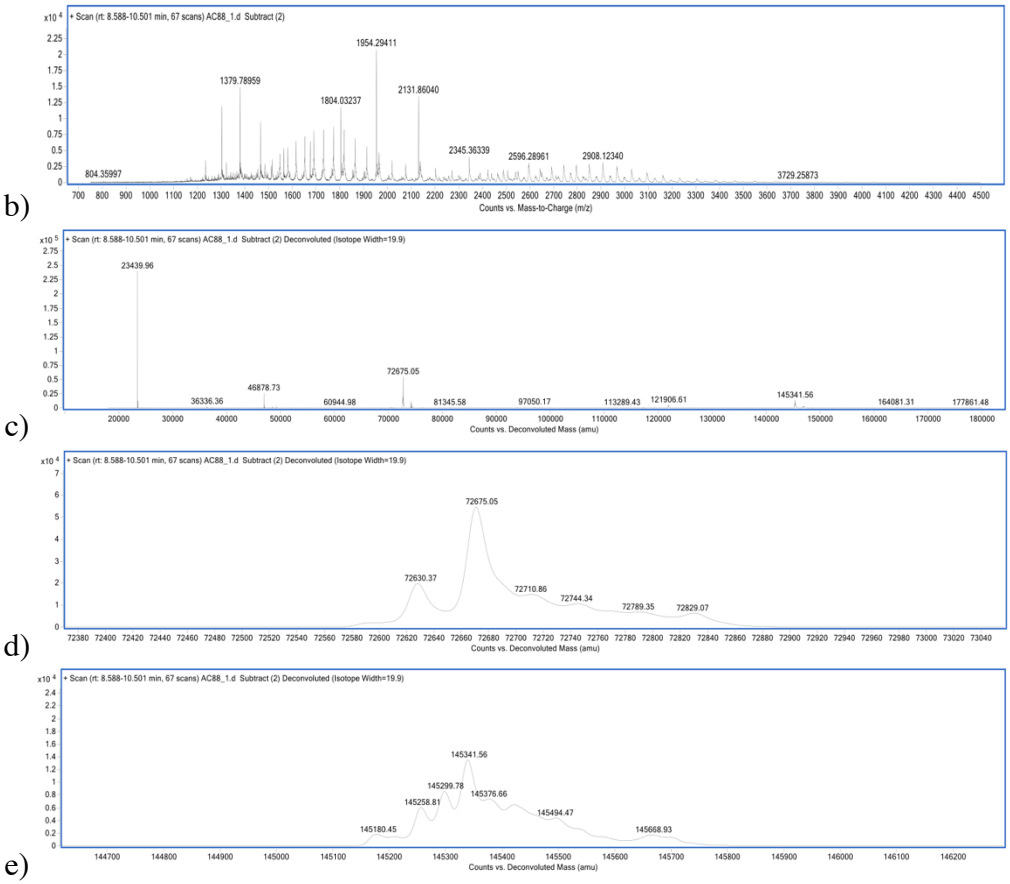

Figure 130. LCMS analysis of rebridging of full antibody with α-chlorothioester **1**; a) TIC, b) non-deconvoluted ion-series, c) full range deconvoluted ion series mass spectrum, d) zoomed deconvoluted ion series mass spectrum HL area, expected mass for formation of two **7** conjugates in the HL area 72669, observed 72675 e) zoomed in deconvoluted ion series mass spectrum, HHLL area, expected mass for formation of four **7** conjugates in the HHLL area 145347, observed 145341.

7.3.45 Rebridging of full antibody with α-chlorothioester (1) and cysteine

Trastuzumab full antibody (50 μL, 30 μM, 4.35 mg/mL) in conjugation buffer was reduced with tris(2-carboxyethyl)phosphine (TCEP) (0.6 μL, 15 mM in diH_2O, 6 eq.). The mixture was incubated at 37 °C for 2 h, 300 rpm. Upon completion of this step, excess of the reagents was removed *via* ultrafiltration (10 kDa MWCO) into conjugation buffer, new Fab concentration was determined. Following that, α-chlorothioester **1** (0.6 μL, 24 mM in DMF, 10 eq.) was added and incubated at 22 °C for 1 h. After that, L-cysteine (1.9 μL, 108 mM in diH_2O, 200 eq.) was added and left at 37 °C, for 16 h, 300 rpm. Lastly, sample was buffer swapped into 50 mM ammonium acetate pH 7.0 (7 kDa MWCO, ZebaSpin) and adjusted to 6.5 μM, following addition of 0.5 μL of PNGase F, the reaction was left at 37 °C for 16 h. Prior LCMS analysis the sample was adjusted

to 2 μM with 50 mM ammonium acetate pH 7.0. Concentration was determined photometrically using $\varepsilon_{280} = 215380\ M^{-1}\ cm^{-1}$.

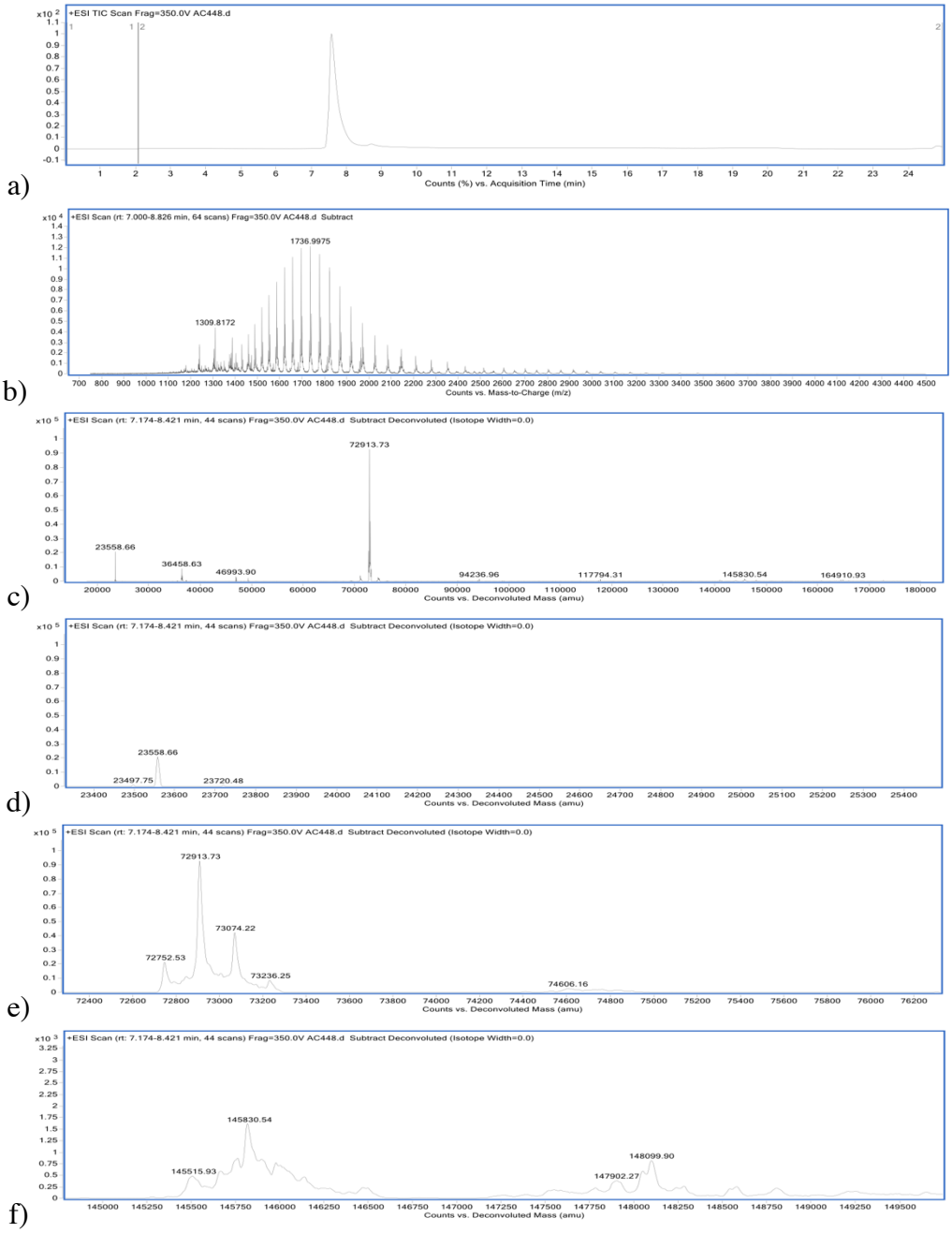

Figure 131. LCMS analysis of rebridging of full antibody with α-chlorothioester **1** and cysteine; a) TIC, b) non-deconvoluted ion-series, c) full range deconvoluted ion series mass spectrum, d) zoomed in deconvoluted ion series mass spectrum, LC area, e) zoomed in deconvoluted ion series mass spectrum, HL area, f) zoomed in deconvoluted ion series mass spectrum, HHLL area.

7.3.46 Reaction of thioester conjugate on full antibody with cysteine, PD and fluorophore

Trastuzumab full antibody (50 μL, 30 μM, 4.35 mg/mL) in conjugation buffer was reduced with tris(2-carboxyethyl)phosphine (TCEP) (0.6 μL, 15 mM in diH_2O, 6 eq.). The mixture was incubated at 37 °C for 2 h, 300 rpm. Following that, α-chlorothioester **1** (0.6 μL, 24 mM in DMF, 10 eq.) was added and incubated at 22 °C for 1 h. After that, L-cysteine (0.6 μL, 105 mM in diH_2O, 50 eq.) was added and left at 37 °C, for 16 h, 300 rpm. Upon completion of this step, excess of the reagents was removed *via* ultrafiltration (10 kDa MWCO) into conjugation buffer, new antibody concentration was determined. TCEP reduction was performed again as before followed by removal of the excess of the reagent. Subsequently, BCN-PD (0.2 μL, 20 mM in DMSO, 10 eq.) was added and left at 37 °C for 2 h, 300 rpm. This was followed by another ultrafiltration to remove excess of the reagent. Finally, Azide fluor 488 (0.5 μL, 10 mM in DMF, 10 eq.) was added and this was left in the dark at 37 °C for 2 h, 300 rpm. The excess reagent was then removed using a desalting column (PD Minitrap G-25, GE Healthcare) followed by ultrafiltration (10 kDa MWCO) into conjugate buffer to concentrate the sample. Lastly, sample was buffer swapped into 50 mM ammonium acetate pH 7.0 (7 kDa MWCO, ZebaSpin) and adjusted to 6.5 μM, following addition of 0.5 μL of PNGase F, the reaction was left at 37 °C for 16 h. Prior LCMS analysis the sample was adjusted to 2 μM with 50 mM ammonium acetate pH 7.0. Concentration was determined photometrically using ε_{280} = 215380 M^{-1} cm^{-1}.

a)

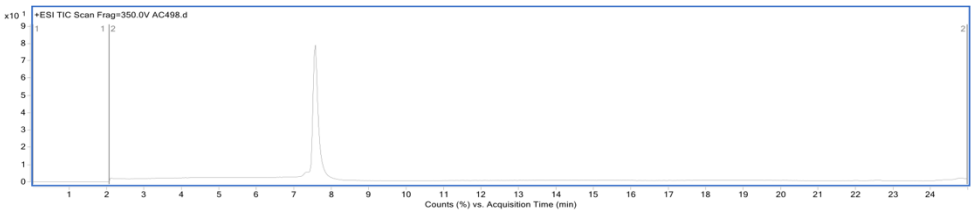

b)

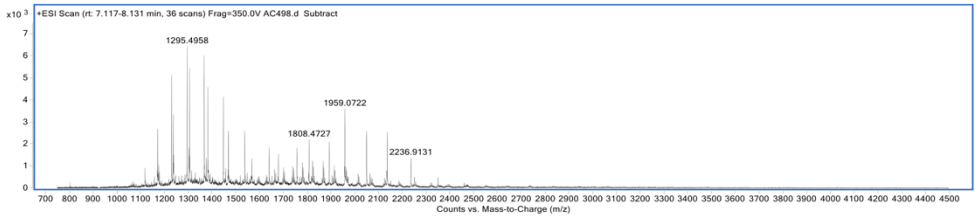

c)

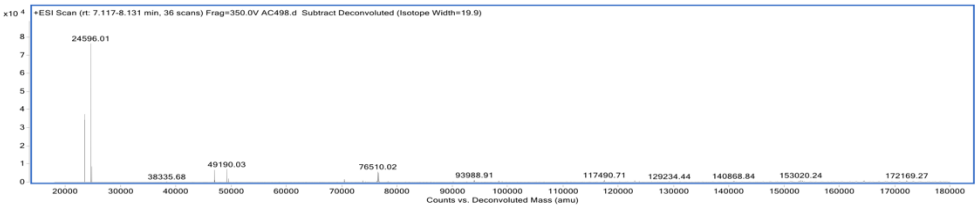

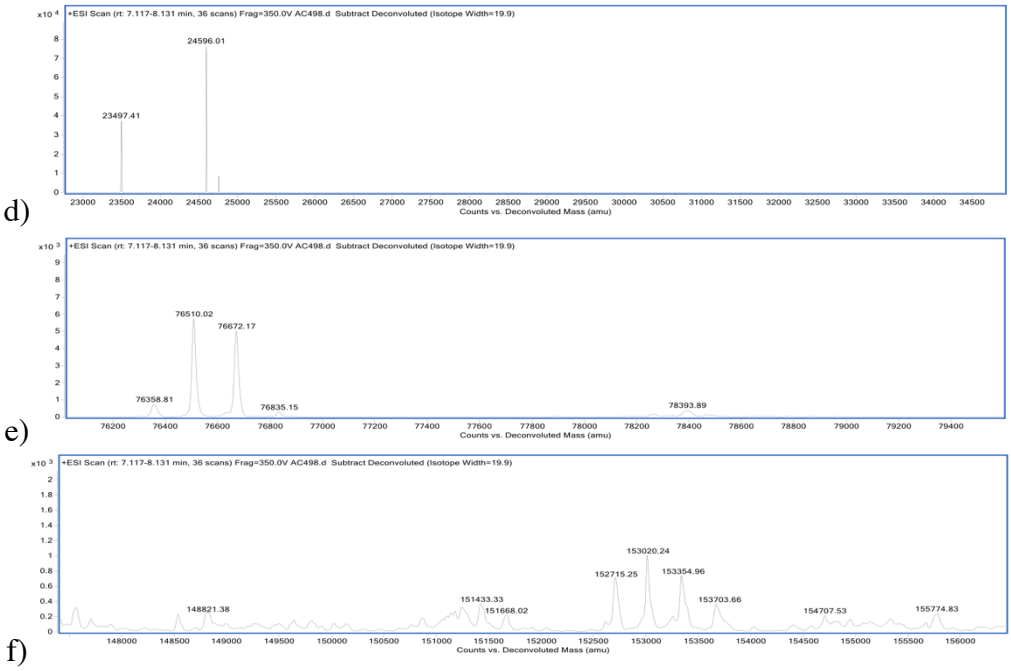

Figure 132. LCMS analysis of rebridging of full antibody with α-chlorothioester **1**, followed by cysteine, PD-BCN and Azide fluor 488; a) TIC, b) non-deconvoluted ion-series, c) full range deconvoluted ion series mass spectrum, d) zoomed in deconvoluted ion series mass spectrum, LC area, e) zoomed in deconvoluted ion series mass spectrum, HL area, f) zoomed in deconvoluted ion series mass spectrum, HHLL area.

7.3.47 Reaction of thioester conjugate on full antibody with TAT peptide

Trastuzumab full antibody (50 μL, 30 μM, 4.35 mg/mL) in conjugation buffer was reduced with tris(2-carboxyethyl)phosphine (TCEP) (0.6 μL, 15 mM in diH_2O, 6 eq.). The mixture was incubated at 37 °C for 2 h, 300 rpm. Following that, α-chlorothioester **1** (0.6 μL, 24 mM in DMF, 10 eq.) was added and incubated at 22 °C for 1 h. After that, TAT peptide (5.2 μL, 10 mM in diH_2O and 15 % MeCN, 50 eq.) was added and left at 37 °C for 16 h, 300 rpm. Lastly, sample was buffer swapped into 50 mM ammonium acetate pH 7.0 (7 kDa MWCO, ZebaSpin) and adjusted to 6.5 μM, following addition of 0.5 μL of PNGase F, the reaction was left at 37 °C for 16 h. Prior LCMS analysis the sample was adjusted to 2 μM with 50 mM ammonium acetate pH 7.0. Concentration was determined photometrically using $\varepsilon_{280} = 215380\ M^{-1}\ cm^{-1}$.

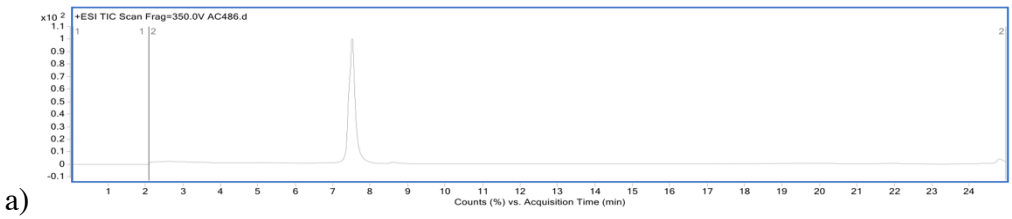

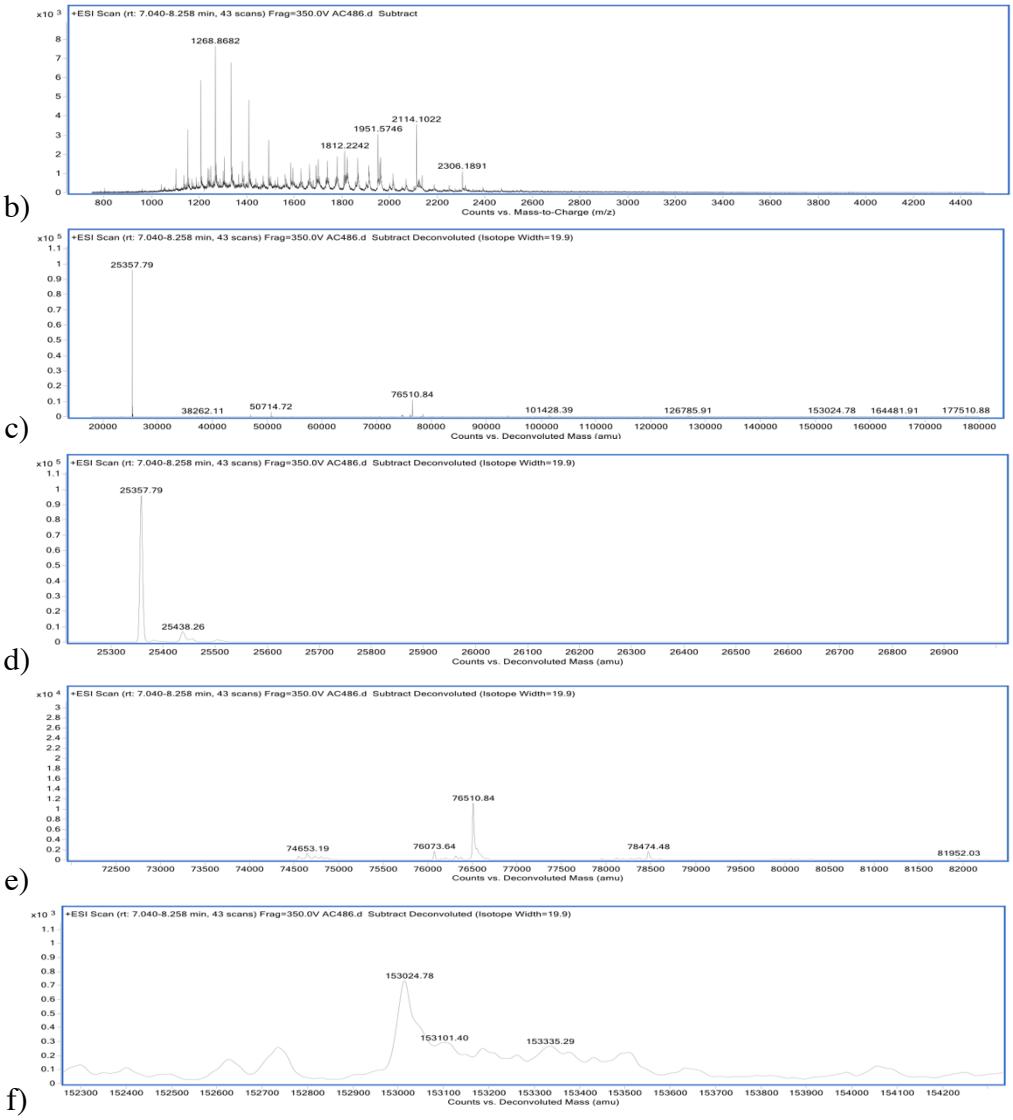

Figure 133. LCMS analysis of rebridging of full antibody with α-chlorothioester **1** and TAT peptide; a) TIC, b) non-deconvoluted ion-series, c) full range deconvoluted ion series mass spectrum, d) zoomed in deconvoluted ion series mass spectrum, LC area, e) zoomed in deconvoluted ion series mass spectrum, HL area, f) zoomed in deconvoluted ion series mass spectrum, HHLL area.

7.3.48 Reaction of thioester conjugate on full antibody with TAT peptide and PD

Trastuzumab full antibody (50 μL, 30 μM, 4.35 mg/mL) in conjugation buffer was reduced with tris(2-carboxyethyl)phosphine (TCEP) (0.6 μL, 15 mM in diH_2O, 6 eq.). The mixture was incubated at 37 °C for 2 h, 300 rpm. Following that, α-chlorothioester **1** (0.6 μL, 24 mM in DMF, 10 eq.) was added and incubated at 22 °C for 1 h. After that, TAT peptide (5.3 μL, 10 mM in diH_2O and 15 % MeCN, 50 eq.) was added and left at 37 °C for 16 h, 300 rpm. Upon completion of this step, excess of the reagents was removed *via* ultrafiltration (10 kDa MWCO) into

conjugation buffer, new antibody concentration was determined. TCEP reduction was performed again as before followed by removal of the excess of the reagent. Subsequently, BCN-PD (0.3 μL, 20 mM in DMSO, 10 eq.) was added and left at 37 °C for 2 h, 300 rpm. Lastly, sample was buffer swapped into 50 mM ammonium acetate pH 7.0 (7 kDa MWCO, ZebaSpin) and adjusted to 6.5 μM, following addition of 0.5 μL of PNGase F, the reaction was left at 37 °C for 16 h. Prior LCMS analysis the sample was adjusted to 2 μM with 50 mM ammonium acetate pH 7.0. Concentration was determined photometrically using $\varepsilon_{280} = 215380\ M^{-1}\ cm^{-1}$.

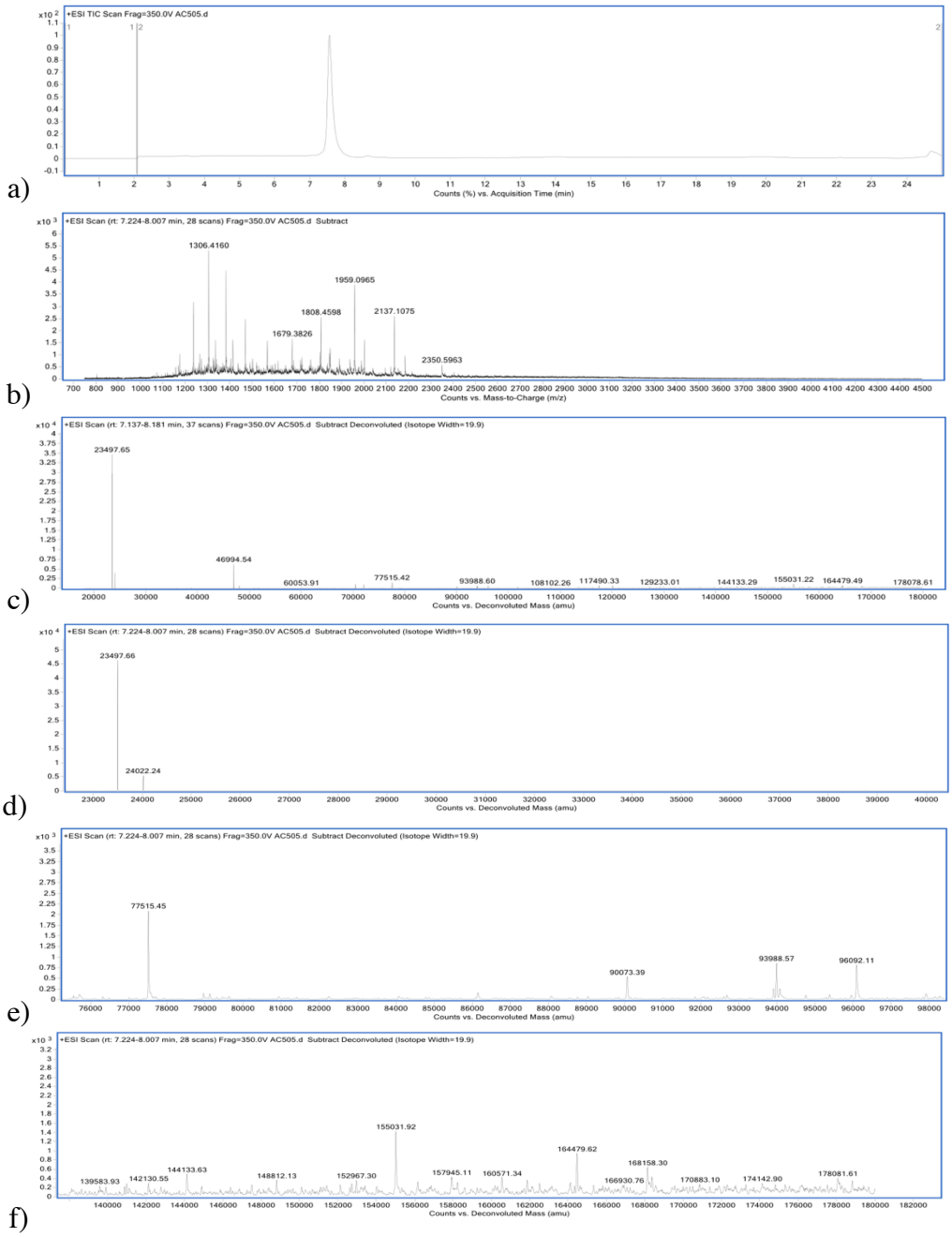

Figure 134. LCMS analysis of rebridging of full antibody with α-chlorothioester **1**, TAT peptide and PD-BCN; a) TIC, b) non-deconvoluted ion-series, c) full range deconvoluted ion series mass spectrum, d) zoomed in deconvoluted ion series mass spectrum, LC area, e)

zoomed in deconvoluted ion series mass spectrum, HL area, f) zoomed in deconvoluted ion series mass spectrum, HHLL area.

7.3.49 Reaction of thioester conjugate on full antibody with TAT, PD and fluorophore

Trastuzumab full antibody (50 μL, 30 μM, 4.35 mg/mL) in conjugation buffer was reduced with tris(2-carboxyethyl)phosphine (TCEP) (0.6 μL, 15 mM in diH_2O, 6 eq.). The mixture was incubated at 37 °C for 2 h, 300 rpm. Following that, α-chlorothioester **1** (0.6 μL, 24 mM in DMF, 10 eq.) was added and incubated at 22 °C for 1 h. After that, TAT peptide (5.6 μL, 10 mM in diH_2O and 15 % MeCN, 50 eq.) was added and left at 37 °C for 16 h, 300 rpm. Upon completion of this step, excess of the reagents was removed *via* ultrafiltration (10 kDa MWCO) into conjugation buffer, new antibody concentration was determined. TCEP reduction was performed again as before followed by removal of the excess of the reagent. Subsequently, BCN-PD (0.2 μL, 20 mM in DMSO, 10 eq.) was added and left at 37 °C for 2 h, 300 rpm. This was followed by another ultrafiltration to remove excess of the reagent. Finally, Azide fluor 488 (0.4 μL, 10 mM in DMF, 10 eq.) was added and this was left in the dark at 37 °C for 2 h, 300 rpm. The excess reagent was then removed using a desalting column (PD Minitrap G-25, GE Healthcare) followed by ultrafiltration (10 kDa MWCO) into conjugate buffer to concentrate the sample. Lastly, sample was buffer swapped into 50 mM ammonium acetate pH 7.0 (7 kDa MWCO, ZebaSpin) and adjusted to 6.5 μM, following addition of 0.5 μL of PNGase F, the reaction was left at 37 °C for 16 h. Prior LCMS analysis the sample was adjusted to 2 μM with 50 mM ammonium acetate pH 7.0. Concentration was determined photometrically using ε_{280} = 215380 M^{-1} cm^{-1}.

a)

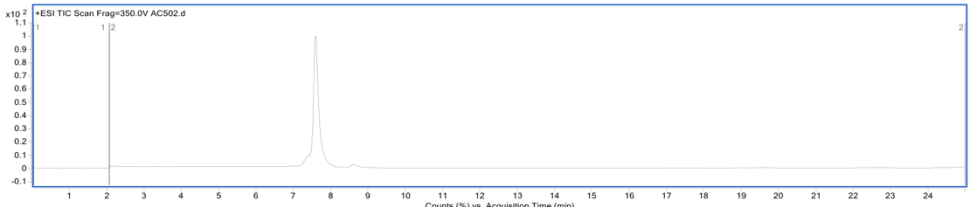

b)

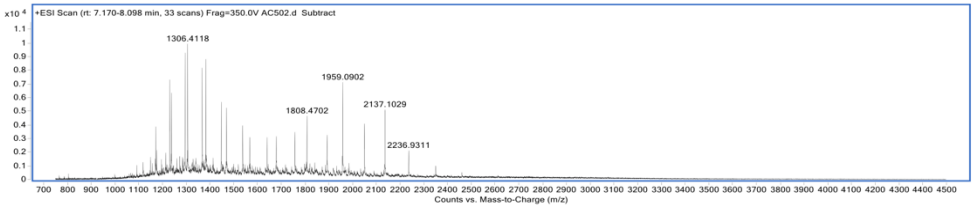

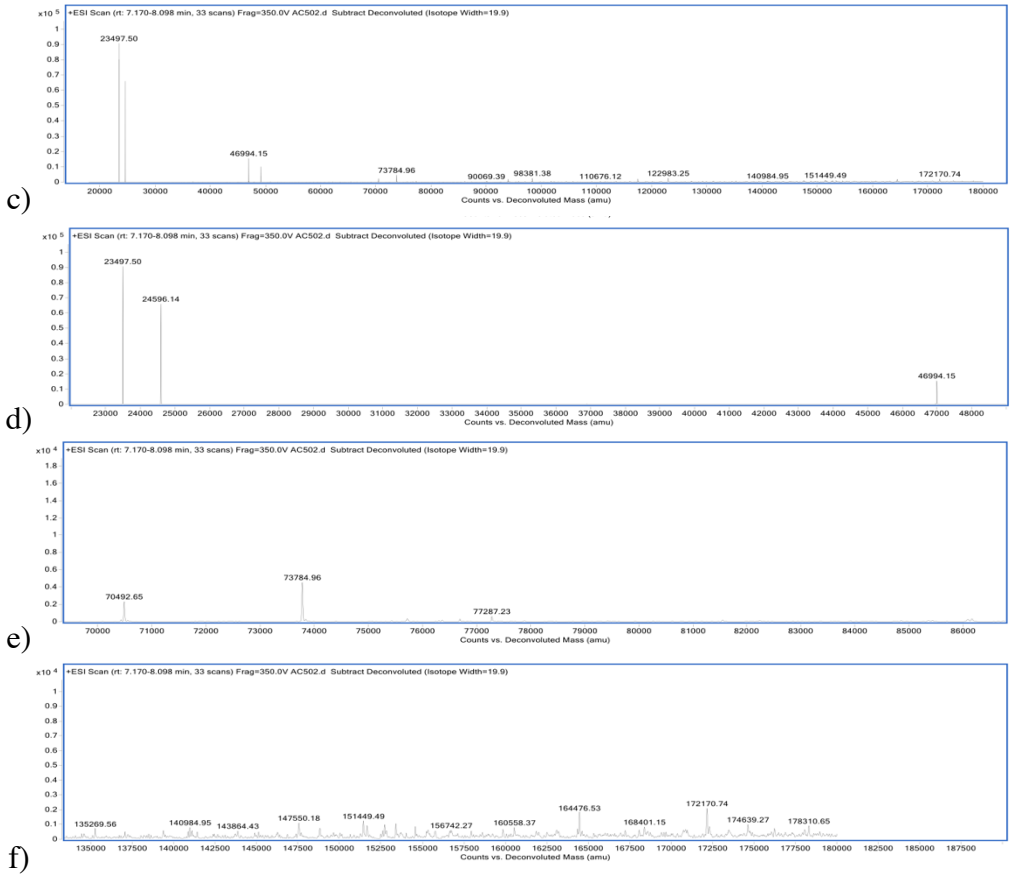

Figure 135. LCMS analysis of rebridging of full antibody with α-chlorothioester **1**, TAT, PD-BCN, and Azide fluor 488; a) TIC, b) non-deconvoluted ion-series, c) full range deconvoluted ion series mass spectrum, d) zoomed in deconvoluted ion series mass spectrum, LC area, e) zoomed in deconvoluted ion series mass spectrum, HL area, f) zoomed in deconvoluted ion series mass spectrum, HHLL area.

References

1 A. Chrzastek, I. A. Thanasi, J. A. Irving, V. Chudasama and J. R. Baker, *Chem. Sci.*, 2022, **13**, 11533–11539.

2 J. Jay, B. Bray, Y. Qi, E. Igbinigie, H. Wu, J. Li and G. Ren, *Antibodies*, 2018, **7**, 18.

3 L. J. Harris, E. Skaletsky and A. McPherson, *J. Mol. Biol.*, 1998, **275**, 861–872.

4 A. V. J. Collis, A. P. Brouwer and A. C. R. Martin, *J. Mol. Biol.*, 2003, **325**, 337–354.

5 G. Vidarsson, G. Dekkers and T. Rispens, *Front. Immunol.*, 2014, **5**, 1–17.

6 P. T. M. walport K. Murphy; C. Janeway, *Janeway's Immunology*, 2013.

7 Q. Zhou, *Biomedicines*, 2017, **5**, 64.

8 H. Kaplon, A. Chenoweth, S. Crescioli and J. M. Reichert, *MAbs*, 2022, **14**, e2014296.

9 H. Kaplon, M. Muralidharan, Z. Schneider and J. M. Reichert, *MAbs*, 2020, **12**, e1703531.

10 H. Kaplon and J. M. Reichert, *MAbs*, 2019, **11**, 219–238.

11 S. A. Beers, M. J. Glennie and A. L. White, *Blood*, 2016, **127**, 1097–1101.

12 A. L. Grilo and A. Mantalaris, *Trends Biotechnol.*, 2019, **37**, 9–16.

13 C. Bahou, E. A. Love, S. Leonard, R. J. Spears, A. Maruani, K. Armour, J. R. Baker and V. Chudasama, *Bioconjug. Chem.*, 2019, **30**, 1048–1054.

14 P. Zhao, Y. Zhang, W. Li, C. Jeanty, G. Xiang and Y. Dong, *Acta Pharm. Sin. B*, 2020, **10**, 1589–1600.

15 P. Dennler, E. Fischer and R. Schibli, *Antibodies*, 2015, **4**, 197–224.

16 J. Z. Drago, S. Modi and S. Chandarlapaty, *Nat. Rev. Clin. Oncol.*, 2021, **18**, 327–344.

17 Y. Chu, X. Zhou and X. Wang, *J. Hematol. Oncol.*, 2021, **14**, 1–20.

18 V. Kostova, P. Désos, J.-B. Starck and A. Kotschy, *Pharmaceuticals*, 2021, **14**, 1–46.

19 S. Ali, H. Dunmore, D. Karres, J. L. Hay, T. Salmonsson, C. Gisselbrecht, S. B. Sarac, O. W. Bjerrum, D. Hovgaard, Y. Barbachano, N. Nagercoil and F. Pignatti, *Oncologist*, 2019, **24**, 171–179.

20 P. R. Hamann, L. M. Hinman, I. Hollander, C. F. Beyer, D. Lindh, R. Holcomb, W. Hallett, H. R. Tsou, J. Upeslacis, D. Shochat, A. Mountain, D. A. Flowers and I. Bernstein, *Bioconjug. Chem.*, 2002, **13**, 47–58.

21 Q. Jiang, B. Patel, X. Jin, D. Di Grandi, E. Bortell, B. Czapkowski, T. F. Lerch, D. Meyer, S. Patel, J. Pegg, A. Arbuckle, J. Lagliva, V. Sriskanda, L. Letendre, H. Li, E. Thomas and D. Nadkarni, *ACS Omega*, 2019, **4**, 6468–6475.

22 J. Lu, F. Jiang, A. Lu and G. Zhang, *Int. J. Mol. Sci.*, 2016, **17**, 561.

23 J. A. Francisco, C. G. Cerveny, D. L. Meyer, B. J. Mixan, K. Klussman, D. F. Chace, S. X. Rejniak, K. A. Gordon, R. DeBlanc, B. E. Toki, C. L. Law, S. O. Doronina, C. B. Siegall, P. D. Senter and A. F. Wahl, *Blood*, 2003, **102**, 1458–1465.

24 C. Vaklavas and A. Forero-Torres, *Ther. Adv. Hematol.*, 2012, **3**, 209–225.

25 J. Katz, J. E. Janik and A. Younes, *Clin. Cancer Res.*, 2011, **17**, 6428–6436.

26 Y. Chen, M. T. Kim, L. Zheng, G. Deperalta and F. Jacobson, *Bioconjug. Chem.*, 2016, **27**, 2037–2047.

27 L. Amiri-Kordestani, G. M. Blumenthal, Q. C. Xu, L. Zhang, S. W. Tang, L. Ha, W. C. Weinberg, B. Chi, R. Candau-Chacon, P. Hughes, A. M. Russell, S. P. Miksinski, X. H. Chen, W. D. McGuinn, T. Palmby, S. J. Schrieber, Q. Liu, J. Wang, P. Song, N. Mehrotra, L. Skarupa, K. Clouse, A. Al-Hakim, R. Sridhara, A. Ibrahim, R. Justice, R. Pazdur and P. Cortazar, *Clin. Cancer Res.*, 2014, **20**, 4436–4441.

28 M. Barok, H. Joensuu and J. Isola, *Breast Cancer Res.*, 2014, **16**, 1–12.

29 E. D. Deeks, *Drugs*, 2019, **79**, 1467–1475.

30 R. Ohri, S. Bhakta, A. Fourie-O'Donohue, J. Dela Cruz-Chuh, S. P. Tsai, R. Cook, B. Wei, C. Ng, A. W. Wong, A. B. Bos, F. Farahi, J. Bhakta, T. H. Pillow, H. Raab, R. Vandlen, P. Polakis, Y. Liu, H. Erickson, J. R. Junutula and K. R. Kozak, *Bioconjug. Chem.*, 2018, **29**, 473–485.

31 A. G. Polson, S. F. Yu, K. Elkins, B. Zheng, S. Clark, G. S. Ingle, D. S. Slaga, L. Giere, C. Du, C. Tan, J. A. Hongo, A. Gogineni, M. J. Cole, R. Vandlen, J. P. Stephan, J. Young, W. Chang, S. J. Scales, S. Ross, D. Eaton and A. Ebens, *Blood*, 2007, **110**, 616–623.

32 Z. Xu, D. Guo, Z. Jiang, R. Tong, P. Jiang, L. Bai, L. Chen, Y. Zhu, C. Guo, J. Shi and D. Yu, *Eur. J. Med. Chem.*, 2019, **183**, 111682.

33 S. J. Keam, *Drugs*, 2020.

34 Y. Ogitani, T. Aida, K. Hagihara, J. Yamaguchi, C. Ishii, N. Harada, M. Soma, H. Okamoto, M. Oitate, S. Arakawa, T. Hirai, R. Atsumi, T. Nakada, I. Hayakawa, Y. Abe and T. Agatsuma, *Clin. Cancer Res.*, 2016, **22**, 5097–5108.

35 P. M. Challita-Eid, D. Satpayev, P. Yang, Z. An, K. Morrison, Y. Shostak, A. Raitano, R. Nadell, W. Liu, D. R. Lortie, L. Capo, A. Verlinsky, M. Leavitt, F. Malik, H. Avina, C. I. Guevara, N. Dinh, S. Karki, B. S. Anand, D. S. Pereira, I. B. J. Joseph, F. Donate, K. Morrison and D. R. Stover, *Cancer Res.*, 2016, **76**, 3003–3013.

36 S. Sahota and L. T. Vahdat, *Expert Opin. Biol. Ther.*, 2017, **17**, 1027–1031.

37 W. Dong, J. Shi, T. Yuan, B. Qi, J. Yu, J. Dai and L. He, *Eur. J. Med. Chem.*, 2019, **167**, 583–593.

38 S. Trudel, N. Lendvai, R. Popat, P. M. Voorhees, B. Reeves, E. N. Libby, P. G. Richardson, A. Hoos, I. Gupta, V. Bragulat, Z. He, J. B. Opalinska and A. D. Cohen, *Blood Cancer J.*, 2019, **9**, 1–10.

39 N. Joubert, A. Beck, C. Dumontet and C. Denevault-Sabourin, *Pharmaceuticals*, 2020, 1–31.

40 F. Zammarchi, S. Corbett, L. Adams, P. C. Tyrer, K. Kiakos, N. Janghra, T. Marafioti, C. E. Britten, C. E. G. Havenith, S. Chivers, F. D'Hooge, D. G. Williams, A. Tiberghien, P. W. Howard, J. A. Hartley and P. H. Van Berkel, *Blood*, 2018, **131**, 1094–1105.

41 X. Zhang, Q. Li, H. Zhao, L. Ma, T. Meng, J. Qian, R. Jin, J. Shen and K. Yu, *Oncotarget*, 2017, **8**, 59086–59102.

42 D. A. Richards, *Drug Discov. Today Technol.*, 2018, **30**, 35–46.

43 S. Jäger, T. R. Wagner, N. Rasche, H. Kolmar, S. Hecht and C. Schröter, *Bioconjug. Chem.*, 2021, **32**, 1699–1710.

44 A. Bates and C. A. Power, *Antibodies*, 2019, **8**, 28.

45 Z. Zhou, J. Zhang, Y. Zhang, G. Ma and Z. Su, *Bioconjug. Chem.*, 2016, **27**, 238–246.

46 R. P. Lyon, T. D. Bovee, S. O. Doronina, P. J. Burke, J. H. Hunter, H. D. Neff-Laford, M. Jonas, M. E. Anderson, J. R. Setter and P. D. Senter, *Nat. Biotechnol.*, 2015, **33**, 733–735.

47 R. Ahamadi-Fesharaki, A. Fateh, F. Vaziri, G. Solgi, S. D. Siadat, F. Mahboudi and F. Rahimi-Jamnani, *Mol. Ther. - Oncolytics*, 2019, **14**, 38–56.

48 C. Spiess, Q. Zhai and P. J. Carter, *Mol. Immunol.*, 2015, **67**, 95–106.

49 A. Pishko and S. D. Nasta, *Transl. Cancer Res.*, 2017, **6**, 93–103.

50 A. Beck, L. Goetsch, C. Dumontet and N. Corvaïa, *Nat. Rev. Drug Discov.*, 2017, **16**, 315–337.

51 B. Nolting, *Methods Mol. Biol.*, 2013, **1045**, 71–100.

52 J. D. Bargh, S. J. Walsh, A. Isidro-Llobet, S. Omarjee, J. S. Carroll and D. R. Spring, *Chem. Sci.*, 2020, **11**, 2375–2380.

53 P. Khongorzul, C. J. Ling, F. U. Khan, A. U. Ihsan and J. Zhang, *Mol. Cancer Res.*, 2020, **18**, 3–19.

54 H. L. Perez, P. M. Cardarelli, S. Deshpande, S. Gangwar, G. M. Schroeder, G. D. Vite

and R. M. Borzilleri, *Drug Discov. Today*, 2014, **19**, 869–881.

55 R. A. Firestone, D. Willner, S. J. Hofstead, H. D. King, T. Kaneko, G. R. Braslawsky, R. S. Greenfield, P. A. Trail, S. J. Lasch, A. J. Henderson, A. M. Casazza, I. Hellström and K. E. Hellström, *J. Control. Release*, 1996, **39**, 251–259.

56 M. Thomas, J. Clarhaut, P. O. Strale, I. Tranoy-Opalinski, J. Roche and S. Papot, *ChemMedChem*, 2011, **6**, 1006–1010.

57 W. C. Widdison, S. D. Wilhelm, E. E. Cavanagh, K. R. Whiteman, B. A. Leece, Y. Kovtun, V. S. Goldmacher, H. Xie, R. M. Steeves, R. J. Lutz, R. Zhao, L. Wang, W. A. Blättler, R. V. J. J. Chari, I. Ojima, X. Geng, X. Wu, C. Qu, C. P. Borella, H. Xie, S. D. Wilhelm, B. A. Leece, L. M. Bartle, V. S. Goldmacher and R. V. J. J. Chari, *J. Med. Chem.*, 2006, **49**, 5620–5623.

58 A. Mukherjee, A. K. Waters, I. Babic, E. Nurmemmedov, M. C. Glassy, S. Kesari and V. M. Yenugonda, *Hum. Antibodies*, 2018, **27**, 53–62.

59 J. E. Koblinski, M. Ahram and B. F. Sloane, *Clin. Chim. Acta*, 2000, **291**, 113–135.

60 S. S. Matikonda, R. McLaughlin, P. Shrestha, C. Lipshultz and M. J. Schnermann, *Bioconjug. Chem.*, 2022, **33**, 1241–1253.

61 H. Luesch, G. Harrigan, G. Goetz and F. Horgen, *Curr. Med. Chem.*, 2012, **9**, 1791–1806.

62 J. Anderl, H. Faulstich, T. Hechler and M. Kulke, in *Antibody–Drug Conjugate Payloads*, Springer Protocols, Totowa, New Jersey, 2013, pp. 51–70.

63 J. M. Lambert and R. V. J. Chari, *J. Med. Chem.*, 2014, **57**, 6949–6964.

64 B. Shor, H. P. Gerber and P. Sapra, *Mol. Immunol.*, 2015, **67**, 107–116.

65 N. K. Damle and P. Frost, *Curr. Opin. Pharmacol.*, 2003, **3**, 386–390.

66 Y. Ogitani, Y. Abe, T. Iguchi, J. Yamaguchi, T. Terauchi, M. Kitamura, K. Goto, M. Goto, M. Oitate, H. Yukinaga, Y. Yabe, T. Nakada, T. Masuda, K. Morita and T. Agatsuma, *Bioorganic Med. Chem. Lett.*, 2016, **26**, 5069–5072.

67 M. S. Kang, T. W. S. Kong, J. Y. X. Khoo and T. P. Loh, *Chem. Sci.*, 2021, **12**, 13613–13647.

68 C. Sornay, V. Vaur, A. Wagner and G. Chaubet, *R. Soc. Open Sci.*, 2022, **9**, 1–39.

69 P. A. Szijj, K. A. Kostadinova, R. J. Spears and V. Chudasama, *Org. Biomol. Chem.*, 2020, **18**, 9018–9028.

70 H. Tagawa, K. Maruyama, K. Sasaki, N. Konoue, A. Kishimura, M. Kanai, T. Mori, K. Oisaki and Y. Katayama, *RSC Adv.*, 2020, **10**, 16727–16731.

71 S. Lin, X. Yang, S. Jia, A. M. Weeks, M. Hornsby, P. S. Lee, R. V. Nichiporuk, A. T. Iavarone, J. A. Wells, F. D. Toste and C. J. Chang, *Science (80-.).*, 2017, **355**, 597–602.

72 V. Gautier, A. J. Boumeester, P. Lössl and A. J. R. Heck, *Proteomics*, 2015, **15**, 2756–2765.

73 M. Haque, N. Forte and J. R. Baker, *Chem. Commun.*, 2021, **57**, 10689–10702.

74 T. Tamura and I. Hamachi, *J. Am. Chem. Soc.*, 2019, **141**, 2782–2799.

75 G. T. Hermanson, in *Bioconjugate Techniques*, 2013, pp. 229–258.

76 O. Koniev and A. Wagner, *Chem. Soc. Rev.*, 2015, **44**, 5495–5551.

77 T. Nakamura, Y. Kawai, N. Kitamoto, T. Osawa and Y. Kato, *Chem. Res. Toxicol.*, 2009, **22**, 536–542.

78 L. Petri, P. A. Szijj, Á. Kelemen, T. Imre, Á. Gömöry, M. T. W. Lee, K. Hegedus, P. Ábrányi-Balogh, V. Chudasama and G. M. Keseru, *RSC Adv.*, 2020, **10**, 14928–14936.

79 M. E. Annunziato, U. S. Patel, M. Ranade and P. S. Palumbo, *Bioconjug. Chem.*, 1993, **4**, 212–218.

80 J. E. T. Corrie, C. T. Davis and J. F. Eccleston, *Bioconjug. Chem.*, 2001, **12**, 186–194.

81 M. J. Matos, B. L. Oliveira, N. Martínez-Sáez, A. Guerreiro, P. M. S. D. Cal, J. Bertoldo, M. Maneiro, E. Perkins, J. Howard, M. J. Deery, J. M. Chalker, F. Corzana, G. Jiménez-Osés and G. J. L. Bernardes, *J. Am. Chem. Soc.*, 2018, **140**, 4004–4017.

82 N. Forte, I. Benni, K. Karu, V. Chudasama and J. Baker, *Chem. Sci.*, 2019, **10**, 10919–10924.

83 K. Yamada, N. Shikida, K. Shimbo, Y. Ito, Z. Khedri, Y. Matsuda and B. A. Mendelsohn, *Angew. Chemie - Int. Ed.*, 2019, **58**, 5592–5597.

84 S. J. Walsh, J. D. Bargh, F. M. Dannheim, A. R. Hanby, H. Seki, A. J. Counsell, X. Ou, E. Fowler, N. Ashman, Y. Takada, A. Isidro-Llobet, J. S. Parker, J. S. Carroll and D. R. Spring, *Chem. Soc. Rev.*, 2021, **50**, 1305–1353.

85 F. F. Schumacher, M. Nobles, C. P. Ryan, M. E. B. Smith, A. Tinker, S. Caddick and J. R. Baker, *Bioconjug. Chem.*, 2011, **22**, 132–136.

86 K. Tsuchikama and Z. An, *Protein Cell*, 2018, **9**, 33–46.

87 S. B. Gunnoo and A. Madder, *ChemBioChem*, 2016, **17**, 529–553.

88 K. G. Byler, Y. Li, R. A. Houghten and K. Martinez-Mayorga, *Org. Biomol. Chem.*, 2013, **11**, 2979–2987.

89 C. Zhang, E. V. Vinogradova, A. M. Spokoyny, S. L. Buchwald and B. L. Pentelute, *Angew. Chemie - Int. Ed.*, 2019, **58**, 4810–4839.

90 C. Jonathan, G. Nick and W. Stuart, *Organic Chemistry*, Oxford University Press, Oxford, Second Edi., 2012.

91 O. Koniev and A. Wagner, *Chem. Soc. Rev.*, 2015, **44**, 5495–5551.

92 J. T. Patterson, S. Asano, X. Li, C. Rader and C. F. Barbas, *Bioconjug. Chem.*, 2014, **25**, 1402–1407.

93 M. Morpurgo, F. M. Veronese, D. Kachensky and J. M. Harris, *Bioconjug. Chem.*, 1996, **7**, 363–368.

94 J. Morales-Sanfrutos, F. J. Lopez-Jaramillo, F. Hernandez-Mateo and F. Santoyo-Gonzalez, *J. Org. Chem.*, 2010, **75**, 4039–4047.

95 B. Bernardim, M. J. Matos, X. Ferhati, I. Compañón, A. Guerreiro, P. Akkapeddi, A. C. B. Burtoloso, G. Jiménez-Osés, F. Corzana and G. J. L. Bernardes, *Nat. Protoc.*, 2019, **14**, 86–99.

96 S. Kolodych, O. Koniev, Z. Baatarkhuu, J. Y. Bonnefoy, F. Debaene, S. Cianférani, A. Van Dorsselaer and A. Wagner, *Bioconjug. Chem.*, 2015, **26**, 197–200.

97 P. Strop, S. H. Liu, M. Dorywalska, K. Delaria, R. G. Dushin, T. T. Tran, W. H. Ho, S. Farias, M. G. Casas, Y. Abdiche, D. Zhou, R. Chandrasekaran, C. Samain, C. Loo, A. Rossi, M. Rickert, S. Krimm, T. Wong, S. M. Chin, J. Yu, J. Dilley, J. Chaparro-Riggers, G. F. Filzen, C. J. O'Donnell, F. Wang, J. S. Myers, J. Pons, D. L. Shelton and A. Rajpal, *Chem. Biol.*, 2013, **20**, 161–167.

98 L. M. Tedaldi, M. E. B. Smith, R. I. Nathani and J. R. Baker, *Chem. Commun.*, 2009, **43**, 6583–6585.

99 P. Moody, M. E. B. Smith, C. P. Ryan, V. Chudasama, J. R. Baker, J. Molloy and S. Caddick, *ChemBioChem*, 2012, **13**, 39–41.

100 F. F. Schumacher, J. P. M. Nunes, A. Maruani, V. Chudasama, M. E. B. Smith, K. A. Chester, J. R. Baker and S. Caddick, *Org. Biomol. Chem.*, 2014, **12**, 7261–7269.

101 N. Forte, V. Chudasama and J. R. Baker, *Drug Discov. Today Technol.*, 2018, 30, 11–20.

102 V. Chudasama, M. E. B. Smith, F. F. Schumacher, D. Papaioannou, G. Waksman, J. R. Baker and S. Caddick, *Chem. Commun.*, 2011, **47**, 8781–8783.

103 C. Bahou, P. A. Szijj, R. J. Spears, A. Wall, F. Javaid, A. Sattikar, E. A. Love, J. R. Baker and V. Chudasama, *Bioconjug. Chem.*, 2021, **32**, 672–679.

104 O. Koniev, I. Dovgan, B. Renoux, A. Ehkirch, J. Eberova, S. Cianférani, S. Kolodych, S. Papot and A. Wagner, *Medchemcomm*, 2018, **9**, 827–830.

105 G. Badescu, P. Bryant, M. Bird, K. Henseleit, J. Swierkosz, V. Parekh, R. Tommasi, E.

Pawlisz, K. Jurlewicz, M. Farys, N. Camper, X. Sheng, M. Fisher, R. Grygorash, A. Kyle, A. Abhilash, M. Frigerio, J. Edwards and A. Godwin, *Bioconjug. Chem.*, 2014, **25**, 1124–1136.

106 S. J. Walsh, S. Omarjee, W. R. J. D. Galloway, T. T. L. Kwan, H. F. Sore, J. S. Parker, M. Hyvönen, J. S. Carroll and D. R. Spring, *Chem. Sci.*, 2019, **10**, 694–700.

107 C. Canovas, M. Moreau, C. Bernhard, A. Oudot, M. Guillemin, F. Denat and V. Goncalves, *Angew. Chemie - Int. Ed.*, 2018, **57**, 10646–10650.

108 N. Griebenow, S. Bräse and A. M. Dilmac, *RSC Adv.*, 2015, **5**, 54301–54303.

109 M. T. W Lee, A. Maruani, J. R. Baker, S. Caddick and V. Chudasama, *Chem. Sci.*, 2016, **7**, 799–802.

110 M. E. B. Smith, F. F. Schumacher, C. P. Ryan, L. M. Tedaldi, D. Papaioannou, G. Waksman, S. Caddick and J. R. Baker, *J. Am. Chem. Soc.*, 2010, **132**, 1960–1965.

111 J. P. M. Nunes, M. Morais, V. Vassileva, E. Robinson, V. S. Rajkumar, M. E. B. Smith, R. B. Pedley, S. Caddick, J. R. Baker and V. Chudasama, *Chem. Commun.*, 2015, **51**, 10624–10627.

112 M. W. Jones, R. A. Strickland, F. F. Schumacher, S. Caddick, J. R. Baker, M. I. Gibson and D. M. Haddleton, *J. Am. Chem. Soc.*, 2012, **134**, 1847–1852.

113 S. A. Fletcher, P. K. B. Sin, M. Nobles, E. Årstad, A. Tinker and J. R. Baker, *Org. Biomol. Chem.*, 2015, **13**, 9559–9563.

114 F. F. Schumacher, V. A. Sanchania, B. Tolner, Z. V. F. Wright, C. P. Ryan, M. E. B. Smith, J. M. Ward, S. Caddick, C. W. M. Kay, G. Aeppli, K. A. Chester and J. R. Baker, *Sci. Rep.*, 2013, **3**, 1–8.

115 D. A. Richards, S. A. Fletcher, M. Nobles, H. Kossen, L. Tedaldi, V. Chudasama, A. Tinker and J. R. Baker, *Org. Biomol. Chem.*, 2016, **14**, 455–459.

116 F. Bryden, A. Maruani, H. Savoie, V. Chudasama, M. E. B. Smith, S. Caddick and R. W. Boyle, *Bioconjug. Chem.*, 2014, **25**, 611–617.

117 M. Morais, J. P. M. Nunes, K. Karu, N. Forte, I. Benni, M. E. B. Smith, S. Caddick, V. Chudasama and J. R. Baker, *Org. Biomol. Chem.*, 2017, **15**, 2947–2952.

118 C. Bahou, D. A. Richards, A. Maruani, E. A. Love, F. Javaid, S. Caddick, J. R. Baker and V. Chudasama, *Org. Biomol. Chem.*, 2018, **16**, 1359–1366.

119 E. Robinson, J. P. M. Nunes, V. Vassileva, A. Maruani, J. C. F. Nogueira, M. E. B. Smith, R. B. Pedley, S. Caddick, J. R. Baker and V. Chudasama, *RSC Adv.*, 2017, **7**, 9073–9077.

120 G. T. Hermanson, *Bioconjugate Techniques*, Elsevier, Third., 2013.

121 P. Agarwal and C. R. Bertozzi, *Bioconjug. Chem.*, 2015, **26**, 176–192.

122 G. Chaubet, F. Thoreau and A. Wagner, *Drug Discov. Today Technol.*, 2018, **30**, 21–26.

123 P. Ochtrop and C. P. R. Hackenberger, *Curr. Opin. Chem. Biol.*, 2020, **58**, 28–36.

124 D. A. Shannon, R. Banerjee, E. R. Webster, D. W. Bak, C. Wang and E. Weerapana, *J. Am. Chem. Soc.*, 2014, **136**, 3330–3333.

125 J. R. Junutula, H. Raab, S. Clark, S. Bhakta, D. D. Leipold, S. Weir, Y. Chen, M. Simpson, S. P. Tsai, M. S. Dennis, Y. Lu, Y. G. Meng, C. Ng, J. Yang, C. C. Lee, E. Duenas, J. Gorrell, V. Katta, A. Kim, K. McDorman, K. Flagella, R. Venook, S. Ross, S. D. Spencer, W. Lee Wong, H. B. Lowman, R. Vandlen, M. X. Sliwkowski, R. H. Scheller, P. Polakis and W. Mallet, *Nat. Biotechnol.*, 2008, **26**, 925–932.

126 F. Tian, Y. Lu, A. Manibusan, A. Sellers, H. Tran, Y. Sun, T. Phuong, R. Barnett, B. Hehli, F. Song, M. J. DeGuzman, S. Ensari, J. K. Pinkstaff, L. M. Sullivan, S. L. Biroc, H. Cho, P. G. Schultz, J. Di Joseph, M. Dougher, D. Ma, R. Dushin, M. Leal, L. Tchistiakova, E. Feyfant, H. P. Gerber and P. Sapra, *Proc. Natl. Acad. Sci. U. S. A.*, 2014, **111**, 1766–1771.

127 M. S. K. Sutherland, R. B. Walter, S. C. Jeffrey, P. J. Burke, C. Yu, H. Kostner, I. Stone, M. C. Ryan, D. Sussman, R. P. Lyon, W. Zeng, K. H. Harrington, K. Klussman, L. Westendorf, D. Meyer, I. D. Bernstein, P. D. Senter, D. R. Benjamin, J. G. Drachman and J. A. McEarchern, *Blood*, 2013, **122**, 1455–1463.

128 E. M. Sletten and C. R. Bertozzi, *Angew. Chemie - Int. Ed.*, 2009, **48**, 6974–6998.

129 J. Liu, R. M. Barfield and D. Rabuka, in *Methods in Molecular Biology*, 2019.

130 M. Zimmer, *Chem. Soc. Rev.*, 2009, **38**, 2823.

131 H. C. Hang, C. Yu, D. L. Kato and C. R. Bertozzi, *Proc. Natl. Acad. Sci. U. S. A.*, 2003, **100**, 14846–14851.

132 T. A. Nigst, A. Antipova and H. Mayr, *J. Org. Chem.*, 2012, **77**, 8142–8155.

133 Y. Zeng, T. N. C. Ramya, A. Dirksen, P. E. Dawson and J. C. Paulson, *Nat. Methods*, 2009, **6**, 207–209.

134 E. Saxon and C. R. Bertozzi, *Science (80-.).*, 2000, **287**, 2007–2010.

135 V. V. Rostovtsev, L. G. Green, V. V. Fokin and K. B. Sharpless, *Angew. Chemie - Int. Ed.*, 2002, **41**, 2596–2599.

136 C. W. Tornøe, C. Christensen and M. Meldal, *J. Org. Chem.*, 2002, **67**, 3057–3064.

137 V. Hong, S. I. Presolski, C. Ma and M. G. Finn, *Angew. Chemie - Int. Ed.*, 2009, **49**,

9879–9883.

138 G. Wittig and A. Krebs, *Chem. Ber.*, 1961, **94**, 3260–3275.

139 N. J. Agard, J. A. Prescher and C. R. Bertozzi, *J. Am. Chem. Soc.*, 2004, **126**, 15046–15047.

140 C. G. Gordon, J. L. MacKey, J. C. Jewett, E. M. Sletten, K. N. Houk and C. R. Bertozzi, *J. Am. Chem. Soc.*, 2012, **134**, 9199–9208.

141 J. M. Baskin, J. A. Prescher, S. T. Laughlin, N. J. Agard, P. V. Chang, I. A. Miller, A. Lo, J. A. Codelli and C. R. Bertozzi, *Proc. Natl. Acad. Sci. U. S. A.*, 2007, **104**, 16793–16797.

142 X. Ning, J. Guo, M. A. Wolfert and G. J. Boons, *Angew. Chemie - Int. Ed.*, 2008, **47**, 2253–2255.

143 J. Dommerholt, S. Schmidt, R. Temming, L. J. A. Hendriks, F. P. J. T. Rutjes, J. C. M. Van Hest, D. J. Lefeber, P. Friedl and F. L. Van Delft, *Angew. Chemie - Int. Ed.*, 2010, **49**, 9422–9425.

144 E. C. B. Johnson and S. B. H. Kent, *J. Am. Chem. Soc.*, 2006, **128**, 6640–6646.

145 D. Macmillan, *Synlett*, 2017, **28**, 1517–1529.

146 V. Agouridas, O. El Mahdi, V. Diemer, M. Cargoët, J. C. M. Monbaliu and O. Melnyk, *Chem. Rev.*, 2019, **119**, 7328–7443.

147 K. Yan, D. Yang, W. Wei, J. Zhao, Y. Shuai, L. Tian and H. Wang, *Org. Biomol. Chem.*, 2015, **13**, 7323–7330.

148 B. Basu, S. Paul and A. K. Nanda, *Green Chem.*, 2010, **12**, 767–77.

149 X. L. Liu, Y. Shi, J. S. Kang, P. Oelschlaeger and K. W. Yang, *ACS Med. Chem. Lett.*, 2015, **6**, 660–664.

150 H. Shinkai, K. Maeda, T. Yamasaki, H. Okamoto and I. Uchida, *J. Med. Chem.*, 2000, **43**, 3566–3572.

151 T. Pillaiyar, P. Flury, N. Krüger, H. Su, L. Schäkel, E. Barbosa Da Silva, O. Eppler, T. Kronenberger, T. Nie, S. Luedtke, C. Rocha, K. Sylvester, M. R. I. Petry, J. H. McKerrow, A. Poso, S. Pöhlmann, M. Gütschow, A. J. O'Donoghue, Y. Xu, C. E. Müller and S. A. Laufer, *J. Med. Chem.*, 2022, **65**, 9376–9395.

152 S. Aksakal, R. Aksakal and C. R. Becer, *Polym. Chem.*, 2018, **9**, 4507–4516.

153 W. Yang and D. G. Drueckhammer, *J. Am. Chem. Soc.*, 2001, **123**, 11004–11009.

154 N. Zhou, L. Shen, Z. Dong, J. Shen, L. Du and X. Luo, *Catalysts*, 2018, **8**, 1–12.

155 A. T. Khan, L. H. Choudhury and S. Ghosh, *European J. Org. Chem.*, 2005, 2782–2787.

156 M. Kazemi and L. Shiri, *J. Sulfur Chem.*, 2015, **36**, 613–623.

157 W. Xuan, D. Collins, M. Koh, S. Shao, A. Yao, H. Xiao, P. Garner and P. G. Schultz, *ACS Chem. Biol.*, 2018, **13**, 578–581.

158 P. G. Hains and P. J. Robinson, *J. Proteome Res.*, 2017, **16**, 3443–3447.

159 P. A. Jackson, J. C. Widen, D. A. Harki and K. M. Brummond, *J. Med. Chem.*, 2017, **60**, 839–885.

160 A. Paasche, M. Schiller, T. Schirmeister and B. Engels, *ChemMedChem*, 2010, **5**, 869–880.

161 R. F. Hartman and S. D. Rose, *J. Org. Chem.*, 2006, **71**, 6342–6350.

162 R. J. Spears, A. Chrzastek, S. Y. Yap, K. Karu, A. E. Aliev, J. R. Baker and V. Chudasama, *Chem. Commun.*, 2022, **58**, 5359–5362.

163 E. A. Hull, University College London, 2014.

164 C. Bechara and S. Sagan, *FEBS Lett.*, 2013, **587**, 1693–1702.

165 S. G. Patel, E. J. Sayers, L. He, R. Narayan, T. L. Williams, E. M. Mills, R. K. Allemann, L. Y. P. Luk, A. T. Jones and Y. H. Tsai, *Sci. Rep.*, 2019, **9**, 1–9.

166 J. Xie, Y. Bi, H. Zhang, S. Dong, L. Teng, R. J. Lee and Z. Yang, *Front. Pharmacol.*, 2020, **11**, 1–23.

167 F. Milletti, *Drug Discov. Today*, 2012, **17**, 850–860.

168 A. Falanga, L. Lombardi, E. Galdiero, V. Del Genio and S. Galdiero, *Future Med. Chem.*, 2020, **12**, 1431–1446.

169 K. Kurrikoff, M. Gestin and Ü. Langel, *Expert Opin. Drug Deliv.*, 2016, 373–387.

170 F. Wang, Y. Wang, X. Zhang, W. Zhang, S. Guo and F. Jin, *J. Control. Release*, 2014, 126–136.

171 J. E. Dixon, G. Osman, G. E. Morris, H. Markides, M. Rotherham, Z. Bayoussef, A. J. El Haj, C. Denning and K. M. Shakesheff, *Proc. Natl. Acad. Sci. U. S. A.*, 2016, **113**, E291–E299.

172 A. Wall, A. G. Wills, N. Forte, C. Bahou, L. Bonin, K. Nicholls, M. T. Ma, V. Chudasama and J. R. Baker, *Chem. Sci.*, 2020, **11**, 11455–11460.

173 M. Maneiro, N. Forte, M. M. Shchepinova, C. S. Kounde, V. Chudasama, J. R. Baker and E. W. Tate, *ACS Chem. Biol.*, 2020, **15**, 1306–1312.

174 E. Vives, *J. Mol. Recognit.*, 2003, **16**, 265–271.

175 U. Niesner, C. Halin, L. Lozzi, M. Günthert, P. Neri, H. Wunderli-Allenspach, L. Zardi and D. Neri, *Bioconjug. Chem.*, 2002, **13**, 729–736.

176 J. Gaston, N. Maestrali, G. Lalle, M. Gagnaire, A. Masiero, B. Dumas, T. Dabdoubi, K. Radošević and P. F. Berne, *Sci. Rep.*, 2019, **9**, 1–12.

177 C. Bahou and V. Chudasama, *Org. Biomol. Chem.*, 2022, **20**, 5879–5890.

178 A. Maruani, P. A. Szijj, C. Bahou, J. C. F. Nogueira, S. Caddick, J. R. Baker and V. Chudasama, *Bioconjug. Chem.*, 2020, **31**, 520–529.

179 C. Bahou, E. A. Love, S. Leonard, R. J. Spears, A. Maruani, K. Armour, J. R. Baker and V. Chudasama, *Bioconjug. Chem.*, 2019, **30**, 1048–1054.

180 H. A. Cooke, J. Arndt, C. Quan, R. I. Shapiro, D. Wen, S. Foley, M. M. Vecchi and M. Preyer, *MAbs*, 2018, **10**, 1248–1259.

181 F. Sert, D. Hız, M. Gülmez, S. E. Cankurtaran, C. I. Kayalan, H. Kurt and M. Yüce, *Sci. Pharm.*, 2022, **90**, 1–13.

182 N. Bai, H. Roder, A. Dickson and J. Karanicolas, *Sci. Rep.*, 2019, **9**, 1–15.

183 L. Wu and B. Xu, *Curr. Protoc. Protein Sci.*, 2015, **79**, 19.

184 R. M. Ionescu, J. Vlasak, C. Price and M. Kirchmeier, *J. Pharm. Sci.*, 2008, **97**, 1414–1426.

185 P. Garidel, A. Eiperle, M. Blech and J. Seelig, *Biophys. J.*, 2020, **118**, 1067–1075.

186 F. Brotzel, C. C. Ying and H. Mayr, *J. Org. Chem.*, 2007, **72**, 3679–3688.

187 Y. C. Huang, G. M. Fang and L. Liu, *Natl. Sci. Rev.*, 2016, **3**, 107–116.

188 L. Benati, G. Calestani, R. Leardini, M. Minozzi, D. Nanni, P. Spagnolo and S. Strazzari, *Org. Lett.*, 2003, **5**, 1313–1316.

189 D. K. Kölmel and E. T. Kool, *Chem. Rev.*, 2017, **117**, 10358–10376.

190 C. D. Spicer, E. T. Pashuck and M. M. Stevens, *Chem. Rev.*, 2018, **118**, 7702–7743.

191 R. Nisal, G. Jose, C. Shanbhag and J. Kalia, *Org. Biomol. Chem.*, 2018, **16**, 4304–4310.

192 E. T. Kool, D. H. Park and P. Crisalli, *J. Am. Chem. Soc.*, 2013, **135**, 17663–17666.

193 H. Bouchard, C. Viskov and C. Garcia-Echeverria, *Bioorganic Med. Chem. Lett.*, 2014, **24**, 5357–5363.

194 Z. Fang, B. Jiang, W. Wu, Z. Xiang, C. Ouyang, T. Huang, J. Chen and L. Zeng, *Chem. Commun.*, 2013, **49**, 6164–6166.

195 P. Kovaříková, Z. Mrkvičková and J. Klimeš, *J. Pharm. Biomed. Anal.*, 2008, **47**, 360–370.

196 M. Trester-Zedlitz, K. Kamada, S. K. Burley, D. Fenyö, B. T. Chait and T. W. Muir, *Proc. 50th ASMS Conf. Mass Spectrom. Allied Top.*, 2002, 273–274.

197 N. Winssinger, *Chimia (Aarau).*, 2018, **72**, A755.

198 C. Hwang, A. J. Sinskey and H. F. Lodish, *Science (80-.).*, 1992, **257**, 1496–1502.

199 L. Pendyala, S. Velagapudi, K. Toth, J. Zdanowicz, D. Glaves, H. Slocum, R. Perez, R. Huben, P. J. Creaven and D. Raghavan, *Clin. Cancer Res.*, 1997, **3**, 793–798.

200 K. West and S. Otto, *Curr. Drug Discov. Technol.*, 2005, **2**, 123–160.

201 S. Santra, C. Kaittanis, O. J. Santiesteban and J. M. Perez, *J. Am. Chem. Soc.*, 2011, **133**, 16680–16688.

202 I. Dovydenko, I. Tarassov, A. Venyaminova and N. Entelis, *Biomaterials*, 2016, **76**, 408–417.

203 R. J. Christie, D. J. Anderson and D. W. Grainger, *Bioconjug. Chem.*, 2010, **21**, 1779–1787.

204 D. P. Humphreys, S. P. Heywood, A. Henry, L. Ait-Lhadj, P. Antoniw, R. Palframan, K. J. Greenslade, B. Carrington, D. G. Reeks, L. C. Bowering, S. West and H. A. Brand, *Protein Eng. Des. Sel.*, 2007, **20**, 227–234.

205 M. L. Geddie, D. B. Kirpotin, N. Kohli, T. Kornaga, B. Boll, M. Razlog, D. C. Drummond and A. A. Lugovskoy, *MAbs*, 2022, **14**, e2083466.

206 M. Acchione, H. Kwon, C. M. Jochheim and W. M. Atkins, *MAbs*, 2012, **4**, 362–372.

207 M. T. W. Lee, A. Maruani, J. R. Baker, S. Caddick and V. Chudasama, *Chem. Sci.*, 2016, **7**, 799–802.